UPPSALA UNIVERSITET

eawe
european academy of wind energy

20TH EAWE PHD SEMINAR

24-26 September 2024, Visby

fortum

SWECO

Region Gotland

Preface

The 20th EAWE PhD Seminar took place in Visby, Sweden, from September 24 to September 26. It was organized and hosted by the PhD Students of the Wind Energy Section of Uppsala University and the PhD Students from the AptWind doctoral network and with the support of the European Academy of Wind Energy.

Chairs:

Henry Korb

Mohammad Mehdi Mohammadi

Reviewers:

Jean Bastin

Keeta Chapman-Smith

Henry Korb

Mohammadreza Manami

Mohammad Mehdi Mohammadi

Ansh Patel

Peter Stammer

Thea Vanelli

The seminar was made possible with the support by:

Program

Tuesday, 24 September

09:00 - 10:00	Opening				
10:00 - 10:30	Coffee Break				
10:30 - 12:10	Wind farm flows and wakes	Wind resources, turbulence, and acoustics	Reliability, monitoring, and sensing technology	Control of wind turbines and wind farms	Production, O&M, decommissioning and lifetime extension
12:10 - 13:10	Lunch				
13:10 - 14:10	Wind farm flows and wakes	Aero-elastic and blade technology	Electrical conversion, energy system and wind power-to-X	Emerging technologies	
14:10 - 15:00	Coffee Break				
15:00 - 17:00	Skillsharing sessions				

Wednesday, 25 September

09:00 - 10:00	**Scientific Keynotes** Sandrine Aubrun Luca Lanzilao Tuhfe Göçmen				
10:00 - 10:30	Coffee Break				
10:30 - 12:00	**Industry Keynotes** Sonia Karl Spansk Sara Fogelström				
12:00 - 13:00	Lunch				
13:00 - 14:40	Wind farm flows and wakes	Wind resources, turbulence, and acoustics	Aero-elastic and blade technology	Production, O&M, decommissioning and lifetime extension	Support structures and geotechnics
14:40 - 15:10	Coffee Break				
15:10 - 16:50	Wind farm flows and wakes	Wind resources, turbulence, and acoustics	Floating wind turbines	Reliability, monitoring, and sensing technology	

Thursday, 26 September

09:00 - 10:00	Wind farm flows and wakes	Reliability, monitoring, and sensing technology	Aero-elastic and blade technology	Emerging technologies	
10:00 - 10:30	Coffee Break				
10:30 - 11:30	Control of wind turbines and wind farms	Support structures and geotechnics	Electrical conversion, energy system and wind power-to-X	Floating wind turbines	Reliability, monitoring, and sensing technology
11:30 - 12:00	Closing				
13:00 - 15:30	Outreach Activity				

Contents

TOPIC 1

Wind farm flows and wakes

1.1 Session 111: Wind farm flows and wakes

24.09.2024, 10:30, Room 1

Chair:

Isaac Bensignor

Presenters:

Delvaux Theo	A large-eddy simulation analysis of wind-farm axial-induction control strategies in conventionally neutral boundary layers
Purohit Shantanu	Effect of wind veer on yawed wind turbine under realistic atmospheric conditions
Bastin Jean	Wind dynamics around large rotors in Baltic Sea conditions
Gaiser Annika	Analysis of vertically staggered wind farm setups as a mitigation strategy for wind farm cluster wakes
Onnen David	Spectral coherence of wake motions with flow structures and turbine responses

20th EAWE PhD Seminar on Wind Energy
24-26 September 2024
Visby, Sweden

A large-eddy simulation analysis of wind-farm axial-induction control strategies in conventionally neutral boundary layers

Théo Delvaux and **Johan Meyers**

Departement of Mechanical Engineering, KU Leuven, Celestijnenlaan 300 - box2421, B-3001 Leuven, Belgium

E-mail:theo.delvaux@kuleuven.be

Keywords: large-eddy simulations, axial-induction control, wind-farm load reduction, flow blockage

1 Introduction

Over the past few years, the design of an optimal wind farm operating strategy has been the focus of numerous research works (Steinbuch et al. (1988) [17], Gebraad (2014) [8], González et al. (2015) [9], Fleming et al. (2017) [6], Annoni et al. (2018) [5]). Those control strategies essentially consist in adjusting either the thrust coefficients (Axial Induction Control) or the yaw angles (Wake Redirection Control) of the turbines in the farm. In the scope of this work, however, the focus is placed on the first approach only.

Although many studies on optimal farm operating points have shown promising results, the majority of them builds upon low-fidelity engineering models, with which only the wake interactions can be represented. Still, recent investigations on the meso-scale effects of wind farms on the Atmospheric Boundary Layer (ABL) indicated non-negligible impacts on the total power production of the farm (Allaerts & Meyers (2018) [3], Lanzilao & Meyers (2022, 2024) [11] [13]). Similar to the way mountains interact with the ABL under stratified conditions, wind farms were observed to trigger gravity waves in the free atmosphere. As a result, an unfavorable pressure gradient establishes at the inlet of the farm, leading to the so-called blockage effect.

To represent the wind-farm-induced pressure effects on the upstream flow, Allaerts & Meyers (2019) [4] developed an atmospheric perturbation model. With this model, they built the farm-averaged power-coefficient curve for two sets of flow conditions. In both cases, they observed a significant drop with respect to the predictions of the wake-only models. In the work of Allaerts & Meyers (2019) [4], only homogeneous distributions of the thrust coefficient were considered. Later, Lanzilao & Meyers (2021) [10] proposed a more-advanced optimization procedure of the wind-farm thrust set-point under specified flow conditions. Overall, their work emphasized the important part played by gravity-wave-induced blockage effects in the design of an optimal wind farm thrust set-point.

In this context, the present work investigates the benefits of a simple control strategy on power maximization and load reduction. The main goal of this study is to build strong evidence for the potential of axial-induction control approaches, that would in turn inform the development of more advanced control strategies in the future. To this end, we perform a series of large-eddy simulations (LES) on the in-house software SP-Wind, from which we build the power-coefficient and thrust coefficient curves of the wind-farm. In this analysis, we discuss the impact of the atmospheric conditions on the shape of the curves by considering three sets of flow conditions. In total, we perform twelve wind-farm LES, together with twelve LES of a turbine operating in isolation.

2 Methodology

In this section, we provide a summary of the different settings retained for the LES simulations. To a large extend, the methodology described below is inspired by the one followed by Lanzilao & Meyers (2024) [13].

First, we use SP-Wind to solve the filtered incompressible Navier-Stokes equations. The thermal effects are accounted for through a transport equation for the filtered potential temperature. An in-depth description of these

equations can be found in Allaerts & Meyers (2017) [2]. We focus on pressure-driven flows, for which a steady background pressure gradient across the domain balances the Coriolis force above the capping inversion, resulting in a geostrophic wind $G = 10\,\mathrm{m/s}$ in the free atmosphere.

In this paper, we consider a wind-farm composed of 100 IEA 15-Megawatt offshore turbines (Gaertner et al. (2020) [7]) placed in a 10-by-10 staggered configuration. Each rotor is modelled using the Actuator Disc Model (ADM), in which the turbine acts as a porous disc that extracts momentum from the flow. The operating regime of each turbine is set by means of the disc-based thrust coefficient, denoted C_T'. Note that we restrict the analysis to uniform distributions of C_T' over the farm. In particular, we select a sample of four distinct values, ranging over the whole set of realistic possibilities: $C_T' = \{0.50;\, 1.25;\, 2.0;\, 2.75\}$.

With regard to the atmospheric conditions, we model a conventionally-neutral boundary-layer profile using the Rampanelli & Zardi model (2004) [15]. We set the potential-temperature $\theta_0 = 288.15\,\mathrm{K}$ in the first layer and denote the height of the capping inversion by H. We refer to the strength and thickness of the capping inversion using $\Delta\theta$ and ΔH, respectively. Note that the effect of the capping inversion thickness is not further discussed here so that ΔH is fixed to 100 m in the remainder of this study. Above the capping inversion, the potential-temperature profile is controlled by the rate Γ in the free atmosphere. Based on the observations of Lanzilao & Meyers (2024) [13], we select a first set of parameters, $\{\mathrm{H}= 150,\, \Delta\theta = 8,\, \Gamma = 1\}$ (referred to as H150-$\Delta\theta$8-Γ1), for which strong blockage effects are expected. Additionally, we enrich the analysis with the cases H300-$\Delta\theta$5-Γ1 and H500-$\Delta\theta$5-Γ4.

The boundary conditions of the numerical domain are specified as follows. On the bottom face, we model the development of shear stresses by means of the classic Monin-Obukhov similarity theory for neutral boundary layer (Moeng (1984) [14], Allaerts (2016) [1]), with a surface roughness $z_0 = 1 \times 10^{-4}\,\mathrm{m}$. Moreover, both the streamwise and spanwise lateral sides of the domain are assigned periodic boundary conditions. Along the streamwise direction, we employ the fringe region technique developed by Lanzilao & Meyers (2023) [12] to ensure the desired inflow conditions. At the top of the domain, we use a rigid-lid condition, together with a Rayleigh-damping layer (Allaerts & Meyers (2017) [2]).

Prior to simulating the flow over a wind farm, it is necessary to run a precursor simulation during which the turbulent flow fully develops and reaches a statistically steady behaviour. This step is carried out for 20 hours, over a domain of dimensions $10 \times 10 \times 3\,\mathrm{km}^3$. Then, the tiling technique of Sanchez Gomez et al. (2023) [16] is employed to extend the precursor field to the main domain of size $50 \times 40 \times 25\,\mathrm{km}^3$, after which the wind-farm is added to the domain. We note, however, that the single-turbine simulations are performed over a smaller domain ($10 \times 10 \times 25\,\mathrm{km}^3$). In both the precursor domain and the main domain, the grid resolution is $\Delta x = 31.25\,\mathrm{m}$, $\Delta y = 21.74\,\mathrm{m}$ along the streamwise and spanwise directions, respectively. Along the vertical direction, a resolution $\Delta z = 5\,\mathrm{m}$ is maintained up to an altitude of 3 km. Above, we use a stretched grid composed of 190 grid points.

Following the precursor phase, a spin-up simulation is performed over 90 minutes to let the flow adapt to the presence of the farm. Eventually, a one-hour-long simulation is performed, during which the different flow quantities as well as the turbine thrusts and powers are collected. During those last two phases, the precursor field is run concurrently and imposed in the fringe region. The gravity-wave reflection on the top of the domain is prevented by the presence of a Rayleigh-damping layer. The corresponding parameters are set following Lanzilao & Meyers (2024) [13].

3 Results

In the paper, the results are discussed both in terms of the velocity fields and the power measurements. The instantaneous streamwise velocity field is provided in Fig. 1 for the the case H300-$\Delta\theta$5-Γ4 with $C_T' = 0.50$ (Fig. 1a) and H150-$\Delta\theta$8-Γ1 with $C_T' = 2.75$ (Fig. 1b). In Fig. 1a, the farm opposes little resistance to the flow so that only minor large-scale effects can be observed. On the contrary, the farm operating at $C_T' = 2.75$ leads to a significant upwards displacement of the capping inversion, in turn creating an unfavorable pressure gradient at the entry of the farm. This can clearly be seen in Fig. 1b, where a region of low velocity forms upstream of the farm.

With regards to the power production, we find that the wind-farm power coefficient curve plotted with respect to C_T' is substantially flatter than its single-turbine counterpart. The same conclusion, although to a lesser extent, applies to the wind-farm thrust coefficient curve. Consequently, by operating the turbines slightly below the design set-point, we show that the farm-averaged thrust coefficient decreases significantly more than the farm-averaged power coefficient. For example, when operating the farm at $C_T' = 1.12$ instead of $C_T' = 2$ under the conditions used in Fig. 1b, the analysis reveals a total load reduction of 17.8%, achieved at the expense of a power reduction of 1%. For the same set of conditions, we show that the maximum power extraction is realized at $C_T' = 1.6$, leading to a load reduction of more than 6% with respect to the classic set-point $C_T' = 2$.

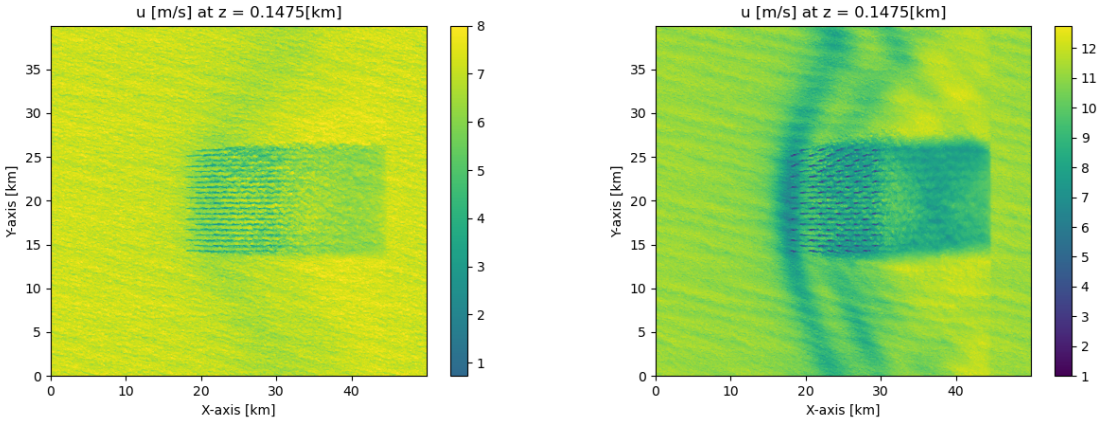

(a) (b)

Figure 1: Streamwise velocity field ($\mathrm{m\,s^{-1}}$) at hub height for the cases H300-$\Delta\theta$5-Γ4 with $C_T' = 0.50$ (a) and H150-$\Delta\theta$8-Γ1 with $C_T' = 2.75$ (b). The color scale is adapted for readability.

In the full paper, we further discuss the impact of the flow conditions on the harnessed power and the corresponding thrust. Thanks to the simulations of the turbine in isolation, we analyse the results in terms of the farm efficiencies. This last step allows us to differentiate between the blockage-induced losses and the wake losses. Eventually, we believe that the results obtained throughout this work constitute a promising starting point towards the development of more advanced axial-induction control strategies.

References

[1] D. Allaerts. Large-eddy simulation of wind farms in conventionally neutral and stable atmospheric boundary layers. phd thesis, kuleuven, leuven, belgium. 2016.

[2] D. Allaerts and J. Meyers. Boundary-layer development and gravity waves in conventionally neutral wind farms. *Journal of Fluid Mechanics*, 814:95–130, 2017.

[3] D. Allaerts and J. Meyers. Gravity waves and wind-farm efficiency in neutral and stable conditions. *Boundary-layer meteorology*, 166:269–299, 2018.

[4] D. Allaerts and J. Meyers. Sensitivity and feedback of wind-farm-induced gravity waves. *Journal of Fluid Mechanics*, 862:990–1028, 2019.

[5] J. Annoni, P. Fleming, K. Johnson, C. Bay, T. Taylor, and L. Pao. Efficient optimization of large wind farms for real-time control: Preprint. *National Renewable Energy Laboratory*, 2017.

[6] P. Fleming, J. Annoni, J. J. Shah, L. Wang, S. Ananthan, Z. Zhang, K. Hutchings, P. Wang, W. Chen, and L. Chen. Field test of wake steering at an offshore wind farm. *Wind Energy Sciences*, 2:229–239, 2017.

[7] E. Gaertner, J. Rinker, L. Sethuraman, F. Zahle, and B. Anderson. Definition of the iea 15-megawatt offshore reference wind. *Golden, CO: National Renewable Energy Laboratory*, 2020.

[8] P. Gebraad. Data-driven wind plant control. *Ph.D. Thesis, Delft University of Technology, Delft, The Netherlands*, 2014.

[9] J. González, M. Payán, J. Santos, and A. Gonzalez. Maximizing the overall production of wind farms by setting the individual operating point of wind turbines. *Renewable Energy*, 80, 2015.

[10] L. Lanzilao and J. Meyers. Set-point optimization in wind farms to mitigate effects of flow blockage induced by atmospheric gravity waves. *Wind Energy Science*, 6, 2021.

[11] L. Lanzilao and J. Meyers. Effects of self-induced gravity waves on finite wind-farm operations using a large-eddy simulation framework. *Journal of Physics: Conference Series*, 2265:269–299, 2022.

[12] L. Lanzilao and J. Meyers. An improved fringe-region technique for the representation of gravity waves in large eddy simulation with application to wind farms. *Boundary-layer meteorology*, 186:567–593, 2023.

[13] L. Lanzilao and J. Meyers. A parametric large-eddy simulation study of wind-farm blockage and gravity waves in conventionally neutral boundary layers. *Journal of Fluid Mechanics*, 979, 2024.

[14] C. Moeng. A large-eddy-simulation model for the study of the planetary boundary-layer turbulence. *Journal of atmospheric science*, 41:2052–2062, 1984.

[15] G. Rampanelli and D. Zardi. A method to determine the capping inversion of the convective boundary layer. *Journal of Applied Meteorology*, 43:925–933, 2004.

[16] M. Sanchez Gomez, J. Lundquist, J. Mirocha, and R. Arthur. Investigating the physical mechanisms that modify wind plant blockage in stable boundary layers. *Wind Energy Science Discussions*, pages 1–28, 2023.

[17] M. Steinbuch, W. de Boer, O. Bosgra, S. Peters, and J. Ploeg. Optimal control of wind power plants. *Journal of Wind Engineering and Industrial Aerodynamics*, 27:237–246, 1988.

20th EAWE PhD Seminar on Wind Energy
24-26 September 2024
Visby, Sweden

Effect of wind veer on yawed wind turbine under realistic atmospheric conditions

Shantanu Purohit[a], **Wei Yu**[a], and **Carlos Simão Ferreira**[a]

[a]Faculty of Aerospace Engineering, Delft University of Technology, Delft, The Netherlands

E-mail: s.purohit@tudelft.nl

Keywords: Turbine yaw, Ekman layer, wake, wind veer

Wind turbines operate in complex atmospheric conditions, including wind shear, veer, and various atmospheric stabilities. As the height of modern wind turbines continues to increase to extract more energy from the wind, understanding the physics of atmospheric flows and their interaction with wind plants becomes essential, highlighted as one of the three grand challenges in wind energy science [1]. A major concern for wind farm operators is power loss due to the so-called "wake effect," which can result in up to 20 % power loss in a wind farm [2]. Wind farm control via wake steering, which is intentionally yawing upstream wind turbines to direct their wakes away from downstream turbines, has been shown to increase the power production of wind turbines in a farm both in field studies and numerical simulations [3]. An important step in the effective implementation of a yaw-based control strategy is the choice of the engineering wake model for yaw that can accurately represent the wake deficit behind the turbine, as numerical modeling tools (such as RANS and LES) are very expensive and not ideal for simulating wind farm control studies. Therefore, developing low-fidelity engineering wake models that can accurately depict wake deficit under realistic atmospheric conditions is important to advance wind farm control via wake steering.

Several such models exist in the literature, such as the classic Jiménez model [4], Bastankhah and Porté-Agel model [5], curled wake model [6], among many others. Although these models have been shown to compare well with the canonical flows under simplistic atmospheric conditions, an important atmospheric phenomenon that these models ignore is the effect of Coriolis force on the vertical change in wind direction with height due to Earth's rotation, also known as "wind veering." This vertical wind veer introduces lateral shear in addition to vertical shear and alters the local inflow vector along the blade profile, impacting lift and drag forces, power production, and wake profile [7]. Wind veer is particularly common in offshore conditions, with field measurements reporting its occurrence up to 70% of the time annually [8]. Studies have shown that in stably stratified flows, low turbulence and high vertical wind veer can cause wake skewness, and this effect has been shown to have a statistically significant impact on wake recovery and power production of downstream turbines [9]. This necessitates the inclusion of wind veering in the engineering wake models. An effort in this direction was made by Abkar *et al.* [10], where the authors developed an analytical model to predict the mean velocity profile of wakes under wind veering conditions. Some efforts have been made to include the combined effects of yaw misalignment and wind veer. Most notably, Narasimhan *et al.* [11] recently introduced a veer correction term to the model proposed by Bastankhah *et al.* [12] and demonstrated, through high-fidelity LES simulations, significant asymmetry in the wake's curled shape. More recently, Mohammadi *et al.* [13] presented a new model of wind turbine wakes in yaw in the presence of wind veer. They proposed two models: the first model separates the effect of wind veering from yaw misalignment, and the second model considers effective yaw angle as seen by the turbine section (because the change in wind direction with height leads to a change in yaw angle seen by the turbine blade section). Although both models give reasonably good predictions for low and medium wind veer, the authors suggest using the second model as it is more physically realistic.

A limitation in the above works on wind veering under a yawed turbine is that all the simulations were performed under a conventionally neutral boundary layer (CNBL). As highlighted before, wind veer occurs predominantly in stable boundary layers (SBL), which differ significantly from neutral boundary layers and are more prominent in offshore wind conditions. For instance, in CNBL, there is no net heat flux between the surface and the atmosphere, whereas in SBL, temperature increases with height, i.e., air near the surface is cooler than the air aloft, which suppresses vertical mixing. Moreover, the level of turbulence is also different in these two stabilities.

To this end, the focus of this work and the questions we want to answer are highlighted below.

Research focus and expected outcomes

This work focuses on using LES simulations to study the effects of wind veer during turbine yaw under a stable boundary layer and examining the extent of wake skewness, its impact on wake recovery and wake structure, power generated, and loads experienced by downstream turbines. Most previous studies on wind turbine yaw in the presence of wind veering have considered non-rotating actuator discs, but whether the wake angular momentum impacts wake deflection and vorticity decay is yet to be ascertained. Key questions include: how does stable stratification affect wake evolution under the combined influence of yaw and veer? Does wind veering have an impact on wake meandering? What is wind veering impact on wake recovery and downstream power production? We will answer these questions by performing LES simulations of wind turbines represented as actuator lines using the NREL tool SOWFA under stable stratification and different wind veering strengths. Precursor simulations will be run by applying different cooling rates to limit the vertical mixing in SBL and different wind veering strengths (from low to high). Each precursor simulation will be run until the quasi-equilibrium state is reached, then turbines will be introduced, and the simulation will be run again until equilibrium is reached. Planes of velocity and pressure fields will be extracted at multiple downstream locations. We will perform a budget analysis of the time-averaged Reynolds stress terms to shed light on the reasons behind faster wake recovery during wind veering and connect the influence of wind veer on turbulence production and transport of mean kinetic energy in the wake during yawing. Additionally, vorticity-based methods will be utilized to develop low-fidelity yaw models for turbine wake for streamwise and lateral velocity components in vertical wind veering. It is unknown whether the existing yaw models that include wind veer will accurately represent the wake deficit under such non-canonical atmospheric stabilities. Answering these questions will provide guidelines on the importance of accommodating wind veer effects in wake steering-based wind farm control and the importance of wake angular momentum on the superposition of wake from wind veer and turbine yaw.

Acknowledgements

This research is part of the project DIAMOND with project number 19882 of the research programme Open Technology which is (partly) financed by the Dutch Research Council (NWO), the Netherlands.

References

[1] Paul Veers, Katherine Dykes, Eric Lantz, Stephan Barth, Carlo L Bottasso, Ola Carlson, Andrew Clifton, Johney Green, Peter Green, Hannele Holttinen, et al. Grand challenges in the science of wind energy. *Science*, 366(6464):eaau2027, 2019.

[2] Rebecca Jane Barthelmie, K Hansen, Sten Tronæs Frandsen, Ole Rathmann, JG Schepers, W Schlez, J Phillips, K Rados, A Zervos, ESa Politis, et al. Modelling and measuring flow and wind turbine wakes in large wind farms offshore. *Wind Energy: An International Journal for Progress and Applications in Wind Power Conversion Technology*, 12(5):431–444, 2009.

[3] Paul Fleming, Jennifer Annoni, Jigar J Shah, Linpeng Wang, Shreyas Ananthan, Zhijun Zhang, Kyle Hutchings, Peng Wang, Weiguo Chen, and Lin Chen. Field test of wake steering at an offshore wind farm. *Wind Energy Science*, 2(1):229–239, 2017.

[4] Ángel Jiménez, Antonio Crespo, and Emilio Migoya. Application of a les technique to characterize the wake deflection of a wind turbine in yaw. *Wind energy*, 13(6):559–572, 2010.

[5] Majid Bastankhah and Fernando Porté-Agel. Experimental and theoretical study of wind turbine wakes in yawed conditions. *Journal of Fluid Mechanics*, 806:506–541, 2016.

[6] Luis A Martínez-Tossas, Jennifer Annoni, Paul A Fleming, and Matthew J Churchfield. The aerodynamics of the curled wake: a simplified model in view of flow control. *Wind Energy Science*, 4(1):127–138, 2019.

[7] Julie K Lundquist. Wind shear and wind veer effects on wind turbines. In *Handbook of Wind Energy Aerodynamics*, pages 1–22. Springer, 2022.

[8] Nicola Bodini, Julie K Lundquist, and Anthony Kirincich. Us east coast lidar measurements show offshore wind turbines will encounter very low atmospheric turbulence. *Geophysical Research Letters*, 46(10):5582–5591, 2019.

[9] Matthew J Churchfield and Senu Sirnivas. On the effects of wind turbine wake skew caused by wind veer. In *2018 wind energy symposium*, page 0755, 2018.

[10] Mahdi Abkar, Jens Nørkær Sørensen, and Fernando Porté-Agel. An analytical model for the effect of vertical wind veer on wind turbine wakes. *Energies*, 11(7):1838, 2018.

[11] Ghanesh Narasimhan, Dennice F Gayme, and Charles Meneveau. Effects of wind veer on a yawed wind turbine wake in atmospheric boundary layer flow. *Physical Review Fluids*, 7(11):114609, 2022.

[12] Majid Bastankhah, Carl R Shapiro, Sina Shamsoddin, Dennice F Gayme, and Charles Meneveau. A vortex sheet based analytical model of the curled wake behind yawed wind turbines. *Journal of Fluid Mechanics*, 933:A2, 2022.

[13] Mohammadreza Mohammadi, Majid Bastankhah, Paul Fleming, Matthew Churchfield, Ervin Bossanyi, Lars Landberg, and Renzo Ruisi. Curled-skewed wakes behind yawed wind turbines subject to veered inflow. *Energies*, 15(23):9135, 2022.

20th EAWE PhD Seminar on Wind Energy
24-26 September 2024
Visby, Sweden

Wind dynamics around large rotors in Baltic Sea conditions

J. Bastin[a,b], **S. Ivanell**[a], **E. Sahlée**[a], **E. Podgrasjsek**[b], and **H. Asmuth**[a]

[a]Uppsala universitet, Institutionen för geovetenskaper, Vindenergi
[b]OX2

E-mail: jean.bastin@geo.uu.se

Keywords: Large rotors, offshore meteorology, LBM

Abstract

The progressive increase of wind turbine dimensions in recent years, coupled with the escalating development of offshore wind farms, has led to the exploration of less comprehended atmospheric regions, necessitating a more thorough understanding. Specifically, the intricate interactions occurring between large rotors and the top of the atmospheric boundary layer (ABL) need to be deeply investigated to significantly improve the precision of wind energy predictions, gain deeper insights into loads affecting turbine blades, and comprehend the impact of these interactions on wake generation behind the turbines.

The Baltic Sea region, characterized by special atmospheric stability conditions, could experience extreme events, notably in the top of the ABL region. To comprehensively investigate the interplay of these events with large turbine rotors, this research proposes conducting Computational Fluid Dynamics (CFD) simulations around expansive wind farms. Emphasis will be placed on innovative CFD techniques, such as the Lattice Boltzmann Method (LBM), which holds the potential to drastically reduce the heavy computational costs associated with such simulations.

Given the academic and industrial significance of this research, the PhD program will be conducted under joint supervision from both the university and industry (OX2) within the Apt Wind doctoral program. The collaboration will extend to the utilization of Large Eddy Simulation (LES) data provided by the industrial partner, enriching the research with practical insights and applications.

Initial research objectives

The initial research objectives are enumerated below:

1. Enhancing comprehension, through CFD simulations, of boundary layer behaviour and characteristics in the Baltic Sea
2. Simulating the interaction between large rotors and the top of the ABL in offshore conditions under varying atmospheric parameters (e.g., stability, wind speed).
3. Investigating the consequences of large rotor wake development within a wind farm and the impact of this latter on neighbouring wind farms.
4. Advancing knowledge of wind distribution over large rotors, potentially leading to revisions to current International Electrotechnical Commission (IEC) standards.

20th EAWE PhD Seminar on Wind Energy
24-26 September 2024
Visby, Sweden

Analysis of vertically staggered wind farm setups as a mitigation strategy for wind farm cluster wakes

Annika Gaiser[a,b]

[a]Carl von Ossietzky Universität Oldenburg, School of Mathematics and Science, Institute of Physics
[b]ForWind - Center for Wind Energy Research, Küpkersweg 70, 26129 Oldenburg, Germany
E-mail: annika.gaiser@uol.de

Keywords: wind farm cluster, cluster wake, vertical staggering, LES

1 Introduction

As part of the energy transition, the utilisation of offshore wind energy resources is expanded, resulting in wind farm clusters, meaning large wind farms being built near other wind farms. The wakes of upstream wind farms can influence downstream wind farms, even if they are tens of kilometres apart, exposing them to reduced wind speeds and increased turbulence that result in lower power production and increased damaging loads [1], [4], [8]. To increase the efficiency of wind farm clusters, it is necessary to mitigate such cluster wakes. Mitigation strategies should thereby ideally consider existing and planned wind farms, addressing the operation and the planning and design phase. So far, studies mainly focused on optimising the power output of single wind farms, which usually creates stronger wind farm wakes due to more power being extracted. In wind farm clusters, this could however negatively impact downstream wind farms. To achieve overall optimal power output in wind farm clusters, it might be necessary to choose wind farm setups, layouts or control strategies that might not be ideal for the isolated upstream wind farm, but reduce the wake for the upstream installation and are therefore beneficial for a downstream wind farm and possibly the entire wind farm cluster. Understanding the influencing factors for wind farm cluster wakes will be the objective of this PhD project. As the PhD project only started a few months ago, the presentation at the PhD seminar will give a brief introduction to the overall plans of the PhD, followed by first results of the first part of the project.

The main objective of this doctoral project is to understand how the extent and intensity of wind farm cluster wakes are influenced by different factors that could affect e.g. shear, vertical mixing and entrainment downstream of wind farms. The project will be divided into three main parts on potential influencing factors, which showed wake impacts for single wind farms or wind turbines and could thereby be relevant strategies to influence wind farm cluster wakes. First, turbine characteristics will be analysed, including different hub heights in the context of vertically staggered wind farms [9], wind turbines with different rotor diameters, and new turbine concepts [7]. Second, the influence of the turbine placement inside the wind farm will be investigated, starting with existing wind farms to derive causes for wake differences, and in a second step optimising the layout of a theoretical wind farm cluster with an optimisation algorithm [5] of the engineering model FOXES. Third, different operation strategies will be analysed, changing e.g. the yaw angle [6], [11] and rotation direction [2]. Besides analysing the impact of the wind farm specifics, the influence of different meteorological conditions like stratification and capping inversion on the cluster wake will be analysed. This will be especially relevant for the different operation strategies, since it could allow the development of condition-specific mitigation strategies. The outputs of these the three parts and meteorological analysis will be integrated into a discussion of differences in the cluster wakes and their causes, yielding potential strategies to mitigate cluster wakes and increase power production for different meteorological conditions.

First results on the influence of the hub height and vertical staggering on cluster wakes will be discussed during the PhD seminar. Most studies so far focused on uniform hub heights within a wind farm, while studies on

vertically staggered wind farms and its impacts on power output are still scarce. For wind farm clusters, vertically staggered setups have generally not been studied, yet. Previous studies on a single wind farm found that vertical staggering can increase the total power output of a wind farm, by either changing the existing wind turbine heights [9, 10] or adding additional smaller turbines [9]. Using a vertically staggered wind farm resulted in the wake extending to higher altitudes [12]. These studies indicate, that the general cluster wake properties and consequent influence on downstream wind farms could be influenced. Analysing the influence of different vertical staggered wind farm setups will be the focus of this first study. The following research questions are intended to be addressed in the PhD seminar presentation:

- How can vertically staggered wind farm layouts be used to affect the properties of wind farm cluster wakes and thereby mitigate them?
- How does the cluster wake differ for ...
  - overlapping rotors vs. no overlap?
  - adding turbines vs. changing the hub height of the existing ones?

2 Methods

2.1 Large-eddy simulations model PALM

The study will be performed with the high-fidelity large-eddy simulations (LES) model PALM as the high resolution and explicitly resolved larger turbulent scales allow a detailed analysis of the spatial structure of the wind farm wakes [3]. The following analyses will be done for an idealised model setup with a wind farm cluster that consists of two wind farms aligned with the flow direction that have the same baseline setup and are at least 10 km apart.

2.2 Simulation setups

Baseline setup

- Two wind farms à 72 (6x12) IEA 15 MW turbines in a rectangular, evenly spaced, aligned layout (the layout will be similar to [8] and [9] to allow comparison)
- The rated power of the wind farms will be kept similar in all sensitivity studies
- Idealised LES runs
- Conventionally neutral stratification

Vertical staggering
Usually, using a wind turbine with a different hub height goes along with different rotor diameters, rated power, etc. that are specific to a turbine type. In this study, we will however only change the height of the nacelle and keep all other specifics constant to only look at the effect of the hub height. It could be interesting, though, to extend the study by using different turbine types for a more realistic setup. The following experiments will be performed, where for experiments two and three, different hub heights will be set for either only the upstream wind farm or both wind farms:

1. Use one hub height for the upstream wind farm and a higher hub height for the downstream wind farm.
2. Increase the height of every second wind turbine of the existing layout with and without overlapping rotor area.
3. Add additional wind turbines with a higher hub height.

To understand and quantify changes to the wind farm cluster wakes the following metrics will be analysed: wake intensity, wake extent, momentum fluxes around the wind farms, boundary layer of the wind farm, atmospheric boundary layer and power output.

3 Expected outcomes

Depending on the approach of how to vertically stagger the wind turbines, the wake properties are expected to be influenced differently. For the first experiment, the downstream wind farm is likely less affected by the upstream wind farm wake, since the upstream wind farm's wake is on a lower level than the rotor area of the downstream wind farm. However, if the rotor areas of upstream and downstream wind farm overlap, the wind speed distribution over the rotor area varies strongly, resulting in stronger loads. By adding higher wind turbines or changing the hub height of the existing wind turbines, it might be possible to reduce the wake. For instance, with a switch to higher turbines the entrainment and therefore wake recovery might be promoted. Also, the vertical wake extent would be larger, while the wake intensity and extent around the lower hub heights might decrease due to a lower rotor density per area.

In a follow up, the experiments are intended to be extended by simulations with different inversion heights and stable stratification to analyse the influence of different atmospheric conditions. Additionally, the hub heights of the two wind farms might be optimised with the engineering model FOXES and compared to the manually designed setups. The way of how the vertical staggering is performed, so either in a more uniform way or more asymmetric as optimised by a model, is additionally expected to affect the wake properties, including the shape of the wake.

Understanding the influence of vertically staggered wind farm clusters could eventually allow a new approach on designing wind farms. One of the most important outcomes will be an increased understanding on how different wind farm cluster setups affect the atmosphere and how this affects downstream wind farms.

Acknowledgements

The PhD is part of the project C^2-Wakes (Controlled Cluster Wakes), which is funded by the Federal Ministry of Economic Affairs and Climate Action (BMWK, grant no. 03EE3087A). The authors acknowledge the computing time made available on the high-performance computer EMMY at the NHR Center NHR-NORD@Göttingen, which is supported by the Federal Ministry of Educarion and Research and the state governments participating in the NHR.

References

[1] J. Cao, Z. Qin, X. Gao, T. Pu, W. Zhu, S. Ke, and X. Shen. Study of aerodynamic performance and wake effects for offshore wind farm cluster. *Ocean Engineering*, 280:114639, 2023.

[2] A. Englberger, A. Dörnbrack, and J. K. Lundquist. Does the rotational direction of a wind turbine impact the wake in a stably stratified atmospheric boundary layer? *Wind Energy Science*, 5:1359–1374, 2020.

[3] B. Maronga, S. Banzhaf, C. Burmeister, T. Esch, R. Forkel, D. Fröhlich, V. Fuka, K. F. Gehrke, J. Geletič, S. Giersch, T. Gronemeier, G. Groß, W. Heldens, A. Hellsten, F. Hoffmann, A. Inagaki, E. Kadasch, F. Kanani-Sühring, K. Ketelsen, B. A. Khan, C. Knigge, H. Knoop, P. Krč, M. Kurppa, H. Maamari, A. Matzarakis, M. Mauder, M. Pallasch, D. Pavlik, J. Pfafferott, J. Resler, S. Rissmann, E. Russo, M. Salim, M. Schrempf, J. Schwenkel, G. Seckmeyer, S. Schubert, M. Sühring, R. V. Tils, L. Vollmer, S. Ward, B. Witha, H. Wurps, J. Zeidler, and S. Raasch. Overview of the palm model system 6.0. *Geoscientific Model Development*, 13:1335–1372, 2020.

[4] N. G. Nygaard and S. D. Hansen. Wake effects between two neighbouring wind farms. *Journal of Physics: Conference Series*, 753:032020, 2016.

[5] M. M. Pedersen and G. C. Larsen. Integrated wind farm layout and control optimization. *Wind Energy Science*, 5:1551–1566, 2020.

[6] G.-W. Qian and T. Ishihara. Wind farm power maximization through wake steering with a new multiple wake model for prediction of turbulence intensity. *Energy*, 220:119680, 2021.

[7] D. Ribnitzky, F. Berger, V. Petrović, and M. Kühn. Hybrid-lambda: a low-specific-rating rotor concept for offshore wind turbines. *Wind Energy Science*, 9:359–383, 2024.

[8] A. Stieren and R. J. A. M. Stevens. Impact of wind farm wakes on flow structures in and around downstream wind farms. *Flow*, 2:21, 2022.

[9] J. M. I. Strickland. *Modelling wakes and blockage in large-scale wind farms*. PhD thesis, University of Twente, Enschede, The Netherlands, 12 2021.

[10] H. Sun and H. Yang. Wind farm layout and hub height optimization with a novel wake model. *Applied Energy*, 348:121554, 2023.

[11] T. Wang, S. Zhou, C. Cai, X. Wang, Z. Wang, Y. Zhang, K. Shi, X. Zhong, and Q. Li. Study on complex wake characteristics of yawed wind turbine using actuator line method. *Journal of Marine Science and Engineering*, 11:1039, 2023.

[12] Y.-T. Wu, T.-L. Liao, C.-K. Chen, C.-Y. Lin, and P.-W. Chen. Power output efficiency in large wind farms with different hub heights and configurations. *Renewable Energy*, 132:941–949, 2018.

Spectral coherence of wake motions with flow structures and turbine responses

David Onnen[a,b], Vlaho Petrović[a,b] and Martin Kühn[a,b]

[a] Carl von Ossietzky Universität Oldenburg, School of Mathematics and Science, Institute of Physics
[b] ForWind - Center for Wind Energy Research, Küpkersweg 70, 26129 Oldenburg, Germany

E-mail: david.onnen@uol.de

Keywords: Wind farm flow control, wake meandering, observability

Introduction

Wind farm flow control relies on wind condition awareness within a wind farm. Especially for closed-loop wake-steering control, the position and trajectory of the wind turbines' wakes are valuable. Various methods for flow field reconstruction and wake estimation from turbine data exist, differing e.g. on the installed sensory or required time- and spatial position resolution. Low-fidelity flow models can be included (see e.g. [1]), where physical knowledge of wake behaviour, such as deflection due to yaw misalignment [2] is represented. Yet, a limiting factor is often the observability of the flow field based on turbine data [3], especially when not the long-term averaged flow but the instantaneous flow situation – subject to wake meandering and dynamic wind direction changes – is of interest. Furthermore, the feedback from a wake-exposed turbine to the wake-causing can partially be considered too late, since the conditions might have changed already, and the wake might have been subject to non-observable distortions. E.g. Raach et al. [4] describe the difficulties of using a delay model for closed-loop wake position control. The consequent next step is to put the wake-causing turbine in focus of the estimation. The Jiménez model [2] describes, how the conservation of momentum translates a turbine's yaw misalignment to a wake deflection and the *dynamic wake meandering model* [5] conjectures that wake meandering is driven by the large-scale transversal flow components. Lejeune et al. [6] show in a simulation environment, how the estimation of the ambient flow field can enhance wake estimation. Muller et al. [7] show the spectral correlation of the lateral inflow components and with a model turbine's load fluctuations and the wake position behind the turbine in a wind tunnel setup.
A similar setup to the one of Muller et al., yet in the field with two utility scale turbines, additional met masts and wind lidars is employed in this study, to unravel

a) the correlation of inflow structures with turbine load data
b) the correlation of a turbine's loads with the trajectory of the wake it causes

By that, relevant spectral scales of wake dynamics and wake propagation through a wind farm in regard to wind farm flow control are identified and the definition *farm effective wind direction* is refined [8,9]. The identified coherences are a direct indictor, which further signals can serve to increase the observability of wind farm flow. The level of instrumentation in the given setup is far beyond of what could be expected in commercial wind farms. This, however, is valuable for validating the approach and to define the minimum requirements of turbine/farm instrumentation for commercial applications.

Methodology

Field setup

A top view of the field setup is shown in Figure 1. Each vertical dashed line indicates a streamwise probing location. Despite the very different probing methodologies (point-probing anemometers / volume averaged lidar probes / rotor effective Kalman filter estimates), comparable quantities are available at each location. The layout constraints the investigations to a limited range of wind directions. However, these are exactly the directions of relevance for wind farm flow control.

For goal a), the upstream met mast with 3D sonic anemometers and a forward-looking hub-mounted spinner lidar are employed and compared with the turbine-estimated wind speeds. The results of a) can be of further use to assess the suitability for lidar-assisted feedforward control [13]. For b), the states of the turbine-based estimation are compared to the wake position found downstream of the turbine. These can be extracted from a downstream facing pulsed lidar on the nacelle [14].

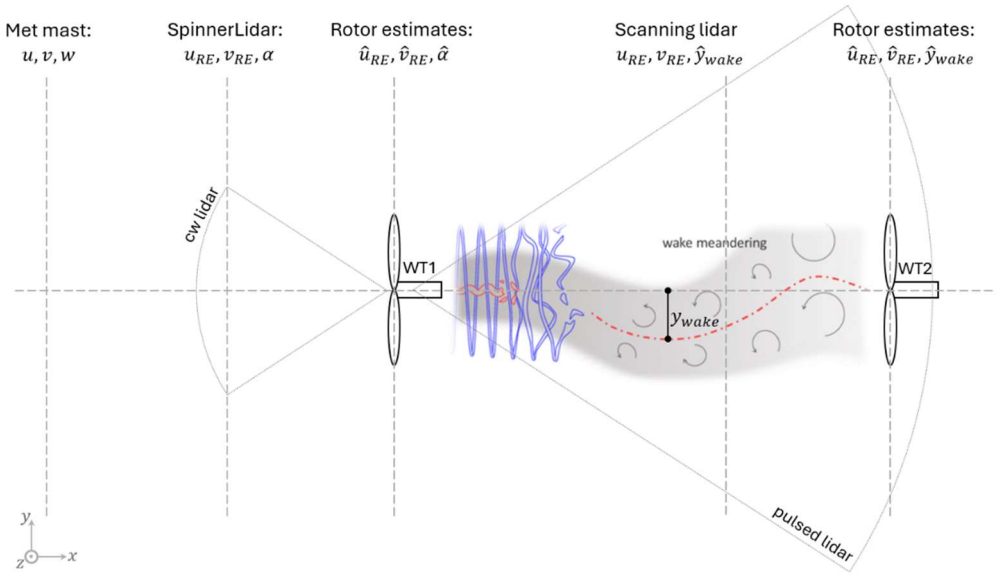

Figure 1 Setup sketch with indications the streamwise probe locations. From left to right: 1. Met mast 2. SpinnerLidar 3. WT1 rotor estimates 4. Pulsed lidar plane 5. WT2 (waked) rotor estimates

Load-based estimation

The streamwise rotor effective wind speed u_{RE} is addressed via a torque balance estimator with a distinction between the slow-changing mean wind speed and the fast-changing turbulent component (see [10]). The latter is driven by a coloured noise term that describes the turbulent characteristics. The EKF is augmented with terms for lateral wind speed v_{RE} and the shear profile (log law coefficient α), by including the in-plane and out-of-plane rotor load harmonics, similar as shown in [6,12]. The BEM-derived relations between flow components and rotor loads, as used by the EKF, are shown non-dimensionalized in Figure 2.

Lidar-based estimation

The forward-looking SpinnerLidar follows a rosette pattern with 312 points per second. The line-of-sight speeds are fitted to a 3-parameter model, resulting in u_{RE}, v_{RE} and α. The nacelle-mounted pulsed lidar records the downstream flow field. After a suitable coordinate transform, the lateral wake position y_{wake} is identified via the convolution of a wake deficit proxy with the lateral distribution of wind speeds [15].

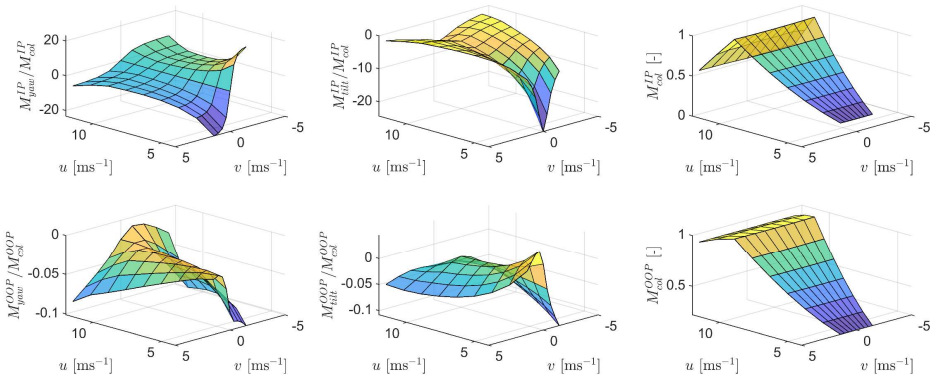

Figure 2 Look-up table for rotor loads in dependency of streamwise and transversal flow component

Spectral coherence

The spectral coherence quantifies the spatial or temporal correlation between two signals (i and j),

$$C_{ij}(f) = \frac{\left|S_{ij}(f)\right|^2}{S_{ii}(f)\, S_{jj}(f)}$$

where S_{ij} is the cross power spectral density and S_{ii} the auto power spectral density. The signals i and j can be any two signals along the five probing locations indicated in Figure 1.

Results & Conclusion

Initial results for a similar measurement setup are shown in the following. In Figure 3, the wake identification from the pulsed lidar measurements is shown, which proves to be very robust even when extracted from a single scan. In Figure 4, EKF results of the lateral wind speed estimation are shown. Meanwhile, the data set is currently being recorded and results for the correlation are expected throughout summer 2024. The analysis profits from a long and consistent data set, which includes different ambient conditions. Especially the atmospheric stability is of interest, since it has an impact on the wind direction variance and the occurrence of large-scale turbulence patters.

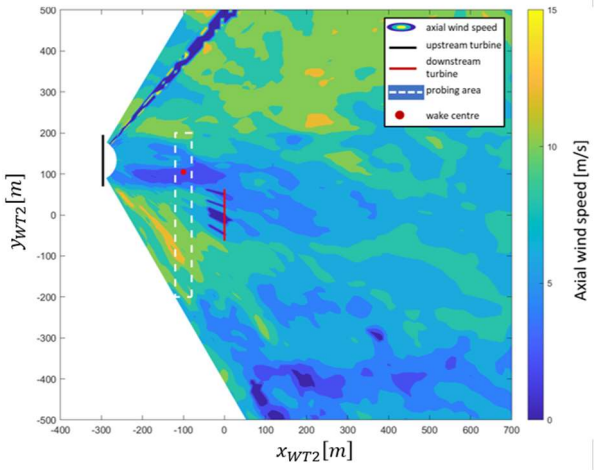

Figure 3 Wake position identification from a lidar scanned wind field

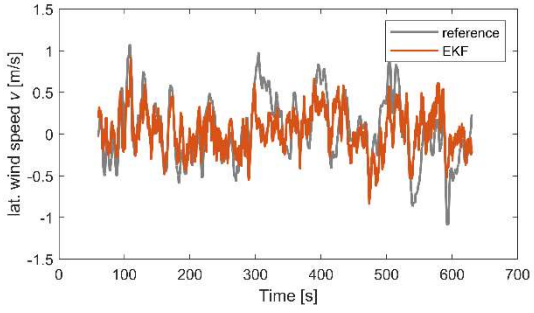

Figure 4 Results of the lateral wind speed estimation

Acknowledgements

This work is partly funded by the Federal Ministry for Economic Affairs and Climate Action according to a resolution by the German Federal Parliament (project DFWind Ph.II, FKZ 0325936H).

References

[1] Becker M, Allaerts D and van Wingerden J W 2022 Ensemble-Based Flow Field Estimation Using the Dynamic Wind Farm Model FLORIDyn *Energies* **15** 1–23
[2] Jiménez Á, Crespo A and Migoya E 2009 Application of a LES technique to characterize the wake deflection of a wind turbine in yaw *Wind Energy* **13** 559–72
[3] Doekemeijer B and van Wingerden J W 2020 Observability of the ambient conditions in model-based estimation for wind farm control: A focus on static models *Wind Energy* **23** 1777–91
[4] Raach S, Schlipf D and Wen Cheng P 2017 Lidar-based wake tracking for closed-loop wind farm control *Wind Energy Sci.* **2** 257–67
[5] Larsen G C, Madsen H A, Thomsen K and Larsen T J 2008 Wake meandering: A pragmatic approach *Wind Energy* **11** 377–95
[6] Lejeune M, Moens M and Chatelain P 2022 A Meandering-Capturing Wake Model Coupled to Rotor-Based Flow-Sensing for Operational Wind Farm Flow Prediction *Front. Energy Res.* **10** 1–20
[7] Muller Y A, Aubrun S and Masson C 2015 Determination of real-time predictors of the wind turbine wake meandering *Exp. Fluids* **56** 1–11
[8] Simley E, Fleming P and King J 2020 Design and analysis of a wake steering controller with wind direction variability *Wind Energy Sci.* **5** 451–68
[9] Braunbehrens R, Tamaro S and Bottasso C L 2023 Towards the multi-scale Kalman filtering of dynamic wake models: observing turbulent fluctuations and wake meandering *JoP Conf. Ser.* **2505** 012044
[10] Soltani M N, Knudsen T, Svenstrup M, Wisniewski R, Brath P, Ortega R and Johnson K 2013 Estimation of rotor effective wind speed: A comparison *IEEE Trans. Control Syst. Technol.* **21** 1155–67
[11] Simley E and Pao L Y 2013 Correlation between rotating LIDAR measurements and blade effective wind speed *51st AIAA Aerosp. Sci. Meet. Incl. New Horizons Forum Aerosp. Expo. 2013* 1–15
[12] Bertelè M, Bottasso C L and Schreiber J 2021 Wind inflow observation from load harmonics: Initial steps towards a field validation *Wind Energy Sci.* **6** 759–75
[13] Guo F, Mann J, Peña A, Schlipf D and Cheng P W 2022 The space-time structure of turbulence for lidar-assisted wind turbine control *Renew. Energy* **195** 293–310
[14] Bromm M, Rott A, Beck H, Vollmer L, Steinfeld G and Kühn M 2018 Field investigation on the influence of yaw misalignment on the propagation of wind turbine wakes *Wind Energy* **21** 1011–28
[15] Vollmer L, Steinfeld G, Heinemann D and Kühn M 2016 Estimating the wake deflection donstream of a wind turbine in different atmospheric stabilities: An LES study *Wind Energy Sci.* **1** 129–41

1.2 Session 121: Wind farm flows and wakes

24.09.2024, 13:10, Room 1

Chair:

Thea Vanelli

Presenters:

Wagner Martin	Stochastic modelling of wind turbine power conversion dynamics using rotor averaged wind speeds
Krishnan Paranjothi Udhaya Chandiran	Analysing the sensitivity of wind farm-induced gravity waves to blockage-induced rotor diameter to hub height ratio
Schøler Jens Peter	Wind Farm Flow Modeling with Neural Operators for Turbine Wake Superposition

20th EAWE PhD Seminar on Wind Energy
24-26 September 2024
Visby, Sweden

Stochastic modelling of wind turbine power conversion dynamics using rotor averaged wind speeds

Martin Wagner[a], **Matthias Wächter**[a], and **Joachim Peinke**[a]

[a]ForWind - Institute of Physics, University of Oldenburg, Germany

E-mail: martin.wagner@uni-oldenburg.de

Keywords: Stochastic model turbine, Langevin equation, Rotational speed dynamics, Turbulent fluctuations

1 Introduction

In the recent years, the power conversion dynamics of wind turbines have been successfully modelled by stochastic Langevin equations [1]. This approach has proven to be more accurate than the standard IEC model on short time scales of minutes and seconds and is also successful in detecting damage to a defective turbine [3][4].
In our work, we try to use the Langevin approach to investigate the alleviation of power fluctuations by wind turbines. The motivation for this idea stems from the fact a wind turbine is exposed to a turbulent inflow. The strong fluctuations of the wind speed are transferred to the power output of a turbine and therefore have a negative impact on the frequency stability of the power grid. However, wind turbines can dynamically use the energy stored in their rotational masses in order to mitigate these power fluctuations. The rotational energy can be accessed by controlling the torque on the generator of a turbine.
In order to correctly capture the short-time turbulent dynamics, we employ the stochastic Langevin model. In this context we identified the rotational speed of a turbine as the central parameter to model. For validation, we compare the model results to data from simulations using the Blade Element Momentum (BEM) Theory. The main questions are: How does the stochastically modelled rotational speed time series compare to the time series from the BEM model? How does the model accuracy depend on the definiton of the inflow wind speed, i.e. the usage of a one-point or a rotor averaged wind speed?
We find a good visual and statistical agreement of the Langevin model and the BEM time series, when we use the rotor averaged wind speed as input to the Langevin model. Instead, when we use a one-point wind speed in the rotor plane as input, the model becomes less accurate.

2 Langevin model

The short time dynamics of the rotational frequency f_{gen} of the generator in a wind turbine are modelled by the Langevin equation

$$\frac{\mathrm{d}}{\mathrm{d}t} f_{gen}(t) = D^{(1)}_{f_{gen}}(f_{gen}(t), u(t)) + \sqrt{D^{(2)}_{f_{gen}}(f_{gen}(t), u(t))} \cdot \Gamma(t). \tag{1}$$

Here, $D^{(1)}_{f_{gen}}$ is the so-called drift coefficient and describes the deterministic part of the frequency dynamics. $\Gamma(t)$ is delta-correlated white noise, so that the second term on the right hand side gives a random contribution to the dynamics. Its amplitude is given by the so-called diffusion coefficient $D^{(2)}_{f_{gen}}$.
Both $D^{(1)}_{f_{gen}}$ and $D^{(2)}_{f_{gen}}$ can be estimated from an existing data set. Knowing both coefficients, an integration of eq. 1 gives an iterative stochastic model for f_{gen}:

$$f_{gen}(t+\Delta t) = f_{gen}(t) + D^{(1)}_{f_{gen}}(f_{gen}(t), u(t))\Delta t + \sqrt{D^{(2)}_{f_{gen}}(f_{gen}(t), u(t))\Delta t} \cdot \eta(t), \tag{2}$$

with the integration time step Δt and white noise $\eta(t)$.

3 Methodology

We use BEM simulations with the simulation package *OpenFAST* and the NREL 5MW reference turbine to generate 1 Hz data for the estimation of $D^{(1)}_{f_{gen}}$ and $D^{(2)}_{f_{gen}}$ [2]. Since both coefficients depend on the inflow wind speed u, we need to cover different wind situations. We therefore generate time series of 10 minutes for average wind speeds from 2 to 15 m/s, in steps of 0.5 m/s, with the submodule *TurbSim*. We use the Kaimal model for turbulence and the turbulence intensity is given by class B, as defined by the IEC standard. For each mean wind speed, we generate 10 time series with different random seeds, in order to increase the statistics for the estimation of our model coefficients.
After estimation of $D^{(1)}_{f_{gen}}$ and $D^{(2)}_{f_{gen}}$, we need a new wind speed time series as input for the stochastic model in eq. 2. We choose a 2 h time series with a mean wind speed of 8.5 m/s, again using the Kaimal model and turbulence class B. Using this time series, we then model the target parameter f_{gen} with eq. 2 and the previously estimated $D^{(1)}_{f_{gen}}$ and $D^{(2)}_{f_{gen}}$. Additionally we conduct a BEM simulation with this wind speed time series, whose result for $f_{gen}(t)$ is used to validate the Langevin model.
We investigate the Langevin model for two choices of the wind speed $u(t)$. In a first step, we estimate the coefficients and calculate the model for the undisturbed one-point wind speed u_{op} at hub height in the rotor plane. Then we consider the averaged wind speed u_{av} instead. Using this quantity, we estimate the coefficients again and re-calculate the model. Eventually, we compare the accuracy of the model for both cases.

4 Results

In Fig. 1, we show the stochastically modelled time series $f_{gen}(t)$ in comparison to the time series from BEM simulations for both the Langevin model with the one-point wind speed u_{op} in (a) and the rotor averaged wind speed u_{av} in (b). The stochastic model for the one-point wind speed roughly follows the BEM result and does not diverge to extreme values. In contrast, the model with the rotor averaged wind speed agrees visually much better with the time series from BEM. A more quantitative evaluation of this similarity using correlation metrics is planned for future work.

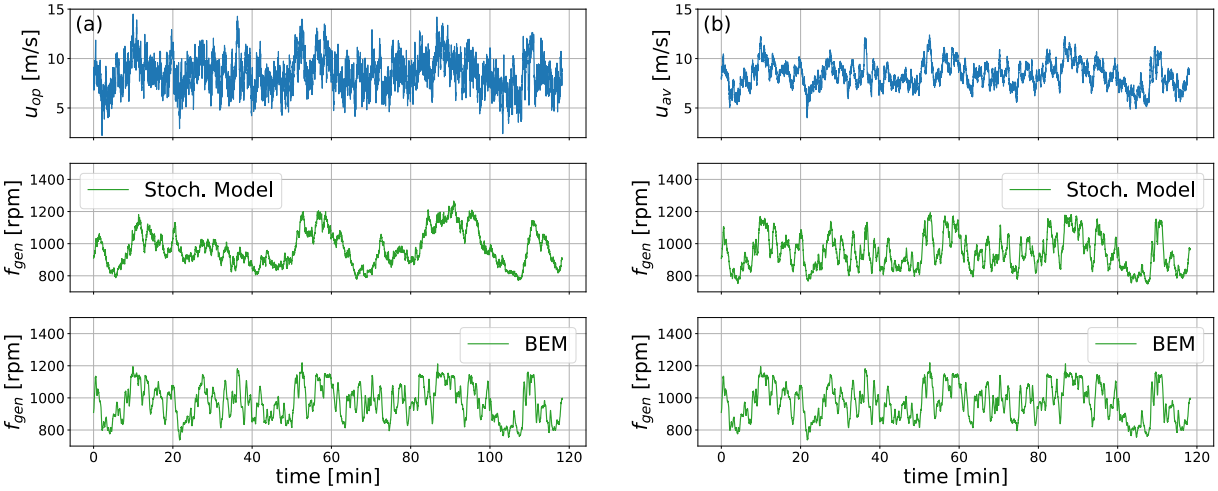

Figure 1: Stochastically modelled time series $f_{gen}(t)$ for Langevin models with two inputs: the one-point wind speed $u_{op}(t)$ in (a) and the rotor averaged wind speed $u_{av}(t)$ in (b). In both cases, the corresponding result of the BEM simulations is shown as a comparison.

In order to validate the two-point statistics of our model, we show the distributions of the generator frequency increments $\Delta f_{gen} = f_{gen}(t+\tau) - f_{gen}(t)$ for the increment steps $\tau \in (1\,\mathrm{s},\ 2\,\mathrm{s},\ 5\,\mathrm{s})$ in Fig. 2, again for both the stochastic model and the BEM simulation results. We note that also statistically, the model with the rotor averaged wind speed seems more precise, especially for the larger increment steps.

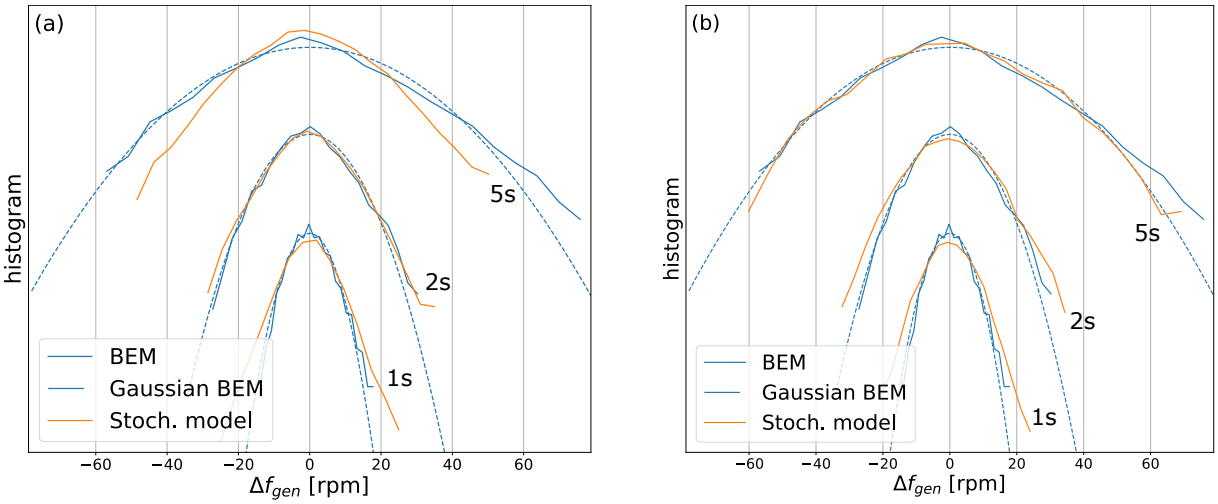

Figure 2: Increments $\Delta f_{gen}(t)$ for both the stochastic model and the data from the BEM simulation. Distributions for different increment time steps $\tau \in (1\,\mathrm{s},\ 2\,\mathrm{s},\ 5\,\mathrm{s})$ are plotted on a logarithmic scale and an arbitrary y-offset was added for reasons of visibility. Gaussian distributions were fitted to the data from the BEM simulation.

Acknowledgements

This work is funded by the Ministry for Science and Culture of Lower Saxony (project "Zukunftskonzept Windenergieforschung").

References

[1] E. Anahua, S. Barth, and J. Peinke. Markovian power curves for wind turbines. *Wind Energy*, 11(3):219–232, May 2008.

[2] J. Jonkman, S. Butterfield, W. Musial, and G. Scott. Definition of a 5-MW Reference Wind Turbine for Offshore System Development. Technical Report NREL/TP-500-38060, 947422, Feb. 2009.

[3] P. Milan, M. Wächter, and J. Peinke. Stochastic modeling and performance monitoring of wind farm power production. *Journal of Renewable and Sustainable Energy*, 6(3):033119, May 2014.

[4] T. A. Mücke, M. Wächter, P. Milan, and J. Peinke. Langevin power curve analysis for numerical wind energy converter models with new insights on high frequency power performance: Langevin power curve analysis for numerical WEC models. *Wind Energy*, 18(11):1953–1971, Nov. 2015.

20th EAWE PhD Seminar on Wind Energy
24 - 26 September 2023
Visby, Sweden

Analysing the sensitivity of wind farm-induced gravity waves to blockage-induced rotor diameter to hub height ratio

Udhaya Chandiran Krishnan Paranjothi[a], Simon J Watson 2[a]

[a] Wind Energy Section, Faculty of Aerospace Engineering, TU Delft, Delft, The Netherlands

E-mail: u.c.krishnanparanjothi@tudelft.nl

Keywords: Atmospheric gravity waves, Wind farm, Flow blockage, Atmospheric flows, Large-eddy simulation

When streamlines are displaced upwards because of the presence of a terrain feature (for example a mountain) in a stratified flow, the combination of this upward force with the downward acting gravitational force triggers a phenomenon called Atmospheric Gravity Waves. The presence of a wind farm, if of sufficient size, can also induce gravity waves especially in a flat homogeneous setting such as offshore and these gravity waves are called wind farm-induced gravity waves.

To lower carbon emissions from electricity generation, it is necessary to drastically increase the capacity of wind energy systems. Increasing the size of the wind turbines and the number of wind turbines in a farm are some of the measures to increase the power generation of a wind farm. Both of these measures result in large wind farms capable of triggering gravity waves. These wind farm-induced gravity waves influence the flow in the vicinity of the wind farm and impact the performance of the wind farm itself. A thorough understanding of these atmospheric gravity waves will assist in better designing future wind farms.

Recently, Allaerts and Meyers [1], through a Large Eddy Simulation framework, analysed wind farm-induced gravity waves in a conventionally neutral boundary layer. This study computationally demonstrated how the wind farm-induced gravity waves can induce a pressure gradient in the wind farm in the streamwise direction. This pressure gradient changes from unfavourable, at the entrance of the wind farm, to favourable, after the first few rows of the wind farm, which impacts the performance of the turbines in a varying manner throughout the different rows. The authors also identified that these effects are pronounced for lower inversion heights. Subsequently, they investigated the impact of stable stratification on the wind-farm induced gravity waves and the performance of the wind farms [2]. They later estimated that the wind farm-induced gravity waves could cause an annual energy loss of the order of 4 to 6 % in the Belgian-Dutch offshore wind farm cluster [3]. Lanzilao and Meyers [4] conducted an extensive investigation of the sensitivity of parameters such as inversion height, inversion strength, inversion thickness, and free atmosphere lapse rate on the self-induced gravity waves and the efficiency of the wind farms. They concluded that a boundary layer characterised by lower inversion height, higher inversion strength and lower free atmosphere lapse rate results in intense gravity waves and pressure gradients, which diminish the efficiency of the wind farm. Aside from Large Eddy Simulations, there have been significant efforts in developing simpler models to account for gravity wave and blockage effects in evaluating wind farm performance [5],[6]. However these models have underlying assumptions, which restrict their applications.

Notwithstanding these research activities, a comprehensive understanding of wind farm-induced gravity waves is yet to be attained. In particular, knowledge of the sensitivity to the turbine diameter and the clearance between the sea surface and the lowest point of the blade tip will assist in better designing the future wind farms. The ability to individually control atmospheric and wind farm parameters and investigate their interaction makes the computational method Large Eddy Simulation suitable for this study. Owing to many advantageous like open-source, state-of-the-art model implementations, good scaling with number of cores, under active development, and full-control over the input data, the incompressible flow solver AMR-Wind [7], developed and maintained by a group of national laboratories in the US, is chosen. For this study, we plan to execute 5 simulations and the details are given in the table below:

Simulation Number	1	2	3	4	5
Parameter Varied	Reference	Vary Diameter		Vary Height	
Turbine Diameter (m)	284	126.91	241.94	284	284
Lowest point of blade tip from sea surface (m)	22.5	22.5	22.5	30	37.5

Table 1: List of simulations

An increase in the turbine diameter is expected to intensify the gravity waves and result in a decrease in the efficiency of the wind farm. However, it is difficult to formulate an expected outcome of an increase in the distance between the lowest point of the blade tip and the sea surface. An increase in the distance between the lowest point of the blade tip and the sea surface leads to both the turbine facing higher velocity wind (thereby higher flow diversion) and an increase in the region available between the turbine and the sea surface for flow diversion from the turbine blockage. Therefore, the outcome depends on how much of the flow diversion happens upwards, which is hard to predict.

Acknowledgements

This work has been partially supported by the MERIDIONAL project, which receives funding from the European Union's Horizon Europe Programme under the grant agreement No. 101084216.

References

[1] D. Allaerts and J. Meyers. Boundary-layer development and gravity waves in conventionally neutral wind farms. *Journal of Fluid Mechanics*, 814:95–130, 2017.

[2] D. Allaerts and J. Meyers. Gravity Waves and Wind-Farm Efficiency in Neutral and Stable Conditions. *Boundary-Layer Meteorology*, 166:269–299, 2018.

[3] D. Allaerts, S.-V. Broucke, N. van Lipzig, and J. Meyers. Annual impact of wind-farm gravity waves on the Belgian–Dutch offshore wind-farm cluster. *Journal of Physics: Conference Series*, 1037:072006, 2018.

[4] L. Lanzilao and J. Meyers. A parametric large-eddy simulation study of wind-farm blockage and gravity waves in conventionally neutral boundary layers. *Journal of Fluid Mechanics*, 979:A54, 2024.

[5] D. Allaerts and J. Meyers. Sensitivity and feedback of wind-farm-induced gravity waves. *Journal of Fluid Mechanics*, 862:990–1028, 2019.

[6] S. Stipa, A. Ajay, D. Allaerts, and J. Brinkerhoff. The Multi-Scale Coupled Model: a New Framework Capturing Wind Farm-Atmosphere Interaction and Global Blockage Effects. Wind Energy Science Discussions, 9:1123–1152, 2024.

[7] M. Sprague, S. Ananthan, G. Vijayakumar, and A.-M. Robinson. ExaWind: A multi-fidelity modeling

and simulation environment for wind energy. *Journal of Physics Conference Series*, 1452:012071, 2020.

20th EAWE PhD Seminar on Wind Energy
24-26 September 2024
Visby, Sweden

Wind Farm Flow Modeling with Neural Operators for Turbine Wake Superposition

J.P. Schøler[a]

[a]DTU Wind and Energy Systems, Frederiksborgvej 399, 4000 Roskilde, Denmark

E-mail: jpsch@dtu.dk

Keywords: Wakes, Wind Turbine Flow, Surrogates, Neural Operators, Scientific Machine Learning (SciML)

Introduction

Within wind farms, the interactions between turbine wakes are important since turbines operating within these wakes generate less power and endure higher loads. When simulating wakes, there are two primary considerations: computational speed and accuracy. Engineering models offer rapid computations but lack precision, while Computational Fluid Dynamics (CFD) models provide high accuracy at a significant computational cost. Training a neural network on CFD data makes it feasible to achieve the computational efficiency of engineering models while retaining accuracy comparable to that of CFD simulations.

Previous works have demonstrated the feasibility of using neural networks as a wake model surrogate [9, 11, 7]. However, engineering models and wake surrogates require super-positioning to construct a farm flow that includes multiple turbine wakes simultaneously. Porté-Agel et al. [6] have reviewed the subject, and they summarize that four superposition principles exist in literature. Two define the velocity deficit related to the incoming boundary layer flow speed: Linear superposition of velocity deficits [3], a linear superposition of energy deficits [2]. The last two define the velocity deficit with respect to the incoming flow speed of the wake-producing turbine. Similarly, these definitions use either linear superposition of velocity deficits [10] or linear superposition of energy deficits [5]. Linear superposition of energy deficits is often termed quadratic sum as the velocity deficits are squared. While these methods produce useful results, they cannot capture non-linear interactions between wakes that are known to be present, these effects grow with the density and amount of turbines in a windfarm. As the price of windfarm lease areas increases, it is reasonable to assume that leaseholders will desire to install turbines more densely, putting existing superposition methods under pressure.

In our proposed work, we want to investigate if learning a better super positioning model from Computational Fluid Dynamics (CFD) data is possible. We suggest using the novel method of Neural Operators as the superpositioning problem can be formulated as an Operator problem.

Neural Operators

An operator acting on a function transforms said function into another function; an example of this could be taking the derivative of a function. A Neural Operator is an approximation of a true Operator using neural networks. Chen and Chen [1] created a universal approximation theorem for Operators in 1995, stating that one can approximate a continuous operator using two shallow neural networks. More recently, this work was re-discovered and led to a variation using two neural networks with depth, leading to the creation of Deep Operator Net (DeepONet) [4]. Seidman *et. al.* [8] improved upon the understanding of neural operators by introducing an explanation of the model architecture, including an encoder $\mathcal{E}$, an approximator $\mathcal{A}$ and a decoder $\mathcal{D}$. Equation (1) below shows how the neural operator can be decomposed into these components when approximating an operator $\mathcal{G}$.

$$\mathcal{G} \approx \mathcal{F} := \mathcal{D} \circ \mathcal{A} \circ \mathcal{E}, \qquad \begin{array}{ccc} L^2(\mathcal{X}) & \xrightarrow{\mathcal{G}} & L^2(\mathcal{Y}) \\ \downarrow \mathcal{E} & & \mathcal{D} \uparrow \\ \mathbb{R}^m & \xrightarrow{\mathcal{A}} & \mathbb{R}^n \end{array} \tag{1}$$

Where $\circ$ is a composition of functions, $\mathcal{F}$ is the combined neural operator approximation of $\mathcal{G}$, $L^2(\mathcal{X})$ and $L^2(\mathcal{Y})$ are two different L^2 Hilbert function spaces.

Wind Farm Flow Superposition Operator

In the context of wind farm flow modeling, we consider the superposition operation that acts on the background flow without turbines, U_{field}, and generates the flow field with the desired turbines, U_{wf}.

$$\mathcal{G}(U_{\text{field}})\left(x^i_{\text{wt}}, \psi^i\right) = U_{\text{wf}} \tag{2}$$

$$\Rightarrow \quad \mathcal{F}(U_{\text{field}})\left(x^i_{\text{wt}}, \psi^i\right) \approx U_{\text{wf}} \tag{3}$$

Here, $\mathcal{G}$ represents the true operator that maps the background flow U_{field} to the wind farm flow U_{wf}, considering turbine positions x^i_{wt} and turbine parameters ψ^i. However, $\mathcal{G}$ is a theoretical construct and is not explicitly known or directly accessible. Despite this, we can approximate $\mathcal{G}$ using a neural operator $\mathcal{F}$. The approximation $\mathcal{F}$ can be learned using Computational Fluid Dynamics (CFD) data, where the background flow and the resulting flow field are available. While $\mathcal{F}$ can provide a practical and usable approximation, it does not represent exactly the true but unknown operator $\mathcal{G}$.

To test the feasibility of the concept, a dataset was constructed using engineering models and using linear superposition of velocity deficits. In Figure 1, the result of this setup is shown; however, as can be seen, the neural operator is struggling to recreate the flow field accurately near the downstream turbines.

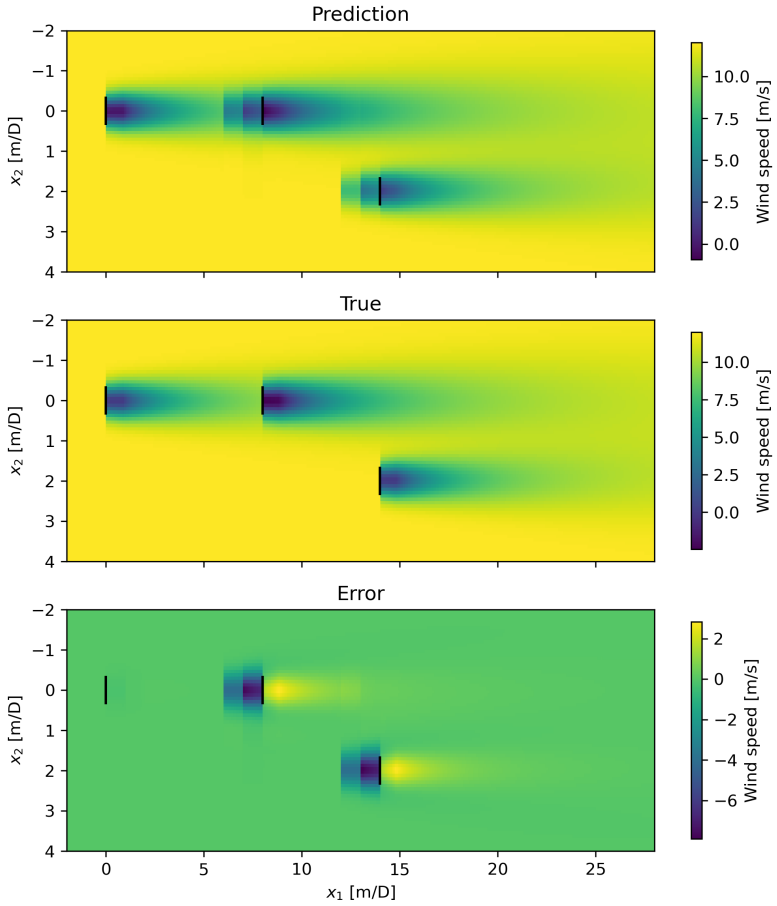

Figure 1: Predicted flowfield, reference flowfield, and error at hub height using a neural operator trained on a simple dataset constructed using engineering models.

Following this initial work, we will train a neural operator using CFD data and address the large errors near the downstream turbines.

References

[1] T. Chen and H. Chen. Universal approximation to nonlinear operators by neural networks with arbitrary activation functions and its application to dynamical systems. *IEEE Transactions on Neural Networks*, 6:911–917, 7 1995.

[2] I. Katic, J. Højstrup, and N. O. Jensen. A simple model for cluster efficiency. volume 1, pages 407–410. APA, 1987.

[3] P. B. S. Lissaman. Energy effectiveness of arbitrary arrays of wind turbines. *Journal of Energy*, 3:323–328, 11 1979.

[4] L. Lu, P. Jin, G. Pang, Z. Zhang, and G. E. Karniadakis. Learning nonlinear operators via deeponet based on the universal approximation theorem of operators. *Nature Machine Intelligence*, 3:218–229, 3 2021.

[5] A. Niayifar and F. Porté-Agel. Analytical modeling of wind farms: A new approach for power prediction. *Energies*, 9:741, 9 2016.

[6] F. Porté-Agel, M. Bastankhah, and S. Shamsoddin. Wind-turbine and wind-farm flows: A review. *Boundary-Layer Meteorology*, 174:1–59, 1 2020.

[7] J. P. Schøler, R. Riva, S. J. Andersen, J. P. Murcia Leon, M. P. van der Laan, J. Criado Risco, and P.-E.. Réthoré. RANS-AD based ANN surrogate model for wind turbine wake deficits. *Journal of Physics: Conference Series*, 2505(1):012022, may 2023. doi: 10.1088/1742-6596/2505/1/012022.

[8] J. H. Seidman, G. Kissas, P. Perdikaris, and G. J. Pappas. Nomad: Nonlinear manifold decoders for operator learning. 6 2022.

[9] Z. Ti, X. W. Deng, and M. Zhang. Artificial neural networks based wake model for power prediction of wind farm. *Renewable Energy*, 172:618–631, 7 2021.

[10] S. Voutsinas, K. Rados, and A. Zervos. On the analysis of wake effects in wind parks. *Wind Engineering*, 14:204–219, 1990.

[11] N. Zehtabiyan-Rezaie, A. Iosifidis, and M. Abkar. Data-driven fluid mechanics of wind farms: A review. *Journal of Renewable and Sustainable Energy*, 14:032703, 5 2022.

1.3 Session 211: Wind farm flows and wakes

25.09.2024, 13:0, Room 1

Chair:

Roko Topić

Presenters:

Krause Jan	Improvement of a double-Gaussian wake model for complex inflow and operation conditions
Mohammadi Mohammad Mehdi	Assessment of wind turbine's loads and power generation in forested areas along the diurnal cycle
Kherlen Jigjid	A simple RANS closure for wind-farms under neutral atmospheric conditions: Model assessment
Clark Ross	Actuator disc analyses - a comparison of numerical results with new analytical formulations
Zengler Clemens	Impact of streamwise pressure gradients on aerodynamic turbine performance – a numerical investigation

20th EAWE PhD Seminar on Wind Energy
24-26 September 2024
Visby, Sweden

Improvement of a double-Gaussian wake model for complex inflow and operation conditions

J. Krause, S. Tamaro, R. Braunbehrens, C. L. Bottasso

Wind Energy Institute, Technische Universität München, Boltzmannstr. 15, 85748 Garching bei München, Germany

E-mail: jan.krause@tum.de

Keywords: analytical wake model, near wake, large eddy simulations

1 Introduction

As a result of energy extraction, a low-velocity region forms behind wind turbines. Through momentum exchange with the surrounding flow, the decelerated fluid particles within this wake gain kinetic energy, reducing the velocity deficit with increasing downstream distance. If a turbine is located within such a wake, not only the power production is lower, but the fatigue loads to which the turbine is subjected are larger as well [12]. These complex phenomena can be modeled using computational fluid dynamics (CFD) frameworks such as SOWFA (Simulator fOr Wind Farm Applications [4]). While the accuracy of these results is high, the computational costs are too. However, for wind farm layout design or wind farm and wake control, faster and computationally cheaper tools are needed. Analytical wake models fill this gap.
Given the limited availability of suitable areas for onshore wind parks, there is a strong interest in a closer spacing of the wind turbines. This necessitates the development of wake models capable of accurately predicting the velocity deficit in the area closer to the turbine, where the wake is not yet self-similar. Double-Gaussian wake models can be used to predict the velocity deficit in this area called near wake. A typical assumption in these models is the symmetry of the velocity deficit. This assumption is not valid anymore, if the turbine is subjected to a sheared inflow or if the turbine is misaligned. The objective of this work is to extend an existing wake model so that it can be applied to such complex inflow and operating conditions.

2 State of the Art

In the field of wake model research, the one proposed by Jensen [6] is considered pioneering work. The author assumed a top-hat shape for the velocity deficit and applied 1D momentum conservation to derive the model. More recently, Bastankhah and Porté-Agel [1] proposed a more comprehensive model assuming a single-Gaussian shape. Although, these models are capable in reliably predicting the velocity deficit in the far wake region [10], they show a poor accuracy in the near wake. In this area, the velocity field is strongly influenced by the shedded tip and root vortex and does not fulfill a single-Gaussian shape.
Keane et al. [8] addressed this issue and derived a model assuming a double-Gaussian shape in the near wake. This shape evolves into a single-Gaussian profile with increasing downstream distance. The normalized velocity deficit at a downstream position x and a radial position r is defined as

$$\frac{\Delta U}{U_\infty} = \frac{U_\infty - U(x,r)}{U_\infty}, \tag{1}$$

with U_∞ being the incoming wind velocity. This deficit is modeled as the product of the normalized double-Gaussian function $g(r,\sigma(x))$ and the amplitude function $C(\sigma(x))$

$$\frac{\Delta U}{U_\infty} = C(\sigma(x)))g(r,\sigma(x)). \tag{2}$$

Within this formulation, the double-Gaussian function is defined as

$$g(r,\sigma(x)) = \frac{1}{2}\left(e^{D_+} + e^{D_-}\right), D_\pm = \frac{-(r \pm r_0)^2}{2\sigma^2(x)} \tag{3}$$

depending on the radial position of the Gaussian extrema r_0 and the standard deviation of the Gaussian function $\sigma(x)$. The latter describes the width of each of the two single-Gaussian profiles. With the goal of deriving a formulation for the wake expansion function $\sigma(x)$, the authors applied the conservation of momentum principle and integrated the resulting equation over the entire rotor disk plane. Schreiber et al. [10] conducted this numerical integration using the same assumptions. However, the authors found that the resulting formulation of the original publications violates the underlying mass and momentum conservation principles in certain conditions. In this case, the wake expansion function is defined as

$$\sigma(x) = k^*(x - x_0) + \varepsilon, \tag{4}$$

with k^* controlling the expansion rate, x_0 being the outlet of the stream tube at a unknown downstream position and the wake expansion ε at this position. The unknown parameter ε is derived enforcing mass conservation between the Betz stream tube and the wake model, leading to a formulation depending on c_T and r_0. The authors propose to tune the remaining parameters x_0 and k^* based on experimental or high-fidelity simulations data.
This model was further improved by Zengler et al. [15], who proposed a new formulation for the initial peak position r_0. This formulation is motivated by the empirical observation that the shape of the velocity deficit depends on the operational state. Additionally, a new formulation for the wake expansion function $\sigma(x)$, assuming a non-linear influence of the the thrust coefficient and the turbulence intensity, is proposed.
Figure 1 shows a comparison of the predicted velocity deficits behind a scaled wind turbine, using models from Schreiber et al. [10] and Zengler et al. [15], with LES data (G1). The workflow for the CFD simulations is described in the following section. Comparing the predictions from the two wake model formulations, two main differences are visible. In Figure 1a) it can be seen, that the new formulation captures the amplitude of the velocity deficit more precisely. Additionally, for a case with a lower thrust coefficient, shown in Figure 1b), the prediction of the shape of velocity deficit is more accurate. Since the amplitude function $C(\sigma(x))$ as well as the shape function $g(r,\sigma(x))$ are both depending on the wake expansion function $\sigma(x)$, these improvements can be attributed to the proposed adjustments.

One common feature among all the introduced models is the assumption of a symmetric velocity deficit. This assumption is not valid, if the turbine is subjected to a sheared inflow, described by the power low coefficient α, or if the turbine is misaligned by a yaw angle γ. To enable the use of double-Gaussian wake models under such complex inflow and operating conditions, the model presented by Zengler et al. [15] will be extended. Preliminary results, along with the future work, are presented in the following section.

3 Preliminary results

The preliminary results presented in this section where generated using an in-house version of SOWFA [4, 13, 14]. This framework couples OpenFOAM [5] directly with the aeroelastic Simulator FAST [7] using the actuator line method for modeling the blades [9, 11]. In this case, the IEA 3.4 MW [3] turbine with a hub height of 110 m and a rotor diameter D of 130 m is used. Nacelle and tower are fully resolved using the snappyHexMesh [5] utility. The domain of size 2080 × 992 × 608 m3 is discretized using a Cartesian grid with five refinement layers, where the cubic cells in the finest layer have an edge length of 1 m.
Figure 2 shows the mean streamwise velocity, non-dimensionalised with the free-stream velocity $U_\infty = 8m/s$ at different downstream distances. A positive vertical distance y is pointing towards the right looking downstream. In all cases, a laminar inflow was used, but with different vertical shear profiles. In the reference case, shown in solid red lines, the turbine is aligned with the non-sheared inflow. The velocity deficit is highly symmetric, but not fulfilling a double-Gaussian shape close to the turbine. The shape of the velocity deficit is strongly influenced by the high gradients at the edges of the wake and close to the wake centerline. Due to the momentum exchange with the more energetic freestream, the gradients decrease with growing downstream distance. To address this issue, the use of a super-Gaussian [2] function will be studied in the course of the future work.
Results for a turbine being aligned with the, now highly sheared inflow are shown in dotted blue. The basic double-Gaussian shape of the velocity deficit remains, but the amplitude of the deficits is highly asymmetric in this case. A

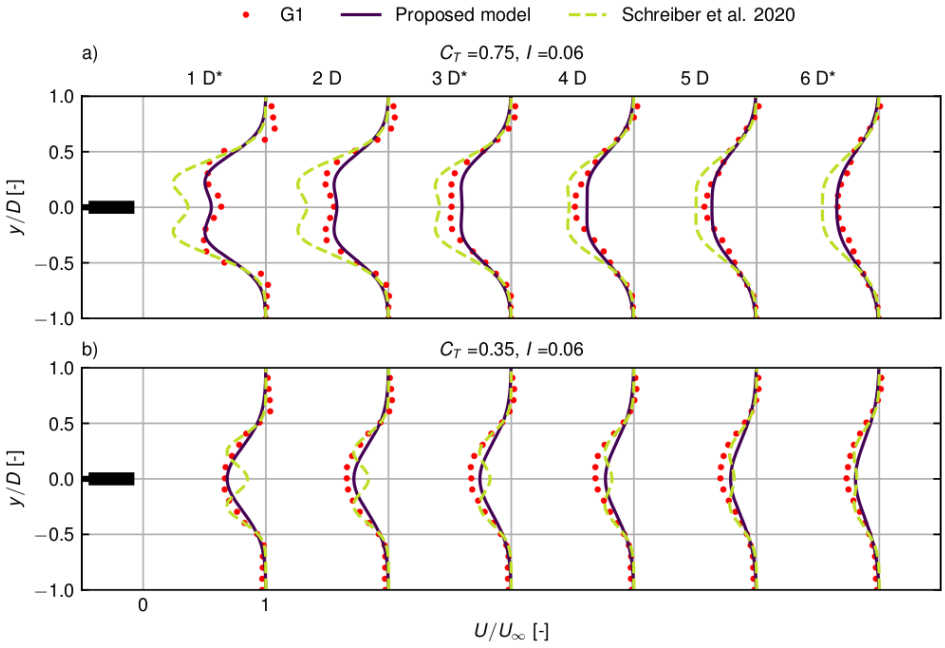

Figure 1: LES results and predictions by the models proposed by [15] and [10] for the velocity deficit behind a scaled wind turbine. This figure is adapted from the publication of Zengler et al. [15].

more complex situation can be observed for a turbine operating under yaw misalignment and a non-sheared inflow. The lower power extraction leads to a lower velocity deficit, which is shifted additionally.

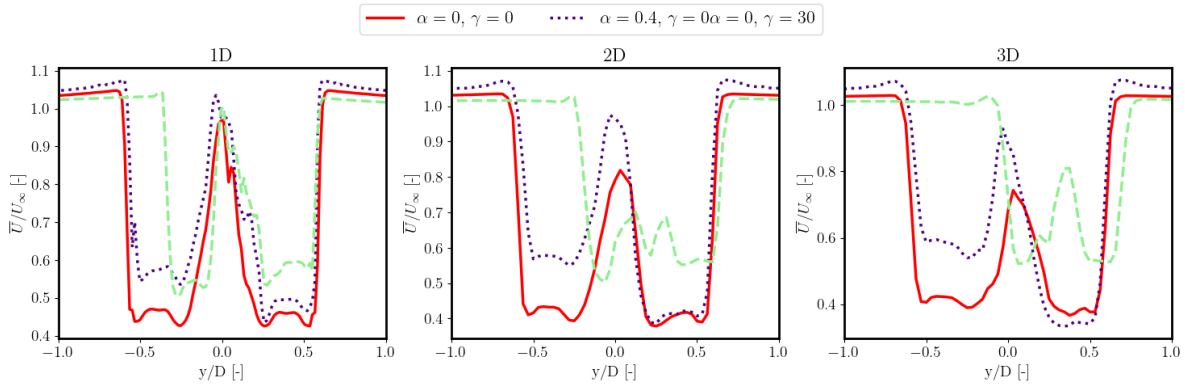

Figure 2: LES results of the normalized mean velocity at different downstream distances D of the IEA 3.4 MW turbine, with α describing the power law coefficient of the laminar inflow and γ the yaw misalignment of the turbine.

The results presented in this section show, that further research is needed to model the velocity deficit with sufficient accuracy in these complex inflow and operation conditions. As future work, a database containing further simulations with different yaw angles and shear exponents will be generated. This simulations will be carried out for both laminar and turbulent inflows. This data will be analysed and used to motivate further adaptions to the double-Gaussian wake model function.

References

[1] M. Bastankhah and F. Porté-Agel. A new analytical model for wind-turbine wakes. *Renewable energy*, 70:116–123, 2014.

[2] F. Blondel and M. Cathelain. An alternative form of the super-gaussian wind turbine wake model. *Wind Energy Science Discussions*, 2020:1–16, 2020.

[3] P. Bortolotti, H. C. Tarres, K. Dykes, K. Merz, L. Sethuraman, D. Verelst, and F. Zahle. Iea wind tcp task 37: Systems engineering in wind energy-wp2. 1 reference wind turbines. 2019.

[4] M. Churchfield, S. Lee, and P. Moriarty. Overview of the simulator for wind farm application (sowfa). *National Renewable Energy Laboratory*, 2012.

[5] C. Greenshields. *OpenFOAM v11 User Guide*. 2023.

[6] N. Jensen. A note on wind turbine interaction. risø national laboratory, roskilde. Technical report, Denmark, Technical Report No M-2411 1983, 1983.

[7] J. M. Jonkman, M. L. Buhl, et al. *FAST user's guide*, volume 365. National Renewable Energy Laboratory Golden, CO, USA, 2005.

[8] A. Keane, P. E. O. Aguirre, H. Ferchland, P. Clive, and D. Gallacher. An analytical model for a full wind turbine wake. In *Journal of Physics: Conference Series*, volume 753, page 032039. IOP Publishing, 2016.

[9] A. R. Meyer Forsting, G. R. Pirrung, and N. Ramos-García. Brief communication: A fast vortex-based smearing correction for the actuator line. *Wind Energy Science*, 5(1):349–353, 2020.

[10] J. Schreiber, A. Balbaa, and C. L. Bottasso. Brief communication: A double-gaussian wake model. *Wind Energy Science*, 5(1):237–244, 2020.

[11] N. Troldborg, J. N. Sørensen, and R. Mikkelsen. Actuator line simulation of wake of wind turbine operating in turbulent inflow. In *Journal of physics: conference series*, volume 75, page 012063. IOP Publishing, 2007.

[12] P. Vølund. Loads on a horizontal axis wind turbine operating in wake. *Journal of Wind Engineering and Industrial Aerodynamics*, 39(1-3):317–328, 1992.

[13] C. Wang, J. Wang, F. Campagnolo, D. Carraón, and C. Bottasso. Validation of large-eddy simulation of scaled waked wind turbines in different yaw misalignment conditions. In *Journal of Physics: Conference Series*, volume 1037, page 062007. IOP Publishing, 2018.

[14] J. Wang, C. Wang, F. Campagnolo, and C. L. Bottasso. Wake behavior and control: comparison of les simulations and wind tunnel measurements. *Wind Energy Science*, 4(1):71–88, 2019.

[15] C. Zengler, R. Braunbehrens, and S. Tamaro. Further improvements to the double-gaussian wake model. *Accepted at TORQUE conference 2024*.

20th EAWE PhD Seminar on Wind Energy
24-26 September 2024
Visby, Sweden

Assessment of wind turbine's loads and power generation in forested areas along the diurnal cycle

Mohammad Mehdi Mohammadi[a]

[a]Department of Earth Sciences, Wind Energy Section, Uppsala University, Cramérgatan 3, 621 67 Visby, Sweden

E-mail: mohammad.mohammadi@geo.uu.se

Keywords: Large eddy simulation, Forest, Stability, Aeroelastic, Actuator sector model, Wind power

The forested areas cover significant parts of the countries such as Sweden and Finland. Due to the availability of land, they can be considered suitable sites for developing wind power projects. In addition, they offer reduced audible and visual impact which can help minimize the opposition from the local population. However, the presence of the forest increases the turbulence intensity and wind shear considerably, which can adversely affect the fatigue loads and thereby turbine lifetime [6]. Also, the modified wind field can affect the wake development, wake recovery, and turbine power generation.

Large eddy simulation (LES) has shown to be a useful tool for investigating the effect of the forest on the wind field and the turbines' performance and loads. For instance, the presence of the forest in the atmospheric boundary layer (ABL) with different stratification is modeled for homogeneous canopies[6, 7]. In another study, the wake of two turbines in an inhomogeneous forest with complex terrain is examined and the results are compared with the measurements in neutral ABL [5]. In addition, the effect of a complex forested site on the turbine's structural loads is studied by extracting the flow field planes and feeding them into a structural solver [1]. In a recent study, a diurnal cycle is modeled over a forested area where the results are in good agreement with the met mast measurements in the wake of a turbine [8].

Despite these advances in forest modeling using LES, we identify a research gap for a study of the effect of the forest on the turbine structural loads and power generation under different stability conditions using an aeroelastically coupled actuator model. This will provide a better and more complete understanding of the turbine's performance and structural response in forested areas. The research questions are as follows.

- How does the forest impact the loading on the turbine's components under different stratification conditions in terms of damage equivalent loads?
- How does the forest impact the turbine power generation and wake development during varying stratification conditions?

To answer these questions, the methodology used in [8] for simulating the diurnal cycle over the forest with different stability conditions is combined with an aeroelastic variant of an actuator sector model presented in [4]. The presence of the forest is modeled by imposing a drag force field into the computational domain [9]. Furthermore, to account for thermal stratification, a source term is added to the temperature equation modeling the heat flux through the canopy [7]. The heat flux varies throughout the day to model the transition between different stability conditions. The increase in dissipation due to the forest is considered by adding an extra term to the turbulent kinetic energy transport equation [7]. Accessing commercial turbines' structural properties required to perform the aeroelastic calculations is often difficult. Therefore, a reference turbine, NREL 5MW [2], is used for the simulations along with the OpenFAST aero-servo-elastic toolbox [3].

It is expected that during the day, there is increased turbulence due to the forest and the unstable condition while the enhanced mixing reduces the velocity at the hub height and the power generation. However, the increased mixing can increase the wake recovery and improve the power generation of the waked turbine downstream. The opposite can happen during the stable hours. The cumulative effects of different mechanisms in action are to be investigated and speculating results is not simple at this stage.

References

[1] H. Abedi, S. Sarkar, and H. Johansson. Numerical modelling of neutral atmospheric boundary layer flow through heterogeneous forest canopies in complex terrain (a case study of a Swedish wind farm). *Renewable Energy*, 180:806–828, 2021.

[2] J. Jonkman, S. Butterfield, W. Musial, and G. Scott. Definition of a 5-mw reference wind turbine for offshore system development. Technical report, National Renewable Energy Laboratory, 2 2009.

[3] J. M. Jonkman and M. L. J. Buhl. FAST User's Guide - Updated August 2005. Technical Report NREL/TP-500-38230, 15020796, NREL, Oct. 2005.

[4] M. M. Mohammadi, H. Olivares-Espinosa, G. P. Navarro Diaz, and S. Ivanell. An actuator sector model for wind power applications: A parametric study. *Wind Energy Science Discussions*, 2023:1–24, 2023.

[5] G. P. Navarro Diaz, J. Arnqvist, and S. Ivanell. Wind turbine wake inflow over a heterogeneous forest - comparison between measurement and LES simulation. *Journal of Physics: Conference Series*, 1934(1):012008, May 2021.

[6] B. Nebenführ and L. Davidson. Influence of a forest canopy on the neutral atmospheric boundary layer-a les study. In *ETMM10: 10th International ERCOFTAC Symposium on Turbulence Modelling and Measurements*, 2014.

[7] B. Nebenführ and L. Davidson. Large-Eddy Simulation Study of Thermally Stratified Canopy Flow. *Boundary-Layer Meteorology*, 156(2):253–276, Aug. 2015.

[8] H. Olivares-Espinosa and J. Arnqvist. Modelling of wind turbine wakes over forests along the diurnal cycle. *Journal of Physics: Conference Series*, 2505(1):012043, May 2023.

[9] R. H. Shaw and U. Schumann. Large-eddy simulation of turbulent flow above and within a forest. *Boundary-Layer Meteorology*, 61(1-2):47–64, Oct. 1992.

20th EAWE PhD Seminar on Wind Energy
24-26 September 2024
Visby, Sweden

A simple RANS closure for wind-farms under neutral atmospheric conditions: Model assessment

Kherlen Jigjid, **Dries Allaerts**, and **Richard P. Dwight**

Faculty of Aerospace Engineering, Delft University of Technology,
Kluyverweg 2, Delft, The Netherlands

E-mail: k.jigjid@tudelft.nl

Keywords: Wake prediction, data-driven RANS, sparse symbolic regression

Introduction

Predicting wind turbine wakes and their interactions is essential for enhancing the efficiency of wind farms, increasing power output, and minimizing land use and maintenance costs. In large and dense wind farms, wakes can significantly impact power generation, potentially reducing it by 10-20% in offshore setups [1]. They also introduce additional turbulence that can cause structural vibrations and premature wear in downstream turbines [2]. Accordingly, an accurate wake prediction method is essential in the wind energy industry.

There are various methods available to predict wind farm wakes. Analytical models are widely used in the industry for their cost-effectiveness. However, they lack accuracy in dense wind farm settings where wake interactions are more frequent [3]. Computational Fluid Dynamics (CFD) methods, such as Large Eddy Simulation (LES) and Reynolds-averaged Navier-Stokes (RANS), offer better accuracy than analytical models but come with varying computational costs. LES is more accurate than RANS, yet its high computational demands, between 10^3 and 10^4 CPU hours, limit its practicality for industrial use [4]. In this regard, RANS could offer a balance between accuracy and cost. Nevertheless, the effectiveness of RANS depends on selecting the appropriate model for its intended application [5].

Due to recent advances in machine learning methods, data-driven model discovery is becoming common in the RANS modeling community, including the symbolic regression framework named Sparse Regression of Turbulent Stress Anisotropy (SpaRTA) [6]. In the framework, the focus is on discovering models for two terms introduced in two-equation RANS models, such as the $k-\varepsilon$ or $k-\omega$ models. The terms are correction to the deviatoric part of the Reynolds Stress Tensor (RST) and the residual term for the k equation. Optimal values for these terms are derived from high-fidelity data sources, such as LES or measurement data, and models for these terms are sought through symbolic regression. Compared to other approaches, symbolic regression provides model that can be formulated in mathematical expression, effectively avoiding the 'black-boxification' commonly associated with neural network based methods. The framework has demonstrated its potential by discovering models for three-dimensional bluff bodies [7], wind-tunnel scaled wind farms [8] and full-scale wind farm cases [9].

In a study [9], it was demonstrated that the framework could discover a simple two-term model for correcting the deviatoric part of the RST in the context of wind farm wake prediction. The model was able to predict power production for an unseen six-turbine case relatively well, even though it was derived from a single turbine case. This suggests that the model can capture the physics present in both cases, indicating its generalization capability. Additionally, the model exhibits behavior similar to the existing $k-\varepsilon-f_P$ model, which modifies the eddy viscosity by changing the value of the constant C_μ via the f_P term. This finding highlights the potential for data-driven methods to rediscover models that resemble or exhibit similar behavior to existing ones, thereby aiding in a better understanding of these models.

Research objectives

Despite the results above, further analysis is needed for the model obtained in the study [9]. Firstly, the model's generalizability could be further explored using more LES datasets. Particularly, scenarios involving staggered and

closely aligned turbines in wind farms, where wake interactions are more significant than in the study's original test case. Secondly, the model needs to be evaluated by comparison with other models. Especially, comparing it to the $k-\varepsilon-f_P$ model is essential, given their similarities in predicting the f_P field.

Considering these, the research objectives of the current research are set as follows:

- Assessment of model generalizability: Evaluate the model's generalizability using additional datasets, including staggered and closely aligned cases, and develop models from these scenarios and assess the differences.
- Model comparison: Conduct a comparative analysis specifically with the $k-\varepsilon-f_P$ model, particularly for the prediction of the f_P field.

References

[1] R. Barthelmie, K. S. Hansen, S. Frandsen, O. Rathmann, J. Schepers, W. Schlez, J. Phillips, K. Rados, A. Zervos, E. Politis, and P. Chaviaropoulos, "Modelling and measuring flow and wind turbine wakes in large wind farms offshore," *Wind Energy*, vol. 12, pp. 431 – 444, 07 2009.

[2] P. Réthoré, *Wind Turbine Wake in Atmospheric Turbulence*. PhD thesis, Oct. 2009.

[3] C. L. Archer, A. Vasel-Be-Hagh, C. Yan, S. Wu, Y. Pan, J. F. Brodie, and A. E. Maguire, "Review and evaluation of wake loss models for wind energy applications," *Applied Energy*, vol. 226, pp. 1187–1207, 2018.

[4] F. Porté-Agel, M. Bastankhah, and S. Shamsoddin, "Wind-turbine and wind-farm flows: A review," *Boundary-Layer Meteorology*, vol. 174, pp. 1 – 59, 2019.

[5] A. Eidi, R. Ghiassi, X. Yang, and M. Abkar, "Model-form uncertainty quantification in rans simulations of wakes and power losses in wind farms," *Renewable Energy*, vol. 179, pp. 2212–2223, 2021.

[6] M. Schmelzer, R. P. Dwight, and P. Cinnella, "Discovery of algebraic reynolds-stress models using sparse symbolic regression," *Flow, Turbulence and Combustion*, vol. 104, pp. 579–603, 12 2019.

[7] J. P. Huijing, R. P. Dwight, and M. Schmelzer, "Data-driven rans closures for three-dimensional flows around bluff bodies," *Computers & Fluids*, vol. 225, p. 104997, 2021.

[8] J. Steiner, R. P. Dwight, and A. Viré, "Data-driven rans closures for wind turbine wakes under neutral conditions," *Computers & Fluids*, vol. 233, p. 105213, 2022.

[9] K. Jigjid, R. Dwight, D. Allaerts, and J. Steiner, "A simple rans closure for wind-farms under neutral atmospheric conditions: Preliminary findings," *Journal of Physics: Conference Series*, vol. 2767, no. 9, p. 092104, 2024.

20th EAWE PhD Seminar on Wind Energy
24-26 September 2024
Visby, Sweden

Actuator disc analyses - a comparison of numerical results with new analytical formulations

Ross Clark[a], **Peter Jamieson**[a], **Laurence Morgan**[a], **Scott McLaren-Gow**[a], and **Edward Hart**[a]

[a]Department of Electronic and Electrical Engineering, University of Strathclyde

E-mail: ross.clark@strath.ac.uk

Keywords: actuator disc, BEM, CFD, vortex ring method

Glauert's blade element momentum (BEM) theory [1], a combination of Froude's blade element theory [2] and Rankine's actuator disc theory [3], has become a ubiquitous method for analysing the aerodynamic behaviour of wind turbine rotors [4, 5]. However, BEM makes a number of assumptions which result in reduced accuracy when compared to other rotor models [6, 7]. In particular, the assertion that each of the infinitesimal rotor annuli shown in fig. 1 can be treated independently has been shown to be false [8].

The result of assuming annuli independence is that BEM does not account for the pressures at the annuli surfaces, leading to a uniform axial wind velocity across the rotor; in fact, this axial velocity has been shown to be non-uniform [9]. It is necessary, then, to modify the actuator disc model used in BEM to account for the axial velocity non-uniformity. An example of the results of uncorrected and corrected BEM is shown in fig. 2.

A large number of BEM correction have been proposed, many of which are empirical or semi-empirical [9, 10]. In this work, an inviscid fluid dynamics model based on the vortex ring method will be used to find numerical results for the flow field through a turbine. This model was previously developed in order to investigate ducted turbines, and has been extensively tested and validated [11]. These numerical results will then be used to investigate the validity of corrected BEM models, including a novel analytical formulation.

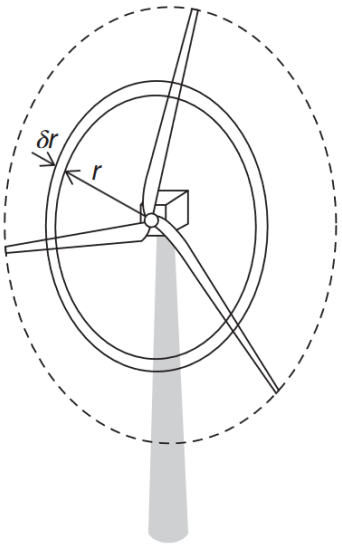

Figure 1: Infinitesimal rotor annuli used in BEM [5].

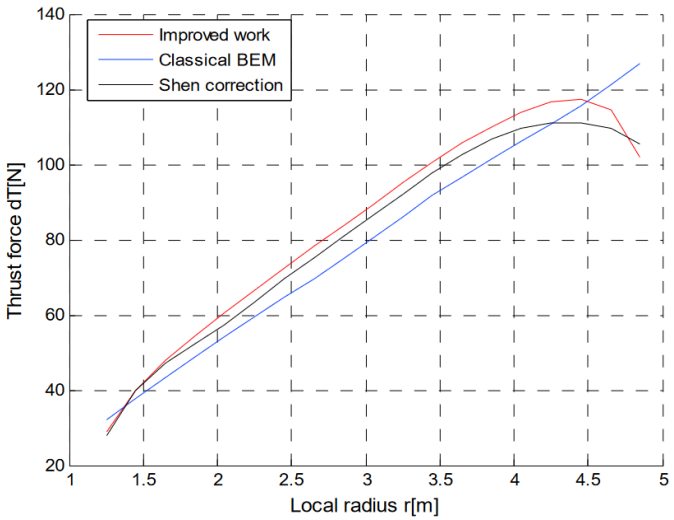

Figure 2: Comparison of thrust force between classical BEM and corrected theories [12].

References

[1] H. Glauert, "Airplane Propellers," in *Aerodynamic Theory*, pp. 169–360, Berlin, Heidelberg: Springer Berlin Heidelberg, 1935.

[2] W. Froude, "On the elementary relation between pitch, slip and propulsive efficiency," *Trans. Roy. Inst. Naval Arch*, vol. 19, no. 47, pp. 47–57, 1878.

[3] W. J. Rankine, "On the mechanical principles of the action of propellers," *Trans. Roy. Inst. Naval Arch*, vol. 6, pp. 13–30, 1865.

[4] S. L. Dixon and C. A. Hall, *Fluid mechanics and thermodynamics of turbomachinery*. Amsterdam Boston: Butterworth-Heinemann, 7th ed., 2014.

[5] T. Burton, N. Jenkins, D. Sharpe, E. Bossanyi, and M. Graham, *Wind Energy Handbook*. Hoboken, NJ: Wiley, third edition ed., 2021.

[6] J. L. Tangler, "The nebulous art of using wind tunnel aerofoil data for predicting rotor performance," *Wind Energy*, vol. 5, no. 2-3, pp. 245–257, 2002.

[7] S. Perez-Becker, F. Papi, J. Saverin, D. Marten, A. Bianchini, and C. O. Paschereit, "Is the Blade Element Momentum theory overestimating wind turbine loads? – An aeroelastic comparison between OpenFAST's AeroDyn and QBlade's Lifting-Line Free Vortex Wake method," *Wind Energy Science*, vol. 5, no. 2, pp. 721–743, 2020.

[8] P. M. Goorjian, "An Invalid Equation in the General Momentum Theory of Actuator Disk," *AIAA Journal*, vol. 10, no. 4, pp. 543–544, 1972.

[9] G. A. M. Van Kuik and L. E. M. Lignarolo, "Potential flow solutions for energy extracting actuator disc flows," *Wind Energy*, vol. 19, no. 8, pp. 1391–1406, 2016.

[10] W. Z. Shen, R. Mikkelsen, J. N. Sørensen, and C. Bak, "Tip loss corrections for wind turbine computations," *Wind Energy*, vol. 8, no. 4, pp. 457–475, 2005.

[11] S. McLaren-Gow, *Rethinking ducted turbines : the fundamentals of aerodynamic performance and theory*. PhD thesis, University of Strathclyde, 2020.

[12] Y. El Khchine and M. Sriti, "Tip Loss Factor Effects on Aerodynamic Performances of Horizontal Axis Wind Turbine," *Energy Procedia*, vol. 118, pp. 136–140, Aug. 2017.

20th EAWE PhD Seminar on Wind Energy
24-26 September 2024
Visby, Sweden

Impact of streamwise pressure gradients on aerodynamic turbine performance – a numerical investigation

Clemens Zengler[a], **Niels Troldborg**[a], and **Mac Gaunaa**[a]

[a]Technical University of Denmark

E-mail: clezen@dtu.dk

Keywords: computational fluid dynamics, actuator disc, site assessment

1 Introduction

Power curve calibration for wind turbines is usually performed in a flat terrain. By doing so, the inflow can be easily characterized, and it can be expected that the flow field does not change significantly between the position of the met mast and the position of the wind turbine. With other words, the flow field is aimed to be lateral and streamwise homogeneous.

However, previous studies have shown, that a power curve obtained under such idealized conditions does not necessarily apply in a non-homogeneous flow field as it can be found in complex terrain [1, 2]. A possible power degradation by up to 33 % is reported [1]. The exact driving mechanism behind this phenomenon is not yet fully understood. Because of this, it is not yet possible to correct for this effect, as no simple model apart from sophisticated computational fluid dynamical (CFD) models exists which can reliably predict this phenomenon. Besides their relatively high computational demand, making them unpractical for detailed site assessment and layout optimization, also CFD models might fail, if the implemented turbine model relies on an induction-thrust relation obtained in flat terrain [2].

As flow accelerates and decelerates in complex terrain, the static pressure fluctuates as well. Thus, one reason for power variations in complex terrain might be the pressure difference between the position of the turbine and the positions up and downstream of the turbine. Previous studies have shown that pressure gradients actually impact the power performance of model wind turbines in the wind tunnel [3, 4].

2 Research question

In this work, the effect of a pressure gradient on aerodynamic turbine performance will be investigated through CFD. Special emphasis is put on the influence of the location of the pressure gradient (before, after, in the turbine plane) on the performance and how the controller of the turbine affects the results. Further, it is intended to validate the numerical results with experimental data.

3 Methodology

Reynolds-averaged Navier Stokes (RANS) simulations – using the k-ε-fp model [5] for closure – of an actuator disc (AD) exposed to various forms of pressure gradients are performed. As solver, EllipSys3D [6, 7] is used. Two different ways of imposing the pressure gradient are considered, as sketched in figure 1. Figure a) shows a domain as it was used in the experimental campaign by Dar et al. [3]. The AD is positioned either at the beginning of the upwards going part of the ramp or at the beginning of the downwards going part of the ramp. The normal vector of the AD is parallel to the tilted ramp, reducing the influence of the vertical component of the flow on the results. The inflow profile is generated and adjusted to match experimental data by performing one-dimensional channel flow simulations with EllipSys1D [8] and adjusting the wall roughness of the top wall or the model constants of the turbulence model. This approach to replicate experimental results is intended as validation scenario for the present investigation. The problem with this setup is, however, that it leads to non-ideal inflow conditions at the AD,

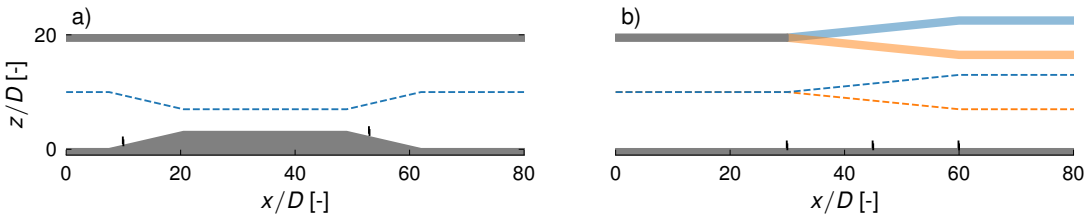

Figure 1: Sketch of the considered computational domains. a) wind tunnel setup as used in [3] and b) ideal setup with pressure gradient imposed by ceiling height variation. Dashed lines indicate idealized pressure variation. Solid black ticks indicate possible AD positions.

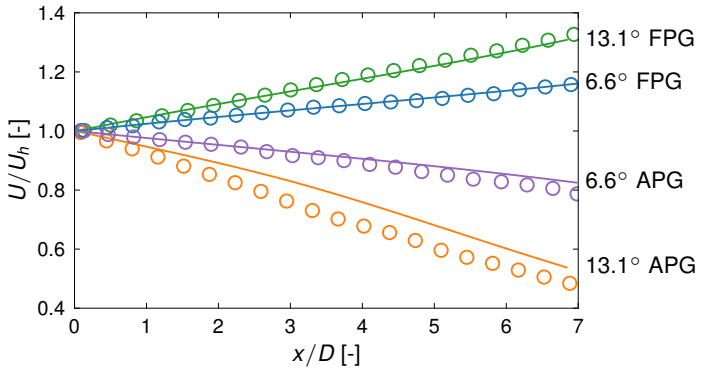

Figure 2: Velocity at hub height behind the turbine position. Comparison of RANS simulations (solid lines) with experimental results (circles) from Dar et al. [3].

making it again difficult to investigate how only the pressure gradient influences power performance. Therefore, the setup in figure 1 b) is considered as well. Varying the domain ceiling is expected to have less impact on the incoming flow field, specifically the relative magnitude of the single components of the velocity vector. Further, varying the position of the AD within this pressure gradient can yield insights into the region of influence of the pressure gradient on power performance.

4 Expected outcomes

Figure 2 shows preliminary results of the undisturbed velocities at hub height behind the turbine position. The favorable pressure gradient (FPG) is located in the domain (figure 1 a)) at the upwards going part of the ramp, and the adverse pressure gradient (APG) at the downwards going part of the ramp. As it can be observed, there is a close agreement between experiments and simulations in case of the FPG. However, in case of the APG, agreement is worse, especially in case of a ramp angle of 13.1 °. Seeking an explanation for this, it appears plausible, that the applied turbulence model needs to be tuned specifically for this case of flow over a complex site since the original model is tuned for a developed boundary layer flow. Hence, it is expected that one outcome of this work will be a new set of model parameters of the k-ε-fp model specifically.

The main outcome however will be insights into how the pressure gradient and its extent up- and downstream of the AD affect the aerodynamic disc performance. Based on these results, it is expected to gain a deeper understanding of the previous results obtained by simulating an AD positioned on top of a ridge [2] where the effect of a pressure gradient was apparent, but not easily separable from other effects as e.g. flow separation and streamline curvature. The impact on power performance will be quantified more accurately and the results verified with previous experimental investigations [3, 4]. Further, also theoretical considerations from a vorticity perspective and a momentum theory perspective will be investigated. These results will be accompanied by insights into the role of the AD controller to reach optimal power performance.

References

[1] N. Troldborg et al. "Brief communication: How does complex terrain change the power curve of a wind turbine?" In: *Wind Energy Science* 7.4 (2022), pp. 1527–1532. DOI: 10.5194/wes-7-1527-2022.

[2] C.P. Zengler, N. Troldborg, and M. Gaunaa. "Is the free wind speed sufficient to determine aerodynamic turbine performance in complex terrain?" In: *The Science of Making Torque from Wind (TORQUE 2024): Wind resource, wakes, and wind farms*. Journal of Physics: Conference Series 9. United Kingdom: IOP Publishing, 2024. DOI: 10.1088/1742-6596/2767/9/092049.

[3] A.S. Dar, A.S. Gertler, and F. Porté-Agel. "An experimental and analytical study of wind turbine wakes under pressure gradient". In: *Physics of Fluids* 35.4 (Apr. 1, 2023), p. 045140. DOI: 10.1063/5.0145043.

[4] T. Cai et al. "Local topography-induced pressure gradient effects on the wake and power output of a model wind turbine". In: *Theoretical and Applied Mechanics Letters* 11.5 (July 2021), p. 100297. DOI: 10.1016/j.taml.2021.100297.

[5] M.P. van der Laan et al. "An improved k - ε model applied to a wind turbine wake". In: *Wind Energy* 18.5 (May 2015), pp. 889–907. DOI: 10.1002/we.1736.

[6] N.N. Sørensen. "General purpose flow solver applied to flow over hills". PhD thesis. Risø National Laboratory, 1995.

[7] J.A. Michelsen. *Basis3D - a Platform for Development of Multiblock PDE Solvers*. Technical University of Denmark, 1992.

[8] M.P. Van Der Laan and Niels N. Sørensen. *A 1D version of EllipSys*. DTU Wind Energy E-0141. Technical University of Denmark, 2017.

1.4 Session 221: Wind farm flows and wakes

25.09.2024, 15:10, Room 1

Chair:

Jean Bastin

Presenters:

Uluocak Sinem	Detection of turbulent structures of wind turbine inflow using dual WindScanner measurements
Devesse Koen	Demonstrating WAYVE: a Code for Modeling Wind-Farm Gravity-Wave Interaction
Ndindayino Olivier	Investigation of the effect of blockage on wind turbine wake development
Bellini Federico	Comparison Among Low and Medium Fidelity Models and Experimental Wind Tunnel Data
Liu Jiaxin	Parametric study on the impact of atmospheric inflow characteristics on turbine performance and loads

20th EAWE PhD Seminar on Wind Energy
24-26 September 2024
Visby, Sweden

Detection of turbulent structures of wind turbine inflow using dual WindScanner measurements

Sinem Uluocak[a,b], **Andreas Rott**[a,b], **Hauke Beck**[a,b], and **Martin Kühn**[a,b]

[a]ForWind - Center for Wind Energy Research, Küpkersweg 70, 26129 Oldenburg, Germany
[b]Carl von Ossietzky Universität Oldenburg, School V, Institute of Physics

E-mail: sinem.uluocak.dincer@uol.de

Keywords: wind turbine wake detection, short-range continuous-wave lidar, free-field, wind field reconstruction.

1 Introduction

Detection of turbulent structures such as gusts or turbine wakes plays a significant role on the wind turbine power output, load estimations and control purposes. In order to accurately detect and characterize these structures, measuring in a large area around the wind turbine is required. Conventional point-wise sensors such as anemometers, which are mounted on a turbine or on a met mast are insufficient for this purpose. Numerous studies have been conducted on wind tunnel experiments to characterize the turbulent structures up to several rotor diameters upstream of a model wind turbine using measurement techniques such as hot wire arrays or Partical Image Velocimetry (PIV). However, the effects of scaled turbine geometries and relatively low Reynolds numbers result in discrepancies with respect to the turbulent flow in free-field.

Lidars are a feasible alternative in the free-field to scan large areas with fast scans without disturbing the flow. Short-range continuous-wave lidars, such as WindScanners, are advantageous in this respect due to their high resolution and flexible scan trajectories. They were used to measure 3D velocity fields in near wake [8] and around turbines, bridges and buildings [5]. van der Laan et al. [7] measured the streamwise velocity fields with a single WindScanner mounted on the top platform of the wind turbine to characterize the multi rotor wake. Recently, dual WindScanners were used to measure 2D velocity fields in the induction zone of a turbine in free-field [3].

New control techniques such as Dynamic Induction Control (DIC) [6] or Helix approach [1] where the recovery of the wake is accelerated through the amplification of the meandering and mixing of the wake, need the information about the change in the turbulence in the flow fields besides the mean velocity to better understand the phenomena.

Although turbulence measurements conducted by lidar systems have not been widely accepted for the standard inflow turbulence measurements due to spatial and temporal averaging, they can be useful to observe changes in the turbulence. Recently, half-wake situations were detected in the Doppler spectrum of a four beam nacelle lidar based on the fact that small-scale turbulence will lead to a broadening of the Doppler spectrum [2].

This study aims to detect turbulent structures within the wind turbine inflow in different wake conditions from the area scans of dual WindScanner measurements. These turbulent structures will be identified using not only the mean wind velocity but also the lidar-based turbulence estimation with different methods including the use of the lidar Doppler spectrum. The results will be compared with point-wise sensor measurements on a met mast array.

2 Measurement test site - WiValdi

Free-field measurements are performed in the inflow of an Enercon E-115 EP3 wind turbine, with a total height of 150 m and a rotor diameter (D) of 115 m at WiValdi with different wake conditions using dual WindScanners.

WiValdi (Wind Validation) is a full-scale test site in Krummendeich, Germany including three fully-equipped turbines (WT1 to WT3) and a total of five meteorological measuring masts (MM1 to MM5) as shown in Figure 1. Two multi-MW (WT1 and WT2) wind turbines, which are positioned in-line with the main wind direction allow for experiments on the wake flow.

The met mast array consists of three masts with 100 m (MM2, MM4) and 150 m height (center mast, MM3), positioned upstream of WT2 and oriented towards the main wind direction. In this way, the array makes it possible to measure the turbulent inflow across the whole rotor area of WT2. They are highly equipped with 32 cup anemometers and 51 3D ultrasonic anemometers in total, which will be used to compare to the lidar-based velocity and turbulence estimations.

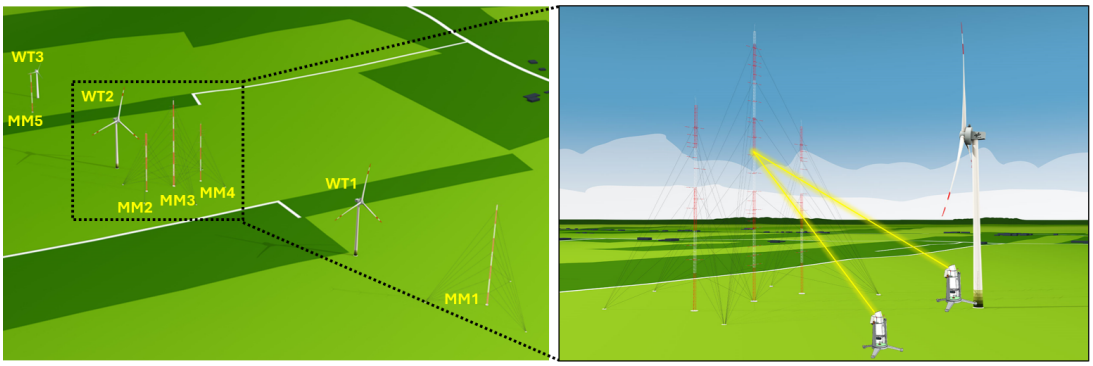

Figure 1: Illustration of the WiValdi test site. The planned measurement area includes wind turbine 2 (WT2) and the met mast array (MM2, MM3, MM4). Wind scanners (WS1 and WS2)

The lidars are two identical short-range continuous-wave WindScanners (WS1 and WS2) developed and manufactured by the Technical University of Denmark [4]. The measurement range is up to 300 m by design and the sampling rate is 450 Hz. They are able to scan different trajectories synchronously with their steerable laser beam having a full opening angle of 120° through the use of two prism motors each. The velocity measurement principle is based on the Doppler shift of the backscattered signal from the aerosols in the air. The WindScanners are used to scan an area between the wind turbines at the triple mast array.

3 Scan strategy

Large vertical and horizontal scans are generated in the inflow of WT´2 to detect turbulent structures. The trajectory can be shifted and can also be rotated according to the flow direction measured by the met mast sensors before each scan.

Examples of a vertical and a horizontal scan with the size of the rotor diameter ($D \times D$) are shown in Figure 2. Note that the vertical scan is along the met mast and perpendicular to the main flow direction. A sinusoidal function is used to generate the scans for an easier movement for the WindScanner motors.

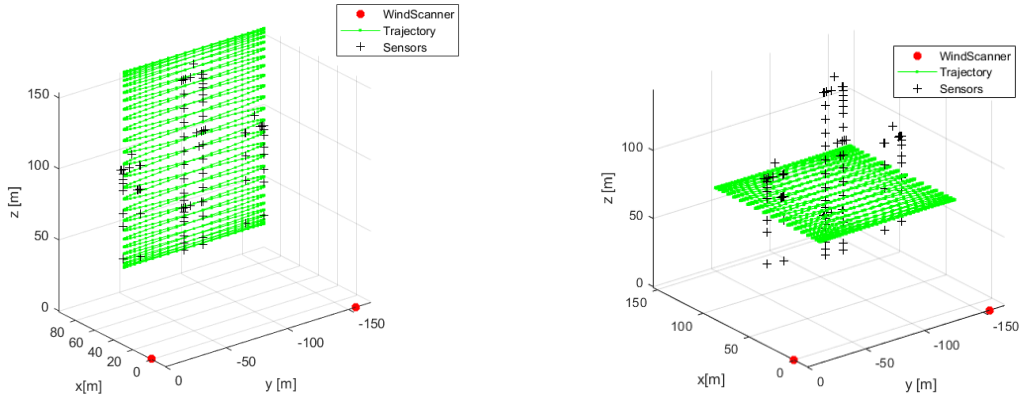

(a) (b)

Figure 2: Vertical area scan along the met mast array (left) and horizontal area scan at 60 m height and centered around the met mast array (right). + symbols shows the sensor locations on the met mast.

4 Preliminary results in undisturbed inflow conditions

First tests were conducted in undisturbed inflow conditions where the upstream turbine is out of operation. The aim of these tests is to define the maximum measurement area by the dual WindScanner configuration and optimize the scan parameters.

The two WindScanners measure two linearly independent line-of-sight velocities which will be used to reconstruct the lateral velocity components (u and v) of the inflow. Here, the preliminary results show only the velocities of the southern WindScanner WS2 ($v_{los,2}$) which is positioned at the origin (0, 0, 0) in the defined coordinate system since the calibration of the northern WindScanner WS1 is on-going. The 10-minute averaged data over the vertical and horizontal area scans are plotted in Figure 3.

The met mast array structures and even the wires can be detected from the low or zero velocity regions in Figure 3a because those stationary objects contribute to the backscattered signal together with the aerosols along the probe volume. The differences between the velocities of the met mast-shaped regions can be explained by the wind direction. Although the wind direction during those test measurements is not known, it can be interpreted from the figures that the wind is coming towards to the southern WindScanner WS2. Therefore, the area to the north (the right side of the figures) has lower line-of-sight velocities. The Figure 3b shows the line-of-sight velocity map of the horizontal plane scan by the same WindScanner. The lines with the low velocity regions are due to the blocking of the laser beam by the met mast structures. It is advisable to detect the hard targets in the measurement area to verify the azimuth and elevation calibration of the lidar. However, in the future, these hard target areas will be removed from the data prior to the averaging process by applying a filter.

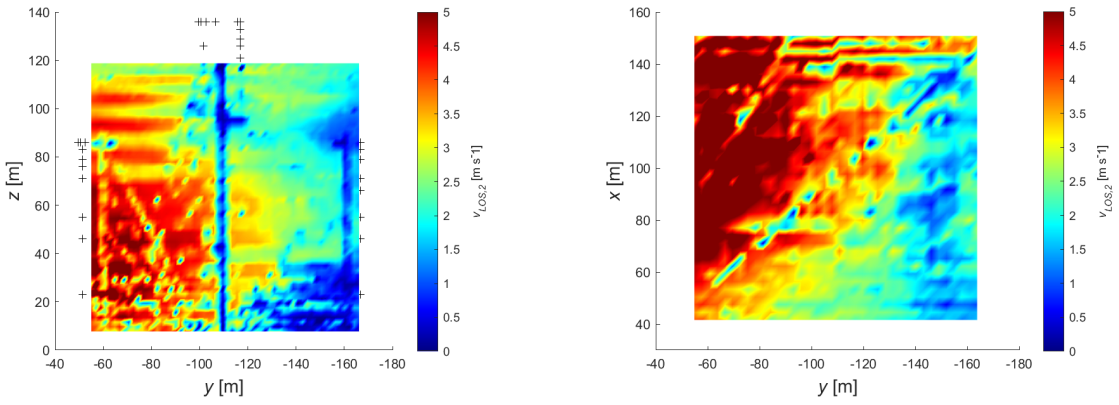

(a) (b)

Figure 3: Averaged line-of-sight velocity measurements over the (a) vertical and the (b) horizontal scans shown in Figure 2. The WindScanner WS2 is positioned at the origin (0, 0, 0). + symbols shows the sensor locations.

The preliminary results show that the dual WindScanner system can scan horizontal and vertical areas of ($D \times D$) around the met-mast array. In the future, the mean and turbulent flow components will be reconstructed from the measured line-of-sight velocities and the Doppler spectrum of the lidar.

Acknowledgements

This work was funded by the German Federal Ministry for Economic Affairs and Climate Action (grant no. 0325936H) on the basis of a decision by the German Bundestag.

References

[1] J. A. Frederik, B. M. Doekemeijer, S. P. Mulders, and J.-W. van Wingerden. The helix approach: Using dynamic individual pitch control to enhance wake mixing in wind farms. *Wind Energy*, 23(8):1739–1751, 2020.

[2] D. P. Held and J. Mann. Detection of wakes in the inflow of turbines using nacelle lidars. *Wind Energy Science*, 4(3):407–420, 2019.

[3] A. P. Kidambi Sekar, P. Hulsman, M. van Dooren, and M. Kühn. Synchronised windscanner field measurements of the induction zone between two closely spaced wind turbines. *Wind Energy Science Discussions*, 2023:1–32, 2023.

[4] T. Mikkelsen. Lidar-based research and innovation at dtu wind energy–a review. In *Journal of Physics: Conference Series*, volume 524, page 012007. IOP Publishing, 2014.

[5] T. Mikkelsen, M. Sjöholm, N. Angelou, and J. Mann. 3d windscanner lidar measurements of wind and turbulence around wind turbines, buildings and bridges. In *IOP Conference Series: Materials Science and Engineering*, volume 276, page 012004. IOP Publishing, 2017.

[6] D. Van der Hoek, J. Frederik, M. Huang, F. Scarano, C. Simao Ferreira, and J.-W. van Wingerden. Experimental analysis of the effect of dynamic induction control on a wind turbine wake. *Wind Energy Science Discussions*, 2022:1–23, 2022.

[7] M. P. van der Laan, S. J. Andersen, N. Ramos García, N. Angelou, G. R. Pirrung, S. Ott, M. Sjöholm, K. H. Sørensen, J. X. Vianna Neto, M. Kelly, et al. Power curve and wake analyses of the vestas multi-rotor demonstrator. *Wind Energy Science*, 4(2):251–271, 2019.

[8] H. Yazicioglu, N. Angelou, T. Mikkelsen, and J. J. Trujillo. Characterization of wind velocities in the wake of a full scale wind turbine using three ground-based synchronized windscanners. *Journal of Physics: Conference Series*, 753(3):032032, 2016.

20th EAWE PhD Seminar on Wind Energy
24-26 September 2024
Visby, Sweden

Demonstrating WAYVE: a Code for Modeling Wind-Farm Gravity-Wave Interaction

Koen Devesse[a] and **Johan Meyers**[a]

[a]Department of Mechanical Engineering, KU Leuven, Leuven, Belgium

E-mail: koen.devesse@kuleuven.be

Keywords: Blockage, Gravity Waves, Atmospheric Boundary Layer, Open-source code

As offshore wind farms grow larger, mesoscale effects such as blockage and gravity waves become increasingly important. To address this, wind farm models will need to include these atmospheric interactions. This is the goal of the recently released code WAYVE, which implements an Atmospheric Perturbation Model (APM) to simulate large wind farms in offshore conditions [2]. WAYVE is relatively fast, and can perform full farm simulations within five minutes on a standard laptop. To promote its use as a research tool, we will give an overview of its capabilities and code structure.

The APM is based on an earlier model by Allaerts and Meyers [1], which predicts the generation and impact of wind-farm induced gravity waves. The model resolves the meso-scale flows, and couples to a wake model to estimate the turbine inflow velocities. Several methods for coupling the APM to wake models have been developed, and all of them are implemented in WAYVE [4]. Additionally, the interface required of the wake model is relatively simple, allowing other wake model codes to be used in combination with WAYVE.

The APM has been validated using 27 LES simulations of a large wind farm under conventionally neutral conditions, with varying boundary layer heights and stratification profiles. The APM and LES results were compared on both meso- and farm-scale, and on turbine power output. The APM captures the overall effects gravity waves have on wind farm power production, and significantly outperforms uncoupled wake models [3, 4].

WAYVE is an open-source code, and is freely available for wind farm researchers, developers, and operators. However, as it is a recent model, it has not yet become widely used. As we believe it is a powerful tool for studying the interaction between wind farms and the atmosphere, we will demonstrate its capabilities and code structure.

References

[1] D. Allaerts and J. Meyers. Sensitivity and feedback of wind-farm-induced gravity waves. *Journal of Fluid Mechanics*, 862:990–1028, 2019.

[2] K. Devesse, L. Lanzilao, D. Allaerts, S. Jamaer, and J. Meyers. Wind-fArm gravitY-waVe and blockagE code, 2023.

[3] K. Devesse, L. Lanzilao, and J. Meyers. A meso-micro atmospheric perturbation model for wind farm blockage. oct 2023.

[4] K. Devesse, S. Stipa, J. Brinkerhoff, D. Allaerts, and J. Meyers. Comparing methods for coupling wake models to an atmospheric perturbation model in wayve. *Journal of Physics: Conference Series*, 2767(9):092079, jun 2024.

20th EAWE PhD Seminar on Wind Energy
24-26 September 2024
Visby, Sweden

Investigation of the effect of blockage on wind turbine wake development

Olivier Ndindayino[a], **Augustin Puel**[a], and **Johan Meyers**[a]

[a]KU Leuven

E-mail: olivier.ndindayino@kuleuven.be

Keywords: Blockage

1 Introduction

Recently [5], LES simulations were performed of a fixed 1.6GW wind farm in different atmospheric stratified conditions to investigate effects on wind-farm efficiency, blockage and related gravity-wave excitation. They noticed that the wind farm blockage induces a favourable pressure gradient throughout the farm. In their work they defined a wake efficiency η_w as the ratio between the average turbine power in the wind farm and the average turbine power of the first row of a wind farm. They identified a strong positive correlation between the favourable pressure gradient in the farm and η_w. This correlation implies that the favourable pressure gradient, induced by blockage, enhances the wake recovery mechanism. This beneficial effect is isolated and further studied in the current work, utilising a set of LES simulations, performed on the numerical solver SP-Wind developed at KU Leuven. For simplicity reasons, the simulated wind farm consists of a single infinitely wide row of turbines in an idealised ABL, i.e. neutral stratification and no wind veer. We systematically study the blockage effect by varying the turbine spacing (S) and boundary layer height (H). First the developed near wake model is discussed, followed by the setup of the numerical solver. Lastly the model is validated against the LES data and the far wake is discussed.

2 Model description

The derivation of the model originates from [6], and is similar to the one proposed by [7]. The model is based on the Froude momentum theory. Figure 1 illustrates the two control volumes used in the derivation, where A_w, A_d and A are the cross-sectional areas of the wake, disk and the entire domain, respectively. U_∞ and p_∞ are the upstream velocity and pressure, respectively. Further, U_d and U_s are the flow velocity at the disk and outside the stream tube. p_d^+ and p_d^- are the pressures at the front and back of the disk, and Δp is the pressure drop over the domain. The derivation assumes uniform in- and outflow in both control volumes.

The model consists of the following six equations that are obtained by, applying the principle of conservation of mass and momentum in the streamwise direction over the control volumes, Bernoulli's principle upstream and

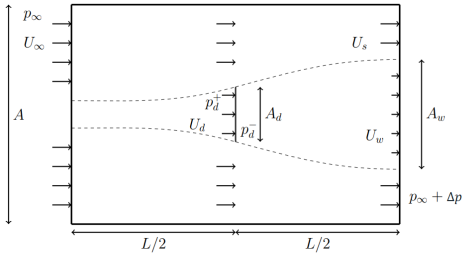

Figure 1: Schematic representation of the control volumes. The dotted line enveloping the actuator disk represents the streamtube. Figure adapted from [6].

downstream of the rotor and inside the outer streamtube and finally using the definition of the disk based thrust coefficient:

$$A_d U_d = A_w U_w, \tag{1}$$

$$A U_\infty = A_w U_w + (A - A_w) U_{s2}, \tag{2}$$

$$(A - A_w) U_{s2}^2 + A_w U_w^2 - A U_\infty^2 = -F - \Delta p A, \tag{3}$$

$$\frac{U_\infty^2}{2} = \Delta p + \frac{U_{s2}^2}{2}, \tag{4}$$

$$F = \left(\frac{U_\infty^2}{2} - \frac{U_w^2}{2} - \Delta p \right) A_d, \tag{5}$$

$$F = \frac{1}{2} C_t' A_d U_d^2. \tag{6}$$

The above six equations form a closed system with six unknowns: $A_w, U_w, U_d, F, \Delta p$ and U_{s2}. The input parameters of the model are A, A_d, C_t' and U_∞. Solving the system of equations analytically leads to complex non-linear analytical expressions. As a result, the model is solved numerically.

3 LES simulations

The governing equations (the momentum and continuity equations) are solved using SP-Wind, an LES solver developed at KU Leuven. The top of the computational domain contains a rigid-lid boundary condition, allowing zero shear stress and vertical velocity. Thus acting as an infinitely strong capping inversion on top of the boundary layer. The bottom of the domain is modelled using a standard wall stress model, which reduces to the log law for the considered neutral cases. The boundary conditions in the horizontal directions are as periodic. To break the periodicity in the streamwise direction and prescribe an inflow condition, we use a fringe-region technique to drive the main domain by turbulent fully developed statistically steady flow fields obtained from concurrent precursor simulations [9]. The turbine thrust force is modelled using a filtered non-rotating actuator disk model corrected with the Shapiro factor [8]. Information such as the implementation of the governing equations, numerical discretization and subgrid-scale model (stability-dependent Smagorinsky model) are provided in e.g. [4, 1, 5].

The streamwise (x) and spanwise (y) length of the computational domain are $L_x = 20$ km and $L_y = 9.6$ km. The height of the domain i.e. the boundary layer height H, is $Lz = 0.35$, 0.5, 0.7 km, for the different cases. The distance between the domain inflow and row of turbines is $L_{ind} = 4$ km. Regarding grid resolution, we set $\Delta x = 40$ m, $\Delta y = 24$ m and $\Delta z = 7.93$ m in the streamwise, spanwise and vertical directions, respectively. The simulations are initialized with a pre-computed turbulent boundary layer, inside an identical computational domain. The boundary layer is characterized by a wall roughness $z_0 = 10^{-4}$ m and friction velocity $u_\tau = 0.274$ m/s. Afterwards, a sufficiently long spin-up simulation is performed for the wind farm, to reach a new statistically steady state. Finally, statistical time averages are calculated over $\Delta t_{av} = 10000s$ and over each turbine in the row.

Utilising the spanwise periodicity of the domain, the simulated wind farm is represented by a single infinitely wide row of turbines. Five cases of different turbine spacing are simulated $S/D = 2.5, 5, 10, 20, 40$, with $D = 240$ m, for $L_z = 0.35$ km and 0.5 km. To save on computational cost, only cases with $S/D = 2.5, 5, 40$ are simulated for $L_z = 0.7$ km. This results in 18 separate LES cases. The actuator disk is modelled after the International Energy Agency (IEA) Wind 15 MW offshore reference wind turbine [3]. The turbine has a hub height $z_h = 150$ m. Since the free-stream inflow velocity varies around 10 m/s, the turbines operate bellow their rated power. As a result the disk-based thrust coefficient is $C_t' = 1.44$ [2]. It is this value of C_t' that is fixed in the LES simulations. However, C_t which is based on the upstream velocity can vary due to blockage, as will be shown in section 4.1, while C_t' is fixed.

4 Results and discussion

4.1 Near wake analysis

Following the actuator disk concept, $C_p = C_t' (U_d/U_\infty)^3$. From the LES data, U_d is retrieved as the average disk velocity, U_∞ is extracted as the inflow velocity at hub height and C_t' is an input parameter of the simulation. The input parameters to the model A, A_d, C_t' are also fixed inputs of the simulation. In the LES results $U_\infty \approx 10$ m/s

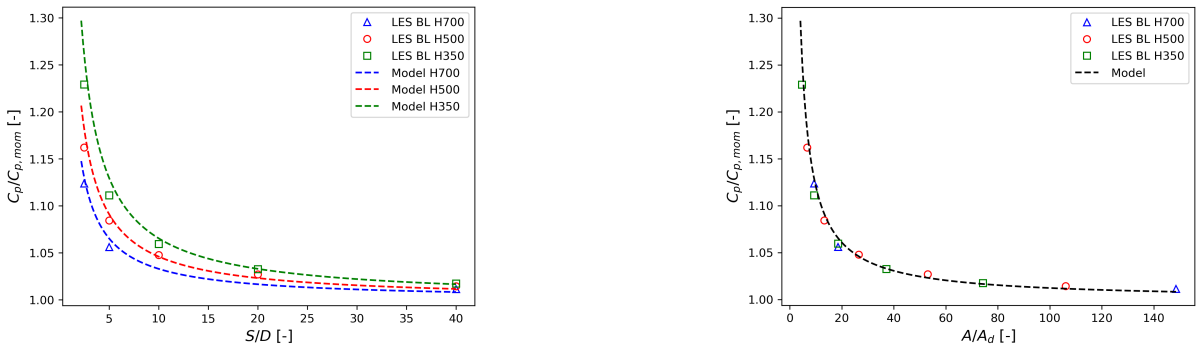

(a) (b)

Figure 2: (a) Power coefficient C_p scaled with $C_{p,mom}$versus spacing S/D, for varying boundary layer heights. (b) C_p versus the inverse wind tunnel blockage ratio A/A_d, for varying H.

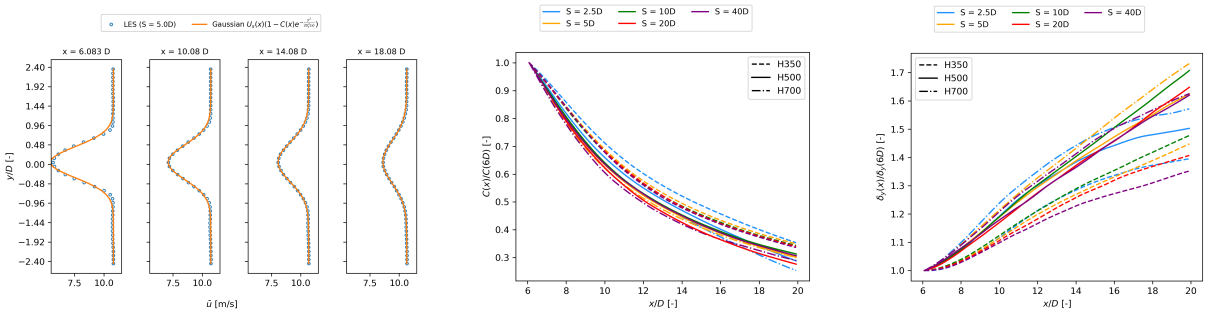

(a) (b) (c)

Figure 3: (a) LES wake profile fitted with a Guassian curve for different downwind distances. (b) Normalised velocity deficit and (c) wake width versus normalized downwind distance.

at hub height, thus for the model $U_\infty = 10$ m/s. It should be noted that the model considers a single turbine, as a result $A = SL_z$ since the turbines have a constant spacing inside the computational domain. Lastly, U_d is an output parameter of the model.

Figure 2a, shows C_p versus S for varying boundary layer heights, for model and LES, scaled with the $C_{p,mom} = 64C_t'/(C_t'+4)^3$ from the classic Froude momentum theory. The model is in good agreement with the LES data. The smaller spacing show a significant increase in C_p, 12%, 8% and 6% for H = 0.35, 0.5, 0.7 km respectively, compared to the momentum theory. Figure 2b shows the same results from figure 2a, but now in function of the typical inverse wind tunnel blockage ratio A/A_d. This results in the collapse of the curves for different H. Since the standard thrust coefficient $C_t = C_t'\,(U_d/U_\infty)^3$, the same trends can be found for C_t as for C_p.

4.2 Far wake analysis

Figures 3b and 3c show the evolution of the normalized maximum velocity deficit $C(x)$ and wake width $\delta(x)$ of the LES results in the far wake, for the different cases. These quantities are obtained by fitting a gaussian shape function on the wake velocity in the LES data as shown in figure 3a. For increasing H, the $C(x)$ curves decrease and the $\delta(x)$ curves increase faster. This is expected since in a deeper boundary layer, the wake is able to mix with more faster moving air from above, resulting in a faster wake recovery and more wake spreading. The $C(x)$ curves overlap well for the varying S, which means that S has a negligible effect on the far wake development. It should be noted that for the case with $S = 2.5D$, $C(x)$ does diverge slightly from the other cases. The reason is that the spacing is so narrow that neighbouring wakes make contact. This is seen in figure 3c, where the wake width evolution of the different cases are similar, except for the smallest S. For this spacing the wake width evolution is similar to the other cases, until a certain streamwise distance ($x/D \approx 14$), after which the wake width plateaus. It should also be noted that for H = 0.35 km, the $\delta(x)$ curves vary irregularly with S.

5 Conclusion

This study set out to analyse the effect of blockage on the wake development behind turbines. To this end, we performed 18 LES simulations of infinitely wide wind farms in an idealised atmospheric boundary layer with varying turbine spacing. The simulations were carried out with an LES solver developed at KU Leuven. First, we concluded that the pressure drop present over the wind farm, induced by blockage, increases C_p and C_t, significantly. Furthermore, we developed an analytical model that predicts the blockage effect on the near wake. Specifically, the model outputs are the wake frontal area, the average wake velocity, the average streamwise disk velocity, the pressure difference between the near wake and the free atmosphere, the thrust, and the velocity far from the wake centre. Additionally, the model inputs are the rotor diameter, turbine spacing, boundary layer height and free stream velocity. The model is based on the theoretical Froude momentum theory applied on a confined domain.

Lastly we concluded that in the far wake, the velocity deficit and wake width are also affected. However, when normalised with near wake deficit and wake width, all the wake profiles collapse, with varying spacing, except for the narrow spacing. Furthermore, increasing boundary layer height shows a faster wake recovery and wake expansion.

Acknowledgements

The computational resources and services used in this work were provided by the VSC (Flemish Supercomputer Center), funded by the Research Foundation - Flanders (FWO) and the Flemish Government. Additionally, the authors express their gratitude to the anonymous reviewers for their insightful comments and relevant observations on this work.

References

[1] D. Allaerts and J. Meyers. Boundary-layer development and gravity waves in conventionally neutral wind farms. *Journal of Fluid Mechanics*, 814:95–130, 2017.

[2] M. Calaf, C. Meneveau, and J. Meyers. Large eddy simulation study of fully developed wind-turbine array boundary layers. *Physics of Fluids*, 22(1):015110, 01 2010.

[3] e. a. Gaertner. Iea wind tcp task 37: Definition of the iea 15-megawatt offshore reference wind turbine. 3 2020.

[4] J. Goit and J. Meyers. Optimal control of energy extraction in wind-farm boundary layers. *Journal of Fluid Mechanics*, 768:5–50, 2015.

[5] L. Lanzilao and J. Meyers. A parametric large-eddy simulation study of wind-farm blockage and gravity waves in conventionally neutral boundary layers. *Journal of Fluid Mechanics*, 979:A54, 2024.

[6] A. Puel and J. Meyers. Analysis of the flow blockage induced by a single-row wind farm and its effect on power production, 2023.

[7] A. Segalini and P. Inghels. Confinement effects in wind-turbine and propeller measurements. *Journal of Fluid Mechanics*, 756:110–129, 2014.

[8] C. R. Shapiro, D. F. Gayme, and C. Meneveau. Filtered actuator disks: Theory and application to wind turbine models in large eddy simulation. *Wind Energy*, 22(10):1414–1420, 2019.

[9] R. J. Stevens, J. Graham, and C. Meneveau. A concurrent precursor inflow method for large eddy simulations and applications to finite length wind farms. *Renewable Energy*, 68:46–50, 2014.

20th EAWE PhD Seminar on Wind Energy
24 - 26 September 2023
Visby, Sweden

Comparative analysis of Wake models for Floating Offshore wind Turbines Using FLORIS and Experimental Validation in Wind Tunnel

Federico bellini, Majid Ebrahimi, Marco De Pascali

Politecnico di Milano – department of mechanical Engineering
E-mail: federico.bellini@polimi.it

Keywords: FLORIS, Wind Tunnel, FAST.Farmf

1 Introduction

The wind energy market has been experiencing a significant shift towards the construction of large offshore wind farms utilizing floating wind turbines. This trend is driven by several factors, including the availability of vast offshore spaces, superior wind conditions, and reduced environmental impact compared to traditional seabed-anchored turbines. However, the current floating technology incurs higher costs, necessitating extensive research and development efforts to enhance efficiency and reduce overall expenses. This study aims to bridge the gap between numerical modeling and experimental validation, focusing on the development of accurate wake models for floating offshore wind turbines.

2 Research Objectives

The primary objective of this study is to develop a comprehensive numerical model of power (Cp) and thrust (Ct) coefficients based on tests previously conducted in a wind tunnel using a 1/150 scale model of the IEA-15-240-RWT turbine. By utilizing FLORIS, a low-fidelity modeling software, we aim to analyse bottom fixed and offshore wind turbines and compare various wake models. The research extends to comparing these models with FAST.Farm a medium-fidelity modeling software, and ultimately comparing the results through wind tunnel experiments. This multi-faceted approach allows for a thorough understanding of how different programs model wake based on input configurations, providing valuable insights for the efficieny of floating offshore wind farms.

3 Methodology

Our research methodology emploFays three approaches to wake modeling using FLORIS:

1. **Jensen Model:** We implement this classic wake model, which represents the spread of velocity deficit as a cone, the model is derived from [1]. Despite its simplicity, the Jensen model provides a baseline for comparison with more complex.
2. **GCH Model:** This Gaussian velocity model offers a more sophisticated approach, considering wake rotation and adjacency effects between turbines. The implementation in FLORIS is based on the work of Bastankhah and Porté-Agel [2] [3], providing a more nuanced representation of wake dynamics.
3. **Empirical Gauss Model:** This model features the familiar Gaussian wake shape seen in other popular FLORIS models. However, the models governing wake width and deflection have been revised for easier tuning and improved data fitting, more information about the model are provided in [4]. Of particular interest for floating applications, as it the vertical deflection of the wake, a technique exploitable exclusively in the floating field.

Here below in figure Figure 3-1 and Figure 3-2 are shown how the wake models are generated.

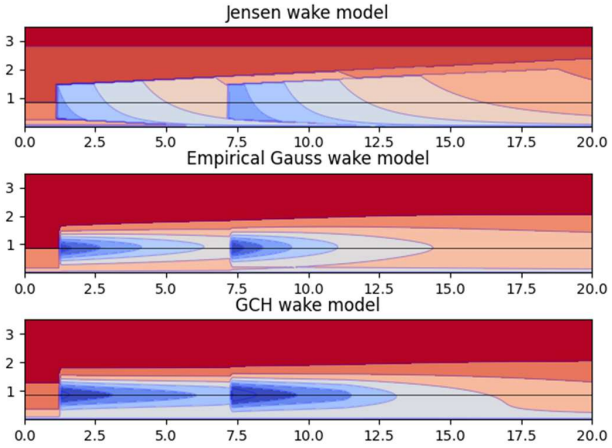

Figure 3-1 Visualization of different wake models in Floris

To ensure a comprehensive analysis, we implemented an initial layout followed by an optimized configuration using an optimization technique proposed by Michael Sinner and Paul Fleming [5] available on the most recent release of FLORIS. Recognizing the importance of pitch angle in floating turbine performance, we simulated wind turbines with three different pitch angles (0°, 10°, 20°) as shown in Figure 3-2 to understand the vertical deflection of the wake. This approach allows us to estimate and model the complex wake interactions that occur in real-world floating wind farm scenarios.

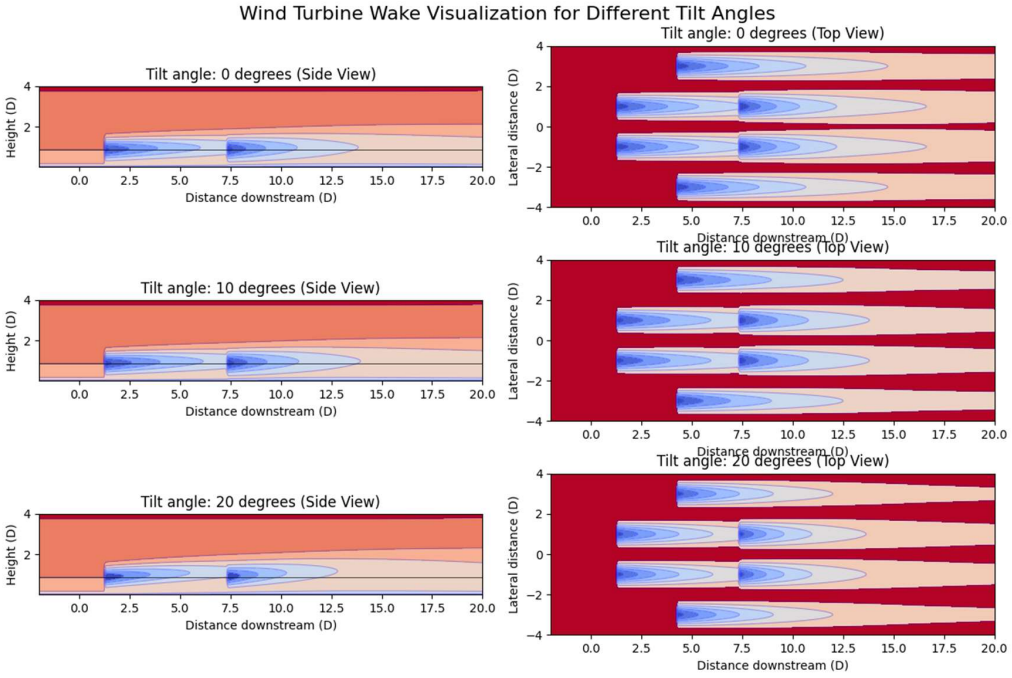

Figure 3-2 Wind farm model with different tilt angles in the horizontal and vertical plane with empirical gauss model.

20th EAWE PhD Seminar on Wind Energy
24 - 26 September 2023
Visby, Sweden

The models were developed using specific input data for the scaled wind turbine and variable configurations to assess their accuracy and versatility. After that we decided to perform the optimization with the random search optimization. The result provides an optimized layout, and it too will be tested within the wind tunnel.

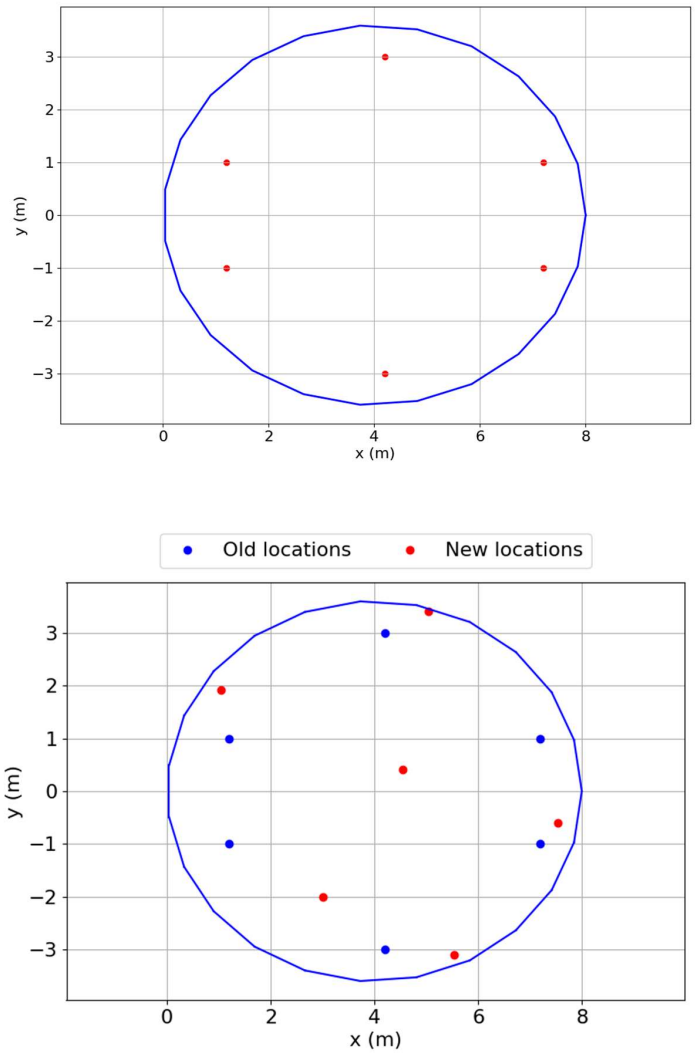

Figure 3-3 Optimized layout obtained with Random search optimization.

4 Expected Results

In the coming months, we will conduct an extensive test campaign at the Politecnico di Milano wind tunnel, utilizing six turbines at a 1/150 scale compared to the IEA-15-240-RWT. These experiments are meticulously designed to provide crucial empirical data for comparison with the simulation results obtained from FLORIS and FAST.Farm. We anticipate that this experimental data will serve as a valuable benchmark, allowing us to refine our understanding of the observed wake phenomena and validate the accuracy of our numerical models. The comparison between experimental and simulated results will likely reveal areas where current models excel and where they may need further refinement.

20th EAWE PhD Seminar on Wind Energy
24 - 26 September 2023
Visby, Sweden

5 Discussion

Our research acknowledges that each wake model has specific advantages and limitations. The Jensen model, while computationally efficient, may lack precision in complex wind farm configurations. The GCH model offers enhanced accuracy but at the cost of increased computational complexity. The Empirical Gauss Model, with its unique ability to model wake deflection, shows promise for floating turbine applications where wake control is crucial for optimizing energy production. It is also interesting to study an optimized model to evaluate the power values generated in the wind tunnel and focus not so much on matching FLORIS values, given the high scale factor, but on comparing the tested layouts.

6 Conclusions

This study aims to advance the understanding and optimization of wake modeling for floating offshore wind turbines through a combined numerical and experimental approach. By utilizing FLORIS and FAST.Farm software, we have explored three distinct wake models: the classic Jensen model, the advanced GCH model, and the revised Empirical Gauss Model tailored for floating applications. Each model offers unique insights into wake dynamics, with the Empirical Gauss Model particularly promising for its ability to model vertical wake deflection, crucial in optimizing energy production in floating wind farms.

The upcoming wind tunnel experiments at Politecnico di Milano will provide empirical data essential for validating our simulation results and refining these wake models further. We anticipate that this empirical validation will highlight areas of strength and areas requiring refinement in current wake models.

Overall, this research contributes to the broader effort of enhancing the efficiency and cost-effectiveness of floating offshore wind farms. By bridging numerical modeling with experimental validation, we aim to provide valuable insights for future developments in this rapidly evolving field.

References

[1] Niels Otto Jensen. *A note on wind generator interaction*. Risø National Laboratory, 1983.
[2] Majid Bastankhah and Fernando Porté-Agel. *Experimental and theoretical study of wind turbine wakes in yawed conditions.* Journal of Fluid Mechanics, 806:506–541, 2016.
[3] Amin Niayifar and Fernando Porté-Agel. *Analytical modeling of wind farms: a new approach for power prediction*. Energies, 9(9):741, 2016.
[4] https://nrel.github.io/floris/empirical_gauss_model.html#empirical-gauss-model.
[5] Michael Sinner and Paul Fleming 2024 J. Phys.: Conf. Ser. 2767 032036J.-O. Mo, A. Choudhry, M.

20th EAWE PhD Seminar on Wind Energy
24-26 September 2024
Visby, Sweden

Parametric study on the impact of atmospheric inflow characteristics on turbine performance and loads

Jiaxin Liu[a], **Delphine De Tavernier**[a], and **Dominic von Terzi**[a]

[a]Delft University of Technology

E-mail: J.Liu-15@tudelft.nl

Keywords: Synthetic inflow, Turbulence intensity, wind shear, veer

Abstract: Modern wind turbines are upscaling due to the growing demand for higher production and lower cost of renewable energy. The atmospheric inflow characteristics play a critical role in the turbine performance and load assessment as the turbine enlarges. In this study, the turbulence intensity, wind shear and veer will be explored systematically to gain a deeper insight into their impact on turbine performance and aerodynamic loads. Herein arbitrary combinations of the three atmospheric parameters will be made to see the integrated effects on turbine power curves and blade aerodynamic loads. Afterwards, specific combinations will be structured to mimic corresponding realistic atmospheric phenomena. The atmospheric inflows are generated by the analytical inflow model Kaimal, which constructs synthetic inflows with empirical turbulence power spectral density functions. The BEM theory, implemented in OpenFAST, is used to calculate the turbine aerodynamic responses. The turbine performance and loads will be compared with the benchmark under uniform inflows.

1 Introduction

The performance and loads of wind turbines can vary drastically depending on the external atmospheric characteristics and turbine operational parameters. The upscaling of wind turbines has contributed to the increasing complexity of the multi-scale interaction between turbines and the turbulent atmospheric boundary layer (ABL), challenging the accuracy of turbine loading assessment and performance prediction. The lower part of the atmospheric boundary layer is the main regime of wind turbines and wind farms. The turbine performance and loads can be affected by a variety of inflow structures in the ABL triggered by mesoscale weather phenomena, Coriolis force, topography, and atmospheric stability[7]. The upwind region of the wind turbine often shows obvious variations in wind speed, wind direction and turbulence scales. According to realistic turbulent wind measurement, the wind velocity varies in the time and space domains, leading to many complex phenomena such as gravity waves, convective structures, and low-level jets, which can hardly be captured from CFD simulations. These complex phenomena are all coupled with various and instantaneous combinations of shear, TI and veer. The general dynamic process of atmospheric conditions in diurnal cycles and in seasons are coupled with corresponding variations in TI, wind shear and veer profiles. Shear and veer represent the variation in height of the horizontal wind velocity component and the wind direction, respectively, while TI represents the unsteadiness of the wind velocity in time.

Previous studies have highlighted the impact of individual atmospheric inflow factors on the power generation and dynamic loads of wind turbines and wind farms, including wind shear, wind veer, turbulence intensity, air density and atmospheric stability[5, 10, 11, 3]. These efforts aim to strengthen the understanding of how turbines interpret the atmospheric inflow information and transform the kinetic energy in the free-stream into electrical output. This information ultimately helps to assess the energy yield more precisely and thus helps wind energy developers avoid prediction errors in the wind farm production process as much as possible. However, the integrated impact of wind shear, veer and TI on turbine performance and loads has not been fully studied.

The performance and load assessment results of current reference turbine models are accessible in standard technical reports and open-source databases. These results commonly adopt steady-state inflows as benchmarks[2]. The artificial atmospheric inflows can be generated through Reynolds-averaged Navier-Stokes equations (RANS), large-eddy simulation (LES) or analytical inflow models, which are based on isotropic and homogeneous assumptions deviating from realistic atmospheric inflows. Besides, inflow data can also be acquired by wind tunnel experiments and field measurements[7]. These methods have diverse application scenarios under different cost

and fidelity requirements. Due to high efficiency and low cost, the analytical inflow models are widely used for engineering purposes, especially in the early stage of wind turbine design. However, artificial inflows generated by analytical inflow models vastly neglect physical mechanisms in the ABL. It is common practice in both experimental and numerical studies to measure the power generation and dynamic responses within the swept area of the rotor by assuming the vertical wind profile near the hub height is linear and using the wind velocity at the hub height instead of the true disk-averaged wind velocity[10, 6]. However, for large rotor discs, the wind shear, veer and TI change within the swept area of turbines, resulting in suboptimal or superoptimal performance. So far, more and more studies have proven a significant deviation in power curves and load testing from the steady-state baselines when different wind profiles and turbulence intensity levels are applied to the inflow within the rotor disk area. As the wind turbine grows, the effects of turbulent inflow characteristics on the rotor dynamics and power generation will become a non-negligible issue.

2 Research objective

This study investigates the integrated effects of multiple atmospheric characteristic parameters on the IEA 15MW turbine's performance and aerodynamic loads in a systematic manner by making combinations of shear, veer and TI. The analytical inflow model Kaimal (represented in Turbsim) is chosen to generate turbulent inflows. OpenFAST, with its BEM implementation, is chosen to model the turbine responses. The parametric study investigates the impact of shear, veer and TI on turbine power curves and aerodynamic loads.

3 Methodology

3.1 Inflow model

In this study, the atmospheric inflow data is generated by the IEC Kaimal turbulence model, which is implemented in the turbulence simulator Turbsim[4]. The IEC Kaimal model provides the turbulent wind with a set of spectral density functions and assumes neutral stability, where the Richardson number is zero. The turbulence spectrum represents the distribution of the power in turbulent eddies across the frequencies, given in longitudinal, lateral and vertical directions as follows:

$$S_k(f) = \frac{4\sigma_k^2 L_k / v_{hub}}{(1+6fL_k/V_{hub})^{\frac{5}{3}}}$$

where f is the frequency, k is the index of three wind velocity components, $sigma_k$ is the standard deviation of wind velocity components, L_K is the integral length scale parameter, V_{hub} is the wind speed at hub height. Considering the longitudinal direction along the inflow, the turbulence spectrum relies on the IEC 61400-1 standard, where the integral length scale is defined as [1]:

$$L_k = 8.1\Lambda_k$$

$$\Lambda_k = 0.7 \cdot min(60m, HubHt)$$

Three inflow parameters are taken into account in this study. TI can be defined either following IEC 61400-1 standard turbulence classes or by percentage. The wind shear and veer are defined in the User-Defined profiles, which include the changes in wind speed and direction with height.

3.2 Turbine model

The aerodynamic loads and power generation can be calculated by OpenFAST, which is based on BEM theory[8]. OpenFAST couples multiple computational modules to enable aeroelastic simulations for wind turbines. In this study, a variety of output parameters are assessed, including generator power, power coefficient, thrust coefficient, lift and drag force and blade root bending moment.

3.3 Case study

The IEA 15MW reference turbine model with a diameter of 240m is used in this study. According to the measurements across diverse sites and atmospheric conditions summarized by [9], the ranges in which the inflow parameters can realistically vary over worldwide installation sites are assessed, including shear profile exponent,

veer, standard deviations of different directional wind speed component and the integral turbulence length scales. To simplify the coherent impact study of wind shear, veer and TI, the wind shear profiles adopt the power law with the exponent α varying from 0 to 0.3. The wind veer (also known as directional shear) β is set as constant values ranging from -10°to 25°. Turbulence intensity is designed based on the IEC turbulence standard in Category A, B, and C, indicating a range from 12% to 16%, and the mean wind speed at hub height $\overline{V}_{hub}$ ranges from cut-in speed $3m \cdot s^{-1}$ to cut-out speed $25m \cdot s^{-1}$, as shown in Table 1. Arbitrary combinations of shear exponent, veer and TI within the reasonable regimes of the inflow parameters are tested. Afterwards, specific combinations that correspond to the diurnal variation in shear, veer, and TI are designed. Besides, the simulation results under uniform inflow with a default power law shear profile and no veer are provided as benchmarks.

Table 1: Inflow parameter ranges

Inflow parameter	Minimum	Maximum
$\overline{V}_{hub}$ $(m \cdot s^{-1})$	3	25
α (-)	0	0.3
$\beta(^{\circ})$	-10	25
TI (-)	12%	16%

4 Results

4.1 Turbine performance

A study has been conducted to show the effect of TI on the turbine power curve, as in Figure 2. Simulations are run at every wind speed for 10 minutes within the operational range. Currently, the generator power is calculated by averaging the last 5-minute output of each simulation to avoid numerical fluctuation errors. The analysis compares the generator power and power coefficient changes over mean wind speed at the hub height with different combinations of TI. The baseline is the nominated power curve under steady-state inflow. in the turbulent cases, turbulence intensity is defined based on the IEC turbulence standard, indicating the turbulence class 1A, 1B, 1C with TI equal to 16%, 14%, 12%, respectively. The general power curves show obvious deviations from the baseline, with suboptimal power output near the rated wind speed and fluctuations near cut-in wind speed.

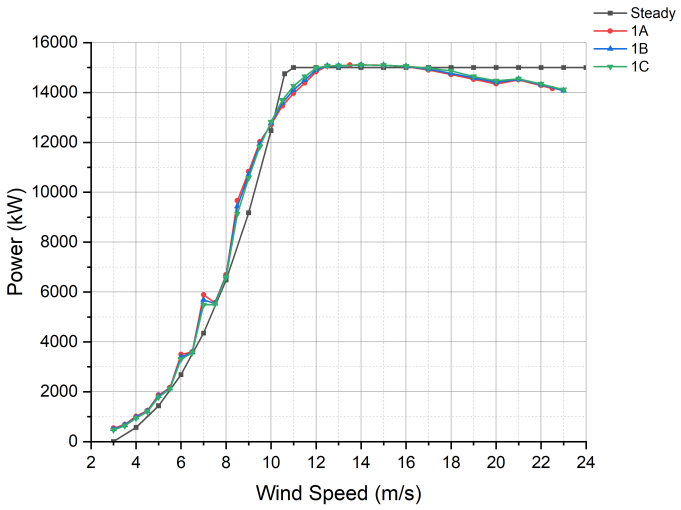

Figure 1: Power curves under different TI levels.

The study will be extended with an analysis of shear, veer, and TI, first independently and then in a coupled manner. The frequency distribution of wind speed, veer and time-resolved power output will also be analysed. The power curves and the power coefficient over the entire wind speed domain will be assessed.

4.2 Turbine loads

Similarly, aerodynamic loads, including lift and drag force, blade root momentum, and thrust coefficient, can be compared and analysed with respect to the above-mentioned combinations of inflow parameters. The loads will be decomposed by power spectra density to assess the fluctuation responses to the turbulent inflows.

5 Conclusions

The preliminary conclusion of this study can be given as follows. TI and shear have the most significant impact on turbine performance and loads. The effect of wind veer is relatively moderate. When the variation levels of the three inflow parameters increase, the power curves will have more differences from the steady-state power curve, especially near the rated wind speed.

Acknowledgements

This work is performed as part of the MERIDIONAL project, funded by the European Union under the Horizon Europe grant no.101084216.

References

[1] L. Dong, W. H. Lio, and E. Simley. On turbulence models and lidar measurements for wind turbine control. *Wind Energy Science Discussions*, 2021:1–16, 2021.

[2] E. Gaertner, J. Rinker, L. Sethuraman, F. Zahle, B. Anderson, G. Barter, N. Abbas, F. Meng, P. Bortolotti, W. Skrzypinski, et al. Iea wind tcp task 37-definition of the iea wind 15-megawatt offshore reference wind turbine-technical report. denver, 2020.

[3] L. Gao, B. Li, and J. Hong. Effect of wind veer on wind turbine power generation. *Physics of Fluids*, 33(1), 2021.

[4] B. Jonkman. Turbsim user's guide v2. 00.00. *Natl. Renew. Energy Lab*, 2014.

[5] D.-Y. Kim, Y.-H. Kim, and B.-S. Kim. Changes in wind turbine power characteristics and annual energy production due to atmospheric stability, turbulence intensity, and wind shear. *Energy*, 214:119051, 2021.

[6] P. Murphy, J. K. Lundquist, and P. Fleming. How wind speed shear and directional veer affect the power production of a megawatt-scale operational wind turbine. *Wind Energy Science Discussions*, 2019:1–46, 2019.

[7] F. Porté-Agel, M. Bastankhah, and S. Shamsoddin. Wind-turbine and wind-farm flows: a review. *Boundary-layer meteorology*, 174(1):1–59, 2020.

[8] J. Rinker, E. Gaertner, F. Zahle, W. Skrzypiński, N. Abbas, H. Bredmose, G. Barter, and K. Dykes. Comparison of loads from hawc2 and openfast for the iea wind 15 mw reference wind turbine. In *Journal of Physics: Conference Series*, volume 1618, page 052052. IOP Publishing, 2020.

[9] A. N. Robertson, K. Shaler, L. Sethuraman, and J. Jonkman. Sensitivity analysis of the effect of wind characteristics and turbine properties on wind turbine loads. *Wind Energy Science*, 4(3):479–513, 2019.

[10] J. Sumner and C. Masson. Influence of atmospheric stability on wind turbine power performance curves. 2006.

[11] M. Talavera and F. Shu. Experimental study of turbulence intensity influence on wind turbine performance and wake recovery in a low-speed wind tunnel. *Renewable Energy*, 109:363–371, 2017.

1.5 Session 311: Wind farm flows and wakes

26.09.2024, 9:0, Room 1

Chair:

Roko Topić

Presenters:

Ebrahimi Majid	Offshore wind farm model validation
Krumbein Sascha	The Underwater Berlin Research Turbine: A Wind Turbine Model for Wake Investigations in a Water Towing Tank
Batista Vasco	Wind farm wake flows under marine conditions

Offshore Wind Farm model validation with mid-fidelity simulator

Majid Ebrahimi [a], Federico Bellini [a], Alessandro Fontanella [b]

a Politecnico of Milano, Department of mechanical engineering

E-mail: majid.ebrahimi@polimi.it

Keywords: Wake model, FAST.Farm, Power, load

1 Introduction

In the European Union's strategic pursuit of renewable energy dominance, wind power emerges as a cornerstone, particularly within the burgeoning offshore sector. As the integration and complexity of wind farms escalate, the fidelity of their modeling becomes paramount for optimizing energy production and ensuring grid stability. This is especially pertinent for offshore installations, where the nuanced understanding of wake effects is crucial for advancing power generation. Our discourse focuses on the validation of offshore wind farm models, a critical phase in ensuring their veracity in real-world applications, encompassing forecasting, control, and strategic decision-making.

2 Objectives

This investigation appraises the precision of a numerical model for offshore wind farms, embedded within the mid-fidelity simulator FAST.Farm. The model's validation is centered on its ability to accurately depict wake dynamics, power generation, and load distributions. The study underscores the significance of wake characteristics in the far wake regions, which profoundly affect the performance and loading of downstream turbines. An assessment of various wake formulations is conducted to ascertain the most precise representation, with a particular focus on vertical and horizontal wake deflection and meandering. The model's efficacy is benchmarked against scholarly literature, concentrating on wake behavior, wind turbine and farm power output, and the resultant loads on turbine towers and blades.

3 Methodology

Employing the FAST.Farm toolbox, we scrutinize a compact array of floating offshore wind turbines (FOWTs) under a spectrum of environmental conditions (see Figure 1). The study utilizes the IEA 15 MW reference semi-submersible model, a design gaining traction in the commercial sector, for validation against academic references. The low-resolution domain, tasked with capturing wake dynamics, is meticulously chosen as 7020 m × 1500 m × 480 m with a spatial resolution of 45m, 20m, and 25m in the X, Y, and Z directions, respectively, and a temporal resolution of 2.5 seconds, in accordance with the FAST.Farm manual [1] and the RAM capacity of our computational cluster. The high-resolution domain, essential for precise load calculations, is set at 280 m × 280 m × 480 m with a uniform spatial resolution of 5 meters and a temporal resolution of 0.25 seconds. This study encompasses a variety of mean wind speeds, turbulence intensities, shear profiles characterized by the power law exponent, and sea states, as delineated in Table 1, to simulate diverse control strategies and environmental conditions.

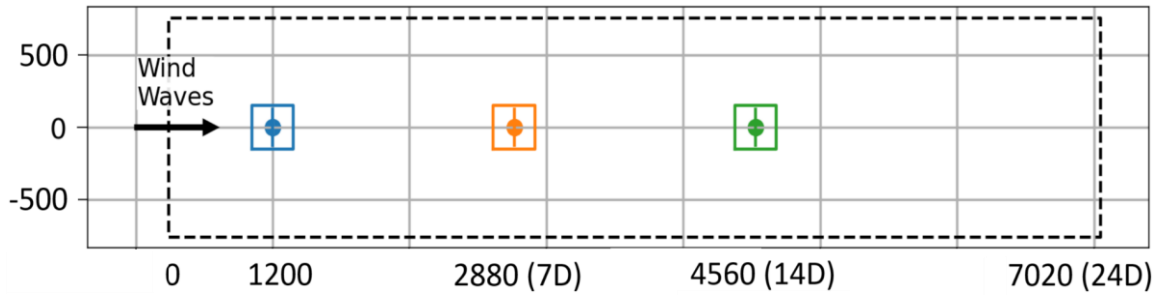

Figure 1: The low- and high-resolution domain considered for the simulations in FAST.Farm, turbines are shown by dots and vertical lines.

Table 1 Environmental conditions considered for model validation.

Parameter	Label	Value
Mean Wind Speed	Below Rated	8 m s^{-1}
	Rated	11.4 m s^{-1}
	Above Rated	18 m s^{-1}
Turbulent Intensity	Low	5%
	Medium	10%
	High	20%
Exponent of shear profile	Low	0.02
	Medium	0.20
	High	0.40
Sea State	Mild	T_p = 8.0 s, H_s= 1.0m
	Medium	T_p = 10.0 s, H_s= 4.0m
	Severe	T_p = 14.0 s, H_s= 8.0m

In our analysis, we meticulously compare the power production, tower-base moments for both floating and fixed turbines across a spectrum of environmental conditions, including varying wind speeds, turbulence intensity levels, shear profiles, and sea states. This comprehensive evaluation extends to both the time and frequency domains for power assessment, complemented by a fatigue load analysis utilizing the Mlife [3] software to compute the short-term damage equivalent load. Our focus on tower base and blade root moments for comparative analysis is conducted under conventional torque and pitch control strategies, providing insights into the operational dynamics of wind turbines under real-world conditions.

FAST.Farm, the simulation tool at the heart of our study, incorporates two distinct wake dynamics formulations: the polar wake and the curled wake. The polar wake formulation posits an axisymmetric wake structure, derived from the principles of momentum and mass conservation. In contrast, the curled wake formulation is engineered to simulate more realistic wake profiles, particularly under yawed or skewed flow conditions. This formulation adeptly captures the asymmetric characteristics of wakes resulting from skewed flow, rotor yaw, and tilt. Our comparative analysis of the polar and curled wake formulations, focusing on generated power and tower base fore-aft moment in the below-rated region, aims to evaluate the productivity of the polar wake formulation and to discern its potential shortcomings. This approach not only enhances our understanding of wake dynamics but also informs the development of more efficient and resilient wind farm designs.

4 Results

This section elucidates the findings pertaining to the wind farm under scrutiny, comprising an ensemble of three IEA 15 MW wind turbines, subjected to a gamut of environmental conditions for both offshore and fixed scenarios. The analysis unfolds with a meticulous examination of power production, tower-base moments, insights into the operational dynamics of these turbines under varying conditions.

4.1 Generator Power

The primary impetus behind our farm analysis is to delve into the impact of wake effects on the power generation of downstream units. Figure 2 elucidates the average power generated by each wind turbine under a variety of conditions. It is evident that floating wind turbines produce less power compared to their fixed counterparts, a phenomenon attributed to the reduction in effective sweep area due to platform motions. Each row in the figure represents an individual wind turbine within the three-unit wind farm array. The colors denote the severity of the sea state, while the shapes indicate the shear of the wind profile. As depicted, there is a discernible decrease in power generation with an increase in shear, a consequence of the reduced average wind speed intercepted by the rotor. In the above-rated region, for low and medium turbulence, there is negligible difference across various shear and sea states. However, under the harshest conditions, the controller struggles to maintain nominal power regulation.

Figure 3 presents the Power Spectral Density (PSD) of the generated power for individual wind turbines (WTs) under conditions of low shear and a Turbulence Intensity (TI) of 5%. The first row focuses on the low-frequency spectrum, capturing the frequency of turbulence, while the second row is dedicated to the wave frequency. In the below-rated region, the amplitude of turbulent frequencies significantly surpasses that of wave frequencies. Conversely, in the above-rated region, the wave frequency associated with severe sea states exhibits higher amplitudes than those observed in turbulent winds.

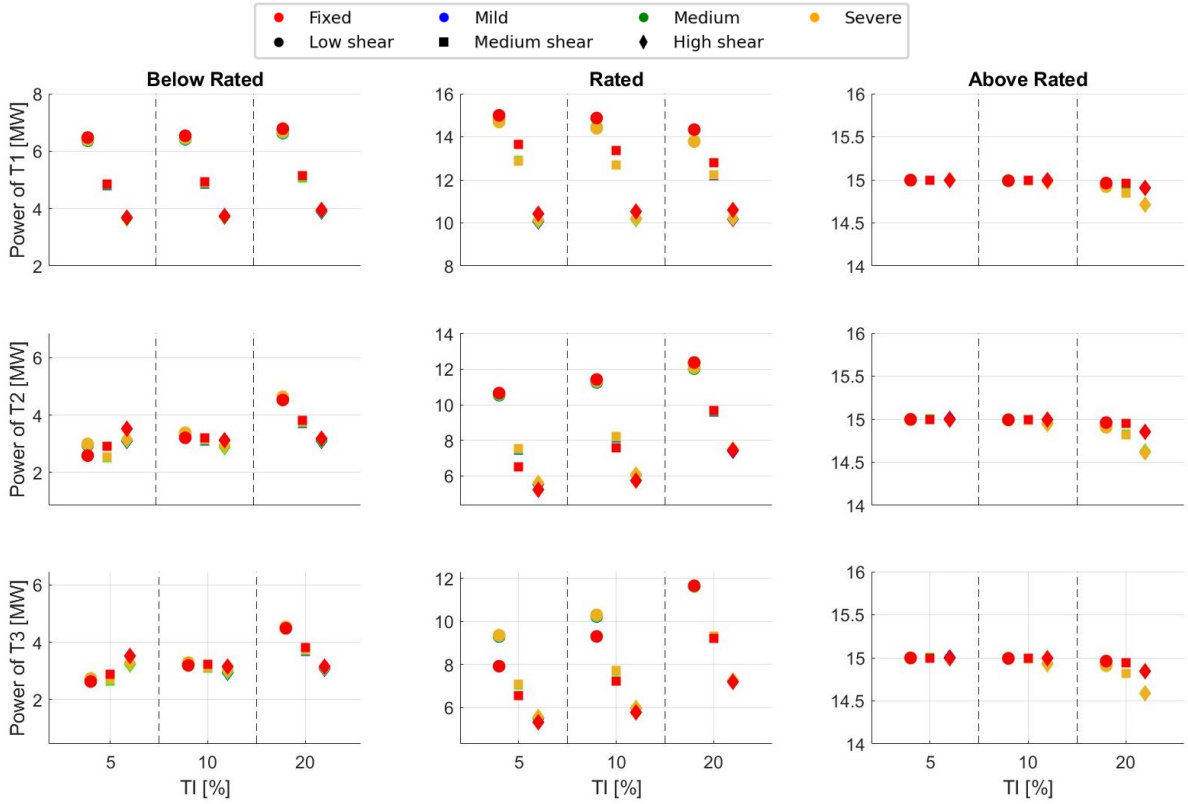

Figure 2: The averaged generated power for individual wind turbines for different environmental conditions.

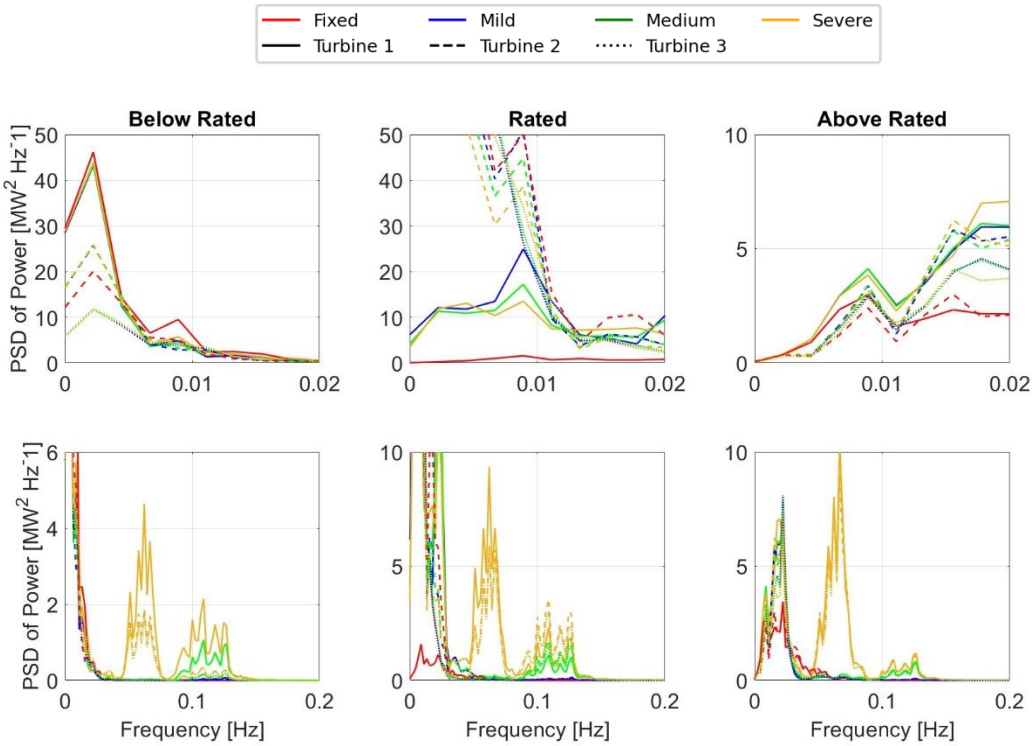

Figure 3: PSD of the generator power of individual WT in an array for low shear and TI= 5%. The first row corresponds to lower frequency to capture the turbulence frequency, and the second row corresponds to the range of frequencies which are excited by wave.

4.2 Fatigue load assessment

Figure 4 delineates the short-term damage equivalent load (DEL) of the tower base fore-aft moment, computed using the Mlife software developed by NREL. This analysis is based on the time series of the tower moment. As evident in the figure, the DEL exhibits an ascending trend with the increase in turbulence intensity, with the highest and lowest values corresponding to the severe sea state and fixed scenarios, respectively. Figure 5 showcases the Power Spectral Density (PSD) of the tower fore-aft moment for cases with a Turbulence Intensity (TI) of 10% and medium shear. The PSD reveals the turbulent frequency at lower frequencies, followed by wave excitations captured in the range of 0.10 to 0.15 Hz. Subsequently, between 0.20 and 0.30 Hz, the 3p frequency is observed for fixed cases, while for offshore cases, this range shifts to between 0.50 and 0.60 Hz.

4.3 Future results

We anticipate that the polar wake formulation will effectively model wake standard deviation in both vertical and horizontal directions but may not accurately represent vertical wake deflection. Conversely, the curled wake model is expected to capture vertical wake deflection and meandering in the far wake. A comparison between polar and curl wake formulation will be conducted in terms of wake characteristic, power, and fatigue loads. Also, Wake shape of this model will be compared to the results generated by lower fidelity simulator, FLORIS for some cases. Another comparison which gives our model more validity is to compare the wake characteristics with Carmo et. al [4] results, since they compared their results to higher fidelity simulations, Large-Eddy Simulations (LES).

5 Conclusion

This research initiative is dedicated to constructing a robust wind farm model that serves as a foundational tool for future academic exploration, encompassing wind farm layout optimization, power output maximization, and load mitigation strategies. The study undertakes a rigorous evaluation of diverse wake calculation formulations, meticulously assessing their accuracy and applicability across a spectrum of parameters. This comprehensive

analysis not only contributes to the refinement of existing models but also paves the way for innovative approaches in wind energy research, ultimately advancing the field towards more efficient and sustainable energy production.

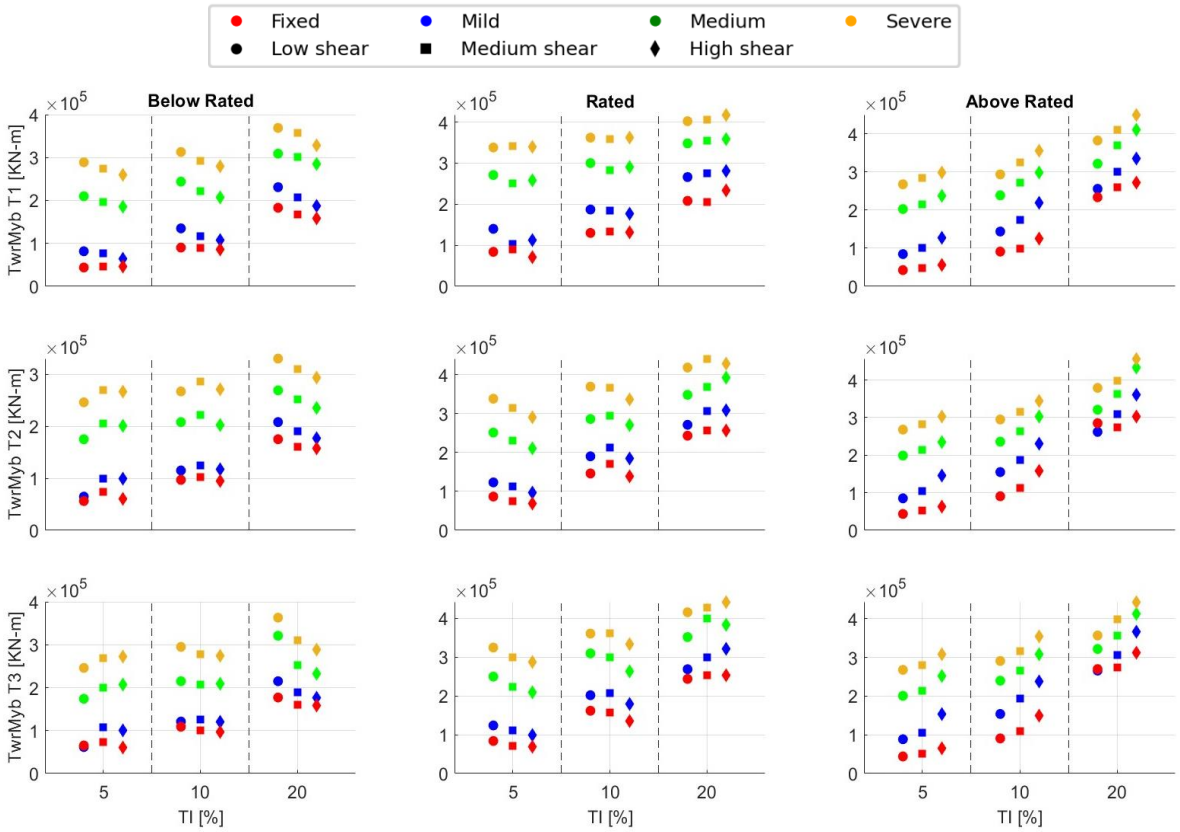

Figure 4: Illustration for DEL tower-base fore-aft moment across all environmental conditions.

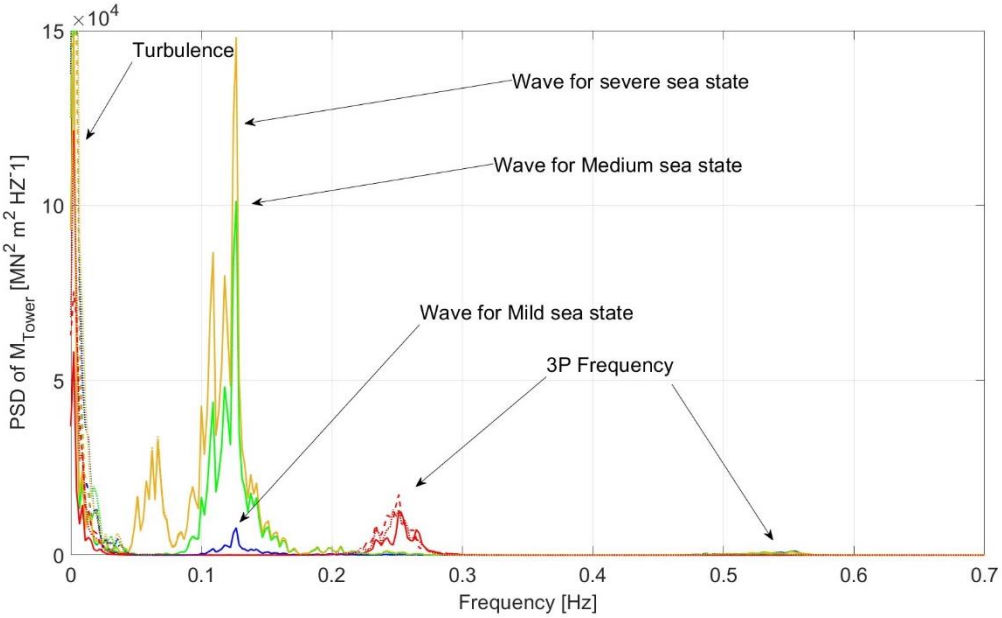

Figure 5: PSD of the fore-aft tower-base moment and the illustration of the frequencies of interest, for the cases with TI= 10% and medium shear.

References

[1] Jonkman, J. M., & Shaler, K. (2021). *Fast. farm user's guide and theory manual*. Golden, CO, USA: National Renewable Energy Laboratory.

[2] Hall, M. (2015). MoorDyn user's guide. *Department of Mechanical Engineering, University of Maine: Orono, ME, USA*, *15*.

[3] Hayman, G. J., & Buhl Jr, M. (2012). Mlife users guide for version 1.00. *National Renewable Energy Laboratory, Golden, CO*, *74*(75), 112.

[4] Carmo, L., Jonkman, J., & Thedin, R. (2024). Investigating the interactions between wakes and floating wind turbines using FAST. Farm. *Wind Energy Science Discussions*, *2024*, 1-32.

The Underwater Berlin Research Turbine: A Wind Turbine Model for Wake Investigations in a Water Towing Tank

Sascha Krumbein[a], Marvin Jentzsch[a], Joseph Saverin[a], and Christian Navid Nayeri[a]

[a]Technische Universität Berlin, Chair of Fluid Dynamics, Müller-Breslau-Straße 8, 10623 Berlin, Germany

E-mail: s.krumbein@tu-berlin.de

Keywords: Wind Turbine Model, Design, Characterization, Simulation

1 Challenge

Water towing tanks allow for wake investigations of horizontal axis wind turbine (HAWT) models at high chordwise Reynolds numbers due to the lower kinematic viscosity of water compared to air [3]. However, the higher density of water induces large loads on the model and its support structure. Assessing the structural loading to dimension HAWT models for towing tank experiments is therefore vital [6]

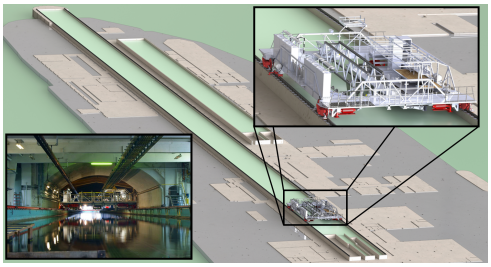

Figure 1: Towing tank and carriage [3].

2 The Underwater Berlin Research Turbine (UBeRT)

The UBeRT is a HAWT with a rotor diameter of 1.3 m. The model is submerged to a depth of 2.5 m inside the 250 m long, 8 m wide, and 5 m deep water towing tank of the Technical University of Berlin. A blockage of 3.3 % is yielded. An underwater stereo particle image velocimetry (uSPIV) system for wake measurements at several downstream positions complements the test setup. The UBeRT enables wake measurements for tip speed ratios (TSRs) between 3 and 10, inflow velocities ranging from 0.5 to 1.75 $\mathrm{m\,s^{-1}}$, and chordwise Reynolds numbers approaching 700 000. [4]
The UBeRT test bed is currently being built and will be commissioned from August until November 2024. In the future, the test rig will be used to develop methods for reducing the near wake length and ultimately accelerating wake recovery of modern HAWTs. To achieve this, various wake control strategies for exciting unstable modes of the tip vortex helix will be investigated. [7, 1, 9, 2]

2.1 Airfoil

The blades of the UBeRT are derived from the SG6040 airfoil. The profile is characterized by a relative thickness of 16 %. For manufacturing reasons, the airfoil sections are gradually thickened, yielding a trailing edge thickness of $0.01c$, where c is the local chord length. [4]

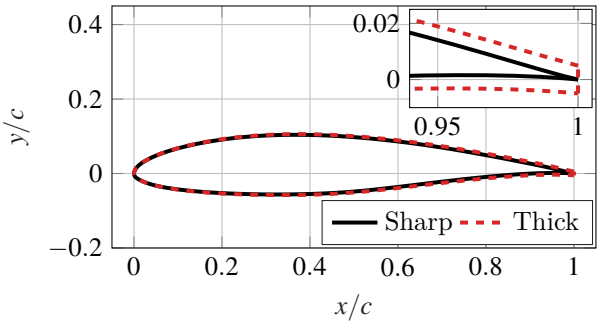

Figure 2: SG6040 airfoil and utilized trailing edge treatment with edge thickness $\Delta = 0.01c$. Chord c.

2.2 Blade

At rated TSR 7, inflow velocity of 1.5 $\mathrm{m\,s^{-1}}$, and rotations per minute (RPM) of 154 $\mathrm{min^{-1}}$, the chordwise Reynolds number at the tip is 400 000.

Comparing the minimum pressure coefficient of the airfoil at a given angle of attack with the local cavitation number allows for considering cavitation during the design process [4]. Up to a chordwise Reynolds number of 700 000, e.g., at inflow velocity $1.75\,\mathrm{m\,s^{-1}}$ and TSR 9, cavitation is not projected to occur. Towards the blade root, two interpolated airfoils are incorporated for smooth geometry transitioning to the circular connection piece with a diameter of 57 mm. The blades have a maximum chord length of 151 mm.

2.3 Tower

The support structure is made from stainless steel tubes with an outer diameter of 219.1 mm and a wall thickness of 8.18 mm. The tower is 5 m long, split into six segments. The whole turbine can be traversed into the streamwise and vertical directions. Several submergence depths can be investigated to quantify the influence of surface waves.

2.4 Instrumentation

The root bending moments on each blade in the flapwise and edgewise directions are measured. The aerodynamic torque of the UBeRT is counteracted by a 7.5 kW planetary gear motor. A frequency converter allows for RPM and torque control. The generated electrical torque is utilized to derive the turbine's power output. An absolute multi-turn encoder measures the RPM. Blade position-dependent uSPIV triggering is enabled. A force gauge measures the thrust and side forces. Water ingress detectors, a temperature sensor, and a triple-axis accelerometer are added for safety and online monitoring.

3 Numerical Considerations

3.1 Model Description

The entire UBeRT test rig is analyzed in the wind turbine simulation suite QBlade using aeroelastic blade-element-momentum and lifting-line-free-vortex-wake simulations [5]. The aerodynamics of the rotor are represented by 2D polars and chord and twist distributions. The structural properties of the blade, the nacelle, and the tower are modeled using Euler-Bernoulli beam elements, based on tabulated cross-sectional data. Hydrodynamic properties such as buoyancy or added-mass are omitted.

3.2 Rotor Characteristics

The power coefficient reaches 43 % at TSR 6. This represents an energy extraction comparable to modern multi-megawatt HAWTs. The thrust coefficient approaches 83 % at TSR 9. For an inflow velocity of $2\,\mathrm{m\,s^{-1}}$, this results in the generation of a design driving thrust of 2200 N.

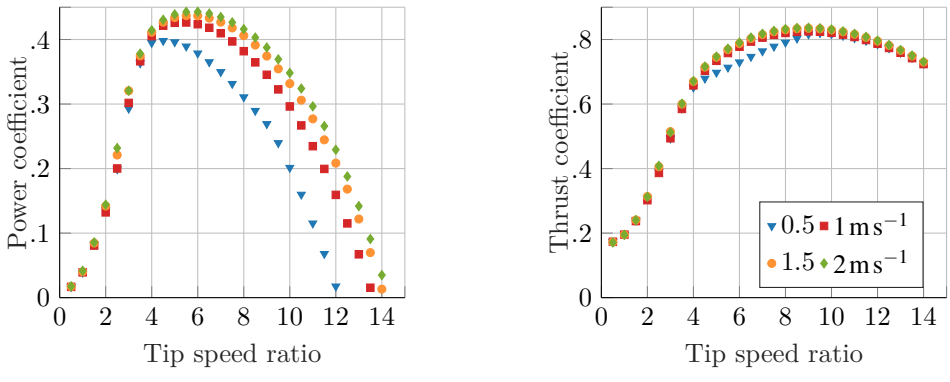

(a) (b)

Figure 3: a) Power and b) Thrust coefficients for various undisturbed inflow velocities, derived in QBlade.

3.3 Modal Properties

QBlade's modal analysis tool reveals several structural modes. The lowest corresponding frequencies are identified as follows: at 6.6 Hz as tower fore-aft mode, at 67.8 Hz as asymmetric flapwise rotor mode, and at 86.3 Hz as combined mode. [5]

4 Test Rig Impressions

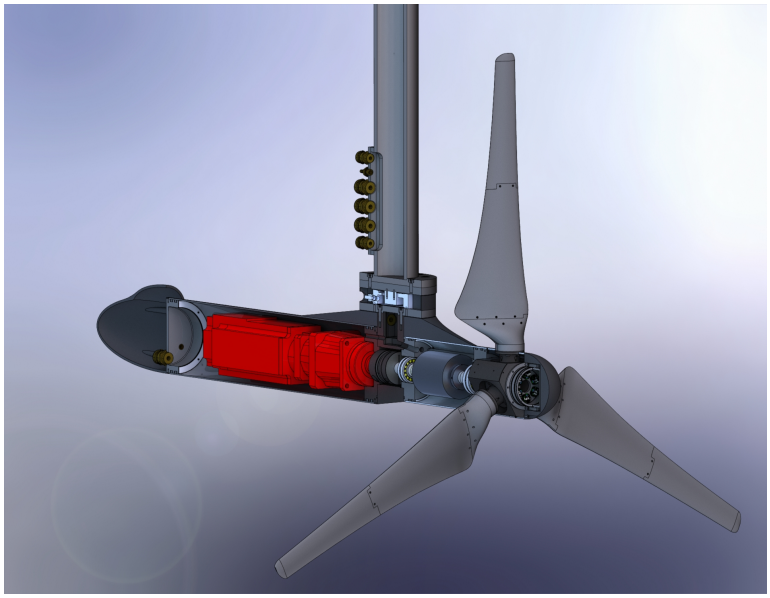

(a)

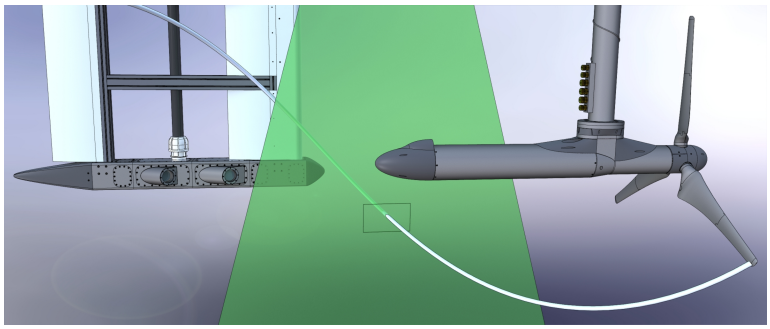

(b)

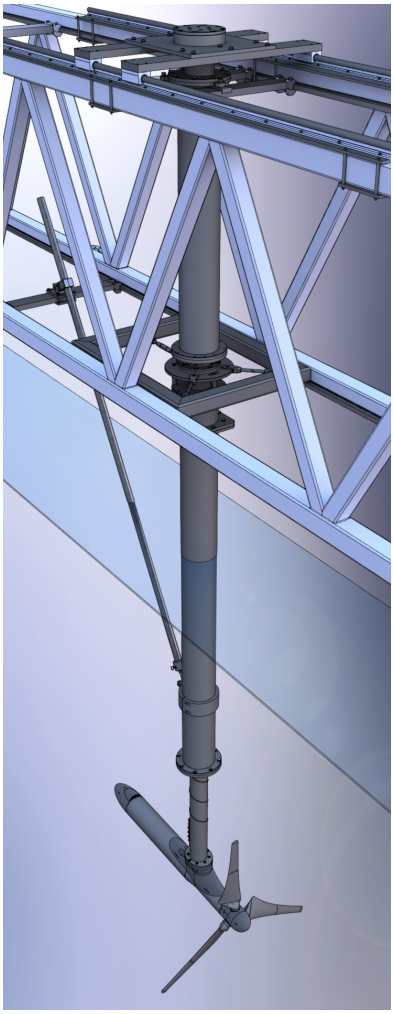

(c)

Figure 4: UBeRT turbine, uSPIV, and test rig. a) UBeRT turbine: Servo motor with planetary gear, rotor brake, and absolute multi-turn encoder for measuring the motor speed and the blade positions. Three-component force gauge for measuring thrust and side forces. Metal bellows coupling. Floating shaft bearing. Slip ring. Fixed shaft bearing. Strain gauge amplifiers for conditioning the blade root bending moment signals. b) Turbine and uSPIV system: Schematic tip vortex. Field of view. uSPIV: Two 14 bit charge-coupled device cameras, 1392 by 1040 pixels (width by height). Max. frame rate 5 Hz. Laser sheet emanating from top. c) UBeRT test rig: Truss system is attached to tow carriage (not displayed). Refer to Figure 1 for overall view. Fixed tower bearing with streamwise brake. Linear traverse for streamwise positioning. Floating tower bearing with streamwise and rotational brake. Large tower member. Small tower member with Scruton strakes. Exemplary stiffening rod. Free water surface.

Acknowledgements

We would like to thank Gregory Payne for providing us with detailed information on his underwater research turbine. His publication on the design of a tidal turbine model proofed abundantly helpful throughout the design process [8]. The UBeRT test rig is funded by the Deutsche Forschungsgemeinschaft as part of project 469304061 "Dynamik und Destabilisierung von helikalen Wirbeln".

References

[1] A. Abraham and T. Leweke. Experimental investigation of blade tip vortex behavior in the wake of asymmetric rotors. Springer Nature, Jan. 2023.

[2] K. Brown, D. Houck, D. Maniaci, C. Westergaard, and C. Kelley. Accelerated Wind-Turbine Wake Recovery Through Actuation of the Tip-Vortex Instability. AIAA Journal, 60(5):3298–3310, Jan. 2022.

[3] M. Jentzsch, H.-J. Schmidt, R. Woszidlo, C. N. Nayeri, and C. O. Paschereit. Challenges and procedures for experiments with steady and unsteady model velocities in a water towing tank. Experiments in Fluids, 62(4):1–20, Jan. 2021. Publisher: Springer; Springer Berlin Heidelberg.

[4] S. Krumbein. Design of a horizontal axis wind turbine for experimental investigation in a large water towing tank. PhD thesis, Technische Universität Berlin, Berlin, Jan. 2023.

[5] S. Krumbein. Numerical Modeling of the Underwater Berlin Research Turbine in a Towing Tank. PhD thesis, Technische Universität Berlin, Berlin, Jan. 2023.

[6] S. Krumbein, M. Jentzsch, J. Saverin, C. N. Nayeri, and C. O. Paschereit. The Underwater Berlin Research Turbine: A Wind Turbine Model for Wake Investigations in a Water Towing Tank. Journal of Physics: Conference Series, Jan. 2024.

[7] T. Leweke, H. U. Quaranta, H. Bolnot, F. J. Blanco-Rodríguez, and S. Le Dizès. Long- and short-wave instabilities in helical vortices. Journal of Physics: Conference Series, 524:012154, Jan. 2014.

[8] G. S. Payne, T. Stallard, and R. Martinez. Design and manufacture of a bed supported tidal turbine model for blade and shaft load measurement in turbulent flow and waves. Renewable Energy, 107:312–326, Jan. 2017.

[9] D. Schröder, T. Leweke, and E. Stumpf. High-speed volumetric particle tracking measurements of unstable helical vortex pairs. Experiments in Fluids, 64(8), Jan. 2023.

20th EAWE PhD Seminar on Wind Energy
24-26 September 2024
Visby, Sweden

Wind farm wake flows under marine conditions

Vasco T. P. Batista[a,b]

[a]Natural Power SARL, 1, Boulevard Salvador Allende, 44100 Nantes, France
[b]Faculty of Engineering of the University of Porto (FEUP), Mechanical Engineering Department, Rua Dr Roberto Frias s/n, 4200-465 Porto, Portugal

E-mail: vtpb@fe.up.pt

Keywords: wind turbine wake, offshore, wind farm, model chain

1 Introduction

The REPowerEU and "Fit for 55" directives have set significant goals for renewable energy production in the European Union, with wind energy expected to be a major contributor. To reach the stipulated targets, atmospheric flow modelling—particularly for site assessment—is one part of the design process requiring further improvements, and the main challenges are summarised in the recent review by Veers et al. [16].

As part of the Atmospheric Physics and Turbulence for Wind Energy (AptWind) project, this work aims to improve upon the modelling of wind farm wake flows in marine environments using the VENTOS® CFD codes [1, 12, 10]. Typically employed for flows over complex [8] and forested terrain [6, 17, 13], the codes have also been used in a model chain approach [10] with the Weather Research and Forecasting model (WRF) [14], successfully capturing observed intricate flow patterns in the form of lee-waves and low-level jets [7].

2 Objectives

Three major objectives can be outlined. The first is understanding the capabilities of VENTOS® in representing offshore wind phenomena impacting wind turbines and farms, initially by modelling idealised atmospheric conditions (e.g., conventionally neutral and stable boundary layers), which pose their own set of challenges [4, 5]. However, the wide range of length-scales in the atmospheric boundary layer (ABL) signals that both large-scale behaviour and local (micro-scale) phenomena must be captured, and coupling remains the most viable solution [4]. Further adaptation of the current approach [10] for offshore and coastal environments is the second step and will bring added complexity throughout the model chain [11, 2]. Thirdly, since accurate capture of intra- and inter-wind-farm flow effects on wakes and turbine performance [9] is of primary interest, the implemented wake model [3] will be expanded upon and compared against currently employed techniques [9]. Large-eddy simulation [12], SCADA [15] or experimental datasets will be considered for validation.

3 Final remarks

In line with current environmental targets, this research work aims to provide commercially-viable solutions for offshore flow and wake modelling, capturing the wide range of scales and complex phenomena in the ABL. This will allow for improved planning of wind farm placement and better forecasts of expected wind energy availability on the day-to-day market, which could translate to a reduction of energy for consumers on the European electricity market.

Acknowledgements

This research is within the scope of the Atmospheric Physics and Turbulence for Wind Energy (AptWind) project (ID 101119550), granted under the Horizon Europe MSCA programme (Call: HORIZON-MSCA-2022-DN-01).

References

[1] F. A. Castro, J. M. L. M. Palma, and A. Silva Lopes. Simulation of the Askervein Flow. Part 1: Reynolds Averaged Navier–Stokes Equations (k-epsilon Turbulence Model). *Boundary-Layer Meteorol*, 107(3):501–530, June 2003.

[2] I. L. Coimbra and J. M. L. M. Palma. Challenges in simulating the wind over a coastal complex-shaped site: Madeira Island. *J. Phys.: Conf. Ser.*, 2767(5):052014, June 2024.

[3] V. Costa Gomes. *Modelling of Wind Turbine Wakes through an Actuator Disk*. PhD thesis, University of Porto, Portugal, 2019.

[4] S. E. Haupt, B. Kosović, L. K. Berg, C. M. Kaul, M. Churchfield, J. Mirocha, D. Allaerts, T. Brummet, S. Davis, A. DeCastro, S. Dettling, C. Draxl, D. J. Gagne, P. Hawbecker, P. Jha, T. Juliano, W. Lassman, E. Quon, R. K. Rai, M. Robinson, W. Shaw, and R. Thedin. Lessons learned in coupling atmospheric models across scales for onshore and offshore wind energy. *Wind Energ. Sci.*, 8(8):1251–1275, Aug. 2023.

[5] M. A. Khan, S. J. Watson, D. J. N. Allaerts, and M. Churchfield. Recommendations on setup in simulating atmospheric gravity waves under conventionally neutral boundary layer conditions. *J. Phys.: Conf. Ser.*, 2767(9):092042, June 2024.

[6] J. R. Monteiro, V. T. P. Batista, and J. M. L. M. Palma. Assessing canopy models across forest edges on flat terrain. *J. Phys.: Conf. Ser.*, 2767(9):092011, June 2024.

[7] J. Palma, A. Silva Lopes, V. Costa Gomes, C. Veiga Rodrigues, R. Menke, N. Vasiljević, and J. Mann. Unravelling the wind flow over highly complex regions through computational modeling and two-dimensional lidar scanning. *J. Phys.: Conf. Ser.*, 1222:012006, May 2019.

[8] J. M. L. M. Palma, C. A. M. Silva, V. C. Gomes, A. Silva Lopes, T. Simões, P. Costa, and V. T. P. Batista. The digital terrain model in the computational modelling of the flow over the Perdigão site: The appropriate grid size. *Wind Energ. Sci.*, 5(4):1469–1485, Nov. 2020.

[9] F. Porté-Agel, M. Bastankhah, and S. Shamsoddin. Wind-Turbine and Wind-Farm Flows: A Review. *Boundary-Layer Meteorol*, 174(1):1–59, Jan. 2020.

[10] C. V. Rodrigues, J. M. L. M. Palma, and Á. H. Rodrigues. Atmospheric Flow over a Mountainous Region by a One-Way Coupled Approach Based on Reynolds-Averaged Turbulence Modelling. *Boundary-Layer Meteorol*, 159(2):407–437, May 2016.

[11] W. J. Shaw, L. K. Berg, M. Debnath, G. Deskos, C. Draxl, V. P. Ghate, C. B. Hasager, R. Kotamarthi, J. D. Mirocha, P. Muradyan, W. J. Pringle, D. D. Turner, and J. M. Wilczak. Scientific challenges to characterizing the wind resource in the marine atmospheric boundary layer. *Wind Energ. Sci.*, 7(6):2307–2334, Nov. 2022.

[12] A. Silva Lopes, J. Palma, and F. Castro. Simulation of the Askervein flow. Part 2: Large-eddy simulations. *Boundary-Layer Meteorol*, 125(1):85–108, Oct. 2007.

[13] A. Silva Lopes, J. Palma, and J. V. Lopes. Improving a two-equation turbulence model for canopy flows using large-eddy simulation. *Boundary-Layer Meteorol*, 149(2):231–257, Nov. 2013.

[14] W. Skamarock, J. Klemp, J. Dudhia, D. Gill, D. Barker, W. Wang, X.-Y. Huang, and M. Duda. A Description of the Advanced Research WRF Version 3. Technical report, UCAR/NCAR, June 2008.

[15] D. van Binsbergen, P.-J. Daems, T. Verstraeten, A. R. Nejad, and J. Helsen. Hyperparameter tuning framework for calibrating analytical wake models using SCADA data of an offshore wind farm. *Wind Energ. Sci.*, 9(7):1507–1526, July 2024.

[16] P. Veers, C. L. Bottasso, L. Manuel, J. Naughton, L. Pao, J. Paquette, A. Robertson, M. Robinson, S. Ananthan, T. Barlas, A. Bianchini, H. Bredmose, S. G. Horcas, J. Keller, H. A. Madsen, J. Manwell, P. Moriarty, S. Nolet, and J. Rinker. Grand challenges in the design, manufacture, and operation of future wind turbine systems. *Wind Energ. Sci.*, 8(7):1071–1131, July 2023.

[17] J. M. Viana Parente Lopes, J. M. L. M. Palma, and A. Silva Lopes. Modelling the flow within forests: The canopy-related terms in the Reynolds-averaged formulation. *J. Fluid Mech.*, 910, Jan. 2021.

TOPIC 2

Wind resources, turbulence and acoustics

2.1 Session 112: Wind resources, turbulence, and acoustics

24.09.2024, 10:30, Room 2

Chair:

Roko Topić

Presenters:

Borowski Johanna	Predicting future wind speeds based on climate model data and MCP methods
Afanasieva Nadiia	LES Reduction for Lidar-Assisted Wind Field Reconstruction
Patel Ansh	Lidar measurements of turbulence characteristics for large wind turbines
Pogumirskis Maksims	Quantifying biases in the wind forecasted by WRF with wind measurements in the Baltics
Sagredo Esperanza	Wind-field characterization using lidar measurements and proper orthogonal decomposition

Predicting future wind speeds based on climate model data and MCP methods

Johanna Borowski[a,b], Sandra Schwegmann[a], Kerstin Avila[bc], Martin Dörenkämper[a]

[a] Fraunhofer IWES, Fraunhofer Institute for Wind Energy Systems IWES
[b] Carl von Ossietzky Universität Oldenburg, School of Mathematics and Science, Institute of Physics
[c] ForWind - Center for Wind Energy Research, Küpkersweg 70, 26129 Oldenburg, Germany

E-mail: Johanna.Borowski@iwes.fraunhofer.de

Keywords: wind energy site assessment, wind climate, climate change, CMIP6, uncertainty, long-term referencing, Measure-Correlate-Predict (MCP)

Precise knowledge of the wind climate at a target site is crucial for estimating the wind potential not only in the planning phase of wind farms, but also during the wind farm projects lifetime of 20 years and more. For this purpose, measurement campaigns are carried out typically covering a full yearly cycle which are then extended with a wind time series based on numerical data (long-term data) covering at least 10 years, in order to investigate a representative period. This is typically done by linking the short-term and long-term data by statistical methods based on the overlapping time period of both data sets, commonly known as Measure-Correlate-Predict (MCP) methods. In current site assessment industry standards (e.g., the German Technical Guideline (TR6) for Wind Turbines) a wind climate persistence is assumed.

In view of climate change, however, it is questionable whether projecting wind speed into the future solely based on historical data is still a reliable assumption. Therefore, this study shows how climate projections and advanced MCP methods can be used to obtain a more representative view on future wind speed. A consistent methodology from short-term over long-term to future climate projection is presented.

Our analysis focuses on several sites in Europe with long-term measurements in varying terrain complexity from simple over heterogeneous to (very) complex terrain. The historical wind climate was predicted based on measurement and ERA5– reanalysis data. To predict the future wind climate, an ensemble of several CMIP6 model data provide additional long-term data in the MCP-method. Based on the resulting ensemble of future predictions an uncertainty estimation for the future wind climate is obtained.

The results indicate that implementing climate model data into the process of determining the future wind resource is promising. In the historical overlap period, the predicted wind speeds based on climate model data reasonably agree with the measurement data and the historical prediction based on classical reanalysis data. This emphasizes that using the MCP method to correct climate model data to a target site, is a great benefit in wind energy site assessment. Analyzing the near future (2041 – 2070) and far future (2071 – 2100) wind speed predictions reveal seasonal changes. The results from the analysis of the corrected climate model data indicate a consistent decrease in wind speed in summer months for both near and far future, however, the spread is relatively wide. In winter months the climate model data show no clear tendency.
This study highlights the significance of climate projections in assessing future wind speeds at specific locations. By incorporating climate model data into the MCP method, more precise predictions of the future wind climate

can be generated, enabling the analysis of seasonal variations. These findings offer valuable insights for evaluating wind energy site suitability and facilitate the incorporation of climate-related changes and uncertainties into long-term planning.

Acknowledgements

The results presented were derived in the framework of the KliWiSt (grant no. 03EE3041A) project. The KliWiSt project is funded by the German Federal Ministry for Economic Affairs and Climate Action (Bundesministerium für Wirtschaft und Klimaschutz– BMWK) due to a decision of the German Bundestag. We thank the ECMWF for providing the ERA5 reanalysis data and making them freely accessible. We further thank the World Climate Research Program, which coordinated and sponsored CMIP6 through its coupled modeling working group, and the climate modeling groups for producing and making available their model results.

20th EAWE PhD Seminar on Wind Energy
24-26 September 2024
Visby, Sweden

LES Reduction for Lidar-Assisted Wind Field Reconstruction

Nadiia Afanasieva[a] and **David Schlipf**[a]

[a]Wind Energy Technology Institute, Flensburg University of Applied Sciences

E-mail: nadezhda.a.afanasieva@gmail.com

Keywords: Wind Field Reconstruction, Incompressible Navier Stokes Equations, Large Eddy Simulation, Lidar

1 Introduction

Wind lidar, though still needing pre- and post-verification, has already been used for wind measurement companies for more than a decade, with successful applications in industry and research. For years, researchers have been motivated by the success of this technology to use it for data-based wind field reconstruction (WFR) and lidar-assisted prediction of wind field mechanics.

Engineering approaches to WFR under the assumption of linear wind dynamics have already been successfully applied in field studies [2]. However, in order to extend the benefits of lidar-assisted WFR to conditions where the assumption of linear wind dynamics is not valid, advanced methods need to be developed.

Atmospheric flows with high Reynolds number require accounting for nonlinearities that are difficult to capture with linear, data-driven approaches, while first-principle approaches are computationally slow for real-time wind field prediction.

On the other hand, the spatial sparsity of lidar measurements constrains the application of sophisticated CFD models. Lidar systems allow the construction of different scan configurations so that a field of points can be measured at one or multiple distances at a time. However, there is always a trade-off that limits the temporal and spatial measurement discretization.

This study focuses on developing a closure model for the nonlinear dynamics in the wind field, which is constrained by the spatial sparsity of lidar measurements and the requirement of real-time computational speed.

2 Methodology

The method formulated in this study was inspired by the study reported in [3]. The authors reduced the incompressible Navier Stokes equations (NSEs) in polar coordinates to 2D nonlinear convection and applied factorized interpolation at boundaries and projection at the axial points.

To ensure that the first-principle physics of the wind flow is preserved, we do not reduce the number of terms in the incompressible NSEs. Instead, we introduce simplification and optimization concepts in the numerical scheme. For the discretization, we use a staggered grid, in Cartesian coordinates.

We are implementing the model in MATLAB in a vectorized form. To achieve real-time capability, the solver's basis is developed in 2D.

3 Results and Outlook

The simulation results for different degrees of spatial resolution show that the calculation at a resolution of 10x10 is about four times faster than the real simulation time (Table 1). At the same time, the accuracy of the estimated position of the gust and the velocity profile formed by the gust due to the non-linear propagation is compromised. The zone of low wind speed behind the maximum wind speed area develops with a delay at the lowest resolution while the position of the gust is overestimated. The resolution of 40x40 yields a much better estimate of the wind field, while the calculation reaches the limit of non-real-time. Using a resolution of 20x20 is, therefore, the compromise.

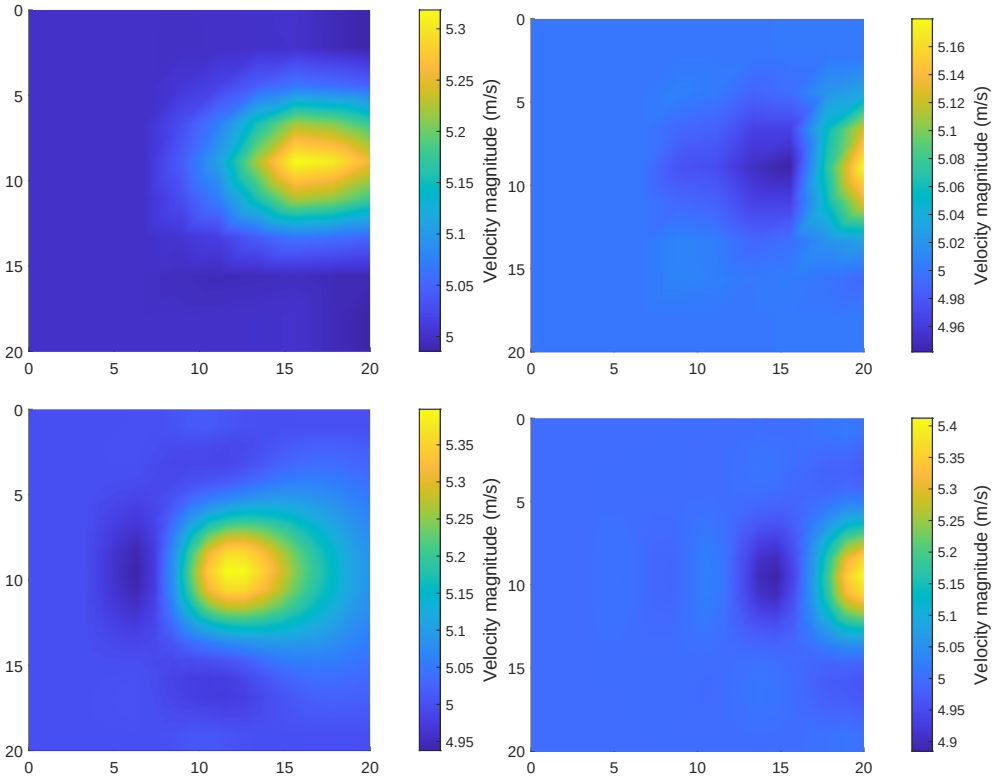

Figure 1: Simulation results with a resolution of 10x10 (top) and 20x20 (bottom) during the simulation (left) and at the last time step (right) (domain: 20x20 m; simulation time = 4,5 s; wind speed = 5 m/s; ρ =1,00 kg/m^3; μ =0,0010 kg/(m · s); flow disturbance: Gaussian gust)

Table 1: Calculation speed versus spatial resolution

Resolution [number of cells]	Calculation speed normalized by simulation time
10x10	0.265
20x20	0.515
25x25	0.704
40x40	1.388

In the current phase, the results of implementing the conceptualized reduction for the numerical approximation of NSEs showed the approach's general capability to be applied as a non-linear solver in data-based wind models. However, the stability of the model under constrained spatial resolution and computation speed needs further optimization.

The following steps involve conducting additional test cases, focusing on further numerical scheme stabilization. The model will then be validated against benchmark LES simulation data, and tested with actual wind lidar data been applied at the boundaries. After being validated, the solver is assumed to be implemented in the Kalman filter-based wind field prediction model [1], which is part of the lidar-assisted model-predictive control set-up being developed in the ABBA-project.

Acknowledgements

This study is part of the ABBA project, funded by the Federal Ministry for Economic Affairs and Climate Action.

ABBA: Adaptive Betriebsstrategien für bestehende Windenergieanlagen / Adaptive Operating Strategies for existing Wind Turbines (FKZ 03EE3068A).

References

[1] N. Afanasieva and D. Schlipf. Improving the quality of wind field reconstruction techniques for lidar-assisted control of wind turbines. In *19th EAWE PhD seminar, Hannover (Germany)*. EAWE, Jun. 2023.

[2] D. Schlipf. *Lidar-Assisted Control Concepts for Wind Turbines*. PhD thesis, University of Stuttgart, 2015.

[3] P. Towers and B. L. Jones. Real-time wind field reconstruction from lidar measurements using a dynamic wind model and state estimation. *Wind Energy*, 19(1):133–150, 2016.

20th EAWE PhD Seminar on Wind Energy
24-26 September 2024
Visby, Sweden

Lidar measurements of turbulence characteristics for large wind turbines

Ansh Patel[a], **Jakob Mann**[a], **Mikael Sjöholm**[a], **Gunhild Rolighed Thorsen**[a], **Elliot Simon**[a], **Lin-Ya Hung**[b], and **Julia Gottschall**[b]

[a]Technical University of Denmark, DTU Wind, Roskilde, Denmark
[b]Fraunhofer Institute for Wind Energy Systems IWES, Bremerhaven, Germany

E-mail: patel@dtu.dk

Keywords: Turbulence, Doppler lidar, Spectra, Coherence, Gusts

1 Introduction

Over the last three decades, wind turbines have undergone a monumental increase in size [7]. Driven by strong economic forces, it is excepted that the growth in rotor diameter and hub height will continue over the coming years [11]. But a number of challenges must be addressed before taller wind turbines can bring about the expected reduction in cost of energy [15]. For example, new models for atmospheric turbulence, more advanced control strategies or a revision in the design process may be required.

The reassessment of inflow conditions is particularly important because wind turbines of the future will operate in a region of the atmosphere of which our knowledge is currently limited, which requires extensive measurements are necessary [14]. The International Energy Commission (IEC) standards for design and certification of wind turbines [1] suggest models for inflow conditions based on measurements from relatively short meteorological masts which are subsequently used as inputs in aero-elastic simulations of structural loads. Hence, it is possible that there may be a significant difference between the simulated and actual structural loads experienced by larger wind turbines [6, 10]. This uncertainty is typically addressed by using large safety factors on the turbine components which results in non-optimal material and energy [15]. Thus, in order to ensure the cost-effectiveness of wind energy in the future, inflow conditions used in wind turbine design must be reassessed.

Some of the parameters of interest when characterizing turbulence are the power spectra and spectral coherence. They are especially relevant in wind energy as they affect the loads and response of a turbine [12]. Consequently, a few measurement campaigns have been carried out using either meteorological masts [4, 5] or lidars [3, 2] at heights relevant for wind turbines. Cheynet *et al.* [4, 5] used data from the FINO 1 met-mast to characterize the spectra and spectral coherence under varying atmospheric stability conditions and compared them with commonly used turbulence models [1]. It was found that the spectral properties of atmospheric turbulence are well described by the IEC turbulence models at high frequencies and under neutral stability. But, the measurement height was limited to 81m and coherence was measured in the vertical direction only. Thus, in the COTUR experiment [3], lidars were used to obtain measurements at heights 100m above sea-level (a.s.l.). This was a novel experiment but the results were limited by the high uncertainty in the pointing directions of the lidar beams. In the Hywind experiment [2], nacelle-based lidars were used to measure coherence in the lateral direction at a height of up to 150m. Despite measuring the coherence for a range of lateral separations, the direction was limited to the direction of the diverging beams and consequently, the true along-wind and cross-wind components were not measured.

Thus, there remains a necessity for characterizing spectral properties of atmospheric turbulence at heights greater than or equal to 150 meters.

2 Research questions

The following research questions will be addressed as part of the PhD:

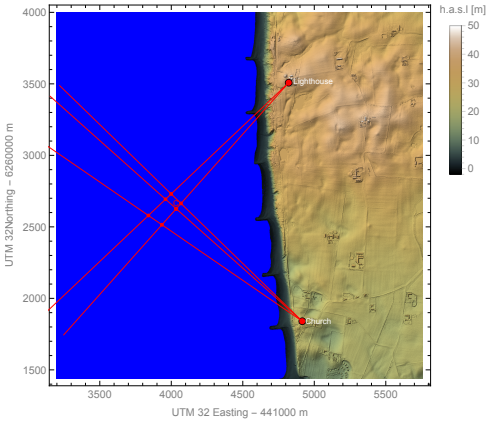

Figure 1: Lidar beams crossing off the coast

1. How well do the Kaimal [8], Mann [9] and Syed *et al.* [13] turbulence models predict the spectra and spectral coherence of the along-wind and cross-wind components for a range of lateral directions and at heights greater than 150 meters?
2. How does atmospheric stability affect the spectra and coherence at these heights? Does it lead to more or less deviations from the aforementioned models?
3. Do wind boxes generated using Large Eddy Simulation (LES) of atmospheric flow compare well with measurements?

3 Methodology

The above research questions will be addressed using concurrent measurements with five pulsed coherent Doppler lidars crossing at six points over the North Sea. The experiment took place on the west coast of Denmark, starting late January 2024 and ended by the end of May 2024. For the data analysed in the paper, the elevation angle was around 5° making the beams cross at 150 m above the mean sea height or slightly higher. Moreover, we used real-time kinematic positioning (RTK) based GPS technique together with drones to lower the uncertainty of the beam directions. Figure 1 shows the lidar beams crossing approximately 2kms from the shore. In absence of direct temperature measurements, the atmospheric stability condition will be deduced from reanalysis data. Lastly, readily available LES data will be used for question 3.

4 Preliminary results

For the results presented in this section, we used a simplified data filtering procedure wherein we divided the time series from the five lidars into 10-min periods and calculated the standard deviation of the line-of-sight or radial velocity (σ_{v_r}). As a crude filtering mechanism, all 10-min periods in which σ_{v_r} was greater than 3m/s were discarded. Subsequently, we reconstructed the horizontal wind components, u_{EW} and v_{NS}, at the crossing points of the lidars while assuming the vertical component to be zero. This was done using the standard approach for a dual lidar system:

$$\underbrace{\begin{bmatrix} v_{r_1} \\ v_{r_2} \end{bmatrix}}_{\mathbf{vr}} = \underbrace{\begin{bmatrix} \cos\theta_1 \cos\phi_1 & \sin\theta_1 \cos\phi_1 \\ \cos\theta_2 \cos\phi_2 & \sin\theta_2 \cos\phi_2 \end{bmatrix}}_{\mathbf{M}} \underbrace{\begin{bmatrix} u_{EW} \\ v_{NS} \end{bmatrix}}_{\mathbf{v}}, \tag{1}$$

and thus

$$\mathbf{v} = \mathbf{M}^{-1}\mathbf{vr}, \tag{2}$$

where the subscripts 1 and 2 refer to the lidars at church and lighthouse respectively. ϕ is the elevation angle of the beam and θ is the azimuth angle.

The along-wind component (u) and the cross-wind component (v) are obtained by rotating u_{EW} and v_{NS} into the mean wind direction over a time period of 1 hour. The data were further filtered to ensure that mean wind

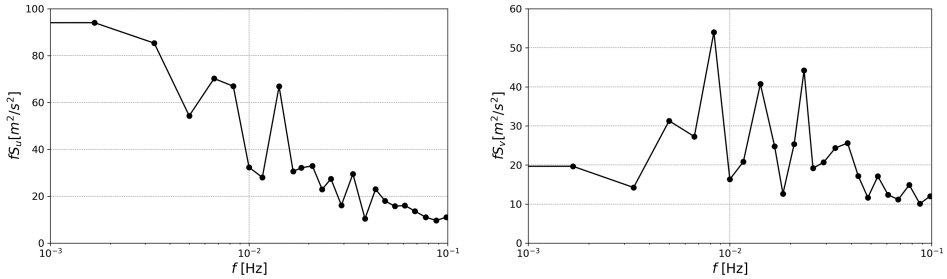

Figure 2: The spectrum of the along-wind component (left) and cross-wind component (right) as computed at one of the lidar crossings.

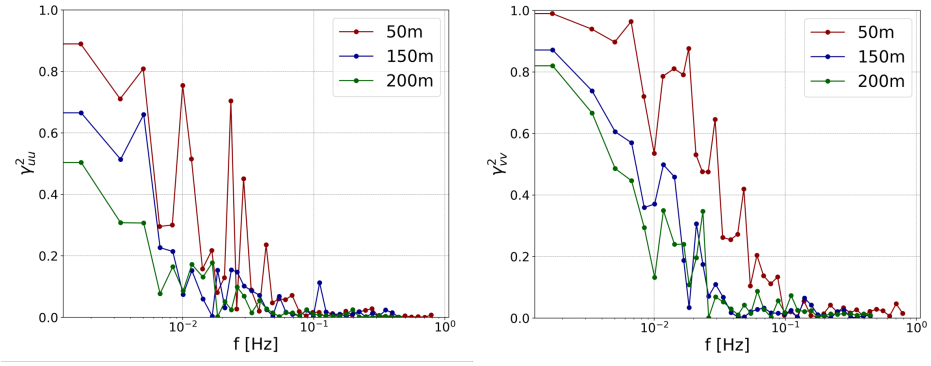

Figure 3: Squared coherence of the along-wind (left) and cross-wind (right) component for three lateral separations at a height of approximately 155m above sea level. The different colors indicate different lateral separations.

direction was approximately perpendicular to the vector connecting the lidar crossings under consideration. We averaged the auto and cross spectra over 10-min periods. The resulting spectra were further bin-averaged on a logarithmic scale. Next, we computed the squared coherence using the following relation:

$$\gamma^2_{ij}(f) = \frac{\left|\chi_{ij}(f)\right|^2}{S_{ii}(f)S_{jj}(f)}, \tag{3}$$

where the subscript i and j stand for either the along-wind component or the cross-wind component.

The spectrum of the along-wind component computed by averaging over six consecutive 10-min periods is shown in Figure 2 and Figure 3 shows the squared coherence of the along-wind and cross-wind component for three different lateral separations. We observe that the coherence at zero frequency decreases with an increase in separation. Moreover, the coherence at higher frequencies decays faster as the separation increases.

Thus, we demonstrate that we can measure spectral coherence at heights and with lateral displacements relevant for wind turbine loads with a number of coordinated Doppler lidars.

5 Expected Outcomes

A profound outcome from this project would be to show that the IEC turbulence models fail at heights relevant for future wind turbines. This can potentially pave the way for new models of turbulence (such as the Syed *et al.* model) or new methods of generating turbulent wind fields (eg. from LES) to become more widely accepted or even included in the standards.

Acknowledgements

This project is funded through the European Union Horizon Europe Framework programme HORIZON-CL5-2021-D3-03-04 under grant agreement no. 10108420 (FLOW) and HORIZON-MSCA-2022-DN-01 under grant agreement no. 10111955 (AptWind).

References

[1] IEC 61400-1:2005 — IEC Webstore — rural electrification, wind power. Technical report.

[2] N. Angelou, J. Mann, and C. Dubreuil-Boisclair. Revealing inflow and wake conditions of a 6 MW floating turbine. *Wind Energy Science*, 8(10):1511–1531, 10 2023.

[3] E. Cheynet, M. Flügge, J. Reuder, J. B. Jakobsen, Y. Heggelund, B. Svardal, P. Saavedra Garfias, C. Obhrai, N. Daniotti, J. Berge, C. Duscha, N. Wildmann, I. H. Onarheim, and M. Godvik. The COTUR project: Remote sensing of offshore turbulence for wind energy application. *Atmospheric Measurement Techniques*, 14(9):6137–6157, 9 2021.

[4] E. Cheynet, J. B. Jakobsen, and C. Obhrai. Spectral characteristics of surface-layer turbulence in the North Sea. *Energy Procedia*, 137:414–427, 10 2017.

[5] E. Cheynet, J. B. Jakobsen, and J. Reuder. Velocity Spectra and Coherence Estimates in the Marine Atmospheric Boundary Layer. *Boundary-Layer Meteorology*, 169(3):429–460, 12 2018.

[6] P. Doubrawa, M. J. Churchfield, M. Godvik, and S. Sirnivas. Load response of a floating wind turbine to turbulent atmospheric flow. *Applied Energy*, 242:1588–1599, 5 2019.

[7] P. Enevoldsen and G. Xydis. Examining the trends of 35years growth of key wind turbine components. *Energy for Sustainable Development*, 50:18–26, 6 2019.

[8] J. C. Kaimal, J. C. Wyngaard, Y. Izumi, and O. R. Coté. Spectral characteristics of surface-layer turbulence. *Quarterly Journal of the Royal Meteorological Society*, 98(417):563–589, 7 1972.

[9] J. Mann. The spatial structure of neutral atmospheric surface-layer turbulence. *Journal of Fluid Mechanics*, 273:141–168, 1994.

[10] K. Müller, M. Reiber, and P. W. Cheng. Comparison of Measured and Simulated Structural Loads of an Offshore Wind Turbine at Alpha Ventus. *International Journal of Offshore and Polar Engineering*, 26(03):209–218, 9 2016.

[11] M. Noonan, T. Stehly, Mora Alvarez, David Fernando, L. Kitzing, G. Smart, V. Berkhout, and Y. Kikuch. IEA Wind TCP Task 26: Offshore Wind Energy International Comparative Analysis - DTU Findit, 2018.

[12] A. Nybø, F. G. Nielsen, J. Reuder, M. J. Churchfield, and M. Godvik. Evaluation of different wind fields for the investigation of the dynamic response of offshore wind turbines. *Wind Energy*, 23(9):1810–1830, 9 2020.

[13] A. H. Syed and J. Mann. A Model for Low-Frequency, Anisotropic Wind Fluctuations and Coherences in the Marine Atmosphere. *Boundary-Layer Meteorology*, 190(1):1–37, 1 2024.

[14] G. A. Van Kuik, J. Peinke, R. Nijssen, D. Lekou, J. Mann, J. N. Sørensen, C. Ferreira, J. W. Van Wingerden, D. Schlipf, P. Gebraad, H. Polinder, A. Abrahamsen, G. J. Van Bussel, J. D. Sørensen, P. Tavner, C. L. Bottasso, M. Muskulus, D. Matha, H. J. Lindeboom, S. Degraer, O. Kramer, S. Lehnhoff, M. Sonnenschein, P. E. Sørensen, R. W. Künneke, P. E. Morthorst, and K. Skytte. Long-term research challenges in wind energy – a research agenda by the European Academy of Wind Energy. *Wind Energy Science*, 1(1):1–39, 2 2016.

[15] P. Veers, C. L. Bottasso, L. Manuel, J. Naughton, L. Pao, J. Paquette, A. Robertson, M. Robinson, S. Ananthan, T. Barlas, A. Bianchini, H. Bredmose, S. G. Horcas, J. Keller, H. A. Madsen, J. Manwell, P. Moriarty, S. Nolet, and J. Rinker. Grand challenges in the design, manufacture, and operation of future wind turbine systems. *Wind Energy Science*, 8(7):1071–1131, 7 2023.

Quantifying biases in the wind forecasted by WRF with wind measurements in the Baltics

Peter Stammer[a,b], **Tija Sīle**[a], **Lasse Svenningsen**[b]

[a] University of Latvia
[b] EMD International A/S

E-mail: pst@emd.dk

Keywords: WRF, hindcast, validation, wind forecast, measurements

The Weather Research and Forecasting (WRF) numerical weather prediction model is a useful tool for assessing the wind resource of prospect wind farm sites. The software tool windPRO, developed by EMD International A/S, provides WRF data of the hourly wind speed and direction as input for the planning and development of wind turbine sites. WRF data is a significant supplement to physical wind measurements, and with improved accuracy may potentially make expensive measurements unnecessary in future site assessments. While the newest data product has shown much improved accuracy compared to predecessor data sets [3, 4], there are also clear indications for specific instances in which the model shows a bias when comparing with measurements [1, 2]. As an example case of a bias, we document and quantify occurrences of low-level jets that are underrepresented in the WRF model simulations. Further relevant quantities to look at outside of low-level jet incidents are wind speed, wind shear and turbulence. We use validation data from weather observations available internally at EMD, public weather stations in the Baltic countries and observations from the Advanced Scatterometer (ASCAT) over the Baltic Sea to compare the WRF modeled wind. The broader aim of this work is to clearly identify systematic problems in WRF wind output as an outset for later work in adjusting various factors of the model and input data to reduce these errors. The final objective is to provide improved WRF data for better and cheaper wind farm development in EMD's software products, facilitating the transition to a 100% renewable future.

References

[1] S. Shimada, T. Ohsawa, 2011: Accuracy of Offshore Wind Speeds Simulated by WRF. SOLA, Vol.7, 021−024, doi:10.2151/sola.2011-006

[2] S. Shimada, T. Ohsawa, S. Chikaoka, K. Kozai, 2011: Accuracy of the Wind Profile in the Lower PBL as Simulated by the WRF Model. SOLA, Vol. 7, 109−112, doi:10.2151/sola.2011-028

[3] K. Solbakken, Y. Birkelund, E. M. Samuelsen, 2021: Evaluation of surface wind using WRF in complex terrain: Atmospheric input data and grid spacing. Environmental Modelling and Software 145 (2021) 105182

[4] L. Svenningsen, M. L. Thøgersen, T. Sørensen, 2020: Technical Note: Validation of EMD-WRF EUROPE+ (ERA5) mesoscale dataset. EMD International A/S

20th EAWE PhD Seminar on Wind Energy
24-26 September 2024
Visby, Sweden

Wind-field characterization using lidar measurements and proper orthogonal decomposition

Esperanza Soto Sagredo[a], **Jennifer M. Rinker**[a], **Michael Courtney**[a], and **Ásta Hannesdóttir**[a]

[a]Department of Wind and Energy Systems, Technical University of Denmark (DTU)
E-mail: espa@dtu.dk

Keywords: wind-field reconstruction, POD, lidar, hub-lidar, LAC, lidar-assisted control

1 Introduction

As the wind industry develops, the increasing size of wind turbines highlights the need for a flow-field-aware controller that can account for the flow-field coming towards the rotor, to optimize wind turbine performance.

The CONTINUE project [1] seeks to design and demonstrate an advanced wind-turbine controller capable of measuring, estimating, and adapting to the turbulent field impacting the entire rotor.

Achievement of this objective requires the development of three essential technologies: 1) a pulsed lidar system affixed to and moving with the rotor's hub (hereafter hub-lidar), which bypasses blade blockage to deliver high-fidelity measurements, 2) a real-time turbulence estimator that takes the raw lidar data and calculates the incoming flow field, and 3) a control algorithm that adjusts to wind-speed fluctuations across the rotor plane to reduce loads on blades and tower.

This PhD project focuses on developing the wind-field reconstruction algorithm, as detailed in [2]. It uses data from the hub-mounted lidar and Proper Orthogonal Decomposition (POD), to accurately estimate the full-flow field across the wind turbine rotor in real time. Meanwhile, the development of the novel control algorithm is being spearheaded by VESTAS. The prototype control system, designed for wind turbines with a rated power exceeding 2 MW, will undergo trials during the demonstration phase.

2 Methodology

The methodology compromises the following steps, from the work presented in [2]:

1. A dataset of turbulence boxes is made with the Mann turbulence generator [3] for a wind speeds of U =11.4 m/s. The wind profile was modeled using a power-law with a shear exponent of 0.2.
2. Fundamental modes of flow fluctuations are extracted from the dataset via Proper Orthogonal Decomposition (POD), creating a reduced-order model of the flow.
3. Synthetic hub-mounted lidar measurements are simulated using the HAWC2 hub-lidar sensor [4] on a rigid, non-tilting tower in HAWC2 v13.1 for the DTU 10MW reference wind turbine [5]. A six-beam configuration is employed, with each beam featuring a half-cone angle of $\theta = 25°$ and azimuthal angles $\phi = [0°, 15°, 30°, 45°, 60°, 75°]$ for beams 1 through 6, respectively. This setup facilitates spatial sampling through rotor rotation and varied range distances, with each beam scanning ten equally spaced distances from 30 to 300 m. Each beam is sampled consecutively, with a 500 ms sampling time per beam, and achieves a 2 Hz sampling frequency per consecutive beam through post-processing, without any switching delay.
4. Measurement selection is carried out by capturing all available measurements within a defined longitudinal range across the wind direction (Fig. 1 a). The width of this range corresponds to a distance covered during a specified number of full scans, n_{scans}. In a six-beam setup, with each beam sampling at 2 Hz, one full scan duration is $t_{fscan} = 3$ s. Thus, for a wind speed of $U = 11.4$ m/s and $n_{scans} = 2$, the longitudinal range is calculated as $U \times n_{scans} \times t_{fscan} = 68.4$ m (Fig. 1 b).

5. The longitudinal velocity component from the lidar measurements, u_{lidar}, is calculated by projecting line-of-sight velocities, V_{LOS}, onto the longitudinal axis, ignoring the v- and w-components, resulting in $u_{lidar} = V_{LOS}/\cos\theta$, where θ is the half-cone angle of each beam.

6. The hub-lidar data is fit to a fixed grid (Fig. 1 c), from which the modal amplitudes (C) are estimated using the Moore-Penrose pseudo-inverse [6, 7], by solving a least squares problem.

7. The full inflow is then reconstructed using the first K POD modes and their corresponding amplitudes C, expressed as $u_{reconstructed} = \sum_{i=1}^{K} g_i C + \hat{u}$, where $\hat{u}$ is the mean from the dataset used to generate the global basis (including the known shear). The result is a low-rank approximation reconstruction based on the selected modes and estimated modal amplitudes.

8. To establish a baseline for comparison, the mean wind field was calculated at each time step, by averaging lidar measurements across the YZ plane, using the data selection method outlined previously.

9. The method is applied at each time step to generate the reconstructed wind-field as turbulence boxes for the longitudinal component, equivalent to a 10-minute period.

10. A sensitivity analysis identifies the optimal number of measurements and modes necessary to maximize reconstruction accuracy.

11. Aeroelastic simulations are conducted for the DTU 10MW wind turbine, using the aeroelastic code HAWC2 [8].

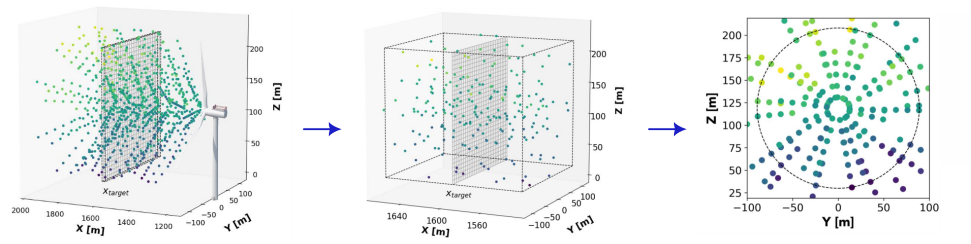

a) Hub-lidar measurements for 100 seconds simulation

b) Measurement selection based on number of scans considered

c) Selected measurements fit into fix grid to sub-sample modes for reconstruction

Figure 1: Schematic for measurement selection at time step $t_{step} = 140$ s, employing $n_{scan} = 4$ full scans.

3 Results

To assess the accuracy of POD-reconstructed wind-fields against reference fields, we calculated the Normalized Root Mean Square Error ($NRMSE = (\sqrt{1/n\sum_i^n (y_i - \hat{y}_i)^2})/U_o$), comparing the reconstructed field (y_i) with the reference field ($\hat{y}_i$). Here, $n = 7168$ represents the grid size in the longitudinal direction for 700 s, and U_o denotes the reference mean wind speed of 11.4 m/s.

Figure 2 presents the NRMSE for the longitudinal component of the wind field, calculated using u_{lidar} values for reconstruction. The plot details errors across various configurations, including different numbers of scans and modes. It is evident that increasing the number of scans consistently decreases NRMSE, thus enhancing performance in all cases. The most effective configuration, utilizing four scans and 30 modes, achieves a 57% reduction in error compared to the baseline.

Performance variations in different configurations of scans and modes stem from two main factors: (1) The count of scans dictates the span of the wind field utilized for lidar measurement selection. An increased number of scans broadens the pool of measurements available, enhancing the alignment with POD modes for accurate reconstruction. (2) The availability of data points significantly critically affects the efficacy of POD reconstructions. Specifically, using a single scan with a high number of modes can lead to overfitting issues. As illustrated in Fig. 2, deploying more modes with fewer scans can result in overfitting; for instance, employing 40 modes with only one scan elevates the error by 131% compared to the most effective baseline scenario.

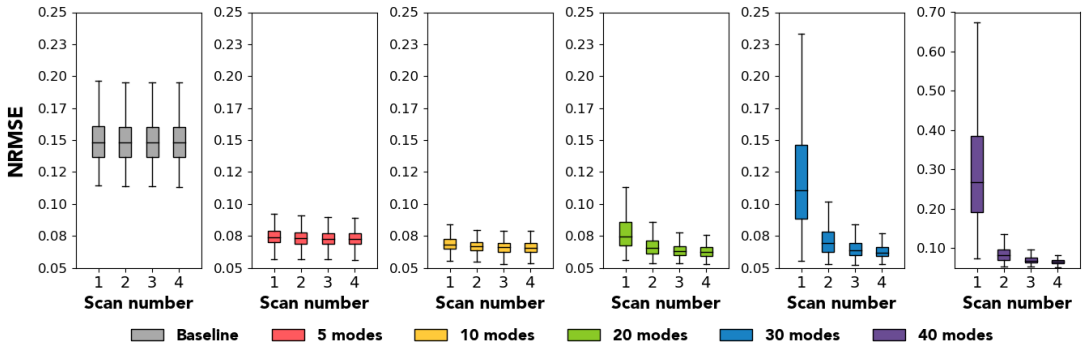

Figure 2: NRMSE for wind-field reconstruction from hub-lidar measurements (u_{lidar}).

Figure 3 illustrates the reconstruction of longitudinal wind speeds using 40 modes at time step 565.3 s for configurations with one (top) and four (bottom) scans. The images, arranged from left to right, display available hub-lidar measurements on the YZ plane, reference and reconstructed longitudinal wind speeds u, and the differences between them. With a single scan, the measurement count drops to 50, leading to overfitting, especially in regions lacking measurements, and results in a NRMSE of 0.3447. In contrast, using four scans increases the measurement tally to 181, significantly reducing the NRMSE to 0.0664. Despite this improvement, areas with no data, such as the upper-left corner, still show noticeable disparities.

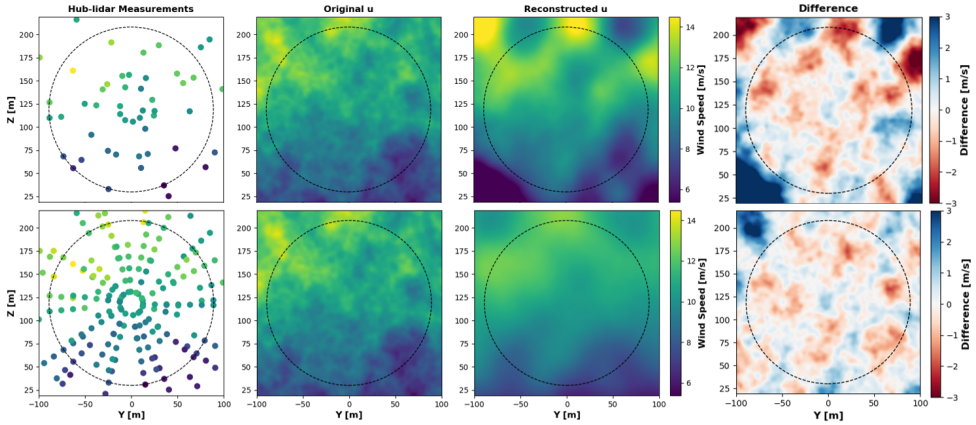

Figure 3: Comparison of longitudinal wind speed reconstruction at time step 565.3 s for two configurations with 40 modes: one scan (top) and four scans (bottom) (Figure 4 from [2]).

Finally, Fig. 4 compares the aeroelastic responses between the reference, baseline, and best performance cases. The reconstruction and baseline perform adequately across Rotor Average Wind Speed (RAWS), power, and rotor speed channels. However, the proposed method more accurately captures fluctuations in the blade root flapwise (MxBR), tower base fore-aft (MxTB), and side-side (MyTB) moments. However, $MyTB$ responses exhibit noticeable lags compared to the reference case.

Overall, the POD reconstruction method proves more effective in reflecting the wind turbine's dynamic response compared to the baseline, primarily due to its capability in capturing the spatial variations of turbulence.

4 Conclusion and Outlook

While the method exhibits sensitivity to measurement distribution and faces challenges in accurately characterizing high-frequency channels, it shows promise for real-time wind field estimation. This capability is advantageous for lidar-assisted turbine control and load validation.

Future efforts will concentrate on validating this method using Large Eddy Simulation (LES) data and investigating the effects of unknown shear profiles on reconstruction accuracy, with these profiles deduced directly from

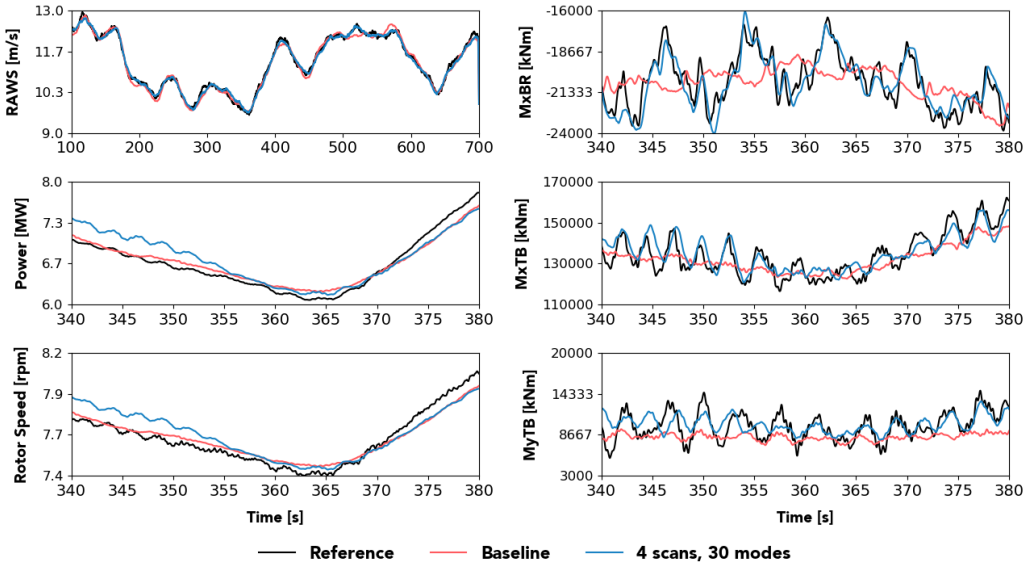

Figure 4: Time series for six turbine response channels for $U_o = 11.4$ m/s, for selected reconstruction case, reference and baseline case.

hub-lidar data. Additionally, the relevance of Taylor's frozen hypothesis in measurement selection requires deeper exploration. Moreover, the method's high sensitivity to the spatial distribution of measurements presents particular challenges for turbines with variable rotor speeds. To address this, future research may develop adaptive strategies or incorporate interpolation techniques to efficiently manage data gaps and enhance reconstruction accuracy.

Acknowledgements

This work is part of the CONTINUE project, which has received funding from the Danish Energy Technology Development and Demonstration Programme (EUDP), under grant agreement 640222-496980.

References

[1] EUDP. Continue - control of next-generation wind turbines. https://eudp.dk/en/node/16680, 2023. Accessed: 2024-14-06.

[2] E. Soto Sagredo et al. Wind-field characterization using synthetic lidar measurements and proper orthogonal decomposition. *J. Phys.: Conf. Ser.*, 2767:052061, 2024.

[3] Jakob Mann. Wind field simulation. *Probabilistic Engineering Mechanics*, 13(4):269–282, 1998.

[4] E. Soto Sagredo et al. Verification of numerical lidars in hawc2: Analysis of nacelle- and hub-mounted lidars. Technical report, DTU Wind Energy, Roskilde, Denmark, 2023.

[5] C. Bak et al. General rights the dtu 10-mw reference wind turbine, 2013.

[6] H. Moore. On the reciprocal of the general algebraic matrix. *Bulletin of the American Mathematical Society*, 26:394–395, 1920.

[7] R. Penrose. A generalized inverse for matrices. *Proceedings of the Cambridge Philosophical Society*, 51: 406–413, 1955.

[8] DTU. Hawc2 horizontal axis wind turbine simulation code 2nd generation. http://www.hawc2.dk/, 2019.

2.2 Session 212: Wind resources, turbulence, and acoustics

25.09.2024, 13:0, Room 2

Chair:

Mohammadreza Manami

Presenters:

Chapman-Smith Keeta	Modelling Tropical Cyclones for Safer Farm Design and Operations
Agarwal Nathan	Evaluation of MYNN and 3DPBL wakes with North Sea in-situ observations
Bührend Lukas	Large Eddy Simulations of Turbulence Regimes in the Stable Boundary Layer
Korb Henry	Simulating Thermally Stratified Boundary Layers with the Lattice Boltzmann Method
Bensignor Isaac	Physics of Rotor Noise of Vehicles Operating in Urban Environments

20th EAWE PhD Seminar on Wind Energy
24 - 26 September 2023
Visby, Sweden

Modelling Tropical Cyclones for Safer Farm Design and Operations

Keeta Chapman-Smith 1[a], Xiaoli Guo Larsén 2[a], Mark Brodersen 3[b], Morten Nielson 4[a], Jana Fishereit 5[a]

[a] Denmark Technical University
[b] Ørsted

E-mail: kechap@dtu.dk

Keywords: tropical cyclones, regional characteristics, re-analysis, best track data, modelling, uncertainty, cost related to hazards

1. Overview

This project aims to accurately model tropical cyclones and quantify uncertainty across different regions for safer wind farm design and operation. The characteristics of tropical cyclones in different regions will be identified followed by conducting a review and case study of models such as the Holland model, Monte Carlo simulations, numerical models, and using machine learning techniques. The model's performance across different global regions with diverse met-ocean conditions and land-sea interactions will be assessed. Understanding these regional conditions is crucial for identifying the unique challenges in tropical cyclone modelling and determining the most suitable model for each area. Additionally, the project will reconstruct re-analysis data by using best track data as the training data. Analysis on the available re-analysis datasets needs to be undertaken before the re-analysis dataset is chosen. This includes a comprehensive uncertainty assessment. Lastly the extreme loads on turbines from different tropical cyclone cases will be investigated to identify the uncertainty of costs related to hazards.

2. Methodology

2.1 Quantification of regional characteristics

Initially, the quantification of diverse characteristics of tropical cyclones in regions such as the US, Taiwan, and Japan using Best Track Data will take place. This comprehensive analysis will involve understanding various attributes, including the path, intensity, size, fetch, given location relative to the eyewall, and the boundary layer height for tropical

cyclones in these different regions, enabling a deeper insight into the regional variability and behavior of these storms.

2.2 Evaluation of tropical cyclone models

Secondly, scientific guidelines of assessing extreme wind and loads related to tropical cyclones in different regions will be developed. This will be done by evaluating the strengths and weaknesses of various tropical cyclone models. A review of existing methods and a case study will be done for each of the models: the Holland model, Monte Carlo Simulations, numerical models and machine learning techniques. The metocean conditions and land-sea interactions for different regions will be considered as part of the review and case study. By understanding regional conditions such as wind speed, direction, gustiness, air temperature, humidity, and water level fluctuations, the specific challenges of modelling in each area can be identified, and the most suitable model for each region can be determined.

2.3 Uncertainty assessment

The next phase of the project will centre on the quantification of uncertainty of calculations of meteorological parameters. Reconstructing reanalysis data using best track data training will be used to do so. Three methods will be used for uncertainty assessment:

2.3.1 Uncertainty propagation

Uncertainty propagation in the training will quantify the uncertainty in the input data and the model parameters which affect the reconstructed re-analysis data. This will be done by identifying the uncertainty in the input data, including uncertainty in the model training process and using Monte Carlo simulations to build a statistical distribution of possible outcome. By using this method a quantified understanding of how the input uncertainties impact the reconstructed re-analysis data will be obtained.

2.3.2 Range of variability

Understanding the range of variability of model results that the reconstructed re-analysis can take is an important step in the uncertainty assessment. This can be done by assessing how input parameters and initial conditions impact outputs, generating a range of different scenarios and comparing several model outputs against each other.

2.3.3 Comparison to high-resolution numerical model

The reconstructed re-analysis data will be compared to a high-resolution numerical model to validate the accuracy and spatial detail of the reconstructed re-analysis data. This entails initial numerical modelling of a tropical cyclone, followed by comparison of the structure to the reconstructed reanalysis data. Analysis of how the reconstructed data captures the metocean conditions and land-sea interactions will be evaluated here.

2.4. Costs related to hazards

Finally, the uncertainty of calculations of cost related to hazards through hazard models will be quantified. The load on a turbine from individual cases of tropical cyclones, one in 50-year events, 10-minute average wind speed and gusts all need to be investigated. To do this it requires an extension of the GASP and the GASPOC models for tropical cyclone impacted areas.

3. Expected Outcome

The expected outcome of this project will be fourfold. Firstly, the improved understanding of tropical cyclones characteristics in different regions and their respective challenges for diverse modelling approaches. Secondly, developed scientific guidelines for accessing extreme winds and loads in various tropical cyclone affected areas. Thirdly, the quantification of uncertainties related to the different calculation approaches. Fourthly, the quantification of the uncertainty of costs related of hazards.

4. Conclusion

This project will aim to assess the characteristics of tropical cyclones in different regions and define which models are most appropriate for each. The assessment of extreme loads related to tropical cyclones will be defined and quantification of uncertainty will be established.

20th EAWE PhD Seminar on Wind Energy
24 - 26 September 2024
Visby, Sweden

Evaluation of MYNN and 3DPBL wakes with North Sea in-situ observations

Nathan J. Agarwal[a,b], Julie K. Lundquist[a,b,c,d], Timothy W. Juliano[e], Alex Rybchuk[c]

[a] Department of Atmospheric and Oceanic Sciences, University of Colorado, Boulder, Boulder Colorado, USA
[b] Johns Hopkins University, Baltimore, MD, USA
[c] National Renewable Energy Laboratory, Golden, CO, USA
[d] Renewable and Sustainable Energy Institute, Boulder, CO, USA
[e] U.S. NSF National Center for Atmospheric Research, Boulder, CO, USA

E-mail: nagarw22@jhu.edu

Keywords: WRF, wind farm wake, mesoscale, Fitch, WFP, PBL, North Sea, WIPAFF

1. Introduction

One open research area in Wind Farm Parameterization (WFP) intercomparison is wake sensitivity based on the planetary boundary layer (PBL) scheme choice. Although the PBL scheme choice has been shown to be important in turbine-free simulations [1], until recently, only one PBL scheme [2] has been available for the default, Fitch [3] WFP in the Weather Research and Forecasting (WRF) model. However, a new, three-dimensional, PBL scheme (NCAR 3DPBL) [4],[5] has been integrated [6],[7] into the Fitch WFP. This 3DPBL scheme has shown to improve observational agreement in cold-air pool events [8] and has also been theorized to be useful for modern, "grey zone" turbulence modelling that characterize multiple wind energy applications [9]. This work leverages this new integration of Fitch with the 3DPBL scheme to explore the sensitivity of PBL scheme choice on wake behavior. We assess wind speeds, temperature, and turbulence kinetic energy (TKE) at a North Sea cluster of wind farms with both the 1D MYNN PBL scheme [2] and the

3DPBL scheme with the PBL approximation [4],[5]. We then compare these two simulations to both FINO1 tower and aircraft in-situ observations from the WIPAFF [10] experiment.

2. Methods

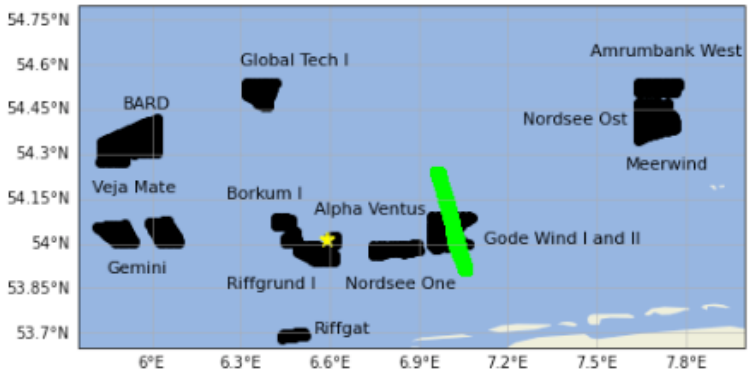

Figure 1: Map of the WRF inner domain where the wind farm areas are defined in black, the FINO1 tower is starred, and the flight transect paths are marked in lime green.

The North Sea's Wind Park Far Field (WIPAFF) project [10] collected aircraft observations to assess mesoscale wind farm wakes. We focus on a 14 October 2017 WIPAFF case study of six aircraft transects that have been previously studied [11],[12],[13] with the 1D MYNN scheme (Figure 1). We perform sixteen numerical simulations that build on the Ali et al. (2023) WRF setup [13] and alter the PBL scheme, adjust the degree of turbine-induced turbulence, and isolate TKE advection. Wind speed, temperature, and TKE output were extracted, interpolated, and compared both to FINO1 tower and aircraft observations. The correlation, bias, root mean square error (RMSE), and earth movers' distance (EMD) were then calculated at both locations [14].

3. Results/Conclusions

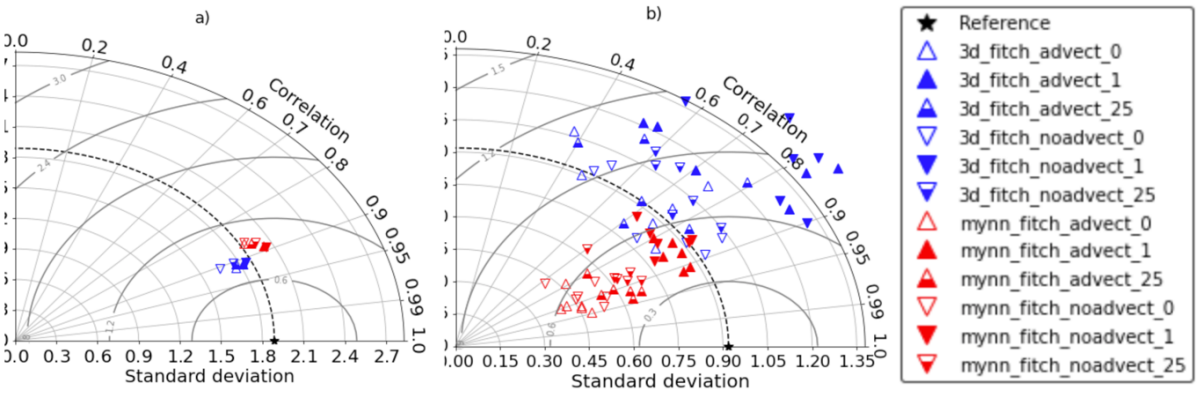

Figure 2: Taylor diagrams [15] comparing modelled wind speeds to wind speed observations at the FINO1 tower (102 m) a) and across the six aircraft transects (~ 250 m) b). The rings represent the root mean square error (RMSE), where markers in rings closer to the observation (star) have closer agreement than markers in rings further away.

Wind speeds at both the FINO1 tower and the aircraft transects show performance differences based on PBL scheme, regardless of the wind farm TKE factor or TKE advection option (Figure 2). The performance difference between PBL schemes could be explained by differences in turbulence characterization. The 3DPBL scheme considers three-dimensional effects not included in the 1D MYNN scheme and therefore, shows slower wind speeds than the 1D MYNN PBL scheme. While the 3DPBL scheme performs better than the 1D MYNN scheme at the FINO1 tower, the 3DPBL scheme performs worse than the 1D MYNN scheme along the aircraft transects. The relative performance difference between sites could be explained by site characteristics. While the FINO1 tower measurements are at altitudes within the turbine rotor region, the aircraft observations are taken at a height where turbulent interactions between the aircraft and turbines may be suppressed by the stably-stratified boundary layer. Therefore, the 3DPBL scheme incorporates more of the turbulence present within the rotor region and overpredicts turbulence aloft for this case study.

Acknowledgements

This work was supported by an agreement with NREL under APUP UGA-0-41026-125. This work was authored in part by the National Renewable Energy Laboratory, operated by Alliance for Sustainable Energy, LLC, for the U.S. Department of Energy (DOE) under Contract No. DE-AC36-08GO28308. Funding was provided by the U.S. Department of Energy Office of Energy Efficiency and Renewable Energy Wind Energy Technologies Office and by the National Offshore Wind Research and Development Consortium under agreement no. CRD-19-16351. The views expressed in the article do not necessarily represent the views of the DOE or the U.S. Government. The U.S. Government and the publisher, by accepting the article for publication, acknowledge that the U.S. Government retains a nonexclusive, paid-up, irrevocable, worldwide license to publish or reproduce the published form of this

work, or allow others to do so, for U.S. Government purposes. Neither NYSERDA nor OceanTech Services/DNV have reviewed the information contained herein and the opinions in this report do not necessarily reflect those of any of these parties. Data storage supported by the University of Colorado Boulder 'PetaLibrary'. This work utilized the Alpine high performance computing resource at the University of Colorado Boulder. Alpine is jointly funded by the University of Colorado Boulder, the University of Colorado Anschutz, and Colorado State University. A portion of this research was performed using computational resources sponsored by the DOE's Office of Energy Efficiency and Renewable Energy and located at NREL. Author TWJ is grateful for support in part from the Department of Energy Wind Energy Technologies Office through Contract #DE-A05-76RL01830 to Pacific Northwest National Laboratory (PNNL). The NSF National Center for Atmospheric Research (NSF NCAR) is a subcontractor to PNNL under Contract #659135. NSF NCAR is a major facility sponsored by the National Science Foundation under Cooperative Agreement No. 1852977.

References

[1] C. Draxl et al. Evaluating winds and vertical wind shear from Weather Research and Forecasting model forecasts using seven planetary boundary layer schemes, *Wind Energy Science*, 17:39-55, 2014.

[2] G. Mellor and T. Yamada. Development of a turbulence closure model for geophysical fluid problems. *Review of Geophysics*, 20:851-875, 1982.

[3] A. Fitch et al. Local and mesoscale impacts of wind farms as parameterized in a mesoscale NWP model, *Monthly Weather Review*, 140:3017-3038, 2012.

[4] B. Kosović et al. Three-dimensional planetary boundary layer parameterization for high-resolution mesoscale simulations, *Journal of Physics: Conference Series*, 1452:12-80, 2020.

[5] T. Juliano et al. "Gray Zone" simulations using a three-dimensional planetary boundary layer parameterization in the Weather Research and Forecasting Model, *Monthly Weather Review*, 150:1585-1619, 2022.

[6] A. Rybchuk et al. The sensitivity of the Fitch wind farm parameterization to a three-dimensional planetary boundary layer scheme, *Wind Energy Science*, 7:2085-2098, 2022.

[7] A. Peña et al. Can we yet do a fairer and more complete validation of wind farm parameterizations in the WRF model?, *Journal of Physics: Conference Series*, 2505:12-24, 2023.

[8] R. Arthur et al. Improved representation of horizontal variability and turbulence in mesoscale simulations of an extended cold-air pool event, *Journal of Applied Meteorology and Climatology*, 61:685-707, 2022.

[9] J. Wyngaard. Toward numerical modeling in the "Tierra Incognita", *Journal of the Atmospheric Sciences*, 61:1816-1826, 2004.

[10] A. Platis et al. First in situ evidence of wakes in the far field behind offshore wind farms, *Scientific Reports*, 8:2163:, 2018.

[11] S. Siedersleben et al. Turbulent kinetic energy over large offshore wind farms observed and simulated by the mesoscale model WRF (3.8.1), *Geoscientific Model Development*, 13:249-268, 2020.

[12] X. Larsén and J. Fischereit. A case study of wind farm effects using two wake parameterizations in the Weather Research and Forecasting (WRF) model (V3.7.1) in the presence of low-level jets, *Geoscientific Model Development*, 14:3141-3158, 2021.

[13] K. Ali et al. Assessment of five wind farm parameterizations in the Weather Research and Forecasting model: a case study of wind farms in the North Sea, *Monthly Weather Review,* 151:2333-2359, 2023.

[14] M. Optis et al. Best practices for the validation of U.S. offshore wind resource models, *NREL technical report*, 1-55, 2020.

[15] K. Taylor. Summarizing multiple aspects of model performance in a single diagram, *Journal of Geophysical Research: Atmospheres*, 112:11 – 24, 2001.

20th EAWE PhD Seminar on Wind Energy
24-26 September 2024
Visby, Sweden

Large Eddy Simulations of Turbulence Regimes in the Stable Boundary Layer

Lukas Bührend[a]

[a]Institute of Atmospheric Physics - German Aerospace Center (DLR)

lukas.buehrend@dlr.de

Keywords: Stable Boundary Layer, Nonlinear Backscatter Subgrid Scale Model, Turbulence

1 Introduction

The impact of the atmospheric boundary layer on wind turbines plays a key role when estimating the efficiency and power output of a wind park. Especially challenging is the stable, sometimes also called nocturnal boundary layer (SBL). It is characterized by surface temperature inversion (i.e. potential temperature increase with height), supergeostrophic windspeeds at rotor height (also called low level jets (LLJ)), weak, intermittent turbulence and strong wind veer (Ekman spiraling) [8]. The DLR WiValdi Research windpark in Krummendeich (northern Germany) is equipped with two wind turbines, lidars, microwave radiometers and sonic anemometers to measure these effects (see windenergy-researchfarm.com). However, measurements alone are not sufficient to fully understand SBL effects on wind turbines and have to be accompanied by numerical investigations.

Large eddy simulations (LES) have proven to provide detailed wind speed, temperature and turbulence fields over time, while remaining computational inexpensive and relatively fast in contrast to direct numerical simulations. The closure of the governing equations for LES requires a parameterization of unresolved or sub grid scales (SGS). In the SBL, the dominance of smaller turbulence eddies increases the influence of SGS parameterization. In addition, the weak turbulence intensity enhances the relative influence of numerical oscillations and boundary conditions.

In summary, the main research question is: how can the SBL in LES be suitably represented for wind turbine simulations including typical SBL features while maintaining relative low computational costs? To answer this question, an intercomparison of three different SGS models is presented in the next section. This is followed by a numerical characterization of the different SBL regimes by varying the geostrophic wind speed in Section 3.

2 The Relevance of the Subgrid Scale Model in Large Eddy Simulations

2.1 Simulation Tool, Initial and Boundary Conditions

The solenoidal zonal, meridonal and vertical windspeeds $\overline{u}_i$ ($\overline{u}_1 = \overline{u}, \overline{u}_2 = \overline{v}, \overline{u}_3 = \overline{w}$) and the potential temperature $\overline{\theta}$ are solved with the finite difference fluid solver EULAG [5] using the nonoscillatory MPDATA advection algorithm [7] (filtered Navier-Stokes equations subject to Boussinesq assumption, inclusion of Coriolis force). $\bar{\cdot}$ is the filtering operation, here realized by grid discretization.

In opposition to most other LES models, no Monin-Obukhov similarity theory is utilized to prescribe surface fluxes. Partial slip Neumann boundary conditions (BC) satisfying the continuity equation are applied to the lower surface (details can be found in [5]). In addition, the surface heat flux is prescribed as BC for the potential temperature at the lower boundary and horizontal periodic BC are applied to all variables.

The closure of the governing equations, i.e. the parameterization of the subgrid scale stress tensor $\tau_{ij} = \overline{u_i u_j} - \bar{u}_i \bar{u}_j$ is achieved by using the widespread Deardorff turbulent kinetic energy (TKE) SGS model [1]. Turbulent fluxes for any variable x (like u_i or θ) are defined via Reynolds decomposition, i.e. $x' = x - \langle x \rangle$, where $\langle \cdot \rangle$ defines the mean value, here over the horizontal plane. TKE is defined as $e = \frac{1}{2} u_i' u_i'$.

The unresolved (i.e. subgrid scale) component e_{SGS} of the TKE is parameterized via the governing equation

$$\frac{\mathrm{d}e_{\mathrm{SGS}}}{\mathrm{d}t} = \underbrace{-\tau_{ij}\bar{S}_{ij}}_{P} \underbrace{-\frac{g}{\theta_0}\nu_\theta\frac{\partial\bar{\theta}}{\partial x_3}}_{B} - \varepsilon + \underbrace{\frac{\partial}{\partial x_i}\left(2\nu_{\mathrm{t}}\frac{\partial e_{\mathrm{SGS}}}{\partial x_i}\right)}_{D}. \tag{1}$$

P is the SGS TKE production term with the resolved strain rate tensor $\overline{S}_{ij} = \frac{1}{2}(\frac{\partial\bar{u}_i}{\partial x_j} + \frac{\partial\bar{u}_j}{\partial x_i})$. B is the buoyancy term with $g = 9.81\,\mathrm{m\,s^{-2}}$, θ_0 a reference potential temperature and ν_θ the eddy diffusivity. ε is the SGS dissipation term and D the diffusion term with ν_t the eddy viscosity.

Three different flavors of the TKE subgrid scale models were tested regarding their suitability for SBL simulations, they will be explained below. The reference for all three SGS model tests is the GABLS LES intercomparison [2] based on the BASE (Beaufort Sea Arctic Stratus Experiment) observations. Initial and boundary conditions are consistent with the GABLS case and briefly revisited here, more details can be found in [2]. The domain size is $L_x = L_y = L_z = 400\,\mathrm{m}$, geostrophic wind speeds are ($U_G = 8\,\mathrm{m\,s^{-1}}$, $V_G = 0\,\mathrm{m\,s^{-1}}$), the latitude is $\phi = +73°$, the physical simulation time was 9 hours. A constant heatflux of $H = -7\,\mathrm{K\,m\,s^{-1}}$ was applied to the lower surface. The initial $\bar{u}$ and $\bar{v}$ velocity profiles correspond to the geostrophic windspeeds, $\bar{w}_{\mathrm{init}} = 0$. The initial potential temperature profile is $\theta_i(z) = 265 + \mathbf{1}_{z>100\mathrm{m}} \cdot 0.01\,\mathrm{K\,m^{-1}}$. A uniform gridsize of $\Delta = 6.25\,\mathrm{m}$ was used. Figure 1 shows the vertical profiles over the height z (horizontal spatial average and temporal mean over last 30 minutes) for the different subgrid scale models. Grey dots show results from the GABLS intercomparison, the grey vertical line shows the critical Richardson number $R_{\mathrm{cr}} = 0.25$.

2.2 The Influence of the Subgrid Scale Model

The default approach readily implemented in EULAG is the parameterization according to Schumann [6]. Here, $\tau_{ij} = -2\nu_t\bar{S}_{ij}$, $\nu_t \propto \sqrt{e_{\mathrm{SGS}}}$, $\nu_\theta = \nu_t/Pr_t$ with a turbulent Prandtl number Pr_t and $\varepsilon \propto e_{\mathrm{SGS}}^{3/2}$. This model results in no resolved turbulence (see Figure 1, TKE plot, red line) and heatflux due to excessive dissipation in the SGS range. The lack in upwards momentum and heatflux leads to a low LLJ height (mean windspeed plot in Figure 1) and less cooling in the upper z range.

One approach to tackle the issue of unresolved turbulence is the anisotropy model developed by Sullivan [9]. Close to the surface, the vertical turbulence length scale decreases (turbulence anisotropy) and the horizontal mean shear dominates turbulent motions. This is taken into account by introducing a mean-field eddy-viscosity model adjusted by an isotropy factor (for a detailed review see [9]). In comparison to the default approach, resolved turbulence and heatflux is visible in Figure 1. The plot of the Richardson number shows that the boundary layer height is increased relative to the default model. However, the mean windspeed and potential temperature profiles still deviate from the reference in the GABLS study.

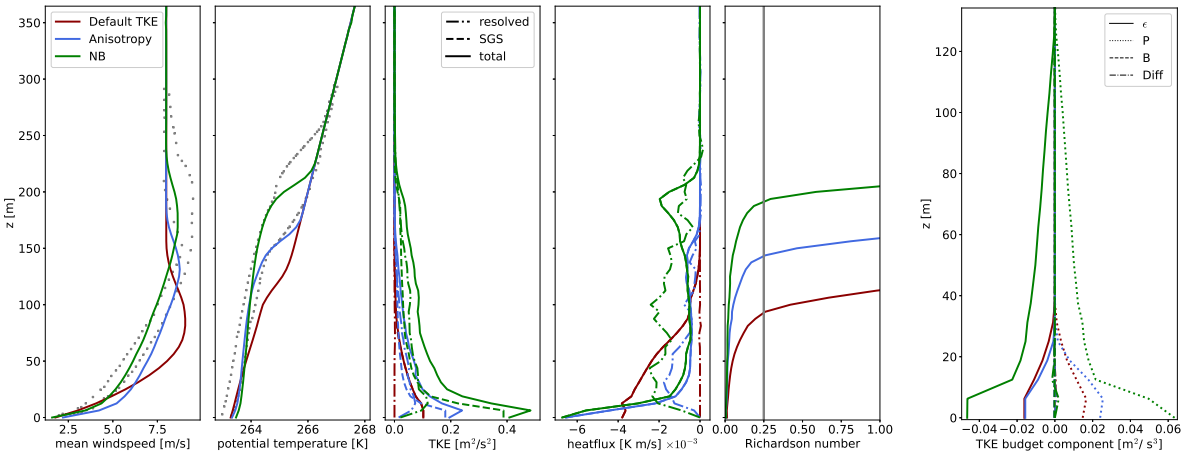

Figure 1: Vertical profiles of different variables resulting from the stable boundary simulation with EULAG with initial and boundary conditions similar to the GABLS LES intercomparison [2]. The colors depict the different subgrid scale models explained in Section 2.2.

Both models mentioned above are purely dissipative, i. e. energy is transferred from large to small scales and then to viscous dissipation and a potential energy backscatter is not taken into account. The nonlinear backscatter (NB) model developed by Kosovic [3] incorporates energy transfer from subgrid to resolved scales by including nonlinear contributions of strain rate tensor and rotation rate tensor products. In comparison to the other models shown in Figure 1, resolved turbulence and heatflux are largest and also the contributions of the TKE budget terms are more significant over height.

In summary, the NB model is the most promising SGS parameterization approach for SBL LES simulations with EULAG. As a side note, it is also implemented in the Weather Research and Forecasting Model WRF.

The NB model can now be applied to a characterization of the different stable boundary layer regimes in the following section.

3 Turbulence Regimes in the SBL

The turbulence regimes within the stable boundary layer can be partitioned into the weakly stable (WSBL) and the very stable boundary layer (VSBL) [4]. The WSBL is characterized by strong winds and weak stratification with continuous turbulence. It normally follows similarity theory relationships like MOST. The VSBL is identified with weak winds, strong stratification and weak, intermittent turbulence. Similarity theories like MOST break down in this regime [4].

In measurements of the atmospheric boundary layer [10], these regimes can be identified by plotting the turbulence intensity (here parameterized as $\sqrt{TKE}$) versus the horizontal averaged mean windspeed (see Fig. 2). In the VSBL regime (1), turbulence increases weakly with windspeed and arises from local instabilities (B). Above a threshold windspeed U_{th} in the WSBL regime (2), the turbulence intensity increases strongly linear with windspeed. Here, turbulence arises mainly from bulk shear. Additionally, intermittent turbulence can occur by temporary windspeed increases above the threshold (A) or top-down turbulence events (C).

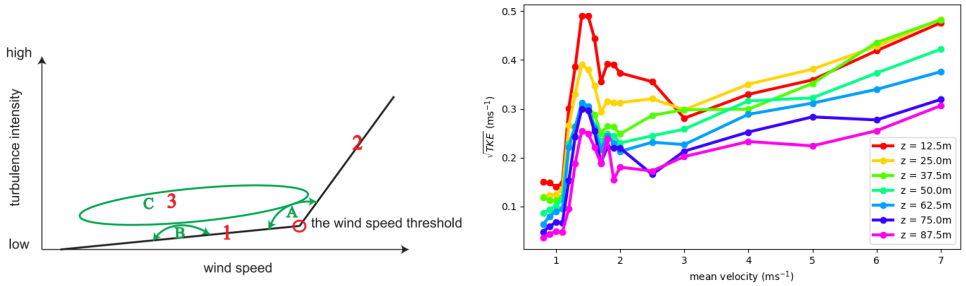

(a) (b)

Figure 2: (a): Schematic representation of different turbulence regimes in the stable boundary layer by the relation of windspeed versus turbulence intensity: 1 depicts the very stable boundary layer (VSBL), 2 the weakly stable boundary layer (WSBL) regime. The different turbulence types (A,B,C) are explained in the text. Image taken from [10]. (b) Results of LES simulations of the SBL with varied geostrophic windspeed, plotted for different height levels z.

All these turbulence events can potentially influence the performance and power output of wind turbines. As a consequence, they should be analyzed and represented in large eddy simulations for the SBL. A first investigation of turbulence regimes is presented here, a detailed analysis will follow in the future. The simulation setup including initial and boundary conditions is similar to the GABLS intercomparison setup presented in Section 2, but some parameters were adapted to closer match the DLR research windpark WiValdi in Krummendeich. The latitude was changed to $\phi_{\text{Kr}} = 53.9°$, the initial temperature profile to $\theta_{\text{l,Kr}}(z) = 280 + \mathbf{1}_{z>100\text{m}} \cdot 0.01\text{K m}^{-1}$. The heatflux was changed to $H = -20\,\text{K m/s}$. These are rough estimates to show the realization of VSBL and WSBL in the simulation. In the future, measurement data of windspeed, potential temperature, surface heat and momentum fluxes at Krummendeich will be used to calibrate and fine-tune the simulations. The nonlinear backscatter model presented in Section 2 was used.

The geostrophic wind was varied in the range of $0.5\,\text{m s}^{-1} \leq U_g \leq 7\,\text{m s}^{-1}$ with a step size of $0.1\,\text{m s}^{-1}$ between 0.5 and $2\,\text{m s}^{-1}$ and a step size of $1\,\text{m s}^{-1}$ from 2 to $7\,\text{m s}^{-1}$. V_g remains $0\,\text{m s}^{-1}$ for all values of U_g.

The resulting relationship between mean windspeed and $\sqrt{TKE}$ is shown in Figure 2b for different heights z. The threshold velocity appears to be around $1.5\,\mathrm{m\,s^{-1}}$. There, a local maximum of $\sqrt{TKE}$ is visible for all height levels, which can be explained with intermittent turbulence (A). For windspeeds below this local maximum, $\sqrt{TKE}$ remains approximately constant, for windspeeds above, a linear increase is visible. This shows, that the VSBL and WSBL can be differentiated in the LES by varying the geostrophic windspeed.

4 Summary / Outlook

It has been shown in Section 2, that the nonlinear backscatter subgrid scale model is more suitable for a simulation of the SBL with EULAG than other SGS models presented in this abstract by comparing the results of a benchmark LES intercomparison. As a first showcase, EULAG with the NB model was used in Section 3 to simulate an ensemble of LES with varying geostrophic windspeeds. The very stable and the weakly stable boundary layer regime were represented in this ensemble. It was shown that these regime changes influence the TKE. This can have significant influences for the loads and power output for wind turbines.

Future analysis of the different stability regimes includes varying parameters like surface heatflux, drag coefficient, initial temperature and windspeed profiles. The dependence of the threshold velocity on this parameters will be evaluated and the sensitivity of the different stability regimes to perturbations will be investigated. An integration of a wind turbine in the simulation, e.g. via the actuator line method will be realized.

Acknowledgements

The author gratefully acknowledges the Gauss Centre for Supercomputing e.V. (www.gauss-centre.eu) for funding this project by providing computing time on the GCS Supercomputer SuperMUC at Leibniz Supercomputing Centre (www.lrz.de).

References

[1] J. W. Deardorff. Stratocumulus-capped mixed layers derived from a three-dimensional model. *Boundary-Layer Meteorology*, 18(4):495–527, June 1980.

[2] B. et al. An intercomparison of large-eddy simulations of the stable boundary layer. *Boundary-Layer Meteorology*, 118(2):247–272, Feb. 2006.

[3] B. Kosovic and J. A. Curry. A large eddy simulation study of a quasi-steady, stably stratified atmospheric boundary layer. *Journal of the Atmospheric Sciences*, 2000.

[4] L. Mahrt. Stably stratified atmospheric boundary layers. *Annual Review of Fluid Mechanics*, 46(1):23–45, Jan. 2014.

[5] J. M. Prusa, P. K. Smolarkiewicz, and A. A. Wyszogrodzki. EULAG, a computational model for multiscale flows. *Computers and Fluids*, 37(9):1193–1207, Oct. 2008.

[6] U. Schumann. Subgrid length-scales for large-eddy simulation of stratified turbulence. *Theoretical and Computational Fluid Dynamics*, 2(5-6):279–290, Aug. 1991.

[7] P. K. Smolarkiewicz and L. G. Margolin. MPDATA: A finite-difference solver for geophysical flows. *Journal of Computational Physics*, 140(2):459–480, Mar. 1998.

[8] R. B. Stull, editor. *An Introduction to Boundary Layer Meteorology*. Springer Netherlands, 1988.

[9] P. P. Sullivan, J. C. McWilliams, and C.-H. Moeng. A subgrid-scale model for large-eddy simulation of planetary boundary-layer flows. *Boundary-Layer Meteorology*, 71(3):247–276, Nov. 1994.

[10] J. Sun, L. Mahrt, R. M. Banta, and Y. L. Pichugina. Turbulence regimes and turbulence intermittency in the stable boundary layer during cases-99. *Journal of the Atmospheric Sciences*, 69(1):338–351, Jan. 2012.

20^{th} EAWE PhD Seminar on Wind Energy
24-26 September 2024
Visby, Sweden

Simulating Thermally Stratified Boundary Layers with the Lattice Boltzmann Method

Henry Korb[a], **Henrik Asmuth**[a], and **Stefan Ivanell**[a]

[a]Wind Energy Section, Department of Earth Sciences, Uppsala University

E-mail: henry.korb@geo.uu.se

Keywords: Stratified Flows, Boundary Layer, Lattice Boltzmann Method

Thermal stratification in the atmospheric boundary layer plays an important role in wind farm flows. Effects of stratification include gravity waves and wind farm blockage, but also altered turbulence characteristics, which in turn affect wake recovery and turbine loads [10, 1, 11]. With growing wind farm size, the effects become even more pronounced. However, accurately simulating such stratified flows requires the use of high-fidelity methods. Large Eddy Simulation is the common choice in research, although advances have been made in applying Reynolds-Averaged Navier-Stokes methods as well [5]. Simulating large offshore wind farms is extremely expensive in terms of computational resources since the simulation domain needs to be both very large and well resolved, especially when simulating stable conditions [2]. In recent years, the Lattice Boltzmann Method (LBM) was developed for the application to neutral boundary layer flows and wind farm flows [3, 4, 8]. By utilizing GPUs (graphical processing units), the computational cost can be greatly reduced compared to traditional approaches based on CPUs (central processing unit). Furthermore, since one GPU contains now up to 80 Gigabytes of memory, much fewer processors are needed to simulate large domains, thus circumventing costly node-to-node communication.

In this presentation, I will show some of our ongoing work in extending the Lattice Boltzmann Method to stratified flows.

In order to simulate stratified flows, the evolution of potential temperature has to be computed. In addition to the momentum equations, which are solved using the cumulant LBM [7, 6], we solve an advection diffusion equation for a scalar representing potential temperature. The Boussinesq approximation is used to compute a buoyancy force that couples the temperature back to the momentum equations. Two alternatives exist for solving the advection diffusion equation for temperature to incorporate thermal effects into LBM [9, 12]. The lesser used approach is the use of finite differences (FD), while the more common approach is to use an adjusted version of LBM , called the double-distribution approach (DDF). While the finite-difference approach has many benefits, such as reduced memory footprint and easier implementation, it requires the combination of two very different numerical approaches. Furthermore, only limited literature is available. The DDF approach on the other hand uses the same numerical scheme, but requires more memory. I will compare both of these approaches for canonical test cases as well as stratified boundary layer flows. Canonical test cases include the advection of a Gaussian hill of concentration, a differentially heated cube and Rayleigh Bénard convection. The results of a convergence study comparing FD and DDF approach are shown in Figure 1a. The converge study shows that both approaches have similar orders of accuracy. However, the FD approach uses only 75% of memory of the DDF approach and consistently has a higher computational performance, as is shown in Figure 1b.

While both approaches perform similar at test cases with finite Reynolds and Rayleigh numbers, only the DDF approach appears to be stable in simulations of conventionally neutral boundary layers. The reason for that instability is not known to us, although we conjecture that it is due to the differences in numerical schemes and consequently inconsistent time integration. Building on that result, I will present some preliminary results from further verification cases conducted with the DDF approach. We reproduce the case of a conventionally neutral marine boundary layer as described in detail in [2], however we only aim to reproduce the precursor without turbines. In order to simulate CNBLs, we require the use of a wall model for momentum and temperature. Extending the approach presented in [4], we develop and approach to impose a heat flux at the surface according to Monin-Obukhov similarity theory. Further adaptations are not necessary.

The results are promising and demonstrate that LBM can be used to simulate stratified ABLs at very low computational cost.

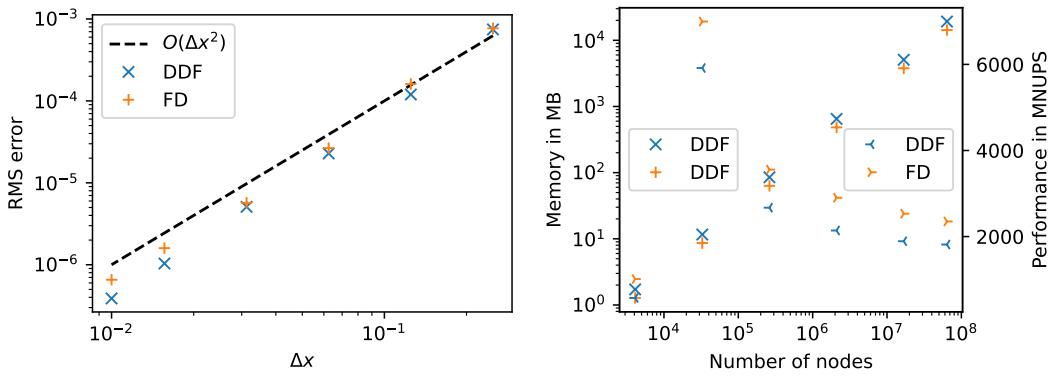

(a) Root mean square error of the numerical to the analytical solution of the advection of a Gaussian hill of concentration.

(b) Comparison of memory usage and computational performance in a converge study of the advection of a Gaussian hill of concentration

References

[1] Dries Allaerts and Johan Meyers. "Gravity Waves and Wind-Farm Efficiency in Neutral and Stable Conditions". In: *Boundary-Layer Meteorology* 166.2 (Feb. 1, 2018), pp. 269–299. DOI: 10.1007/s10546-017-0307-5.

[2] Dries Allaerts and Johan Meyers. "Large Eddy Simulation of a Large Wind-Turbine Array in a Conventionally Neutral Atmospheric Boundary Layer". In: *Physics of Fluids* 27.6 (June 10, 2015), p. 065108. DOI: 10.1063/1.4922339.

[3] Henrik Asmuth, Hugo Olivares-Espinosa, and Stefan Ivanell. "Actuator Line Simulations of Wind Turbine Wakes Using the Lattice Boltzmann Method". In: *Wind Energy Science* 5.2 (May 26, 2020), pp. 623–645. DOI: 10.5194/wes-5-623-2020.

[4] Henrik Asmuth et al. "Wall-Modeled Lattice Boltzmann Large-Eddy Simulation of Neutral Atmospheric Boundary Layers". In: *Physics of Fluids* 33.10 (Oct. 1, 2021), p. 105111. DOI: 10.1063/5.0065701.

[5] M. Baungaard et al. "A Numerical Investigation of a Wind Turbine Wake in Non-Neutral Atmospheric Conditions". In: *Journal of Physics: Conference Series* 2265.2 (May 2022), p. 022015. DOI: 10.1088/1742-6596/2265/2/022015.

[6] Martin Geier, Andrea Pasquali, and Martin Schönherr. "Parametrization of the Cumulant Lattice Boltzmann Method for Fourth Order Accurate Diffusion Part I: Derivation and Validation". In: *Journal of Computational Physics* 348 (Nov. 2017), pp. 862–888. DOI: 10.1016/j.jcp.2017.05.040.

[7] Martin Geier et al. "The Cumulant Lattice Boltzmann Equation in Three Dimensions: Theory and Validation". In: *Computers & Mathematics with Applications* 70.4 (Aug. 2015), pp. 507–547. DOI: 10.1016/j.camwa.2015.05.001.

[8] Henry Korb, Henrik Asmuth, and Stefan Ivanell. "Validation of a Lattice Boltzmann Solver Against Wind Turbine Response and Wake Measurements". In: *Journal of Physics: Conference Series* 2505.1 (May 2023), p. 012008. DOI: 10.1088/1742-6596/2505/1/012008.

[9] Timm Krüger et al. *The Lattice Boltzmann Method: Principles and Practice*. 1st ed. Graduate Texts in Physics. Springer International Publishing, 2017. 694 pp.

[10] Luca Lanzilao and Johan Meyers. "Effects of Self-Induced Gravity Waves on Finite Wind-Farm Operations Using a Large-Eddy Simulation Framework". In: *Journal of Physics: Conference Series* 2265.2 (May 2022), p. 022043. DOI: 10.1088/1742-6596/2265/2/022043.

[11] Fernando Porté-Agel, Majid Bastankhah, and Sina Shamsoddin. "Wind-Turbine and Wind-Farm Flows: A Review". In: *Boundary-Layer Meteorology* 174.1 (Jan. 1, 2020), pp. 1–59. DOI: 10.1007/s10546-019-00473-0.

[12] Keerti Vardhan Sharma, Robert Straka, and Frederico Wanderley Tavares. "Current Status of Lattice Boltzmann Methods Applied to Aerodynamic, Aeroacoustic, and Thermal Flows". In: *Progress in Aerospace Sciences* 115 (May 1, 2020), p. 100616. DOI: 10.1016/j.paerosci.2020.100616.

20^{th} EAWE PhD Seminar on Wind Energy
24-26 September 2024
Visby, Sweden

Physics of Rotor Noise of Vehicles Operating in Urban Environments

Isaac S. Bensignor, **Tercio Lima Pereira**, and **Daniele Ragni**

Delft University of Technology, Faculty of Aerospace Engineering, 2629 HS Delft, Netherlands

E-mail: i.bensignor@tudelft.nl

Keywords: rotor, aeroacoustics, aeromechanics, pressure sensitive paint. acoustic wind tunnel

1 Introduction

This research project will study the noise emitted by rotors akin to those used by small drones and advanced air mobility vehicles for flight in urban environments. Flying in urban areas demands that vehicles make rapid maneuvers, maintain a desired attitude, and keep to a set flight path under dynamic, gusting, and turbulent flow conditions. Controlling the noise emissions, which is altered by each of the aforementioned flight characteristics, is of paramount importance for ensuring public acceptance of urban air operations [1].

Studying the noise emitted by rotors is a challenging task. Experiments and numerical simulations with rotating bodies have long been realized [2, 3]. However, reliable cross-validation between both has always been difficult to achieve. This is mostly because experimental campaigns are subject to higher uncertainties and less information. For example, experimental isolated rotor performance data is usually restricted to integral steady loads and torques at a fixed or a range of rotational speed(s). These types of experimental campaigns fall short on two crucial issues. First, the lack of blade surface information or detailed flow-field measurements hampers the full understanding and identification of the sources and aeromechanics of acoustic noise. Second, the conditions assessed are usually not representative of rotors in (urban) flight where large-scale gusts, turbulent flows, the propeller control system, flow-body interactions, and flight maneuvers can significantly modify the (perceived) noise emissions. Moreover, the rotors operate in low Reynolds number flow, where 1) the usage of statistical methods for estimating flow fluctuations is not well established, and 2) where the interaction of rotors with "slow-moving" turbulence – whose scales are on the same order as the size of the rotor chord or span – is not well understood.

This research project aims to study noise emission from rotors in conditions that represent flight in urban environments. The project encompasses three main research goals. The first is the definition, development, and creation of a bench test case where the physics of rotors and their emitted noise in simulated urban environments can be quantified. This first phase also will validate and verify the novel experimentation technique to be implemented so that a baseline capability is determined. The second main goal is characterizing relationships between various rotor aerodynamic and geometric conditions with the emitted noise observed/estimated. Characterization of such relationships may show that there are means for exploitation for rotor noise reduction. The third main goal is to employ the lessons learned with an application, like with a demonstrator vehicle or technology. Alongside the experiment-focused research project will be complementary computational and numerical validation studies, which require the use and development of semi-analytical formulations and simulations. Given that the scale and operational range (i.e. rotor radius, Reynolds number, Mach number) of the tests to be performed are on the same order as that of real flight vehicle rotors, the results of the studies will be directly applicable to those seeking to reduce the noise signature of their urban flight vehicle.

2 Proposed Method and Example Results

This first phase is currently underway with the development of a new rotor test stand; one that is designed such that typical rotor airfoil sections can be assessed in quasi-isolation for noise emission characterization. An example

of the custom rotor head is shown in Fig. 1. The Phase 1 experiments will be performed in the TU Delft Anechoic Wind Tunnel (AWT), where much of the testing infrastructure and support already exists and can be relied upon. The rotor test stand is being designed such that employment of a novel experimental method, pressure sensitive paint (PSP), can be leveraged as a non-intrusive optical pressure measurement technique. PSP will be deposited on the surfaces of the rotor blade sections to be evaluated. With the necessary lighting conditions, cameras, data acquisition systems, and post-processing techniques the results obtained will yield pressure distributions maps on the suction and pressure sides of the rotor. Obtaining experimental rotor pressure maps – which is notoriously difficult, and provides greater data resolution than pointwise measurements, like from pressure taps – allows for coupling of such information with the Ffwocs-William Hawking (FWH) equations or Hanson's formulation to determine the far field noise heard by an observer.

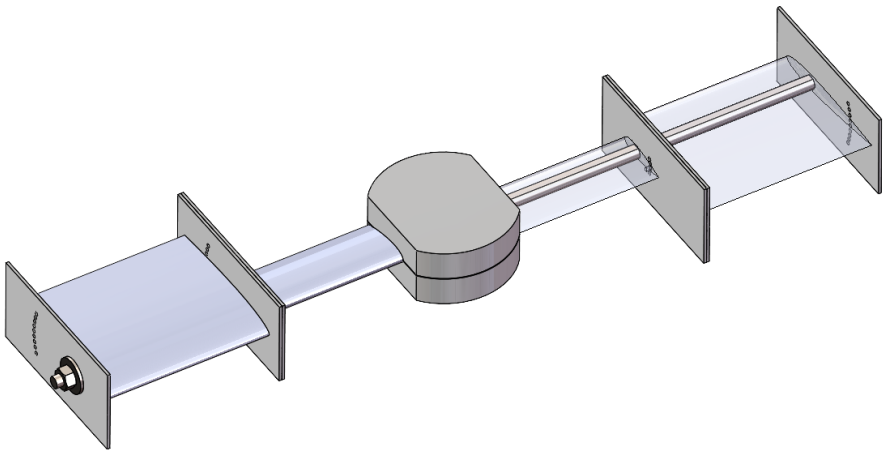

Figure 1: Preliminary custom rotor head designed for studying isolated rotor airfoil characteristics.

Two primary questions to be answered by the end of Phase 1 are: "can PSP-derived noise emission estimates produce the same fidelity of acoustic information as acoustic microphones for characterizing rotor noise?" and "can PSP visualizations of the blade surfaces demonstrate that there are multiple aerodynamic scenarios which produce the same (or similar) rotor noise profiles?" If these question's answers prove to be "yes," then environments in which rotor noise are not as well easily assessed (like outside of anechoic facilities) can be used for testing other relevant urban flight like scenarios (which is expanded upon in Phases 2 and 3). Moreover, the results from PSP will have shown that there are underlying aerodynamics and aeromechanics that have yet to be understood or uniquely identified and associated with the acoustic phenomena measured. Therefore, the successful employment of PSP lends towards acoustic characterization in any environment and to analyze scenarios that may not be well suited by other methods.

PSP (and its counterpart, temperature sensitive paint (TSP)) have been used for rotor performance and aerodynamic visualization research [4, 5, 6], and for acoustic analysis of arbitrary bodies (like cavities, which possess analytical formulations for which PSP results can be directly compared with) [7, 8, 9]. Assessments of noise via source localization with PSP and microphone correlation has been performed for airfoil wind tunnel testing [10]. However, using PSP for acoustic analysis of rotor noise has never been proposed and such a project will be the first of its kind. Using PSP in this scenario requires having a precise experimental setup and extensive post-processing of the raw data obtained. Klein *et al.* [11] and Kulesh *et al.* [12] have shown that PSP studies on rotors can estimate integrated rotor performance (i.e. thrust and torque loads). Weiss *et al.* [13] demonstrated that aerodynamic phenomena, like transition and separation locations, can be decomposed from the data. Therefore, use of PSP and TSP allows for a more holistic and global analysis of the aerodynamic phenomena occurring, while simultaneously providing blade surface information. No other experimental method (PIV, stereo-PIV, oil flow interferometry, laser-doppler anemometry, etc.) provides such detailed information about the object studied without the experiment including a second analysis method. Another advantage of using PSP to analyze low Reynolds number rotor flow and noise is that the turbulence and non-uniform pressure fluctuations expected to be measured occur at a low enough frequency that PSP can capture them (due to PSP's low response time to pressure changes

[14]). Moreover, PSP results provide a favorable spatial and temporal resolution for making aeroacoustic characterizations. An example wind tunnel setup and PSP results from rotor testing is shown in Fig. 2 from Disotell *et al.* [15].

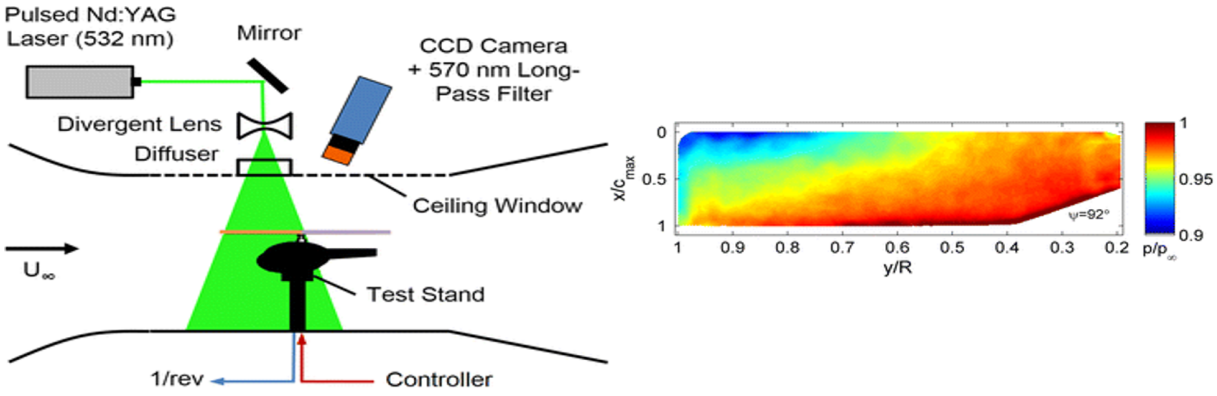

Figure 2: Left: an example experimental setup using PSP on rotor blades. Right: an example rotor suction side pressure map obtained via PSP and calibration data; from Disotell *et al.* [15]

The successful validation of Phase 1 lends towards performing further studies on the aeromechanics and physics of rotor noise due to differing aerodynamic and geometric conditions (like aspect ratio; twist; airfoil shape and spanwise distribution; subjection to turbulence and gusts; simulation of rotor flight-like profiles; non-uniform RPM modulation; and induction of time-varying rotor loading). Each of these varied conditions can produce starkly different aerodynamic phenomena which possess different acoustic profiles. Further review of the literature will inform which of those conditions are best suited or are of most interest to assess. Testing of the identified aerodynamic and geometric conditions of interest will be the focus of Phase 2 and would occur in the TU Delft AWT and Open Jet Facility (OJF) (where a turbulence and gusting environment can be created). The OJF is not as well suited to make aeroacoustic characterization compared to the AWT due to its lack of wall-lined acoustic dampeners. However, since PSP/TSP is expected to be a sufficient substitution for acoustic microphones, the tests in the OJF are meaningful to perform.

Given the amount of data to be collected via PSP/TSP and with acoustic microphones, it's reasonable to assume relationships can be drawn between acoustic phenomena and aerodynamic phenomena. It is speculated that use of such a method to produce blade pressure maps will help decompose the sources of aeroacoustic noise measured via characterization of pressure fluctuations. Moreover, with a detailed blade pressure map, the higher harmonics (e.g. $>= 3$) of the blade passage frequency response can be characterized and lend towards development of better prediction tools. Its also possible that prior rotor noise characterizations were not able to detect and separate the sources of acoustic phenomena that appear as the same integrated result, but with high resolution blade pressure distributions, its speculated this will indeed be possible. Exploitation of to-be-determined aeroacoustic relationships could lead to qualitatively and quantitatively lower (perceived) noise emissions from rotors. The results of Phase 2 will also intend to show that there is a clear and discreet relationship between an aerodynamic source and an acoustic observation – a characterization that would be a first of its kind.

Lastly, Phase 3 will showcase an ability to demonstrate the more clearly "extracted" physics uncovered by the results of Phases 1 and 2. An application case will be selected (based on the feasibility of what could successfully be demonstrated) where the lessons learned in the controlled studies are implemented in the assessment of noise from an integrated system. Examples of such a system could be a flying drone, a large-scale multicopter model, or a flight test. Having previously identified the aeromechanical means in which noise is generated via rotor operation in dynamic flight conditions, there is the potential for demonstrating the reduction of a rotor's aeroacoustic signature noise (or, equally important, its psychoacoustic impression) via these experiments. Depending on the results of Phase 3, the lessons learned may be able to inform regulatory bodies on the mechanics and propagation of rotor noise and where commercial and hobby UAS vehicles may be restricted to flying within urban areas. The results of this study can also help substantiate a public repository on rotor noise for different geometric and aerodynamic conditions.

References

[1] EASA. Study on the societal acceptance of urban air mobility in europe. *Technical report, European Union Aviation Safety Agency (EASA)*, 2021. https://www.easa.europa.eu/full-report-study-societal-acceptance-urban-air-mobility-europe.

[2] F.d. Monteiro, R. Merino-Martínez, and L. T. L. Pereira. Psychoacoustic evaluation of an array of distributed propellers under synchrophasing operation. *30th AIAA/CEAS Aeroacoustics Conference*, 2024.

[3] A. Piccolo, R. Zamponi, F. Avallone, and D. Ragni. Towards a novel physics-based correction to amiet's theory for inflow-turbulence noise prediction. *30th AIAA/CEAS Aeroacoustics Conference*, 2024. https://doi.org/10.2514/6.2024-3121.

[4] W. Lang, A. Gardner, S. Mariappan, C. Klein, and M. Raffel. Boundary-layer transition on a rotor blade measured by temperature-sensitive paint, thermal imaging and image derotation. *Experiments in Fluids*, 56:1–14, 2015. https://doi.org/10.1007/s00348-015-1988-5.

[5] A. Watkins, B. Leighty, W. Lipford, K. Goodman, J. Crafton, and J. Gregory. Measuring surface pressures on rotor blades using pressure-sensitive paint. *AIAA Journal*, 54:206–215, 2016. https://doi.org/10.2514/1.J054191.

[6] J. Gregory, H. Sakaue, T. Liu, and J. Sullivan. Fast pressure-sensitive paint for flow and acoustic diagnostics. *Annual Review of Fluid Mechanics*, 46:303–330, 2014. https://doi.org/10.1146/annurev-fluid-010313-141304.

[7] J. Gössling, T. Ahlefeldt, and M. Hilfer. Experimental validation of unsteady pressure-sensitive paint for acoustic applications. *Experimental Thermal and Fluid Science*, 2020. https://doi.org/10.1016/j.expthermflusci.2019.109915.

[8] K. Disotell and J. Gregory. Measurement of transient acoustic fields using a single-shot pressure-sensitive paint system. *The Review of Scientific Instruments*, 82, No. 7:75–112, 2011. https://doi.org/10.1063/1.3609866.

[9] J. Li, N. Roozeboom, E. Lara Lash, M. Shaw-Lecerf, J. Baerny, T. Garbeff, L. Hand, C. Henze, D. Murakami, and N. Smith. Aeroacoustic analysis using dynamic mode decomposition of unsteady pressure-sensitive paint measurements. *AIAA SciTech Forum*, 2024. https://doi.org/10.2514/6.2024-0882.

[10] K. Nakakita and H. Ura. Aeroacoustic noise source identification using unsteady psp and microphone correlation measurement. *AIAA SciTech Forum*, 2020. https://doi.org/10.2514/6.2020-0513.

[11] C. Klein, U. Henne, W. E. Sachs, S. Hock, N. Falk, V. Ondrus, U. Beifuss, and S. Schaber. *Pressure Measurement on Rotating Propeller Blades by Means of the Pressure-Sensitive Paint Lifetime Method*, pages 535–544. Springer International Publishing, Cham, 2014.

[12] V. Kulesh, V. Mosharov, A. Orlov, S. Ostroukhov, and V. Radchenko. Application of pressure sensitive paint for determination of aerodynamic loads and moments on propeller blade. In *Optical Methods of Flow Investigation, Proceedings of SPIE, vol. 6262*, 2006. https://doi.org/10.1117/12.683025.

[13] A. Weiss, R. Geisler, T. Schwermer, D. Yorita, U. Henne, C. Klein, and M. Raffel. Single-shot pressure-sensitive paint lifetime measurements on fast rotating blades using an optimized double-shutter technique. *Experiments in Fluids*, 58:1–20, 2017. https://doi.org/10.1007/s00348-017-2400-4.

[14] Y. Egami, Y. Sato, and S. Konishi. Development of sprayable pressure-sensitive paint with a response time of less than 10 μs. *AIAA Journal*, 2019. https://doi.org/10.2514/1.J057434.

[15] K. Disotell, D. Peng, T. Juliano, J. Gregory, J. Crafton, and N. Komerath. Single-shot temperature- and pressure-sensitive paint measurements on an unsteady helicopter blade. *Experiments in Fluids*, 55:1–15, 2014. https://doi.org/10.1007/s00348-014-1671-2.

2.3 Session 222: Wind resources, turbulence, and acoustics

25.09.2024, 15:10, Room 2

Chair:

Thea Vanelli

Presenters:

Topić Roko	Assessment of modelling strategies on complex and forested terrains
Hernandez Alan	Optimization of the WRF configuration for accurately predicting operational wind farm data
Silva Caballero Adrián	Wind flow dynamics under extreme situations in complex terrains
Hamzeloo Sima	Investigation of wind-wave interaction on Marine Atmospheric Boundary Layer: One-Way Coupling between MIKE 3 wave and WRF-LES
Menken Julia	Impact of atmospheric turbulence and stability on wind turbine wakes measured with a nacelle lidar at WiValdi

20^{th} EAWE PhD Seminar on Wind Energy
24-26 September 2024
Visby, Sweden

Assessment of modelling strategies on complex and forested terrains

Roko Topić

Wind Energy Section, Uppsala University

E-mail: rokkotopic@gmail.com

Keywords: flow modelling, complex terrain, atmospheric stability

Estimating wind resources and wind park efficiency is crucial for both the financial and environmental sustainability of a wind energy facility. Additionally, accurately describing wind flow within a wind park is important for addressing the operational capabilities of a wind turbine. This is usually represented by numerical models that simulate the interactions between the airflow and the turbines on selected temporal and spatial scales.

Forests and mountains present significant challenges for parameterization in modeling setups due to their complexity and impact on wind flow [1]. The variations in atmospheric stability throughout the diurnal cycle further complicate this [2]. Consequently, when assessing the wind potential of these complex sites, the wind industry often makes compromises and simplifies these features. The effects of these simplifications on evaluating the performance and production of wind parks are largely overlooked and not well understood.

Therefore, this PhD project will focus on assessing the consequences of simplifying features such as the representation of topography and terrain, including elevation differences, forest distribution, and leaf density.
Additionally, it will evaluate the outcomes of forecasting wind flows when compromises are made in atmospheric conditions, such as considering discrete stability regimes instead of continuous transitions during diurnal cycles.

To demonstrate this, results from Large-Eddy Simulations (LES) performed using the OpenFOAM framework will be directly compared to observed on-site wind load values. This will enable accuracy and reliability evaluation of wind load representation for models with simplified terrain, forest, and stability features, as well as for more complex models where these features are represented more robustly. The ultimate goal is to improve load prediction and make wind farm planning more viable in the future.

References

[1] Mahmoud Elgendi, Maryam AlMallahi, Ashraf Abdelkhalig, and Mohamed Y.E. Selim. A review of wind turbines in complex terrain. *International Journal of Thermofluids*, 17, 2023.

[2] C. Pérez Albornoz, M.A. Escalante Soberanis, V. Ramírez Rivera, and M. Rivero. Review of atmospheric stability estimations for wind power applications. *Renewable and Sustainable Energy Reviews*, 163, 2022.

20th EAWE PhD Seminar on Wind Energy
24-26 September 2024
Visby, Sweden

Optimization of the WRF configuration for accurately predicting operational wind farm data

A.S. Hernández-Acosta[a], **E. Ramos**[a], and **C.A. López-Villalobos**[*a]

[a]Instituto de Energías Renovables, Universidad Nacional Autónoma de México
E-mail*: calovi@ier.unam.mx

Keywords: PBL, LSM, complex terrain, WRF, power

Wind energy prediction over complex terrain is a challenging task because of the difficulty of describing atmospheric flux interaction with the land surface topography. A versatile and widely used tool in atmospheric research and operational forecasting is the Weather Research and Forecasting (WRF) model. However, this model relies on a configuration that encompasses different Planetary Boundary Layer (PBL) and Land Surface Model (LSM) schemes to describe the physics near the surface. This work aims to optimize the configuration of the WRF model by evaluating the impact of the PBL and LSM schemes using different vertical levels to obtain the best representation of the wind field to calculate the power production of a wind farm located in the complex terrain at La Rumorosa, Baja California, Mexico. The best statistical metrics are obtained by coupling the Mellor-Yamada-Nakanishi–Niino (MYNN) PBL scheme with the Noah-Multiphysics LSM and utilizing 61 vertical levels. This setup is used in the assessment of the wind farm performance, increasing the accuracy of power prediction.

1 Introduction

Although there is wind technological maturity, there is a need to improve the understanding of the atmospheric wind flow to have reliable production systems, which requires increased accuracy and detail about turbulence, shear, extreme-large-scale events, and features related to the terrain [2]. A convenient and affordable method to obtain useful wind data is Numerical Weather Prediction (NWP) models [1]. However, the results obtained with NWP models are highly dependent on the ability of the model to represent and simulate the processes in the PBL correctly. Besides, near the land, transfer coefficients are usually estimated using the Atmospheric Surface Layer (ASL) scheme. Analogously, the fluxes occurring in the soil are estimated by Land Surface Models (LSM). It should be added that the surface information calculated by the ASL and LSM schemes serve as a basis for the PBL scheme, which estimates the vertical variation of the wind field.

Therefore, we present a sensitivity analysis of the different WRF PBL schemes and two different resolutions of the lower part of the atmospheric boundary layer in La Rumorosa, Baja California, Mexico, which is a region with complex terrain. Daily simulations were carried out with a spatial resolution of 3 km. The results are compared with data from an anemometrical mast in order to determine the optimal vertical levels, WRF-PBL, and WRF-LSM scheme. Additionally, in a test case scenario, the best WRF configuration model is used to estimate wind power production. The results are compared against field wind power production of a wind farm located in La Rumorosa.

2 Field wind and wind turbine performance data

The site where the atmospherical data and wind turbine efficiency from a five-turbine wind farm are taken is in the northern extreme of the Baja California peninsula in northwestern Mexico (see Figure 1).

Measured data with a resolution of 10 minutes were obtained from a meteorological mast (M01) located at La Rumorosa (32°28′50.5″N, 116°06′46.7″W). The horizontal wind speeds were measured at four heights: 80, 60, 40, and 20 m. The wind direction was measured at 58 and 78 m. The field data is one hour averaged to be compared with the WRF model results.

Operational wind turbine data is obtained from a wind power plant. The farm is located at 1350 meters above sea level and is composed of five Gamesa G87/2000 wind turbines with a nominal power output of 2 MW, a rotor diameter of 87 m, and a hub height of 78 m above surface level. The data sampling in each turbine consists of a 10-minute time series of wind power and wind speed and direction measured by anemometers at each turbine.

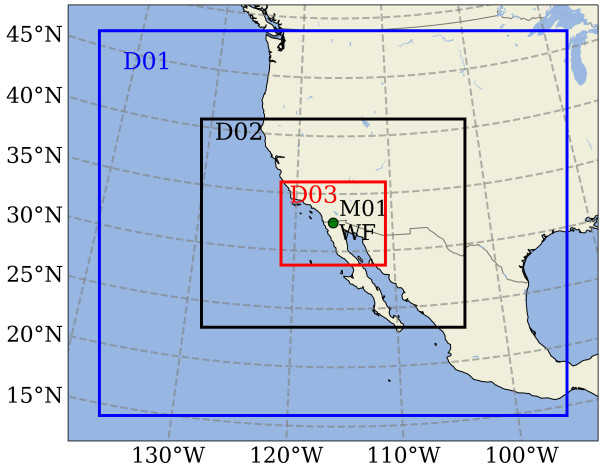

Figure 1: WRF domains and locations of M01 tower and wind farm.

3 WRF Set-Up and tests

Figure 1 shows the three domains centered at the M01 meteorological mast. The spatial resolutions of the domains labeled D01, D02, and D03 are 27, 9, and 3 km, respectively. D01 was designed to capture the large-scale wind patterns that influence the wind behavior of the site of interest. Hence, it extends into the Pacific Ocean and captures part of the Gulf of Mexico. D02 is expected to be a smooth transition between the largest and smallest domains. The innermost domain, D03, is employed to compare with the measured data.

The WRF model was set up to run for February 2018. Using the parameters suggested in the New European Wind Atlas (NEWA) calculations [3] and taking ERA5 data as initial and boundary conditions.

In order to evaluate the impact of the vertical levels and the different PBL and LSM schemes, several tests with different WRF model configurations are proposed. The setup for each test is shown in Table 1.

4 Methods to evaluate the WRF model

The accuracy of WRF model set-ups is evaluated by measuring the difference between the WRF outputs and measured values. The metrics employed are root mean squared error (RMSE), Bias, and Pearson Correlation Coefficient (PCC). RMSE evaluates the quality of predictions by measuring the Euclidean distance between the WRF prediction and the observed wind speed. Bias and PCC account for the degree of relationship between the predicted WRF model and the measured atmospheric wind flow.

Table 1: Test configurations: the first column refers to the name of the test. The second and third columns refer to the Planetary Boundary Layer (PBL) schemes and Land Surface Model (LSM) schemes used. The last column means the full σ-levels.

Test name	PBL scheme	LSM	σ-levels
MYNN_44L	MYNN2	Noah	44
MYJ_44L	MYJ	Noah	44
YSU_44L	YSU	Noah	44
MYNN_61L	MYNN2	Noah	61
MYJ_61L	MYJ	Noah	61
YSU_61L	YSU	Noah	61
MYNN_61L_MP	MYNN2	Noah-MP	61
MYJ_61L_MP	MYJ	Noah-MP	61
YSU_61L_MP	YSU	Noah-MP	61

Table 2: Pearson coefficient, RMSE and bias for nine combinations of PBL, LSM schemes and vertical level numbers at 40, 60, and 80 meters. See Table 1 for nomenclature.

	40 m			60 m			80 m		
	Pearson	RMSE	Bias	Pearson	RMSE	Bias	Pearson	RMSE	Bias
MYNN_44L	**0.800**	**2.229**	0.411	0.789	2.530	0.657	0.788	2.639	0.684
MYJ_44L	0.791	2.262	0.505	0.782	2.518	0.770	0.780	2.641	0.793
YSU_44L	0.792	2.295	0.604	0.788	2.469	0.677	0.785	**2.578**	0.676
MYNN_61L	**0.800**	2.451	0.774	**0.802**	2.564	0.785	**0.803**	2.667	0.805
MYJ_61L	0.791	2.350	0.723	0.785	2.552	0.842	0.779	2.708	0.905
YSU_61L	0.782	2.364	0.596	0.777	2.549	0.687	0.771	2.698	0.739
MYNN_61L_MP	0.797	2.339	**0.400**	0.800	2.473	**0.444**	0.802	2.579	**0.482**
MYJ_61L_MP	0.776	2.740	1.153	0.773	2.954	1.313	0.774	3.093	1.420
YSU_61L_MP	0.796	2.240	0.457	0.793	**2.424**	0.572	0.787	2.581	0.639

5 Results

5.1 Sensitivity of Planetary Boundary Layer (PBL), Land Surface Model (LSM) schemes and vertical levels

Table 2 shows the statistical metrics for the tests at 40, 60, and 80 meters, where field data are available from an anemometrical mast. In all cases, the best results are obtained for MYNN, except for the RMSE metric corresponding to 60 and 80 m, where the YSU scheme leads to a substantially better result. For all schemes, using a larger number of vertical levels has a lower impact on Pearson and RMSE metrics. However, when the Noah-Multiphysics LSM is added to the MYNN scheme with 61 $\sigma-$levels, the bias is significantly reduced (0.4 m/s for all heights).

5.2 Test Case

To evaluate the performance of the optimal configuration identified in the previous section, two simulations were carried out. The first one is the control test with the default parameters of WRF, and the second corresponds to MYNN_61L_MP. The cases are labeled *default* and *test*, respectively. There are two major differences between the two configurations. The first one lies in the number of vertical levels, being 44 for the default and 61 for the test case. The second difference is the LSM used, being NOAH for the default case and NOAH-MP for the test case. Two specific times were chosen to analyze, t_1=06:00:00 2020-02-27, and t_2=18:00:00 2020-02-29 local time. This pair was chosen because the wind speed difference is small (<0.7 m/s), but the direction is almost opposite (181°) as it is described in Table 3. As mentioned in previous sections, the study was focused in La Rumorosa, which is a region with irregular topography and was chosen because of the availability of data.

Cross-sections of terrain profiles and velocity fields are shown in Figure 2. Land formations are represented by black regions. The cross-sections are parallel to the wind flow direction in each case, and the wind turbine rotors are oriented facing the wind. Figures 2 a) and b) correspond to t_1 and the differences between default and test cases configurations can be compared. The dynamics shown in Figures 2 a) and b) have similar features except for a larger low velocity region on the front side of the hill calculated with the default configuration. The flow circumvents the obstacle and runs downhill with the relatively large velocity. For the two configurations, the wind speed at the wind farm site is approximately 9 m/s. For the second time analyzed, t_2, the wind velocity fields are shown in Figures 2 c) and d). The wind enters from the left and accelerates going downhill after reaching the top of the hill. Note that this effect is also influenced by the fact that the profiles of the hills are not exactly the same. The main difference between the two configurations is that the test set-up yields a higher wind speed at the wind farm site (approximately 10 m/s) than the default simulation (approximately 9 m/s).

The instantaneous measurements of a single wind turbine of the five ones that compose the wind farm are compared to the results using different setups (see Table 3). For February 27th, the wind velocity and direction obtained by default simulation are higher than the observed. Therefore, the difference in power production is lower using the test configuration, where the wind speed and direction are better predicted. Besides, for February 29th, the wind speed was underestimated by the default simulation, and the wind direction deviated more. For this instant, the wind speed given by the test simulation is very close to the measured. Again, the power output difference is significantly lower when is used the test configuration (about 15% better).

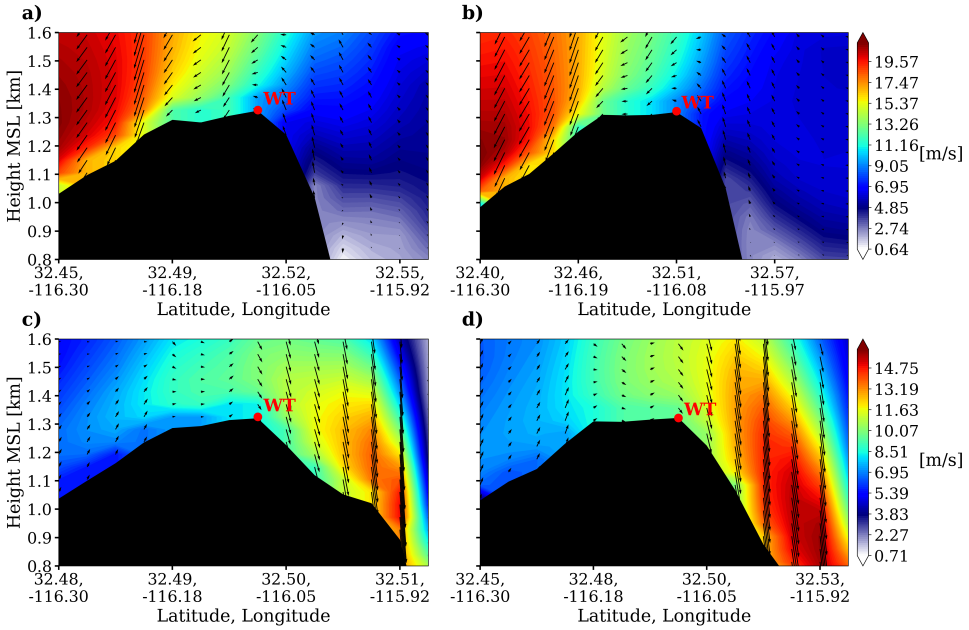

Figure 2: Cross section for wind speed. a) and b) correspond to t_1=06:00:00 2020-02-27. c) and d) correspond to t_2=18:00:00 2020-02-29. a) and c) were obtained using the default set-up. b) and d) were obtained by using the test set-up.

Table 3: Performance of default and test configurations compared with field data.

	t_1=06:00:00 2020-02-27			t_2=18:00:00 2020-02-29		
	Field data	Default	Test	Field data	Default	Test
Wind speed [m/s]	9.73	10.81	9.77	10.37	9.41	10.27
Direction [°]	45.47	73.06	61.06	226.58	267.37	256.06
Power output [kW]	1030.09	1337.95	987.01	1243.27	999.93	1299.04
Power difference [%]		29.89	4.18		19.57	4.49

6 Conclusions

Results were presented using different WRF model configurations to improve the reproduction of wind power over complex terrain in La Rumorosa, Mexico. The vertical levels number, PBL, and LSM scheme are sensitive parameters within the WRF model for wind flow prediction; therefore, these variables were explored for optimal WRF configuration. It was found that the optimal configuration for this site was coupling the MYNN 2.5 PBL and NOAH-MP LSM schemes with 61 vertical levels.

The results using the optimal configuration show a power production maximum error of 4.5% compared to the field data. This is a substantial improvement on the 30.0% maximum error for power production obtained with the default configuration.

References

[1] S. Al-Yahyai, Y. Charabi, and A. Gastli. Review of the use of Numerical Weather Prediction (NWP) Models for wind energy assessment. *Renewable and Sustainable Energy Reviews*, 14:3192–3198, 2010.

[2] P. Veers, K. Dykes, E. Lantz, S. Barth, C. L. Bottasso, O. Carlson, A. Clifton, J. Green, P. Green, H. Holttinen, et al. Grand challenges in the science of wind energy. *Science*, 366:eaau2027, 2019.

[3] B. Witha, A. Hahmann, T. Sīle, M. Dörenkämper, Y. Ezber, E. García-Bustamante, J. F. González Rouco, G. Leroy, and J. Navarro. Report on WRF model sensitivity studies and specifications for the mesoscale wind atlas production runs. 2019.

20th EAWE PhD Seminar on Wind Energy
24-26 September 2024
Visby, Sweden

Wind flow dynamics under extreme situations in complex terrains

Adrián Silva Caballero[a]

[a]Uppsala University — Department of Earth Sciences

E-mail: adsic12358@gmail.com

Keywords: Onshore Wind Farms, Atmospheric Boundary Layer, Turbulent Flows, Complex Terrains, Large Eddy Simulations

The progressive increase of wind turbine projects in recent years, coupled with the escalating development of onshore wind farms under forests, has led to the exploration of less comprehended atmospheric regions, necessitating a more thorough understanding. Specifically, the intricate interactions occurring between turbulent flows over complex terrains, and the top of the atmospheric boundary layer (ABL) need to be deeply investigated to significantly improve the precision and understanding of how does these adverse conditions affect the operation life and maintenance of the wind turbines elements, in order to be able to predict and minimise their impacts on wind farms.

Forested regions have been increasingly seeked by stakeholders for wind projects, as their costs are lower than offshore projects and the wind project's public negative view of not in my backyard is minimized. Nonetheless, they are characterized by complex terrains, in terms both of topography and terrain, which increase the overall rugosity of the terrain and escalate the extreme events number in the ABL, consequently increasing the loads experience by the wind turbine's components. In order, to properly understand how the turbulence flow in the ABL changes over time under these complex terrains does, this research proposes conducting Computational Fluid Dynamics (CFD) simulations, in particular Large Eddy Simulations (LES) to predict and understand the underlying aerodynamic and meteorological phenomena. Emphasis will be placed to develop modelling techniques to capture the most relevant physics to reproduce design loads aiming at reducing the number of CFD runs, where machine learning, statistical analysis and LES hold the potential to reduce the order modelling, and consequently the heavy computational costs associated with such simulations. The initial research objectives are:

- To develop advanced modelling techniques (CFD simulations) for capturing the ABL behaviour, and fluid mechanics of individual wind turbines and wind farms in complex terrains.
- To enhance understanding of design loads and extreme working conditions in complex terrain.
- To reduce computational efforts by combining Large-Eddy Simulation (LES) with machine learning techniques.
- To identify the coupling between environmental parameters and instantaneous/extreme working conditions associated with intense load events.

20th EAWE PhD Seminar on Wind Energy
24-26 September 2024
Visby, Sweden

Investigation of wind-wave interaction on Marine Atmospheric Boundary Layer: One-Way Coupling between MIKE 3 wave and WRF-LES

Sima Hamzeloo[a], **Xiaoli Guo Larsén**[a], **Alfredo Peña**[a], **Jacob Tornfeldt Soerensen**[b], and **Stephan Kistner**[b]

[a]DTU Wind and Energy Systems, Frederiksborgvej 399, 4000 Roskilde, Denmark
[b]DHI, Agern Allé 5, 2970 Hørsholm, Denmark

E-mail: siham@dtu.dk

Keywords: wind-wave interactions, WRF-LES, MIKE 3 wave, Marine atmospheric boundary layer

1 Introduction

Wind-wave interactions have a significant impact on the wind and turbulence structure within the marine atmospheric boundary layer (MABL). As a result, enhancing atmospheric flow simulations over the seas can benefit a wide range of atmospheric and engineering applications. One such example is offshore wind energy, which has been growing significantly in recent decades [2]. Wind interactions directly influence the performance and loads of offshore wind turbines. Therefore, improved models for wind-wave interactions can reduce the uncertainty in offshore wind energy simulations, ultimately enhancing financial reliability [1].

2 Methodlology

In this study, we couple the Weather Research and Forecasting model under Large Eddy Simulation mode (WRF-LES) with the MIKE 3 wave FM model. The new coupling system developed so far is one-way and offline. The purpose is to investigate WRF-LES's performance in simulating atmospheric flow within the marine atmospheric boundary layer (MABL) with underlying irregular long-crested waves generated by the M3W model. M3W generates these waves using wave spectrum parameters such as significant wave height and peak wave period. These waves from the M3W model are applied as the surface boundary condition for the WRF-LES model. The WRF-LES model simulates flow within the MABL, and we initialize it with an ideal neutral boundary layer.

3 Validation

We use the highest storm during the measurement period to test and validate the WRF-LES-M3W modeling system. For this case, we have both wave and atmospheric measurements from a site in the North Sea. Additionally, we conduct a non-coupled WRF-LES simulation with a flat surface (no waves) to study the difference when simulating the effect of waves on atmospheric flow during this storm condition over the North Sea.

4 Preliminary results

The comparison of simulated and measured wave heights in Figure 1 indicates that the M3W model accurately represents the sea state.

Figure 2 presents the simulations and measurements of the atmospheric flow for both flat and coupled simulations. This figure shows that both simulated profiles are in agreement with the measurements. However, there is a better match between measurements and the coupled model up to 150 meters for mean wind speed.

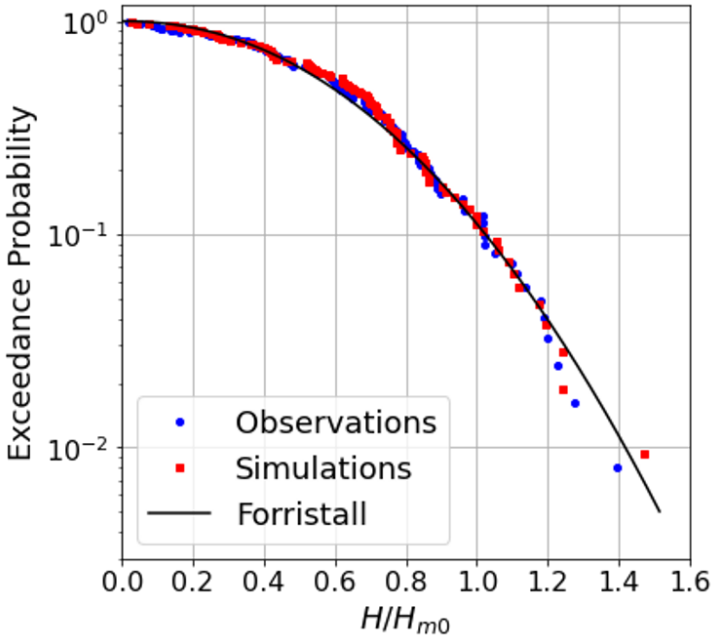

Figure 1: Wave height distribution.

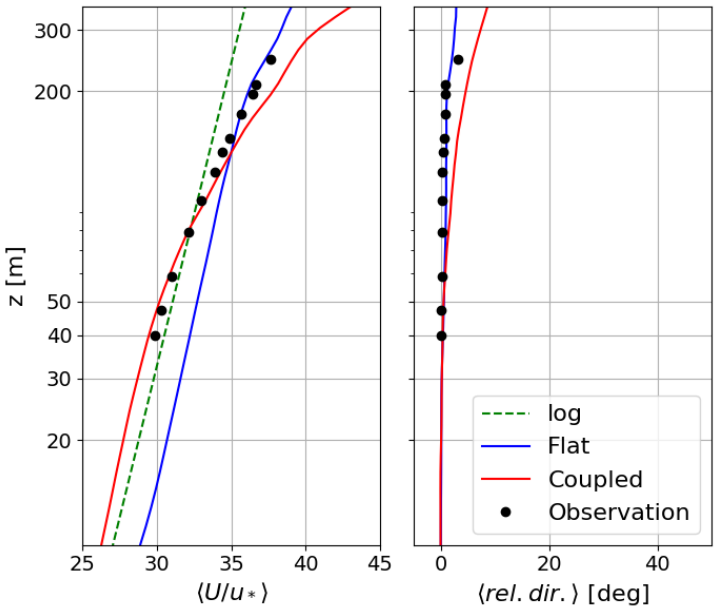

Figure 2: The vertical profiles of spatial-average of normalized wind speed (left) and relative direction (right). The logarithmic profile (log.) is also included.

5 conclusion

The comparison of simulated and measured wave heights indicates that the M3W model accurately represents the sea state. Furthermore, the simulations and measurements of the atmosphere flow for both flat and coupled simulations show good agreement. However, the coupled model aligns more closely with the measurements for mean wind speed up to a height of 150 meters.

Acknowledgements

This work is funded by the Independent Research Fund Denmark (Danmarks Frie Forskningsfond DFF) through the 'Multi-scale Atmospheric Modeling Above the Seas (MAMAS)' project. In addition, we would like to acknowledge the contribution of DHI team. Their support and expertise have greatly contributed to the success of this research.

References

[1] G. Deskos, J. C. Y. Lee, C. Draxl, and M. A. Sprague. Review of wind–wave coupling models for large-eddy simulation of the marine atmospheric boundary layer. *Journal of the Atmospheric Sciences*, 78(10):3025 – 3045, 2021.

[2] IEA. Renewables data explorer. Technical report, IEA, Paris, 2022.

20th EAWE PhD Seminar on Wind Energy
24-26 September 2024
Visby, Sweden

Impact of atmospheric turbulence and stability on wind turbine wakes measured with a nacelle lidar at WiValdi

Julia Menken[a], **Norman Wildmann**[a], and **Jeffrey D. Thayer**[a]

[a]Institute of Atmospheric Physics, Deutsches Zentrum für Luft- und Raumfahrt e.V., Oberpfaffenhofen, Germany

E-mail: julia.menken@dlr.de

Keywords: nacelle lidar, turbine wake, field observations, turbulence, atmospheric stability

1 Introduction

One of the challenges in wind energy is the impact of turbine wakes, i.e. the flow behind a wind turbine (WT) characterized by reduced wind speeds and increased turbulence. These wakes can substantially affect the performance of downstream turbines, leading to reduced overall efficiency and increased loads on the turbine. Accurate wake measurements are essential for validating and refining engineering models used to predict wake behavior, optimize wind farm layouts, and improve overall energy yield. Engineering wake models, while computationally efficient, often rely on simplified analytical formulas to describe wake deficits, limiting their ability to fully resolve the complex turbulent structures within the wake.

For validation and improvement of these models, field measurements provide valuable data. Probing the atmosphere in and around wind farms aids to understanding wake dynamics and their interaction with the atmospheric boundary layer (ABL). Remote sensing techniques like light detection and ranging (lidar) mounted on the nacelle of a turbine have proven to be powerful tools for measuring wind turbine wakes [1]. Unlike traditional in-situ measurements, such as those from meteorological masts, nacelle-mounted lidars can capture the wind field over large areas with high spatial and temporal resolution, providing a more comprehensive understanding of wake dynamics.

Both experimental and numerical investigations have highlighted that atmospheric stability significantly affects the evolution of wind turbine wakes. Stable atmospheric conditions tend to result in longer, more pronounced wakes with higher velocity deficits and increased turbulence intensities. Conversely, unstable conditions promote faster wake recovery and dispersion due to stronger mixing within the ABL [2]. The influence of atmospheric turbulence is also significant, with higher turbulence levels leading to faster wake recovery and more rapid dissipation of the wake [3].

To more efficiently use the space required for a wind farm the spacing between the wind turbines can be reduced which makes understanding and modeling the near-wake region crucial. Located immediately downstream of the turbine, the near-wake region is characterized by highly turbulent and complex flow structures caused by tip and root vortices [4]. This region has a significant impact on the wake recovery process and characterizing the near-wake is essential for understanding the transition to the far-wake. However, engineering wake models currently do not sufficiently take into account the processes in the near-wake.

My study aims to measure wind turbine wakes under different atmospheric conditions using a nacelle-mounted lidar. In particular, I will analyze the effects of atmospheric stability and turbulence on wake dynamics and additionally focus on the near-wake. Data will be collected from the research wind farm WiValdi including data from a nacelle lidar, a ground-based lidar, a microwave radiometer, in-situ observations from meteorological masts and data from the turbines themselves.

Within my work I would like to work on the following research questions:

- How do atmospheric stability and turbulence influence the structure, propagation, and dissipation of wind turbine wakes, and how can these effects be measured using nacelle-mounted lidar?
- What are the defining characteristics of the near wake of a wind turbine, and at what point does the transition from the near wake to the far wake occur?

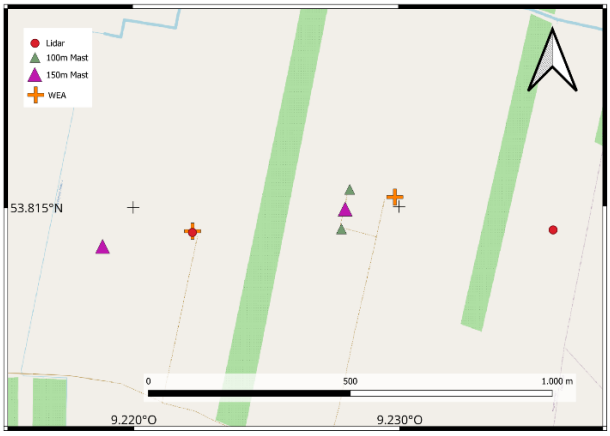

Figure 1: Map of the WiValdi research park

2 Methods

The research wind farm WiValdi in North Germany features two utility-scale WTs with a total height of 150m and a rotor diameter of 116m. One of them is located in the wake of the other turbine in the main wind direction. This offers a unique possibility to study the impact of WT wakes and their interaction. The two WTs are accompanied by an inflow mast of 150m height upstream of the turbines and by a set of three measurement masts, the mast array, located between the two WTs (Fig. 1). All masts are equipped with wind-measuring sensors at different heights and the inflow mast (conforming to IEC-61400) additionally with sensors to measure further atmospheric parameters, like temperature, humidity, and rain. From this data, stability and turbulence characteristics of the atmosphere can be determined. In addition, a microwave radiometer yields measurements of stability further east of the two turbines.

We operate two Doppler wind lidars of the type Leosphere Windcube 200s in the wind farm. One serves as a ground-based profiling lidar yielding statistics about wind and turbulence. The other is mounted on the nacelle of the turbine which is in the main wind direction in front of the second WT. The nacelle-mounted lidar measures the wind field behind the rotor which is affected by the WT wake. Plan position indicator (PPI) scans (Tab. 2) have been performed for our long-term scanning strategy since November 2023 to capture the main wake properties. Three different elevation angles of $-7°$, $0°$ and $7°$ are chosen to cover the vertical extent of the wake across the rotor area at 4D downstream. The azimuth angle has a total opening angle of $90°$ and a resolution of $2°$. With this strategy the total time for one complete scan takes about 27s.

To reduce noisy and erroneous measurements, the lidar data is filtered to use only data with CNR values between -25 and 5dB. To make the filtering even more robust, a 2D median filter is applied to the CNR values and radial velocities. A robust algorithm for detecting and describing wakes is essential for investigating wake characteristics under different atmospheric conditions. As has been shown before [5], the horizontal structure of a wake can be described by a Gaussian function (Eq. 1) in the far wake, where the impact of the rotor is less relevant

Parameter	Value
Physical resolution	50m
Range gate separation	20m
Min. range gate	100m
Max. range gate	4080m
Azimuth opening angle	90°
Elevation angles	-7, 0, 7°
Angular resolution	2°
Accumulation time	200ms

Table 1: PPI scan settings

for the shape of the wake.

$$u(x) = A \exp - \frac{(x-b)^2}{2\sigma^2} + d \tag{1}$$

$u(x)$ is the function of horizontal wind speeds in dependency of the position x, A the amplitude, b the maximum position, σ the standard deviation and d an additional offset.

Closer to the WT, in the near-wake, the rotor shape is important for the structure of the wake and it can typically be approximated by a double Gaussian shape (Eq. 2).

$$u(x) = A \left[\exp - \frac{(x-b_1)^2}{2\sigma^2} \exp - \frac{(x-b_2)^2}{2\sigma^2} \right] + d \tag{2}$$

where $b1$ and $b2$ are the respective center positions and σ is the same standard deviation for both overlapping functions.

For each distance downstream starting at the minimum range gate of 100m, both functions are fitted to the data to determine the wake center, wake width, and the wind velocity deficit. To decide which function best fits the wake structure, an extra-sum-of-squares F-test is used. For the first distance, the wake center initial guess is set to be at the WT position itself, and for the subsequent distances the wake center from the prior distance is used [6]. The wake detection stops once the fit to Equations 1 or 2 is impossible or one of the following conditions is met:

- the detected wake center plus wake width is out of bounds of the observed region in x-direction,
- the difference of the wake position of two succeeding wake centers is greater than 3 times the grid distance in x-direction (10m)
- the amplitude A is smaller than $1\,\mathrm{m\,s^{-1}}$
- σ is greater than 2 rotor diameters

Additionally, the first wake detection should be valid close to the WT (200m), otherwise the whole case is neglected.

3 Preliminary Results and Outlook

The collected Doppler wind lidar measurements provide a rich data set for the detailed analysis of WT wakes under different atmospheric conditions. Preliminary analyses show promising insights into the spatio-temporal dynamics of these phenomena. Our study will involve filtering of the nacelle-mounted lidar data, applying the Gaussian wake algorithm to detect wakes and their characteristics, and retrieving atmospheric characteristics like stability and turbulence from other remote sensing and in-situ measurements at the wind farm. An example of a wake measurement downstream from the nacelle-mounted lidar is displayed in Figure 2. The WT with the lidar are located at the zero point. It shows radial wind speeds on the 13.02.2024 averaged over 30 minutes, with the detected wake center line along with the outer lines indicating the wake width. In this case, the wake could be detected about 17 rotor diameters downstream. We will then perform an analysis of wake decay under different conditions of atmospheric stability and background turbulence to understand the complex interactions between turbulent flows and WT wakes.

To investigate the near-wake, the measurements at WiValdi need to be adapted, as the standard measurements do not resolve the wake high enough and the nacelle lidar itself only measures radial wind speeds, which requires assumptions to derive wake parameters. Therefore, a ground-based lidar will be configured to determine the three-dimensional extent of the wake together with the nacelle lidar. Additional measurements at several points inside the wake will be carried out using a fleet of unmanned aerial systems (UAS) that measures wind, turbulence, temperature and pressure with high temporal resolution. UAS have already been successfully used before to study wake dynamics [7]. This data set enables to study the turbulent processes in the near wake and the transition to decaying blade tip vortices in the far wake in detail.

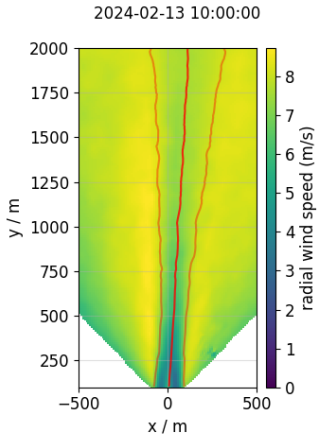

Figure 2: Time-averaged wind field with wake center line and wake width

Acknowledgements

The research was carried out in the framework of the projects DFWind2 (FKZ 0325936A) and NearWake (FKZ 03EE3097B) funded by the German Federal Ministry for Economic Affairs and Energy (BMWK) based on a resolution of the German Bundestag.

References

[1] M. L. Aitken and J. K. Lundquist. Utility-scale wind turbine wake characterization using nacelle-based long-range scanning lidar. *Journal of Atmospheric and Oceanic Technology*, 31(7):1529–1539, 2014.

[2] E. Machefaux, G. C. Larsen, N. Troldborg, M. Gaunaa, and A. Rettenmeier. Empirical modeling of single-wake advection and expansion using full-scale pulsed lidar-based measurements. *Wind Energy*, 18(12):2085–2103, 2014.

[3] M. Abkar, A. Sharifi, and F. Porté-Agel. Wake flow in a wind farm during a diurnal cycle. *Journal of Turbulence*, 17(4):420–441, 2016.

[4] F. Porté-Agel, M. Bastankhah, and S. Shamsoddin. Wind-turbine and wind-farm flows: A review. *Boundary-Layer Meteorology*, 174(1):1–59, 2019.

[5] M L. Aitken, Robert M. Banta, Yelena L. Pichugina, and Julie K. Lundquist. Quantifying wind turbine wake characteristics from scanning remote sensor data. *Journal of Atmospheric and Oceanic Technology*, 31(4):765–787, 2014.

[6] N. Wildmann, S. Kigle, and T. Gerz. Coplanar lidar measurement of a single wind energy converter wake in distinct atmospheric stability regimes at the perdigão 2017 experiment. *Journal of Physics: Conference Series*, 1037:052006, 2018.

[7] T. Wetz and N. Wildmann. Multi-point in situ measurements of turbulent flow in a wind turbine wake and inflow with a fleet of uncrewed aerial systems. *Wind Energy Science*, 8(4):515–534, 2023.

TOPIC 3

Reliability, monitoring and sensing technology

3.1 Session 113: Reliability, monitoring and sensing technology

24.09.2024, 10:30, Room 3

Chair:

Keeta Chapman-Smith	

Presenters:

Zacharias Konstantin	Wind measurements in complex terrain: A combination of met mast and drone-based measurements
Lüdemann Dana Sarah	Validation of CFD simulations for urban wind flow using Wind Scanner building wake measurements
Edirisinghe Dylan S.	Development of a Computational Model to simulate the Whirling Arm Rain Erosion Rig (WARER) Experiments
Piovesan Francesco	Risk-based feasibility assessment and life cycle cost modelling of next generation wind turbine components
Leone Tiziano	Wind tunnel numerical modeling for wind farm control strategies

Wind measurements in complex terrain: A combination of met mast and drone-based measurements

Konstantin Zacharias[a], William Thielicke[b], Waldemar Huebert[b], Ulrich Mueller[b], Alexander Buchele[a]

[a] University of Applied Sciences Ansbach
[b] OPTOLUTION Messtechnik GmbH

E-mail: Konstantin.zacharias@hs-ansbach.de

Keywords: complex terrain, drone-based measurements, meteorological mast

Abstract. Wind flow measurements in complex terrain are still challenging due to inhomogeneous flow fields and high turbulence. In this study, we combined drone-based measurements with those from a meteorological mast in a complex terrain to enhance the understanding of wind flow characteristics. First, we validated our measurement drone by hovering next to the anemometers of the met mast and showed good agreement between these two techniques. The analysis of longitudinal coherence revealed a weak correlation at distances of 100 m and 200 m indicating a high complexity in the flow field. Finally, we presented an example of a meander flight path technique that indicated an expected flow pattern for the lowest leg.

1 Introduction

Wind energy plays an important role in achieving the EU's renewable energy targets and making the EU carbon neutral by 2050. Onshore wind energy expansions are leading to more wind turbines in complex terrain, which remain challenging due to their inhomogeneous wind fields and turbulence. Meteorological masts can provide high frequency measurements with a small probe volume but only at fixed locations and at several heights. To improve the understanding of flow fields in complex terrain, multiple measurement locations need to be utilized.

Currently, there are no measurement solutions that provide: low cost, accurate measurements over diverse terrain; a simple method to perform atmospheric measurements at multiple locations; high frequency measurements with minimal probe volume and long measurement duration [1]. Drone-based measurements can meet all requirements except for extended measurement duration.

In the present study we combine met tower measurements with drone-based measurements to obtain a better understanding of flow fields in complex terrain.

2 Methodology

In this section, we provide a brief overview of our previous drone validation campaign and describe the measurement setup conducted in this study.

2.1 Wind measurement drone

The drone was developed and optimized by OPTOLUTION Messtechnik GmbH. It is a multicopter drone equipped with an ultrasonic anemometer (Gill WindMaster) to measure 3D wind speeds up to 20 m/s with a sampling rate of 20 Hz. The ultrasonic anemometer is mounted 1 m away from the propellers to avoid propeller-

induced flow, as shown in Figure 1. During a measurement campaign in a wind tunnel, the 3D wind sensing capabilities of the Gill WindMaster and the effects of propeller-induced flow were tested. The measurements showed that the bias and RMSE of the Gill WindMaster are minimal and that the mount didn't influence the measurements [2].

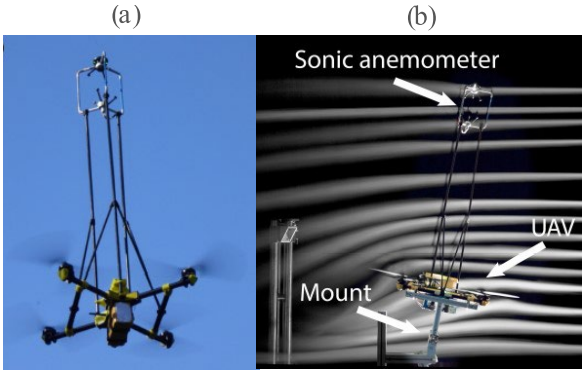

Figure 1: (a) Drone with mounted sonic anemometer during a measurement. (b) Propeller-induced flow investigation in a wind tunnel [2]

2.2 Experimental campaign

The test site is in the Black Forest, south of Freiburg and known for the complex topography. Figure 2(a) shows the elevation map of that specific area, which was derived from airborne laser scanning with a resolution of 1 m. Due to this, some artifacts remain in the figure. The met tower is indicated by a red triangle and is located on a mountain ridge with an elevation of 813 m above sea level. It is equipped with two ultra sonic anemometers (954 m a.s.l. and 913 m a.s.l.), three wind cup anemometers (960 m a.s.l., 933 m a.s.l. and 913 m a.s.l.) and a wind fan (954 m a.s.l.). The main wind direction during our measurements on 3rd May 2024 was southwest with wind speeds up to 8 m/s (see Fig. 2(b)). For this direction, the resulting terrain slope is 17° and the landscape is covered with forest.

We conducted three different measurements that are marked in Figure 2(a) and the results are presented in the following chapter.

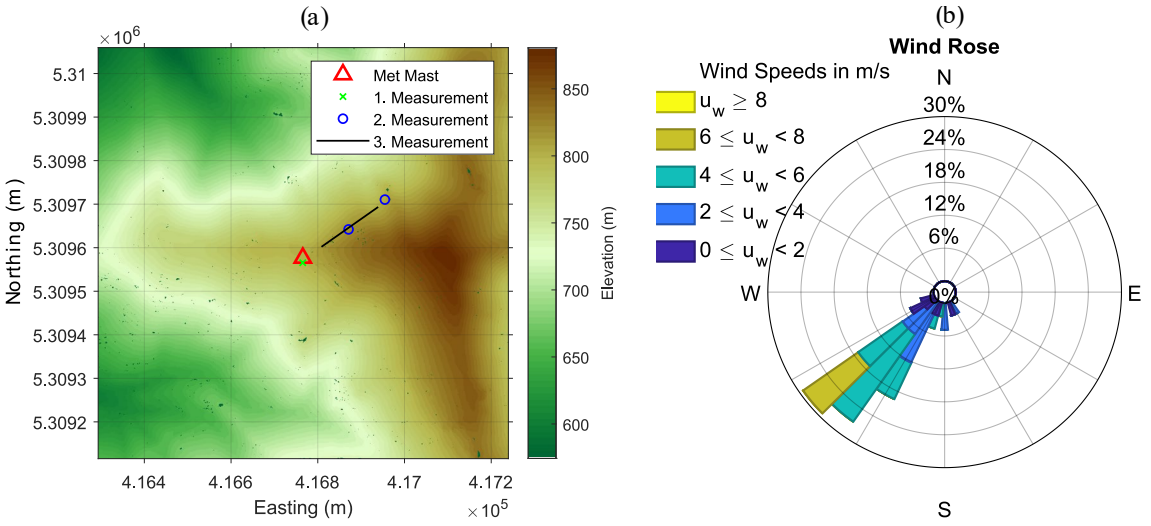

Figure 2: (a) Elevation map with marked positions of the met mast and conducted drone measurements. (b) Wind rose [3] extracted from the met mast wind vane (954 m a.s.l.) and the met mast cup anemometer (960 m a.s.l.) during all measurements.

3 Results

1. Measurement

Our first experiment aimed to validate our wind measurement drone against the meteorological mast by hovering 10 m upstream of the met tower at anemometer heights. For both cup heights we see a good agreement between our drone-based measurement and the met tower (Fig. 3), even though we used the 10 Hz data. For some reason, the met tower sonic anemometer doesn't fit well with our drone measurement. If we compare the cup anemometer on top of the tower, which is slightly higher but shifted about 5 m to the northwest direction, then we see a much better match. Although there is a slightly height shift, we consider the cup anemometer at 960 m a.s.l for the following drone measurements at 954 m a.s.l. The shift is also noticeable in longitudinal coherence (see Fig 3(a)), where we see a sharper decrease in coherence magnitude γ^2 at the frequencies compared to the other heights.

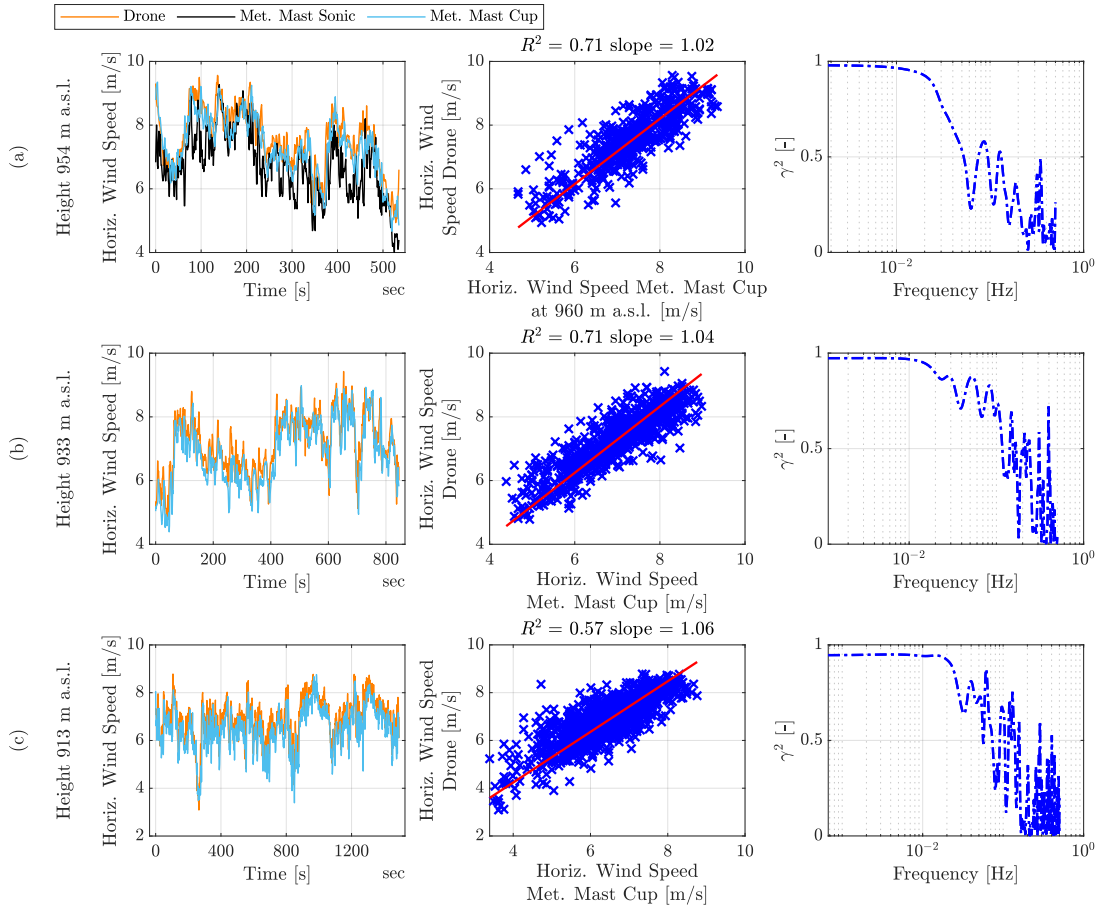

Figure 3: Comparison of horiz. wind speed between met mast and drone in 10 m distance, linear regression plot and longitudinal coherences for different heights a.s.l. (a) 954 m (b) 933 m (c) 913 m

2. Measurement

Next, we analyzed longitudinal coherences at 954 m a.s.l. at 100 m and 200 m distance (see Fig. 4(a)). Therefore, we used the data of the cup anemometer at 960 m a.s.l. as mentioned before. A coherence magnitude of γ^2=1 indicates a perfect correlation of both signals. As the longitudinal distance increases, coherent structures are expected to decrease due to the evolving of wind. Small eddies correspondence to low frequencies and decay faster than large eddies with higher frequencies. These assumptions are included in most longitudinal coherence models and were investigated by Simley et al. based on large eddy simulations [4]. For our measurements, we see a weak coherence, especially for the 100 m distance, where no decay pattern can be observed. However, for the 200 m distance we see a more expected linear decay up to 10^{-1} Hz. During our measurements, we observed a high turbulence level of TI~16% which corresponds to an increase in coherence in a low frequency range.

3. Measurement

Finally, we flew horizontal paths downstream at distances of 50-200 m from the mast, as shown in Figure 4(b). These flights followed a meandering pattern: we flew downstream for the lowest leg, then against the wind for the middle one and once again downstream for the highest leg. One meander cycle takes 150 s and we conducted in total 14 cycles. Figure 4(b) shows cycle 12 where we are nearly parallel with the wind direction during that cycle. Wind speeds are averaged within a distance of 10 m and the standard deviation is plotted as error bars. As expected, we see an increase in horizontal wind speed with higher heights as known from atmospheric boundary layer theory. Due to the steep slope of the terrain, we would expect a positive vertical wind component, which decreases to highest elevation and after that, a recirculation zone could appear behind the mountain ridge. For the lowest leg, we can see this trend in vertical wind speeds. But this could also be a transient effect. To get a clearer picture of the flow field, all cycles need to be included and averaged. This analysis is still ongoing. Furthermore, we want to use the mast data as inlet boundary for a high-fidelity simulation to confirm our measurements.

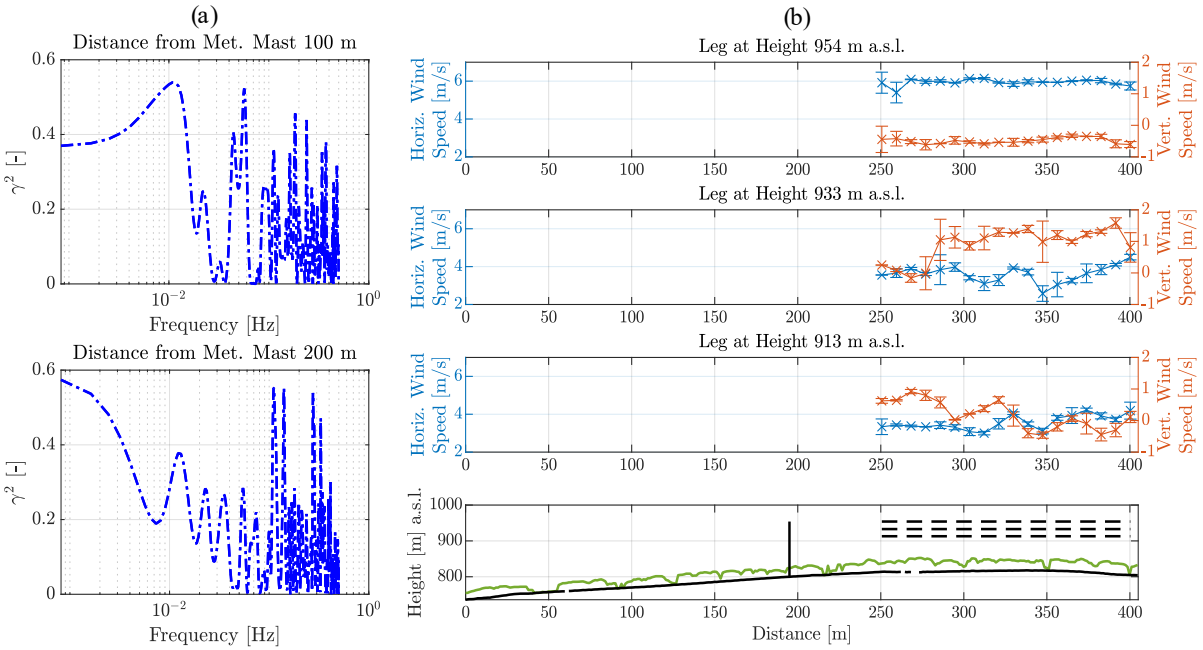

Figure 4: Longitudinal coherences of the 2. Measurement (a). Wind speeds of the meander flight path legs at different heights and elevation profile through meander path with forest height and met mast (b)

Conclusions

We can conclude that drone-based measurements can add value to wind measurements in complex terrain by providing a simple and accurate method to perform atmospheric measurements at multiple locations. By adding these measurements to static methods such as profiling lidar or a met mast, drones can enhance the understanding of wind flow characteristics in complex terrain.

References

[1] N. Vasiljevic, M. Harris, A. Tegtmeier Pedersen, G. Rolighed Thorsen, M. Rasmussen, C. B. Munk Pedersen, P. Hansen, and M. Courtney. Wind sensing with drone-mounted wind lidars: proof of concept. *Atmos. Meas. Tech.*, 13, 521–536, https://doi.org/10.5194/amt-13-521-2020, 2020.

[2] W. Thielicke, W. Hübert, U. Müller, M. Eggert, P. Wilhelm, P. Towards accurate and practical drone-based wind measurements with an ultrasonic anemometer, *Atmos. Meas. Tech.,* 14, 1303–1318, https://doi.org/10.5194/amt-14-1303-2021, 2021.

[3] D. Pereira. Wind Rose (https://www.mathworks.com/matlabcentral/fileexchange/47248-wind-rose), *MATLAB Central File Exchange*. access 6. June 2024.

[4] E. Simley and L. Y. Pao. A longitudinal spatial coherence model for wind evolution based on large-eddy simulation, *2015 American Control Conference (ACC)*, Chicago, IL, USA, pp. 3708-3714, https://doi.org/10.1109/ACC.2015.7171906, 2015.

Validation of CFD simulations for urban wind flow using Wind Scanner building wake measurements

Dana Lüdemann*[1], Niels Troldborg[2], Nikolas Angelou[3], Jan Pehrsson[4], and Ebba Dellwik[3]

[1]Technical University of Denmark, Department of Wind and Energy Systems – Denmark
[2]Technical University of Denmark, Department of Wind and Energy Systems, Frederiksborgvej 399, 4000 Roskilde – Denmark
[3]Technical University of Denmark, Department of Wind and Energy Systems – Denmark
[4]PDC-ARGOS ApS – Denmark

Abstract

In order to understand the small-scale flow around buildings and predict the wind field in urban environments, we often rely on results from computational fluid dynamics (CFD) simulations. This understanding is important for several applications such as wind resource modeling or urban wind energy exploitation, dispersion of atmospheric pollutants, as well as wind risk assessment for building design. Since urban wind field changes are characterized by abrupt and sharp gradients, it is challenging to validate the model with single-point sensors. This work aims to advance the validation of CFD simulation results and increase our knowledge in urban simulations by investigating the flow around a single building located on a sloping grass hill on DTU Risø Campus.
Another challenge in urban areas is including sufficient detail in the geometric model of the urban area. Here, we use an algorithm called Geoflow (2), which outputs a watertight geometrical model at a specified level of detail (LoD). The resulting models are then utilized in the CFD solver EllipSys (1) with a novel implementation of the immersed boundary method (IBM) (3). The simulated wind field is compared to measurements from a campaign with the DTU short-range Wind Scanner, which used continuous wave lidar to map the wake flow behind the building at a similar resolution as the numerical simulations.

Key research questions include: (1) How accurately do CFD simulations replicate observed wind flow patterns? (2) How do the LoD reconstructions influence simulation accuracy?
Expected outcomes include increasing the robustness and reliability of CFD simulations, understanding the impact of model detail, and establishing a validated approach for future urban flow and dispersion research. Improving the reliability of CFD for urban wind prediction will enable better-informed urban flow estimations and air quality modeling.

*Speaker

Development of a Computational Model to simulate the Whirling Arm Rain Erosion Rig (WARER) Experiments

Dylan S. Edirisinghe[a], Lilibeth A. Zambrano M.[a], Edmond Tobin[a], Ashish Vashishtha[a]

[a] Department of Aerospace and Mechanical Engineering,
South-East Technological University, Carlow Campus, Ireland

E-mail: ashish.vashishtha@setu.ie

Keywords: Some keywords here

1. Introduction

The Rain Erosion Test (RET) is one of the experiments conducted to determine the material degradation due to the repetition impacts of rain droplets. The RET facility, known as the Whirling Arm Rain Erosion Rig (WARER) located at Limerick University- Ireland, was particularly developed to study the wind turbines' blade erosion since eroded blades affect the turbine's performance. Figure 1 shows the WARER test facility with the zoomed 3D model to understand the droplet impact phenomenon. WARER consists of two major systems. The first system is to generate the artificial rain by randomly releasing 2 mm diameter droplets using the needles. Here rain intensity is determined by controlling the water flowrate into the system. The second system is the whirling arm holding the test specimen called 'coupon'. The coupon is a sample of wind turbine's blade coating. When the whirling arm rotates at pre-define speeds the coupon is affected with some of the droplets, damaging the coating over the time. Damage is quantified by measuring the mass loss while indicating the time takes to initiate the erosion. In addition to these two main systems, WARER is equipped with several safety gears and a cooling coil to maintain the temperature during the test period.

This study aimed to build a computational model to simulate the physical WARER test facility by identifying the erosion pattern and assign values for damage accumulation at different location of the coupon. Once the computational model is validated with the WARER experiment, the model is intended to be enhanced by incorporating real rain scenarios, which are limited in the WARER test.

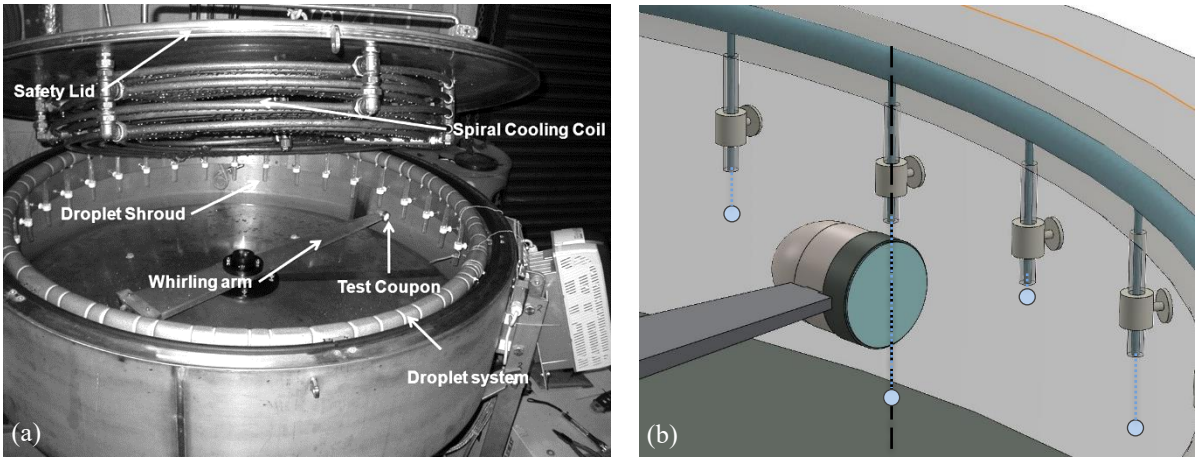

Figure 1: (a) WARER experiment facility at Limerick University-Ireland, (b) Zoom view of 2D model of whirling arm holding the test coupon and needles releasing droplet

2. Methodology

The current modelling of the WARER test developed as a python code following three main steps.

As the first steps, droplet and coupon impacts were identified by comparing the droplet releasing time and specimen alignment time under each needle whereas the impacts were recorded with their location and time. Furthermore, the regional impacting probability was observed on the specimen by dividing the specimen into five regions as shown in Figure 2. The number of impacts were observed for different periods of test time, flow rates and gaps between the needle tip and the specimen, as indicated in Figure 2.

In the second step, a pre-prepared coating material stress profile was loaded corresponding to the impact location and time. The stress profile was prepared by performing CFD study of single droplet impact in Ansys CFX and transient Structural simulations. These profiles provide the von-Misses stress variation over the impact time for each nodal point of mesh denoted by x-y-z coordinates.

In the third step, stress-time history was developed for a point of interest on the specimen considering all effective droplets impacts near that point. Then this stress-time history was prepared for fatigue analysis using the rain-flow cycle counting method and material S-N curve. Miner's rule for fatigue damage accumulation is used to quantify the possibility of erosion referred as damage intensity in this article. The third step was conducted for twelve different locations on the specimen to develop the contour map of damage intensity.

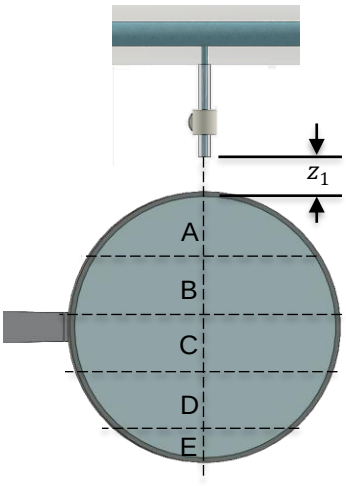

Figure 2: Regional division of the specimen and the gap between needle tip and specimen (z_1)

3. Results and Discussion

The number of impacts was observed for different test periods, flow rates and z1 gaps under the first stage, whereas the resulting impact variations are shown in Table 1. The needles were assumed to be perfectly aligned with the specimen central axis, so that the released droplets impact at the different locations on the central axis only.

When the test time increases, the total number of droplets released from the needles increase proportionally, so that the numbers of impact also increase. A similar trend can be seen in the case of increasing the flow rate. Most of these impacts happen closer to the top part of the specimen (Figure 2, Region A), having 30-33% impact probability. The other observation is that the impact probability decays from top to bottom along the central axis. In the cases of varying z1 gap, while the amount of released droplet is same, a smallest gap results in a high number of impacts, having 42% dense regional impact probability at location A. This implies that the closer the specimen to the needles, the higher the droplet impacts and intense the impact on top part of the specimen.

Table 1: Droplet impact distribution for different test times, flow rates and z_1 gaps

Variable		Test time (s)			Flow rate (ml/min)			z_1 gap (mm)		
Value		30	60	120	60	80	100	0.1	1	5
Impacted droplets		236	438	924	342	449	590	633	588	458
Impact probability (%)	P_A	32	30	33	33	33	31	42	38	30
	P_B	28	24	25	25	21	23	20	24	24
	P_C	22	21	19	16	22	19	15	17	21
	P_D	12	16	16	18	18	19	16	13	16
	P_E	7	8	7	8	7	7	7	8	9

A case study was conducted to quantify the damage accumulation strength on the specimen considering 12 sample points simulating the whole process explained in section 2. The selected case runs for 60 seconds under the flow rate of 80 ml/min for a 5 mm gap distance. Figure 3(a) shows the contour map developed using the twelve-

damage accumulation strength indicated in Figure 3(b). In each level from top to bottom, three bars represent the damage intensity where the black bar indicates the central axis, dark and light blue bars indicate the left and right side of central axis respectively. Damage intensity decreases from top to bottom, since many impacts happen at the top region, calculated in the regional impact probability. Even though the impacts happen only at the central axis, the impact effect seems to spread away to the side from the central axis showing a symmetric behaviour. This spreading effect is significant, since damage intensity of L_1 side values (2.47×10^{-5}) reached nearly to L_2 damage intensity at the central axis (2.56×10^{-5}).

The contour patten obtained from the computational model was compared with the experimented test coupon shown in Figure 3(c). The erosion pattern qualitatively matched between the experiment and modelling where the highest damage in experiment recorded at the top region of the specimen and damage is decay from top to bottom and away from the central axis.

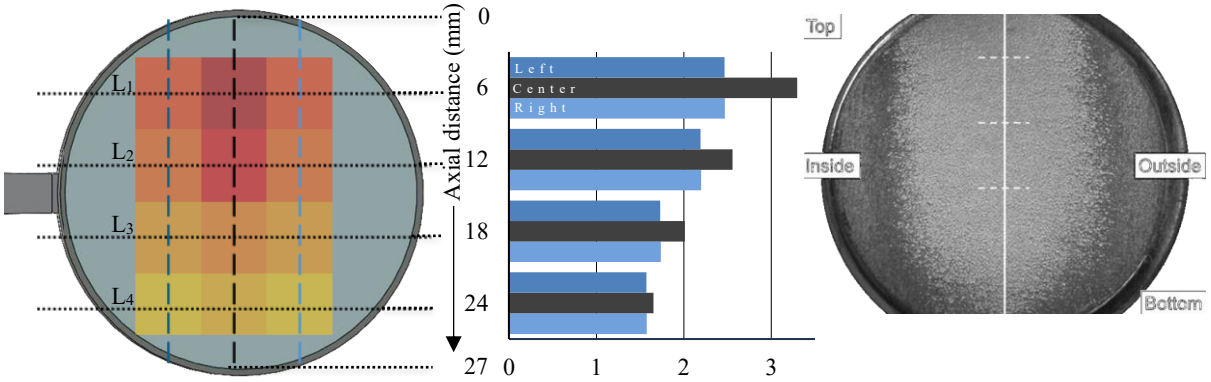

Figure 3: Left- Contour map for damage intensity, Middle- Magnitude of damage intensity, Right- Experimented test coupon

4. Conclusions

Primarily the computational model is validated for the erosion pattern with the WARER test, indicating severe erosion damage on the top region of the specimen. Furthermore, the developed damage intensity contour shows the damage intensity distribution on the specimen where the intensity decays from top to bottom and away from the central axis. Calculated damage intensities are only referred during the stage of erosion incubation period prior to the material removal. Currently, the study is navigating to validate the time taken for erosion initiation considering the experimental robustness. Once the computational model is validated both qualitatively and quantitatively reliable enough to represent the WARER experiment, the final version will be used to implement to evaluate the erosion of wind turbine's blades under real rain scenarios.

Acknowledgements

This study is supported by the Sustainable Authority of Ireland under the SEAI Research, Development & Demonstration Funding Program 2021 (Grant number 21/RDD/671 as part of the project SPOTBlade- Strategies for erosion and fouling Protection of Offshore Turbine Blades)

References

[1] E.F. Tobin, T.M. Young, D. Raps and O. Rohr, Comparison of liquid impingement results from whirling arm and water-jet rain erosion test facilities, Wear 271 (2011) 2625–2631, 2011
[2] B. Amirzadeh, A. Louhghalam, M. Raessi and M. Tootkaboni, A computational framework for the analysis of rain-induced erosion in wind turbine blades, part II: Drop impact-induced stresses and blade coating fatigue life, Journal of Wind Engineering & Industrial Aerodynamics 163 (2017) 33–43.
[3] Doagou-Rad S, Mishnaevsky L Jr, Bech JI. Leading edge erosion of wind turbine blades: Multiaxial critical plane fatigue model of coating degradation under random liquid impacts. Wind Energy. 2020;23:1752–1766. https://doi.org/10.1002/we.2515
[4] Antonios Tempelis and Leon Mishnaevsky Jr, Surface roughness evolution of wind turbine blade subject to rain erosion, Materials & Design 231 (2023) 112011, https://doi.org/10.1016/j.matdes.2023.112011

20th EAWE PhD Seminar on Wind Energy
24-26 September 2024
Visby, Sweden

Risk-based feasibility assessment and life cycle cost modelling of next generation wind turbine components

Francesco Piovesan[a], **Athanasios Kolios**[a], **Nikolay Dimitrov**[a], **Mohammed Fajar**[b], **Marianna Rondon**[b], and **Matteo Capaldo**[b]

[a]DTU, Department of Wind & Energy Systems
[b]TotalEnergies OneTech, France

E-mail: frpi@dtu.dk

Keywords: Feasibility Assessment, Risk-based Feasibility Assessment, Life cycle cost, Large scale wind turbine blades

1 Introduction

The escalating global energy demands, the urgent need for sustainable solutions and the advancement of renewable energy technologies, particularly wind power, has become a pivotal aspect of the green energy transition. Successful transition to renewable energy requires that the newly installed wind energy capacities provide reliable energy supply at low risk and low cost. New offshore wind farm projects are associated with a degree of uncertainty, as they may be located further offshore, in deeper waters, and with harsher environmental conditions than existing offshore wind farms. Additional uncertainty comes from the continuous evolution of wind turbine technology (primarily towards bigger turbines). This evolution, combined with the fairly long wind farm project development process (typically 7-10 years), means that the planning process is based on turbines that are not fully designed yet. The primary goal of this PhD project is to develop methodologies for risk-based technology feasibility assessment for large offshore wind turbine rotors. The primary outcome of the project is a framework that evaluates the feasibility and suitability of a given rotor technology for a particular site and operating conditions. It utilizes risk assessment, uncertainty quantification, wind turbine loads and performance modelling, and impact assessment, to assess the technology performance over its entire life cycle, and identify potential unexpected challenges and failure modes - and how these may affect the cost of energy produced. For the development of this framework and methodologies probabilistic design assessments, uncertainty quantification, and data-driven approaches using AI/ML [1] will be integrated, with the objective of seeking to advance wind energy systems towards higher technological readiness levels, ensuring their viability and cost-effectiveness. The integration of risk-based models in feasibility assessment and life cycle cost analysis is not just an academic pursuit but a strategic move towards reducing development costs and expediting market uptake [2, 3].

2 Background and Objectives

The quest for sustainable energy sources has led to significant growth in wind energy, yet this sector faces complex challenges in feasibility assessment and cost-effectiveness. Current methodologies in risk assessment and life cycle cost modeling in wind energy are often fragmented and lack comprehensive integration with advanced data-driven techniques [4, 5]. This gap hinders the accurate prediction and mitigation of risks, thereby impacting the economic feasibility and reliability of wind turbines [6].

The project's rationale is rooted in the need for a holistic approach to bridge this gap by combining probabilistic risk assessment with sophisticated cost modeling. This approach ensures a more accurate, reliable, and economically viable deployment of wind energy technologies [7]. The urgency for such a framework is underscored by the increasing scale and complexity of modern wind turbine systems, particularly with the advent of large-scale,

floating offshore turbines [8].

To develop a comprehensive framework for the risk-based feasibility assessment of large-scale wind turbine blades, DNV-RP-A203's qualification plan is used as a foundational guideline [9], analyzing and addressing the challenges associated with the design, reliability, and cost-efficiency of large-scale blades. A case study on the development of this component offers a tangible context to apply and validate the proposed methodologies. The objectives of this research project therefore are:

- Development of a Feasibility Assessment Framework: Adapt and apply the DNV-RP-A203 [9] feasibility assessment plan specifically for large-scale wind turbine blades. This ensures a rigorous and industry-relevant qualification process;
- FMEA (Failure Modes and Effects Analysis): Conduct a detailed Failure Modes, Effects and Criticality Analysis (FMECA), in particular on scale-based failure modes. The goal is to identify potential reliability risks unique to large-scale blades and adopt subsequent design optimization strategies [5];
- Establishing a multi-KPI (Key Performance Indicator) Scheme for comprehensive cost and impact assessment: The objective of the scheme is the evaluation of the economic, environmental and technical aspects of blade development, providing a balanced view of its feasibility and sustainability, adapted to the specific call for tender [10];
- Development of Guidelines for Future Projects based on the integration of the research insights to formulate practical guidelines: These guidelines, which will include the possible technology showstoppers related to the very large rotors, will aid in future large-scale blade development projects, ensuring they are economically viable, technologically advanced, and environmentally responsible.

3 Methodology

To perform this research a comprehensive and innovative methodology, integrating multiple sources and approaches, is adopted:

- In-depth FMECA analysis: Extending conventional risk policies to focus on the feasibility assessment [6, 11]; this is carried out by specifically targeting scale-based failure modes relevant to large-scale blades, identifying potential risks and criticalitites to direct the subsequent stages of the project;
- Collaborative Workshops: Engage with leading industry experts to ensure that the research is aligned with real-world applications and technological advancements. These workshops will validate the FMECA results and refine the focus for modelling and the analytical phases;
- Development of Sophisticated Numerical Models: Utilize Python and ANSYS to simulate the blade's structural behavior and operational response. These models will be informed by the FMECA and workshops outcomes to guarantee their relevance and accuracy [12, 13, 14, 15, 16];
- Surrogate Models using Machine Learning: Develop surrogate models to approximate the behavior of the complex numerical simulations, reducing the dimensionality and the computational load while keeping the model accuracy. These models will provide important insights in terms of performance and reliability of the blade designs [17, 18, 19, 20];
- Reliability Analysis: Implement first-order methods (FORM) and Monte Carlo simulations [4, 15], to quantify the reliability of different blade designs, incorporating findings from both the numerical and surrogate models;
- Life Cycle Cost Model Development: Create a comprehensive life cycle cost model, potentially with the integration of time-domain simulations to include maintenance and operational scenarios [21]. This model considers various cost factors under different risk conditions;
- Guideline Development: Based on the results obtained in the previous steps, develop guidelines offering a balanced perspective on performance, risk, and cost for the development and assessment of large-scale wind turbine blades.

Acknowledgements

This PhD project is fully sponsored by Total Energies as part of the DTEC TREND Research project, encompassing all associated costs and resources required for the completion of the research.

References

[1] Nikolay Dimitrov and Anand Natarajan. From SCADA to lifetime assessment and performance optimization: how to use models and machine learning to extract useful insights from limited data. *Journal of Physics: Conference Series*, 1222(1):012032, May 2019. Publisher: IOP Publishing.

[2] S. M. Samindi M. K. Samarakoon and R. M. Chandima Ratnayake. Technology Qualification of Offshore Wind Turbine Supporting Concrete Constructions: Mitigation of Future Catastrophic Incidents via Quantification of Unknown. American Society of Mechanical Engineers Digital Collection, September 2017.

[3] S. M. Samindi M. K. Samarakoon and R. M. Chandima Ratnayake. On the Necessity for Minimizing Risk Based Technology Qualification Variability: An Application to Offshore Floating Wind Turbines. American Society of Mechanical Engineers Digital Collection, December 2020.

[4] Mareike Leimeister and Athanasios Kolios. A review of reliability-based methods for risk analysis and their application in the offshore wind industry. *Renewable and Sustainable Energy Reviews*, 91:1065–1076, August 2018.

[5] Javier Contreras Lopez and Athanasios Kolios. Risk-based maintenance strategy selection for wind turbine composite blades. *Energy Reports*, 8:5541–5561, November 2022.

[6] Matti Niclas Scheu, Lorena Tremps, Ursula Smolka, Athanasios Kolios, and Feargal Brennan. A systematic Failure Mode Effects and Criticality Analysis for offshore wind turbine systems towards integrated condition based maintenance strategies. *Ocean Engineering*, 176:118–133, March 2019.

[7] Anastasia Ioannou. Stochastic financial appraisal of offshore wind farms. *Renewable Energy*, 2020.

[8] Mareike Leimeister, Athanasios Kolios, Maurizio Collu, and Philipp Thomas. Larger MW-Class Floater Designs Without Upscaling?: A Direct Optimization Approach. American Society of Mechanical Engineers Digital Collection, November 2019.

[9] DNV-RP-A203: Qualification of New Technology, 2011.

[10] Martin Colla, Anastasia Ioannou, and Gioia Falcone. Critical review of competitiveness indicators for energy projects. *Renewable and Sustainable Energy Reviews*, 125:109794, June 2020.

[11] Athanasios J. Kolios and Ursula Smolka. Risk-based Maintenance Strategies for Offshore Wind Energy Assets. In *2020 Annual Reliability and Maintainability Symposium (RAMS)*, pages 1–6, January 2020. ISSN: 2577-0993.

[12] Shaikha Al-Sanad, Lin Wang, Jafarali Parol, and Athanasios Kolios. Reliability-based design optimisation framework for wind turbine towers. *Renewable Energy*, 167:942–953, April 2021.

[13] Shaikha Al-Sanad, Jafarali Parol, Lin Wang, and Athanasios Kolios. Design optimisation of wind turbine towers with reliability-based calibration of partial safety factors. *Energy Reports*, 9:2548–2556, December 2023.

[14] Mareike Leimeister, Maurizio Collu, and Athanasios Kolios. A fully integrated optimization framework for designing a complex geometry offshore wind turbine spar-type floating support structure. *Wind Energy Science*, 7(1):259–281, February 2022. Publisher: Copernicus GmbH.

[15] Mareike Leimeister and Athanasios Kolios. Reliability-based design optimization of a spar-type floating offshore wind turbine support structure. *Reliability Engineering & System Safety*, 213:107666, September 2021.

[16] Abdulhakim Adeoye Shittu, Ali Mehmanparast, Lin Wang, Konstantinos Salonitis, and Athanasios Kolios. Comparative Study of Structural Reliability Assessment Methods for Offshore Wind Turbine Jacket Support Structures. *Applied Sciences*, 10(3):860, January 2020. Number: 3 Publisher: Multidisciplinary Digital Publishing Institute.

[17] Filippo De Girolamo, Lorenzo Tieghi, Giovanni Delibra, Valerio Francesco Barnabei, and Alessandro Corsini. Surrogate Modeling of the Aeroacoustics of an NM80 Wind Turbine. *International Journal of Turbomachinery, Propulsion and Power*, 8(4):43, December 2023. Number: 4 Publisher: Multidisciplinary Digital Publishing Institute.

[18] Juan Pablo Murcia, Pierre-Elouan Réthoré, Nikolay Dimitrov, Anand Natarajan, John Dalsgaard Sørensen, Peter Graf, and Taeseong Kim. Uncertainty propagation through an aeroelastic wind turbine model using polynomial surrogates. *Renewable Energy*, 119:910–922, April 2018.

[19] Rafael Valotta Rodrigues, Mikkel Friis-Møller, Katherine Dykes, Nicolò Pollini, and Morten Jensen. A surrogate model of offshore wind farm annual energy production to support financial evaluation. *Journal of Physics: Conference Series*, 2265(2):022003, May 2022.

[20] Yihan Wu and Steven Jige Quan. A review of surrogate-assisted design optimization for improving urban wind environment. *Building and Environment*, 253:111157, April 2024.

[21] Anastasia Ioannou, Andrew Angus, and Feargal Brennan. A lifecycle techno-economic model of offshore wind energy for different entry and exit instances. *Applied Energy*, 221:406–424, July 2018.

20th EAWE PhD Seminar on Wind Energy
24-26 September 2024
Visby, Sweden

Wind tunnel numerical modeling for wind farm control strategies

Tiziano Leone[a], **Filippo Calamelli**[a], **Paolo Schito**[a], and **Alberto Zasso**[a]

[a]Department of Mechanical Engineering, Politecnico di Milano, Milan, Italy

E-mail: tiziano.leone@polimi.it

Keywords: Atmospheric boundary layer, Wind tunnel numerical modeling, Large eddy simulation, Actuator line model, Wake recovery

Abstract

In wind energy and wind engineering research it is of fundamental importance to reproduce correctly the Atmospheric Boundary Layer (ABL). During wind tunnel testing various techniques are utilized, and the resulting ABL is borne out of the interaction of the peculiar chamber configuration with the incoming flow. Correctly reproducing this interaction in a numerical setting it is important to be able to validate the codes' performance through the experimental measurements performed in the wind tunnel. This study aims to reproduce numerically the Politecnico di Milano wind tunnel (Hereafter GVPM) by comparing the performance of the numerical model with complete experimental mapping obtained through 3D hot-wire anemometer measurements. Subsequently, the results achieved by a numerical wind turbine model immersed in the wind tunnel simulation will be compared to the ones obtained with a standard precursor ABL simulation and to experimental data.

1 INTRODUCTION

To study the action of the wind on man-made structures in the lower part of the atmosphere (wind turbines, buildings, etc.) ad-hoc wind tunnels have been developed to reproduce the peculiar characteristics of the Atmospheric Boundary Layer (ABL). Engineering codes prescribe the characteristics of the ABL to be taken into account depending on the location of the structure. Correctly representing the wind characteristics during wind tunnel testing is a fundamental aspect of the craft [8, 2], both from an experimental and a numerical point of view. During wind tunnel testing it is thus necessary to reproduce a target boundary layer, through the use of turbulence-generating geometrical objects, such as spires and blocks, arranged in various configurations [5]. The resulting ABL is a product of the configuration chosen and the flow entering the test section, which depends on a lot of factors. It is often discounted, but the inlet flow at the beginning of the test section is affected by the objects inside the chamber, depending on their blockage ratio.

In the context of numerical simulations that have as objective the reproduction of the ABL with its unsteady characteristics, multiple approaches have been proposed [9]. Recycling methods and synthetic turbulence are very useful for reducing computational costs by replacing the physical modeling of the wind tunnel. Nevertheless, they are not usually able to fully capture the behavior of the flow that actually impinges on the object during the experiments. This is why, for validating numerical codes for wind energy applications, such as the Actuator Line Models (ALM) developed in-house [7, 3, 6], with experiments performed in the wind tunnel, the correct representation of the behavior of the flow actually acting on the wind turbine cannot be discounted. This is especially true for wind farm control, due to the relevant impact of the length scales of the flow [4].

It is thus important for a facility such as GVPM to be able to reproduce with fidelity, through the means of Large Eddy Simulations (LES), the behavior of the flow inside its test section under multiple ABL configurations. The GVPM facility is an interesting example, characterized by the presence of two test sections arranged in a vertical layout, as shown in Fig. 1. Moreover, the entrance of the ABL section comes after a pressure drop due to the presence of the heat exchanger, resulting in a background turbulence in the order of 2% throughout all the section. The numerical results will be validated against the experimental measurements performed during the CL-Windcon test campaigns, in which the mapping of the chamber through the use of 3D-hotwire anemometers has been carried out at 2 plane locations, in different roughness configurations.

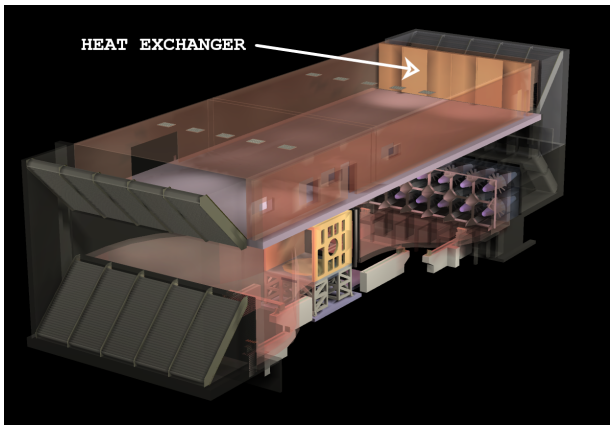

Figure 1: GVPM Wind tunnel rendering

In the context of wake control strategies, a complete numerical model of the GVPM wind tunnel will then allow us to compare the results obtained by the ALM codes with the experiments that will be performed in the GVPM wind tunnel. We will be able to quantify more accurately the impact of the length scales of the actual flow on the wake recovery behavior, by comparing the results with the ones obtained through more conventional practices, such as precursor-successor simulations or synthetic generation. Moreover, for what concerns synthetic turbulence generation for ABL, a numerical model of the GVPM wind tunnel will help us validate such methods by offering a complete insight into the wind to be matched at the test location. Lastly, such a model will also be able to inform the test engineers on the complete wind behavior varying the turbulence-generating objects configuration, to develop new ones more representative of the wind behavior at real scale.

2 METHODOLOGY

2.1 Part 1: GVPM numerical model

The first part of the work aims to accurately reproduce numerically the flow inside the test section of GVPM. Therefore, wall-modeled Large Eddy Simulations will be employed, describing as accurately as possible the wind tunnel geometry. The peculiar characteristics of the GVPM wind tunnel pose some challenges from the numerical point of view. It is incorrect to reproduce the flow impinging on the initial spires as a uniform zero-turbulence flow. The flow entering the chamber presents a background turbulence of 2%, and the presence of the spires close to the entrance generates a vertically non-uniform blockage, thus a non-uniform wind velocity profile. Initially, it is fundamental to reproduce the flow condition due to the simultaneous contribution of both spires and the porous media, representing the heat exchanger. To model the heat exchanger without resolving its geometry a Darcy-Forchaimer model will be employed. A first analysis will be carried out to evaluate the length of the upstream fetch, shown in Fig. 2, necessary to correctly reproduce the interaction of the flow with the spires and the porous media. The validation will be performed with the two configurations mapped during CL_Windcon, one off-shore low-turbulence, and the other on-shore high-turbulence. Since the high-turbulence configuration presents some brick elements, computationally expensive to mesh accurately, the results' dependency on grid refinement will be analyzed. To assess the predictive performances of the model, simulations of other different configurations will be carried out. For these, the model's performance will be evaluated on the wind profiles obtained at the test table location.

2.2 PART 2: Validation of ALM codes in ABL flow

Once the GVPM numerical model has been validated, it will be possible to assess the results obtained with the in-house ALM codes. Extensive testing campaigns have already been carried out [1], and others will be in the near future in which a Particle Image Velocimetry (PIV) mapping of the wind turbine wake will be produced in different tilt/yaw configurations. The ALM will be implemented in the simulations through the use of the SOWFA OpenFOAM open-source module. Comparing the results obtained through the use of precursor-successor simulations, the numerical wind tunnel simulations and experimental tests will offer insights into the wake recovery

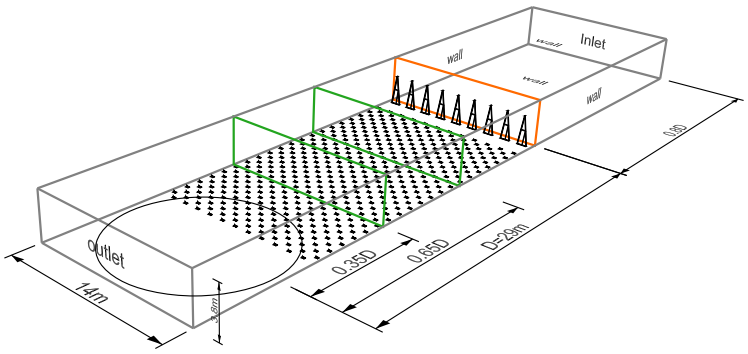

Figure 2: Scheme of the CFD model in the on-shore configuration. The orange plane indicates the heat exchanger, while the green planes represent the mapping made by 3D-hotwire anemometers. D indicates the distance between the center of the rotating test table and the heat exchanger.

mechanisms for wind turbines immersed in the ABL, as well as a method to validate more accurately the ALM models.

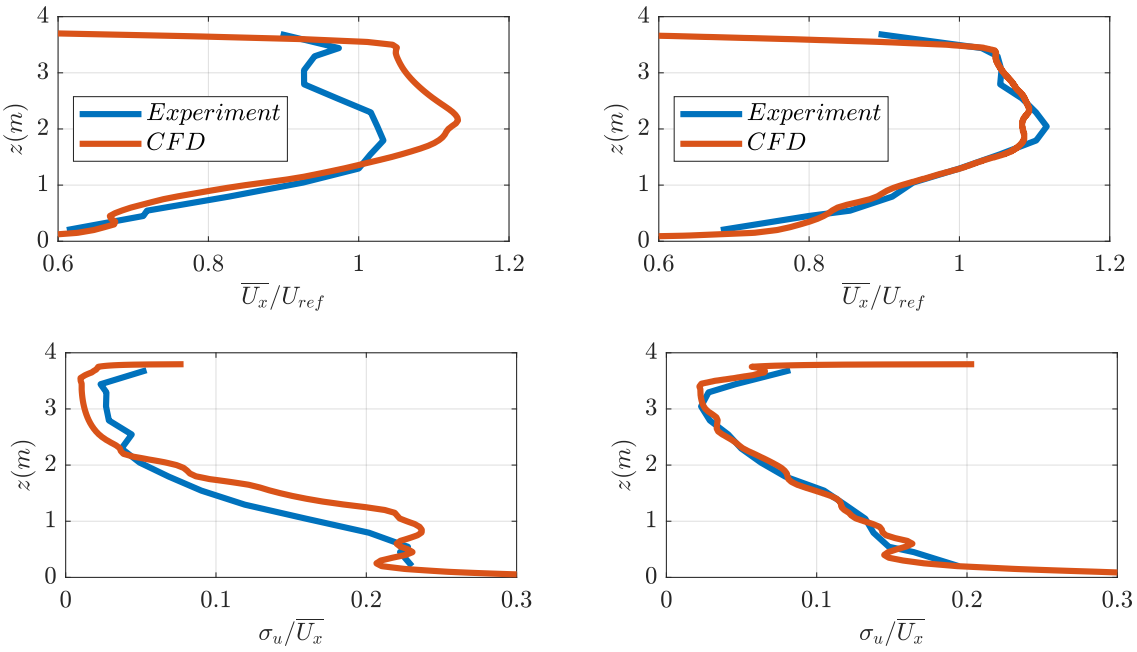

Figure 3: Normalized wind velocity (with respect to the velocity at z=1.3m) and longitudinal turbulence intensity profiles comparison for the on-shore configuration at 0.65D (**left column**) and 0.35D (**right column**) before the center of the test table, where D is defined in fig. 2.

3 PRELIMINARY RESULTS

The presentation of results will first focus on the performance of the GVPM model compared to the measurements performed during the CL_Windcon testing campaign. The impact of the most important modeling choices, i.e. the antecedent fetch, the modeling of the porous layer, and the mesh refinement, will be investigated. Some preliminary results in terms of velocity and turbulence intensity profiles are shown in Fig.3, at different distances from the entrance of the chamber. The simulated profiles show a good agreement with the experimental ones,

specifically at the location near the rotating table. Moreover, the velocity profiles present a knee at around 2m height, which could have a potential impact on the wake recovery mechanisms.

Subsequently, the results obtained by placing the modeled wind turbine in the numerical GVPM flow will be compared to the ones derived using a standard precursor-successor approach. Their performance with respect to experimental PIV data will be assessed in terms of wake recovery behavior.

References

[1] I. Bayati, M. Belloli, L. Bernini, D. Boldrin, K. Boorsma, M. Caboni, M. Cormier, R. Mikkelsen, T. Lutz, and A. Zasso. Unaflow project: Unsteady aerodynamics of floating wind turbines. In *Journal of Physics: Conference Series*, volume 1037, page 072037. IOP Publishing, 2018.

[2] B. Blocken. Les over rans in building simulation for outdoor and indoor applications: A foregone conclusion? In *Building Simulation*, volume 11, pages 821–870. Springer, 2018.

[3] A. Cioffi, C. Muscari, P. Schito, and A. Zasso. A steady-state wind farm wake model implemented in openfast. *Energies*, 13(23):6158, 2020.

[4] E. L. Hodgson, M. H. A. Madsen, and S. J. Andersen. Effects of turbulent inflow time scales on wind turbine wake behavior and recovery. *Physics of Fluids*, 35(9), 2023.

[5] H. Irwin. The design of spires for wind simulation. *Journal of wind engineering and industrial aerodynamics*, 7(3):361–366, 1981.

[6] C. Muscari, P. Schito, A. Vire, A. Zasso, and J.-W. van Wingerden. An advanced approach to velocity sampling in actuator line models. *Authorea Preprints*, 2023.

[7] A. G. Sanvito, G. Persico, P. Schito, V. Dossena, and A. Zasso. Comparative assessment of actuator-line modeling of fowt rotor aerodynamics to wind tunnel experiments. In *Journal of Physics: Conference Series*, volume 2626, page 012063. IOP Publishing, 2023.

[8] X. Wu. Inflow turbulence generation methods. *Annual Review of Fluid Mechanics*, 49:23–49, 2017.

[9] B. Yan and Q. Li. Inflow turbulence generation methods with large eddy simulation for wind effects on tall buildings. *Computers & Fluids*, 116:158–175, 2015.

3.2 Session 224: Reliability, monitoring and sensing technology

25.09.2024, 15:10, Room 4

Chair:

Ansh Patel

Presenters:

Thurn Jonathan	Damage detection and localisation of a lattice tower using autocovariance functions of acceleration measurements
Ladopoulou Domna	Probabilistic Multi-Layer Perceptrons for Wind Farm Condition Monitoring
Manami Mohammadreza	Novel Wind Lidar Configurations For Wind Energy Applications
Cadavid Gil Esteban	Finite element analysis of the structural behaviour and fatigue life of a dynamic power cable
Bull Thomas Serup	Treatment of uncertainties in digital twin modelling

20th EAWE PhD Seminar on Wind Energy
24-26 September 2024
Visby, Sweden

Damage detection and localisation of a lattice tower using autocovariance functions of acceleration measurements

Jonathan Thurn[a], **Clemens Jonscher**[a], **Tanja Grießmann**[a], and **Raimund Rolfes**[a]

[a]Leibniz Universität Hannover, Institute of Structural Analysis

E-mail: jonathan.thurn@stud.uni-hannover.de

Keywords: Structural Health Monitoring, Damage Detection, Damage-Sensitive Feature

1 Introduction

In structural health monitoring (SHM), civil structures like wind turbines are continuously monitored to detect, localise and quantify damages and predict the remaining lifetime of the structure [5]. This study focuses on the first SHM level: damage detection. In damage detection, the structural state is classified as either ”healthy” or ”damaged” based on the information available in damage-sensitive features. A deviation of these features from their known values during the training period indicates damage. Therefore, damage detection is possible even if training data is only available from the undamaged condition [9].
In the initial step of an SHM process, damage-sensitive features have to be extracted from the vibration measurement. These features carry information about the system state, which is influenced by both damages and environmental conditions (ECs) [6]. Commonly used features include modal parameters such as natural frequencies and mode shapes [2]. However, extracting these modal parameters from vibration data involves parameter-dependent and potentially time-consuming system identification. Auto-covariance functions (ACFs) offer an alternative, as they can be estimated without system identification while still providing noise reduction and data reduction compared to actual measurements. As ACFs are connected to the power spectral density and the Fourier transformation of a signal through the Wiener-Chintschin-Theorem, they contain information about the vibrational properties of the monitored structure [1].

This study investigates a method for damage detection presented by Kullaa [3] is investigated. In this method, ACFs are used as the damage-sensitive feature and the influence of varying ECs is compensated via a whitening transformation, thus eliminating the need for direct EC measurements. This step is commonly referred to as normalisation. The ACFs are estimated from the measurement data in the first step. The correlation between the ACFs of different sensors provides spatial information alongside temporal information. This spatial-temporal information is utilised by simultaneously processing ACFs with different time lags, forming a new data matrix consisting of multiple ACFs shifted by one time lag each. In the second step, the whitening matrix is calculated from training data and subsequently applied to each measurement. In the final step, a damage indicator (DI) is calculated as the maximum score on the first principal component of the whitened data. The method is applied to the Leibniz University Test Structure for Monitoring (LUMO) [8], an ambiently excited lattice tower of 9 m height featuring reversible damage mechanisms at six levels. A more detailed description of LUMO can be found in [7].

Kullaa et al. already validated this method using measurements from LUMO under a single damaged condition [4]. Based on this, the method is now applied to six different damage scenarios. Additionally, two extensions to the method are proposed and presented here for the first time.

2 Application

For this study, acceleration measurements from October 2020 to July 2021 from LUMO are utilised. During the investigated period, six different damage scenarios were tested in LUMO, covering three different damage locations (P1, P2, P3) with two different damage severities each. In the first three damage scenarios, all three struts at the damage location were removed, while for the last three damage scenarios only one strut was removed respectively. The damage positions are shown in Figure 2 (a).

The ACFs are estimated from 10-minute measurements separately for each acceleration sensor. To ensure that all relevant modes are present in the ACFs, 100 time-lags are considered in the ACFs. To eliminate the excitation dependency of the ACFs magnitude, all ACFs from one measurement are scaled to a single sensor. Subsequently, the ACFs are time-shifted to account for spatial-temporal information. To compensate for the influence of varying ECs the whitening transformation is used. The whitening matrix is calculated from pooled training data covering a wide range of ECs. The training data consisted of 600 measurements. The time-shifted ACFs of each measurement are normalised using the whitening matrix and are subsequently subjected to a principal component analysis. The maximum value on the first principal component is used as a damage indicator. A threshold for classification as "healthy" or "damaged" is determined from the DIs of the training data. For each damage scenario, a new whitening matrix and threshold are calculated using data collected after restoring the undamaged condition.
The evolution of the DI during the investigated period is shown in Figure 1. For all six damage scenarios, a system change is visible from the changing magnitude of the DI as soon as damage is introduced, although no alarm is triggered in (f). However, false positives do occur, particularly in (c), where ECs not included in the training data are interpreted as damage.

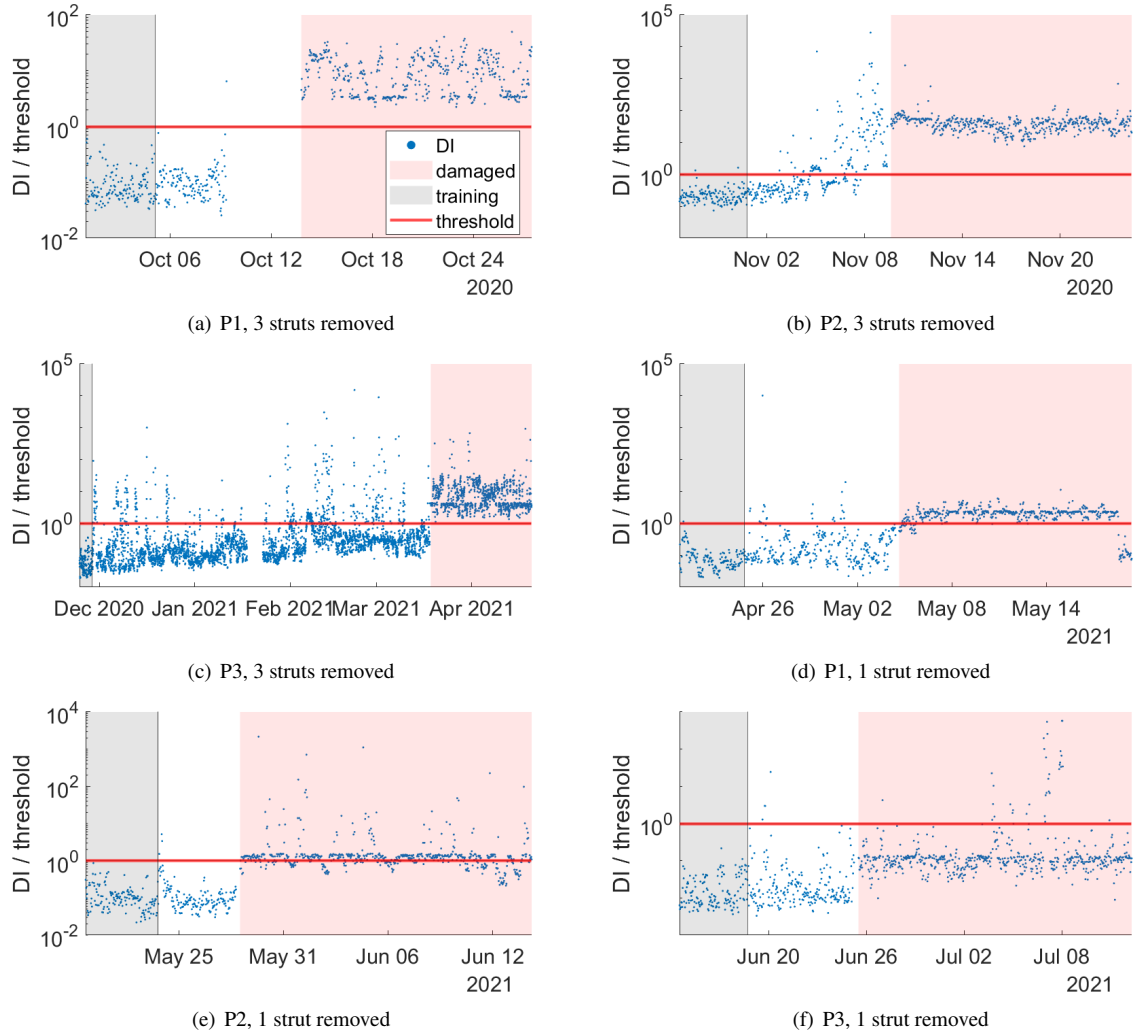

(a) P1, 3 struts removed

(b) P2, 3 struts removed

(c) P3, 3 struts removed

(d) P1, 1 strut removed

(e) P2, 1 strut removed

(f) P3, 1 strut removed

Figure 1: Evolution of the Damage Indicator (DI), scaled to the threshold, for all investigated damage scenarios.

To evaluate the damage detection, the F-score is calculated from the number of true positives (TP), false positives (FP) and false negatives (FP) for all six damage scenarios according to Equation 1.

$$F = \frac{2 \cdot TP}{2 \cdot TP + FP + FN} \tag{1}$$

The F-score for the six damages is presented in Figure 2 (b). The F-score of five of the six investigated damage scenarios is larger than 80%, indicating that those five damages can be detected reliably.

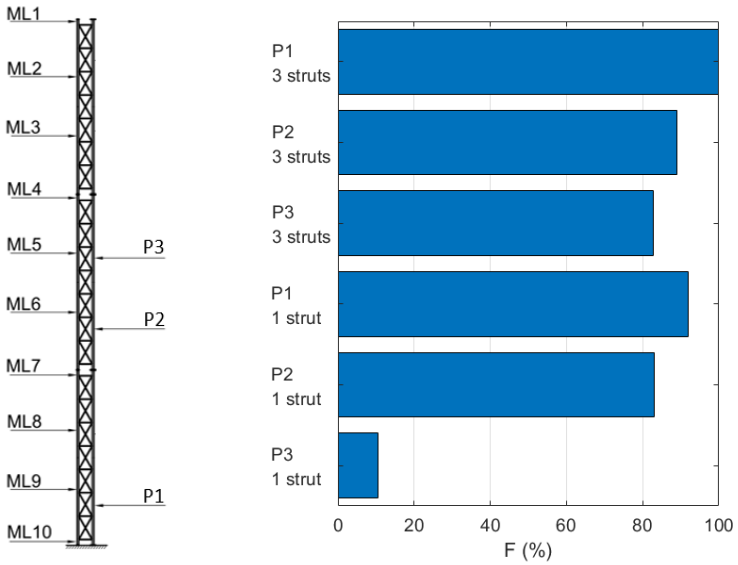

(a) LUMO (b) F-score

Figure 2: (a) Schematic drawing of LUMO including the measurement levels (ML) and the damage positions (P). (b) F-score calculated from the results in Figure 1.

3 Results

This study demonstrates that damage-sensitive features are not limited to modal parameters, as shown in previous research, but can also include different features such as the ACF used here. Furthermore, this method utilises a normalisation technique that does not rely on measurements of the ECs. The investigation shows that even though no measurements of the ECs were used for normalisation, it is still crucial for the training data to encompass a wide range of ECs to effectively compensate the influence of varying ECs.

References

[1] J. S. Bendat and A. G. Piersol. *Random data: analysis and measurement procedures*. John Wiley & Sons, 2011.

[2] S. W. Doebling, C. R. Farrar, M. B. Prime, et al. A summary review of vibration-based damage identification methods. *Shock and vibration digest*, 30(2):91–105, 1998.

[3] J. Kullaa. Damage detection and localization using autocorrelation functions with spatiotemporal correlation. In *Experimental Vibration Analysis for Civil Engineering Structures: Select Proceedings of the EVACES 2021*, pages 83–95. Springer, 2022.

[4] J. Kullaa, C. Jonscher, L. Liesecke, and R. Rolfes. Damage detection with closely spaced modes using auto-covariance functions [unpublished], 2024.

[5] A. Rytter. Vibration based inspection of civil engineering structures ph. d. *Aalborg University, Aalborg, Denmark*, 1993.

[6] H. Sohn. Effects of environmental and operational variability on structural health monitoring. *Philosophical Transactions of the Royal Society A: Mathematical, Physical and Engineering Sciences*, 365(1851):539–560, 2007.

[7] S. Wernitz, B. Hofmeister, C. Jonscher, T. Grießmann, and R. Rolfes. A new open-database benchmark structure for vibration-based structural health monitoring. *Structural Control and Health Monitoring*, 29(11):e3077, 2022.

[8] S. Wernitz, B. Hofmeister, C. Jonscher, T. Grießmann, and R. Rolfes. Lumo - leibniz universtity test structure for monitoring, 2021.

[9] K. Worden, C. R. Farrar, G. Manson, and G. Park. The fundamental axioms of structural health monitoring. *Proceedings of the Royal Society A: Mathematical, Physical and Engineering Sciences*, 463(2082):1639–1664, 2007.

20th EAWE PhD Seminar on Wind Energy
24-26 September 2024
Visby, Sweden

Probabilistic Multi-Layer Perceptrons for Wind Farm Condition Monitoring

Filippo Fiocchi[a], **Domniki Ladopoulou**[a], and **Petros Dellaportas**[a,b]

[a]University College London, London, United Kingdom
[b]Athens University of Economics and Business, Athens, Greece

E-mail: domna.ladopoulou.22@ucl.ac.uk

1 Introduction

There is a need to reduce the high operational and maintenance costs of wind turbines via a cost-effective and high-precision condition monitoring system. One cost-effective way of developing a condition monitoring system is by using the supervisory control and data acquisition (SCADA) data which are currently recorded in most of the wind farms. A typical approach to the problem is to produce a model using features extracted from SCADA data that predicts the output power of a wind turbine under normal behaviour. Then the model can be used to inspect whether the observed and model-predicted output deviate in some statistical sense. Although this is a sensible, well-known approach, practical and effective condition monitoring of a wind farm requires a modelling perspective with four particular characteristics outlined below.

First to accommodate weather fluctuations, the model needs to be able to scale well with the data size since it requires to be trained for at least one calendar year which is $52,560$ 10-minute intervals. Second, it should be able to extract all the wealth of information available in SCADA data. Third, the model needs to provide probabilistic predictions in the form of predictive density so that proper probabilistic assessment of the deviation of the observed from the expected output can be performed. Last but not least, the model should be able to deal with the peculiarities of wind farm SCADA data recording in the following sense. It is common that historical SCADA data may have many missing data in a particular wind turbine because it was out-of-order for a long period of time or it has been recently installed. A good model should be able to predict the output power of this wind turbine with an inferential procedure that borrows strength from the features and output power of all other wind turbines in the wind farm.

We develop a condition monitoring system based on a model that has all the four necessary characteristics described above using a probabilistic multi-layer perceptron (PMLP) with transfer learning via fine-tuning. We assume that the output power follows a normal distribution with input-dependent mean and input-dependent variance which form our predictive density for each 10-minute interval. For the probabilistic condition monitoring we propose the use of CUSUM control charts. We illustrate its performance in a real data application by comparing it with two other probabilistic models: a Gaussian process and a Bayesian neural network. Both probabilistic methods mentioned above are well-known probabilistic approaches in the literature, see for example [3, 4, 5] for Gaussian processes and [1] for a long short term memory (LSTM) Bayesian neural network. We found that our model predicts better with respect to root mean square error, mean absolute error and maximum calibration error. We demonstrate that by transfer learning we can use information from all turbines in a wind farm to improve the prediction of the output power of a single wind turbine. We also provide a real data example in which our proposed condition monitoring system expressed via a CUSUM control chart reveals an early warning in a particular wind turbine failure.

2 Proposed Methodology

In section 2.1 we describe a fully connected deep neural network that predicts both the mean and the variance of output power at a particular 10-minute interval. In section 2.2 we present the second ingredient in our model that is the incorporation of transfer learning. Finally, our proposed probabilistic condition monitoring system is based on a CUSUM control chart. Anomalous operational behaviour is reported when the observed output power departs, in

a probabilistic sense, from the expected predicted normal density under the trained model. The overall flowchart of the proposed probabilistic condition monitoring system is presented in Fig. 1.

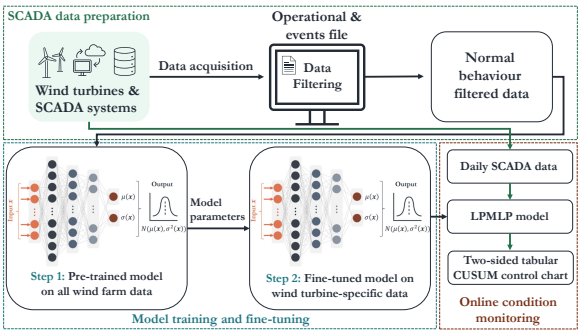

Figure 1: Overall flowchart of the proposed probabilistic condition monitoring system. LPMLP: Large probabilistic multi-layer perceptron.

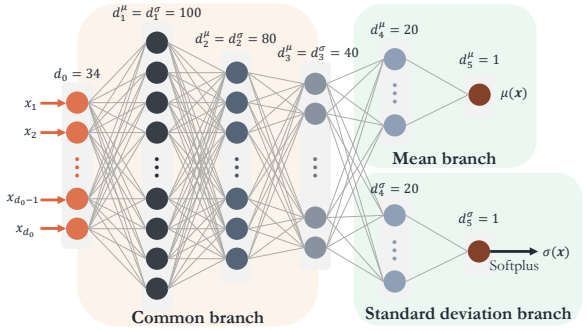

Figure 2: Indicative PMLP architecture used in the application of Section 3 and named as *PMLP arch. A1* with shared initial layers and independent branches for mean and standard deviation.

2.1 Probabilistic multi-layer perceptron

To model a heteroscedastic output noise we assume that for each 10-minute interval the power output of a wind turbine y conditioned on the SCADA input features $\mathbf{x} \in \Re^{d_0}$ follows a normal distribution with unknown mean and variance that both depend on $\mathbf{x}$, so $y \sim \mathcal{N}(\mu(\mathbf{x}), \sigma^2(\mathbf{x}))$. We will approximate $\mu(\mathbf{x})$ and $\sigma(\mathbf{x})$ by a probabilistic multi-layer perceptron (PMLP) with branching prediction heads, see for example, Figure 2 for an indicative PMLP architecture.

Given an input vector $\mathbf{x} = (x_1, x_2, \ldots, x_{d_0})$ that represents the d_0 SCADA input features at a particular time interval, the predicted PMLP power output $\hat{y} \in \Re$ follows a normal density with parameters $\mu(\mathbf{x})$ and $\sigma^2(\mathbf{x})$ which are continuous functions of the inputs $\mathbf{x}$. In fact, our proposed PMLP models $\mu(\mathbf{x})$ as a linear piecewise function of $\mathbf{x}$ and $\sigma(\mathbf{x})$ as a nonlinear piecewise function of $\mathbf{x}$.

For a number of k hidden layers with widths $d_1, d_2, \ldots, d_k$ and input and output dimensions d_0 and $d_{k+1} = 1$ respectively, we adopt the linear functions $g_i : \Re^{d_{i-1}} \to \Re^{d_i}$ for $i = 1, \ldots, k$ defined as $g_i(\mathbf{x}) = \mathbf{W}_i\mathbf{x} + \mathbf{b}_i$, where $\mathbf{W}_i \in \Re^{d_i \times d_{i-1}}$, $\mathbf{x} \in \Re^{d_{i-1}}$ and $\mathbf{b}_i \in \Re^{d_i}$. Furthermore, we adopt the Rectified Linear Unit function $ReLU_i : \Re^{d_i} \to \Re^{d_i}$ defined as $ReLU_i(\mathbf{x}) = (\max\{0, x_1\}, \max\{0, x_2\}, \ldots, \max\{0, x_{d_i}\})$, and the Softplus function $S : \Re \to \Re$ defined as $S(x) = \log(1 + e^x) + \delta$ for a small $\delta > 0$ used for numerical stability needed when x becomes very small. These three functions are the basic ingredients of our PMLP.

To define the branching structure of the PMLP, we use two sets of functions g and $ReLU$, corresponding to predictions of $\mu(\mathbf{x})$ and $\sigma(\mathbf{x})$ and indexed by the superscripts μ and σ respectively. Different functions g have different sets of parameters $\mathbf{W}_i, \mathbf{b}_i$ where by different functions $ReLU$ is meant that they operate on different dimensions d_i. We further assume that there exist two corresponding numbers of hidden layers k_μ and k_σ with widths $d_1^\mu, d_2^\mu, \ldots, d_{k_\mu}^\mu$ and $d_1^\sigma, d_2^\sigma, \ldots, d_{k_\sigma}^\sigma$. Then, the output $\hat{y}$ of the PMLP with k_μ and k_σ hidden layers is represented as

$$\begin{aligned} \mu(\mathbf{x}) &= g_{k_\mu+1}^\mu \circ ReLU_{k_\mu}^\mu \circ g_{k_\mu}^\mu \circ \cdots \circ g_2^\mu \circ ReLU_1^\mu \circ g_1^\mu(\mathbf{x}) \\ \sigma(\mathbf{x}) &= S \circ g_{k_\sigma+1}^\sigma \circ ReLU_{k_\sigma}^\sigma \circ g_{k_\sigma}^\sigma \circ \cdots \circ g_2^\sigma \circ ReLU_1^\sigma \circ g_1^\sigma(\mathbf{x}) \\ \hat{y} &\sim \mathcal{N}(\mu(\mathbf{x}), \sigma^2(\mathbf{x})) \end{aligned} \tag{1}$$

where $\circ$ denotes the function decomposition operator.

The branching mode of the PMLP is achieved by setting a layer k^* such that $1 \le k^* \le \min\{k_\mu, k_\sigma\}$ and setting $ReLU_i^\mu(\mathbf{x}) = ReLU_i^\sigma(\mathbf{x})$, $g_i^\mu(\mathbf{x}) = g_i^\sigma(\mathbf{x})$ and $d_i^\mu = d_i^\sigma$ for all $1 \le i \le k^*$. Thus, before the k^*-th layer there is a common deep neural network; after the k^*-th layer, the network branches into two paths for predicting $\mu(\mathbf{x})$ and $\sigma(\mathbf{x})$ with each path having its own sequence of hidden layers with potentially different widths and depths.

The training of the PMLP is achieved by solving the following empirical risk minimisation problem. Given n data points $(\mathbf{x}_i, y_i) \in \Re^{d_0} \times \Re$, $i = 1, 2, \ldots, n$, and number and widths of the hidden layers, find $\hat{y}_i$ that is represented with an PMLP and minimises $\min_{\mathbf{W},\mathbf{b}} \mathscr{L}_1$ where $\mathbf{W} = \{\mathbf{W}_i\}_{i=1}^{k_{\text{total}}}$, $\mathbf{b} = \{\mathbf{b}_i\}_{i=1}^{k_{\text{total}}}$ denoting all parameters, and $\mathscr{L}_1$ is a

loss function. By assuming independence between $\hat{y}_i$, the product of normal densities $\prod_{i=1}^{n}\mathcal{N}(\mu(\mathbf{x}_i),\sigma^2(\mathbf{x}_i))$ can be viewed as a multivariate predictive density so a plausible loss function for our PMLP is the minus logarithmic score, see for example [2], defined as

$$\mathscr{L}_1 = -\sum_{i=1}^{n}\log\left(\mathcal{N}(y_i \mid \mu(\mathbf{x}_i),\sigma^2(\mathbf{x}_i))\right) \tag{2}$$

where $\mathcal{N}(y|\mu,\sigma)$ denotes the p.d.f. of a normal density with mean μ and variance σ^2 evaluated at y.

2.2 Transfer Learning

The realistic application of condition monitoring of a wind turbine should necessarily take into account the fact that the wind turbine is part of a wind farm. Thus, instead of training a model for each wind turbine separately, we could use the PMLP model of subsection 2.1 to train all wind turbines simultaneously.

We can apply model (1) to all wind turbines of the wind farm by just denoting $\mathbf{x}$ as the features from all wind turbines and $\hat{y}$ as a vector power output for a particular 10-minute period. The loss function (2) is just the sum of log-normal densities of each wind turbine at each 10-minute interval. The mathematical formulation of this model is as follows. Let $\mathbf{x}_{ij}$ be the input feature vector of the j-th wind turbine at the i-th 10-minute interval with corresponding output power y_{ij}. Then, the model is defined as

$$\begin{aligned}
\mu(\mathbf{x}_{ij}) &= g^{\mu}_{k_\mu+1}\circ ReLU^{\mu}_{k_\mu}\circ g^{\mu}_{k_\mu}\cdots g^{\mu}_{2}\circ ReLU^{\mu}_{1}\circ g^{\mu}_{1}(\mathbf{x}_{ij})\\
\sigma(\mathbf{x}_{ij}) &= S\circ g^{\sigma}_{k_\sigma+1}\circ ReLU^{\sigma}_{k_\sigma}\circ g^{\sigma}_{k_\sigma}\cdots g^{\sigma}_{2}\circ ReLU^{\sigma}_{1}\circ g^{\sigma}_{1}(\mathbf{x}_{ij})\\
\hat{y}_{ij} &\sim \mathcal{N}(\mu(\mathbf{x}_{ij}),\sigma^2(\mathbf{x}_{ij})).
\end{aligned} \tag{3}$$

If we have data for n_j time intervals for wind turbine j for $j=1,\ldots,J$, the loss function of model (3) is

$$\mathscr{L}_2 = -\sum_{j=1}^{J}\sum_{i=1}^{n_j}\log\left(\mathcal{N}(y_{ij} \mid \mu(\mathbf{x}_{ij}),\sigma^2(\mathbf{x}_{ij}))\right). \tag{4}$$

Notice that the possibly different number of available data n_j from each wind turbine indicates that this model utilizes all available data from all wind turbines. This is of huge practical importance in realistic applications since SCADA data typically contain many missing data.

However, by training all data of wind farms in the same model, the amount of available data may become prohibitively vast to allow frequent re-training. The usual treatment of such huge datasets is to adopt some transfer learning techniques so that knowledge gained from pre-training the model based on all wind turbines data can be used to boost performance in predicting the power of a single wind turbine. We call such a PMLP model that uses pre-training based on loss function $\mathscr{L}_2$ and then predicts the power of only one wind turbine using fine-tuning and the loss function $\mathscr{L}_1$ a Large PMLP (LPMLP) model. When new data arrive, re-training of the PMPL model based on $\mathscr{L}_2$ is not anymore necessary. Moreover, additional important practical advantages arise. First, consider the very realistic scenario in which a wind turbine has fewer data points because, for example, it has been out-of-order for a long period of time or has been recently installed. Normal behaviour modelling of this wind turbine might be very hard or even impossible to achieve. Our LPMLP model is capable of producing a predictive density for such low-information wind turbines by using the data from all wind turbines in the wind farm. Second, transfer learning can be used to improve the predictive power of model (1) as we empirically show in Section 3.

Our proposed transfer learning is achieved via the following fine-tuning. We first train the LPMLP model (3) with the loss function (4). Then, we use the parameters of the pre-trained model as initial values, and we predict the mean and standard deviation of the output power of the wind turbine we are interested in. Thus, the training uses the loss function (2) that refers to one only wind turbine and is achieved very fast.

3 Application

For all our experiments, we used a randomly selected $80-20$ data ratio for the train and test data, respectively. When a validation set was required, the train-validation data ratio was $72-8$. The PMLP and LPMLP models were trained using the Adam optimiser with a learning rate of 0.001, a batch size of 32, and 100 and 500 epochs respectively. This was done for both A1 and A2 architectures. Note that architecture A2 has $91,002$ parameters while architecture A1 has $16,508$ parameters. Additionally, the LPMLP models were fine-tuned for 50 epochs using learning rates of 10^{-3} and 10^{-4} for A1 and A2 respectively. The Softplus activation function $S(x)$, used a $\delta = 0.001$. Early stopping on a validation set was employed during all training stages. All results refer to the out-of-sample prediction of the output power of only one randomly chosen wind turbine of the wind farm.

The results shown in Table 1 are based on 151,504 and 37,877 training and test 10-minutes intervals respectively. Note that the models have been trained with SCADA data which have the size of nearly three years of wind turbines operation. We base our comparison with the usual root mean square and mean absolute error defined as RMSE $= (n^{-1}\sum_{i=1}^{n}(y_i - \mu(\mathbf{x}_i))^2)^{1/2}$ and MAE $= n^{-1}\sum_{i=1}^{n}|y_i - \mu(\mathbf{x}_i)|$ respectively. Although these metrics provide a good indication on how well our model predicts the output power, it is based only on the predicted means $\mu(\mathbf{x}_i)$. An issue of more importance to our condition monitoring methodology is the out-of-sample coverage probabilities that are defined as the probabilities that a confidence interval region will include the true power output. These are empirically estimated in our test data and shown in Fig. 3 where the calibration error, defined as the difference between observed and theoretical coverage probabilities are plotted for all six models and for twenty different intervals. The maximum calibrated error, which is the maximum observed deviation, is reported in Table 1.

Table 1: Out-of-sample performance metrics. SGP: Sparse Gaussian process; BNN: Bayesian neural network; PMLP: probabilistic multi-layer perceptron; LPMLP: large probabilistic multi-layer perceptron; arch.: architecture; RMSE: root mean square error; MAE: mean absolute error; MCE: maximum calibration error. Best performance is indicated in bold.

Metric	*SGP*	*BNN*	*PMLP arch. A1*	*LPMLP arch. A1*	*PMLP arch. A2*	*LPMLP arch. A2*
RMSE	45.17	30.06	28.19	25.38	26.09	**23.73**
MAE	30.44	16.47	14.99	13.62	14.17	**12.67**
MCE	17.79	1.83	1.12	1.91	**1.04**	1.77

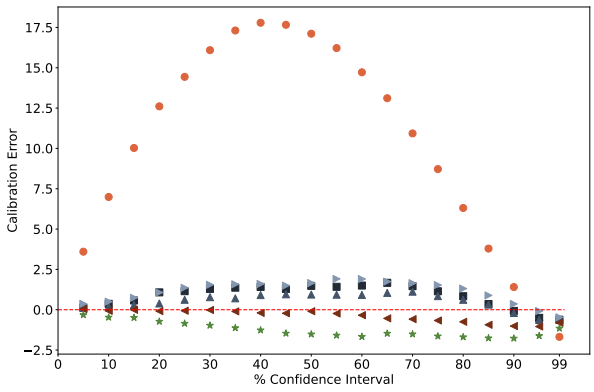

Figure 3: Calibration error of twenty binned confidence levels including the 95% and 99% confidence intervals. ● Sparse Gaussian process (RBF kernel); ▲ PMLP with architecture A1; ◀ PMLP with architecture A2; ■ Bayesian neural network; ▶ LPMLP with architecture A1; ★ LPMLP with architecture A2.

It is important to note that our condition monitoring system is based on testing model adequacy by testing the hypothesis that the observed output power observations have been generated by our trained model. This requires, of course, some evidence that our model has sufficiently good coverage probability so that in an out-of-sample healthy wind turbine environment the observed power output indeed follow the normal density indicated by the trained model.

For the data we used, our probabilistic model outperforms other probabilistic methods in terms of RMSE and MAE and has good coverage probabilities in large out-of-sample empirical exercises. Although it is an unsupervised monitoring system, we were able to illustrate its immediate applicability by inspecting the fault events file after an anomaly is detected.

References

[1] Z.-G. Deng, X. Zhang, Z. Li, J. Yang, X. Lv, Q. Wu, and B. Zhu. Probabilistic prediction of wind power based on improved Bayesian neural network. *Frontiers in Energy Research*, 11, 1 2024.

[2] T. Gneiting and A. E. Raftery. Strictly proper scoring rules, prediction, and estimation. *Journal of the American statistical Association*, 102(477):359–378, 2007.

[3] J. Li, L. Xiao, H. Li, and R. Li. Normal behavior models for the condition assessment of wind turbine generator systems. *Electric Power Components and Systems*, 42(11):1201–1212, 2014.

[4] R. Pandit, D. Infield, and A. Kolios. Gaussian process power curve models incorporating wind turbine operational variables. *Energy Reports*, 6:1658–1669, 2020.

[5] T. J. Rogers, P. A. Gardner, N. Dervilis, K. Worden, E. Maguire, E. Papatheou, and E. J. Cross. Probabilistic modelling of wind turbine power curves with application of heteroscedastic gaussian process regression. *Renewable Energy*, 148:1124–1136, 2020.

Novel Wind Lidar Configurations For Wind Energy Applications

Mohammadreza Manami[a,b], Mikael Sjöholm[a], Jakob Mann[a], Guillaume Léa[b], Guillaume Gorju[b]

[a] DTU Wind and Energy Systems, Technical University of Denmark, Roskilde, Denmark
[b] Lidar Division, LUMIBIRD, Lannion, France

E-mail: manami@dtu.dk, misj@dtu.dk

Keywords: Six-Beam Method, Lidar Configuration, Turbulence Measurements, Wind Energy

Accurate measurement of wind turbulence is a key factor affecting wind resource prediction, power production, turbine load and lifespan. Wind lidar provides high accuracy for wind speed measurements [1–3], however, measuring turbulence with high precision is still a challenge [4]. This research aims to develop state-of-the-art algorithms for the design space of lidar configurations tailored for capturing atmospheric turbulence in wind energy applications.

Most commercially available lidars utilize the velocity azimuth display (VAD) technique or the Doppler beam swinging (DBS) for wind profile measurements. However, an alternative method employing six lidar beams has been proposed to address limitations associated with only using one single elevation angle in characterizing atmospheric turbulence [4]. The six-beam method measures the radial velocity variances at five equally spaced azimuth angles along the base of a scanning cone, with an additional measurement at the center of the scanning circle (Figure 1). This method utilizes measurements at two distinct elevation angles, offering a significant improvement over the VAD and DBS techniques for determining the Reynolds stress tensor and turbulence parameters.

In this study, the modification to the aforementioned six-beam configuration is proposed for a prototype lidar with six flexible oriented telescopes, in order to achieve high accuracy for measuring turbulence parameters. The methodology includes signal processing and analysis algorithms from ongoing research campaigns. Besides, identifying the performance limitations is suggested by a detailed data analysis. Following the implementation of a novel configuration and new lidar line-of-sight geometry, the optimized retrievals of turbulence and atmospheric flow structures are expected.

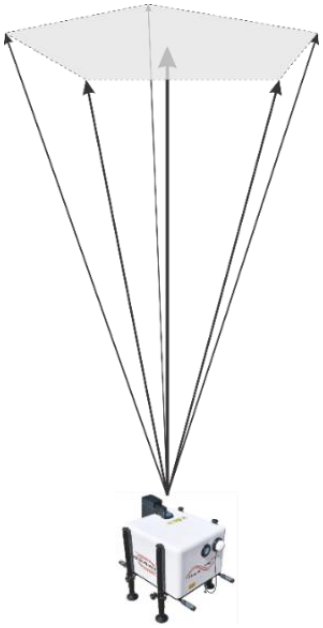

Figure 1: Schematic of the six-beam method utilized in lidar wind profiler "Streamline BEAM 6X" manufactured by the LUMIBIRD group [5].

References

[1] D.A. Smith, M. Harris, A.S. Coffey, T. Mikkelsen, H.E. Jørgensen, J. Mann, R. Danielian, Wind lidar evaluation at the Danish wind test site in Høvsøre, Wind Energy 9 (2006) 87–93. https://doi.org/https://doi.org/10.1002/we.193.

[2] A. Peña, C.B. Hasager, S.-E. Gryning, M. Courtney, I. Antoniou, T. Mikkelsen, Offshore wind profiling using light detection and ranging measurements, Wind Energy 12 (2009) 105–124. https://doi.org/https://doi.org/10.1002/we.283.

[3] R. Wagner, M. Courtney, J. Gottschall, P. Lindelöw-Marsden, Accounting for the speed shear in wind turbine power performance measurement, Wind Energy 14 (2011) 993–1004. https://doi.org/https://doi.org/10.1002/we.509.

[4] A. Sathe, J. Mann, N. Vasiljevic, G. Lea, A six-beam method to measure turbulence statistics using ground-based wind lidars, Atmos Meas Tech 8 (2015). https://doi.org/10.5194/amt-8-729-2015.

[5] METEK, Doppler Wind LIDAR Streamline | Streamline Beam 6X, METEK Meteorologische Messtechnik GmbH (n.d.). https://metek.de/product/streamline-beam-6x/ (accessed June 20, 2024).

Finite element analysis of the structural behaviour and fatigue life of a dynamic power cable

Esteban Cadavid Gil[a], Kris Hectors[a], Wim De Waele[a]

[a] Ghent University / OWI-Lab, Faculty of Engineering and Architecture, Department of Electromechanical, Systems, and Metal Engineering, Technologiepark-Zwijnaarde 46, Belgium

E-mail: esteban.cadavidgil@ugent.be

Keywords: Offshore Wind, Fatigue, Power Cable, Nonlinear Behavior, Finite Element

Abstract

This extended abstract introduces an approach based on a 3D finite element model aimed at analyzing the local stress state of a three-core dynamic power cable subjected to cyclic loading conditions. The study emphasizes detailed modelling of the cable and its components such as the conductors, metal screens, and armouring. Key aspects include the helical shape of components, inelastic material behaviour, friction and normal separation between cable components, and large deformations. The selection of the element types, the formulation of the friction effect, and the constitutive properties of inelastic material behaviour will be determined by balancing the computational cost with results accuracy. This approach is intended to contribute to a deeper understanding of the mechanical performance of dynamic power cables, vital for ensuring their reliable operation in the offshore floating wind industry.

1. Introduction

Floating offshore wind installations represent a clean and sustainable technology for renewable electric energy generation by exploiting the wind power. The electric energy generated by wind turbines is transported through dynamic power cables, which are subjected to rough environmental and operational conditions, such as wind- and wave-induced motions. These harsh loading conditions represent a risk of fatigue damage in dynamic power cables, potentially reducing their operational lifespan. Therefore, the dynamic, mechanical behaviour of power cables must be carefully predicted to ensure a reliable mechanical design that can fulfill the economic and technical challenges that arise [1].

For this purpose, both global and local analyses of dynamic power cables will be performed. The global analysis estimates the global loads on the power cables in response to the actions of the currents, waves, wind and the movements of the floating platform itself. These global loads (bending, tension and torsion) can then be transferred to the local analysis, which uses sub-models of the power cable to calculate the time series of stresses acting in individual components and their fatigue life [2]. Consequently, these sub-models must incorporate accurate representations of all cable components, such as electrical conductors, metal screens, insulations, fillers, inner and outer sheaths, and armouring (as illustrated in Figure 1). Due to the complex and heterogeneous geometry of the cable components, together with the variety of types of materials resulting in different mechanical properties, detailed 3D FE models are necessary for the local analysis.

This study is part of the BEL-Float project funded by FPS Economy through the Energy Transition Fund of the Federal Government of Belgium. The main goal is to assess the dynamic power cable deformation, stress and integrity using numerical modelling. The next section summarizes a review of the state of the art in finite element modeling of the structural behaviour of dynamic power cables. Next, a strategy is proposed to perform a local

analysis of stresses acting on cable components with greater modelling detail compared to the state of the art. Finally, some preliminary results are presented, followed by a discussion of the forthcoming work.

2. State-of-the-art

From the global analysis point of view, a case study of a point-absorber wave energy converter system is reported in [3]. In this work, the fatigue damage analysis was carried out by modelling the cables using beam elements with constant cross sections. Although the developed model was shown to be useful for analysing the dynamics and fatigue characteristics of the power cables, a detailed local model was required to simulate the interaction between the cable components. In [4], the global analysis of a floating offshore wind turbine (FOWT) was performed using the software SIMO/RIFLEX. In this analysis, the mooring lines were modelled as bar elements with only axial stiffness included, whereas the power cables were modelled as beam elements with specified axial, bending, and torsional stiffness. The achieved results showed that the mechanical response of the mooring lines and dynamic cables was dominated by the floater motions and sea current.

A local analysis, on the other hand, requires a more detailed modelling approach since dynamic power cables comprise an assembly of several components with different geometries and material properties. Moreover, some components such as the conductor and the armouring are formed by individual wires creating a complex helical shape. In [1], stresses in the armouring were estimated using a 3D finite element model along with periodic boundary conditions to reduce the computational time. In addition, this FE model accounted for the contact and friction effects between cable components. In [5], two finite element models with different cable lengths were implemented. One model considered a portion of 250 mm in length, while the other, represented by a RUC (Repeated Unit Cell), had a length of 20 mm. The former was dedicated to evaluating the cable's overall response in terms of the curvature-bending curve. The latter, validated using the longer model, was developed to compute the stresses in individual components with particular focus on the armouring. In [1] and [5], individual wires forming the armouring were represented as 3D solid elements. Furthermore, the helical shape of other components such as the conductor was not considered. In [6], and based on the results of their previous work [7], the authors reduced the computational expense of the numerical model by using 3D beam element modelling of armouring components. This modelling strategy provided an effective balance between accuracy and numerical efficiency and, compared with 3D solid elements, it resulted in lower computational time. This 3D FE model focused on the local analysis, also using periodic boundary conditions and including the contact between different components, was validated by experimental data and analytical results. The experimental data served to evaluate the overall behavior of the dynamic power cable under a cyclic bending load, whereas analytical models available in literature were used to validate the local analysis results. In [8], both experimental tests and finite element simulations were carried out to study the non-linear reciprocating bending response of a copper conductor.

3. Methodology for local stress analysis

This work focuses on the local analysis of stresses in individual components of a dynamic power cable, which will be used to assess the cable integrity and fatigue life.

Contrary to 3D FE models found in literature that tend to focus only on the armouring, and as a consequence only the helical shape and individual wires of this cable component are included, this research also intends to account for the helical geometry and composition of the conductor and metal screen. The conductor serves the purpose of transmitting the produced electrical power through the dynamic power cable. The metal screen provides electromagnetic shielding that protects the cable from electromagnetic interference. Both components are made up of a large number of wires. The metal screen is formed by winding thin copper wires around the metal conductor (made of aluminium or copper) at a particular laying angle. In the conductor, from the mechanical point of view, interaction between each individual wire in the same layer and among different layers leads to contact and friction effects. As a result, and together with the non-linear constitutive behaviour of some cable components, the whole structure undergoes a non-linear response under bending loading.

Since reciprocating bending behaviour is the key factor leading to fatigue damage of dynamic power cable components, research on the reciprocating bending response of power cables tends to focus solely on the mechanical properties of the steel wires in the armouring, which are designed to give the cable the required bending flexibility and axial and torsional resistance to withstand the severe operational conditions. As a result, other components such as the conductor, are often ignored. For this reason, this work also aims to analyze the non-linear bending response of the conductor and metal screen needed to accurately predict the fatigue life of the power cable.

In addition, the 3D FE model aims to consider each cable component separately. Contact mechanisms such as stick-slip behaviour and allowed normal separation between components will be taken into account.

As shown in image (b) of Figure 1, the cross section of a preliminary 3D FE model of the dynamic power cable under analysis is depicted. The three metal components of interest - conductor, metal screen and armouring - are highlighted. Furthermore, a flowchart illustrating the general procedure of this research is presented in image (c).

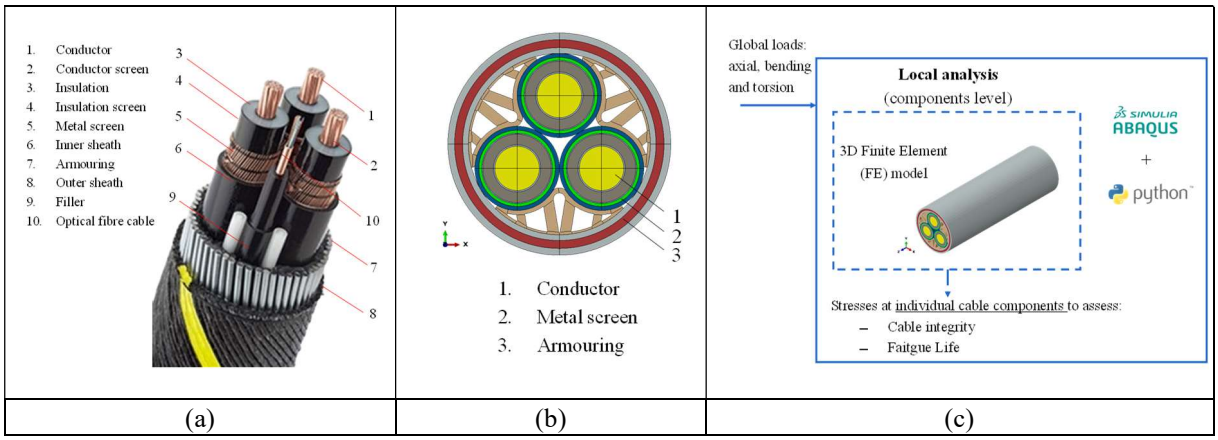

(a) (b) (c)

Figure 1: (a) Power cable components [9]. (b) Cross section of the studied power cable. (c) Flowchart of local stress analysis of a power cable segment

Preliminary benchmark results were obtained by performing finite element simulations of a 3D model in the commercial software Abaqus (version 2023). A 500 mm long segment of a dynamic power cable was modelled and subjected to a concentrated bending moment at one end, while the other end was fixed. The purpose of this preliminary study was to compute the axial stress in the metal screen as a function of the bending curvature. It is important to highlight that linear material behaviour was considered for this study. All components were modelled using first-order 3D elements with reduced integration scheme (C3D8R). In this preliminary study, the individual wires of the armouring, conductor and metal screen and tangential friction were not included to reduce computational time. Thus, these components were represented as cylinders and their helical shape was neglected. To compensate for the effect of these geometrical simplifications on the mechanical response of the power cable, the Young's modulus of these components was adjusted to (i) account for the angled orientation with respect to the main loading direction (using analytical equations available in literature [10]), and (ii) realize similar axial and bending stiffness of the real and simplified geometries. . Normal separation between all cable components was allowed. The following image illustrates the obtained results:

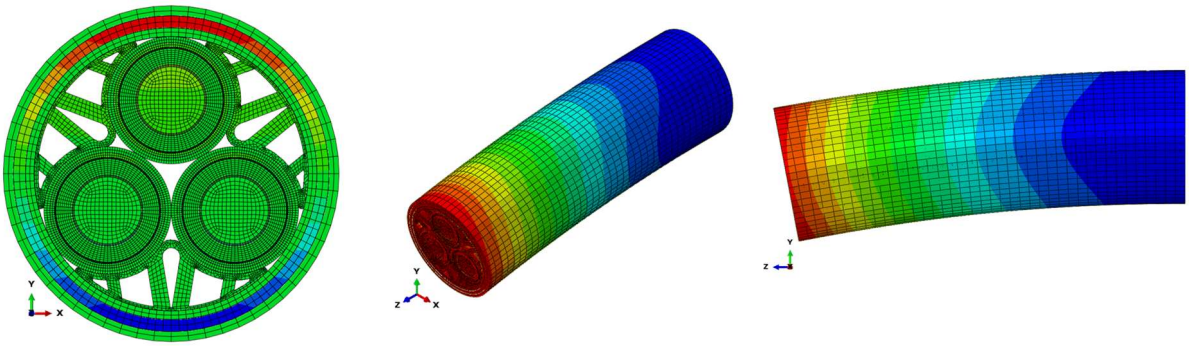

(a) (b) (c)

Figure 2: Axial stress distribution over the cross section. (b) and (c) Deformed cable segment.

4. Future work

To accurately compute the stresses in the individual components of the dynamic power cable, the preliminary 3D FE model will be enhanced to account for factors that significantly affect the non-linear bending response of the power cable. The primary modifications are the following:

- The helical geometry of the armouring, conductor and metal screen will be included, as well as individual wires that constitute these components.
- Two types of finite elements will be considered to model the individual wires of the aforementioned components: (i) 3D solid elements and (ii) 3D beam elements. The selection of one of both element types will be based on balancing computational cost and results accuracy.
- Friction between all cable components will be included, and a sensitivity analysis will be performed to determine whether it has significant effect on the results.
- Inelastic material behaviour of the cable components will eventually be considered. However, its inclusion in the FE model will depend on the computational cost.
- The calculated stress states in individual components will serve as input to fatigue damage models to assess the lifetime of the dynamic power cable.

5. Acknowledgements

This work is financially supported by the FPS Economy under the call 2022 of the Energy Transition Fund of the Belgian Federal Government through the BEL-Float project.

References

[1] J.-M. Leroy, Y. Poirette, N. Brusselle Dupend, and F. Caleyron, 'Assessing Mechanical Stresses in Dynamic Power Cables for Floating Offshore Wind Farms', in *Volume 10: Ocean Renewable Energy*, Trondheim, Norway: American Society of Mechanical Engineers, Jun. 2017, p. V010T09A050. doi: 10.1115/OMAE2017-61630.

[2] D. G. Young, C. Ng, S. Oterkus, Q. Li, and L. Johanning, 'Assessing the mechanical stresses of dynamic cables for floating offshore wind applications', *J. Phys. Conf. Ser.*, vol. 1102, p. 012016, Oct. 2018, doi: 10.1088/1742-6596/1102/1/012016.

[3] S.-H. Yang, J. W. Ringsberg, and E. Johnson, 'Parametric study of the dynamic motions and mechanical characteristics of power cables for wave energy converters', *J. Mar. Sci. Technol.*, vol. 23, no. 1, pp. 10–29, Mar. 2018, doi: 10.1007/s00773-017-0451-0.

[4] S. Zhao, Y. Cheng, P. Chen, Y. Nie, and K. Fan, 'A comparison of two dynamic power cable configurations for a floating offshore wind turbine in shallow water', *AIP Adv.*, vol. 11, no. 3, p. 035302, Mar. 2021, doi: 10.1063/5.0039221.

[5] P. Fang, X. Li, X. Jiang, H. Hopman, and Y. Bai, 'Bending study of submarine power cables based on a repeated unit cell model', *Eng. Struct.*, vol. 293, p. 116606, Oct. 2023, doi: 10.1016/j.engstruct.2023.116606.

[6] F. Ménard and P. Cartraud, 'A computationally efficient finite element model for the analysis of the non-linear bending behaviour of a dynamic submarine power cable', *Mar. Struct.*, vol. 91, p. 103465, Sep. 2023, doi: 10.1016/j.marstruc.2023.103465.

[7] F. Ménard and P. Cartraud, 'Solid and 3D beam finite element models for the nonlinear elastic analysis of helical strands within a computational homogenization framework', *Comput. Struct.*, vol. 257, p. 106675, Dec. 2021, doi: 10.1016/j.compstruc.2021.106675.

[8] H. Hu, J. Yan, S. Sævik, N. Ye, Q. Lu, and Y. Bu, 'Nonlinear bending behavior of a multilayer copper conductor in a dynamic power cable', *Ocean Eng.*, vol. 250, p. 110831, Apr. 2022, doi: 10.1016/j.oceaneng.2022.110831.

[9] B. Taormina *et al.*, 'A review of potential impacts of submarine power cables on the marine environment: Knowledge gaps, recommendations and future directions', *Renew. Sustain. Energy Rev.*, vol. 96, pp. 380–391, Nov. 2018, doi: 10.1016/j.rser.2018.07.026.

[10] E. A. W. De Menezes and R. J. Marczak, 'Comparative analysis of different approaches for computing axial, torsional and bending stiffnesses of cables and wire ropes', *Eng. Struct.*, vol. 241, p. 112487, Aug. 2021, doi: 10.1016/j.engstruct.2021.112487.

20th EAWE PhD Seminar on Wind Energy
24-26 September 2024
Visby, Sweden

Treatment of uncertainties in digital twin modelling

Thomas Bull[a,b]

[a]Aalborg University, Department of the Built Environment

[b]LICengineering A/S - part of the NIRAS group

E-mail: tbl@liceng.dk

Keywords: Epistemic uncertainty, Offshore wind turbines, Digital twin, Structural health monitoring

1 Introduction

Information gathered from Structural Health Monitoring (SHM) on structures in operation enhances the understanding of structural systems, such as those represented by finite element (FE) models. A calibrated FE model, often referred to as a digital twin (DT), can represent the physical system because it has been adjusted based on the available SHM information. In practice, it is common to calibrate a single best system representation using modal properties, see for example [1]. Once a model is selected, subsequent conclusions are drawn under the assumption that this model accurately represents the true system.

However, this approach overlooks the fact that there is no absolute truth in modeling, and a digital twin cannot fully replicate reality. It is known that multiple different system representations can have similar or identical likelihoods based on the available (often sparse) measurements [7], yet yield completely different predictions of unobserved quantities, such as stresses in structural details. Moreover, accurately accounting for the propagation of uncertainties in nonlinear models is crucial for obtaining unbiased results. Unfortunately, current state-of-the-art approaches often neglect this critical aspect, leading to biased results that are suboptimal and potentially unsafe.

The present extended abstract serves to showcase the influence of different DT models, with similar likelihood of explaining the data, on the inspection times of fatigue sensitive details of a monopile wind turbine structure exposed to typical environmental loading. The results are illustrated based on the probabilistic digital twin updating approach provided in Figure 1 combined with traditional fatigue limit state analysis and risk-based inspection (RBI) procedures.

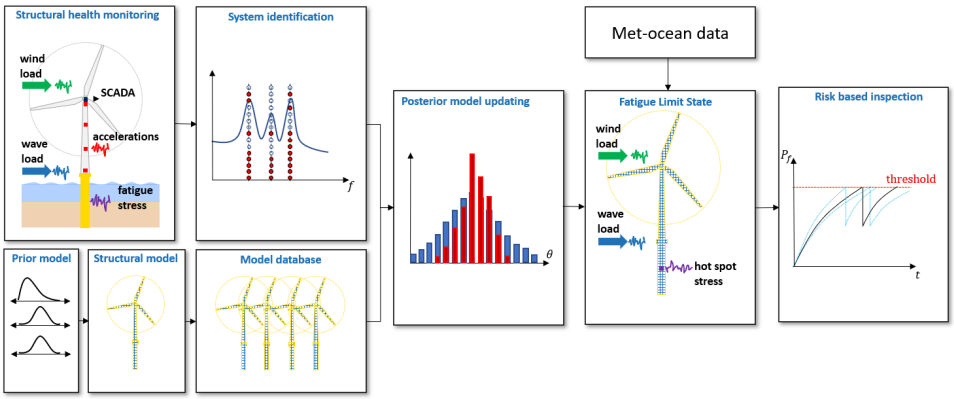

Figure 1: Probabilistic digital twin for risk-based inspection planning.

2 Probabilistic digital-twin based RBI

2.1 System identification

Modal properties (natural frequencies, damping ratios, and mode shapes) of the physical system are estimated using a covariance-driven stochastic subspace-based system identification (SSI) algorithm applied to SHM measurements. This algorithm requires the user to specify only one parameter: the model order n_o of the system. The SSI algorithm estimates the discrete-time state and output matrices, $\hat{\boldsymbol{A}}_d \in \mathbb{R}^{n_o \times n_o}$ and $\hat{\boldsymbol{C}} \in \mathbb{R}^{n_y \times n_o}$ (where n_y is the number of output channels) from which modal properties, $\hat{\lambda} \in \mathbb{C}$ and $\hat{\boldsymbol{\phi}} \in \mathbb{C}^{n_y}$, can be derived:

$$\hat{\lambda} = \frac{\ln \hat{\mu}}{\Delta t} \quad \text{and} \quad \hat{\boldsymbol{\phi}} = \hat{\boldsymbol{C}}\hat{\boldsymbol{\varphi}}. \tag{1}$$

As n_o is unknown in practice, the algorithm is typically run for multiple model orders and the identified frequencies, derived from system poles $\hat{\lambda}$ are arranged in a stabilization diagram allowing for manual classification of physical stable modes based on visual interpretation. To process large amount of available data, an automated approach is adopted in this work. To this end, the SSI algorithm is embedded in an automated operational modal analysis (AOMA) setting in which physical modes are classified through multistage clustering; the approach is outlined in detail in [2].

2.2 Posterior model

A design FE model and as-built drawings of the system is typically the starting point for the calibration based on prior model assumptions, $\boldsymbol{\theta} \in \mathcal{T}$ (with $\mathcal{T}$ being the prior samples drawn from the prior distribution). Subsequently, the calibration is solved by updating the prior distribution $f_{\boldsymbol{\Theta}}$ to a posterior distribution $f_{\boldsymbol{\Theta}|\mathcal{Y}}$ that considers the available measurements $\mathcal{Y}$. Formally, this is achieved using Bayes' theorem that gives the posterior distribution in a discrete setting by

$$\mathrm{f}_{\boldsymbol{\Theta}|\mathcal{Y}}(\boldsymbol{\theta}) = \frac{\mathcal{L}(\boldsymbol{\theta},\mathcal{Y})}{\sum_{\boldsymbol{\theta}\in\mathcal{T}} \mathcal{L}(\boldsymbol{\theta},\mathcal{Y})}, \quad \boldsymbol{\theta} \in \mathcal{T}. \tag{2}$$

For an explanation of the likelihood function and the distance metric the reader is referred to [2].

2.3 Reliability-based inspection

RBI is a specialized application of Bayesian decision theory [8] used to determine the optimal strategy for inspecting deteriorating structures [9]. RBI methods integrate reliability assessment with probabilistic updating to create a time-history of the reliability of hot spots—specific locations within the structure that have a high probability of failure. A hot spot subjected to cyclic loading accumulates fatigue damage with each cycle. To compute the damage for a specific stress collective, the Palmgren-Miner linear damage accumulation hypothesis is employed. The damage D at a hot spot is determined using a suitable S-N curve η and the stress spectra σ obtained from typical fatigue assessments with

$$D = \eta(\sigma, x_v) \tag{3}$$

where x_v represents realizations of an uncertain parameters vector specifying the SN-curve and its uncertainties. Given the damage, the normalized crack growth model (NCGM) [5] can be used to compute the crack length with

$$a(D,\alpha) = D_{\text{crit}} 10^{\frac{\log_{10}\left(\frac{D-\frac{\iota}{\alpha}}{1-\frac{\iota}{\alpha}}\right)}{\alpha(1+sD)f_{\text{plate}}}}, \tag{4}$$

where D_{crit} is the critical crack depth at which failure occurs, f_{plate} is the plate-thickness factor that depends on the thickness of the hot spot plate, ι and s are fitting parameters and α is a parameter describing the crack growth.

Finally, the quality of an inspection technique can be characterized through its PoD function. For a given crack length a, it returns the probability of detecting that crack with said inspection technique.

The PoD used in this study is given by [4]

$$\mathrm{PoD}(a) = 1 - \frac{1}{1 + \left(\frac{a}{x_0}\right)^h}, \tag{5}$$

where x_0 and h are parameters of the inspection method. This function can be inverted to obtain a probabilistic model of the detectable crack size with $c(u) = \mathrm{PoD}^{-1}(u)$, where u is a realization of a standard uniformly distributed random variable.

3 Case study

The case study examines the sensitivity of the model choice on two hot spot stress positions located in the monopile support structure. The wind turbine model used in the study is the 5 MW NREL wind turbine subjected to a typical fatigue limit state (FLS) load case with four accelerometers assumed mounted in the tower section. The monopile has a diameter of 6 m, a wall thickness of 50 mm, and an overall height of 60 m, including 30 m of soil penetration. The met-ocean and soil data utilized in the simulations are based on site-specific information from a region in the Baltic Sea. Wind conditions are simulated according to [3] with the normal turbulence model, while wave conditions are simulated using first-order theory and a JONSWAP spectrum.

The database is populated (utilizing Latin hypercube sampling) with 4,000 realizations of the independent marginals defined in Table 1. The marginals comprise stiffness related properties of the soil, monopile, tower and blades. The depth-dependent soil strength is assumed to follow a log-normal distribution with a mean of 1 and a coefficient of variation (COV) of 33 % [6], while the stiffness properties of the structure are assumed to be normal distributed with COVs of 5 %.

Table 1: Database variable marginal distribution.

Variable	Distribution	Mean	COV	Description
Θ_1	Log-normal	1	0.33	Undrained shear strength multiplier
Θ_2	Normal	2.1e11 Pa	0.05	Young's modulus of monopile
Θ_3	Normal	1	0.05	Tower stiffness multiplier
Θ_4	Normal	1	0.05	Blade stiffness multiplier

The RBI results, as illustrated in Figure 3, show that all the inspection plans, when using the PDT-informed stress estimates, are scattered around the inspection plan when using the "exact" stress from the simulations (which is only known in the present setting).

Any of the PDT-informed inspection plans represent sparse information at measurement positions, indicating that they could originate from a conventional "best" representation DT, though the exact inspection plan depends on the calibration routine. Depending on the DT model the inspection times can vary up to 10 years and can provide either overly conservative estimates of the failure probability or unconservative and potentially unsafe estimates of the failure probability.

The PDT-RBI approach provides a set of inspection plans, thus incorporating model uncertainty in evaluating the most cost-effective inspection plan.

The increased complexity introduced by the probabilistic RBI plans, stemming from multiple system representations, can be handled by introducing a life-cycle cost optimization approach for informing the decision-making process [10].

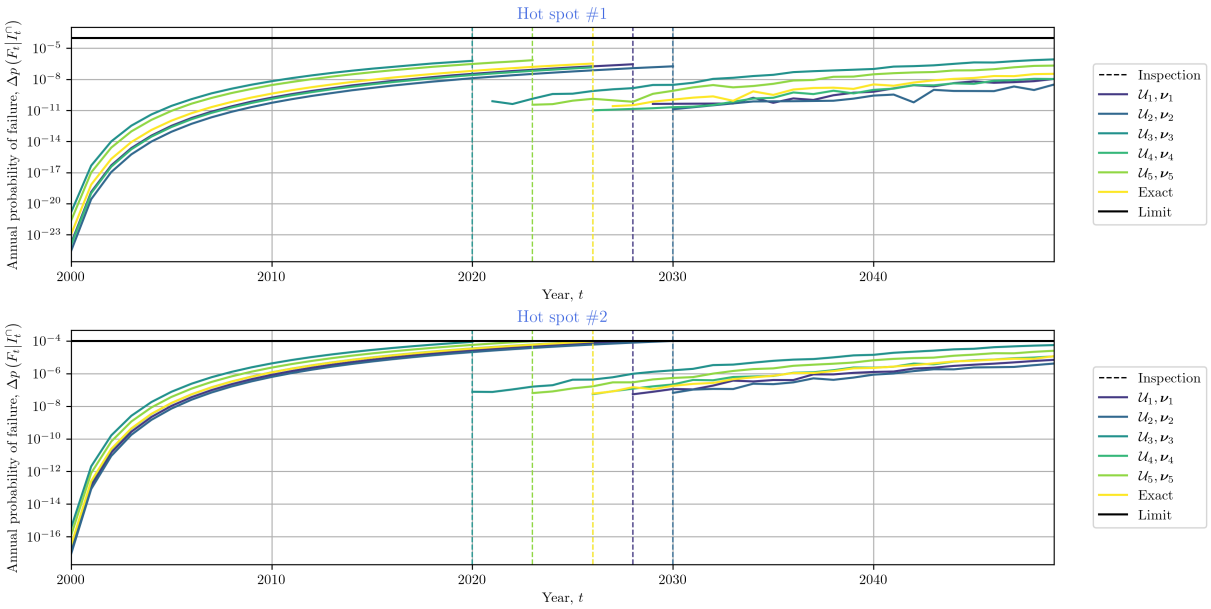

Figure 2: RBI plans for five posterior model realizations for the two hot spot groups Hot spot #1 and Hot spot #2. The inspection plan when using the actual stresses from the simulation is called "Exact".

References

[1] T. Bull, D. V. Muff, P.-R. Wagner, M. Schubert, H. J. Riber, W.-H. Zhang, and M. H. Faber. Digital twin and shm informed risk based inspection planning for offshore wind turbine structures. *14th International Conference on Applications of Statistics and Probability in Civil Engineering (ICASP14), Dublin, Ireland, 2023*, aug 2023.

[2] T. Bull, D. V. Muff, P. R. Wagner, W. H. Zhang, M. H. Faber, M. Schubert, and H. J. Riber. Probabilistic digital twin-informed risk based inspection planning for offshore wind turbine structures. *Submitted to Applied Energy*, 2024.

[3] DNV-ST-0437. Loads and site conditions for wind turbines. Standard, Det Norske Veritas, 2021.

[4] M. H. Faber and J. D. Sørensen. Reliability and risk based inspection planning for jacket structures, 2002.

[5] S. T. Glavind, H. Brüske, and M. H. Faber. On normalized fatigue crack growth modeling. *Proceedings of the ASME 2020 39th International Conference on Ocean, Offshore and Arctic Engineering*, 2A, aug 2020.

[6] A. L. Jones, S. L. Kramer, and P. Arduino. Estimation of uncertainty in geotechnical properties for performance-based earthquake engineering. Report, University of Washington, 2002.

[7] L. Nielsen, S. Tølbøll Glavind, J. Qin, and M. H. Faber. Faith and fakes–dealing with critical information in decision analysis. *Civil Engineering and Environmental Systems*, 36(1):32–54, 2019.

[8] H. Raiffa and R. Schlaifer. *Applied statistical decision theory*. Harvard University, fifth edition, 1961.

[9] D. Straub and M. H. Faber. Risk based inspection planning for structural systems. *Structural Safety*, 27(4):335–355, oct 2005.

[10] W. H. Zhang, T. Bull, P. R. Wagner, D. V. Muff, H. J. Riber, M. Schubert, and M. H. Faber. On risk-informed inspection planning in the face of epistemic uncertainty. *Submitted to Reliability Engineering and Safety*, 2024.

3.3 Session 312: Reliability, monitoring and sensing technology

26.09.2024, 9:0, Room 2

Chair:

Maksims Pogumirskis	

Presenters:

Oliveira Catarina	Population-based monitoring of wind turbines
Galhardo António	Improving OpenFAST models for wind turbine lifetime prediction using experimental measurements
Plets Jelle	Remaining fatigue lifetime of welded tubular joints of offshore structures using detailed stress analysis based on 3D scans

Population-based monitoring of wind turbines

Catarina Oliveira[a,b,c], João Santos[a], Elsa Caetano[b], Min Xu[c]

[a] Faculty of Engineering, University of Porto (FEUP), Rua Dr. Roberto Frias, s/n, 4200 - 465 Porto, Portugal
[b] Ventient Energy Limited, Rua João Chagas, 53A Piso 0, 1495 - 072 Algés, Portugal
[c] National Laboratory of Civil Engineer (LNEC), Avenida do Brasil, 101 1700 - 066 Lisboa, Portugal
E-mail: up202111325@edu.fe.up.pt

Keywords: Structural health monitoring, populations of structures, deep learning, wind turbines.

1 Introduction

The rapid adoption of renewable energy, driven by consumption needs and environmental concerns, highlights challenges in maintaining aging wind turbine infrastructure [1], [2]. As these turbines near the end of their operational life, early damage detection through Structural Health Monitoring (SHM) is crucial, yet integration faces obstacles such as data scarcity, high SHM system costs, and the need for reliable diagnostics [3]. The study of Supervisory Control and Data Acquisition (SCADA) high frequency and SHM data and their correlation aims to contribute as initial e exploratory analysis to address these challenges by employing Population Based Structural Health Monitoring (PBSHM) techniques [4].

2 Data

SCADA data is recorded from each wind turbine with a high sampling rate but is generally stored using 10-minute features (average, maximum, minimum, and standard deviation) [5]. According to the literature review, SCADA data is used for operation monitoring and SHM, most cases for power curve modelling, wind speed prediction, and prediction of another operational variable [6], [7].

In the case study, the SHM data is acquired from sensors installed in Candeeiros Wind Farm, located in Portugal. Four wind turbines are instrumented with strain gauges, accelerometers, and thermometers. From each system acquiring, time series are obtained for variables measured by the abovementioned sensors. Examples of time series of structural responses associated with accelerations and stresses are presented in Figure 1. An example of a temperature time series is also shown, which becomes relevant to measure despite being an action on the structure, considering its possible influence on the stress measurements.

Although 10-minute averages of data may be sufficient for operation monitoring, for SHM data processing, it is important to combine SCADA data with a higher temporal discretization and the data acquired from the instrumentation systems, particularly regarding the transformation of the values of the stresses measured at four points of the sections to the two main directions: fore-aft (FA) and side-to-side (SS).

Figure 2 shows examples of the combination of these two types of data, particularly strain. Considering only the operational data, the high similarity between the patterns of wind speed and power generated, both with a high correction with the generated generator speed (Figure 2(a)), is observed. Moreover, Figure 2(b) shows a variation in wind speed and direction, reproduced in a decrease of power produced shown in Figure 2(b). Regarding the combination of the data, the observed strain patterns follow the variations of wind speed and, consequently, of the generator speed and the power generated by the wind turbine (Figure 2(a)). Additionally, an untwist phenomenon is noted at the end of the day (change of the nacelle direction represented by red in Figure 2(b) and Figure 2(c)).

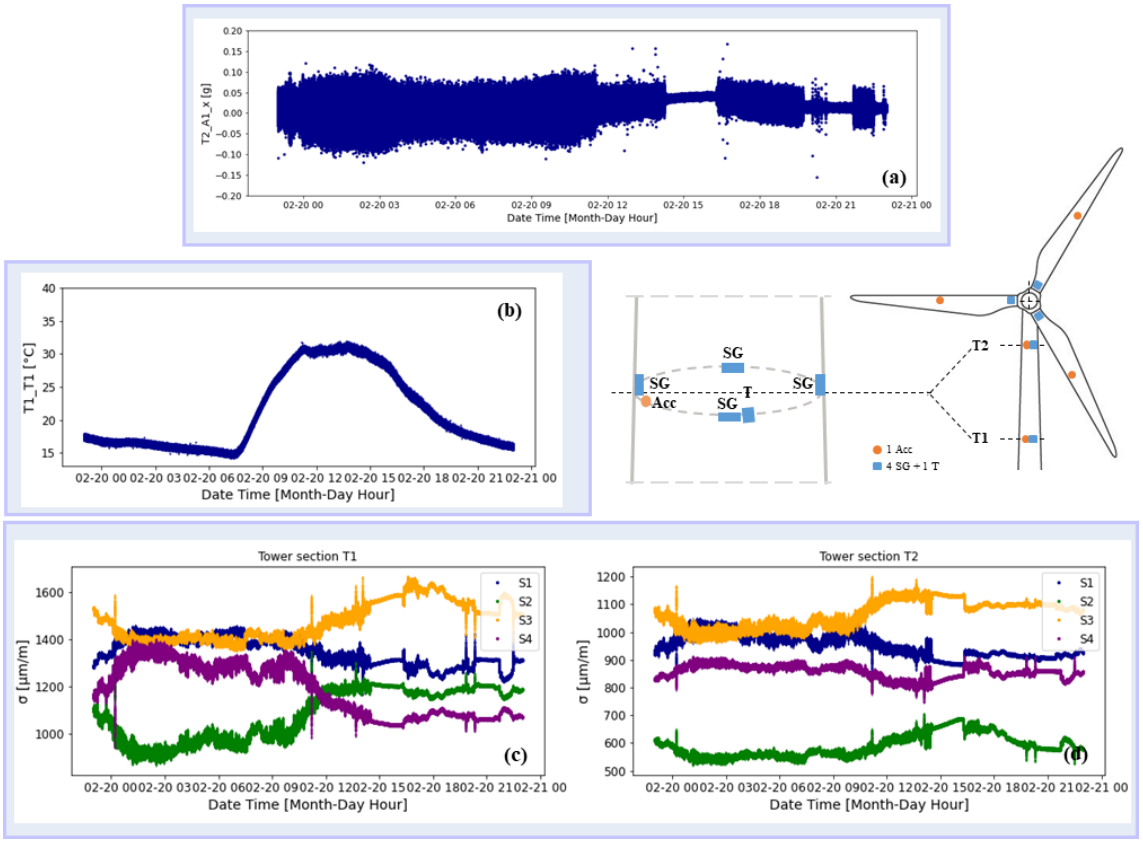

Figure 1: Examples of time series of acceleration and strains as structural responses and temperature as action measured from WTG35 of Candeeiros Wind Farm.

3 Operation monitoring

Before employing Population Based Structural Health Monitoring (PBSHM) techniques, understanding of the operational behaviour of each wind turbine as an individual structure is important ain in this sense modelling and predict the main operation curves is essential. These curves are being modelled with a Gaussian Process Regressor using SCADA 10-min data. For these models, a set of variable combinations are tested, and the best results are obtained for the case where just wind speed is considered the input variable.

In Figure 3, the measured and the modelling power, pitch, and generator speed curves can be observed. A good approximation between the real curves and the modelling curves is achieved in a global view. Furthermore, and for the specific case of the predicted power curve in Figure 4, it is possible to observe a good correlation between the two wind turbines regarding the test data and the predicted power. Although the wind turbines are not precisely equal, they present high similarity.

This example demonstrates the feasibility of applying the concept of populations of structures in the wind farm under study not only in the modelling and prediction of operational quantities but also in structural responses.

4 Conclusions and future work

The studies that have been developed highlight the high importance of considering high-frequency data in the analysis of operation and structural health monitoring, emphasizing that understanding this aspect is crucial. It is further concluded that the modes of operation of this type of structure influence the modelling of the main operating curves. It is suggested that future studies include analyses of wind direction sectors to improve the models. In future analyses, operational data should be modelled using SCADA-10min data related to a population of wind turbines with a tentative to represent the behaviour of the wind farm. It is also expected that structural data will be used to model and predict structural responses, using data from instrumented wind turbines.

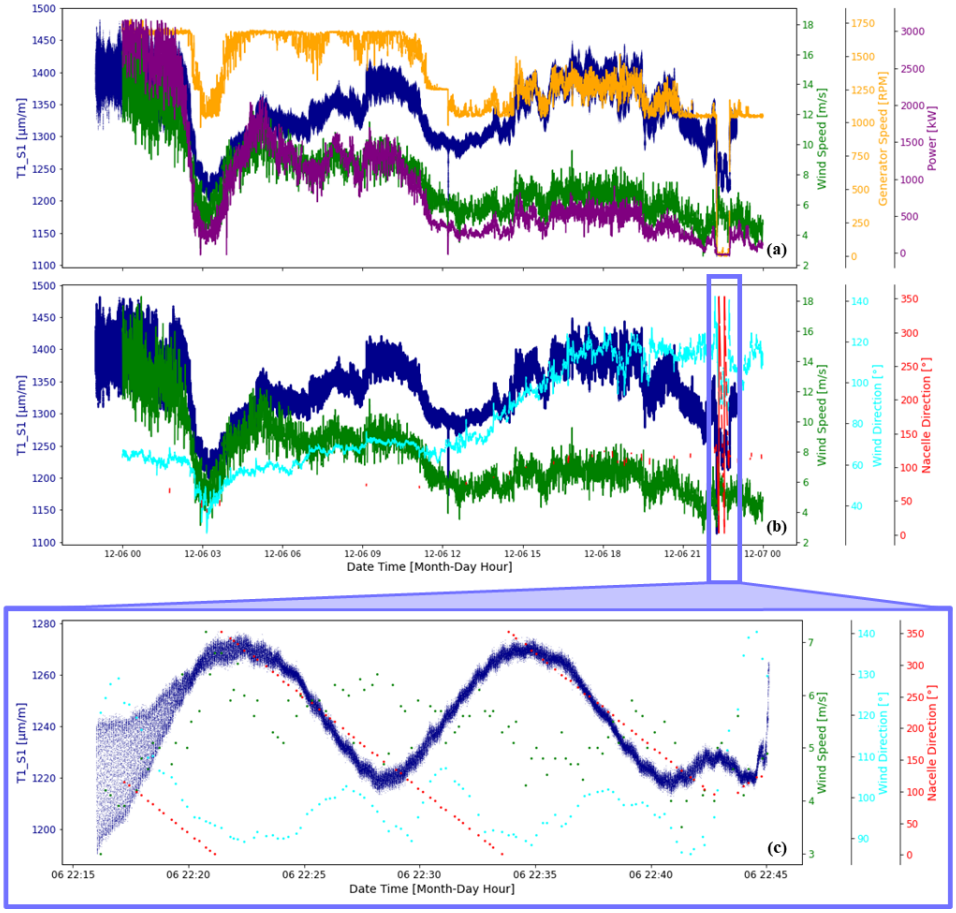

Figure 2 Time series of examples of strain S1 combined with operational high frequency data: (a) wind speed, generator speed and power, and (b) and (c) wind speed, wind direction and nacelle direction, measured on the tower section T1 of Candeeiros WTG35.

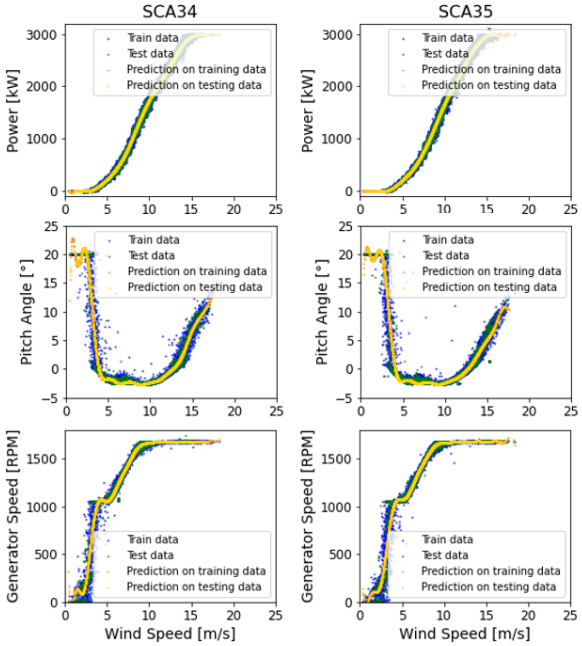

Figure 3 Results of operations curves modelling for wind turbines of Candeeiros Wind Farm: power in the first, pitch in the second and power in the third rows.

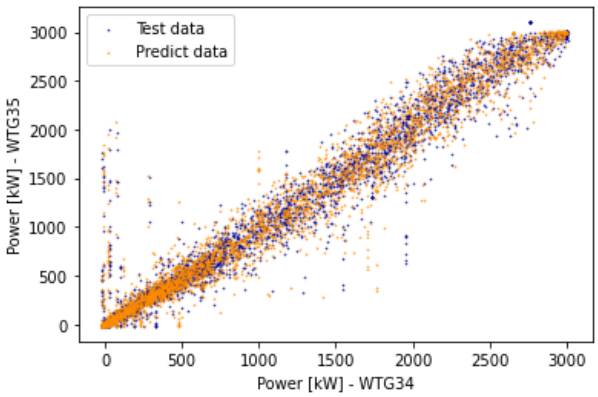

Figure 4 Results of correlations between the test and the predicted data for wind turbines WT34 and WT35 of Candeeiros Wind Farm.

Acknowledgements

This work is funded by the PhD Grant ref. 2021.06078.BD. This work is also a part of the ongoing research project: "M4WIND – Monitoring, Modelling and Machine learning for Managing the operating life of WIND farms", ref. 2022.08120.PTDC (https://doi.org/10.54499/2022.08120.PTDC). Funded by national funds through the FCT/MCTES (PIDDAC).

Furthermore, an acknowledgement to Ventient Energy for founding the opportunity to participate in the 20th PhD Seminar.

References

[1] Á. M. Costa, J. A. Orosa, D. Vergara, and P. Fernández-Arias, "New tendencies in wind energy operation and maintenance," *Applied Sciences (Switzerland)*, vol. 11, no. 4. MDPI AG, pp. 1–26, Feb. 02, 2021. doi: 10.3390/app11041386.

[2] S. Pfaffel, S. Faulstich, and K. Rohrig, "Performance and reliability of wind turbines: A review," *Energies*, vol. 10, no. 11. MDPI AG, Nov. 01, 2017. doi: 10.3390/en10111904.

[3] J. Gosliga, P. A. Gardner, L. A. Bull, N. Dervilis, and K. Worden, "Foundations of Population-based SHM, Part II: Heterogeneous populations – Graphs, networks, and communities," *Mech Syst Signal Process*, vol. 148, Feb. 2021, doi: 10.1016/j.ymssp.2020.107144.

[4] G. Tsialiamanis, N. Dervilis, D. J. Wagg, and K. Worden, "A Meta-Learning Approach to Population-Based Modelling of Structures," Feb. 2023, [Online]. Available: http://arxiv.org/abs/2302.07980

[5] A. Kusiak, H. Zheng, and Z. Song, "Models for monitoring wind farm power," *Renew Energy*, vol. 34, no. 3, pp. 583–590, Mar. 2009, doi: 10.1016/j.renene.2008.05.032.

[6] Y. Zhang, L. Liu, X. Xiong, G. Li, G. Wang, and L. Lin, "Long-term Wind Power Forecasting with Hierarchical Spatial-Temporal Transformer," May 2023, [Online]. Available: http://arxiv.org/abs/2305.18724

[7] S. M. Malakouti, "Improving the prediction of wind speed and power production of SCADA system with ensemble method and 10-fold cross-validation," *Case Studies in Chemical and Environmental Engineering*, vol. 8, Dec. 2023, doi: 10.1016/j.cscee.2023.100351.

20th EAWE PhD Seminar on Wind Energy
24-26 September 2024
Visby, Sweden

Improving OpenFAST models for wind turbine lifetime prediction using experimental measurements

António Galhardo[a,b], **Filipe Magalhães**[a], and **João Santos**[b]

[a]Faculty of Engineering, University of Porto (FEUP), Rua Dr. Roberto Frias 4200-465 Porto, Portugal
[b]Ventient Energy Limited, Rua João Chagas 53A Piso 0, 1495 072 Algés, Portugal
E-mail: up202202385@up.pt

Keywords: Structural health monitoring, aeroelastic modelling, OpenFAST, digital twin, optimization

1 Introduction

The ageing of wind turbines is a significant obstacle to the growth of wind energy in electricity production, with many assets approaching the typical design life of 20 years. In many cases, some years of lifetime extension are found to be profitable before repowering or decommissioning. However, this must not compromise structural stability, necessitating a technical analysis that ensures safe operation beyond design life. This work focuses on developing a tool for that analysis, combining structural health monitoring (SHM) systems with numerical aeroelastic modelling to create a digital twin. This takes advantage of the detailed response prediction in numerical models while using experimental results to tune model parameters that would otherwise have high uncertainty.

2 Background

The structural health monitoring of wind turbines has received extensive research. SHM systems usually consist of accelerometers and strain gauges, which can be used to study the frequency response and perform Rainflow cycle counting to estimate fatigue damage [1, 2]. Fatigue life assessments of towers are common and typically conclude that the design lifetime of 20 years is very conservative [3, 4]. For blades, however, SHM systems are more difficult to install and therefore rarer; some existing examples of instrumentation of blades during operation include [5, 6, 7].

Numerical aeroelastic modelling, using software such as OpenFAST [8], is an alternative and complementary strategy in order to analyse a wind turbine's behaviour. Works such as [9, 10] have developed faithful replications of a turbine's structural response and operational curves, but the uncertainty of several modelling parameters was highlighted. It is hypothesised that experimental results may be used to decrease those uncertainties by formulating optimization problems where unknown inputs are updated so that the output matches the measured response. This has been successfully done with finite element models [11, 12]. However, a similar approach using OpenFAST or similar codes was not found to have been deeply investigated so far.

3 Wind turbine monitoring

The present work relies on an experimental database measured at two Portuguese wind farms, each with two wind turbines equipped with the SHM systems schematised in figure 1. In wind farm 1, two sections at the tower top and bottom are instrumented with 8 strain gauges. Farm 2 has 2 instrumented tower sections in one turbine and only one in the other, which contain 4 strain gauges and 1 accelerometer. Furthermore, this farm has rotor instrumentation systems, consisting of 4 strain gauges in a section near the blade root (at radius $r = 3\,\text{m}$, and an accelerometer in the blade sections with $r = 14\,\text{m}$). All strain gauges are of the resistive kind.

The work developed thus far has focused mainly on farm 1, which has been instrumented for longer and thus has a larger database. The strain measurements were used to calculate the bending moments in the two sections,

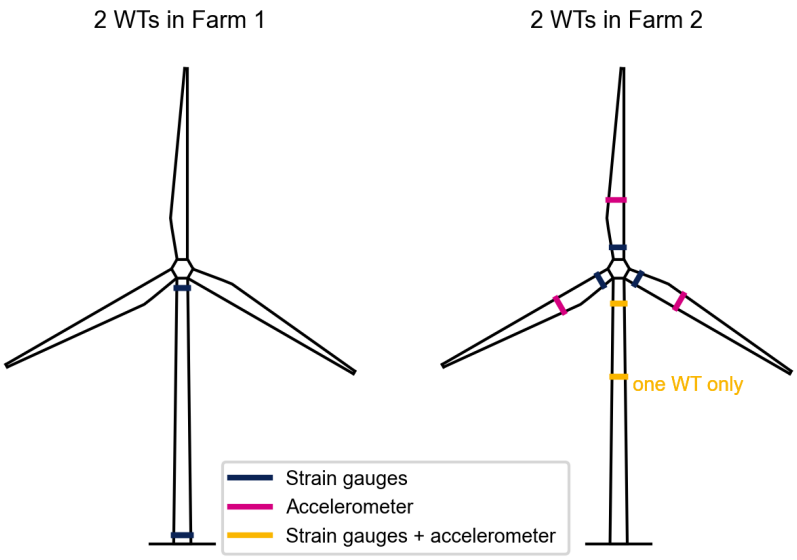

Figure 1: Experimental setups

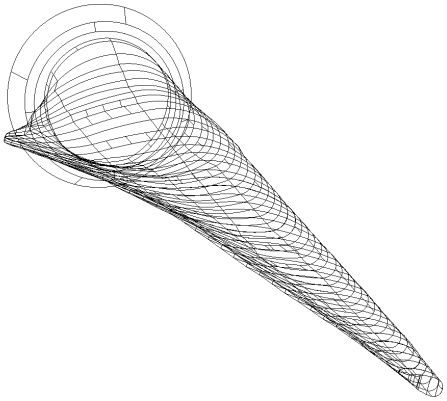

Figure 2: Laser scan results

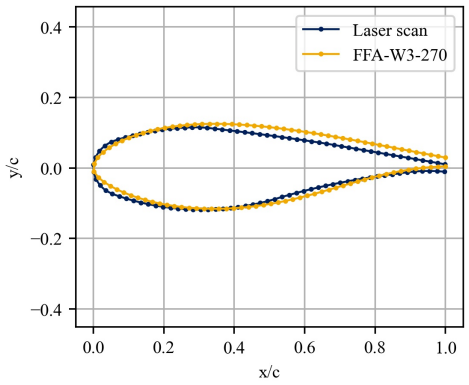

Figure 3: Comparison between laser scan and fitted foil

which required some pre-processing. The 360° rotations of the nacelle, during which the strains should measure a sinusoidal signal, were used to validate the sensors and calculate their drift as a function of time. In the top section, this also required removing the effect of stress concentrations due to interaction with the yaw mechanism. Subsequently, the bending moments were calculated by assuming plane stress in both sections and finding the mean plane defined by the sensor measurements at each time instant. Finally, the SCADA-logged yaw angle was used to convert the moments to the fore-aft and side-to-side directions.

In addition to the installation of SHM systems, a laser scan of the blade used in the farm 1 turbines was performed. This contributes to the knowledge of the blades geometry, a crucial modelling parameter which is difficult to obtain from the manufacturer, due to intellectual property protection. The laser scan results, illustrated in figure 2, estimated the cross-sectional geometry at 44 sections along the blade span. Thus the chord, twist, and airfoil shapes can be known. To know the airfoil shapes, the laser-scanned cross sections were compared with a database of airfoils with known geometry; for each section, the best fit was selected. Figure 3 shows an example.

4 OpenFAST modelling

Since the key idea of this work is to develop numerical models whose parameters are optimised using experimental measurements, two OpenFAST models were developed to mimic one of the turbines in farm 1. The first, named "Baseline", is meant to replicate a situation where no information is known about the blade's geometry. In this model, the blade properties were estimated by applying scaling laws to a reference wind turbine with similar rated power. The second model, named "Calibrated Model 1" or "CM1" for short, incorporates the laser scan results to establish a more accurate blade modelling approach. In both cases, the tower was modelled using information from manufacturer drawings and the controller was modelled with ROSCO [13], using SCADA measurements to calibrate parameters.

A comparison between the two models and the experimental results, in two variables which were considered to be particularly illustrative, is shown in figure 4. Firstly, the pitch curve shows that the wrong airfoils in the baseline model cause significant deviation from the SCADA measurements above rated wind speed. Regarding the tower base FA moment (an important variable for tower fatigue assessment), the models only differ in the below-rated regime, and both agree well with experimental results.

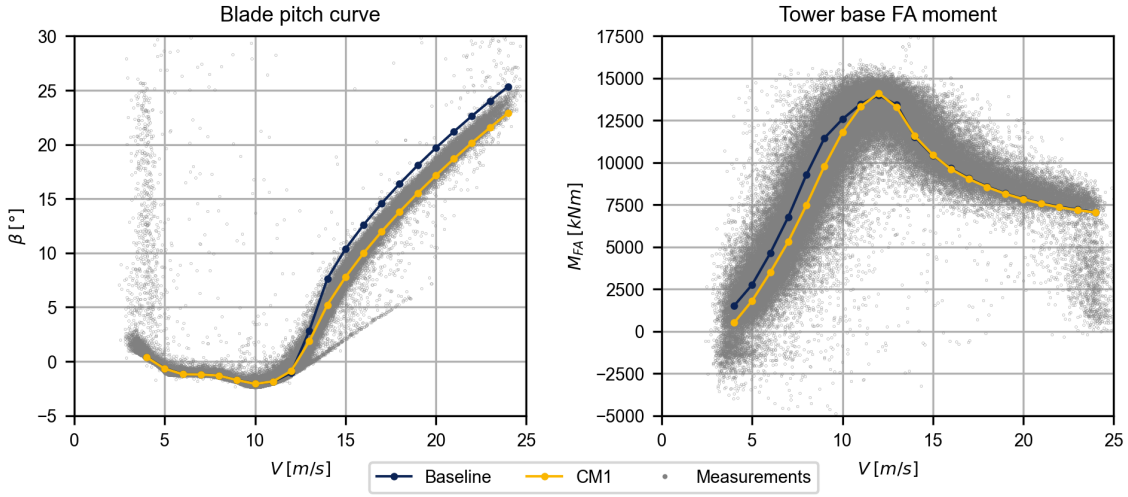

Figure 4: Comparison between models and SHM: blade pitch and tower base fore-aft moment

5 Conclusions and future work

The key idea of this work is to use experimental measurements in operational wind turbines to calibrated OpenFAST models. Thus far, a rich database of experimental results has been acquired, with SHM measurements at two wind farms and blade laser scans. Meanwhile, two OpenFAST models with different degrees of calibration have been developed. From the presented results, it is clear that the CM1 (which uses laser scan measurements) is superior to the baseline model, showcasing the importance of using those measurements.

The subsequent work will focus on developing additional models (CM2, CM3, etc.), which incorporate the SHM measurements in the calibration process. The measurements are expected to be crucial in optimising unknown structural parameters such as the blades mass and stiffness distributions. This may be done by establishing an optimisation problem, where the shape of those two functions is optimised to minimise the difference between modal parameters in the simulated and experimental results. Similarly, the SCADA pitch curves and the measured blade root bending moments may be used to develop alternative ways of estimating the chord, twist, and airfoil shapes, to avoid the large costs associated with laser scans.

Finally, the calibrated models will be used for fatigue assessment and remaining useful lifetime estimation. The detailed structural response given by numerical models is expected to help define transfer functions between instrumented and non-instrumented sections. Additionally, the instrumented wind turbines and their corresponding models will train machine learning models which learn the relationship between critical SHM indicators and easily

measurable SCADA parameters, thus extending the tool's applicability to non-instrumented turbines.

Acknowledgements

This work is funded by the PhD Grant ref. 2022.12813.BD. This work is also a part of the ongoing research project: "M4WIND – Monitoring, Modelling and Machine learning for Managing the operating life of WIND farms", ref. 2022.08120.PTDC (https://doi.org/10.54499/2022.08120.PTDC). Funded by national funds through the FCT/MCTES (PIDDAC).

References

[1] G. Oliveira, F. Magalhães, A. Cunha, and E. Caetano, "Development and implementation of a continuous dynamic monitoring system in a wind turbine," *Journal of Civil Structural Health Monitoring*, vol. 6, pp. 343–353, July 2016.

[2] J. Pacheco, F. Pimenta, S. Pereira, A. Cunha, and F. Magalhães, "Fatigue Assessment of Wind Turbine Towers: Review of Processing Strategies with Illustrative Case Study," *Energies*, vol. 15, p. 4782, Jan. 2022.

[3] C. Loraux and E. Brühwiler, "The use of long term monitoring data for the extension of the service duration of existing wind turbine support structures," *J.Phys.:Conf.Ser*, vol. 753, p. 072023, Sept. 2016.

[4] T. Rubert, G. Zorzi, G. Fusiek, P. Niewczas, D. McMillan, J. McAlorum, and M. Perry, "Wind turbine lifetime extension decision-making based on structural health monitoring," *Renewable Energy*, vol. 143, pp. 611–621, Dec. 2019.

[5] D. Tcherniak and G. C. Larsen, "Application of OMA to an Operating Wind Turbine: now including Vibration Data from the Blades," in *5th International Operational Modal Analysis Conference*, 2013.

[6] J. Zierath, R. Rachholz, S.-E. Rosenow, R. Bockhahn, A. Schulze, and C. Woernle, "Experimental identification of modal parameters of an industrial 2-MW wind turbine," *Wind Energy*, vol. 21, no. 5, pp. 338–356, 2018.

[7] J. Pacheco, S. Guimarães, C. Moutinho, M. Marques, J. C. Matos, and F. Magalhães, "New strategies for optimized structural monitoring of wind farms: experimental campaign," *Wind Energy Science*, vol. 5, pp. 983–996, Aug. 2020.

[8] B. Jonkman, R. M. Mudafort, A. Platt, E. Branlard, M. Sprague, jjonkman, H. Ross, HaymanConsulting, M. Hall, G. Vijayakumar, M. Buhl, P. Bortolotti, S. Ananthan, M. S, J. Rood, rdamiani, nrmendoza, sinolonghai, pschuenemann, D. Slaughter, ashesh2512, kshaler, S. Housner, psakievich, K. Bendl, L. Carmo, E. Quon, mattrphillips, N. KUSUNO, and A. G. Salcedo, "OpenFAST/openfast: v3.4.1," Feb. 2023.

[9] F. Pimenta, J. Pacheco, C. M. Branco, C. M. Teixeira, and F. Magalhães, "Development of a digital twin of an onshore wind turbine using monitoring data," *Journal of Physics: Conference Series*, vol. 1618, p. 022065, Sept. 2020.

[10] B. Moynihan, B. Moaveni, S. Liberatore, and E. Hines, "Estimation of Blade Forces in Wind Turbines Using Strain Measurements Collected on Blades," in *Dynamics of Civil Structures, Volume 2* (K. Grimmelsman, ed.), Conference Proceedings of the Society for Experimental Mechanics Series, (Cham), pp. 43–48, Springer International Publishing, 2022.

[11] B. Moynihan, A. Mehrjoo, B. Moaveni, R. McAdam, F. Rüdinger, and E. Hines, "System identification and finite element model updating of a 6 MW offshore wind turbine using vibrational response measurements," *Renewable Energy*, vol. 219, p. 119430, Dec. 2023.

[12] M. Song, B. Moaveni, H. Ebrahimian, E. Hines, and A. Bajric, "Joint parameter-input estimation for digital twinning of the Block Island wind turbine using output-only measurements," *Mechanical Systems and Signal Processing*, vol. 198, p. 110425, Sept. 2023.

[13] N. J. Abbas, D. S. Zalkind, L. Pao, and A. Wright, "A reference open-source controller for fixed and floating offshore wind turbines," *Wind Energy Science*, vol. 7, pp. 53–73, Jan. 2022.

20th EAWE PhD Seminar on Wind Energy
24-26 September 2024
Visby, Sweden

Remaining fatigue lifetime of welded tubular joints of offshore structures using detailed stress analysis based on 3D scans

Jelle Plets[a], **Kris Hectors**[a], and **Wim De Waele**[a]

[a]Ghent University / OWI-Lab, Faculty of Engineering and Architecture, Department of Electromechanical, Systems and Metal engineering, Laboratory Soete, Belgium
E-mail: Jelle.Plets@UGent.be

Abstract

Corrosion and fatigue damage are the primary factors contributing to the degradation of offshore steel substructures. In the FlexWind project, funded by the Energy Transition Fund of the Belgian federal government, an innovative approach will be developed to assess the remaining fatigue resistance of offshore wind turbine foundations. Instead of relying solely on design documentation, the as-built conditions will be considered. More specifically, the aim is to enhance the analysis of local aspects, such as surface degradation and the actual weld geometry, beyond current standard practices. To this end, a framework for semi-automated reconstruction of finite element models based on 3D scanned data is developed. The required local geometrical data is obtained using a handheld 3D laser scanner. As only the outer surfaces are accessible to the scanner, the framework needs to reconstruct the inaccessible parts. The finite element model is used to determine the fatigue governing local stresses that serve as the input for fatigue life prediction of the welded joints.

Keywords: Fatigue, Life extension, 3D laser scanning, Offshore wind

1 Introduction

Offshore wind turbines and their foundations are typically designed to have an operational lifetime of 20 years [1]. From 2029 onwards, many wind turbines in the North Sea will reach their design lives, as shown in Figure 1. Once the design life is reached, there are three possible scenarios for the substructures of these turbines; decommissioning, lifetime extension or repowering. The latter two are economically and ecologically more beneficial, but require an extensive investigation to ensure the continued safe operation of the substructure. The goal of the FlexWind project is to develop a framework to determine the remaining lifetime of fixed-bottom substructures. This paper focuses on a jacket-type substructure, which is the second most common substructure type in European offshore wind farms, alongside monopiles [16]. With respect to structural integrity, the welds of the tubular joints are the most critical locations for fatigue.

In the design stage, lifetime calculations of the substructure are based on the as-designed geometry and idealized welds. High safety factors are included to account for the deviations of the as-built geometry. By performing a more detailed analysis of the tubular joints, the lifetime can be assessed more accurately and lower safety factors can be incorporated. Previous research [11, 6] has shown that the actual weld geometry significantly influences the local stresses and, consequently, the fatigue life. This work aims to develop a new method for fatigue life analysis that accounts for the as-built geometry of the welds and any surface degradation due to (pitting) corrosion, based on 3D laser scans of the joints.

2 Literature study

In 2016, Lang et al. [8] applied 3D laser scanning for the quality assessment of welds. They highlighted that using 3D laser scanning, the quality control can be done independently from the operator, resulting in greater

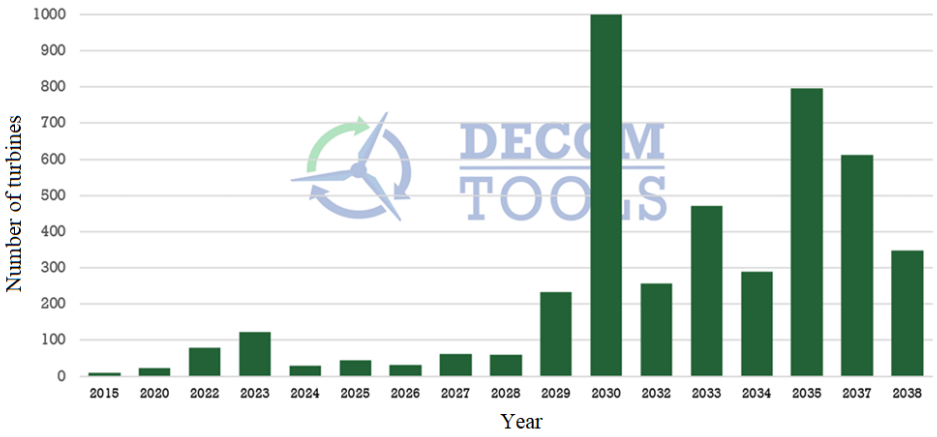

Figure 1: Number of wind turbines that reach their design lifetime in the North Sea [10].

consistency. In a follow-up paper, they showed the potential of using laser scanning data as input for finite element models for fatigue analysis [7]. Inspired by Tovo et al. [15], Lang et al. applied the stress gradient approach to determine fatigue governing effective stresses. These were then used as input for a probabilistic Weibull-based crack initiation framework to calculate the fatigue life of a variety of components.

Stenberg et al. [13] investigated the use of laser scanning technology for online monitoring of weld quality. They developed a system called ONWELD to assess the weld quality of fillet, overlap, and butt welds. A few years later, Hultgren et al. [2, 4, 3] from the same research group published several papers on the fatigue assessment of welded joints based on data collected from laser scans. They evaluated the importance of variations in the weld geometry features, such as weld toe radius, weld toe angle and throat thickness, on the fatigue strength. They used a probabilistic framework focusing on the weld geometry features to evaluate the fatigue strength. One of the conclusions drawn from their work was that surrounding geometry can reduce the influence of a very small local defect. The main advantage of using laser scanning data is thus also the biggest challenge of the technology, namely that much smaller defects can be detected compared to weld property measurements.

Shojai et al. [12] investigated the influence of pitting corrosion on the fatigue strength of steel structures. To quantify the corrosion damage, they used 3D surface scans. The influence on the local stress of the pitting corrosion is captured with stress concentration factors. These can then be used for the evaluation of the remaining fatigue life based on S-N curves. In previous research at Laboratory Soete, finite element models haven been generated based on 3D scans of corrosion pitted surfaces [5]. The result of such an analysis is shown in Figure 2. The main challenge faced in this research was the convergence of the local stress values at the sharp features of the model.

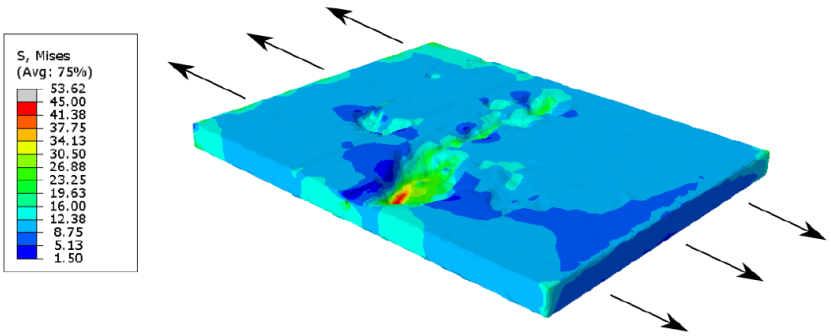

Figure 2: Distribution of von Mises stress in a finite element model based on a 3D scan of a corrosion pitted surface [5].

3 Methodology

First, a 3D scanner is used to capture the geometrical data of tubular joints. In this work, the Creaform HandySCAN3D is used, which projects structured blue light on the surface of the specimen. The deformed pattern is observed by two cameras and is used by the software to recreate the outer surface based on the triangulation principle. The output of the scan is a point cloud.

The downside of laser scanners is that only the outer surface can be scanned. Besides, only the outer walls of the tubular members are accessible. Therefore, a framework is developed to (semi-)automatically reconstruct the inaccessible parts of the specimen. This requires assumptions to be made about the inner walls of the tubular members and the geometry of the weld roots. The reconstruction steps followed by the framework are shown in Figure 3.

The reconstructed point cloud forms the basis for a finite element model. The finite element models of the joints include as much geometrical detail as possible. However, it is expected that stress singularities will occur at sharp features in the finite element model.

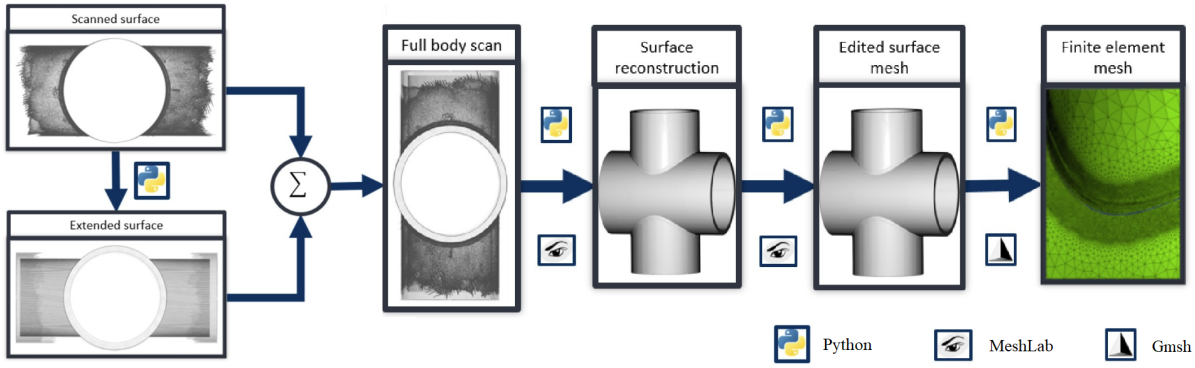

Figure 3: Flowchart illustrating the process of mesh reconstruction from 3D scan data.

To deal with the stress singularities, different stress analysis methods will be compared, such as the theory of critical distances (TCD) [14] and the implicit gradient approach [15]. The results of these stress analysis methods is an effective stress, which is not sensitive to the stress singularities. Especially, the implicit gradient approach seems promising since it is a non-local method. This means it can be applied to the whole specimen at once, contrary to the more popular TCD variants.

Appropriate loading conditions for the high-fidelity tubular joint models will be determined from global aero-hydro-elastic simulations on a full-scale lower-fidelity model. Within the scope of this work, these simulations will be performed in the QBlade software [9]. These simulations will be used to determine the loads on the members of the studied joints, which can then be applied to the high-fidelity joint models.

4 Expected outcomes

The expected outcomes of this research are:

- The development of a numerical framework that is able to convert welded joint scanning data to highly detailed solid finite element models. The 3D scans are made with a handheld laser scanner.
- The development of a stress-based fatigue analysis method for long continuous welds of tubular joints based on surface scanned data. The output of this method is an effective stress, which can be used together with S-N curves to determine the remaining fatigue lifetime of the joint.
- Hindcasting the accumulated fatigue damage and forecasting the remaining fatigue life of offshore jacket structures. To this end, the high-fidelity submodels of welded tubular joints will be one-way coupled to aero-hydro-elastic global models.

The expected outcomes of this research will contribute to the advancement of knowledge in the field of fatigue damage accumulation of welded tubular joints, leading to improved design practices and lifetime calculations for offshore jacket substructures.

Acknowledgements

This work is supported by the ETF (Energy Transition Fund) of the Federal Government of Belgium through the FlexWind project.

References

[1] DNV-ST-0126: Support structures for wind turbines. *Det Norske Veritas*, 2021.

[2] G. Hultgren and Z. Barsoum. Fatigue assessment in welded joints based on geometrical variations measured by laser scanning. *Welding in the World*, 64:1825–1831, 2020. doi: 10.1007/s40194-020-00962-8.

[3] G. Hultgren, R. Mansour, et al. Fatigue strength assessment of welded joints incorporating the variability in local weld geometry using a probabilistic framework. *International Journal of Fatigue*, 167, 2023. doi: 10.1016/j.ijfatigue.2022.107364.

[4] G. Hultgren, L. Myrén, et al. Digital scanning of welds and influence of sampling resolution on the predicted fatigue performance: modelling, experiment and simulation. *Metals*, 11, 2021. doi: 10.3390/MET11050822.

[5] L. Jacobs. Constructing a finite element model from a 3d scanned corrosion pitted surface. Master's thesis, Ghent University, 2021.

[6] K. Hectors and W. De Waele. Influence of weld geometry on stress concentration factor distributions in tubular joints. *Journal of Constructional Steel Research*, 176, 2021. doi: 10.1016/J.JCSR.2020.106376.

[7] R. Lang and G. Lener. Application and comparison of deterministic and stochastic methods for the evaluation of welded components' fatigue lifetime based on real notch stresses. *International Journal of Fatigue*, 93:184–193, 2016. doi: 10.1016/j.ijfatigue.2016.08.023.

[8] R. Lang, G. Lener, et al. Welded seam evaluation based on 3D laser scanning. *Stahlbau*, 85:336–343, 2016. doi: 10.1002/STAB.201610375.

[9] D. Marten, J. Wendler, et al. Qblade : An open source tool for design and simulation of horizontal and vertical axis wind turbines. *International Journal of Emerging Technology and Advanced Engineering*, 3, 2013.

[10] Safety4Sea. Offshore wind decommissioning in North Sea to increase from 2020, new study shows, 2020. https://safety4sea.com/offshore-wind-decommissioning-in-north-sea-to-increase-from-2020-new-study-shows/.

[11] B. Schork, P. Kucharczyk, et al. The effect of the local and global weld geometry as well as material defects on crack initiation and fatigue strength. *Engineering Fracture Mechanics*, 198:103–122, 2018. doi: 10.1016/j.engfracmech.2017.07.001.

[12] S. Shojai, P. Schaumann, et al. Influence of pitting corrosion on the fatigue strength of offshore steel structures based on 3d surface scans. *International Journal of Fatigue*, 164, 2022. doi: 10.1016/j.ijfatigue.2022.107128.

[13] T. Stenberg, Z. Barsoum, et al. Quality control and assurance in fabrication of welded structures subjected to fatigue loading. *Welding in the World*, 61:1003–1015, 2017. doi: 10.1007/S40194-017-0490-5.

[14] D. Taylor. The theory of critical distances. *Engineering Fracture Mechanics*, 75:1696–1705, 2008. doi: 10.1016/J.ENGFRACMECH.2007.04.007.

[15] R. Tovo and P. Livieri. An implicit gradient application to fatigue of sharp notches and weldments. *Engineering Fracture Mechanics*, 74:515–526, 2007. doi: 10.1016/J.ENGFRACMECH.2006.06.009.

[16] WindEurope. Offshore wind in europe - key trends and statistics 2019, 2020. https://windeurope.org/wp-content/uploads/files/about-wind/statistics/WindEurope-Annual-Offshore-Statistics-2019.pdf.

3.4 Session 325: Reliability, monitoring and sensing technology

26.09.2024, 10:30, Room 5

Chair:

Vasco Batista

Presenters:

Marini Rebeca	Insights in wind field reconstruction from LiDAR measurements
O'Neill Niall	Optimization under uncertainty applied to wind farm design and control

20th EAWE PhD Seminar on Wind Energy
24-26 September 2024
Visby, Sweden

Insights in wind field reconstruction from LiDAR measurements

Rebeca Marini[a], **Konstantinos Vratsini**[a], **Pieter-Jan Daems**[a], **Timothy Verstraeten**[a,b], and **Jan Helsen**[a]

[a]OWI-Lab, Vrije Universiteit Brussel, Pleinlaan 2, Brussels, 1050, Belgium
[b]Artificial Intelligence lab, Vrije Universiteit Brussel, Pleinlaan 2, Brussels, 1050, Belgium

E-mail: rebeca.marini@vub.be

Keywords: Wind Field Reconstruction, Offshore wind farm, LiDAR

The global rise in offshore wind farms underscores the need to cut costs and optimise energy production. As turbines increase and wind farms become more concentrated, mitigating downstream wake effects is crucial for operational efficiency. LiDAR technology, offering advantages like eliminating the need for meteorology masts, has been extensively discussed in the literature. However, it indirectly measures wind parameters, relying on assumptions and embedded algorithms. Wind field reconstruction (WFR) methods empower users with more control over LiDAR measurements, allowing tailored flow assumptions and parameter estimation. Using LiDAR data from two sequential campaigns at a wind farm, the research analyses LiDAR performance validated with SCADA measurements and applies WFR for wind field parameters estimation. Comparative analyses of wind parameters from different sources, particularly downstream turbines, demonstrate the robustness of WFR. The reconstructed wind field is compared with SCADA data for a comprehensive assessment.

1 Introduction

The European Union (EU) has set guidelines and targets to fulfil the United Nations' Agenda for 2030 to ensure a better future for the next generations. One of these is to further decarbonise the current energy system, for example, by further investing in renewable energy research. Wind energy in the last two decades has been rapidly growing, representing more than 35% of the produced renewable energy in the EU during 2020 [1]. The European Wind Energy Association (EWEA) estimates this growth to reach almost 400 GW production by 2030, with 25% produced in offshore wind farms [2].

Wind field reconstruction methods are techniques to infer the wind field over a specific area of interest, typically using wind measurements from one or more sensors. These methods are necessary since the LiDAR retrieves the backscattered light detected along a line-of-sight of the direction of the emitted laser beam. This limitation causes an ambiguity in the WFR, also known as Cyclops dilemma [3]. The Cyclops Dilemma is a challenge encountered in remote sensing measurements of wind speed and direction using a single monostatic LiDAR. To determine the full wind vector, multiple sensors measuring the same position or the sensor measuring at distinct locations can be used to reconstruct the wind field. The former is an expensive solution, so the latter is implemented at the cost of using simplification assumptions of the wind field.

In the current work, an established wind field reconstruction (WFR) method is implemented and further validated with offshore LiDAR measurements. The 2-beam WFR method is implemented, a widely used methodology by researchers due to its straightforward application and acceptable wind speed and direction estimations [4]. The reconstruction is made in two locations within the same wind farm, namely in two sequentially downstream wind turbines, and the correspondent time series of estimated wind speed and direction are compared. The difference between the reconstructed wind field is noticeable, indicating a possible negative influence from wakes on the accuracy of the estimated wind field from the 2-beam WFR method.

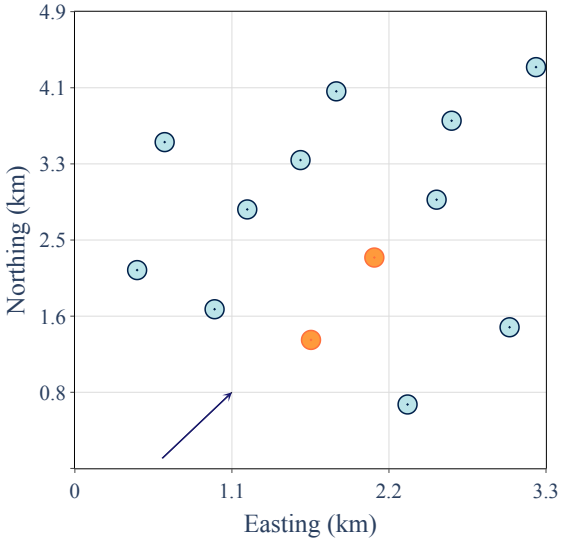

Figure 1: The LiDAR was installed on top of the nacelle of two turbines of the same wind farm. Specifically, in the first and second rows, seen in orange, the neighbouring turbines are highlighted in blue. The dominant wind direction, i.e., south-west, is denoted by a dark blue arrow.

2 Methodology

The objective is to derive the horizontal wind speed and direction using LiDAR measurements. The current paper focuses on implementing a method called 2-beam reconstruction. However, it must be implemented under certain wind flow assumptions, such as horizontal homogeneity, a two- or three-dimensional wind vector, and a predefined shear profile [5]. The implementation uses Python with the default mathematical algorithms, such as the least squares optimisation in the module *scipy*. Different authors, for example, in [6, 7], have implemented a 2-beam reconstruction method with slight differences in methodologies but with the same principle basis.

This study analysed two field experiments executed in a wind farm in the Belgian North Sea. Each campaign gathered several months of measurements with the same LiDAR in different wind turbines and different years, one in 2022 and then in 2023. The chosen wind turbines are positioned in a sequential downstream of each other, as in Figure 1, where a schematic of a section of the wind farm is shown. The second measurement campaign is made in the first row of the wind farm, where there are no installed wind turbines in the region's dominant wind direction. The wind farm consists of several rows of wind turbines Vestas V164 with 9.5MW rated power, a hub height of 104 m and a diameter of 164 m.

In the first field experiment, the LiDAR was installed in the second row of wind turbines from winter to spring of 2022. The following year, the second field experiment started with two different measurement periods, between winter and spring and from the end of summer of the following year. The same LiDAR was installed in the first row of wind turbines for the second field experiment. Furthermore, for the scope of the current research, the final date for the second field experiment was set at the end of autumn. So, although there was no simultaneous measurement campaign, some of the same meteorological seasons were captured in both experiments.

3 Results

The methodology is applied to the LiDAR and SCADA data set described in Section 2. All reconstruction results are made at 420m from the wind turbine at hub height. As mentioned, LiDAR's fit-derived wind components are used to compare and validate the experimental setup and the wind parameters estimation with the presented method. After deploying the measurement campaign, LiDAR's fit-derived records were compared with the wind data captured by the sensors installed by the wind turbine manufacturer, which is designated SCADA. It was determined that, for the studied time window, the measurements show a good agreement between them, validating the LiDAR's functioning and positioning.

After the validation process, which enhances confidence in the measurements, implementing the WFR method becomes more reliable. The 2-beam method demonstrates an excellent agreement with SCADA for wind speed, as the correlation factor is very high in both reconstructions. For this analysis, the data is filtered for the undisturbed wind direction of the wind farm, with the second row decreasing to a R^2 with a value of 0.95. Nevertheless, there is a high correlation, but the potential presence of wake effects can explain the decrease from a R^2 of 0.98. To this end, the reconstruction method's behaviour in free flow and waked conditions is investigated. However, these strong correlations show the method's effectiveness in providing precise wind speed estimations.

Figure 2 highlights the variations in wind direction reconstruction errors when the LiDAR was placed in two different locations, i.e., on a turbine in the free flow and a turbine in waked conditions from all cardinal directions. As seen, regions without turbines have a minor reconstruction error due to minimal wake influence. Moreover, there is a relationship between the distance of neighbouring turbines and the reconstruction error. Specifically, the reconstruction error increases when a neighbouring turbine is closer to a specific direction. Compared to Figure **??**, the sectors influenced by wake effects depict higher deviations in wind direction but do not seem to influence wind speed estimation. There is a better agreement between the south and west in the cardinal locations without wind turbines. However, it is significantly less accurate when considering north and east, where a higher density of wind turbines is present. This indicates a more substantial wake influence on the free-flow wind turbine in these directions.

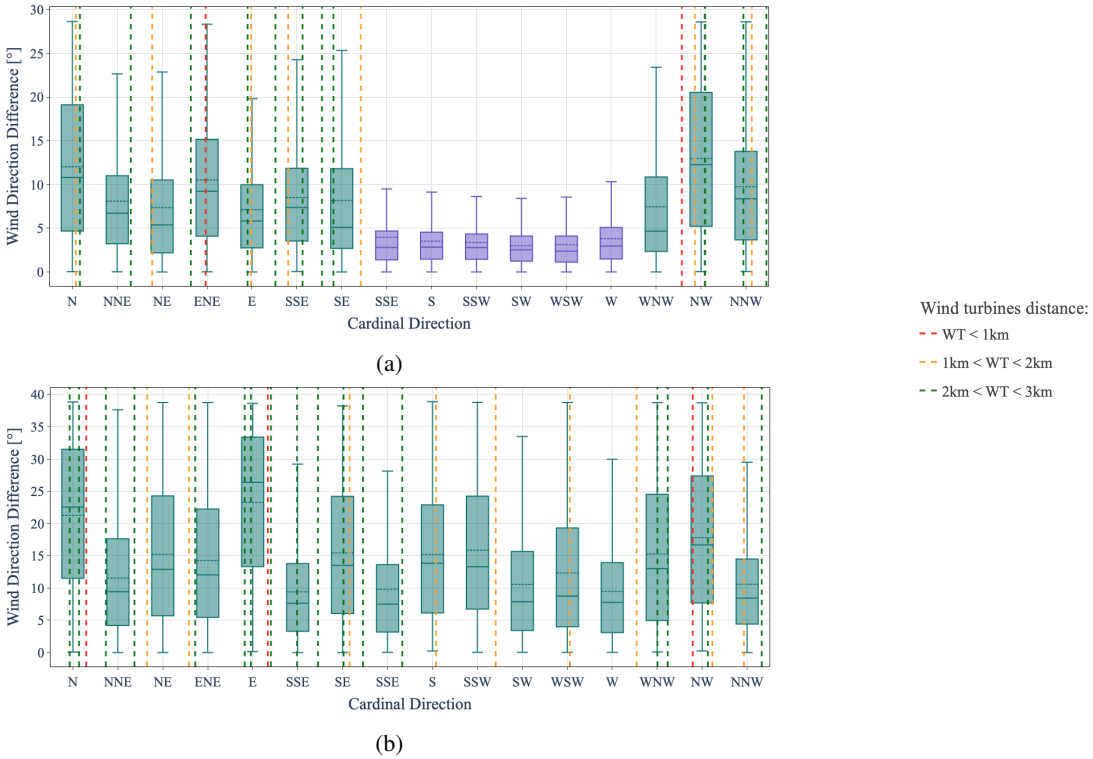

(a)

(b)

Figure 2: Box plot of the absolute difference between estimated and measured wind directions of the first row (a) and the second row (b) -mounted LiDAR. The boxes for the cardinal locations without wind turbines, signifying free-flow conditions, are coloured blue, while in-wake conditions are coloured green. Dashed red lines denote the presence of a wind turbine less than 1 km away. The yellow dashed lines denote the presence of a wind turbine between 1 km and 2 km, while green lines denote between 2 km and 3 km.

4 Conclusions

Following a measurement campaign on an offshore wind turbine, it is necessary to analyse and interpret the measured data with appropriate methodologies. This research is currently underway, representing the first steps towards extracting wind field insights from the LiDAR measurements. The initial findings are shared and discussed in this

paper to provide insights on the possible wake effect in wind field reconstruction, namely in the context of offshore wind energy.

Due to the assumed flow simplifications, the 2-beam WFR method has higher errors in more dynamic weather conditions [8]. These are more noticeable in wind direction estimations, where the wake affects the line-of-sight measurement. To increase the current level of accuracy, it is necessary to detect and correct these measurements. Further investigation is needed on handling in-wake conditions, where samples are taken in a mixture of wakes.

The methodology proposed by Borraccino et al. [9] introduces a less simplistic, potentially more accurate, static WFR method. This approach was applied with nacelle-mounted LiDAR measurements from an experimental campaign conducted on an onshore wind turbine. The comprehensive insights from this research underscore the potential of nacelle-mounted LiDAR as a valuable tool for measuring and optimising wind energy systems. This paper presents a practical application of leveraging LiDAR technology. It provides a methodological framework for reconstructing the wind field from LiDAR measurements, paving the way for further advancements in wind energy performance optimisation.

Acknowledgements

This research was supported by funding from VLAIO (Flemish Agency for Innovation and Entrepreneurship) and Blue Cluster through project SBO CORE and the intercluster SIM-Blue Cluster ICON Rainbow. The authors, moreover, acknowledge the support via the Flemish Government under the “Onderzoeksprogramma Artificiële Intelligentie (AI) Vlaanderen” program.

References

[1] H. Ritchie and M. Roser, “Energy,” *Our World in Data*, 2020.

[2] EWEA, “Aiming high rewarding ambition in wind energy,” *The European Wind Energy Association*, 2015.

[3] F. Guillemin, D. D. Domenico, N. Nguyen, G. Sabiron, M. Boquet, N. Girard, and D. Coupiac, “Nacelle lidar online wind field reconstruction applied to feedforward pitch control,” in *Journal of Physics: Conference Series*, vol. 753, p. 052019, IOP Publishing, 2016.

[4] R. Wagner, R. L. Rivera, I. Antoniou, S. Davoust, T. F. Pedersen, M. Courtney, and B. Diznabi, “Procedure for wind turbine power performance measurement with a two-beam nacelle lidar,” 2013.

[5] A. Borraccino, M. Courtney, and R. Wagner, “Generic methodology for field calibration of nacelle-based wind lidars,” *Remote Sensing*, vol. 8, p. 907, 2016.

[6] D. Schlipf, L. Y. Pao, and P. W. Cheng, “Comparison of feedforward and model predictive control of wind turbines using lidar,” in *51st IEEE Conference on Decision and Control (CDC)*, pp. 3050–3055, IEEE, 2012.

[7] R. Wagner, T. F. Pedersen, M. Courtney, I. Antoniou, S. Davoust, and R. L. Rivera, “Power curve measurement with a nacelle-mounted lidar,” *Wind Energy*, vol. 17, pp. 1441–1453, 2014.

[8] H. Wang, R. J. Barthelmie, A. Clifton, and S. C. Pryor, “Wind measurements from arc scans with doppler wind lidar,” *Journal of Atmospheric and Oceanic Technology*, vol. 32, pp. 2024–2040, 2015.

[9] A. Borraccino, D. Schlipf, F. Haizmann, and R. Wagner, “Wind field reconstruction from nacelle-mounted lidar short-range measurements,” *Wind Energy Science*, vol. 2, pp. 269–283, 2017.

20th EAWE PhD Seminar on Wind Energy
24 - 26 September 2023
Visby, Sweden

Optimization Under Uncertainty Applied to Wind Farm Design & Control

Niall O'Neill

[a] Technical University of Denmark
[b] Électricité de France

E-mail: ntion@dtu.dk

Keywords: Uncertainty Quantification, Multi-Fidelity Modelling, Wind Farm Layout Optimization

1. Context & research question

To meet EU targets for increased capacity of wind energy and to take advantage of the large offshore wind resource, wind turbines are becoming larger and entering environments where understanding of the flow physics is currently insufficient. Improvements in multi-fidelity flow modelling, to meet these demands will play a vital role in the design of next generation wind farms. Such models often require many input parameters, all containing a degree of uncertainty. With multiplicity, these uncertainties propagate through the model, leading to higher uncertainties in overall predictions [1]. It follows that the development of a tool to quantify uncertainty will play an important role in achieving the higher-level objective of improving wind farm flow models.

An improved knowledge of the effect of model and parameter uncertainties on turbine selection and layout design is a key target. Currently, IEC 61400-1 design standard for offshore wind turbines does not consider uncertainties in environmental loading, blade shape or material properties when evaluating the structural performance. The assumption of deterministic values and use of high factors of safety result in expensive project costs [2]. Considering the large investments required for offshore wind farms, quantifying uncertainties in AEP holds a strong potential to reduce financial costs from high factors of safety. Uncertainty in the wind condition can lead to high variation in the yearly AEP. This variation is harmful to the economic viability of offshore wind farms [3].

2. Research methods/objectives

A comprehensive literature review of current uncertainty quantification (UQ) approaches must be carried out to identify gaps and limitations. At a high level, the methodology for optimization under uncertainty may be categorized in sections 2.1-2.4.

2.1. Identification of which input parameters significantly affect the output:

Sensitivity analyses for offshore wind farm models [1] have shown that wind turbulence parameters may be the most sensitive parameters influencing turbine loads and overall system response. With a focus on atmospheric flow simulations and downscaling in this work, there may be additional parameters such as downscaling methods and multi-fidelity modelling parameters that cause additional uncertainties in the output.

2.2. Quantification of uncertainties associated with the selected parameters:

If available, data may be fit to a probability distribution to quantify the uncertainty. Knowledge gained from the EU HiperWind project [4] may be used in this stage to inform UQ methodologies.

2.3. Sampling strategies:

To minimize the number of costly simulations, sampling strategies such as random sampling or latin hypercube sampling may be used. A unique sampling strategy may be developed to suit the needs of the specific problem.

2.4. Uncertainty Propagation:

Surrogate models may be trained on the samples from multiple levels of fidelity to approximate the entire design space and allow for more efficient propagation of uncertainties. Robust optimization techniques may be used to achieve the multi-objective optimization goal of maximization of the value for AEP whilst minimizing the variability and sensitivity to uncertainty in model inputs [3]. Achieving a trade-off between minimizing variation in AEP, whilst also maximizing the mean AEP value is key to making wind farm proposals more attractive.

3. Expected outcomes

The first expected research outcome includes the demonstration of a systematic approach to quantifying uncertainty in the context of multi-fidelity flow modelling and down-scaling. Once a clear approach has been laid out to deal with uncertainty, an approach to couple multi-fidelity tools in the design process will be

developed. The targeted use case is robust wind farm design optimisation under uncertainty. Finally, an advancement in open-loop (wake/noise/load) control under uncertainty.

Acknowledgements

This work is part of the AptWind Industrial Doctoral Network granted under the Horizon Europe Marie Sklodowska-Curie Actions.

References

[1] W. Wiley, J. Jonkman, A. Robertson, and K. Shaler, "Sensitivity analysis of numerical modeling input parameters on floating offshore wind turbine loads," *Wind Energ. Sci*, vol. 8, pp. 1575–1595, 2023, doi: 10.5194/wes-8-1575-2023.

[2] Y. Shao and J. Liu, "Uncertainty quantification for dynamic responses of offshore wind turbine based on manifold learning," *Renew Energy*, vol. 222, Feb. 2024, doi: 10.1016/j.renene.2023.119798.

[3] Y. Wen, M. Song, and J. Wang, "Wind farm layout optimization with uncertain wind condition," *Energy Convers Manag*, vol. 256, p. 115347, Mar. 2022, doi: 10.1016/J.ENCONMAN.2022.115347.

[4] N. K. Dimitrov *et al.*, "End-to-end wind turbine design under uncertainties: A practical example," *J Phys Conf Ser*, vol. 2767, no. 8, 2024, doi: 10.1088/1742-6596/2767/8/082017.

TOPIC 4

Control of wind turbines and wind farms

4.1 Session 114: Control of wind turbines and wind farms

24.09.2024, 10:30, Room 4

Chair:

Mohammadreza Manami

Presenters:

Vanelli Thea	Wind farm modeling for enhanced performance
Duthé Gregory	On the potential of graph neural network surrogates for fatigue-aware control and design of wind farms
Bortolin Davide	An Experimental and Numerical Study of Static and Dynamic Yaw-based Wake Mixing
Mirzaei Mohammad Javad	Enhanced robust control of floating wind conversion system using neural network observer
Sun Haoyuan	Verifying engineering steady yaw models using actuator disc simulations

20th EAWE PhD Seminar on Wind Energy
24-26 September 2024
Visby, Sweden

Wind farm modelling for enhanced performance

Thea Vanelli[a,b], **Ebba Dellwik**[a], **Mahmood Mirzaei**[b], **Jakob Mann**[a], and **Mark Žagar**[b]

[a]Technical University of Denmark
[b]Vestas Wind Systems A/S

E-mail: thevan@dtu.dk

Keywords: Wind farm modelling, wake modelling, lidar, power performance, complex terrain

As wind energy is becoming an important electricity source in the energy market, there is a need to improve its predictability over daily and seasonal cycles. Additionally, in order to maximize power production and project revenue, advanced wind farm control strategies can be implemented. To answer both these needs, the correct understanding of the complex interactions between the atmospheric conditions and the power production of wind farms is important.

In this context, the proposed project aims at exploring new possibilities to study both the power performance and control settings of the individual wind turbines and their resulting wakes under the daily and seasonally varying atmospheric conditions. A unique database of both meteorological data and SCADA data is available from a wind farm located in complex terrain and cold climate. The wind farm is composed of 25 turbines and every turbine is equipped with a nacelle-mounted lidar. Data analysis will be performed on the available database and results will be compared to existing wind farm and wake models, such as PyWake [2] and Floris [1]. For this task, the selection of specific case studies from the field is important due to the limitations of the aforementioned models in modeling, for example, unstable and stable inflow or land surface-atmosphere interaction.

The research plan is divided in the following steps:

1. Understand how accurate lidars are in characterizing atmospheric conditions in complex terrain by analysis of the nacelle-mounted wind-lidars, meteorological masts and simulation models;
2. Understand under what atmospheric conditions the data from the nacelle-mounted wind-lidars can be used to identify wind turbine wakes;
3. Understand how the power performance is influenced by the wind flow and the seasonal and daily variation of atmospheric conditions by additionally considering observational datasets from the turbines' SCADA system;
4. Identify the key parameters that describe the interactions between wind flow and wind turbines within the wind park and their dependence on atmospheric conditions, and validate the wake models used in simulations and wind farm control;
5. Enhance the performance of wind parks through innovative modeling and control strategies.

References

[1] C. Bay, J. King, P. Fleming, L. Martinez, R. Mudafort, E. Simley, and M. Lawson. Floris: A brief tutorial, 2019.

[2] M. M. Pedersen, A. M. Forsting, P. van der Laan, R. Riva, L. A. A. Romàn, J. C. Risco, M. Friis-Møller, J. Quick, J. P. S. Christiansen, R. V. Rodrigues, B. T. Olsen, and P.-E. Réthoré. Pywake 2.5.0: An open-source wind farm simulation tool. 2 2023.

20th EAWE PhD Seminar on Wind Energy
24-26 September 2024
Visby, Sweden

On the potential of graph neural network surrogates for fatigue-aware control and design of wind farms

Gregory Duthé[a] and **Eleni Chatzi**[a]

[a]ETH Zürich

E-mail: duthe@ibk.baug.ethz.ch

Keywords: graph neural networks, surrogates, load-aware optimization

1 Introduction

Optimizing the performance of modern, large scale wind farms is a complex challenge that requires balancing power production with the minimization of turbine fatigue loads to reduce downtime and maintenance costs [10]. Research in this field has led to promising control strategies, such as yaw control or turbine-specific power curtailment. Yet, despite the potential benefits of these methods, their real-world implementations remain rare [9], hindered by concerns over increases in fatigue loads and the subsequent reduction in turbine lifespan. Simulations could potentially be used to dispel these kinds of concerns by demonstrating reduced economical costs over the full lifespan of a wind farm. However, the sheer amount of necessary computations that are required to optimize these strategies over such long periods has been so far prohibitive with current simulation tools.

Machine learning surrogates trained on high-fidelity simulations offer a computationally efficient alternative that could be coupled with advanced optimization tools, provided that they are sufficiently flexible and accurate. Here, we discuss the potential of using graph neural network (GNN) surrogates for efficient and accurate load-aware optimization and control of wind farms. Previous work has demonstrated that GNN surrogates can accurately predict wake-affected fatigue loads and power output in wind farms, while being computationally efficient [4, 3]. These surrogates leverage the power of graph representations to encode the inherent layout-affected structure of wind farms, capturing the complex interactions between turbines and their wakes.

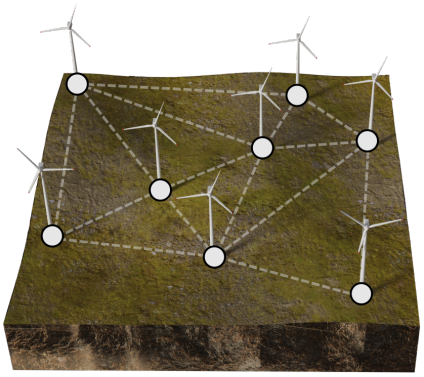

Figure 1: A wind farm can naturally be represented as a graph.

Moreover, GNN surrogates can provide gradients through automatic differentiation [7], enabling the use of gradient-based optimization techniques, which are necessary for analyses relating to sensitivity, uncertainty quantification, and inverse problem solutions. By combining GNN surrogates with optimization algorithms such as reinforcement learning, gradient descent, and evolutionary algorithms, we propose a tractable framework for load-aware optimization of wind farms. This framework can be applied to both the design of new wind farms and the control of existing ones. We illustrate the potential of such a framework by discussing three possible optimization

cases that were previously infeasible: (1) long-term fatigue-aware wake steering and curtailment, (2) dynamic repositioning of floating offshore wind turbines to minimize loads, and (3) load-aware layout optimization for complex terrain.

2 Graph neural network surrogates

GNN-based surrogates offer a promising approach for modeling wind farms and wake effects. Unlike regular neural networks (MLPs, convolutional neural networks, etc.), GNNs are not constrained to a fixed size input, which means that farms of any size can be modeled using a single GNN. These models can leverage the inherent graph-like structure of wind farms, where turbines are represented as nodes and their interactions as edges, allowing for intuitive and effective capture of complex spatial relationships (see Figure 1). This flexibilty gives GNNs remarkable generalization capabilities, adapting to unseen wind farm layouts and varying inflow conditions without retraining, which is crucial to obtain widely applicable models.

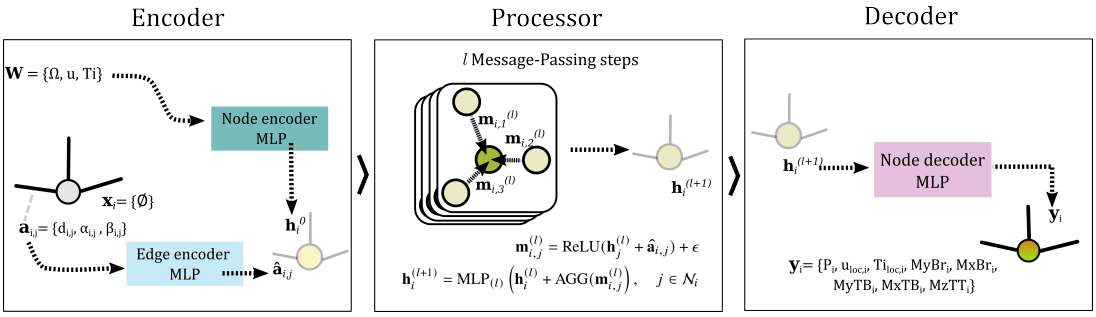

Figure 2: Typical Encode-Process-Decode setup for a GNN surrogate. At the output, we retrieve for each turbine the predicted power, local flow properties and damage equivalent loads.

The geometrical properties of the farm can be naturally fed into the GNN model through the edge features, while quantities of interest such as inflow conditions through graph-level attributes. The GNN itself is built with an Encode-Process-Decode structure, (for increased expressivity) and is trained in a supervised node regression scheme. At the output of the GNN, we retrieve mutlivariate node features for each turbine: power, local flow properties and the damage equivalent loads (DELs). This process is summarized in Figure 2. Empirical evaluations indicate that our trained GNN surrogates achieve inference times approximately ten times faster than leading reduced-fidelity simulators like PyWake [8].

3 Potential optimization cases

As an illustration of the potential of GNN-based surrogates for wind farm optimization, we highlight here three cases that could be of significant interest to the wind energy community, as shown in Figure 3. Furthermore, Table 1 gives a high-level overview on how to setup a GNN surrogate for these cases.

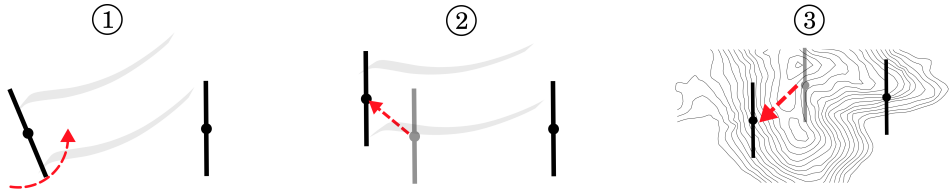

Load-aware wake steering and/or curtailment

Dynamic repositioning of floating offshore turbines

Fatigue-considerate layout optimization for complex terrain

Figure 3: Three illustrative optimization cases are selected to showcase the potential of GNN-based surrogates.

Load-aware wake steering and/or curtailment Wake steering and curtailment are now well-established strategies for wind farm control, with recent research suggesting potential benefits from their co-optimization [6]. While some researchers have begun to incorporate load considerations into these strategies [2], this approach is still in its early stages. To address this challenge using our GNN framework, modifications would be necessary to include individual yaw angles or derating values as node input features. This adaptation would allow the model to predict power output and fatigue loads for various control settings. Given the stochastic nature of this problem, the long time horizon and the need for continuous decision-making, reinforcement learning is suggested as an appropriate optimization technique. This approach could enable the development of adaptive control strategies that balance energy production with turbine load management.

Dynamic repositioning of floating offshore turbines Recent trends have seen floating wind emerge as a promising technology, attracting significant investment and research attention due to its ability to tap into deep-water offshore wind resources previously deemed inaccessible. Floating platforms offer the possibility to dynamically adjust the positions of the turbines to minimize wake-induced power losses [5]. Interestingly, dynamic repositioning could also be used to minimize loads. This case requires no changes to the existing GNN framework, as it can already handle varying turbine positions. The model can directly predict the impact of different turbine arrangements on power production and structural loads. For optimization, a gradient-based approach is recommended, leveraging the GNN's ability to provide gradients through automatic differentiation. This method could efficiently guide the real-time repositioning of turbines to maximize farm performance under changing wind conditions.

Fatigue-considerate layout optimization for complex terrain Although layout optimization has long been a key focus in computational wind energy research, the incorporation of complex terrain effects is a relatively recent development [1], and the simultaneous consideration of fatigue loads is non-existent. To address this challenge, the GNN framework would need to be extended to three dimensions and incorporate additional nodes representing terrain features. These modifications would allow the model to capture the complex interactions between turbines and the surrounding topography. For optimization, either gradient-based methods or evolutionary algorithms could be employed, depending on the specific problem characteristics and computational resources available. This approach could lead to more efficient and durable wind farm designs in challenging terrains.

Table 1: Details of required GNN changes and suggested optimization techniques for the three example cases.

Case	Required changes to GNN framework	Suggested optimization technique
Wake steering and/or curtailment	individual yaw or curtailment values as node input features	reinforcement learning
Dynamic repositioning of floating turbines	none	gradient-based optimization
Layout optimization for complex terrain	make graph 3D, add terrain nodes	gradient-based or evolutionary algos

4 Conclusion

GNN surrogates present a powerful tool for wind farm modeling and optimization. Their ability to rapidly and accurately predict wake effects, power output, and fatigue loads for any farm layout, coupled with their adaptability to various optimization challenges, makes them a promising alternative to traditional high-fidelity simulations. By enabling more efficient design and control strategies, GNN surrogates have the potential to markedly enhance wind farm performance and longevity.

Acknowledgements

This work was supported by the BRIDGE Discovery Program of the Swiss National Science Foundation and Innosuisse (Grant No. 40B2-0_187087), as well as the French-Swiss project MISTERY funded by the French National Research Agency (ANR PRCI Grant No. 266157) and the Swiss National Science Foundation (Grant No. 200021L_212718).

References

[1] J. Allen, R. King, and G. Barter. Wind farm simulation and layout optimization in complex terrain. In *Journal of Physics: Conference Series*, volume 1452, page 012066. IOP Publishing, 2020.

[2] R. Braunbehrens, A. Anand, F. Campagnolo, and C. Bottasso. First experimental results on lifetime-aware wind farm control. In *Journal of Physics: Conference Series*, volume 2767, page 032042. IOP Publishing, 2024.

[3] F. de Nolasco Santos, G. Duthé, I. Abdallah, P.-É. Réthoré, W. Weijtjens, E. Chatzi, and C. Devriendt. Multivariate prediction on wake-affected wind turbines using graph neural networks. In *EURODYN 2023. Proceedings of the XII International Conference on Structural Dynamics*. IOP Publishing, 2024.

[4] G. Duthé, F. de Nolasco Santos, I. Abdallah, P.-É. Réthore, W. Weijtjens, E. Chatzi, and C. Devriendt. Local flow and loads estimation on wake-affected wind turbines using graph neural networks and pywake. In *Journal of Physics: Conference Series*, volume 2505, page 012014. IOP Publishing, 2023.

[5] T. Jard and R. Snaiki. Real-time repositioning of floating wind turbines using model predictive control for position and power regulation. *Wind*, 3(2):131–150, 2023.

[6] J. Liew, K. Heck, and M. F. Howland. Enhanced modeling of joint yaw and axial induction control using blade element momentum methods. In *Journal of Physics: Conference Series*, volume 2767, page 032018. IOP Publishing, 2024.

[7] A. Paszke, S. Gross, F. Massa, A. Lerer, J. Bradbury, G. Chanan, T. Killeen, Z. Lin, N. Gimelshein, L. Antiga, et al. Pytorch: An imperative style, high-performance deep learning library. *Advances in neural information processing systems*, 32, 2019.

[8] M. M. Pedersen, A. M. Forsting, P. van der Laan, R. Riva, L. A. A. Romàn, J. C. Risco, M. Friis-Møller, J. Quick, J. P. S. Christiansen, R. V. Rodrigues, B. T. Olsen, and P.-E. Réthoré. Pywake 2.5.0: An open-source wind farm simulation tool. 2 2023.

[9] E. Simley, P. Fleming, N. Girard, L. Alloin, E. Godefroy, and T. Duc. Results from a wake-steering experiment at a commercial wind plant: investigating the wind speed dependence of wake-steering performance. *Wind Energy Science*, 6(6):1427–1453, 2021.

[10] P. Veers, K. Dykes, E. Lantz, S. Barth, C. L. Bottasso, O. Carlson, A. Clifton, J. Green, P. Green, H. Holttinen, et al. Grand challenges in the science of wind energy. *Science*, 366(6464):eaau2027, 2019.

An Experimental and Numerical Study of Static and Dynamic Yaw-based Wake Mixing

Davide Bortolin[a], Filippo Campagnolo [a], Doruk H. Aktan [a] and Carlo L. Bottasso [a]

Affiliation a. Wind Energy Institute, Technical University of Munich, Boltzmannstr. 15, 85748 Garching bei München, Germany

E-mail: davide.bortolin@tum.de

Keywords: dynamic yaw, wind tunnel experiments, LES validation

1. Motivation

Wind tunnel experiments using scaled models of wind turbines are extensively utilized in current research to investigate and model the wake interactions between turbines [1]. Additionally, Large Eddy Simulation (LES) has seen increasing adoption within the wind farm research community. LES offers the ability to more accurately resolve relevant flow dynamics, providing enhanced insights into the flow characteristics within a wind farm. Together, experimental and computational approaches allow researchers to explore wake control strategies and gain a comprehensive understanding of turbine interactions.
Both approaches face obstacles, for instance, achieving precise control over the wind tunnel inflow conditions presents challenges in experimental setups. Accurately representing aerodynamic forces on the mesh grid requires meticulous tuning in high-fidelity simulations [2],[3].
This study examines and compares three different wake mixing techniques: static yaw steering, dynamic yaw, and a combination of both static and dynamic yaw steering, in terms of power output, both individually and at the cluster level.
Additionally, the initial, ongoing, and future stages of validating LES simulations using SOWFA (Simulator for Wind Farm Applications) solvers [7] are briefly presented.
The abstract is divided into the following sections: the first segment discusses the experimental setup and results, the second delves into the future and ongoing development of the CFD simulations.

2. Experimental set-up and results

Figure 1 shows the experimental setup, a cluster of two scaled wind turbines is installed in the test section of the wind tunnel of the Politecnico di Milano [4].
The turbines are designed to have wake characteristic in good accordance with the full-scale machine, the models are designed with individual pitch, yaw and torque control that enables different turbine and farm strategy, [5]
During the tunnel test campaign, dynamic yaw control (DYC) is tested due to its potential to enhance wake mixing and achieve power gains at the cluster level [6].
The front turbine is subjected to a sinusoidal yaw control $\gamma(t) = \gamma_0 + \hat{\gamma}\sin(2\pi f_\gamma t)$, where γ_0 is the initial yaw angle, $\hat{\gamma}$ is the amplitude of the oscillation and f_γ is the frequency of the periodic yaw control. The second turbine, positioned 4D behind the first, is operated as a sensor to calculate the total power of the cluster. To be able to better compare the DYC excitation methodology with other dynamic control strategies, the frequency can also be

expressed in terms of the Strouhal number: $St = \frac{f_\gamma D}{U_\infty}$ being $D = 2$ the rotor diameter and U_∞ the free stream wind velocity.

Figure 1: Wind Tunnel Experimental set-up.

The measurements are divided in three different stages. In the first stage the amplitude $\hat{\gamma}$ is kept constant at a value of 10[deg], and the excitation frequency f_γ was varied between 0.1 and 1.24 [Hz]. This allowed for the identification of the optimal Strouhal number, which provides the best performance in terms of power at the cluster level see **Error! Reference source not found.**.
The second stage aims to identify the optimal oscillation amplitude, based on the best frequency determined in the first part of the experiments see Figure 1
The first two sets of experiments enable the identification of the optimal point for overall cluster performance. In the final stage, this optimal point (best oscillation frequency and amplitude) is used to investigate the potential gains achieved by combining dynamic yaw with a static steering technique. Figure 2 presents a comparison between simple steering (-20[deg]) and the combined dynamic yaw plus static steering approach.

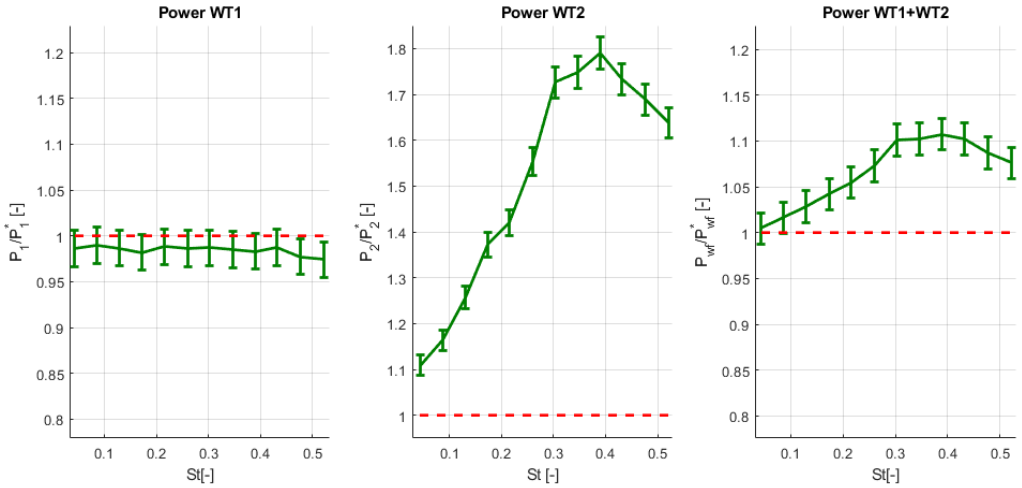

Figure 2: Extracted power of the upstream/actuated turbine, downstream/sensor turbine, and combined turbine array for changing yaw frequencies f_γ= (0.1:1.24) normalized to the respective baseline case without any actuation (dashed red line).

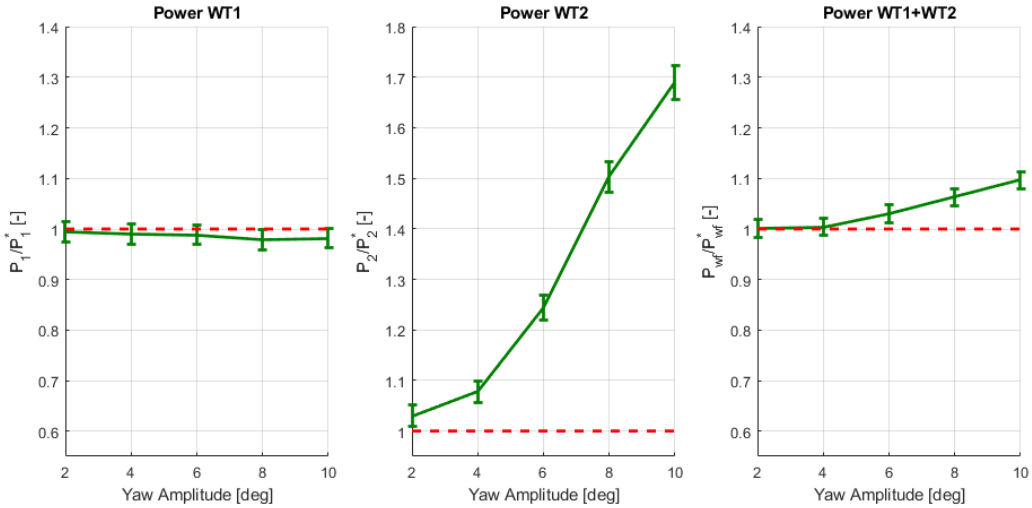

Figure 1 Extracted power of the upstream/actuated turbine, downstream/sensor turbine, and combined turbine array for changing yaw amplitudes $\hat{\gamma}$ = (2:10) normalized to the respective baseline case without any actuation (dashed red line).

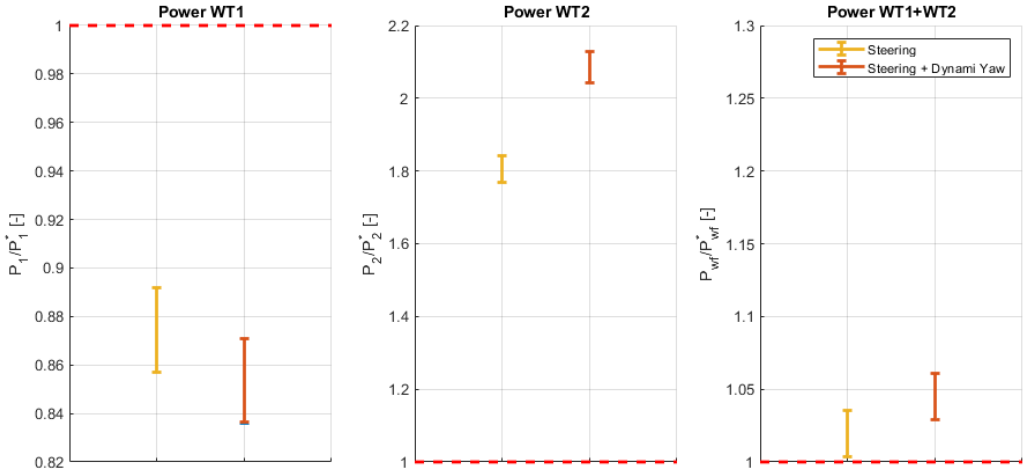

Figure 2 Extracted power of the upstream/actuated turbine, downstream/sensor turbine, and combined turbine array for stating yaw steering (yellow point) and combined mixing and steering (orange point) normalized to the respective baseline case without any actuation (dashed rep line)

The peak performance of the cluster was observed at a Strouhal number of approximately 0.4. Additionally, an increase in the values of $\hat{\gamma}$ corresponds to an enhancement in the farm's performance, justified by an increased in wake recovery.

To ensure realistic and applicable results for real-world turbine applications, a yaw amplitude of 8 degrees was selected for the comparisons between the steering technique and the combined steering plus mixing technique.

The results highlight an overall performance gain at the cluster level for all the control strategy: approximately 2% for simple steering, 5% for dynamic yaw, and 4.5% for the combined steering and dynamic yaw technique. The reason why the combined technique performs worse than dynamic yaw alone is unknown to the authors and remains to be explained.

These results indicate a potential for increasing the farm's performance, with dynamic yaw demonstrating the best overall improvement for the specific experimental conditions.

3. Ongoing and Future work

Following the methodology described by Wang et al. (2019) [5], an LES framework that models the nacelle, tower, and airfoil polars was used to represent the scaled model of the turbine.
The CFD model was tuned by matching the power output generated by SOWFA with that obtained from a simple blade element momentum solver (OpenFAST) [8]. Additionally, the forces normal and tangential to the rotor plane were compared to study the correlation between the two methods.
As future work, a precursor simulation will be employed to generate the turbulent inflow, replicating the conditions at the inlet of the Milan wind tunnel. This approach will ensure that the simulation matches the operational conditions of the experiment, leading to a better correlation between the software and the physical model. Once a match between the simulation and the experiment is achieved, the LES framework will be used to investigate a wider range of oscillation frequencies and amplitudes as well as other different dynamic and static wake mixing strategy. The CFD simulations will also aim to understand in detail the interaction and propagation of the wake, advancing progress toward addressing the unresolved questions raised from the experimental work.

4. Conclusions

This study experimentally demonstrates and compares the potential for power enhancement using static steering, dynamic yaw, and a combination of the two. The validation process will further confirm the accuracy of the results and provide an opportunity to expand the range of operational point and strategies.

References

[1] Campagnolo, F., Weber, R., Schreiber, J., and Bottasso, C. L.: Wind tunnel testing of wake steering with dynamic wind direction changes, Wind Energy Science., 5, 1273–1295, https://doi.org/10.5194/wes-5-1273-2020, 2020.

[2] Sørensen, J. N. and Shen, W. Z.: Numerical Modeling of Wind Turbine Wakes, J. Fluids Eng., 124, 393-399, 2002.

[3] E. L. Hodgson, S. J. Andersen and N. Troldborg, A. M. Forsting, R. F. Mikkelsen and J. N. Sørensen.: A Quantitative Comparison of Aeroelastic Computations using Flex5 and Actuator Methods in LES, Journal of Physics: Conference Series, 2021

[4] Carlo L. Bottasso, Filippo Campagnolo, Vlaho Petrović.: Wind tunnel testing of scaled wind turbine models: Beyond aerodynamics, Journal of Wind Engineering and Industrial Aerodynamics, Volume 127, 2014.

[5] Wang, J., Wang, C., Campagnolo, F., and Bottasso, C. L.: Wake behavior and control: comparison of LES simulations and wind tunnel measurements, Wind Energy Science., 4, 71–88, https://doi.org/10.5194/wes-4-712019, 2019.

[6] M. Lin and F. Porté-Agel.: Wake meandering of wind turbines under dynamic yaw control and impacts on power and fatigue, Renewable Energy journal, 2024.

[7] Churchfield, M. and Lee, S. (2012) NWTC Design Codes (SOWFA).URL: http://wind.nrel.gov/designcodes/simulator

[8] Jonkman J. NWTC Design Codes (FAST) 2012. URL: http://wind.nrel.gov/designcodes/simulator s/fast/

20th EAWE PhD Seminar on Wind Energy
24-26 September 2024
Visby, Sweden

Enhanced robust control of floating wind conversion system using neural network observer

Mohammad Javad Mirzaei[a], **Mohamed Assaad Hamida**[a], and **Franck Plestan**[a]

[a]Ecole Centrale de Nantes - LS2N UMR CNRS 6004, Nantes, France

E-mail: mohammad-javad.mirzaei@ec-nantes.fr

Keywords: RBF neural network, wind turbines, uncertain nonlinear systems, super twisting sliding mode, offshore platforms

The rising energy demand due to industrialization and increased use of electrical devices has led to a focus on renewable energy sources. Wind energy is prominent due to its safety and minimal environmental impact, with a global installed capacity of 732 GW, whereas modern turbines have significantly higher capacities, with onshore turbines ranging from 3-4 MW and offshore turbines from 8-12 MW (IRENA, 2022). Floating wind turbines (FWTs) offer promising solutions but face challenges such as high wind speeds and wave heights, leading to increased mechanical fatigue. Robust and accurate control strategies are essential to ensure high power production and limit mechanical fatigue in FWTs. Then, the control objectives in Region III are mainly power regulation, limitation of platform pitch motion and related fatigues, and blade fatigue load reduction.

Linear control approaches, such as optimal control [6] and PI controllers with scheduled gains (GSPI) [1, 4], require tuning and linearization, making them time-consuming to tune and less efficient. Adaptive super twisting (STW) as a robust approach [10, 3, 8] dynamically evolves gains and has shown promising results for FWT control [11, 13, 12, 7]. Neural network-based strategies offer another adaptation approach for model approximation. This work proposes an adaptive STW controller using a radial basis function (RBF) neural network to estimate unknown model components, enhancing FWT control. The RBF neural network's generalization ability, straightforward structure, and efficient computation make it suitable for control design. Previous studies [9, 2, 5] demonstrate the efficacy of combining neural networks with control strategies for wind turbines. This paper develops a neural network-based STW strategy for CBP control of spar-buoy FWTs, addressing the challenges of unknown system models.

Problem Statement

The control of an FWT system with unknown dynamics and external disturbances is investigated. A neural network-based STW controller is proposed to observe and compensate for these unknown parts, ensuring system stability and improved performance. Consider the nonlinear system:

$$\dot{\sigma} = f(\sigma,t) + u + \delta(t) \tag{1}$$

where σ is the sliding variable, u is the control input, and $\delta(t)$ represents external disturbances. The objective is to direct σ and its derivative to zero using an STW sliding mode control approach. However, the function $f(\sigma,t)$ is difficult to get and often unknown in practical systems. To address this, an RBF neural network is employed for its approximation capabilities, enhancing the controller's accuracy and adaptability. The network's architecture includes input, hidden, and output layers with the activation functions as

$$h(x) = [h_1(x), h_2(x), \ldots, h_m(x)]^T \tag{2}$$

where $h_j(x)$ are Gaussian basis functions. The weights of the network are adaptively updated based on Lyapunov stability criteria:

$$\dot{\hat{W}}_j = \gamma_j \sigma h_j(\sigma) \tag{3}$$

The neural network-based STW controller integrates the RBF neural network to estimate the unknown function $f(\sigma,t)$, defined as:

$$\hat{f}(\sigma,t) = \hat{W}^T h(\sigma) \tag{4}$$

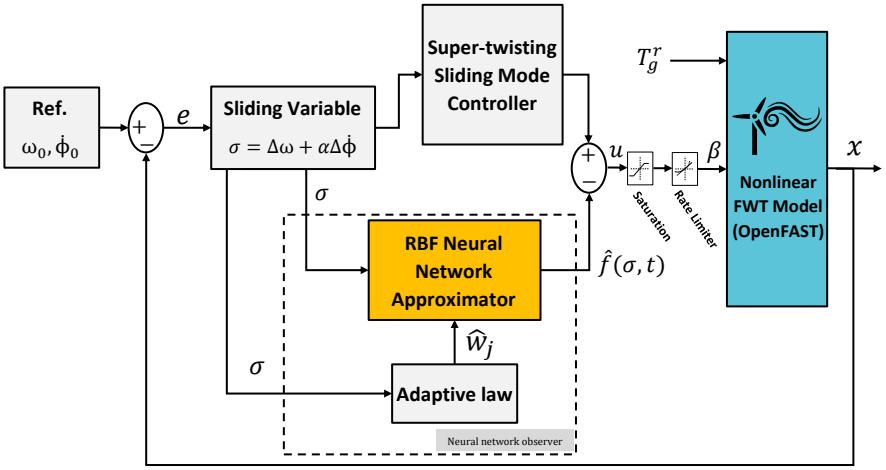

Figure 1: Block diagram of the STW control strategy based on artificial neural network approximation with co-simulation scheme of the control and the OpenFAST model. The OpenFAST block output is $x = [\phi, \dot{\phi}, \Omega]$ and T_g^r is the rated torque.

The control input is then:

$$\begin{aligned} u &= -\hat{f}(\sigma,t) - k_1|\sigma|^{1/2}\text{sign}(\sigma) + v \\ \dot{v} &= -k_2\text{sign}(\sigma) \end{aligned} \tag{5}$$

where k_1 and k_2 are positive constants. Simulation results demonstrate the effectiveness of the neural network-enhanced controller, showing significant improvements in system stability and performance compared to traditional methods.

Application to the Floating Wind Turbine

To demonstrate the efficiency of the proposed control method for the FWT, a simulation study using Matlab/Simulink and co-simulation with OpenFAST is conducted. The block diagram of the control strategy is shown in Fig. 1. The control strategy is applied to the CBP control of an FWT in Region III, aiming to:

- Regulate the output power to the rated value P_0;
- Decrease platform pitch motions and oscillations.

The control objective is to regulate rotor speed, defined by the sliding variable σ:

$$\sigma = (\Omega - \Omega_0) + \alpha(\dot{\phi} - \dot{\phi}_0) = \Delta\Omega + \alpha\Delta\dot{\phi} \tag{6}$$

where $\alpha > 0$ is a constant, and $\dot{\phi}_0 = 0$ to reduce platform pitch oscillations. When the sliding mode is established ($\sigma = \dot{\sigma} = 0$), the rotor speed error is related to the platform pitch rate $\Delta\Omega = -\alpha\Delta\dot{\phi}$. The dynamics of σ can be expressed as:

$$\dot{\sigma} = \Psi(\cdot) + \Phi(\cdot)u \tag{7}$$

where $\Psi(\cdot)$ and $\Phi(\cdot)$ include nominal and uncertain parts. Due to the boundedness of the uncertain parts and by considering that the nominal parts are bigger than uncertain ones, the derivative of σ can be presented in the right structure for applying the STW controller with the neural network-based approach in Eq. (5) previously detailed (see Chapter 2-[11]). It is noted that because the FWT model is complex, it is considered unknown [11, 7]. Here, the unknown model is estimated by the proposed approximation algorithm to improve the performance of the STW sliding mode controller. Based on the adaptive protocol, $\hat{f}(\sigma,t)$, which is achieved from the neural network structure, is utilized as the estimated value of $f(\sigma,t)$.

Table 1: Parameters of 5MW OC3 FWT

Parameters	Value
Rotor, hub diameter	126 m, 3 m
Hub height	90 m
Rated rotor speed Ω	12.1 rpm
Minimum, maximum blade pitch angle	0 deg, 90 deg
Maximum blade pitch rate	$\pm$ 8 deg/s

Simulations and Analysis

The proposed neural network-based strategy is implemented on a 5MW OC3 FWT using MATLAB and OpenFAST software co-simulation. The structural parameters of the FWT are detailed in Table 1. All 24 DOFs in the FWT are activated in the OpenFAST simulation. The performance of the neural network-based approach is evaluated by comparing STW results *with & without* the neural network approximator and against the GSPI controller as the baseline method.

Various criteria are used to analyze the performance of the proposed strategy. The root mean square (RMS) index is computed for the main variables to compare power, rotor speed precision, and platform oscillations. The damage equivalent loads (DEL) index is used to evaluate possible fatigue loads on different structural sections of the FWT, such as the tower base, blade root, fair-lead force, and anchor force of the mooring lines. Blade pitch angle variation (VAR) is also analyzed.

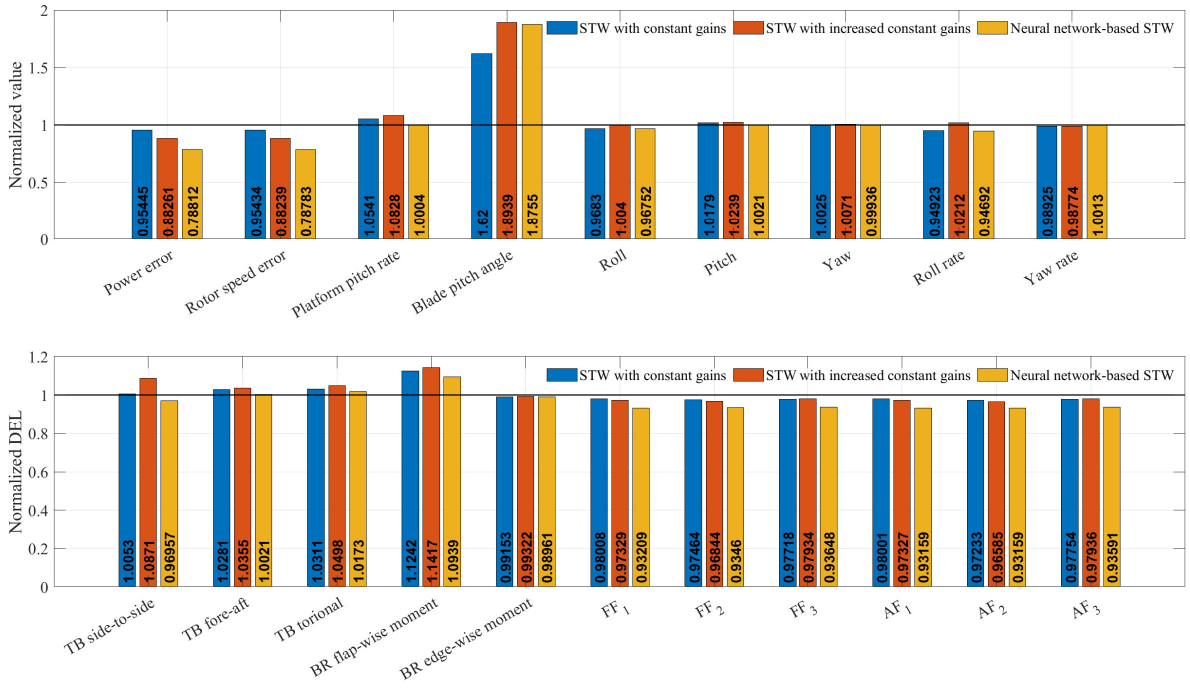

Figure 2: Normalized RMS/VAR indexes for STW with constant gains (blue), STW with increased constant gains (red), and neural network-based STW (orange) approaches. TB, BR, FF, and AF stand for tower base, blade root, fair-lead force, and anchor force, respectively.

A detailed comparison with GSPI is shown in Figure 2. The neural network-based STW controller reduced power and rotor speed errors by 21.1 % compared to STW with constant gains and by at least 11.9 % compared to other approaches. Increasing gains without the neural network resulted in higher errors and increased blade pitch angle, platform pitch rate, and DEL values. In contrast, the neural network-based adaptive approach improves tracking accuracy, reduces platform pitch rate, and decreases DEL values, demonstrating the effectiveness of the

neural network-based control strategy.

Acknowledgements

This work was supported in part by the Agence Nationale de la Recherche (ANR) project CREATIF under Grant ANR-20-CE05-0039.

References

[1] O. Bagherieh and R. Nagamune. Gain-scheduling control of a floating offshore wind turbine above rated wind speed. *Control Theory and Technology*, 13(2):160–172, 2015.

[2] H. Chojaa, A. Derouich, S. E. Chehaidia, O. Zamzoum, M. Taoussi, and H. Elouatouat. Integral sliding mode control for dfig based wecs with mppt based on artificial neural network under a real wind profile. *Energy Reports*, 7:4809–4824, 2021.

[3] S. V. Gutierrez, J. De León-Morales, F. Plestan, and O. Salas-Peña. A simplified version of adaptive super-twisting control. *International Journal of Robust and Nonlinear Control*, 29(16):5704–5719, 2019.

[4] C. Han and R. Nagamune. Platform position control of floating wind turbines using aerodynamic force. *Renewable Energy*, 151:896–907, 2020.

[5] I. U. Haq, Q. Khan, I. Khan, R. Akmeliawati, K. S. Nisar, and I. Khan. Maximum power extraction strategy for variable speed wind turbine system via neuro-adaptive generalized global sliding mode controller. *IEEE Access*, 8:128536–128547, 2020.

[6] Y. Ma, P. D. Sclavounos, J. Cross-Whiter, and D. Arora. Wave forecast and its application to the optimal control of offshore floating wind turbine for load mitigation. *Renewable Energy*, 128:163–176, 2018.

[7] M. J. Mirzaei, M. A. Hamida, and F. Plestan. Super-twisting control of offshore wind turbine in region iii with self-tuning adaptive gains. In *2022 16th International Workshop on Variable Structure Systems (VSS)*, pages Rio de Janeiro, Brazil, 2022.

[8] M. J. Mirzaei, M. A. Hamida, F. Plestan, and M. Taleb. Super-twisting sliding mode controller with self-tuning adaptive gains. *European Journal of Control*, 2022.

[9] I. Sami, S. Ullah, S. U. Amin, A. Al-Durra, N. Ullah, and J.-S. Ro. Convergence enhancement of super-twisting sliding mode control using artificial neural network for dfig-based wind energy conversion systems. *IEEE Access*, 10:97625–97641, 2022.

[10] Y. Shtessel, M. Taleb, and F. Plestan. A novel adaptive-gain supertwisting sliding mode controller: Methodology and application. *Automatica*, 48(5):759–769, 2012.

[11] C. Zhang. *A contribution to the nonlinear control of floating wind turbines*. Ph.D. Thesis, École Centrale de Nantes, Nantes, France, 2021.

[12] C. Zhang and F. Plestan. Adaptive sliding mode control of floating offshore wind turbine equipped by permanent magnet synchronous generator. *Wind Energy*, 2021.

[13] C. Zhang and F. Plestan. Individual/collective blade pitch control of floating wind turbine based on adaptive second order sliding mode. *Ocean Engineering*, 228:108897, 2021.

20th EAWE PhD Seminar on Wind Energy
24-26 September 2024
Visby, Sweden

Verifying engineering steady yaw models using actuator disc simulations

Haoyuan Sun[a], **Wei Yu**[a], and **Carlos Simão Ferreira**[a]

[a]Faculty of Aerospace Engineering, Delft University of Technology, Delft, 2628 CD, The Netherlands

E-mail: H.Y.Sun@tudelft.nl

Abstract

Yaw models are implemented as corrections to the industrial wind turbine design workhouse — BEM to improve the loads and power estimation accuracy. However, most engineering models were developed under uniform inflow considerations, excluding realistic inflow conditions like wind shear, veer, and atmospheric stability. Meanwhile, significant disagreements with high-fidelity results have been observed in previous studies. This research aims to comprehensively evaluate mainstream engineering models for the induction prediction of a static yawed wind turbine. By applying the actuator disk, computational fluid dynamics (CFD) simulations are performed on the NREL 5MW wind turbine under different inflow and yaw angle settings to validate the capability of existing engineer models. The effects of different inflow conditions are quantified numerically by conducting the analysis. Furthermore, it will provide a deeper insight into the azimuthal variation of the aerodynamic induction field on a static yawed rotor plane representing a typical and commercial wind turbine.

Keywords: Wind turbine, Static Yaw, Aerodynamics, Induction field, Engineering model, CFD

1 Introduction

Under the sustainable development background, wind turbines are designed and implemented to capture the kinetic energy from the wind, with its origin tracing back to early in the last century. During past decades, considerable studies and literature have grown around wind turbine design and simulation. Central to the entire field of wind energy is the discipline of wind turbine unsteady aerodynamics, which deals with the flow field around a wind turbine in reality and is essentially relevant to the power production and loads. From a practical perspective, a wind turbine constantly experiences fluctuating inflow and control actions during its operational process due to complex inflow conditions, including wind shear, veer, pitch, yaw, wake dynamics, etc. These unsteady phenomena are recognized as severe factors influencing the performance and reliability of wind turbines; they are difficult but necessary to reproduce in simulation [1], especially under industry application scenarios. Among all these unsteady phenomena, yawing alignment has obtained increasing interest from researchers owing to its application potential in the layout and power output optimization of a wind farm in recent years. However, much of the available literature regarding yaw aerodynamics focuses on the performance optimization and wake mitigation of wind farms [2]. The aerodynamics of a single static yawed wind turbine rotor and the validation of industry prediction, in other words, engineering models, are less concerned.

Along with this growing scale of wind energy, engineering models gain an increasing application throughout the wind turbine design process. Engineering models are the optimum solution for widespread industry simulation with reliable results. However, observations have indicated notable discrepancies between measurements, high-fidelity simulations, and widely utilized yaw engineering models in contemporary aeroelastic simulation code. One of those great disagreements was witnessed by a blind comparison between the Unsteady Aerodynamics Experiment (UAE) and modelling codes sourced globally launched by Simms et al. [3]. Samara et al. [4] measured the load of a yawed wind turbine and compared it with NREL FAST code predictions. Some imperative disagreements emerged and pointed out the model's weakness in depicting tip loss, stall, 3D flow effect, and airfoil corrections. Until now, few published studies have systematically investigated the capability of yaw engineer models. Rahimi et al.[5] investigated the current yaw engineering models: Glauert, Schepers and a free vortex wake model by comparing simulation results against CFD and experiments under uniform inflow conditions. It is observed that the

Glauert model assumed a sinusoidal distribution for the induced velocity, which coincided more with high-fidelity simulation at the blade tip region since it is based on tip vortex. In contrast, the Schepers model showed better agreement at the blade root region by taking the root vortex into account, but it also weakened its performance at the blade tip. Hur et al.[6] compared different engineering yaw models: Coleman, White and Blake, Pitt and Pitters and Øye, all of which are based on Glaurt formulation, in actuator disk momentum theory with fixed and free wake vortex models. It is proved that Øye's model shows the best agreement, but significant deviations in radial-induced velocity can still be observed. To the best of the authors' knowledge, insufficient yaw model validations by high-fidelity simulations are available in the literature. Besides, previous studies on model developments and validation are carried out under uniform inflow conditions, which conflicts with realistic wind turbine fluctuating inflows. To fill these two gaps, the present study contributes to accurately modeling yawed wind turbines in the following ways. For example, 1) A detailed investigation of the skewed wake effect on a static yawed rotor plane is presented and explained. 2) The effects of non-uniform inflow conditions are quantified by a comparative study of the induction field under different inflow setups, including uniform and non-uniform.

In conclusion, few studies have deeply explored the capability of Yaw engineer models. However, predicting a yawed rotor induction field is essential for estimating wind turbine performance, especially in a wind farm context. Therefore, it proposes the need for a more comprehensive exploration and understanding of engineering models undertaken in this study.

2 Methodology

In this study, the main objective is to conduct the validation of yaw engineer models through comparison with CFD simulations, with a focus on the induction field on the rotor disk. The simulation is conducted based on an NREL 5MW wind turbine with main parameters in Tab.1.

Table 1: Main parameters of the turbines NREL 5MW

Turbine Parameter	NREL 5MW
Rated power [MW]	5
Rotor diameter [m]	126
Axial induction [-]	0.25
Rated rotor speed [rpm]	12.1
Tip speed [m/s]	80
Hub height [m]	90

CFD simulations of this work are performed by applying a yawed actuator disk source in *OpenFOAM v2206*, an open-source finite-volume-based CFD solver. Yaw engineer models deal with skewed wake effect and have gained different forms in low fidelity simulations [7]. It describes the non-uniform distribution of axial induced velocity from the upwind to the downwind direction on the rotor plane. Glauert [8] firstly proposed the skewed wake model with an unknown term K. It applies the correction factor to the axial induced velocity in the form of:

$$a = a_{i,x}(1 + K\frac{r}{R}\sin\psi) \tag{1}$$

where $a_{i,x}$ is the axial induction factor, r and R are radial positions along the blade and rotor plane radius, respectively, and K is the correction factor related to yaw angle γ.

This form of the model has been employed in Blade element momentum to (BEM) for wind turbine simulation and gained widespread application in the industry by follow-up studies centering on the determination of K parameter in Eq.(1). Diverse modeling techniques for the function K are presented below.

Coleman et al.[9]:

$$K = \tan\frac{\chi}{2} \tag{2}$$

White and Blake [10]:

$$K = \sqrt{2}\sin\chi \tag{3}$$

Pitts and Peters [11]:

$$K = \frac{15\pi}{32}\tan\frac{\chi}{2} \tag{4}$$

Howleet [12]:

$$K = \sin^2 \chi \tag{5}$$

where χ is the skew angle, the angle between the inclined wake center and rotor axis, and can be expressed as:

$$\chi = \arctan \frac{V_0 \sin \gamma}{V_0 \cos \gamma - V_{i,x}} \tag{6}$$

Øye [13] modified the radial dependent term in Glauert's skewed wake model with a function F as:

$$a = a_{i,x}(1 + F \tan \frac{\chi}{2} \sin \psi) \tag{7}$$

$$F = \frac{r}{R} + 0.4(\frac{r}{R})^3 + 0.4(\frac{r}{R})^5 \tag{8}$$

3 Expected outcomes

The low and high-fidelity simulations of a static yawed wind turbine are expected to provide insights into three main aspects:

1. Engineering model validation. The prediction from the static yaw models can be validated against the induction field predicted by the high-fidelity simulations. It can be used to examine the capability of engineering models.
2. Effect of unsteady inflow conditions. Different inflow conditions are considered to reproduce the realistic operating conditions that a commercial wind turbine could experience. Different inflow conditions are decomposed to quantify effects on the induction field compared with uniform non-yawed and yawed scenarios.
3. Induction distribution. A better understanding of aerodynamics on a yawed rotor plane is expected to be obtained, including the induction distribution from upwind to downwind direction and its radial distribution tendency.

Acknowledgements

This publication is part of the project Diamond with project number 19882 of the research programme Open Technology which is (partly) financed by the Dutch Research Council (NWO).

References

[1] J. Gordon Leishman. "Challenges in Modelling the Unsteady Aerodynamics of Wind Turbines". In: *Wind Energy* 5.2-3 (2002), pp. 85–132. ISSN: 1099-1824. DOI: 10.1002/we.62.

[2] Jian Yang et al. "Review of Control Strategy of Large Horizontal-Axis Wind Turbines Yaw System". In: *Wind Energy* 24 (Sept. 2020). DOI: 10.1002/we.2564.

[3] D. Simms et al. *NREL Unsteady Aerodynamics Experiment in the NASA-Ames Wind Tunnel: A Comparison of Predictions to Measurements*. Tech. rep. NREL/TP-500-29494. National Renewable Energy Lab. (NREL), Golden, CO (United States), June 2001. DOI: 10.2172/783409.

[4] F Samara and D A Johnson. "Experimental Load Measurement on a Yawed Wind Turbine and Comparison to FAST". In: *Journal of Physics: Conference Series* 1618.3 (Sept. 2020), p. 032031. ISSN: 1742-6588, 1742-6596. DOI: 10.1088/1742-6596/1618/3/032031.

[5] H. Rahimi et al. "Investigation of the Current Yaw Engineering Models for Simulation of Wind Turbines in BEM and Comparison with CFD and Experiment". In: *Journal of Physics: Conference Series* 753.2 (Sept. 2016), p. 022016. ISSN: 1742-6596. DOI: 10.1088/1742-6596/753/2/022016.

[6] Chihoon Hur et al. "A Review of Momentum Models for the Actuator Disk in Yaw". In: *AIAA Scitech 2019 Forum*. AIAA SciTech Forum. American Institute of Aeronautics and Astronautics, Jan. 2019. DOI: 10.2514/6.2019-1799.

[7] L. J. Vermeer, J. N. Sørensen, and A. Crespo. "Wind Turbine Wake Aerodynamics". In: *Progress in Aerospace Sciences* 39.6 (Aug. 2003), pp. 467–510. ISSN: 0376-0421. DOI: 10.1016/S0376-0421(03)00078-2.

[8] H. Glauert. *A General Theory of the Autogyro*. Technical Report. H. M. Stationery Office, 1926.

[9] Carl W. Stempin. *Evaluation of the Induced-Velocity Field of an Idealized Helicopter Rotor*. June 1945.

[10] F. White and B.B. Blake. "Improved Method Of Predicting Helicopter Control Response And Gust Sensitivity". In: *Vertical Flight Society Annual Forum & Technology Display - Forum*. The Vertical Flight Society, May 1979.

[11] Dale Pitt and David Peters. "Theoretical Prediction of Dynamic-in Ow Derivatives". In: *Vertica* 5 (Jan. 1981).

[12] J. J. Howlett. *UH-60A Black Hawk Engineering Simulation Program. Volume 1: Mathematical Model*. Tech. rep. SER-70452. Dec. 1981.

[13] S Øye. "Induced velocities for rotors in yaw". In: *Proceedings of the Sixth IEA Symposium* (1992).

4.2 Session 321: Control of wind turbines and wind farms

26.09.2024, 10:30, Room 1

Chair:

Ansh Patel

Presenters:

Aslmostafa Jarchelou Ehsan	Nonlinear robust control approaches for maximizing power generation in floating offshore wind turbines in low-wind Regions
Nilsen Marcus	Autonomous Data-driven Wind Farm Control
Duvivier Alban	Optimizing Electrical Stability in Offshore Energy Hubs: An Analysis of Topologies and Solutions

20th EAWE PhD Seminar on Wind Energy
24-26 September 2024
Visby, Sweden

Nonlinear robust control approaches for maximizing power generation in floating offshore wind turbines in low-wind Regions

Ehsan Aslmostafa[a], **Mohamed Assaad Hamida** [a], and **Franck Plestan** [a]

[a]Nantes Université, École Centrale Nantes, CNRS, LS2N, UMR 6004 F-44000, Nantes, France
E-mail: ehsan.aslmostafa-jarchelou@ec-nantes.fr

Keywords: Robust control, maximum power point tracking, floating offshore wind turbine, super-twisting control.

This research investigates robust control methods for floating offshore wind turbines (FOWTs) in Region II, aiming to maximize power point tracking (MPPT) and minimize fatigue loads within wind speed limits. Achieving optimal tip speed ratio (TSR) ensures MPPT, while setting platform pitch rate to zero reduces fatigue. Due to the complex dynamics of FOWTs, nonlinear robust control approaches are proposed, requiring minimal system knowledge and adapting to parameter changes. Simulations validate the effectiveness of this control method.

1 Introduction

The NREL 5MW OC3-Hywind wind turbine operates in four regions of wind speed [5]. In low-wind area (Region 2), achieving maximum power is challenging. Techniques like TSR control optimize torque to maintain peak power coefficient to have an MPPT control.
Due to the complex dynamics of FOWTs, advanced control strategies are necessary. Nonlinear control strategies provide an advantageous, simplifying tuning and improving performance by handling wind fluctuations and turbulence [4]. Advanced algorithms such as higher-order sliding mode control (HOSMC) effectively address model nonlinearities. This paper employs super-twisting (STW) algorithms which offer robustness, finite-time convergence, reduced chattering, and less reliance on detailed system models [7].
Two adaptive versions of super-twisting control are applied to a FOWT with uncertain parameters in Region II. These control strategies are compared using the OpenFAST platform against the decreasing torque gain (DTG) control in realistic conditions.

2 System description and modeling

2.1 Description of FOWT

This study focuses on the NREL 5MW OC3-Hywind wind turbine, which is mounted on a spar-buoy platform and simulated using the OpenFAST [4]. The investigation is carried out within Region II, where the primary objective is to maximize power production within a wind speed range spanning from 3 m/s to 11.4 m/s [4]. To achieve MPPT and maintain the optimal TSR, the controller design regulates rotor speed ω to follow a reference value ω^*. Additionally, the study explores reducing fatigue on the FOWT platform. The proposed robust control strategies aim to meet both objectives. Modeling a FOWT is complex due to factors like the elasticity of turbine components (tower, blades, drive train) and the interplay of aerodynamic forces on the rotor and hydrodynamic effects on the platform. This makes representing a FOWT mathematically challenging due to its highly nonlinear nature. The reference rotor speed is determined as a function of the platform pitch velocity and the wind speed, resulting in the following desired value

$$\omega^* = \frac{\lambda^*}{R} V - k\dot{\varphi}, \tag{1}$$

where $\lambda^* = 7.55$ is the optimal TSR and k is a positive constant. When the platform pitches forward, $\dot{\varphi}$ becomes negative, increasing the reference rotor speed ω^*. This control strategy increases aerodynamic torque and rotor

speed, preventing forward pitching by increasing aerodynamic thrust, thus stabilizing $\dot{\varphi}$ and converging the rotor speed reference to its optimal value [9]. If there is no platform pitch velocity ($\dot{\varphi} = 0$), the reference is optimal and equal to $\lambda^* V/R$.

3 Control design

In Region II, the primary goals are to maximize power output and reduce platform fatigue by controlling the generator torque based on rotor speed. The turbine operates near the optimum power efficiency point $C_p(\lambda, \beta)$, adjusting rotor speed to match the wind speed and maintaining the optimal TSR with a blade pitch angle of 0 degrees to maximize lift. The generator torque T_g is used as the control input. In this work, first, an improved method of a torque control approach which is called decreasing torque gain (DTG) is considered as a baseline control [3], and then a robust control strategy is going to be discussed.

3.1 Decreasing torque gain control

In this method, the reference value for the generator torque is expressed as $T_g^* = k_d k_{\text{opt}}\, \omega^2$ [2]. Here, k_d represents the torque gain coefficient, with the constraint that $0 < k_d < 1$. The term k_{opt} is calculated as $k_{\text{opt}} = \frac{\rho \pi R^5 C_p^*}{2\lambda^{*3}}$.

3.2 Robust control design

The work discusses the necessity of a robust control strategy due to the limitations of linear controls in managing changes. It proposes a STW-based control approach that is robust to perturbations and requires minimal information about the dynamic model, relying instead on available measurements. Given the complexity of wind turbine mechanics and the challenge of accurate modeling, the work suggests an adaptive version of STW control. This approach addresses issues from unmodeled dynamics and perturbations, preventing sudden failures and ensuring satisfactory performance.
Based on a discussion in [1], a solution ensuring the establishment of a second order sliding mode, *i.e.* $\sigma = \dot{\sigma} = 0$ in a finite time, is based on the super-twisting algorithm defined as [6]

$$\begin{aligned} w &= -k_1 |\sigma|^{\frac{1}{2}} \operatorname{sign}(\sigma) + v \\ \dot{v} &= -k_2 \operatorname{sign}(\sigma) \end{aligned} \tag{2}$$

where k_1 and k_2 have to fulfilled conditions depending on upper bound of perturbation. As a result, the system trajectories can converge towards the manifold $\sigma = \dot{\sigma} = 0$ within a finite time.
In practical applications, accurately determining uncertainty bounds is challenging and often overestimated, degrading control performance. Adaptive gain approaches address this by dynamically adjusting gains, increasing them when accuracy is insufficient and decreasing them when control objectives are achieved. Here, two adaptive versions of super-twisting algorithms are adopted, differing in their adaptation laws.
The first one is the adaptive super-twisting (ASTW) controller, as proposed in [10]. It requires the tuning of a set of parameters, and the gain adaptation law reads as follows:

- **ASTW** : The controller gains k_1 and k_2 are defined as

$$\dot{k}_1 = \begin{cases} \alpha \operatorname{sign}(|\sigma| - \varepsilon) & \text{if } k_1 > k_{1m} \\ \eta & \text{if } k_1 < k_{1m} \end{cases} \quad \text{and} \quad k_2 = \gamma k_1 \tag{3}$$

  Take the positive constants $\eta, \alpha, \varepsilon, \gamma$, and k_{1m} as the minimal value admissible for k_1.

The second one is the self-tuning adaptive super-twisting (STAS) controller [8]. This offers a single tuning parameter, ε, to ensure system stability. This method ensures that the gains k_1 and k_2 dynamics are adapted as below:

- **STAS**:

$$\begin{cases} \dot{k}_1 = \frac{\alpha(t)}{|\hat{\sigma}| + \varepsilon} \quad \& \quad \dot{k}_2 = \frac{\alpha(t)}{2|\sigma|^{\frac{1}{2}}} & \text{if} \quad |\sigma| > \varepsilon \\ \dot{k}_1 = -k_1 \quad \& \quad \dot{k}_2 = -k_2 & \text{if} \quad |\sigma| \leq \varepsilon \end{cases} \tag{4}$$

with any positive initial conditions and the self-tuning dynamics obtained as

$$\begin{cases} \alpha(t) = |k_1||\sigma|^{\frac{1}{2}} + |\hat{\sigma}| + |z| \\ \dot{z} = k_2 \operatorname{sgn}(\sigma), \quad z(0) = 0 \end{cases} \tag{5}$$

According to above definitions and detailed discussion at [1], to satisfying the control objectives, the following control is applied to the discussed FOWT

$$u = T_g = -\frac{J_0}{n_g}(\dot{\omega}^* + w). \tag{6}$$

where J_0 is the inertia, n_g is the gearbox ration and w defined by (2)-(3) or (2)-(4)-(5).

4 Simulations and analysis

4.1 Simulation set-up

A 5MW OC3 FOWT developed by NREL is simulated using the OpenFAST platform. The parameters for this FOWT are obtained from [4]. The control strategies are developed in Matlab/SIMULINK and integrated with the OpenFAST simulation. It's worth noting that while a control strategy is initially designed for a simplified model, all 24 degrees of freedom (DOFs) are activated and considered in the OpenFAST simulation. All simulations are conducted over 1200 seconds, with the first 200 seconds considered as startup time. The integration algorithm used is ODE1 (Euler) with a fixed step equal to 0.0125 sec. The two adaptive super-twisting-based controllers previously recalled, ASTW and STAS, as proposed by [10] and [8] respectively, are used for comparison. The initial values of the adaptive gains are $k_1(0) = 5$ and $k_2(0) = 0.01$. The controller proposed in [8] requires only one parameter for tuning, the controller accuracy ε, and is set to $\varepsilon = 10^{-3}$. For the other control that has been proposed in [10], the tuning parameters are configured as $\alpha = 0.001, k_{1m} = 0.01, \varepsilon = 0.01, \mu = 0.01, \gamma = 0.01$. Also, the method explained in [3] requires tuning the parameter k_d and set as $k_d = 0.001352$. This approach is also taken as a baseline control in this work.
As for the environmental conditions, the controllers are implemented under an irregular wave with a significant height of 3.25 m and a peak spectral period of 9.7 s, and the stochastic wind with a mean value equal to 7 m/s and 10% turbulence intensity.

4.2 Results and analysis

Based on Table 1, the first evaluation parameter is the mean value of the generated power by each control. The second criterion evaluates the effectiveness of each control in performing the MPPT operation, according to the power coefficient error, calculated as $|C_p^* - C_p|$. For successful MPPT, the control must maintain the tip speed ratio λ at its optimal value λ^*, maximizing the power coefficient C_p at it maximal value C_p^*. A smaller error indicates better control performance. The obtained results suggest that the STAS generates more power and is more efficient in achieving MPPT compared to the two other approaches. It is evident that DTG does not offer acceptable performance for achieving MPPT. STAS, on the other hand, shows a 0.28% better performance than ASTW, generating even more power than both ASTW and DTG. To analyze the performance of the proposed strategies, platform motions and corresponding rates are presented in Figure 1. Here, a smaller value indicates better control performance. Based on this, except for the roll motion, the STW-based controls work well and almost have the same performance.

Table 1: Power production and MPPT performance

Parameters	STAS	ASTW	DTG (baseline)
Mean value of power (MW)	1.1410	1.1385	1.1046
Power coefficient error (%)	3.84%	4.12%	10.07%

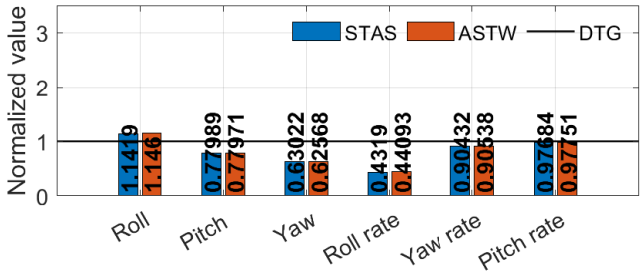

Figure 1: Motion indicators

5 Conclusion

The research enhanced FOWT operations in Region II using robust control approaches to optimize MPPT and reduce fatigue loads. Despite the complexity of the OpenFAST platform model, these nonlinear control methods effectively managed parameter variations with minimal system information. Simulations validated the control strategies, improving FOWT performance and reliability. The findings offer promising implications for sustainable energy systems.

Acknowledgements

This work has been partially supported by *Région Pays de la Loire* and is a part of ANR CREATIF project (No. ANR-20-CE05-0039).

References

[1] E. Aslmostafa, M. A. Hamida, and F. Plestan. Nonlinear control strategies for a floating wind turbine with pmsg in region 2: A comparative study based on the openfast platform. *Ocean Engineering*, 300:117507, 2024.

[2] H. Chen, Y. Sun, Y. Cai, J.-F. Charpentier, J. Han, N. Aït-Ahmed, and M. Benbouzid. Improved torque compensation control based-maximum power point tracking strategy for large scale floating offshore wind turbines. *Ocean Engineering*, 273:113974, 2023.

[3] K. E. Johnson, L. J. Fingersh, M. J. Balas, and L. Y. Pao. Methods for increasing region 2 power capture on a variable-speed wind turbine. *J. Sol. Energy Eng.*, 126(4):1092–1100, 2004.

[4] J. Jonkman, S. Butterfield, W. Musial, and G. Scott. Definition of a 5-mw reference wind turbine for offshore system development. Technical report, National Renewable Energy Lab.(NREL), Golden, CO, USA, 2009.

[5] D. Kumar and K. Chatterjee. A review of conventional and advanced mppt algorithms for wind energy systems. *Renewable and sustainable energy reviews*, 55:957–970, 2016.

[6] A. Levant. Sliding order and sliding accuracy in sliding mode control. *International Journal of Control*, 58(6):1247–1263, 1993.

[7] A. Levant. Higher-order sliding modes, differentiation and output-feedback control. *International journal of Control*, 76(9-10):924–941, 2003.

[8] M. J. Mirzaei, M. A. Hamida, F. Plestan, and M. Taleb. Super-twisting sliding mode controller with self-tuning adaptive gains. *European Journal of Control*, 2022.

[9] H. Namik and K. Stol. Individual blade pitch control of a spar-buoy floating wind turbine. *IEEE transactions on control systems technology*, 22(1):214–223, 2013.

[10] Y. Shtessel, M. Taleb, and F. Plestan. A novel adaptive-gain supertwisting sliding mode controller: methodology and application. *Automatica*, 48:759–769, 2012.

20th EAWE PhD Seminar on Wind Energy
24-26 September 2024
Visby, Sweden

Autonomous Data-driven Wind Farm Control

Marcus Binder Nilsen[a], **Tuhfe Göçmen**[a], **Nikolay Dimitrov**[a], and **Pierre-Elouan Réthorén**[a]

[a]Department of Wind and Energy Systems, Technical University of Denmark, Roskilde, Denmark

E-mail: manils@dtu.dk

Keywords: Wind farm control, Reinforcement Learning

1 Background

For reliable and affordable operation of wind turbines located in wind farms, coordinated control solutions that take aerodynamic interactions into account play an important role. Referred as wind farm flow control (WFFC), these collective control actions primarily aim to mitigate wake effects; hence maximizing power/revenue, reducing structural loads and increasing component lifetime.

Given the prospects of the technology, WFFC is one of the most 'dynamic' fields within wind energy, that is increasingly popular across the globe. There are, on average, more than 20 WFFC-related journal articles published on Wind Energy Science journal alone in a year – for the past 5 years.

As highlighted in the Grand Challenges article for WFFC [9], the synergies between Artificial Intelligence (AI) applications and WFFC domain are prominent, and they are gaining wider research attention following the advances in applied data science techniques and increasing availability of data. A relatively new but rapidly growing application for data-driven WFFC is reinforcement learning (RL) based control, allowing optimal control strategies to be learnt purely from data collected from the turbulent, and ever-changing wind farm environment.

However, even though research has started to look into RL for wind farm control, it is still a relatively new area. Most research is either done on smaller wind farms and/or static wind conditions, or with low fidelity turbine representation, using e.g. actuator discs to represent the turbines [1].

2 Research state of the art

This project will be built on two pillars, where recent advancements has been made.

The first is inside the field of RL. Here, a number of advancements has been made over the last couple of years.

- Advancements with more sample efficient algorithms such as TD7 [4] or TQC [5] have shown great promise to be able to control even more advanced systems with less training. These improved models means that the models used in [1] already has improved iterations that might increase performance significantly.

- Another interesting advancement in RL is within offline learning. Models that incorporate the transformer architecture [2] or make use of *Upside Down RL* [10] are both interesting approaches which could be explored.
  Both of these methods "flip" the normal RL objective, where instead of maximising a reward, the goal of the agent is to produce a specific reward over a given time frame. These methods might learn the environment dynamics better. Also in being offline learners, they can take advantage of the already generated data that exist from real wind farms.

- A very recent innovation is with the KAN network architecture [8]. This could be incorporated with RL, to increase the interpretability of otherwise black box or hard to understand models.

The second pillar of the PhD project is the research within medium-fidelity wind farm simulators. New computational efficient dynamic wake meandering (DWM) methods are now able to model the farm interactions, and

with the development of Dynamiks [3], on top of HAWC2Farm [7], HAWC2 [6] and DWM is combined in a way that is deemed fast enough to be utilized for RL. The coupling with HAWC2 makes it possible to get more realistic control input parameters then before, and the 3D multibody formulation of the turbine makes the structural loads and turbine responses more realistic. This coupling enables not only the optimisation based on power production, but also to investigate what impact the farm level control will have on the structural loads and the lifetime of the turbine components.

3 Objectives

The overall objective of this PhD project is to identify optimal operation strategies for wind farms based on the health status of the turbine(s), external conditions (e.g., environmental effects, electricity/energy markets) and the long-term implications of the control actions without humans in the loop. Several data sources will be integrated into the workflow, developing and demonstrating the state-of-the-art digital skills, competences and synergies within wind energy research, implemented in a brand-new facility.

4 Research questions

Research questions for this PhD are:

- **How to best implement RL for wind farm control?**
  To answer this question, the following ”sub questions” arise:
  - **What are the best currently available algorithms?**
    It needs to be investigated what RL algorithms that already exist, and which one(s) seems most promising for the task.
  - **How is the training conducted optimally?**
    When implementing RL there are multiple ”tricks” that can be applied to increase the performance or to speed up the learning. For example the use of reward shaping, or transfer learning.
  - **How to integrate several data sources relevant for wind farm control?**

- **How to implement AI driven wind farm control in the field?**
  It is important that the developed control strategies can actually be implemented on a real life turbine.

- **Can theoretical/numerical benefits of AI-driven control be reproduced in the field?**
  To help advance the field of RL in wind farm control, the simulated benefits should also be seen in the field.

References

[1] M. Abkar, N. Zehtabiyan-Rezaie, and A. Iosifidis. Reinforcement learning for wind-farm flow control: Current state and future actions. *Theoretical and Applied Mechanics Letters*, 13(6):100475, 2023.

[2] L. Chen, K. Lu, A. Rajeswaran, K. Lee, A. Grover, M. Laskin, P. Abbeel, A. Srinivas, and I. Mordatch. Decision Transformer: Reinforcement Learning via Sequence Modeling, 2021.

[3] DTU. Dynamiks, 2024. `https://gitlab.windenergy.dtu.dk/DYNAMIKS/dynamiks` [Accessed: 11-03-2024].

[4] S. Fujimoto, W.-D. Chang, E. J. Smith, S. S. Gu, D. Precup, and D. Meger. For SALE: State-Action Representation Learning for Deep Reinforcement Learning, 2023.

[5] A. Kuznetsov, P. Shvechikov, A. Grishin, and D. Vetrov. Controlling Overestimation Bias with Truncated Mixture of Continuous Distributional Quantile Critics, 2020.

[6] T. Larsen and A. Hansen. *How 2 HAWC2, the user's manual*. Number 1597(ver. 3-1)(EN) in Denmark. Forskningscenter Risoe. Risoe-R. Risø National Laboratory, 2007.

[7] J. Liew, T. Göçmen, A. W. H. Lio, and G. C. Larsen. Extending the dynamic wake meandering model in HAWC2Farm: a comparison with field measurements at the Lillgrund wind farm. *Wind Energy Science*, 8(9):1387–1402, 2023.

[8] Z. Liu, Y. Wang, S. Vaidya, F. Ruehle, J. Halverson, M. Soljačić, T. Y. Hou, and M. Tegmark. KAN: Kolmogorov-Arnold Networks, 2024.

[9] J. Meyers, C. Bottasso, K. Dykes, P. Fleming, P. Gebraad, G. Giebel, T. Göçmen, and J.-W. van Wingerden. Wind farm flow control: prospects and challenges. *Wind Energy Science*, 7(6):2271–2306, 2022.

[10] J. Schmidhuber. Reinforcement Learning Upside Down: Don't Predict Rewards – Just Map Them to Actions, 2020.

20th EAWE PhD Seminar on Wind Energy
24-26 September 2024
Visby, Sweden

Optimizing Electrical Stability in Offshore Energy Hubs: An Analysis of Topologies and Solutions

Alban J. F Duvivier[a], **Daniel Müller**[a], **Mirza Nuhic**[a], and **Nicolaos Cutululis**[a]

[a]Technical University of Denmark (DTU)

E-mail: ajdu@dtu.dk

Keywords: Offshore Wind Farms, HVDC, Converters, Electrical Stability

1 Introduction

The European Union has set ambitious targets to reduce its greenhouse gas emissions by 55% by 2030 and to become carbon neutral by 2050 [1]. This target must be met if global warming is to be limited to 1.5°C above pre-industrial levels [2]. Among others, offshore wind energy in the North Sea is an important part of this strategy [3]. Indeed, offshore wind capacity in the North Sea is expected to increase significantly [4], which poses technological challenges for this large decentralised power generation. In addition, the intermittency of sustainable energy solutions is driving the need for more international connections. In this context, energy islands have emerged as a promising solution to collect, convert and export large amounts of energy [5].

This report serves as an introduction to the potential major electrical risks and challenges in the implementation of such offshore structures. The report discusses the concept of an offshore energy hub, then presents the three types of connection that have been selected, and finally concludes with an explanation of the methods that can be used to overcome the challenge of electrical stability and ensure the smooth operation of the platform.

2 Offshore energy hub

2.1 General layout

An offshore Energy Hub (OEH) is one of the solutions to address the critical challenges of large-scale offshore wind power integration. Among other things, OEHs can be used to distribute wind production and interconnect different countries through an offshore grid, potentially integrating PtX (Power to X) production for cost-effective energy transmission and flexibility.

A key difference with an onshore grid is the inertia of the system. Onshore grids are fed by large rotating machines that provide stability in the event of disturbances/sudden changes in power. Such machines also have the ability to provide large amounts of power for short periods in the event of a fault. On the other hand, offshore networks have power electronic converters at both ends, which are controlled solely by the converters' controllers and have no intrinsic inertia. During a fault scenario, the limited overload capability of the converters makes fault management more difficult for such networks.

2.2 Offshore wind energy transmission

Onshore power systems use alternating current (AC) to transfer power on the grid. The main problem with long AC lines is the transmission of reactive power on the lines, which increases the current and therefore the losses. However, the DC converters and circuit breakers (for multiple DC circuits) increase the CAPEX of DC technologies [6]. According to [7], expected break-even distance at which DC becomes more advantageous than AC is around 50 km for submarine cables. As wind farms need to be sited further out to sea, DC cables have become the main option for offshore power transmission. [6].

DC connections are not a new topic. Many wind farms are now connected to the onshore grid via point-to-point HVDC connections, and the behaviour of such devices is well understood. The main goal of the OEH is to

connect various hubs and countries using DC cable transmission. This approach aims to reduce losses and costs while increasing the transmission capacity between countries. Although there are only a few multi-terminal DC networks currently in place, none of these infrastructures have been interconnected yet.

2.3 Design of hub topologies

Interconnections between terminals (on a similar platform or with other hubs) can be made by two main connection designs: connected on the DC side (Figure 1) or on the AC side (Figure 2). A third possible solution, the hybrid hub (Figure 3), would be connected to both sides of the converters, allowing both connections to be in operation, depending on requirements.

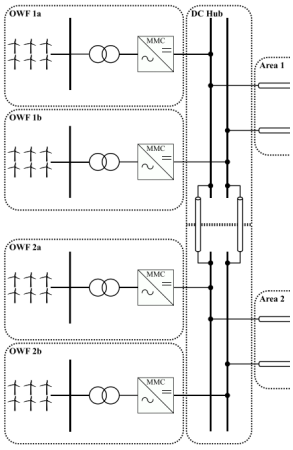

Figure 1: DC Hub

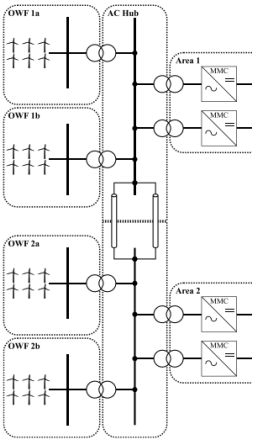

Figure 2: AC Hub

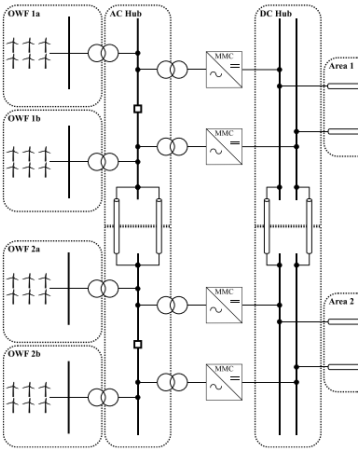

Figure 3: Hybrid Hub

Figure 4: Different design for hub topologies [8]

Both AC and DC hub options have pros and cons. The main advantage of a DC connected energy hub is its ability to transfer power between two countries. As the power flows through the hub on the DC busbar, no converters are used and losses are limited. In the case of AC interconnection, the DC power is converted to AC and back to DC, resulting in large losses in the converters. In addition, the connection capacity is limited by the converters and the actual wind power generation conditions. [8]

On the other hand, a major advantage of the AC connected topology is the connection between the poles before the converters. This makes it possible, in the event of a converter failure, to transfer the power production from the affected wind farm to the other converters. This scenario is developed in [9], which investigates the power dispatch for DC faults that render the connected converter out of service.

Furthermore, according to the economic simulations carried out in [8], the AC hub appears to have a lower CAPEX in the base case and in many different expansion scenarios [1]. In the case of a 4GW hub with two DC connections (2GW spokes, 1GW per DC cable), the DC solution is 14% more expensive than the equivalent AC topology in the base case scenario.

Finally, the hybrid solution essentially combines the advantages and disadvantages of both options, while providing partial redundancy as the connection can be secured at both sides [10]. However, the price of this solution is not negligible, with a CAPEX of up to 120% of the AC hub price for a simple implementation [8].

The main differences between the two options are summarised in the table below 1.

[1] In general, the AC topology is cheaper when the wind capacity is equal to or greater than the interconnection capacity. DC becomes more competitive when there is more interconnection capacity than connected wind capacity. Since less converters are required offshore

	AC Hub	DC Hub
Cost	Lower in most cases	Higher for the base case (+14%) [8]
Interconnection	Current flows twice through the converters Limited by the converter capacity	Lower losses Larger transmission capacity [10]
Maturity	Mainly mature technology	No multi-vendor case yet No operational HVDC CB in EU [10]
Electrical stability	AC potential instabilities [10]	Control of DC grid
Converter fault	Power dispatched	WF switched off [8]
Main Advantage	Power dispatch during converter fault	Interconnection capacity between countries

Table 1: Principal characteristic for AC and DC topologies

3 Challenges Addressed and Proposed Solutions

To ensure the correct operation of such a system, it is essential to ensure that it is electrically stable in a steady state. A general approach to this is to analyse the stability of small signals using a state space representation of the system. Behind this mathematical concept lies a method which, by linearising the equations, makes it easy to model the behaviour of the system when it is subjected to a small change in amplitude. It would efficiently analyse the interactions between the components of the specific system: converters, grid, wind farms, collector network, DC cables,... This analysis should provide more internal arguments to decide on the specific and optimal topology, as well as give input to the requirements to ensure safe operation.

Because the offshore system is decoupled from the onshore system it requires elements that have grid-forming capability, which in the current state-of-the-art is provided by the HVDC converters. Tuning the parameters in a zero-inertia system with a short electrical distance between the converters is not trivial, as the converters may interact negatively. This topic is discussed in detail in [11], where the different stability options for parallel grid-forming converters are analysed. Among other things, the benefits of using a virtual impedance to virtually increase the electrical distance between the controllers are confirmed.

4 Conclusion

This extended abstract has examined the challenges and potential risks involved in implementing offshore wind energy hubs, with a particular emphasis on electrical topologies and stability issues. It introduced the concept of this unprecedented technology, its use and its main characteristics.

Some preliminary studies have already investigated the economic aspects of the various options, without definitively establishing which is the best option. Although the AC topology generally appears to be cheaper, the cost savings are not significant enough to make it the definitive choice. The DC topology, while slightly more expensive, offers better interconnection capacity and should also be considered.

In the first instance, further research will address stability analysis for small signals using state space analysis for both options. Based on eigenvalue analysis, the study will aim to determine the optimal topology and the best control scheme for an offshore energy hub, ensuring efficient and stable operation.

Acknowledgements

This work is part of the Offshore Energy Hub research project funded by EUDP (Energy Technology Development and Demonstration Program), case no. 64022-1011.

References

[1] European Commission. Press release - completion of key 'fit for 55' legislation, 2023. Brussels. Retrieved from https://ec.europa.eu/commission/presscorner/detail/en/ip_23_4754.

[2] IPCC. *Contribution of Working Groups I, II and III to the Sixth Assessment Report of the Intergovernmental Panel on Climate Change*. 2023. Geneva. Sections 3. doi:10.59327/IPCC/AR6-978929169164.

[3] European Commission. A clean planet for all: A european strategic long-term vision for a prosperous, modern, competitive and climate neutral economy, 2018. Brussels. Retrieved from https://eur-lex.europa.eu/legal-content/EN/TXT/?uri=CELEX:52018DC0773.

[4] European Commission. Communication from the commission to the european parliament, the council, the european economic and social committee and the committee of the regions and eu strategy to harness the potential of offshore renewable energy for a climate neutral future, 2020. Brussels. Retrieved from https://eur-lex.europa.eu/legal-content/EN/TXT/?uri=COM:2020:741:FIN&qid=1605792629666.

[5] J. Juhl and A. Kristensen. Energy island in the north sea. In *Wodcon XXIII Proceedings*, 2022.

[6] Alberto Bertinato, Serge Poullain, Donaël Muret, and Kosei Shinoda. Nswph validation technical requirements. Technical Report 3636, SuperGrid Institute SAS, 23 Rue Cyprian, CS 50289, 69628 Villeurbanne Cedex, France, 3 2022. Confidential.

[7] Roland Ryndzionek and Łukasz Sienkiewicz. Evolution of the hvdc link connecting offshore wind farms to onshore power systems. *Energies*, 13(8):1914, 2020.

[8] Daniel Müller, Mirza Nuhic, Domagoj Hart, Gustavo Figueiredo Gontijo, and Syed Hamza Hasan Kazmi. Feasibility assessment of hub topologies. (31/01), 2024.

[9] Patrick Düllmann, Christina Brantl, Philipp Tünnerhoff, Philipp Ruffing, and Albert Moser. European offshore grid: On protection system design for radial bipolar multi-terminal hvdc networks. *Proceedings of the ...*, Session 2022:B4 – DC SYSTEMS AND POWER ELECTRONICS PS1 – HVDC SYSTEMS AND THEIR APPLICATIONS 2, 2022.

[10] Energinet. Offshore energy hubs - high-level system description and requirements, 2023. Document number 20/07386-44.

[11] Benjamin Hartmann Vilmann, Daniel Müller, Gustavo Figueiredo Gontijo, and Hjörtur Johannsson. Stability analysis and mitigation of power oscillations between parallel mmc-hvdc connections operating in grid-forming mode in offshore energy hubs. *CIGRE Paris Session, B4 - DC Systems and Power Electronics*, 2024.

TOPIC 5

Production, O&M, Decommissioning and lifetime extension

5.1 Session 115: Production, O&M, decommissioning and lifetime extension

24.09.2024, 10:30, Room 5

Chair:

Vasco Batista

Presenters:

Vetters Jade	From water to resource: A multi-actor techno-economic analysis of offshore wind farm decommissioning
Ahmad Yusof Nur Ain Wahidah Binti	Design and implementation of a novel technique to measure the tensile strength of recycled glass fibres taken from wind turbine blades
Bouzolin Daniel	Design for Repowering of Wind Farms
Shah Anik Hirenkumar	Impact of low-frequency fatigue cycles on the lifetime of wind turbines
Moynihan Bridget	Probabilistic offshore wind farm fatigue life estimations to inform decommissioning policy and repowering decision making

20th EAWE PhD Seminar on Wind Energy
24 - 26 September 2023
Visby, Sweden

From water to resource: A multi-actor techno-economic analysis of offshore wind farm decommissioning

Jade Vetters[a], Maxime Louis[a], Gwenny Thomassen[a,b,c], Steven Van Passel[a,b]

[a] Department of Engineering Management, University of Antwerp, Belgium
[b] Flanders Make @UAntwerp
[c] Research Group Sustainable Systems Engineering (STEN), Ghent University, Belgium

E-mail: jade.vetters@uantwerpen.be

Keywords: Renewable energy, Wind energy, Circular economy, End-of-life, Techno-economic Assessment, Mass and energy balance, Supply chain management, Stakeholder analysis

1 Introduction

Offshore wind energy (OWE) has rapidly emerged as a significant source of renewable energy, driven by global efforts to reduce carbon emissions and transition towards sustainable energy sources. The development of offshore wind farms (OWFs) began with Vindeby, the first OWF established in 1991, and has since expanded dramatically. By 2020, European waters hosted 116 OWFs across 12 countries, highlighting the growing role of offshore wind in the renewable energy landscape [1]. Belgium has become a key player in this sector, ranking as the fourth-largest European producer of OWE with an installed capacity of 2.3 GW by the end of 2021 [2]. The country currently operates eight OWFs in the Belgian part of the North Sea (BPNS), generating an average annual output of 8 TWh, which meets approximately 8% of the national electricity demand [3], [4].

Despite this progress, the operational lifespan of wind turbines is limited, typically ranging from 20 to 25 years [5]. As installations approach their end-of-life (EoL), decommissioning becomes a critical concern. Decommissioning involves dismantling and removing OWF components and restoring the seabed to its original state, as mandated by legal obligations [5], [6], [7]. Although decommissioning efforts have been minimal to date, Topham et al. [8] predict a significant increase in these activities as many turbines near their EoL. For the Belgian Part of the North Sea (BPNS), decommissioning of existing OWFs is anticipated between 2034 and 2047 [9].

The literature identifies three main EoL strategies: life extension, repowering, and decommissioning, with the latter often being legally mandated [5]. Accurately estimating decommissioning costs for an OWF is widely acknowledged as challenging, with key contributing factors encompassing limited experience, evolving regulatory frameworks, and uncertainties in timing, weather, and methods [10], [11], [12]. Additionally, stakeholders underscored the uncertainty surrounding efficient dismantling and removal approaches, a challenge further intensified by the difficulty in accurate cost estimation [13]. Moreover, Vetters et al. [14] shed light on the coexistence of this challenge with financial and insolvency risks for OWF owners, ambiguous liabilities, and insufficient removal legislation.

Given the complexities and significant economic impacts associated with decommissioning offshore wind farms, this study seeks to answer the following research question: "What are the preferable scenarios for the economic feasibility of offshore wind farms at end-of-life, considering the entire supply chain?" This question aims to explore the economic viability of different decommissioning strategies from the perspectives of various stakeholders within the supply chain, including OWF owners, marine contractors, ports, and recycling companies.

2 Methodology

2.1 Multi-Actor Techno-Economic Analysis (MATEA)

To address the multifaceted challenges of OWF decommissioning, we propose the novel Multi-Actor Techno-Economic Analysis (MATEA) framework. This framework is designed to integrate the techno-economic analysis (TEA) with a life cycle costing approach to provide a comprehensive evaluation of decommissioning scenarios from both societal and individual actor perspectives. This study represents a pioneering effort to apply such an integrated and multi-perspective approach to OWF decommissioning, offering novel insights and methodologies to the field.

The MATEA framework is structured to consider the EoL supply chain, and the decisions of each actor involved in the decommissioning process. This approach aims to facilitate informed decision-making, enhance collaboration, and improve the economic feasibility of decommissioning operations.

To identify the most economically feasible scenarios, the framework will be applied to an OWF in the BPNS equipped with 3 MW turbines and monopile foundations. The analysis will utilize the MATEA framework to examine various scenarios, including a base case with the most likely level of OWF removal, an alteration to this base case involving different offshore and onshore operations, a limited removal scenario, a maximum removal scenario, and a scenario considering alternative design choices.

2.2 Approach

In this study, the steps of a techno-economic analysis, as outlined in Thomassen et al. [15], will be followed:

1 **Market Study**: This step involves analyzing market conditions, regulatory requirements, and economic factors affecting decommissioning and post-decommissioning. The market study provides an understanding of the current landscape and helps identify key drivers and barriers to decommissioning.

2 **Process Flow Diagram / Mass & Energy Balance**: Detailed process flow diagrams are developed to map out the decommissioning activities, as presented in Figure 1 for the transition piece and monopile for the base case scenario. Mass and energy balance calculations are conducted to quantify the material and energy flows involved in the dismantling, removal, transport, and recycling processes. Technical data will be collected through interviews with experts from relevant sectors, supplemented by desk research to comprehensively map the energy consumption of offshore and onshore machinery and the equipment required for dismantling, removal, processing, and recycling.

3 **Economic Analysis**: The economic analysis is conducted using a four-headed integrated approach, considering the perspectives of different actors in the EoL supply chain. This involves evaluating the costs and benefits associated with decommissioning from the viewpoints of OWF owners, marine contractors, ports, and recycling companies. In this study, technical analysis is integrated within the economic calculations to provide a thorough assessment of economic feasibility.

4 **Uncertainty Analysis**: This step involves evaluating uncertainties related to technical and economic factors to enhance the robustness of the assessment.

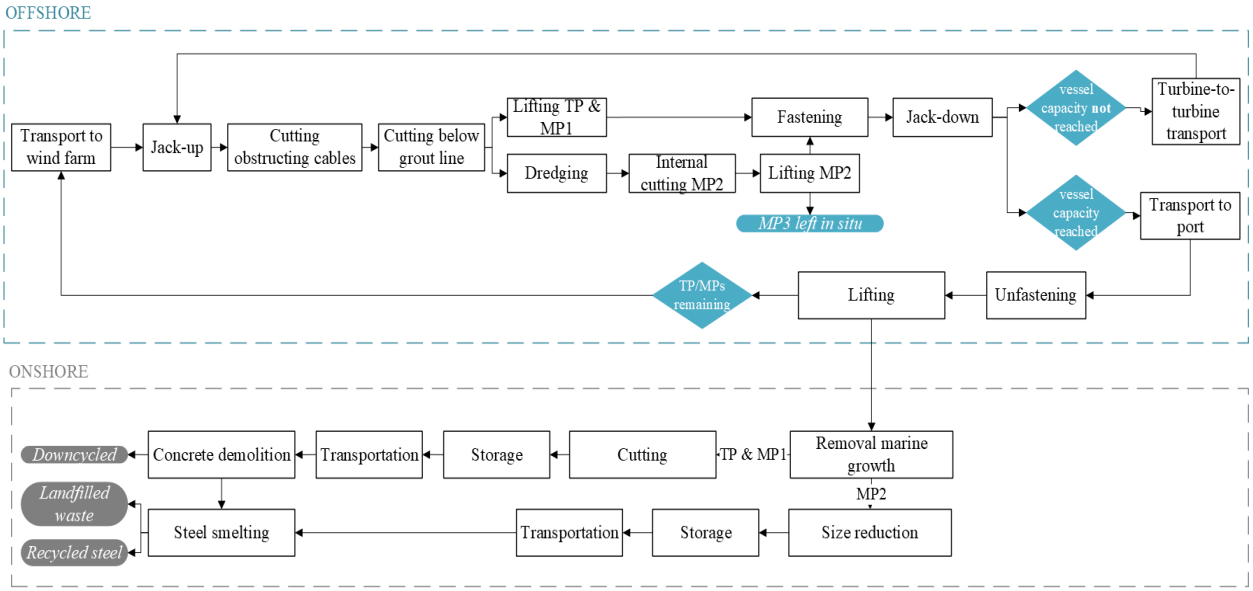

Figure 1: Process flow diagram for transition piece and monopile decommissioning in a base case scenario with monopile removal two meters below the seabed.

3 Expected Outcomes

While this study is in process, this section elaborates on some expected outcomes. Firstly, by evaluating the decommissioning process from multiple perspectives, this study aims to uncover the interdependencies and potential conflicts among different stakeholders. For instance, while full removal may be economically challenging for OWF owners, it could benefit marine contractors by providing more extensive dismantling work.

Secondly, the findings are expected to inform policymakers about the economic implications of different decommissioning regulations. Understanding the costs and benefits associated with various decommissioning strategies can help in designing regulations that balance economic feasibility with environmental protection.

Thirdly, the study will provide recommendations for enhancing collaboration among stakeholders to optimize the decommissioning process. This includes strategies for cost-sharing, resource pooling, and joint planning efforts to reduce overall costs and improve efficiency.

By adopting a multi-actor approach, this study aims to identify the most economically desirable decommissioning strategies for both society and individual stakeholders. This method promotes more efficient and sustainable offshore wind energy transitions by fostering collaboration and informed decision-making among all parties involved in the decommissioning process.

References

[1] WindEurope, "Offshore Wind in Europe - Key trends and statistics 2020," Feb. 2021. Accessed: Oct. 12, 2022. [Online]. Available: https://proceedings.windeurope.org

[2] L. V. De Luca Peña *et al.*, "Monetized (socio-)environmental handprint and footprint of an offshore windfarm in the Belgian Continental Shelf: An assessment of local, regional and global impacts," *Appl Energy*, vol. 353, p. 122123, Jan. 2024, doi: 10.1016/j.apenergy.2023.122123.

[3] Belgian Offshore Platform, "Projects." Accessed: Jan. 29, 2024. [Online]. Available: https://www.belgianoffshoreplatform.be/en/projects/

[4] Belgian Offshore Platform, "Wind farms in Belgian North Sea provided green power for nearly 2 million Belgian households in 2021," Jan. 04, 2022. Accessed: Oct. 30, 2023. [Online]. Available: https://www.belgianoffshoreplatform.be/en/news/wind-farms-in-belgian-north-sea-provided-green-power-for-nearly-2-million-belgian-households-in-2021/

[5] A. M. Jadali, A. Ioannou, K. Salonitis, and A. Kolios, "Decommissioning vs. repowering of offshore wind farms—a techno-economic assessment," *International Journal of Advanced Manufacturing Technology*, vol. 112, no. 9–10, pp. 2519–2532, Feb. 2021, doi: 10.1007/S00170-020-06349-9.

[6] C. T. Nieuwenhout, "Regulating offshore wind energy," *Elgar Encyclopedia of Environmental Law*, vol. 9, pp. 535–545, 2021, doi: 10.4337/9781788119689.IX.45.

[7] E. Topham, D. McMillan, S. Bradley, and E. Hart, "Recycling offshore wind farms at decommissioning stage," *Energy Policy*, vol. 129, pp. 698–709, Jun. 2019, doi: 10.1016/J.ENPOL.2019.01.072.

[8] E. Topham, E. Gonzalez, D. McMillan, and E. Joao, "Challenges of decommissioning offshore wind farms: Overview of the European experience," *J Phys Conf Ser*, vol. 1222, no. 012035, 2019, Accessed: Oct. 13, 2022. [Online]. Available: https://iopscience.iop.org/article/10.1088/1742-6596/1222/1/012035/pdf

[9] A. Goethals and F. Maes, "Decommissioning Offshore Windfarms and Grid Infrastructure: To Remove or Not to Remove?-A Belgian Law Perspective," *Ocean Development & International Law*, vol. 54, no. 3, pp. 304–326, 2023, doi: 10.1080/00908320.2023.2265297.

[10] M. J. Kaiser and B. Snyder, "Modeling the decommissioning cost of offshore wind development on the U.S. Outer Continental Shelf," *Mar Policy*, vol. 36, no. 1, pp. 153–164, Jan. 2012, doi: 10.1016/J.MARPOL.2011.04.008.

[11] C. Mackie and A. P. M. Velenturf, "Trouble on the horizon: Securing the decommissioning of offshore renewable energy installations in UK waters," *Energy Policy*, vol. 157, Oct. 2021, doi: 10.1016/J.ENPOL.2021.112479.

[12] L. Winkler, O. Kilic, and J. Veldman, "Collaboration in the offshore wind farm decommissioning supply chain," *Renewable and Sustainable Energy Reviews*, vol. 167, Oct. 2022, doi: 10.1016/J.RSER.2022.112797.

[13] J. Vetters, G. Thomassen, and S. Van Passel, "Getting stakeholders aboard at the final blow of offshore wind: A qualitative study on end-of-life challenges [Manuscript submitted to Energy Research & Social Science]," 2024.

[14] J. Vetters, G. Thomassen, and S. Van Passel, "Sailing through end-of-life challenges: A comprehensive review for offshore wind," *Renewable and Sustainable Energy Reviews*, vol. 199, p. 114486, Jul. 2024, doi: 10.1016/J.RSER.2024.114486.

[15] G. Thomassen, M. Van Dael, S. Van Passel, and F. You, "How to assess the potential of emerging green technologies? Towards a prospective environmental and techno-economic assessment framework," *Green Chemistry*, vol. 21, no. 18, pp. 4868–4886, Sep. 2019, doi: 10.1039/C9GC02223F.

Design and implementation of a novel technique to measure the tensile strength of recycled glass fibres taken from wind turbine blades

Nur Ain Wahidah Binti Ahmad Yusof [a], Ross Minty[b], Liu Yang[b]

[a] CDT in Wind and Marine Energy Systems and Structures, Department of Electronic and Electrical Engineering, University of Strathclyde, 75 Montrose Street, Glasgow G1 1XJ, UK

[b] Department of Mechanical and Aerospace Engineering, University of Strathclyde, 75 Montrose Street, Glasgow G1 1XJ, UK

E-mail: nur.ain-wahidah@strath.ac.uk

Keywords: wind turbine, recycling, glass fibres, mechanical properties, microbond testing

1.0 Introduction

Over the past decades, glass fibre has been the primary reinforcement material for polymer composites due to its high specific properties and cost-effectiveness. As a result, glass fibre-reinforced composites have been extensively used across various industries with their usage is now expanding further, driven by sectors such as transportation, construction, and the rapidly growing wind energy sector. This widespread application has created significant challenges regarding the disposal of glass fibre-reinforced composites at the end of their lifecycle [1]. In 2019, the global consumption of reinforcement-grade glass fibre likely surpassed six million tons. Alongside this consumption is the generation of up to one million tons of glass fibre manufacturing waste, much of which ends up in landfills [2]. The rising costs and decreasing availability of landfill space, coupled with increasing national and international regulations, make the disposal of end-of-life composites both economically and socially unsustainable. Therefore, there is an urgent need to develop alternative methods for managing end-of-life composites.

In particular, the wind energy sector has rapidly developed over the past twenty years into a promising source of renewable energy. However, wind turbine blades, primarily composed of glass fibre-reinforced thermosets, are currently deemed non-recyclable [3]. Consequently, the recycling of glass fibre-epoxy composite materials from wind turbine blades has emerged as a critical area of research with particular focus on evaluating the mechanical properties of the recycled fibres due to the increasing demand for sustainable practices and the need to manage the significant volume of decommissioned blades.

Current methods for assessing the mechanical properties of recycled fibres are limited, particularly at sub-mm gauge lengths, due to the fibres' brittleness and degradation during the recycling process. This limitation necessitates the development of new techniques to ensure accurate measurement and reliable assessment of the recycled fibres' tensile strength.

2.0 Objective

The objective of this project is to design and implement a novel technique capable of accurately measuring the mechanical properties, specifically the tensile strength, of recycled glass fibres at very low gauge lengths. Given the challenges associated with the brittleness and reduced mechanical performance of these fibres post-recycling, traditional methods have proven inadequate, particularly for gauge lengths below 5 mm. This project seeks to overcome these limitations by developing a method based on the microbond technique, enabling reliable testing at sub-millimetre scales. By starting with a 20 mm gauge length to benchmark against existing methods and progressively reducing to 1 mm and below, the project aims to provide a comprehensive characterization of the tensile properties of recycled glass fibres. This will ultimately facilitate improved recycling processes and the effective utilisation of these materials in various industrial applications.

3.0 Methodology

3.1 Sample Preparation

To prepare recycled glass fibres from wind turbine blades for mechanical testing, fluidised bed method is employed. Figure 1 shows a schematic of the in-house fluidised bed recycling process. In the fluidised bed reactor, the thermosetting polymer matrix undergoes thermal decomposition. The reactor uses silica sand fluidised with pre-heated air from an electric heater. The composite feedstock enters the reactor via an access pipe situated above the expanded bed. A centrifugal fan supplies the fluidising air, which is sufficient to carry the liberated glass fibres from the bed into the reactor's freeboard. An induced draft fan maintains a slight negative pressure in the reactor by drawing the glass fibres and polymer volatiles from the freeboard. The glass fibres are then recovered from the gas stream using a cyclone separator. During the process, the bed temperature is maintained at 500°C, the static bed height at 150 mm, and the fluidisation velocity at 1.5 m/s.

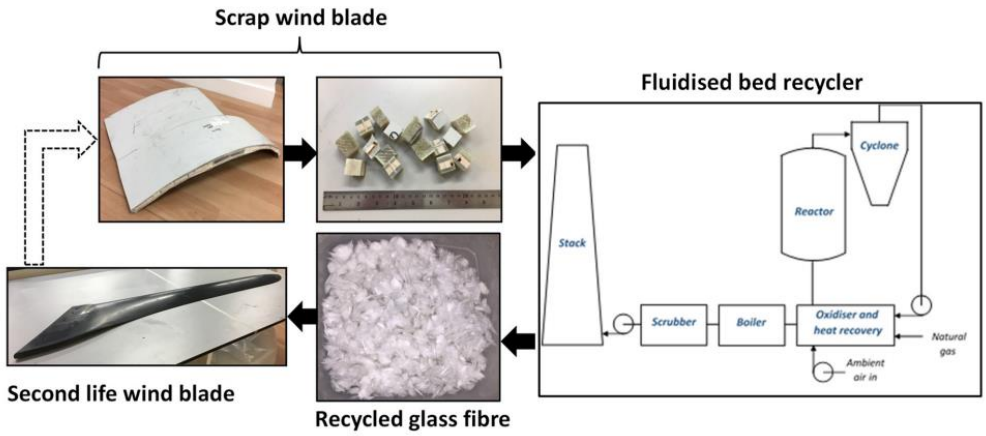

Figure 1: Wind turbine blade recycling described in [4]

3.2 Microbond Testing

A fibre is carefully selected, and small droplets of resin are then deposited along the gauge lengths of the fibre. After the resin droplets are applied, the sample is cured, usually by heating, to solidify the resin and firmly attach the droplets to the fibre.

Unlike the conventional procedure of the microbond test, where small resin droplets are used to measure the interfacial shear strength by observing the debonding of the fibre from the resin, in this experiment, larger droplets are created. The objective is to cause the fibre to break at any point rather than debond from the resin. When a load is applied, the point of failure will be the fibre itself rather than the fibre-resin bond. This method allows us to determine the ultimate tensile strength of the fibre. As we are trying to evaluate the tensile strength of fibres at very short gauge lengths (below 1 mm), using a tensile machine to measure the tensile strength of these fibres

presents limitations. Therefore, this modified approach aims to overcome those limitations by focusing on the fibre's fracture rather than debonding.

4.0 Expected Outcomes

By comparing results from the microbond-based technique with traditional methods at 20 mm gauge lengths, this study aims to validate the effectiveness of the new approach in assessing the tensile strength and other mechanical properties of recycled fibres. Additionally, investigating gauge lengths of 1 mm and below will provide valuable insights into the behaviour of recycled fibres at shorter lengths, which is crucial for accurately characterising their performance in composite materials.

5.0 References

[1] P. G. Jenkins, L. Yang, J. J. Liggat, and J. L. Thomason, 'Investigation of the strength loss of glass fibre after thermal conditioning', *J Mater Sci*, vol. 50, no. 3, pp. 1050–1057, Feb. 2015, doi: 10.1007/s10853-014-8661-x.

[2] J. L. Thomason and L. Yang, 'Towards a New Generation of Glass Fibre Products Based on Regenerated Fibres Recycled from End-Of-Life GRP and GRP Manufacturing Waste'.

[3] K. Pender and L. Yang, 'Regenerating performance of glass fibre recycled from wind turbine blade'.

[4] K. Pender and L. Yang, 'Glass fibre composites recycling using the fluidised bed: A study into the economic viability in the UK', *Clean Technologies and Recycling*, vol. 3, no. 3, pp. 221–240, 2023, doi: 10.3934/ctr.2023014.

Design for Repowering of Wind Farms

Daniel Bouzolin[a], Kyle Settelmaier[a], D. Todd Griffith[a]

[a] The University of Texas at Dallas

E-mail: dan@utdallas.edu

Keywords: Repowering, Wind Farm Design, Lifetime, Optimization, Techno-Economic Analysis

1 Introduction

Wind energy technologies supply a significant portion of the renewable energy market in many countries, but what happens when those technologies begin to age out? In countries like Denmark and Spain, more than half of the cumulative capacity of onshore wind energy consists of turbines which are greater than 10 years old [1]. Most wind farms today are designed for a 20-year lifespan, after which there are three main options: 1) decommissioning, 2) life-extension, or 3) repowering [2].

Repowering refers to the process of retrofitting wind farms with new technologies or refurbishing existing wind turbines in some capacity. This can include either a full repowering (replacement of the entire wind turbine) or a partial repowering (replacement of only certain components such as blades) process [3]. Because wind farm repowering projects can utilize existing infrastructure and initial investments (grid connections, land leases, etc.), repowering greatly simplifies the process of installing or upgrading wind farm capacity [4]. With this process also comes the ability to overcome the economic, regulatory, and societal barriers that typically come with installing new wind farms. Despite these benefits of repowering, there are still significant challenges that create uncertainty in decisions regarding repowering to be made by wind farm operators.

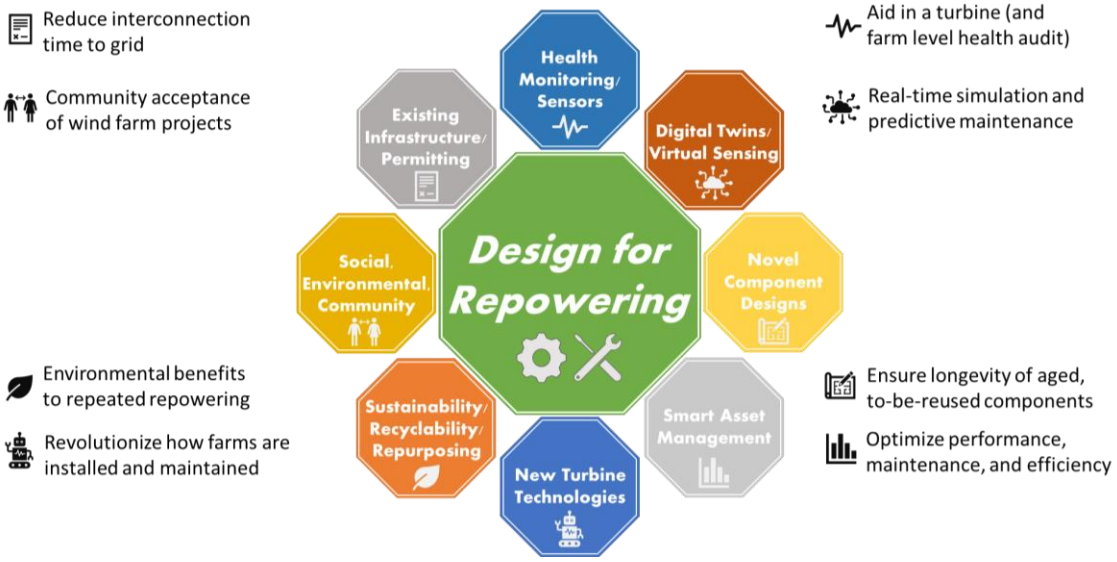

Figure 1: Overview of the Design for Repowering Framework.

This paper aims to develop a comprehensive repowering framework that can be used to "design for repowering" and thus address the uncertainties faced in repowering decisions. The benefits of such a framework

are twofold: 1) this framework can be applied to existing wind farms to address open questions about repowering and best understand how to maximize real-time repowering benefits, and 2) the Design for Repowering framework has the potential to revolutionize the way we future wind farms, wherein the wind farms of the future are designed with ultra-long life and planned repowering in mind. An initial concept for our Design for Repowering framework is presented in Figure 1, where we envision the combined use of new technologies (e.g., sensors and loads monitoring, and new installation and maintenance techniques) along with new repowering cost models, to provide more certainty in decisions regarding the state of health of a components and what action should be taken.

2 Methods

While repowering is attractive as an option for extending or renewing wind farm service life, some open questions about repowering remain: 1) the financial benefits of repowering have yet to be quantified through a well-defined financial model, 2) repowering carries inherent risk due to the uncertainty in the reliability of age to-be-reused components (such as towers and foundations), and 3) the optimal timing and strategy for repowering projects has yet to be explored.

An economic analysis framework for repowering is proposed to address uncertainty in the financial benefits of repowering. In addition, this framework will be applied to identify the optimal timing for repowering (balancing factors such as lost opportunity cost from repowering early against factors like increased power production with newer technology or increased financial incentives). Such a framework can not only support decision-making regarding today's repowering needs but can also be leveraged to design future wind farms for repowering. Accompanying this economic framework is a turbine component loads analysis to better guide decisions about reusing or replacing aged components for long-life repowered projects. This loads analysis includes OpenFAST-based digital twin models used to simulate long-term wind turbine loads in all major components. Such analyses, coupled with the economic framework, will guide repowering decisions by answering key questions about the durability of components, component suitability for continued service, and cost impacts of designing components for longer lifetimes.

3 Results and Conclusions

The initial exploration of the Design for Repowering framework focuses on two main factors. The first is a turbine component loads analysis and levelized-cost-of-energy (LCOE) calculation, designed to inform decisions about repowering through quantification of turbine component durability. Figure 2 below contains results illustrating just one of the key factors of the Design for Repowering framework — smart asset management — and how new turbine technologies like Active Load Control [5] can be utilized to reduce turbine loads and maximize longevity of reusable turbine components.

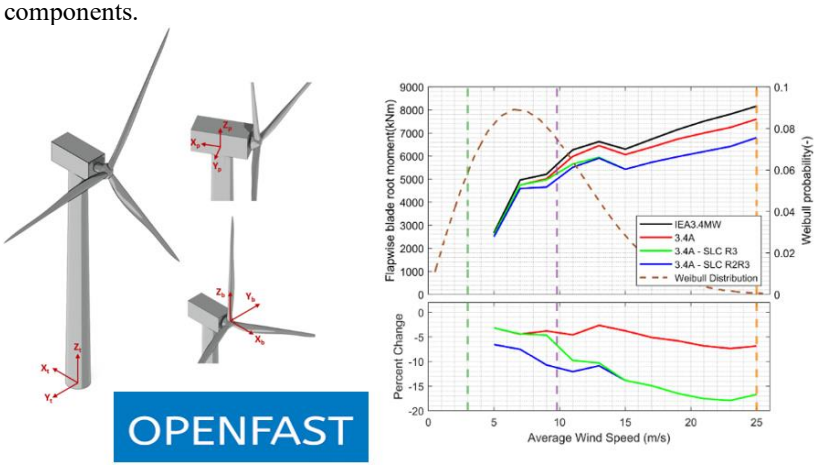

Figure 2: Turbine component loads analysis via OpenFAST.

The second focus topic of this framework is a financial study utilizing the NREL System Advisor Model (SAM) to quantify the financial benefits of repowering. Figure 3 below shows the preliminary analysis demonstrating the

benefits of repowering through the net present value (NPV) of a sample wind farm repowered in year 20 and operated for 20 additional years until 40 years of life. In addition to NPV, other financial parameters including LCOE, return on investment, production tax credits, PPA variability, and EBITDA will impact the viability of repowering.

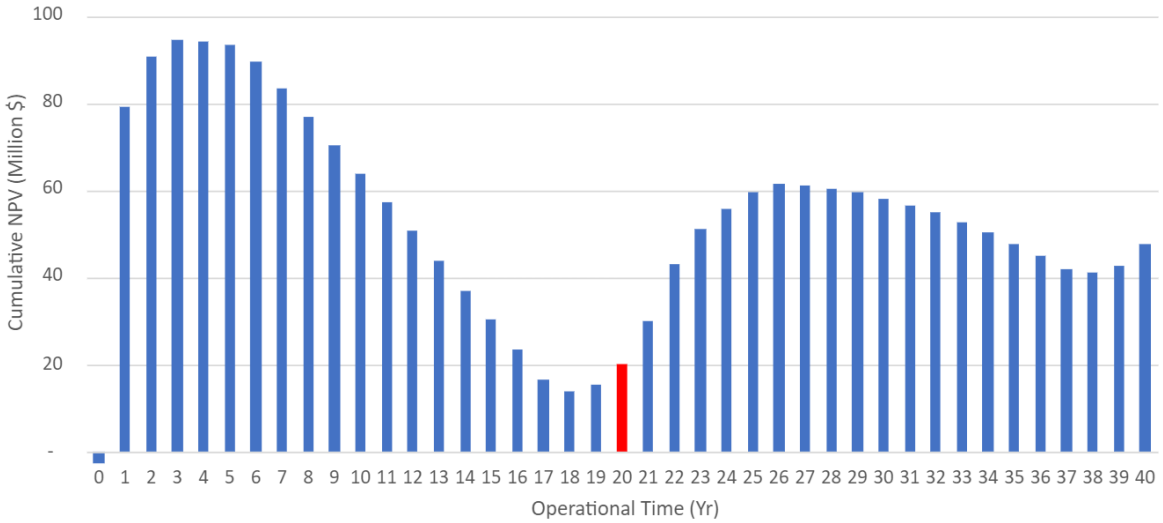

Figure 3: Net present value of a 40-year wind farm repowered at the end of year 20.

Future work will include the following: (1) a comprehensive presentation of the Design for Repowering framework, (2) development of a robust health audit framework based on component loads monitoring to aid in repowering decisions, (3) development of a repowering economics model, and (4) the results of case studies utilizing the framework from point (1) along with data from points (2) and (3). Envisioned case studies for repowering have been identified and include: 1) Baseline: 20-year wind farm with decommissioning, 2) Conventional Repower: 40-year wind farm with partial (e.g., tower repowering) or full repowering at 20 years, and 3) Advanced Repower: 100-year wind farm designed for repowering.

Acknowledgements

The presenting author acknowledges the Eugene McDermott Graduate Fellowship program (award number 202303) for providing support for conference travel.

References

[1] Lena Kitzing, Morten Kofoed Jensen, Thomas Telsnig, and Eric Lantz, “Multifaceted drivers for onshore wind energy repowering and their implications for energy transition,” Nature Energy, 2020.

[2] Katherine Ortegon, Loring F. Nies, John W. Sutherland, “Preparing for end of service life of wind turbines,” Journal of Cleaner Production, Volume 39, 2013, Pages 191-199, ISSN 0959-6526, https://doi.org/10.1016/j.jclepro.2012.08.022.

[3] Eric Lantz, Michael Leventhal, and Ian Baring-Gould, “Wind Power Project Repowering: Financial Feasibility, Decision Drivers, and Supply Chain Effects,” National Renewable Energy Laboratory, 2013

[4] Jadali, A.M., Ioannou, A., Salonitis, K. et al. Decommissioning vs. repowering of offshore wind farms—a techno-economic assessment. Int J Adv Manuf Technol 112, 2519–2532 (2021). https://doi.org/10.1007/s00170-020-06349-9

[5] Chetan, M., Sakib, M.S., Griffith, D.T., Gupta, A., and Rotea, M.A., “Design of a 3.4MW Wind Turbine with Integrated Plasma Actuator-based Load Control” Wind Energy, September 2021, DOI: 10.1002/we.2684

Impact of low-frequency fatigue cycles on the lifetime of wind turbines

Anik H. Shah[a], Andreas Vad[a], Carlo L. Bottasso[a]

[a] Wind Energy Institute, Technical University of Munich, Garching, Germany
E-mail: anik.shah@tum.de

Keywords: low cycle fatigue, wind turbines, remaining useful lifetime

1. Introduction

With 13% of the onshore wind turbine (WT) capacity in Europe expected to be more than 20 years old by 2030 [1], majority of the wind industry in Europe faces the challenge of making an informed decision on lifetime extension of WTs. Remaining useful lifetime (RUL) of WTs is evaluated by comparing Lifetime DELs for original design wind class and site-specific environmental and operating conditions using 10-min aeroelastic simulations [2]. The resulting load time series at critical positions are analysed by applying the rainflow counting (RFC) method and the Palmgren-Miner rule on the resulting load spectrum [3]. While this method determines the fatigue accumulated and damage equivalent loads (DELs) corresponding to cycles within the 10-minute interval, cycles that exceed the 10-minute duration are cut-off. Since these low-frequency cycles (i.e. during wind speed variations, change in operating modes) often exhibit high stress ranges, they are also the most damaging cycles. Therefore, they need to be considered for RUL prediction. In this study, the impact of low-cycle fatigue is evaluated on the lifetime of wind turbines. Moreover, a deep dive into the various factors that affect the impact low-cycle fatigue is also outlined. Lastly, the challenges associated with reconstructing low cycle fatigue for RUL calculation are highlighted.

2. Methodology

Typically, the 10-minute load time series for all inflow and operating conditions (bins) are cycle-counted separately. Cycle-counting a 10-minute subset results in full cycles and half cycles. Based on the standard approach, the damage due to both these cycles is added by weighting. The total damage accumulated is calculated statistically from the overall load spectrum. However, if all load time series were to be concatenated and then cycle-counted, not only would some of the residuals or half cycles finish and create more damage, but also new cycles would emerge representing the "slow" dynamics of wind speed variations and transitions in operating modes. These additional cycles are highlighted by new green full cycles in Figure 1.

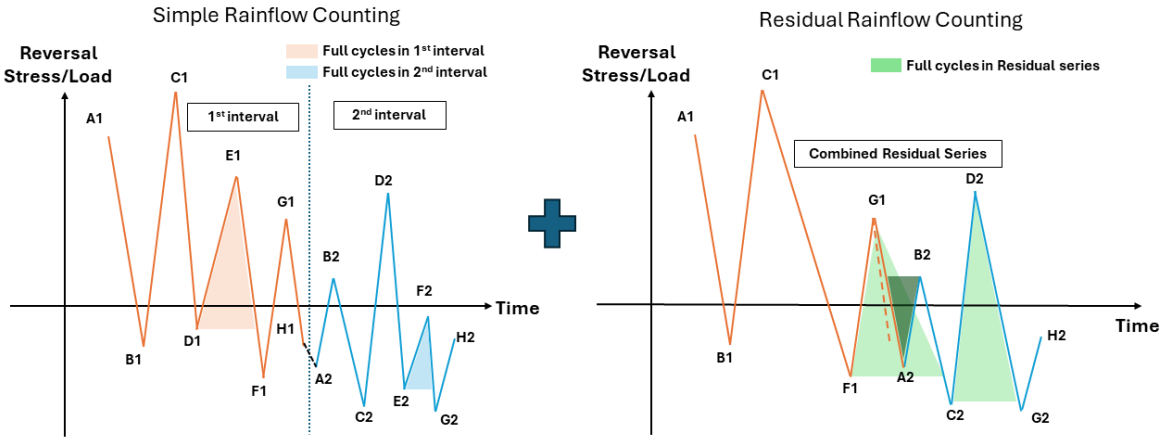

Figure 1 - Additional cycles captured with Residual Rainflow Counting

Amzallag et al. standardized the RFC method and included a way to allow successive time periods to be processed, considering cycles that last beyond the individual time periods while maintaining the efficiency of the 10-min

approach and the accuracy of the concatenation approach [4]. This method is validated in [5] [6] and summarized in Figure 2.

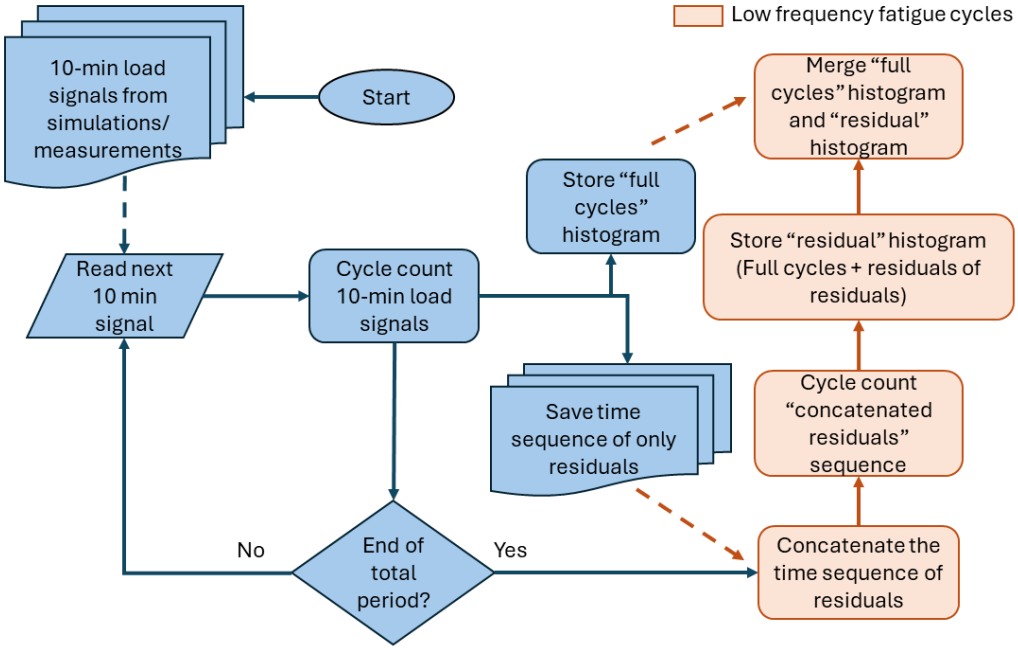

Figure 2 - Framework to account for low-frequency fatigue cycles

Damage ratio can be used to highlight the added damage contribution of low-frequency fatigue cycles (LFFC). It is defined based on the Palmgren-Miner rule as follows:

$$D_{ratio} = \frac{D_{SRFC}}{D_{RRFC}} = \frac{\sum_{i=1}^{N_{SRFC}} n_i \cdot (\Delta\sigma)_i^m}{\sum_{i=1}^{N_{RRFC}} n_i \cdot (\Delta\sigma)_i^m},$$

where, m is the Wöhler exponent, n is the fraction of the no. of cycles for the load/stress range $\Delta\sigma$, and N are the total no. of load/stress ranges in the load spectrum. Additionally, by plotting the ratio of the cumulative damage with respect to the total damage over the cycle length, the percentage of damage that occurs longer than 10-minutes can be quantified.

3. Initial Results

Almost 12 months of tower base load measurements and met-mast data are used from a WT at an onshore site in Germany. The data has been filtered for free-stream and normal power production conditions. Damage ratio is calculated for different wöhler exponents and shown in Figure 3a. Lower damage ratio indicates a higher impact of low frequency fatigue cycles. The damage ratio appears to be converging towards the 1-year mark which is in accordance with other studies [5][6]. However, the current ratios are different from those studies (offshore) indicating a site-specific and perhaps even a WT-specific nature of low-frequency fatigue cycles. Additionally, the impact of LFFC is highly sensitive to the wöhler exponent.

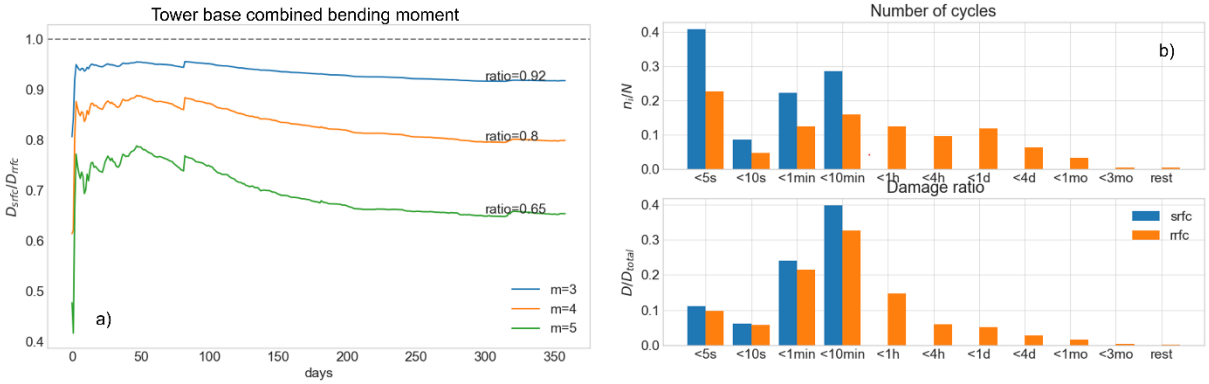

Figure 3 - Damage ratio over days (left) and Damage ratio over cycle lengths (right)

Figure 3b shows the distribution of the fraction of cycles for a given cycle length and the associated damage for both the standard 10-min SRFC and the proposed RRFC method which accounts for low frequency cycles. Cycles beyond 10-min contribute to a significant amount of the damage to the wind turbine over a period of 12 months. Beyond the typical wind speed variations over periods longer than 10 minutes, we also see the impact of diurnal cycles and seasonal effects on low-frequency fatigue damage.

4. Conclusions & Outlook

Residual rainflow counting leads to an increase of the damage at tower and is highly dependent on the wöhler exponent. Low-frequency fatigue cycles span a wide range of time periods. Additionally, the impact of wind direction variation, wake effects and transition cycles could play a significant role. Reconstructing a long-term artificial load series for different components for RUL calculation based on 10-min SCADA measurements introduces significant uncertainties to the formulation of RRFC, specifically due to the stochasticity of turbulent seeds on the residual cycles.

Acknowledgements

This work is funded by the German Federal Ministry for Economic Affairs and Climate Action within the Life-Odometer Project (FKZ: 03EE3037B).

References

[1] WindEurope (2022): Wind energy in Europe: 2023 Statistics and the outlook for 2024-2030 | WindEurope. Available online at https://windeurope.org/intelligence-platform/product/wind-energy-in-europe-2023-statistics-and-the-outlook-for-2024-2030/#overview

[2] Ziegler, Lisa; Gonzalez, Elena; Rubert, Tim; Smolka, Ursula; Melero, Julio J. (2018): Lifetime extension of onshore wind turbines: A review covering Germany, Spain, Denmark, and the UK. In *Renewable and Sustainable Energy Reviews* 82, pp. 1261–1271. DOI: 10.1016/j.rser.2017.09.100.

[3] DKE/K 383 Windenergieanlagen. 2019. *Wind energy generation systems – Part 1: Design requirements (IEC 61400-1:2019); German version EN IEC 61400-1:2019.*

[4] Amzallag, C., Gerey, J., Robert, J., and Bahuaud, J. 1994. Standardization of the rainflow counting method for fatigue analysis. *International Journal of Fatigue* 16, 4, 287-293.

[5] Marsh, G., Wignall, C., Thies, P. R., Barltrop, N., Incecik, A., Venugopal, V., and Johanning, L. 2016. Review and application of Rainflow residue processing techniques for accurate fatigue damage estimation. *International Journal of Fatigue* 82, 757–765

[6] Sadeghi, N., Robbelein, K., D'Antuono, P., Noppe, N., Weijtjens, W., and Devriendt, C. 2022. Fatigue damage calculation of offshore wind turbines' long-term data considering the low frequency fatigue dynamics. *J. Phys.: Conf. Ser.* 2265, 3, 32063

20th EAWE PhD Seminar on Wind Energy
24 - 26 September 2023
Visby, Sweden

Probabilistic offshore wind farm fatigue life estimations to inform decommissioning policy and repowering decision making

Bridget Moynihan[a], Eleonora M. Tronci[b], Babak Moaveni[a], Eric Hines[a]

[a] Civil and Environmental Engineering, Tufts University, Medford, MA, USA
[b] Civil and Environmental Engineering, Northeastern University, Boston, MA, USA

E-mail: bridget.moynihan@tufts.edu

Keywords: Offshore wind, structural health monitoring, lifetime extension, fatigue, repowering, decommissioning, monitoring and instrumentation

1 Introduction

Offshore wind will play a significant role in decarbonizing the U.S. electric grid. Numerous projects are in the development process, and more lease areas are expected to be auctioned in the coming years. The performance and longevity of offshore wind turbines are important to manage for the sake of renewable energy reliability in the energy transition. The measured and predicted capacity of offshore wind turbines throughout their lifetime will become important information for decision-makers, particularly as projects reach the end of a lease term.

The use of Structural health monitoring (SHM) instrumentation systems involving accelerometers and strain gauges [1] can enhance offshore wind turbine reliability and provide information to decision-makers. The data collected from such instrumentation is used to monitor structural dynamics [2, 3], track fatigue consumption [4], reduce the time between inspections, and ultimately extend turbine lifetimes [5]. Typical offshore wind project lengths are 25-30 years. Over this period, operations and maintenance (O&M) costs make up over a quarter of total project costs [6]. SHM will also reduce the cost of offshore wind energy by reducing the need for trips offshore by promoting predictive O&M strategies instead of preventative [5].

Regarding lifetime extension, fatigue assessment provides an up-to-date evaluation of the damage incurred through the operational life [7]. While other components experience more frequent breakages, the foundations (monopiles) of offshore wind turbines are often considered to be overly conservative in design. Fatigue life analyses of instrumented offshore wind turbines have shown that the tower and substructures could last much longer than a wind farm's 25-year design life [8], as well as that when evaluated using measured and reconstructed bending moment responses, these structures experience less fatigue than is predicted in traditional fatigue analyses using simulations [9].

These results could be used by wind farm operators and decision-makers regarding offshore wind farms at the end of a project term or lease length. At the end of a project lifetime, operators can either decommission the infrastructure or instead choose to repower some or all wind turbines. Repowering consists of replacing or repairing components in the farm to increase electricity production and avoid decommissioning. The foundation and tower are the most critical components for a successful repowering effort [10] because of their purpose as the anchor of the entire structure to the seabed. Repowering efforts can increase electricity production while reducing the number of turbines in a farm, but in the case of onshore wind in Europe, less than 10% of turbines are repowered, mostly due to slow and complicated permitting and regulatory regimes around the topic [11].

To avoid a similar situation around repowering efforts, the U.S. industry would benefit from robust predictions of the remaining useful life of every offshore wind turbine in our waters. This information can inform decisions to repower turbines or to decommission and rebuild which will help retain the reliability of renewable energy sources in the grid system. However, current laws in the U.S. state that wind farm operators must decommission all infrastructure after the lease length and project lifetime end [12]. U.S. offshore wind policy calls for a more

20th EAWE PhD Seminar on Wind Energy
24 - 26 September 2023
Visby, Sweden

comprehensive framework for deciding when and how to decommission wind turbine infrastructure. Given the high capital cost and permitting delays related to offshore development, it would be beneficial for the U.S. grid and the energy transition at large if offshore wind farms were allowed to operate beyond their lease length.

This research will work to answer two questions: 1) what does instrumentation data tell us about the expected lifetime of offshore wind turbine towers and foundations as compared to simulations conducted in the design stage? 2) How can accurate fatigue life estimations of a wind farm inform end-of-life decision-making and promote repowering efforts?

This work seeks to answer these questions using a combination of SHM methodologies, physics-based modeling, machine learning algorithms, and agent-based simulations. First, an instrumented turbine is used to build a digital twin using Bayesian model updating techniques. To address non-instrumented turbines, machine learning algorithms are introduced to extrapolate relationships between measured bending moment responses and SCADA data parameters which are widely available in a wind farm. This enables limited predictions of bending moment responses across the wind farm. The digital twin is then utilized in virtual sensing techniques to predict moment responses at fatigue-sensitive locations on the tower and foundation. Fatigue damage or remaining useful life estimates are computed from the predicted bending moment responses. We leverage probabilistic or Bayesian methods in order to quantify the uncertainty in predictions which will be propagated through fatigue life estimations. Methods are applied to real wind turbines located on the U.S. East Coast, where the first offshore wind farms in the country are being built. Turbines are instrumented with accelerometers and strain gauges, as well as SCADA systems. Results will be used to inform a discussion around decommissioning policy and repowering decision-making. This can enable more informed decision-making at the end of wind farm lease lengths, which can ultimately improve overall renewable energy reliability in the U.S. grid and support long-term energy goals.

2 Probabilistic fatigue life estimations for a wind farm

To address the first research questions described above, this section of work seeks to create a digital representation of instrumented offshore wind turbines for use in making predictions of the bending moment or stress response of the structure under varying conditions. The digital twin captures uncertainty in our model, which can be propagated into virtual sensing predictions. Machine learning techniques are introduced to extrapolate what instrumentation tells us about one turbine onto the remaining turbines in a farm, enabling farm-wide virtual sensing. These results are used in fatigue life estimations to provide a predicted distribution of the remaining useful life of the towers and monopiles in a wind farm.

2.1 Digital Twinning of an instrumented offshore wind turbine

Digital twins are a virtual model of an operational offshore wind turbine that has been tuned (updated) to match the behavior of the true structure. This process is carried out through model updating of a finite element model of the turbine and informed by modal parameters obtained from the operational turbine equipped with an SHM instrumentation system [3]. Model updating can be carried out in a probabilistic manner—known as hierarchical Bayesian model updating—which estimates optimal virtual model parameters while quantifying uncertainty and accounting for variability with environmental conditions [13, 14].

Probabilistic digital twins allow us to predict the distribution of natural frequency, damping ratios, and mode shapes of operational wind turbines using SCADA data only. Figure 1 provides an example of predicted natural frequencies according to power output and wind speed. Results show that our model captures the range of frequencies identified as well as the unique relationship between fore-aft frequencies and wind speed for operational (power-producing) conditions.

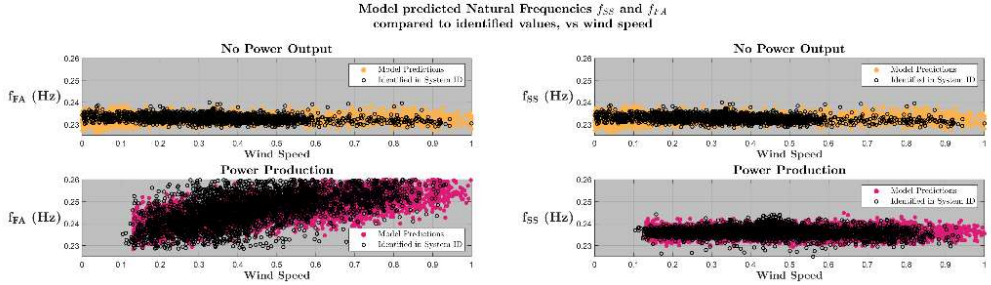

Figure 1: Model-predicted natural frequencies using hierarchical Bayesian digital twin

20th EAWE PhD Seminar on Wind Energy
24 - 26 September 2023
Visby, Sweden

The updated model can be used in virtual sensing techniques to obtain bending moment time histories at non-instrumented locations. Using measured stress or bending moment responses at locations along the tower and foundation which have strain gauges, the stress or bending moment response can be predicted at alternative locations using modal parameters (mode shapes) of the digital twin. This process allows for fatigue estimations at any height along the foundation and tower beyond instrumented locations.

2.2 Transfer learning from instrumented turbine to wind farm

As stated in 2.1, a digital twin which is tuned to match the behavior observed from real data allows us to comprehensively assess the fatigue of the entire tower and foundation of the instrumented turbine. However, turbines at a wind farm are not all routinely instrumented with strain gauges and accelerometers. Therefore, to make farm-wide fatigue predictions, we must predict the stress or moment response of the other turbines in the farm using the information learned on the instrumented turbine. For this task, we leverage the SCADA data which is available at every turbine in a farm. Specifically, the machine learning algorithm Gaussian process regression is used to build a data-driven predictive model for bending moment responses taking only SCADA data as inputs [15]. Figure 3 shows an example of the predictive quality of these models on a bending moment response measured by strain gauges. Due to the similar design and behavior of wind turbines in a farm, next steps of this work will conduct transfer learning on Gaussian process models. This consists of extrapolating the trained models from the instrumented turbine to the remainder of the wind farm, providing bending moment reconstructions for non-instrumented towers and foundations. Gaussian process regression is a probabilistic machine learning algorithm that—similar to hierarchical Bayesian model updating—provides uncertainty quantification. This uncertainty will also be propagated through virtual sensing techniques on the non-instrumented turbines in the farm.

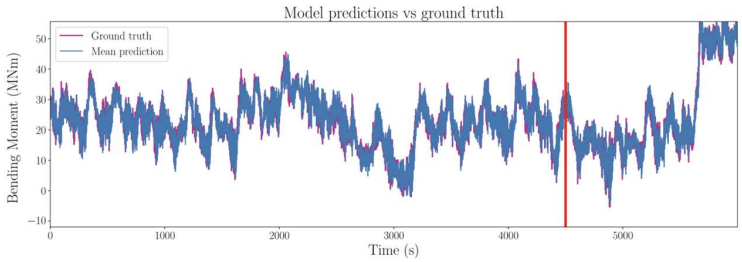

Figure 2: Bending moment response prediction using gaussian process regression taking SCADA data as inputs

2.3 Fatigue life estimation using bending moment response

The bending moment or stress response time histories are used directly in fatigue estimates. Using virtual sensing techniques and the digital twin described in 2.1, the bending moment response can be estimated at critical locations to estimate the remaining useful life. Using machine learning techniques described in 2.2, the same predictions can be made for the entirety of a wind farm without widespread instrumentation. Next steps in this work include the fatigue damage calculations for the entire wind farm using the measured and predicted bending moment responses. Since uncertainty has been propagated to bending moment response predictions, we will continue to treat the problem probabilistically. Existing fatigue analyses of real offshore wind farms have not propagated uncertainty into remaining useful life predictions. Our work will take this step, therefore providing a probability distribution on the fatigue life of structures in the wind farm.

3 Decommissioning and repowering policy analysis

The fatigue life estimations provided by the above work should inform wind farm operators and policy makers who dictate end-of-life decisions in offshore wind. This information will be used to address the second research question laid out in this work about repowering policy and incentives. Next steps in this work will involve a policy simulation analysis in which the fatigue estimations described in 2.3 will serve as model inputs. In these agent-based modeling simulations, various decommissioning and repowering policies can be compared to understand how operators may make decisions at the end of wind farm design lives. Developers have not cited profitability as drivers in deciding to repower wind farms [16], so our simulations will seek to understand what type of policies or incentives could promote repowering efforts.

20th EAWE PhD Seminar on Wind Energy
24 - 26 September 2023
Visby, Sweden

4 Conclusions

This work has shown the first stages of probabilistic digital twinning and farm-wide virtual sensing methods which are conducted for use in fatigue life estimations. Next steps will include propagating the quantified uncertainty into fatigue estimations, and the use of these predictions in a policy simulation analysis to compare the effectiveness of different incentives for increasing repowering efforts in the U.S. offshore wind industry.

Acknowledgements

Partial support of this study is provided by the National Science Foundation grant 2230630 and the Massachusetts Clean Energy Center AmplifyMass program.

References

[1] E. M. Hines *et al.*, "Structural instrumentation and monitoring of the Block Island Offshore Wind Farm," *Renew Energy*, vol. 202, pp. 1032–1045, Jan. 2023, doi: 10.1016/j.renene.2022.11.115.

[2] M. Song, N. Partovi Mehr, B. Moaveni, E. Hines, H. Ebrahimian, and A. Bajric, "One year monitoring of an offshore wind turbine: Variability of modal parameters to ambient and operational conditions," *Eng Struct*, vol. 297, Dec. 2023, doi: 10.1016/j.engstruct.2023.117022.

[3] B. Moynihan, A. Mehrjoo, B. Moaveni, R. McAdam, F. Rüdinger, and E. Hines, "System identification and finite element model updating of a 6 MW offshore wind turbine using vibrational response measurements," *Renew Energy*, vol. 219, Dec. 2023, doi: 10.1016/j.renene.2023.119430.

[4] A. N. Iliopoulos, C. Devriendt, S. N. Iliopoulos, and D. Van Hemelrijck, "Continuous fatigue assessment of offshore wind turbines using a stress prediction technique," in *Health Monitoring of Structural and Biological Systems 2014*, SPIE, Mar. 2014, p. 90640S. doi: 10.1117/12.2045576.

[5] M. Vieira, B. Snyder, E. Henriques, C. White, and L. Reis, "Economic Viability of Implementing Structural Health Monitoring Systems on the Support Structures of Bottom-Fixed Offshore Wind," *Energies (Basel)*, vol. 16, no. 13, Jul. 2023, doi: 10.3390/en16134885.

[6] T. Stehly, P. Duffy, and D. Mulas Hernando, "2022 Cost of Wind Energy Review," 2023.

[7] J. Pacheco, F. Pimenta, S. Pereira, Á. Cunha, and F. Magalhães, "Fatigue Assessment of Wind Turbine Towers: Review of Processing Strategies with Illustrative Case Study," *Energies*, vol. 15, no. 13. MDPI, Jul. 01, 2022. doi: 10.3390/en15134782.

[8] N. Partovi-Mehr *et al.*, "Fatigue Analysis of a Jacket-Supported Offshore Wind Turbine at Block Island Wind Farm," *Sensors*, vol. 24, no. 10, p. 3009, May 2024, doi: 10.3390/s24103009.

[9] F. Pimenta, D. Ribeiro, A. Román, and F. Magalhães, "Predictive model for fatigue evaluation of floating wind turbines validated with experimental data," *Renew Energy*, vol. 223, p. 119981, Mar. 2024, doi: 10.1016/j.renene.2024.119981.

[10] B. Connaghan, E. Decristofaro, E. Soderlund, M. Thibodeau, and X. Wang, "Wind Project Repowering Best Practices and Insights: Focus on Partial Repowering," 2000. [Online]. Available: www.sargentlundy.com

[11] "Repowered wind farms show huge potential of replacing old turbines," Wind Europe, https://windeurope.org/newsroom/news/repowered-wind-farms-show-huge-potential-of-replacing-old-turbines/.

[12] Vineyard Wind LLC, "Construction & Operation Plan (COP)," 2020.

[13] I. Behmanesh and B. Moaveni, "Accounting for environmental variability, modeling errors, and parameter estimation uncertainties in structural identification," *J Sound Vib*, vol. 374, pp. 92–110, Jul. 2016, doi: 10.1016/j.jsv.2016.03.022.

[14] M. Song, B. Moaveni, C. Papadimitriou, and A. Stavridis, "Accounting for amplitude of excitation in model updating through a hierarchical Bayesian approach: Application to a two-story reinforced concrete building," *Mech Syst Signal Process*, vol. 123, pp. 68–83, May 2019, doi: 10.1016/j.ymssp.2018.12.049.

[15] B. Moynihan, E. M. Tronci, M. C. Hughes, B. Moaveni, and E. Hines, "Virtual sensing via Gaussian Process for bending moment response prediction of an offshore wind turbine using SCADA data," *Renew Energy*, vol. 227, Jun. 2024, doi: 10.1016/j.renene.2024.120466.

[16] L. Kitzing, M. K. Jensen, T. Telsnig, and E. Lantz, "Multifaceted drivers for onshore wind energy repowering and their implications for energy transition," *Nat Energy*, vol. 5, no. 12, pp. 1012–1021, Dec. 2020, doi: 10.1038/s41560-020-00717-1.

5.2 Session 214: Production, O&M, decommissioning and lifetime extension

25.09.2024, 13:0, Room 4

Chair:

Maksims Pogumirskis	

Presenters:

Lipari Tiago	Impact of Foundation Repair on Wind Turbine Natural Frequencies: A Case Study
Issa Mahmoud	Investigation of Life Extension Impact and the Financial Viability of Frequency Support Provision from Wind Farms
Benzohra Abdelmalek	Inspection and Maintenance Planning for Offshore Wind Turbine Support Structures: New Insights
Vukobrat Antonina	Assessing the economic and environmental performance of onshore wind farms

20th EAWE PhD Seminar on Wind Energy
24-26 September 2024
Visby, Sweden

Impact of Foundation Repair on Wind Turbine Natural Frequencies: A Case Study

Tiago Lipari[a,b], **Filipe Magalhães**[a], and **João Santos**[b]

[a]Faculty of Engineering, University of Porto (FEUP), Rua Dr. Roberto Frias 4200-465 Porto, Portugal
[b]Ventient Energy Limited, Rua João Chagas 53A Piso 0, 1495 072 Algés, Portugal

E-mail: up202312031@edu.fe.up.pt

Keywords: Foundations, Natural Frequencies, Structural Repair

1. Introduction

As some wind farms age, various types of problems arise that compromise their electrical production. Although not as common as other types of damage, damage to foundations can compromise the stability of the wind turbine and lead to high repair costs [1]. This work focuses on a specific type of damage identified in a large number of existing onshore concrete foundations [2] in which gaps develop between the concrete and the steel tower. The gradual increase in these gaps may have consequences that are yet to be studied in detail. A wind turbine with this damage was analyzed using LVDTs on the foundation to measure the gaps and accelerometers on the tower to estimate natural frequencies. The foundation was then repaired and the results obtained before and after the repair are presented in this work.

2. Case Study background and analysis methodology

The present work relies on data from one wind turbine at a Portuguese wind farm. It is a GE Energy 2.5xl with a rotor diameter of 100m, 85m high and a power of 2,500 kW. The foundation is a concrete gravity based structure with an octagonal shape and 16.5m between the parallel sides. See below for an illustration [1],[2]. Gaps were detected during visual inspection and the wind turbine was experiencing several stops due to excessive vibrations. After measuring the gaps, and following industry practices, it was decided to repair the foundation.

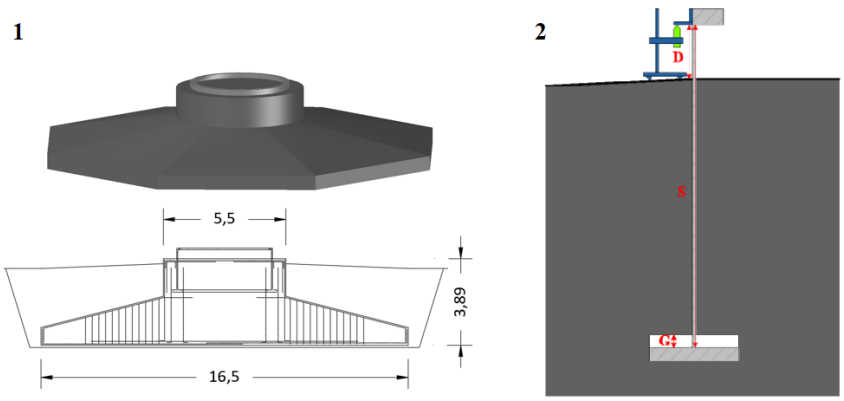

Figure 1: (a) Foundation Geometry. (b) Gap illustration and measurement.

2.1 Gaps estimation - LVDT´s

To estimate the gaps between the concrete foundation and the steel tower 4 LVDT´s were displaced along the based and an emergency stop was performed to promote a quick variation in the bending moment at the base. One test was done before the repair and another after.

2.2 Natural frequency estimation

To gather data that would allow estimating the natural frequencies of the turbine, two accelerometers were placed on the tower. One was placed at the top and the other at 2/3 of the height as shown in figure 2. Data was acquired during one month and the repair was performed during this period. COVariance driven Stochastic Subspace Identification method (SSI-COV Algorithm) was used to indentify the natural frequency values and modal damping ratios for each vibration mode. The algorithm used in this work was developed and described in [3, 4, 5].

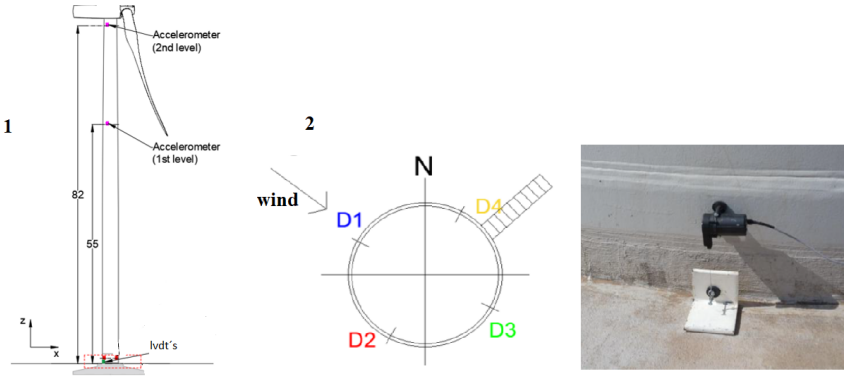

Figure 2: (a) Accelerometer´s layout. (b) LVDT´s layout.

3. Foundation Repair

The foundation repair consisted of reestablishing the original steel-concrete connection. For this, injections of epoxy resin were carried out (compressive strength of 70 Mpa at 7 days). Eight holes were drilled in the pedestal to reach the lower steel flange. See below for an illustration [1],[2]. After injection, surface waterproofing was carried out to prevent water from entering the steel-concrete interface, which is one of the factors that increases the evolution of cracks and gaps in the foundation [6].

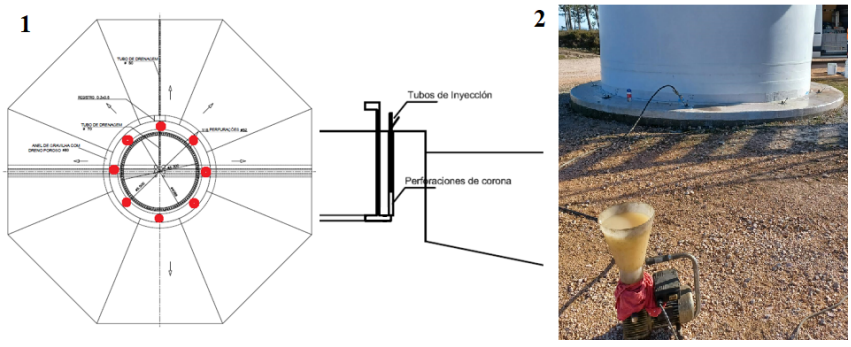

Figure 3: (a) Epoxi resin injections layout. (b) Foundation being injected

4. Results

The measurement of relative displacements between the foundation concrete and the tower steel (gaps) was carried out before and after the repair. Both tests were done with wind speeds between 15 and 20 m/s. Bellow are the results obtained before the repair.

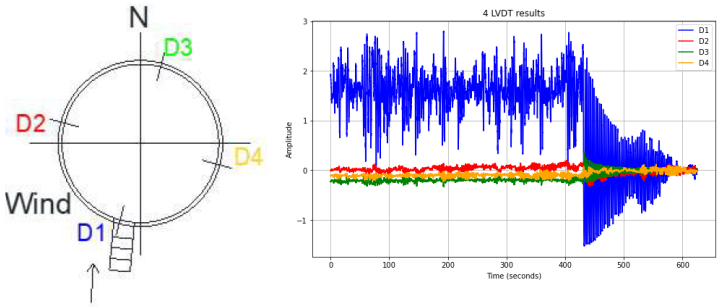

Figure 4: (a) LVDT´s layout. (b) LVDT results before repair

As shown in figure 4, the biggest amplitude was recorded in LVDT D1 indicating an existing gap of around 4.3 mm. The decay time period was 3.42 seconds (corresponding to 0.29 Hz). Bellow are the results obtained after the foundation repair. As shown in figure 5 all LVDT´s recorded amplitudes bellow 0.5mm. The decay

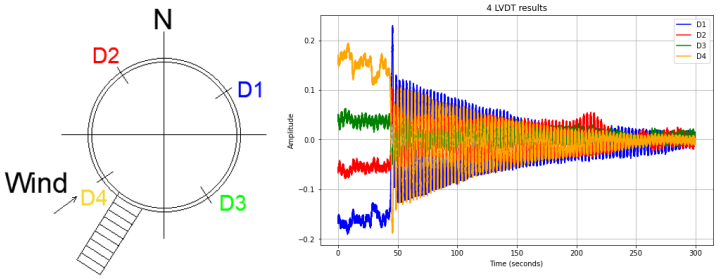

Figure 5: (a) LVDT´s layout. (b) LVDT results after repair

time period was 2.91 seconds (corresponding to 0.34 Hz) clearly indicating a stiffer behavior. Displacements were relatively low and reflect elastic behaviour of the steel tower. This shows the effectiveness of the repair in restoring a monolithic behavior between the foundation and the embedded steel tower. Regarding the estimation of natural frequencies, Figures 6 and 7 present the results obtained from the processing of data set collected in parked (idling) conditions.

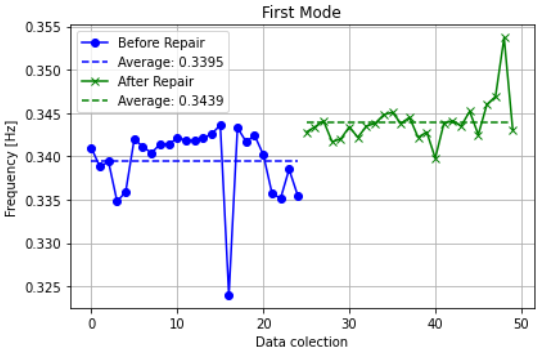

Figure 6: First mode frequencies

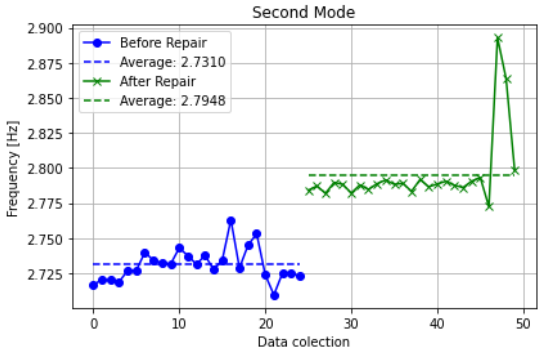

Figure 7: Second mode frequencies

5. Conclusions

The main goal of this work was to assess if reestablishing the monolithic behavior between the foundation and the steel tower would have impact on the main frequencies of a wind turbine. This assessment was carried out and the results seem promising in identifying damage to foundations through natural frequency analysis. For the first mode the main frequency increased 1.3 % while for the second mode it increased 2.3 %. This increment shows the repair increased the overall stiffness of the structure which at the same indicates that this type of damage may decrease the original stiffness. The subsequent work will focus one more wind turbines with the same type of damage and also wind turbines that will face foundation repairs. Monitoring systems are to be implemented in order to try to detect foundation issues. The work will also focus on other consequences of foundation damage that are not yet sufficiently studied in order to assist decisions on whether or not to repair a foundation.

Acknowledgements

This work is part of the ongoing research project: “M4WIND – Monitoring, Modelling and Machine learning for Managing the operating life of WIND farms”, ref. 2022.08120.PTDC (https://doi.org/10.54499/2022.08120.PTDC). Funded by national funds through the FCT/MCTES (PIDDAC).

References

[1] Kirk Morgan, Eric Ntambakwa, and G Hassan. Wind turbine foundation behavior and design considerations. In *Proceedings of the American Wind Energy Association Windpower Conference*, 2008.

[2] Magnus Currie, Mohamed Saafi, Christos Tachtatzis, and Francis Quail. Structural integrity monitoring of onshore wind turbine concrete foundations. *Renewable energy*, 83:1131–1138, 2015.

[3] Filipe Magalhães and Álvaro Cunha. Explaining operational modal analysis with data from an arch bridge. *Mechanical systems and signal processing*, 25(5):1431–1450, 2011.

[4] Gustavo Oliveira. Vibration-based structural health monitoring of wind turbines, 2016.

[5] Bart Peeters. System identification and damage detection in civil engeneering. 2000.

[6] Jack McAlorum, Marcus Perry, Grzegorz Fusiek, Pawel Niewczas, Iain McKeeman, and Tim Rubert. Deterioration of cracks in onshore wind turbine foundations. *Engineering structures*, 167:121–131, 2018.

Investigation of Life Extension Impact and the Financial Viability of Frequency Support Provision from Wind Farms

Mahmoud Issa*[1], Matthew Cole[1], David Campos-Gaona[1], and Abbas Kazemi Amiri[1]

[1]Department of Electronic and Electrical Engineering [Univ Strathclyde] – United Kingdom

Abstract

- **1. Motivation**

In an era where the urgent need for sustainable energy solutions is growing, wind energy emerges as a crucial element in the renewable energy landscape. Moreover, wind power integration into power systems has rapidly expanded and advanced (1). However, historically, the stability of electrical grids has relied heavily on inertia provided by synchronous generators. With the ascent of renewable energy sources, which typically operate asynchronously, there is a critical need for innovative solutions to deal with the reduced synchronised rotational inertia in the grid to avoid system instability and provide system support (2).

The impact of grid frequency support through droop control on the fatigue of wind turbine components has not been extensively researched in the academic literature. To properly investigate this impact, composite grid frequency profiles need to be compiled as grid frequency shows greater variability as wind energy integrates into the power system. Additionally, cross-referencing ancillary service data during these periods could further assess the financial viability of wind farms offering grid support. Currently, the business model in the wind sector is structured to maximize power extraction from wind resources without adequately considering the trade-off between energy pricing and the resultant deterioration to the turbine components. In light of the substantial increase in renewable energy integration and the associated need for curtailment, it is imperative to assess the effects of curtailment on the operational lifetime of turbine components.

- **2. Objective**

The objective is to examine the impact of ancillary service provision from wind in terms of lifetime extension and financial viability.

- **3. Methodology**

Strathfarm, an in-house wind farm modelling software developed by the University of Strathclyde, will be employed in this investigation. Strathfarm encompasses various aspects of wind farm analysis, including structural models for individual wind turbines, wake interactions between turbines, wind farm control, and the newly incorporated grid model designed to assess a farm's influence on grid frequency.

*Speaker

The plan for this investigation will start by studying the existing Strathfarm power system modelling approach and the set-point power tracking algorithms, which is extensively discussed in (3). Subsequently, composite grid frequency profile scenarios will be generated through the analysis of historical grid frequency data. Following this, the existing Strathfarm power system model will undergo modification to incorporate the generated frequency scenarios derived from the preceding step. Then, an analysis will be conducted to study the impact of frequency support provision by a wind farm in terms of lifetime extension and financial viability

4. **References**

(1) A. Al-Shetwi. Sustainable development of renewable energy integrated power sector: trends, environmental impacts, and recent challenges. *Science of The Total Environment,* 822:153645, 2022

(2) H. Golpîra, A. Messina and H. Bevrani. Emulation of Virtual Inertia to Accommodate Higher Penetration Levels of Distributed Generation in Power Grids. *IEEE Transactions on Power Systems.* 34:3384 – 3394, 2019.

(3) M. Cole. Investigation and Assessment of the Benefits For Power Systems From Wind Farm Control. *Doctoral thesis, Wind and Marine Energy Systems CDT, University of Strathclyde,* Dec. 2023. (Online). Available: https://stax.strath.ac.uk/concern/theses/1j92g8062.

Inspection and Maintenance Planning for Offshore Wind Turbine Support Structures: New Insights

Abdelmalek BENZOHRA [a], **Felipe GIRO** [a], and **Philippe RIGO** [a]

[a] ANAST, ArGEnCO, University of Liege, Liege, Belgium

E-mail: abenzohra@uliege.be

Keywords: Offshore wind turbine, fatigue deterioration, inspection, predictive maintenance.

1 Introduction

Offshore wind energy is gaining importance in the shift towards renewable energy. As wind turbines become progressively larger and wind farms are installed in deeper waters, the support structures of offshore wind turbines (OWTs) must withstand larger loads, ultimately increasing the costs associated with these structures. Maintaining the structural integrity of OWTs remains a significant challenge due to their due to their susceptibility to environmental factors like wind, waves, and corrosion, which can lead to structural degradation and ultimately structural failure.

Typical maintenance strategies often rely on reactive approaches can be explained in Figure 1, commonly referred as corrective maintenance, which can lead to increased downtime, maintenance costs, and operational risks. Industrial standards and guidelines for determining design loads for maintenance strategies, such as those from DNV [1], are conservative and subject to high levels of uncertainty. DNV acknowledges these uncertainties and recommends conservative evaluations to mitigate risks, ensuring that structures are over-designed to handle worst-case scenarios, thereby prioritizing safety and reliability.

Inspection and maintenance planning relies on conservative assumptions at design stage without exposing the structure to unnecessary risks. Inspection identifies defects in the structural components, while maintenance improves their condition. In practice, I&M planning can, for instance, decrease some design safety factors, possible resulting in lighter and therefore cheaper structures. Traditionally, heuristic-based plannings are often employed to establish the I&M strategy. Although fast and satisfactory, heuristic-based solutions are likely suboptimal. A fully optimized solution depends on complex models that might demand significant computational resources [2].

This article discusses three perspectives to enhance I&M planning for OWT support structures. They approach deterioration modelling of fatigue cracks and techniques to incorporate diverse sources of information to increase the accuracy of the reliability models necessary for I&M planning. These perspectives provide different insights to reduce the uncertainties related to the deterioration modelling with feasible computational efforts.

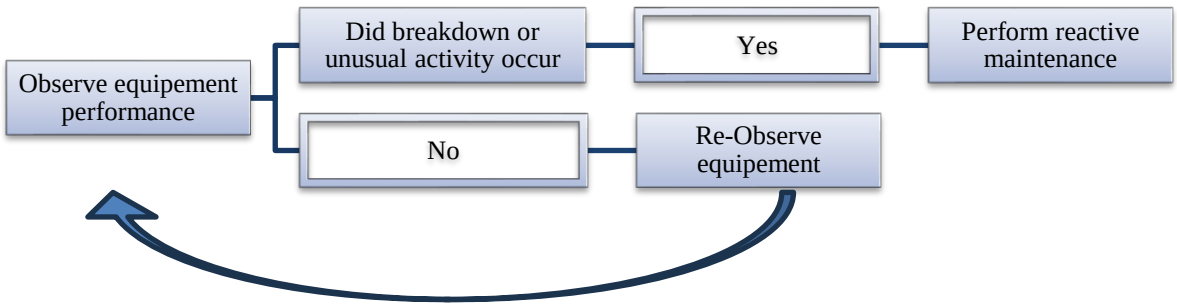

Figure 1: What is Reactive Maintenance used for?

2 Insights for I&M planning

This study presents a synthesis of research conducted by various researchers at University of Liège (ULiège), aimed at tackling challenges in I&M from diverse perspectives. Specifically, the study aims to support I&M planning by integrating multiple sources of information. By doing so, this enhances predictive maintenance capabilities, optimize resource allocation, and mitigate operational risks effectively. This approach not only refines maintenance strategies but also adapts these strategies to changing environmental conditions and operational requirements, ensuring the long-term structural integrity and performance of OWT foundations.

2.1 Fatigue Crack Interaction in Monopile Substructures

The challenges faced by OWT support structures due to combined cyclic loading from wind, waves, and currents, which lead to fatigue and corrosion have been investigated. Notably, research has delved into the interaction between fatigue cracks in monopile substructures has been investigated [3]. This advanced model aims to improve the accuracy and reliability of structural integrity assessments, thereby enhancing the overall reliability of OWT support structures.

2.2 Inter-dependencies among deteriorating components

The support structure can be considered as system composed by different structural components. Groups of these components are often under the same deterioration process. The submerged components, for instance, are subjected to corrosion and present similar degrees of thickness loss and pitting formation. Cyclic loads caused by wind and turbine's rotor expose all structural components to fatigue. Waves, in other hand, mainly affect the components close to the water level, contributing the fatigue damage with additional cyclic loads. The intensity variation of any mentioned deterioration processes affects all components related to it. These components are, thus, correlated by the same deterioration process. In other words, these components are correlated by the deterioration process or inter-dependent.

This part of the work addresses the feasibility and advantage of modelling the inter-dependencies among structural components for I&M planning. It explores inspection and maintenance actions to diverse components of the monopile structure, adding flexibility to the I&M strategies [4].

2.3 Neural Networks for Cyclic Load Estimation

Neural networks (NN) were also employed to estimate cyclic fatigue loads of structural components based on SCADA data, marks a notable advancement in structural health monitoring [5].

These methodologies offer adaptive policies in I&M planning, considering factors like deterioration models, failure criteria, and inspection method sensitivity. Moreover, Bayesian neural networks (BNN) enable stochastic modelling and uncertainty quantification, presenting an advantage in announcing model uncertainty for farm-wide monitoring. Looking forward, further enhancements in virtual monitoring, including improved data estimation and uncertainty measurement, promise to refine decision-making processes and optimize infrastructure maintenance practices for greater efficiency and reliability.

3 Conclusion & remarks

This study offers an insight study that presents a forward-thinking approach to ensuring the structural integrity and operational efficiency OWTs. Through detailed articles, the research provides advanced exploration into structural reliability modelling and integrated Inspection and Maintenance (I&M) planning, highlighting current challenges and proposing innovative approaches to improve the reliability and sustainability of OWT systems.

By identifying key areas for further research and development and leveraging advanced computational techniques such as neural networks and structural analysis, this study contributes to the optimization of I&M strategies and the resilience of engineering structures, paving the way for continued progress in offshore wind energy. The research offers a new approach to address challenges in infrastructure monitoring and maintenance. One of the key suggestions is to employ virtual monitoring to measure uncertainties better. This means trying different ways to estimate information and finding better ways to know if our data is accurate. Doing this can make virtual monitoring systems more dependable and precise, which is pivotal for keeping OWTs running smoothly.

Acknowledgements

The authors would like to acknowledge the financial support granted by the Belgian Energy Transition Fund (FPS Economy) through Phairywind (https://www.phairywind.be) and MAXWind. project.

References

[1] DNV. DNVGL-RP-C203 Fatigue design of offshore steel structures. (Recommended Practice). *Veritasveien 1, 1363 Hovik, Norway*, 2016.
[2] Hlaing, N. Data-driven Virtual Monitoring and Life-cycle Management of Offshore Wind Support Structures. *Doctoral thesis, University of Liege*, *Belgium* 2024.
[3] Jose Mishael, Pablo G. Morato, and Philippe RIGO. Numerical fatigue modelling and simulation of interacting surface cracks in offshore wind structural connections. *Marine Structures 92; 103472,* 2023
[4] Felipe Giro. Inspection and maintenance planning for offshore wind support structures: modelling reliability and inspection costs at the system level. *Proceedings of the ASME 2022 41st International* Conference on Ocean, Offshore and Arctic Engineering OMAE2022, Hamburg, Germany, 2022.
[5] Hlaing, N., Morato, P. G., de Nolasco Santos, F., Weijtjens, W., Devriendt, C., & Rigo, P. Farm-wide virtual load monitoring for offshore wind structures via Bayesian neural networks. Structural Health Monitoring. 2023.

Assessing the economic and environmental performance of onshore wind farms

Antonina Vukobrat, Samuel Kainz, Adrien Guilloré, Carlo L. Bottasso

Wind Energy Institute, Technical University of Munich, Boltzmannstr. 15,
85748 Garching bei München, Germany
E-mail: antonina.vukobrat@tum.de

Keywords: environment, cost, onshore wind

1. Introduction

The Paris Agreement set a global course for tackling climate change, yet the ambitious target of keeping temperature rise below 2°C is proving difficult due to the relentless increase in greenhouse gas (GHG) emissions from human activities, as emphasized by the Intergovernmental Panel on Climate Change [1]. Hence, it is essential to establish a metric quantifying the environmental impact on one hand and to identify the key sources of emissions on the other. The former led to the adoption of carbon footprint, while the energy sector has been ascertained as the main contributor to GHG emissions worldwide. The energy sector also holds the key to sustainability through expansion of renewable energy, particularly wind power. Being crucial in this transition, both onshore and offshore wind capacities are expected to increase [2].

Wind energy is not entirely climate neutral as emissions occur throughout each phase of its lifecycle. Therefore, this work includes the carbon footprint as a key parameter for assessing emissions relative to the electricity generated over the wind farm's lifetime. Moreover, adopting a holistic approach, the study integrates both the environmental and economic aspects of onshore wind farms, aiming to detect the drivers responsible for major emissions and costs. A computational model has been developed and applied to a real-life wind farm, with the objective of utilizing the insights from this analysis to guide the sustainable and economically viable design of future wind energy projects.

2. Methodology

The computational model is designed at TUM to determine both the economic and environmental cost of energy of wind energy systems. This coupled approach has been previously applied to onshore wind turbines [3] and offshore wind plants [4]. The current work expands this methodology to encompass the design of onshore wind farms. The economic cost is evaluated building upon the existing mass and cost models, while the climate change impact is estimated by employing the Life Cycle Assessment (LCA) method. Unlike previous LCA studies [5], this work considers every life cycle stage, resulting in an LCA model that evaluates the carbon footprint of an onshore wind farm as realistically as possible. The incorporated sub-models will be detailed in the following subsections and are illustrated in Figure 1.

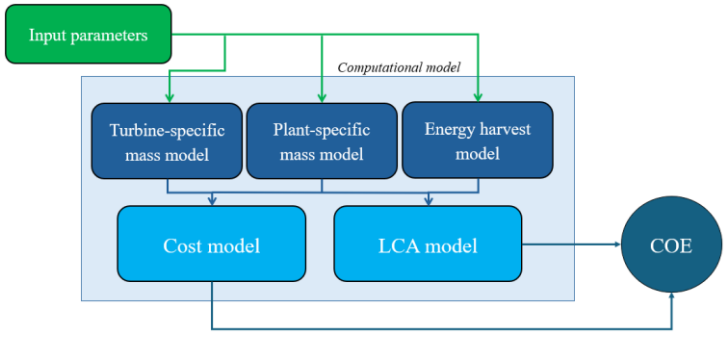

Figure 1: Toolchain framework for the economic and environmental cost assessment.

The first step in calculating cost of energy is the estimation of the mass bill. To achieve this, an open-source tool provided by National Renewable Energy Laboratory (NREL) is utilized for the turbine mass and cost model [6], while for the remaining wind farm components, the Land-based Balance of System Systems Engineering (LandBOSSE) framework is employed [7]. It includes mass and cost models for Balance of Plant (BoP) components as well as project-related costs.

The turbine-specific model comprises onshore wind turbine mass model and the foundation mass model. All components of the rotor nacelle assembly (RNA) and the wind turbine tower are sized according to [6], while the foundation is scaled based on the methodology described in [7]. Additionally, the corrosion protection is designed assuming both inner and outer surfaces of the tower are covered, and paint thickness determined in accordance with ISO 12944-5.

The plant-specific model determines layout of the wind farm, electrical infrastructure, and roads needed to access the site. An advanced approach considers site-specific, user-defined turbine positions and substation locations, allowing for realistic and detailed analysis beyond the basic rectangular layout. Array cabling is dimensioned using the data from XLPE land-based cable system datasheets [8]. Cables are selected for each section based on the predefined voltage level for array system and the cable type with smallest capacity with respect to the transferred rated power. The onshore substation is sized following the guidelines from [9]. Mass of the crushed stone for the construction of access roads is calculated [7].

The energy harvest model utilizes FLORIS [10] to evaluate the annual energy production (AEP) considering wake losses. Moreover, the calculation incorporates performance losses, availability of turbines, and power losses occurring in array cables and the main transformer [4].

Outputs from the previously described models are processed within the economic cost model, namely by evaluating labour, equipment, and material costs based on the mass and quantity of specific components. The model is built on the following pillars: turbine costs [6], balance of plant costs [7], project costs [7], and operational expenditures (OPEX) [11]. Capital expenditures (CAPEX) include the first three sub-models, representing one-time investment, while OPEX covers annual operational expenses. Additionally, escalation and conversion of incurred costs is implemented based on annual inflation rates [12], and exchange rates [13]. Finally, the economic cost of energy is computed as a function of total life cycle costs (*TLCC*), *AEP* and capital recovery factor (*CRF*):

$$COE_{€} = \frac{TLCC \cdot CRF}{AEP}$$

The Life Cycle Assessment (LCA) model has been developed to calculate the environmental cost of energy COE_{CO2}. This automated tool adheres to standardized methodologies from ISO 14040 and ISO 14044 to quantify the climate change impact associated with electricity generated by an onshore wind farm. It evaluates the global warming potential (GWP) over 100 years using the IPCC 2021 life cycle impact assessment method. Activities and processes from the *ecoinvent* database v3.9 are employed to model the life cycle of all wind farm components from cradle to grave, with their selection based on the material breakdown of component masses. Furthermore, the circular footprint formula [14] has been implemented to distribute environmental burdens and benefits between primary and secondary product system, accounting for differences in material quality and various end-of-life (EoL) scenarios.

Emission factors related to the extraction of virgin materials and the manufacturing of components are taken from the *ecoinvent* database. Transport to the wind plant site is modelled assuming transport distances from [15] and emission factors from *ecoinvent* associated with different means of transport. The total time of crane operation required for the installation of wind turbines determined within the cost model is utilized further to calculate emissions linked to this life cycle stage. Moreover, cranes are assumed to be used for maintenance and the installation of new components. In both cases, the emissions are computed by multiplying the number of hours of crane operation and the representative emission factor taken from *ecoinvent*. In addition to crane operation, the impact of O&M stage includes emissions related to regular inspection, lubricant replacement, and repair & replacement of failed components. The average replacement rates are assumed due to the lack of more detailed dataset and spare parts are modelled from cradle to grave. Decommissioning of wind farm components and their transport to the designated regional recycling or disposal plant is considered as the reversed installation. Components replaced within the last five years of operation are resold, attributing only 20 % of emissions to the primary user. Other components are recycled with the recycling rates suggested by [15]. The remaining components are either incinerated or landfilled, following the guidelines from [15]. Lastly, COE_{CO2} expressed in $kgCO_2eq/MWh$ is calculated as a function of the total life cycle emissions (*TLCE*), *AEP*, and design lifetime *Y*:

$$COE_{CO2} = \frac{TLCE}{AEP \cdot Y}$$

3. Results and discussion

The King Plains wind farm located in Oklahoma, USA is selected as case study to evaluate both its economic cost and carbon footprint. With a total capacity of 248 MW, the wind plant consists of 88 GE 2.8-MW wind turbines. The main parameters characterizing this case study are listed in Table 1.

Table 1: Main characteristics of the case study.

Parameter	Value	Parameter	Value
Rated power	2.82 MW	Nominal discount rate	5.37 %
Number of turbines	88	Inflation rate	2.5 %
Rotor diameter	127 m	Array voltage	30 kV
Hub height	89 m	Export voltage	60 kV
Turbulence intensity	18.04 %	Array frequency	60 Hz
Wind shear exponent	0.0898	Assumed lifetime	25 years

Calculation of the economic cost yields a result of **57.5 €/MWh**. The estimated value aligns with the range reported in [16] and [17]. Figure 2 depicts the breakdown of $COE_€$. Turbine costs represent over half of the total expenditures for a wind plant, followed by operation and maintenance costs, and balance-of-plant costs. This cost distribution generally aligns with the LCOE breakdown for onshore wind plants [16], although turbine costs are slightly higher in this analysis. The RNA accounts for more than 80% of the turbine costs, primarily due to extensive material use in blade manufacturing, and the presence of gearbox in the nacelle. Balance-of-plant is driven by key components such as electrical equipment, road construction, and turbine foundations. Wind farm layout design greatly affects these costs, suggesting that strategic optimization could reduce expenses. However, this study does not include grid connection or export cable costs, which would likely increase the share of electrical equipment costs.

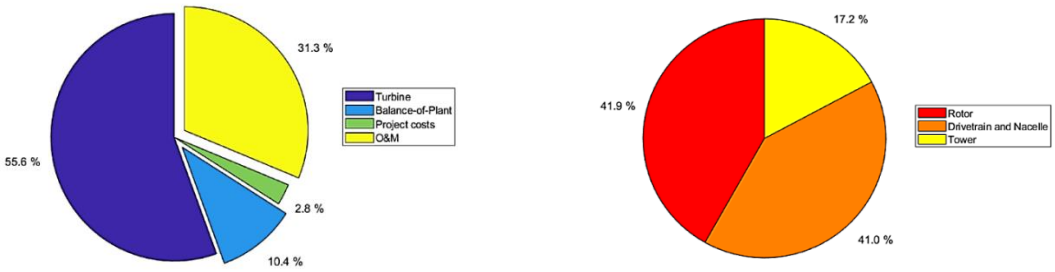

a) b)

Figure 2: Breakdown of economic cost a) total, and b) turbine.

Assessment of the carbon footprint for the presented case study resulted in an COE_{CO2} of **12.2 kgCO2eq/MWh**. This result is broken down by life cycle stage, components, and materials, which is illustrated in Figure 3. The production of wind farm components is a major contributor to the total carbon footprint, encompassing material extraction, transport to the factory, and manufacturing. On the other hand, recycling of components provides environmental credit at the end-of-life. The turbine is identified as the primary source of overall emissions, with more than 50 % attributed to the RNA and an additional 20 % to the tower, due to substantial material requirements. The foundation also significantly contributes to the climate change impact, mainly due to concrete and reinforced steel used for its construction. Steel is the most impactful material, essential for components within the RNA as well as in tower, foundation, and electrical equipment.

The results can be utilized further to reach desired trade-offs between costs and emissions, thereby informing decision makers during the wind farm design phase. Moreover, the holistic evaluation offers a better understanding of the entire life cycle of the wind plant, identifying key areas for performance improvement. Enhancements can be made by selecting more environmentally friendly materials, optimizing layout configurations, and extending the lifespan of critical components. Future work should incorporate other impact categories, such as land use or resource depletion, to enable complete assessment of the environmental friendliness of onshore wind farms.

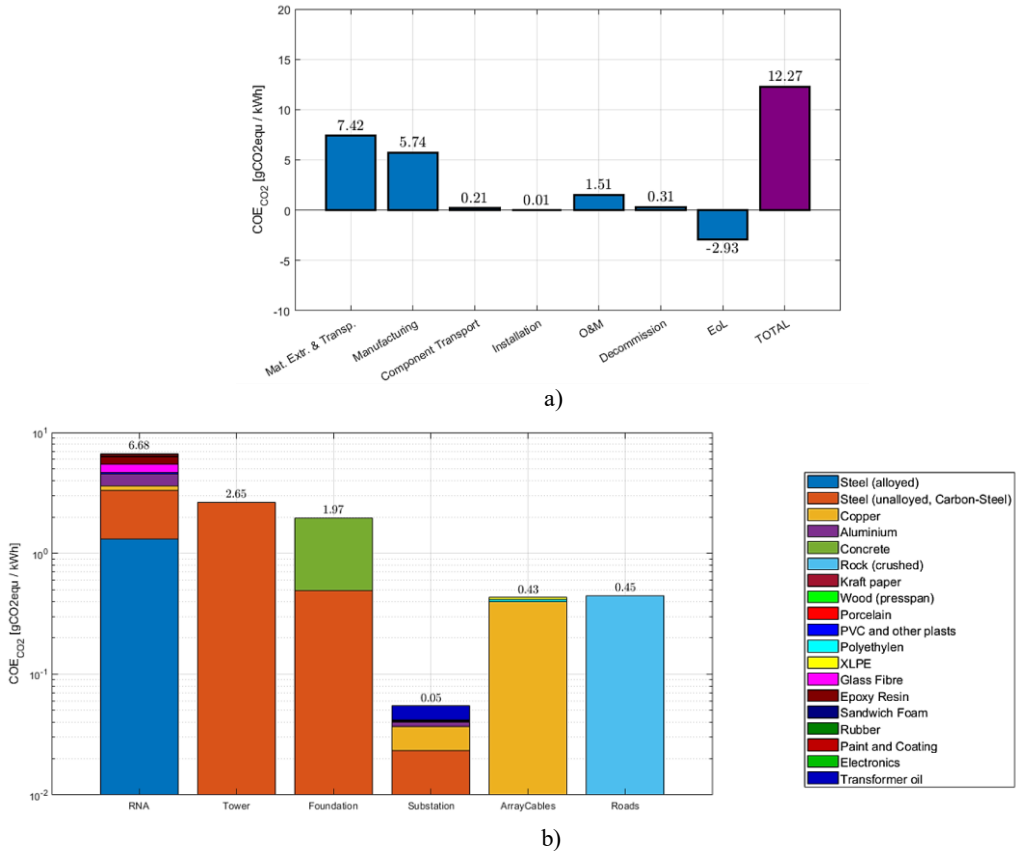

Figure 3: Breakdown of environmental cost a) by life cycle stage, and b) by components and materials.

References

[1] IPCC. Climate Change 2023 Synthesis Report: Summary for Policymakers. 2023.
[2] IEA Wind TCP. Annual Report 2021. Dec. 2022.
[3] H. Canet, A. Guilloré, and C. L. Bottasso. The eco-conscious wind turbine: design beyond purely economic metrics. *Wind Energy Science*, 8: 1029-1047, 2023.
[4] S. Kainz, A. Guilloré, C. L. Bottasso. How do technological choices affect the economic and environmental performance of offshore wind farms? *Journal of Physics: Conference Series*, 2024.
[5] M. Ozoemena, W. M. Cheung, and R. Hasan. Comparative LCA of technology improvement opportunities for a 1.5-MW wind turbine in the context of an onshore wind farm. *Clean Technologies and Environmental Policy*, 20:173–190, 2018.
[6] NREL. WISDEM: The Wind-Plant Integrated System Design and Engineering Model.
[7] A. Eberle, O. Roberts, A. Key, P. Bhaskar, and K. Dykes. NREL's Balance-of-System Cost Model for Land-Based Wind. 2019.
[8] ABB. XLPE Cable Systems: User's Guide.
[9] NREL National Wind Technology Centre. Offshore Renewable Balance-of-system Installation Tool (ORBIT). 2021.
[10] NREL. Flow Redirection and Induction in Steady State (FLORIS) tool.
[11] L. Fingersh, M. Hand, and A. Laxson. Wind Turbine Design Cost and Scaling Model. 2006.
[12] Statista. Projected annual inflation rate in the United States from 2010 to 2028. 2023.
[13] European Central Bank. Euro foreign exchange reference rates: US dollar (USD). 2023.
[14] M. A. Wolf, U. Hofstra, G.J. Vroege, A.D. Schryver, L. Zampori, and K. Wolf. Circular Footprint Formula. Webinar: Environmental Footprint (EF) transition phase. 2019
[15] S. Mali and P. Garrett. Life Cycle Assessment of Electricity Production from an onshore V136-4.2 MW Wind Plant. Mar. 2022.
[16] T. Stehly and P. Duffy. 2021 Cost of Wind Energy Review. Dec. 2022.
[17] C. Kost, S. Shammugam, V. Fluri, D. Peper, A. D. Memar, and T. Schlegl. Levelized Cost of Electricity - Renewable Energy Technologies. 2021.

TOPIC 6

Aero-elastic and blade technology

6.1 Session 122: Aero-elastic and blade technology

24.09.2024, 13:10, Room 2

Chair:

Ansh Patel

Presenters:

Varouxis Theodoros	An Assessment of Kolmogorov-Arnold Network (KAN) in Estimating Wind Turbine Blade Fatigue
Meckelnborg Simon	Methods for Simulation of Vortex-induced-Vibrations and for Site Specific Design of High Wind Turbine Towers
Shah Anik	Parameterizing low-frequency fatigue cycles to reconstruct lifetime fatigue in wind turbines

20th EAWE PhD Seminar on Wind Energy
24 - 26 September 2023
Visby, Sweden

An Assessment of Kolmogorov-Arnold Network (KAN) in Estimating Wind Turbine Blade Fatigue

Theodoros Varouxis [a], Vikram Pakrashi [b], Abdollah Malekjafarian [a]

[a] Structural Dynamics and Assessment Laboratory, School of Civil Engineering, University College Dublin, Dublin, Ireland
[b] UCD Centre for Mechanics, Dynamical Systems and Risk Laboratory, School of Mechanical and Materials Engineering, University College Dublin, Dublin, Ireland

E-mail: theodoros.varouxis@ucdconnect.ie

Abstract

Wind energy is steadily becoming a focus in reaching net zero CO2 emissions by 2050, as stated by the Paris agreement. Towards this goal wind farm installations, both onshore and offshore are needed. Performing Operations and Maintenance (O&M) can contribute up to 35% of the structure's total levelized cost per KWh produced. A substantial part of that is attributed to the wind turbine blade (WTB) related O&M . Estimating the remaining useful life of WTBs can mititgate the associated O&M costsIn the present study, a novel WTB fatigue estimation approach is presented. This approach is based on a Kolmogorov-Arnold network (KAN) trained on modelling the strain time-series of a simulated WTB, which can be leveraged in progressive fatigue damage modelling techniques. The strain time series is obtained from a simple Finite Element (FE) model of the 5MW NREL reference model WTB, leveraging the load modelling capabilities of the OpenFast framework. The aero-servo-elastic simulations in OpenFast are based on weather data obtained from a SCADA unit over the course of 15 years. The proposed methodology attempts to give probabilistic estimates for the fatigue accumulation in WTB using data available from a SCADA unit.

Keywords: Wind turbine blades, fatigue life estimation , Kolmogorov-Arnold networks

1 Introduction

EU targets and subsequent policies are aiming for an increase in total wind energy capacity until 2030, increasing the current capacity of 290GW to an expected to surpass value of 500GW [1]. This increase in capacity requires an equal increase in operating wind turbines (WT), with modern-larger structures being used. These structures offer geometrically higher energy yields, compared to the more mature-smaller structures. However, they create challenges due to their increased size and complexity; especially in the offshore setting. While incident frequency and severity do not change, downtime and repair costs drive the levelized cost per KWh up. It is of utmost importance to refine the current O&M procedures, mitigating the high O&M costs associated with fatigue-induced WTB incidents.

Damage mechanisms in WTB contain, but are not limited to, environmental wear, lightning strikes, fatigue accumulation, leading edge (LE) erosion and trailing edge (TE) cracks [2]. With current O&M procedures detecting and intervening for the aforementioned mechanisms is expensive, labour-intensive and sometimes

20th EAWE PhD Seminar on Wind Energy
24 - 26 September 2023
Visby, Sweden

ineffective. In addition, they normally do not include fatigue damage accumulation, which poses a big technical problem due to its uncertain nature [3]. As a result WTB are designed to be operated for 20-30 years, mostly founded on alleviating the incidence of catastrophic fatigue failure. However, under load and wind variability (turbulence and extreme weather cases), environmental conditions and operating time uncertainty can influence the useful life of WTB . This variability can be observed among two wind farms located in different areas as well as two WT from the same farm, prompting for a data-driven probabilistic approach for fatigue life estimation.

In recent years, fatigue life estimation using Neural Network (NN) based probabilistic models has gained attention. Deep-learning based approaches are popular as they may offer an alternative to the computationally expensive aero-servo-elastic simulations and the associated full-field flow simulations [4].Veloz Parra [5] proposed a novel methodology for fatigue life prediction of WTB under wind uncertainty. The proposed methodology contains deep neural network (DNN) surrogates integrated with Monte Carlo simulations. This integration highlights the robustness of the DNN surrogates in capturing the probabilistic nature of fatigue accumulation. Mylonas et al. [4] presented a novel surrogate modelling method leveraging a Conditional Variational Auto Encoder (CVAE) network. The CVAE is trained to map the probabilistic distribution of accumulated fatigue on a WTB root cross-section, under 10-min long loading intervals. The robustness of the CVAE in mapping the fatigue distribution is demonstrated from using unseen samples to validate. Ziane et al. [6] explored the performance of different optimizations algorithms - Backpropagation, Particle Swarm Optimization and Cuckoo Search [7] – in the use of NNs for fatigue life prediction of WTB materials under variable mechanical, thermal and hygrometric conditions. The Cuckoo Search optimization algorithm yielded the best results in terms of predictive accuracy and computational efficiency, highlighting the potential of these NN optimization algorithm as a fatigue life prediction tool.

While the use of NNs, especially deep-learning based approaches has yielded satisfactory results, there are two main challenges in which they need improvement, interpretability and plasticity. Interpretability refers to the model's ability to give other useful information, rather than just an output to the user's input and Plasticity refers to the model's ability to be altered after training without explicitly retraining it. Both of these attributes are desirable in the formulation of a surrogate model for the purposes of WTB fatigue life prediction, even more when the aero-servo-elastic simulations of a structure deteriorating in real-time is considered. A promising alternative to these mature networks are Kolmogorov-Arnold Networks (KANs), addressing the issues of interpretability and plasticity. KANs allow for models that can be updated with new data over time, leveraging the ability of spline functions to be adjusted locally. So, in this study ….?

2 Kolmogorov-Arnold Networks (KANs)

Fully connected feed-forward neural networks are inspired by the universal approximation theorem. In a similar fashion Liu et al. [8] leverage the Kolmogorov-Arnold representation theorem to formulate a new type of NN appropriately called Kolmogorov Arnold Networks (KAN). The approach considers if f is a multivariate continuous function defined on a bounded domain, then f can be expressed as the superposition of a finite amount of continuous univariate functions. For a continuous $f: [0,1]^n \rightarrow \mathrm{R}$ and continuous functions $\psi_i : [0,1]^n \rightarrow \mathrm{R}$ for $i = 1,2,..2n+1$

$$f(x_1, x_2, .., x_n) = \sum_{i=1}^{2n+1} \varphi_i \left(\sum_{j=1}^{n} \psi_{ij}(x_j) \right) \qquad \text{(Eq. 1)}$$

The use of Kolmogorov-Arnold representation in Machine Learning however dismissed received challenges. Even though approximating univariate functions using the superposition of univariate functions and the sum operation seems trivial, in practice these univariate functions can be non-smooth and even fractal. These attributes can yield them unlearnable in practice, rendering them "useless" [9].

20th EAWE PhD Seminar on Wind Energy
24 - 26 September 2023
Visby, Sweden

This obstacle can be overcome by formulating a NN based on explicitly parameterizing these univariate functions as a B-spline curve, with learnable coefficients of local B-spline basis functions [8]. This yields a 2-layer equivalent network. The original representation from Eq.1 corresponds to a 2-layer network with a $[n, 2n + 1,1]$ architecture. With this analogy, it is possible to generalize the network into an L-layer deep network. For a more detailed mathematical description and a detailed explanation of an L-layer deep KAN the reader is referred to [8]. To understand and assess such new approaches and their applicability, it is thus important to implement them for real applications. The wind energy sector is one such area where artificial intelligence has become popular but there is often a lack of performance comparison of different approaches.

3 Case study description

The focus of the present study is the fatigue life estimation of a WTB from the NREL 5MW offshore reference turbine [10]. The WTB geometry and composite layup have been simplified using Classic Lamination Theory [11]. Accumulated fatigue damage can be estimated from the turbine's historical data, leveraging the OpenFAST [12] modelling capabilities. Part of the OpenFAST workflow is the TurbSim tool [12]. The TurbSim stochastic inflow turbulence tool has been developed to provide a numerical simulation of a full-field flow that contains coherent turbulence structures. The full-field flow can then be inputted to OpenFAST, which in turn will result in the loading time series. BeamDyn, a time-domain structural-dynamics module for slender beam structures incorporated into the OpenFast workflow, is used to perform the analysis yielding the strain time series. Finally, the BECAS, BEam Cross-section Analysis Software is used to both discretise the blade into a set of 6X6 effective stiffness matrices, corresponding to the various cross-sections and post-process the strain time series into stress.

Considering the mean stress effect and the shifted Goodman relation [13], the cycles to failure N can be calculated from

$$N_{f,\sigma_\alpha,\sigma_\mu} = \left(\frac{\sigma_t + |\sigma_c| - 2\sigma_\mu - \sigma_c + |\sigma_c|}{2\sigma_\alpha}\right)^m \qquad \text{(Eq. 2)}$$

with σ_c the ultimate tensile strength, σ_t the ultimate compressive strength, σ_μ the mean stress of the loading cycle using the mean stress effect and m, the Wöhler exponent. This relation is applied to the material level for each of the composite layers, using the mean stress.

4 Fatigue estimation using KANs

Considering the full-field wind as an input to the proposed KAN with the desired output being the strain time series, the network will be trained so that it models the relationship between the full-field wind and the corresponding strain time-series. The necessary depth is going to be selected by experimenting with various numbers of hidden layers, aiming for accuracy and reduced computational complexity. KANs require fewer parameters than regular NNs, however, they are more computationally expensive per parameter [8]. Different configurations are tested, focusing on a good balance between learning complex relationships and avoiding over-parameterization. Networks with layer widths of 10, 20, and 50 are considered for training, along with varying depths. To ensure efficient and stable training, we evaluated several optimizers, including stochastic gradient descent (SGD), and the Adam optimizer. Additionally, fine-tuning will be performed for the learning rate and other hyperparameters through cross-validation to refine the model's performance on our validation set. This iterative process of adjusting the depth, width, and optimizer settings is crucial in developing a robust and accurate neural network model tailored to model the complex relationships of the case study. Comparison with other NNs will be presented to assess the performance of KAN.

20th EAWE PhD Seminar on Wind Energy
24 - 26 September 2023
Visby, Sweden

5 Discussion

Kolmogorov Arnold Network (KAN) presents promises in machine learning due to their unique structure and functionality. Unlike traditional NNs with fixed activation functions at the nodes, KANs employ learnable activation functions along the edges, allowing for the optimization of both compositional structure and univariate functions. This may enhance efficiency and accuracy, in complex tasks. However, KAN has also come under challenges in terms of its usefulness for complex, real-life data and this paper addresses the ability of KAN to estimate fatigue in wind turbine blades as compared to traditional neural networks (NNs). The comparison will provide an evidence base for the ability of KAN to be useful in the wind energy sector, while also identifying potential limitations. This comparison will be presented during the PhD seminar, as the relevant results are not yet ready to be included.

Commented [AM1]: You need to mention somewhere that the results are still not ready to be included in this paper, but will be presented at the seminar.

Commented [TV2R1]: I was trying to hint that. I am using future and present tenses, rather than past. Should I be explicitly stating as much?

Commented [AM3R1]: Yes, you should be explicit.

6 Acknowledgements

The research conducted in this publication was funded by Science Foundation Ireland and co-funding partners under grant number 21/SPP/3756 through the NexSys Strategic Partnership Programme. Vikram Pakrashi would also like to acknowledge Sustainable Energy Authority of Ireland funded RemoteWind RDD/613 TwinFarm RDD/604 , SFI MaREI RC2302_2.

References

[1] WindEurope, "Wind energy in Europe: 2023 Statistics and the outlook for 2024-2030," WindEurope, Brussels, Feb. 2024. [Online]. Available: https://windeurope.org/intelligence-platform/reports/
[2] L. Mishnaevsky, "Root Causes and Mechanisms of Failure of Wind Turbine Blades: Overview," *Materials*, vol. 15, no. 9, p. 2959, Apr. 2022, doi: 10.3390/ma15092959.
[3] K. L. Reifsnider, *Fatigue of composite materials*. Elsevier, 2012.
[4] C. Mylonas, I. Abdallah, and E. Chatzi, "Conditional variational autoencoders for probabilistic wind turbine blade fatigue estimation using Supervisory, Control, and Data Acquisition data," *Wind Energy*, vol. 24, no. 10, pp. 1122–1139, 2021.
[5] W. J. Veloz Parra, "Probabilistic approach for fatigue life estimation of wind turbine blades using deep neural network," 2020.
[6] K. Ziane, A. Ilinca, S. S. Karganroudi, and M. Dimitrova, "Neural network optimization algorithms to predict wind turbine blade fatigue life under variable hygrothermal conditions," *Eng*, vol. 2, no. 3, pp. 278–295, 2021.
[7] N. M. Nawi, A. Khan, and M. Rehman, "CSBPRNN: a new hybridization technique using cuckoo search to train back propagation recurrent neural network," presented at the Proceedings of the First International Conference on Advanced Data and Information Engineering (DaEng-2013), Springer, 2014, pp. 111–118.
[8] Z. Liu *et al.*, "Kan: Kolmogorov-arnold networks," *arXiv preprint arXiv:2404.19756*, 2024.
[9] F. Girosi and T. Poggio, "Representation properties of networks: Kolmogorov's theorem is irrelevant," *Neural Computation*, vol. 1, no. 4, pp. 465–469, 1989.
[10] Jonkman, Jason M., "Definition of a 5-MW reference wind turbine for offshore system development," National Renewable Energy Lab.(NREL), Golden, CO (United States), 2009.
[11] Y.-C. Ng, "Deriving composite lamina properties from laminate properties using classical lamination theory and failure criteria," *Journal of composite materials*, vol. 39, no. 14, pp. 1295–1306, 2005.

[12] OpenFAST, "OpenFAST." [Online]. Available: https://github.com/OpenFAST
[13] R. P. L. Nijssen, "Fatigue life prediction and strength degradation of wind turbine rotor blade composites," *Contractor Report SAND2006-7810P, Sandia National Laboratories, Albuquerque, NM*, 2006.

Methods for Simulation of Vortex-induced-Vibrations and for Site Specific Design of High Wind Turbine Towers

Simon Meckelnborg*[1], Joachim Peinke[1], and Michael Hölling[1]

[1]Institut für Physik [Oldenburg] – Germany

Abstract

To tackle the problem of climate change, the demand for renewable energies is increasing. As
a result, wind turbines are getting bigger in order to produce more energy. This leads to decreasing stiffness of components of a wind turbines and thus to increased risk of aeroelastic instability. One of which is vortex-induced vibrations (ViV) at the tower, which can lead to a
critical upswing by a resonance between the towers natural frequency and cyclically shedding,
transient vortex streets in the wake.

Since circular shapes play an important role in many areas, there has been a remarkable research effort in the last century to understand the effects that occur more precisely (2). However, the focus of these studies differs significantly from the objectives of this project. On the one hand, the range of Reynolds numbers, based on the diameter, investigated is well below 1e5, whereas wind turbine towers are exposed to ranges well above 1e6. Secondly, most of the studies do not cover the parameter space of vibrating cylinders.
Some studies report difficulties in identifying, recording and describing the resulting vibrations
(2),(1) and (3), which underlines the complexity of the problem and makes it clear that descrip-
tion in general is a major challenge.

As part of the MeTuSA project new methodology is to be developed to simulate these vortex-
induced vibrations. For this purpose, a semi-empirical method is developed that enables the integration of tower vibrations in transient load simulations. A semi-empirical model will be improved, calibrated and validated with the help of simulations and measurements and then used in conjunction with findings from detailed flow physics analyses to develop countermeasures.

This study contributes to this project by wind tunnel experiments which creates a database for

*Speaker

the modelling and to validate the simulations. The experiments are carried out in a wind tunnel
with an 3 m x 3 m outlet and a 30 m long test section. An active grid for the individual modulation of the inflow is used to investigate simplified tower models in various flow situations such as turbulence intensities and shear.

During the investigations, the flow around the tower models is measured in both static and dynamic cases. For the dynamic measurements, a setup will be designed that allows the models to be set into movements that are comparable in frequency and amplitude to real oscillations occurring in the field. The pressure distribution on the surface of the tower models is measured,so that it can be compared with simulations. Particle-Image-Velocimetry and hot-wire anemometry is used to measure the flow in the wake of the models.

The experimental setup and measurement parameters will be presented at the conference. It
will be explained why certain parameters are chosen and where the difficulties lie in realising them.

References

(1) P.Bearman. Vortex shedding form oscillating bluff bodies. Annual Review of Fluid Mechanics, 16:195 – 222,
1984.
(2) T.Sarpkaya. A critical review of the intrinsic nature of vortex induced vibrations. Journal of Fluids and
Structures, 19:389 – 447, 2004.
(3) X.Wu, F.Ge, and Y.Hong. A review of recent studies on vortex-induced vibrations of long slender cylinders.
Journal of Fluids and Structures, 28:292 – 308, 2012.

Parameterizing low-frequency fatigue cycles to reconstruct lifetime fatigue in wind turbines

Anik H. Shah[a], Andreas Vad[a], Adrien Guilloré[a], Carlo L. Bottasso[a]

[a] Wind Energy Institute, Technical University of Munich, Garching, Germany
E-mail: anik.shah@tum.de

Keywords: low cycle fatigue, wind turbines, remaining useful lifetime

1. Introduction

While modern wind turbines (WTs) have longer lifetimes, the older WTs in Europe have an operating lifetime of 15-25 years. In 2023, 9% of the installed onshore WT capacity in Europe was more than 20 years old. This share would increase to 13% by 2030 [1]. The entire wind industry in Europe faces the challenge of making an informed decision on maintenance of their aging assets, lifetime extension, or decommissioning of the existing assets and repowering the site with modern WTs. Remaining useful lifetime (RUL) of WTs becomes the driving force for such decisions. It can be evaluated through a combination of inflow reconstruction and aeroelastic simulations for original design wind class and site-specific environmental and operating conditions [2]. These simulations are generally carried out for 10-minute periods. The resulting load time series at critical positions are analysed by applying the rainflow counting (RFC) method and the Palmgren-Miner rule on the resulting load spectrum [3]. While this method determines the fatigue accumulated and damage equivalent loads (DELs) corresponding to cycles within the 10-minute interval, cycles that exceed the 10-minute duration are cut-off. Since these low-frequency cycles (i.e. during wind speed variations, change in operating modes) often exhibit high stress ranges, they are also the most damaging cycles. Therefore, they need to be considered for RUL prediction. In this study, a preliminary step is taken to parameterize the low frequency load cycles as a function of 10-min environmental and operating conditions so that they can be incorporated in the standard methods for RUL calculation.

2. Methodology

Typically, the 10-minute load time series for all inflow and operating conditions (bins) are cycle-counted separately. Cycle-counting a 10-minute subset results in full cycles and half cycles. Based on the standard approach of Simple Rainflow Counting (SRFC), the damage due to both these cycles is accumulated by weighting. The total damage accumulated is calculated statistically from the overall load spectrum. However, if all load time series were to be concatenated and then cycle-counted, not only would some of the residuals or half cycles finish and create more damage, but also new cycles would emerge representing the "slow" dynamics of wind speed variations and transitions in operating modes. These additional cycles due to Residual Rainflow Counting (RRFC) are highlighted by new green full cycles in Figure 1.

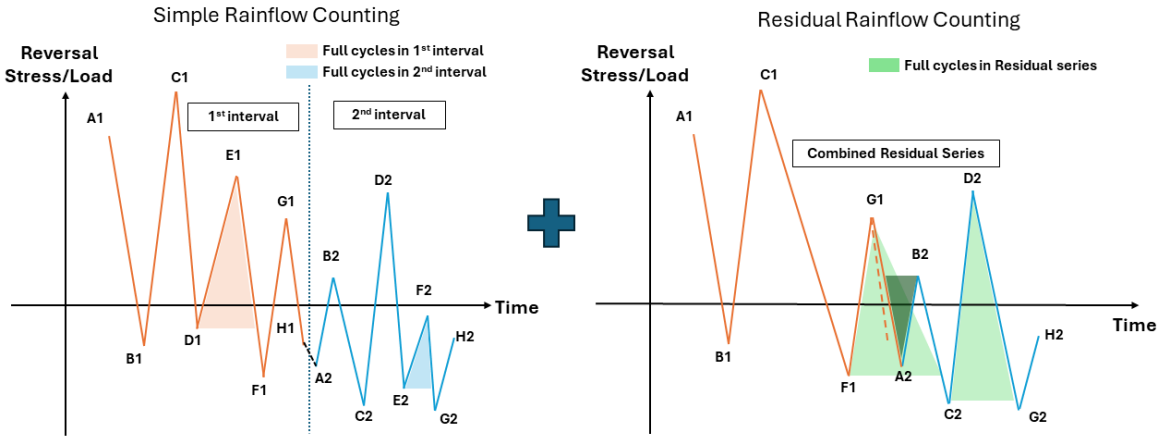

Figure 1 - Additional cycles captured with Residual Rainflow Counting

Amzallag et al. standardized the RFC method that allows successive time periods to be processed, considering cycles that last beyond the individual time periods while maintaining the efficiency of the 10-min approach and the accuracy of the concatenation approach. This method is validated in [4] [5] and summarized in Figure 2.

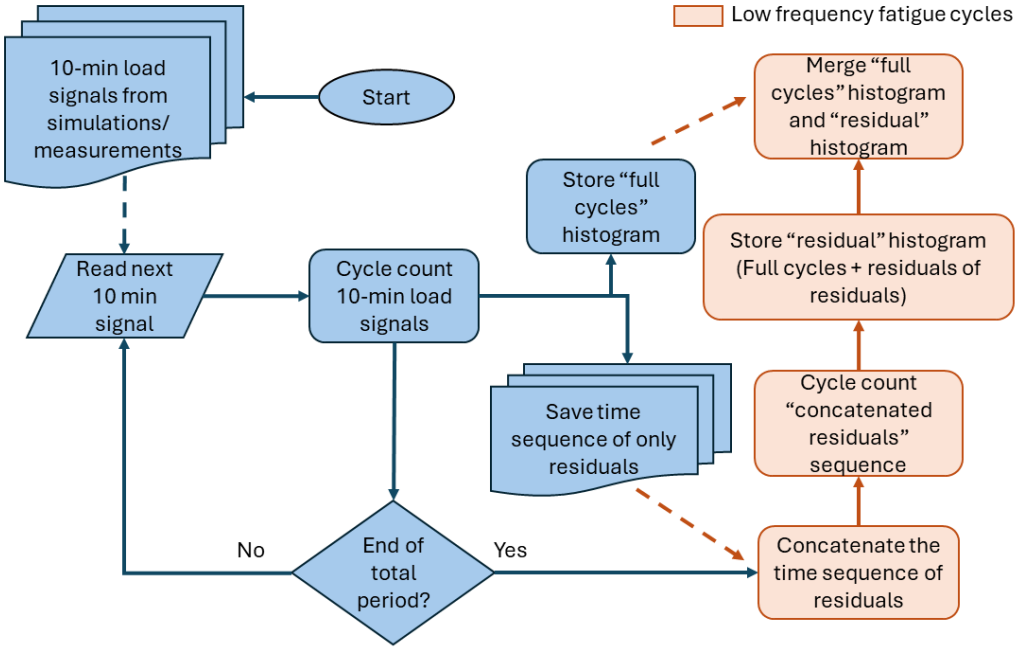

Figure 2 - Framework to account for low-frequency fatigue cycles

Damage ratio can be used to highlight the added damage contribution of low-frequency fatigue cycles (LFFC). It is defined based on the Palmgren-Miner rule as follows:

$$D_{ratio} = \frac{D_{RRFC}}{D_{SRFC}} = \frac{\sum_{i=1}^{N_{RRFC}} n_i \cdot (\Delta\sigma)_i^{\,m}}{\sum_{i=1}^{N_{SRFC}} n_i \cdot (\Delta\sigma)_i^{\,m}}$$

where, m is the Wöhler exponent, n is the fraction of the no. of cycles for the load/stress range $\Delta\sigma$, and N is the total no. of load/stress ranges in the load spectrum. Damage equivalent loads are used as proxy for the damage accumulated within the 10-min period from the load signal. There are studies carried out to map these 10-min DELs to WT-specific inflow and operating conditions using a surrogate [7] [8]. However, to the author's knowledge, there has not been an attempt to map the WT-specific inflow and operating conditions to a proxy for the additional damage due to the 10-min residuals. In this study, as a "step 0", these low-frequency fatigue cycles are parameterized so that they can be later estimated as a function of inflow and operating conditions through surrogate modelling.

After cycle counting a sample 10-min load signal, the residual sequence is shown in Figure 3. It is hypothesized that majority of the new cycles would come by concatenating the maximum and minimum load residuals within each period and the rest of the intermediate residuals would account for the stochastic contribution to the low-frequency fatigue damage (LFFD). Hence, three parameters are identified to describe the residual sequence within a 10-min period –

i. Maximum load residue
ii. Minimum load residue
iii. Number of residual points

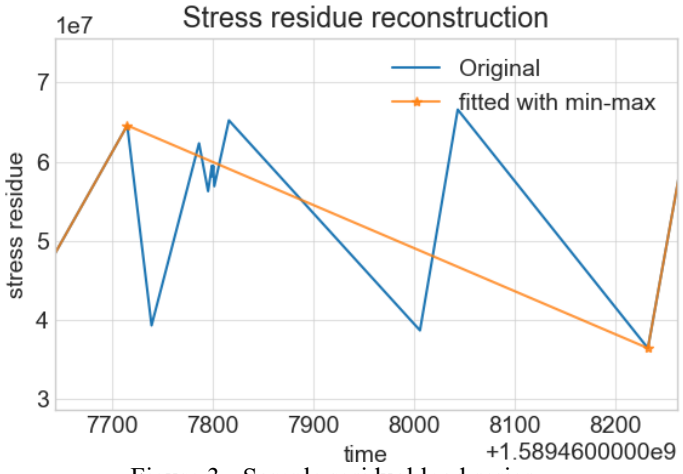

Figure 3 - Sample residual load series

Based on these parameters, two methods to approximate the residual sequence are analysed – "Min-Max" and "Uniform" distribution. The "Min-Max" method approximates the residual sequence in a 10-min interval with just two values – minimum and maximum load residues. The "Uniform" method uses the min-max load residues as bounds and samples the no. of residual points obtained in that period between these bounds while enforcing the sampling of min-max values. Damage ratios are calculated to evaluate the fraction of LFFD approximated by these methods in comparison to the exact residual sequence and to the standard approach of SRFC without LFFD.

3. Initial Results

Almost 12 months of tower base load measurements and met-mast data are used from a WT at an onshore site in Germany. It is filtered for free-stream and normal power production conditions. As a proxy to surrogate modelling, 10-min wind speed (WS) and turbulence intensity (TI) bins are obtained from the met-mast data. Residuals after rainflow counting the measurement load signals are combined for each instance of the wind condition (WS, TI) bin. This mimics the stochasticity of variable seeds from aeroelastic simulations. The three parameters – min & max load residues, along with the no. of residual points are obtained for each of these bins. Fig. 4 shows a clear dependency of the min-max load residues on the WS (x-axis) and TI (color-coded). Both values increase with an increase in WS until rated wind conditions (~11 m/s) and then decrease in region 3 but the gap increases between them. For WS below rated conditions, there is more spread in maximum values due to TI whereas for near-rated conditions, the minimum value is more sensitive to the TI. These indicate complicated but physical correlations and could be estimated with surrogate modelling. No clear trend is observed in the no. of residuals with (WS, TI) bins and hence, an average value over the measurement intervals n=8 is used.

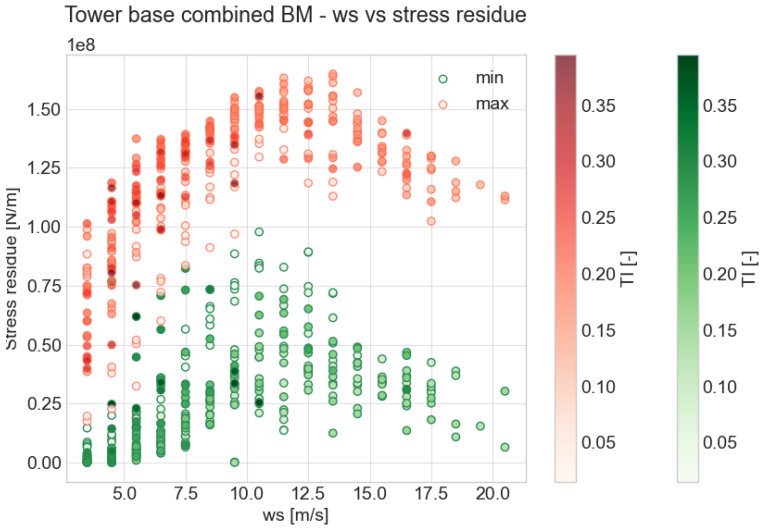

Figure 4 - Influence of inflow conditions on Min-Max load residuals

Table. 2 shows the damage ratios for the two methods of residue reconstruction. Additionally, the last column highlights the increase in damage with these residual counting methods in comparison to the standard approach without any LFFC.

Case	Damage ratio (m=5) $(D_{approx\ RRFC}/D_{exact\ RRFC})$	Damage ratio (m=5) (D_{RRFC}/D_{SRFC})
Exact	1.0	1.49
Min-max	0.95	1.41
Uniform	1.01	1.50

4. Conclusions & Outlook

Low frequency fatigue cycles increase the damage at tower base by 49% for a wöhler exponent m=5. These low frequency fatigue cycles could be parameterized by surrogates as a function of 10-min environmental and operating conditions. Approximating the load residuals with simple values such as the min-max residues already incorporates 95% of the LFFD. This is further improved by incorporating the stochasticity of the intermediate residual using uniform distribution. Further investigation would include accounting for transitions between operating conditions and sensitivity analysis of the parameters for other load channels.

Acknowledgements

This work is funded by the German Federal Ministry for Economic Affairs and Climate Action within the Life-Odometer Project (FKZ: 03EE3037B).

References

[1] WindEurope (2022): Wind energy in Europe: 2023 Statistics and the outlook for 2024-2030 | WindEurope. Available online at https://windeurope.org/intelligence-platform/product/wind-energy-in-europe-2023-statistics-and-the-outlook-for-2024-2030/#overview

[2] Ziegler, Lisa; Gonzalez, Elena; Rubert, Tim; Smolka, Ursula; Melero, Julio J. (2018): Lifetime extension of onshore wind turbines: A review covering Germany, Spain, Denmark, and the UK. In *Renewable and Sustainable Energy Reviews* 82, pp. 1261–1271. DOI: 10.1016/j.rser.2017.09.100.

[3] DKE/K 383 Windenergieanlagen. 2019. *Wind energy generation systems – Part 1: Design requirements (IEC 61400-1:2019); German version EN IEC 61400-1:2019.*

[4] Amzallag, C., Gerey, J., Robert, J., and Bahuaud, J. 1994. Standardization of the rainflow counting method for fatigue analysis. *International Journal of Fatigue* 16, 4, 287-293.

[5] Marsh, G., Wignall, C., Thies, P. R., Barltrop, N., Incecik, A., Venugopal, V., and Johanning, L. 2016. Review and application of Rainflow residue processing techniques for accurate fatigue damage estimation. *International Journal of Fatigue* 82, 757–765

[6] Sadeghi, N., Robbelein, K., D'Antuono, P., Noppe, N., Weijtjens, W., and Devriendt, C. 2022. Fatigue damage calculation of offshore wind turbines' long-term data considering the low frequency fatigue dynamics. *J. Phys.: Conf. Ser.* 2265, 3, 32063

[7] Guilloré, A., Campagnolo, F., and Bottasso, C L. (2024): A control-oriented load surrogate model based on sector-averaged inflow quantities: capturing damage for unwaked, waked, wake-steering and curtailed wind turbines, *J. Phys.: Conf. Ser*. 2767 032019, DOI 10.1088/1742-6596/2767/3/032019

[8] Dimitrov, Nikolay; Kelly, Mark C.; Vignaroli, Andrea; Berg, Jacob (2018): From wind to loads: wind turbine site-specific load estimation with surrogate models trained on high-fidelity load databases. In *Wind Energ. Sci.* 3 (2), pp. 767–790. DOI: 10.5194/wes-3-767-2018.

6.2 Session 213: Aero-elastic and blade technology

25.09.2024, 13:0, Room 3

Chair:

Vasco Batista

Presenters:

Ribnitzky Daniel	Advancements on the Hybrid-Lambda blade design and control methodology
Cespedes Moreno Juan Felipe	Impact on loads and AEP from lift correction models in wind turbine roots with thick airfoils
Wiegant Evert	Verification of coupling OpenFAST to a GPU-resident LES solver with actuator line model
Popi George	Morphing wind turbine blades for turbulence absorption: a preliminary study
Noroozi Marjan	Enhanced characterization and modeling of structural damping in Wind Turbine Blade Composites

20th EAWE PhD Seminar on Wind Energy
24-26 September 2024
Visby, Sweden

Advancements on the Hybrid-Lambda blade design and control methodology

Daniel Ribnitzky[a,b], **Vlaho Petrović**[a,b], and **Martin Kühn**[a,b]

[a]Carl von Ossietzky Universität Oldenburg, Institute of Physics
[b]ForWind - Center for Wind Energy Research, Küpkersweg 70, 26129 Oldenburg, Germany

E-mail: daniel.ribnitzky@uol.de

Keywords: Low specific rating, low-wind turbine, blade design, systems engineering

1 Introduction

The large scale exploitation of offshore wind energy will play a crucial role in the transition to a renewable energy supply but it will come along with certain challenges. Wind energy is a fluctuating source and the power feed-in growths with the wind speed to the power of three. This leads to a lack of power feed-in in light winds and to an oversupply during strong winds. Countries with a high share of wind energy already suffer from very low (or even negative) market prices during strong wind periods while the market price is still high in light winds when conventional wind turbines don't produce much power [5]. This is often named self-cannibalization of wind energy [3] since the effect is self-amplifying with the increasing share of wind energy in the total energy system. The ongoing trend of upscaling the turbines to larger rated power will not solve the problem. Future wind turbine designs should focus on increasing the power feed-in in light winds, while the rated power could be partially reduced in strong winds in order to reduce extreme and fatigue loads on the turbine [7]. This could facilitate light weight and cost effective designs and increase the turbine lifetime. A second problem to be mentioned is the increasing clustering of available offshore areas with wind farms. Cluster wake effects are most prominent below rated wind speed and can reduce the wind speed up to 50 km behind a wind farm [9]. This effect is rarely considered in the single turbine design process. The design of tremendously large turbines that capture more energy in light winds will require load limiting techniques below rated wind speed. This can go hand in hand with blade design methodologies and control strategies that reduce the wake effects by operating at reduced thrust coefficients [8]. There is a need for a change of mindset when designing future wind turbines moving away from an optimization on a single turbine level with the sole objective of reducing the levelized cost of energy. In contrast, future designs should incorporate the demands in the energy system as a whole and they should consider the large scale construction of wind turbines in closely spaced offshore wind farms.
The specific rating of a wind turbine describes the ratio of rated power to rotor swept area. Several studies have shown that low-specific-rating rotor concepts can help to counter balance the self-cannibalization effect [1], [10]. These turbines feature a larger rotor diameter compared to their rated power and capture more energy in light winds. The rated power is not increased as it is commonly done for the ongoing upscaling trends which leads to a reduced load level and further load limiting techniques help to foster a light weight and cost effective rotor design.

In this contribution, we will present how low-specific-rating rotor concepts can overcome the aforementioned challenges. We introduce the Hybrid-Lambda Rotor design methodology and we show how the design methodology was refined starting with a 15 MW offshore wind turbine and advancing to a 22 MW offshore wind turbine.

2 The Hybrid-Lambda Rotor - a 15 MW offshore wind turbine

In this section, we explain the Hybrid-Lambda Rotor concept on the basis of a 15 MW offshore wind turbine with a diameter of 326 m, as described in [7]. Limiting the loads of very long blades to a certain value (even below

rated wind speed) is a widely discussed topic. Usually this is done by pitching the blades to feather once a certain load level is reached which comes along with severe losses in the aerodynamic efficiency and thus a reduced power output. This is often referred to as peak shaving. Madsen et al. [4] and Ribnitzky et al. [7] pointed out that peak shaving can be optimized if not only the pitch angle is increased but simultaneously the operational tip speed ratio (TSR) is reduced. Like this, the loads can be limited to the same value but the power output is higher compared to the conventional peak shaving. Since a reduction in operational TSR in the peak-shaving region is beneficial, it makes sense to account for that already in the blade design process. This idea is integrated in the Hybrid-Lambda Rotor concept.

This concept features a blade design for two operational TSRs. The outer part of the blade (e.g. outer 30% of the blade length) is designed for a high TSR of 11 and a reduced axial induction (see Fig. 1a). In light winds, the rotor is operated at the high TSR and the outer part of the rotor is operating in its design conditions. The inner part of the rotor is designed for a lower TSR of 9 and a higher axial induction. As the wind speed increases and the limiting loads are reached, the operational TSR is reduced and the pitch is increased (see Fig. 1c). Like this, the inner part operates in it's design conditions in stronger wind speeds. In contrast, the loading on the outer part is now relived as it is operated at a lower TSR than the design TSR and the axial induction is even further reduced due to the increased pitch. This leads to a higher power output in the peak-shaving region as can be seen in Fig. 1b. Here, we compare the Hybrid-Lambda Rotor (solid red) to the IEA 15 MW reference turbine (blue) which both constrain the same maximum loads. The larger diameter of the Hybrid-Lambda Rotor (326 m vs. 240 m for the reference turbine) enables 1.8 times the power output in light winds (around 7 m s^{-1}). The green dashed line represents an upscaled version of the reference turbine with the same diameter as the Hybrid-Lambda Rotor and the loads are limited to the same maximum value by means of conventional peak shaving. Here, the advantages of the Hybrid-Lambda Rotor becomes clear as the power losses are less pronounced.

Paulsen et al. [6] investigated the Hybrid-Lambda Rotor on a wind farm level using meso-scale weather research models. They showed that the benefits in a wind farm application even outperform those of the single turbine due to the reduced wake losses. In certain atmospheric conditions, the power output is twice as big compared to a wind farm equipped with IEA 15 MW reference turbines. Over the course of a representative year, the annual energy production is increased by 15% with the use of Hybrid-Lambda turbines.

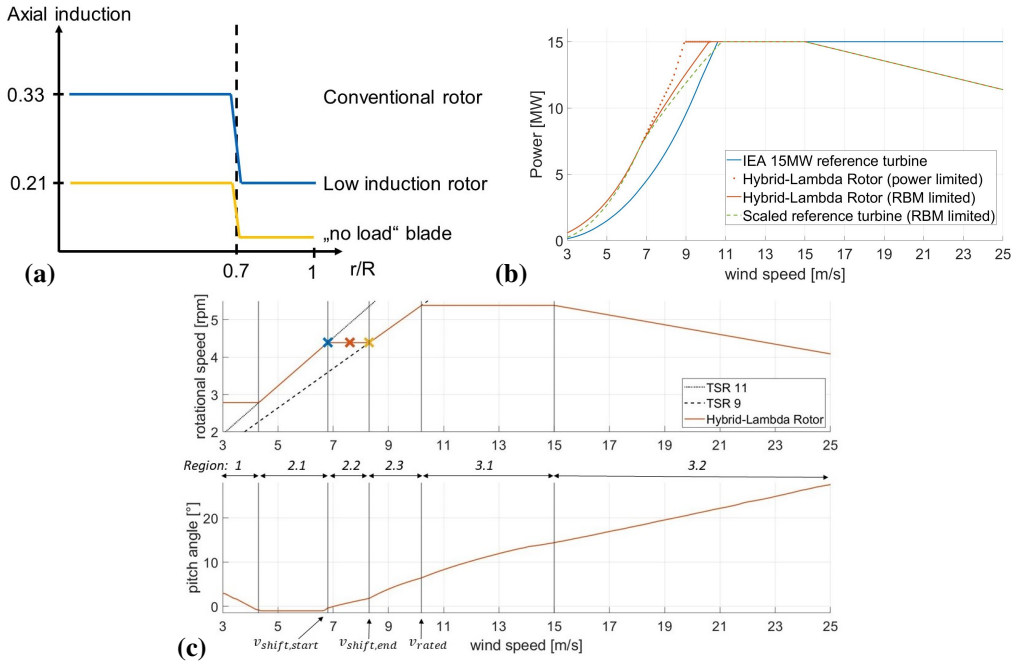

Figure 1: a: Desired axial induction along the blade span for the operating modes in light wind (blue) and strong wind (yellow). b: Power output from BEM simulations. c: Rotational speed and pitch schedule over wind speed.

3 Advancements to the 22 MW Hybrid-Lambda Rotor

One of the objectives of the initial Hybrid-Lambda design methodology was to separate the aerodynamic effects on the outer and the inner part of the rotor as best as possible. This involved a step-like distribution of axial induction along the blade span. Subsequently, the authors investigated to what extend the assumption of independent blade elements in the BEM theory is violated, using free-vortex wake (FVW) simulations [8].

A revised version of the Hybrid-Lambda design methodology was therefore applied to a 22 MW offshore wind turbine with a diameter of 374 m. The updates on the methodology feature a smoother transition of the design TSR along the blade span, as can be seen in Fig. 2a. Further, the desired axial induction distribution is adopted from Jamieson [2] (see Fig. 2b) who analytically derived an optimal axial induction distribution for the design problem of enlarging the rotor diameter while maintaining the same load constraints. Further, the difference between the light wind and strong wind design TSR was increased with a design TSR of 12 for the outer part of the blade. Like this, the outer part of the blade features an extremely slender design (Fig. 2c) and the wind speed range for the transition from the light wind to the strong wind mode is broadened thus opening up new opportunities for the control strategies. When deriving the control strategy, we applied a new optimization framework which simultaneously optimizes the pitch angle and the TSR in order to maximize the power coefficient while constraining the flapwise root bending moment (RBM). Results are displayed in Fig. 3. The optimal control schedule does not follow the strong wind TSR of 9 for wind speeds greater than 10 m s^{-1}. Higher power coefficients are found by reducing the TSR even further until rated power is reached. Figure 3 compares the power curve of the 22 MW Hybrid-Lambda turbine (red) with reference turbines which all share the same maximum RBM. Compared to the standard IEA 22 MW reference turbine with a diameter of 284 m (blue), the power output is greatly enlarged for low wind speeds. We introduce a second comparison which is a scaled version of the IEA 22 MW turbine (black) with the same diameter (374 m) as the Hybrid-Lambda turbine and further constraining the same loads. Here, we once applied the prescribed TSR schedule (black dotted), similar to as in Fig. 1 and once used the control optimization framework (black dashed). Advancements of the control optimization can be seen close to rated wind speed. The comparison further shows how important a compromise finding is when designing a blade for the application of peak shaving. The scaled reference blade (black) was not optimized for peak shaving and shows advantages in the wind speed range below 7 m s^{-1} where the loads are below the limit. Above the aforementioned wind speed, the loads need to be constrained and here the Hybrid-Lambda turbine (red) outperforms the scaled reference turbine, since it was optimized for the application of peak shaving.

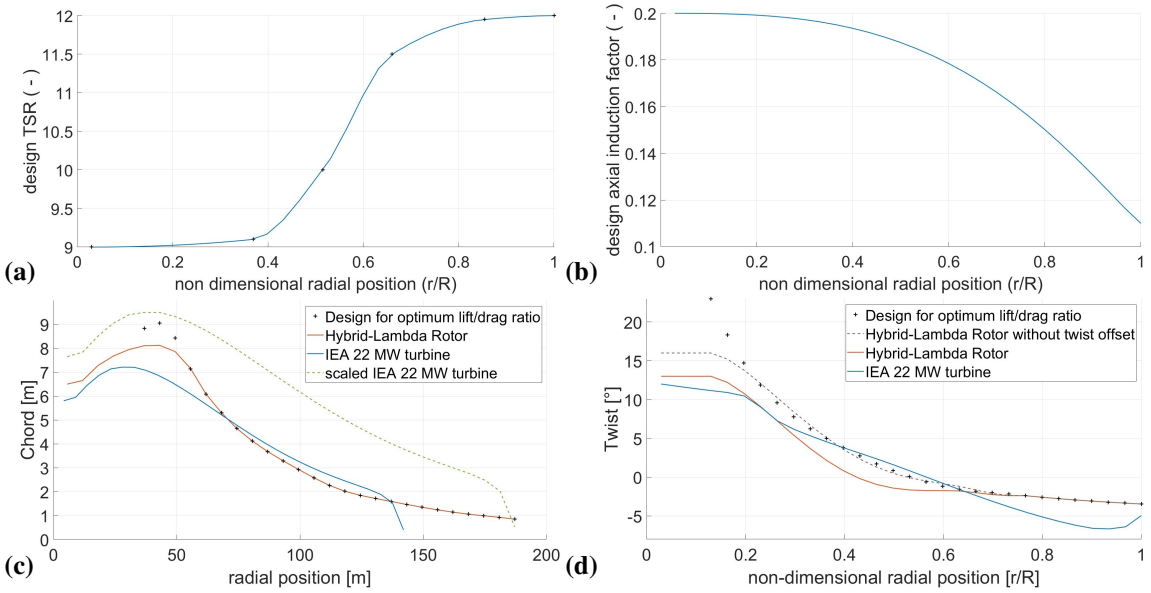

Figure 2: a: Design TSR distribution over blade length. b: Design axial induction. c: Chord distribution. d: Twist distribution

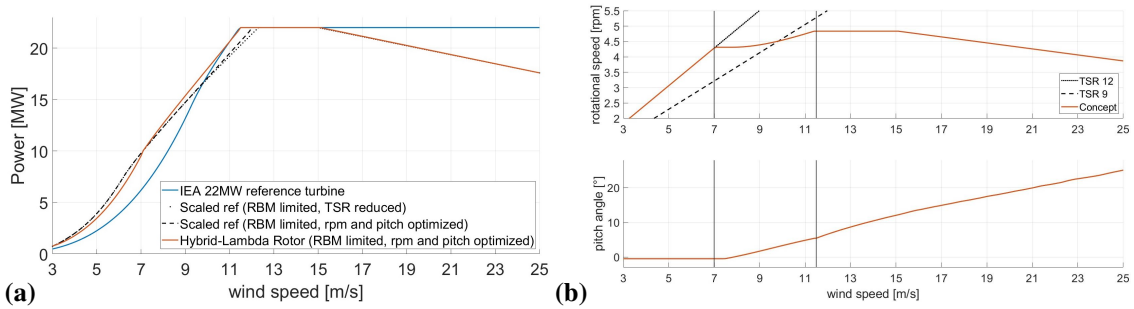

Figure 3: a: Power curve. b: Control schedule, rotational speed and pitch over wind speed.

4 Conclusion and outlook

In this paper, we showed how low-specific-rating turbines can help to overcome the self-cannibalization of wind energy. We further summarized our work on a new blade design methodology. This enables the design of tremendously long blades while still constraining the loads to the same level as a conventional turbine with the same rated power and a conventional specific rating. Advancements in the design and control methodology are shown on the basis of a new 22 MW Hybrid-Lambda turbine. In future work we will address an aero-servo-elastic coupled design process where the structural layup of the blade will be defined. Advanced techniques such as a panel-meta-model with the fibre orientation as a free design variable will allow for an optimization including the effect of bend-twist-coupling into to design methodology.

Acknowledgements

The work presented in this paper was funded by the Deutsche Forschungsgemeinschaft (DFG, German Research Foundation) – Project-ID 434502799 – SFB 1463.

References

[1] M. Bolinger, E. Lantz, R. Wiser, B. Hoen, J. Rand, and R. Hammond. Opportunities for and challenges to further reductions in the “specific power” rating of wind turbines installed in the united states. *Wind Engineering*, 45(2):351–368, 2021.

[2] P. Jamieson. Top-level rotor optimisations based on actuator disc theory. *Wind Energy Science*, 5(2):807–818, 2020.

[3] J. López Prol, K. W. Steininger, and D. Zilberman. The cannibalization effect of wind and solar in the california wholesale electricity market. *Energy Economics*, 85:104552, 2020.

[4] H. A. Madsen, F. Zahle, F. Meng, T. Barlas, F. Rasmussen, and R. T. Rudolf. Initial performance and load analysis of the lowwind turbine in comparison with a conventional turbine. *Journal of Physics: Conference Series*, 1618(3):032011, 2020.

[5] N. May, K. Heuhoff, and F. Borggrefe. Market incentives for system-friendly designs of wind turbines. *DIW Economic Bulletin No. 24/2015*, (24):313–321, 2015.

[6] J. Paulsen, M. Dörenkämper, and G. Steinfeld. Power production and large-scale wake effects of offshore wind turbines with low specific rating. *Journal of Physics: Conference Series*, 2767(9):092060, 2024.

[7] D. Ribnitzky, F. Berger, V. Petrović, and M. Kühn. Hybrid-lambda: a low-specific-rating rotor concept for offshore wind turbines. *Wind Energy Science*, 9(2):359–383, 2024.

[8] D. Ribnitzky, P. Bortolotti, E. Branlard, and M. Kühn. Rotor and wake aerodynamic analysis of the hybrid-lambda concept - an offshore low-specific-rating rotor concept. *Journal of Physics: Conference Series*, 2626(1):012008, 2023.

[9] J. Schneemann, A. Rott, M. Dörenkämper, G. Steinfeld, and M. Kühn. Cluster wakes impact on a far-distant offshore wind farm’s power. *Wind Energy Science*, 5(1):29–49, 2020.

[10] P. Swisher, J. P. Murcia Leon, J. Gea-Bermúdez, M. Koivisto, H. A. Madsen, and M. Münster. Competitiveness of a low specific power, low cut-out wind speed wind turbine in north and central europe towards 2050. *Applied Energy*, 306:118043, 2022.

20th EAWE PhD Seminar on Wind Energy
24-26 September 2024
Visby, Sweden

Impact on loads and AEP from lift correction models in wind turbine roots with thick airfoils

J F Céspedes[a], **C Bak**[a], and **F Zhale**[a]

[a]Department of Wind and Energy Systems, Technical University of Denmark, Frederiksborgvej 399, Roskilde, 4000, Denmark

E-mail: jfcm@dtu.dk

Keywords: Thick airfoils, Lift corrections, Engineering models, 3D effects, aeroelastic simulations.

The main difficulties of the flow in wind turbine root blades are that cross-sections are very thick, with relative thickness above 30%, and the existence of three-dimensional effects with centrifugal and Coriolis forces that create a strong radial flow [1, 2, 3]. Multiple authors have addressed these three-dimensional effects and several models have been developed to capture them [4, 5, 6, 7]. These models are suitable for aeroelastic codes and account for the 3D effects when calculating loads, tuning the controller, and estimating the Annual Energy Production (AEP).

However, traditional models of the 3D effects at the root are based on stall-delay context derived from non-thick airfoils (relative thickness below 30%). In a previous work, presented in Torque 2024 [8], it was shown with CFD computations that the lift coefficient prediction from traditional correction models is significantly worse with thick airfoils. As shown in Figure 1, the error significantly increases for thick sections in all operating conditions. This is a concern because the thickest airfoils constitute the most inner part of the blade.

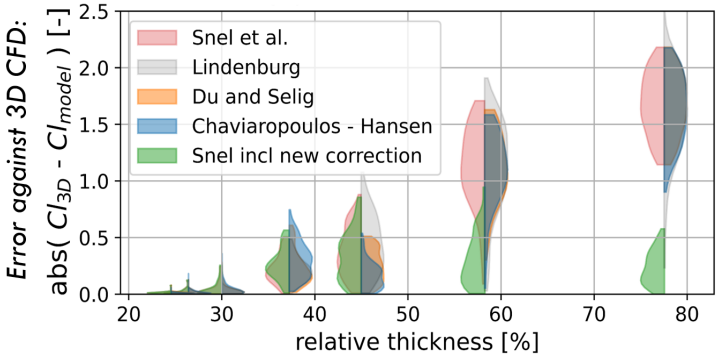

Figure 1: Error in the prediction of 3D lift from several correction models as a function of airfoil relative thickness. At each thickness, each distribution covers a wide range of operating conditions. Plot directly taken from [8]

In the same work [8], a simple extra correction was proposed to account for the increase in lift purely due to the thickness of the airfoil section, resulting in the green series in figure 1. So far this correction is not general, as it has only been tested for the turbine of the study, the DTU 10 MW reference wind turbine [9]. However, at least for this case, it shows a significant reduction in the error for lift prediction on sections with thickness beyond 40%, without disturbing predictions for non-thick airfoils.

The lift correction model has the following form [8]:

$$C_{l-3D} = C_{l-2D} + f(c/r, ...)\,\Delta C_l + g(th, c/r) \tag{1}$$

Where C_{l-3D} is the 3-dimensional lift, C_{l-2D} is the 2-dimensional lift that can come from 2D CFD calculations or wind tunnel experiments, $f(c/r, ...)$ is one of the traditional correction models, which can depend on several parameters, like c/r. Finally, $g(th, c/r)$ is the extra correction proposed to account for the thickness. Eq 2 shows that $g(th, c/r)$ is a logistic function that boosts C_{l-3D} as c/r and the relative thickness (th) increase. In this case, $g(th, c/r)$ was calibrated to minimize the error using $L = 3$, $k = 20$, and $th_0 = 0.5$.

$$g(th, c/r) = \frac{c}{r} \frac{L}{1 + e^{-k(th - th_0)}} \tag{2}$$

The green series in figure 1 shows how much better the three-dimensional lift predictions are when the thickness effects are included. However, it begs the question of how this impacts the loads and AEP prediction. For that reason, this work compares the aeroelastic simulations with no lift corrections at the root, with only the traditional corrections, and with the traditional corrections plus $g(th, c/r)$ to account for the thickness.

The aeroelastic simulations cover all operating wind speeds and, as all the terms in Eq 1 are calculated from a steady state, the first comparison is done without including turbulence. Further studies can be conducted to include turbulent cases and determine the trends of the fatigue loads.

These simulations were performed in HAWC2 [10], with the default parameters for the DTU 10 MW reference wind turbine. All cases have the same geometry, structural parameters, and controller. The only difference between the simulations is the file containing the aerodynamic coefficients of the different airfoil sections. These were modified to suit the three cases in question: no aerodynamic corrections at the root, only traditional lift correction, and traditional lift correction plus $g(th, c/r)$ to account for the thickness. In this case, the traditional correction used is the Snel model [4] due to its simplicity and wide use; furthermore, this is the default correction implemented in HAWC2. Note that only the lift coefficient is modified, the drag and aerodynamic moment coefficients are the same for all cases.

Preliminary results

As the correction increases the lift coefficient, the flapwise bending moment at the blade's root, shown in figure 2, is one of the loads that most clearly shows the differences between the cases. The discrepancies between the three cases are more pronounced after rated conditions, i.e. after 11 m/s, where the loads predicted with just the Snel correction are slightly lower than in the case of no root correction, with a difference lower than 2%. However, when comparing the case of the Snel correction with the Snel + thickness correction, the difference is greater, with the latter case being lower by 3 to 7%. It is also seen that before rated, the Snel + thickness correction is slightly higher than just the Snel correction, with a maximum difference of 1.5%.

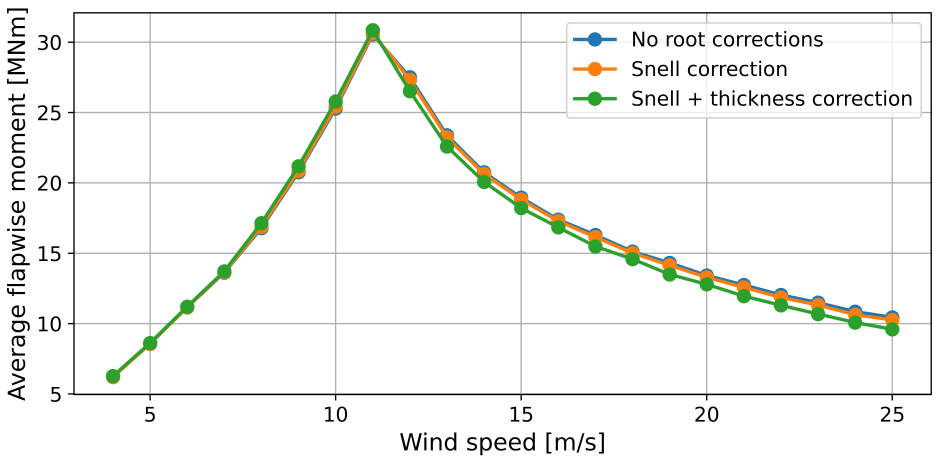

Figure 2: Average flapwise moment at the blade root as a function of wind speed for the computations without corrections at the root, with the Snel correction model, and with the Snel model plus the thickness corrections.

For the maximum load, encountered at rated conditions (11 m/s), the average value is higher by 0.3% if the thickness correction is included. However, suppose instead of the average at each wind speed, the maximum load in time is considered, which includes an overshot as the wind changes and the controller reacts. In that case, the load without the thickness correction is approximately 2.5% larger.

The annual energy production was calculated for the turbine in question which is class IA. According to the standard IEC 61400-1:2019 [11], this implies a Weibull distribution with shape parameter $k = 2$ and scale parameter of 10 m/s. The AEP results are presented in Table 1, they show that including the thickness correction increases the AEP estimate by 1.5%. This is because, before rated power if the thickness correction is included, a little bit more power can be extracted; which is consistent with a slightly higher root bending moment shown in figure 2 for wind speeds bellow 11 m/s.

However, these corrections only address the lift coefficient. If three-dimensional root effects of the drag are also included, likely, the drag would also increase and the AEP increase would be slightly lower.

Case	AEP [MWh]	Difference with respect to no correction	Difference with respect to just Snel correction
No correction	41354	-	-0.44%
Snel	41535	0.44%	-
Snel + thickness correction	42152	1.9%	1.5%

Table 1: Annual energy production comparison

Conclusions

Although further studies are required for the generalization of the thickness correction, for example, for different airfoil families, this study shows that it can be consequential in terms of loads and energy production prediction. Load differences between 3 and 7% are not negligible for the aeroelastic design and should be included. For the AEP, even small changes can have a big impact when scaled for an entire wind farm, which is why a difference in the order of 1% could be very significant. Overall, including three-dimensional corrections at the root could potentially improve the aerodynamic modeling of the blade, which could reduce the uncertainty in practical aspects such as applied loads and energy produced.

Acknowledgements

Ana M. Antunes for her insights in setting up and post-processing the aeroelastic simulations.

References

[1] M Caboni, K Boorsma and S Kanev 2018. Development of thick airfoils for outboard sections and investigation into their application for large rotors. *Wind Engineering* **42** 177-193. ISSN 0309-524X. doi 10.1177/0309524X17736480

[2] F Grasso 2020. Thick Sections.*Handbook of Wind Energy Aerodynamics* ed Bernhard Stoevesandt and Gerard Schepers and Peter Fuglsang and Sun Yuping, Springer International Publishing, chapter 11 pp 353-374

[3] A Muñoz, B Méndez and X Munduate 2016. Thick airfoil designs for the root of the 10MW INNWIND.EU wind turbine. *Journal of Physics: Conference Series* **753**. ISSN 1742-6588. doi 10.1088/1742-6596/753/2/022046

[4] H Snel, R Houwink, G J W van Bussel and A Bruining 1993. Sectional Prediction of 3-D Effects for Stalled Flow on Rotating Blades and Comparison with Measurements. *Wind Energy Conference*. Proceedings of the international conference held at Lubeck-Travemunde, Germany. pp 395-399.

[5] C Lindenburg 2004. Modeling of rotational augmentation based on engineering considerations and measurements. *European Wind Energy Conference*, London. ECN-RX–04-131

[6] Z Du and M Selig 1998. A 3-D stall-delay model for horizontal axis wind turbine performance prediction *ASME Wind Energy* Symposium held in Reston, Virginia. doi 10.2514/6.1998-21

[7] P K Chaviaropoulos and M O L Hansen 2000. Investigating Three-Dimensional and Rotational Effects on Wind Turbine Blades by Means of a Quasi-3D Navier-Stokes Solver. *Journal of Fluids Engineering* **122** 330-336. ISSN 0098-2202. doi 10.1115/1.483261

[8] J F Cespedes, C Bak and F Zhale 2024. Limitations of lift correction models for thick airfoils in wind turbine roots. *Journal of Physics: Conference Series 2767, Torque 2024*. Issue 2. ISSN 1742-6588. doi: 10.1088/1742-6596/2767/2/022029.

[9] C Bak, F Zhale, R Bitsche, T Kim, A Yde, Henriksen, M H Hansen, J P A A Blasques, M Gaunaa and A Natarajan 2013. The DTU 10-MW Reference Wind Turbine. *Danish Wind Power Research*. Conference held in Trinity, Fredericia, Denmark. Report-I-0092

[10] T J Larsen, A M Hansen and DTU Wind Energy HAWC2 Development Team 2019. How 2 HAWC2, the user's manual. *Risø National Laboratory - Technical University of Denmark*. Risø-R-1597(version 12.7)(EN)

[11] European Committee for Electrotechnical Standardization (CENELEC) 2019. DS/EN IEC 61200-1:2019.

20th EAWE PhD Seminar on Wind Energy
24-26 September 2024
Visby, Sweden

Verification of coupling OpenFAST to a GPU-resident LES solver with actuator line model

Evert Wiegant[a], **Delphine de Tavernier**[a], and **Axelle Viré**[a]

[a]Wind energy section, Faculty of Aerospace Engineering, TU Delft

E-mail: e.i.wiegant@tudelft.nl

Keywords: Floating offshore wind turbine, LES, ALM, OpenFAST, GPU

1 Research objective

The objective of this research is to perform a grid study and find the optimal setup, regarding accuracy and computational cost, for an atmospheric large eddy simulation (LES) solver coupled with a wind turbine engineering tool using ALM. We then demonstrate how the coupled model adds value to the simpler stand-alone engineering tool when applied to floating offshore wind turbines (FOWT).

2 Introduction

To be able to capture more of the wind resource, wind energy production is moving further offshore to increasingly deeper waters. The current bottom-fixed technology, widely used for offshore wind turbines, is reaching the limit of economic feasibility around 60m water depth. The use of floating platforms is an attractive alternative for deeper waters. However, when subject to aerodynamic (wind) and hydrodynamic (waves) forcings, while being allowed to move along 6 degrees of freedom, the FOWT is subject to an increased range of structural and aerodynamic loads [2, 15], larger variations in power production [7, 16], and reduced lifetime [1]. Power production and loads find their origin in processes that happen at the blades of the wind turbine. The forces acting on which are often expressed using coefficient that vary with angle of attack. We have observed that for moderate wave conditions, the angle of attack shows larger variations at the blades of a FOWT than it does for bottom-fixed turbines (figure 1). The underlying (unsteady) aerodynamic phenomena prevailing at the blades and rotor of the FOWT have been the topic of active research, yet consensus is not reached on the underlying phenomena and how to describe/model their effects [12, 4]. Both wind tunnel (e.g. [13]) and numerical models (e.g. [11, 3]) are addressed to study the aerodynamics of the FOWT. However, these studies often simplify platform motions (e.g. studying imposed

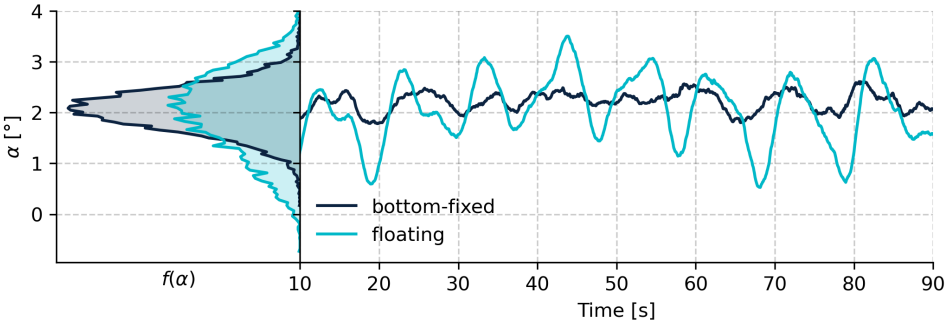

Figure 1: Angle of attack timeseries (after applying a 2s time filter) and distributions at $r/R = 0.8$ of bottom-fixed and FOWT blades. The wind speed at hub height is about 5m/s.

motions and/or only pitch and surge) or simplify the atmosphere (e.g. often limited to neutral stratification, or a predefined TI, wind speed, shear, etc).

With our study, we aim to understand unsteady aerodynamics at the blades of a FOWT in realistic environmental conditions, through numerical simulations that are both accurate enough to capture phenomena on the spatial and temporal scales of the FOWT, as well as fast enough to study a wide range of metocean conditions. We use the GPU-resident atmospheric large eddy simulation (LES) model GRASP (see section 3) to simulate the atmosphere, thus inflow to the wind turbine. Being a multi-scale problem, atmospheric modelling is generally done using global or mesoscale models, with LES filling the niche of simulating atmospheric phenomena up to the smallest scales. Yet, LES are scarcely used to simulate real weather (i.e. as it occurs at a specified location and time). GRASP is developed and used for exactly this purpose, which demonstrates the novelty of our method. We immerse into the LES a aero-elasto-servo-hydrodynamically coupled wind turbine representation, OpenFAST (see section 3), that we couple using the actuator line method (ALM) as implemented by Taschner et al. [14].

By establishing the coupled model, we are moving outside the calibration range of any of the models involved. Therefore, we must verify whether, or to what extent, our coupled setup accurately represents a wind turbine. The present study aims to do this by considering flow at the blades, which is where the models interface. We initially forego the FOWT and focus on a case well within the calibration of the stand-alone OpenFAST; a bottom-fixed wind turbine with uniform inflow. We expect this case to correctly represent wind turbine behaviour, such that we can verify our coupled setup against it. Doing so, we find how we can set up the model to yield accurate results for reasonable computational costs. We conclude with simulations of the FOWT, with which we demonstrate the added value of our coupled tool to the stand-alone OpenFAST.

3 Method

Our verification is of the GRASP-OpenFAST tool, coupled through the ALM. Each tool and the coupling method are briefly described in this section.

GRASP: Flow around the turbine is represented by GRASP. GRASP is a proprietary LES code owned and maintained by Whiffle, which is a company that specializes in high resolution weather simulations. It is based on DALES [5], of which a port to GPU code was created [10] which allowed for fast computations on relatively cheap computing hardware. It is has since been further developed within Whiffle and has seen applications in industry [9, 6], and in academia [14].

OpenFAST: The wind turbine is represented by OpenFAST, a code maintained by NREL (`https://github.com/OpenFAST`). It allows for representation of the elastic response of the wind turbine structure as it is subject to forcings from hydrodynamics, mooring lines, aerodynamics while modulated by its servo system, etc. Its modular framework allows for multiple ways of modelling any of these dynamics, or excluding them entirely.

Actuator line: The actuator line used in our study is the filtered ALM first described by [8] and implemented as described by [14].

Table 1: Model settings used in the verification study.

variable	values	units
Δx	4, 8, 16, 32	m
Δt	1, 0.5, 0.25	$\frac{\Delta x}{U_{rot}}$
ε	10, 15, 20, 30	m
	1, 2, 3, 4	Δx

Set-up: The simulated wind turbine is the IEA 15MW reference wind turbine. We discretize the blades using at least 300 nodes. This is the recommended number of blade nodes for use of the filtered actuator line.

Verification set-up: We fix the wind speed using an initial value of 8m/s and applying no pressure gradient across the domain. We apply no subgrid scheme to ensure the profile remains uniform. This is justified as lift is an inviscid phenomenon. The value of 8m/s is chosen because the turbine is designed to operate without pitch at this wind speed, plus-minus a few m/s.

In our verification against the stand-alone OpenFAST, we exclude most dynamics (e.g. stiff tower and blades, bottom-fixed, constant rotor speed and blade pitch). Since we only aim to verify induction of the ALM, we only consider aerodynamics and force on the generator. We generate 2 reference cases each using a different different aerodynamic modules, namely BEM (using blade element momentum theory) and OLAF (a free vortex wake method).

The spatial and temporal resolutions and ALM kernel width is evaluated in the verification study. The choice of values for these parameters are listed in table 1. Note that limits apply to each of parameters; the timestep (Δt) is limited such that the blade moves no more than $1\Delta x$ per timestep, for small ALM kernel width (around $\varepsilon \lesssim 1\Delta x$ or $\varepsilon \lesssim 2\Delta x$ depending on other settings) we observe oscillations in induction, which acts as a "soft" limit to small

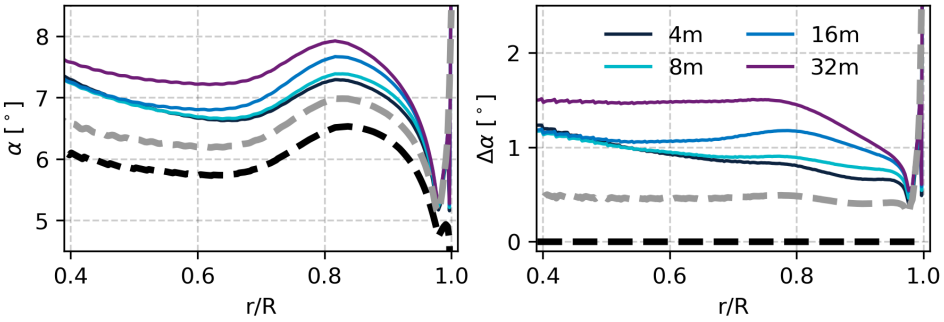

Figure 2: Angles of attack along the blade at different spatial resolutions. The coloured solid lines correspond to output of coupled simulations. The thick dashed lines indicate the references using BEM (black) and OLAF (grey). The left panel shows actual values, the right panel shows the difference to the BEM reference.

ε values, the grid cell size (Δx) determines computational cost to the largest extent and is limited by computational resource. The mesh is uniformly spaced.

Demonstration set-up: In our demonstration we simulate a FOWT, including (at least[1]) hydrodynamics and the 6 degrees of freedom (DOF) related to floater motions.

The demonstration case will use the spatial/temporal resolution and kernel width values we deem optimal from the verification study. We perform a parameter sweep of environmental conditions (wind and wave parameters[1]) and compare the coupled model to the BEM reference case.

4 Results

Resolution study & verification We compare the results from the coupled model, using different values of spatial and temporal resolutions and ALM kernel widths, to the standalone OpenFAST using both BEM and OLAF to describe aerodynamic forces.

We find that the power is overestimated for most cases, resulting from an underestimated induction. In addition, we find that when increasing resolution, the resulting power does not converge. Both are well-known problems for the ALM, hence the use of the filtered ALM (FALM), which partially alleviated the problem.

We have identified the following sensitivities: Increasing Δx increases generated power. Increasing Δt decreases generated power, yet also increases convergence. Increasing ε increases generated power.

Further insight is acquired when we dissect the power into its 2 main constituents at the blade; angle of attack (α) and relative velocity (V_{rel}). Due to fixing the rotor speed, the relatively velocity does not change (much). Any deviation in induction then translates to deviations in α. We therefore consider the best setting to be that which yields best agreement in α. Figure 2 shows α as it varies along the blade. Although the α agreement is best at 4m resolution, we may argue that the 8m resolution is a good trade-off between accuracy and runtime, since halving the resolution to 4m adds a factor 16 more runtime.

Demonstration of coupled simulations of a FOWT We demonstrate the added value of our model coupling by comparing its results to the BEM reference under varying environmental conditions. Turbine motions that are known to express unsteady aerodynamic behaviour (e.g. [12, 4, 13, 11, 3]), reveal the most interesting comparison between the coupled model and the reference.

5 Conclusions

By characterizing the sensitivities of the 2 models coupled through the ALM, as well as recognizing numerical limits, we have identified a set-up that we consider a good compromise between accuracy and computational cost.

The coupled model allows us to simulate FOWT behaviour in real weather conditions.

[1]The exact set-up is to be determined.

6 Acknowledgement

This research has received funding by the Dutch National Research Council (NWO) under the Talent Programme Vidi scheme (project number 19675).

References

[1] Assessment of failure rates and reliability of floating offshore wind turbines. *Reliability Engineering & System Safety*, 228:108777, 2022.

[2] A. AlShuwaykh and K. T. Sharman. Analysis of platform motions effect on the fatigue loads and aerodynamic unsteadiness in floating offshore wind turbines. In *Journal of Physics: Conference Series*, volume 1452, page 012030. IOP Publishing, 2020.

[3] J. Dong and A. Viré. Predicting the occurrence of the vortex ring state for floating offshore wind turbines. In *Journal of Physics: Conference Series*, volume 1618, page 052044. IOP Publishing, 2020.

[4] C. Ferreira, W. Yu, A. Sala, and A. Viré. Dynamic inflow model for a floating horizontal axis wind turbine in surge motion. *Wind Energy Science*, 7(2):469 – 485, 2022.

[5] T. Heus, C. Van Heerwaarden, H. J. Jonker, A. Pier Siebesma, S. Axelsen, K. Van Den Dries, O. Geoffroy, A. Moene, D. Pino, S. De Roode, et al. Formulation of the dutch atmospheric large-eddy simulation (dales) and overview of its applications. *Geoscientific Model Development*, 3(2):415–444, 2010.

[6] J. Kantharaju, R. Storey, A. Julian, F. Delaunay, and D. Michaud. Wind resource modelling of entire sites using large eddy simulation. In *Journal of Physics: Conference Series*, volume 2507, page 012015. IOP Publishing, 2023.

[7] C. Lienard, R. Boisard, and C. Daudin. Aerodynamic behavior of a floating offshore wind turbine. *AIAA Journal*, 58(9):3835–3847, 2020.

[8] L. A. Martínez-Tossas and C. Meneveau. Filtered lifting line theory and application to the actuator line model. *Journal of Fluid Mechanics*, 863:269–292, 2019.

[9] A. Oldroyd, H. Hussin, W. Pustjens, P. Rooijmans, E. Holtslag, L. Garcia, R. Verzijlbergh, and E. Wiegant. Wind resource assessment: Hollandse kust (noord) wind farm zone. Technical Report WOZ2180116, October 2019.

[10] J. Schalkwijk, E. J. Griffith, F. H. Post, and H. J. Jonker. High-performance simulations of turbulent clouds on a desktop pc: Exploiting the gpu. *Bulletin of the American Meteorological Society*, 93(3):307–314, 2012.

[11] C. W. Schulz, S. Netzband, U. Özinan, P. W. Cheng, and M. Abdel-Maksoud. Wind turbine rotors in surge motion: new insights into unsteady aerodynamics of floating offshore wind turbines (fowts) from experiments and simulations. *Wind Energy Science*, 9(3):665 – 695, 2024.

[12] T. Sebastian and M. Lackner. Characterization of the unsteady aerodynamics of offshore floating wind turbines. *Wind Energy*, 16(3):339–352, 2013.

[13] F. Taruffi, F. Miranda Novais, and A. Viré. An experimental study on the aerodynamic loads of a floating offshore wind turbine under imposed motions. *Wind Energy Science*, 9(2):343–358, 2024.

[14] E. Taschner, M. Folkersma, L. A Martínez-Tossas, R. Verzijlbergh, and J.-W. van Wingerden. A new coupling of a gpu-resident large-eddy simulation code with a multiphysics wind turbine simulation tool. *Wind Energy*, 2023.

[15] D. Ward, M. Collu, and J. Sumner. Reducing tower fatigue through blade back twist and active pitch-to-stall control strategy for a semi-submersible floating offshore wind turbine. *Energies*, 12(10):1897, 2019.

[16] B. Xu, T. Wang, Y. Yuan, and J. Cao. Unsteady aerodynamic analysis for offshore floating wind turbines under different wind conditions. *Philosophical Transactions of the Royal Society A: Mathematical, Physical and Engineering Sciences*, 373(2035):20140080, 2015.

Morphing wind turbine blades for turbulence absorption: a preliminary study

George Popi*[1], Delphine De Tavernier , and Dominic Von Terzi

[1]Delft University of Technology – Netherlands

Abstract

Background and motivation
The size of wind turbines has steadily increased in the last decades, with the largest operational wind turbine,
the Mingyang MySE 16.0-260, already reaching a rotor diameter of 260 m (12). It is generally believed that the
scale-up trend is maintained for future-generation turbines, as this would allow both access to the stronger wind
resources found at larger heights, as well as power extraction across larger actuator areas. In turn, this would
boost sustainable electricity generation, one of the main requirements to sustain the worldwide energy transition
according to the Paris Agreement (1).

One of the challenges related to using larger rotors is maximizing the power output under dynamic wind conditions.
During operation, the power generated by the rotor is dependent on multiple factors, such as the wind
shear and the turbulent structures that are locally present at the blades. It is expected that the impact of both will
increase for larger-diameter rotors for two reasons. On the one hand, the larger actuator surfaces will cover a larger
portion of the atmospheric boundary layer (ABL), thus increasing the wind shear encountered by the blades within
a revolution. On the other hand, the larger blade sizes could be exposed to more pronounced non-homogeneity
of the turbulent flow-field in the rotor plane. In turn, these stronger local variations would have a greater influence
over the performance of individual wind turbine sections than is the case for current, smaller-size rotors.
To counteract unwanted effects in power extraction, the state-of-the-art is to control the pitch angle of each wind
turbine blade individually. Nevertheless, this already does not offer enough freedom to mitigate the losses in performance
compared to the (static) conditions for which the wind turbine was designed. This can be proven by

*Speaker

analyzing the data of currently operating megawatt-turbines. For this, one can sample the power output of wind turbines at different average velocities computed over a measurement interval of 10 minutes. In doing so, it can be found that for the same average velocity, the extracted power may differ based on the specific instantaneous environmental conditions that existed during a particular measurement. Kim et al. (18) analyzed field data from a 2 MW individual-pitch controlled turbine located within an onshore wind farm, and found that the variation of the power output for 10-minute averaged measurements is dependent on the measured turbulent intensity (TI). To correspond to the design power of the wind turbine, it is desirable to neutralize the variation of the power with respect to the instantaneous local flow-field fluctuations at all wind speeds above the cut-in velocity.

Given that the state-of-the-art of individually pitching blades does not offer enough control over the flow for large future-generation wind turbines, a more localized solution is needed. In principle, one could simply resort to using pitch control for separate parts of each blade. However, the current pitching actuation systems need to produce large forces, which are attainable only for low actuation frequencies proportional to the first three harmonics of the rotational velocity of the blades (6). By contrast, given the broad turbulent spectrum of the atmosphere, to fully neutralize the unwanted instantaneous effects, an actuation frequency higher than 6 Hz would be needed (5). This is one order of magnitude larger than what is currently used in industry and carries a significant risk of pitch bearing failures for state-of-the-art technologies at such high actuation frequencies (6).

Given the negative effect of atmospheric turbulence, it is desirable to create dynamic aerodynamic control devices that have low inertia, high energy density, a small size, and low power consumption. Since wind turbines are often located in remote areas, it is desired that low maintainability of the solutions is also achieved. Based on these criteria, a possible solution is the use of morphing technologies. Such concepts had first been tested for the aviation industry, with twist-morphing already used for manoeuvring by the Wright Brothers more than a century ago (19). Moreover, high-lift devices, a simplistic example of wing morphing, are widely used for most modern aircraft.

Research question

Based on the environmental conditions, the state-of-the-art and the requirements formulated in the previous section, it was concluded that morphing technologies are a potential candidate for reducing the wind turbine power output variability caused by the unsteady inflow conditions at the rotor. Before presenting concrete solutions to this problem, it is desired to first analyze the work that has been previously done on morphing technologies, in particular for wind turbines. Thus, the question formulated for this study is:

What is the state-of-the-art of morphing technologies in the wind energy industry, and how does it relate to power optimization?

Literature review

Up to now, the current research mainly focused on studying trailing edge (TE) morphing configurations, given that this appears to be the most studied and most mature morphing technology to date. There have been numerous projects in the past which (partially) focused on using a morphing TE for smart control of wind turbines, most notably UpWind (15) and ADAPWING (10). This general preference can be attributed to the fact that changing the aerodynamic shape only in the vicinity of the TE of a given wind turbine blade has specific advantages. For one, it requires less actuation power compared to locally pitching the entire chord of the blade, thus being conducive to higher actuation frequencies. At the same time, the local lift generated by the rotor is highly sensitive to shape modifications close to the TE (21), further supporting the feasibility of this technology for actuation purposes.

The main aerodynamic function of previously used morphing TE technologies was to modify the camber of the blade (2). Based on the configuration morphed shape, two distinct types of TE morphing solutions are distinguished: flap and active trailing edge geometry (ATEG) (2). The former is similar to the high-lift device routinely used for airplanes, where the trailing portion of the wing is hinged rigidly. Although this is a relatively inexpensive approach, it can introduce a discontinuity in the camber of the wind turbine blade, which in turn acts as a source of aerodynamic instability and of unwanted acoustic emissions (6). On the other hand, these issues are mitigated by using the ATEG, where one can ensure that the camberline remains smooth during morphing. In the following, the two approaches are presented separately.

In studies related to flaps, a large body of the literature appears to be presenting controllers that are designed for load alleviation under normal and extreme conditions. Yu et al. (22) propose a proportional–integral–derivative (PID) approach, where the effect of the flap deformation is computed using XFOIL. This controller design is integrated into OpenFAST (17), an aeroservoelastic model, and improvements between 10% and 20% are obtained for both root bending moment and tip deflection under normal and extreme turbulence conditions when a flap over 20% of each blade is used. On the other hand, Cai et al. (13) used a much simpler strategy to minimize the unwanted effects of turbulent fluctuations, where the current flap angle is simply obtained as an average of the ones used in the previous second of operation. Further, the considered effects of the morphing are purely aerodynamic, where a free vortex wake model is used. It is shown that even this simple approach, if calibrated correctly and used

over 22% of the blade, can significantly reduce the transient variations of torque and thrust experienced by the
wind turbine. The utility of rigid flaps for load alleviation was also shown experimentally at TU Delft by Barlas
and van Wingerden (7), who proposed a feedback strategy which was shown to reduce the root bending moments
by up to 50% when using two separate flaps spanning a total of 23% of the blade. Flapped solutions were also
analyzed within a short-duration field test by Castaignet et al. (14) within short-duration field tests on a 225 KW
pitch-regulated wind turbine, where a single flap spanning 5% of the blade's length was used. When coupled with
a model predictive control (MPC) strategy, this setup is shown to reduce the 1P loads by 20%, despite its modest
size. Based on these numerical and experimental studies, it can be concluded that rigid flaps are feasible for the
load alleviation of wind turbines.

Solutions employing ATEG have also been extensively researched in the past, with different designs put forward
(2). In particular, the Wind Energy group at DTU has released a large number of studies, including both
numerical and experimental work, which proved the aerodynamic superiority over the rigid flaps configuration
(20), the benefits of using multiple small-sized independent flaps for each blade compared to a single larger one
(4), the strong unwanted impact of delays in the control system (4), as well as the feasibility of different potential
control strategies (11, 16, 3). Building on these results, aeroelastic (8) and aeroservoelastic (9) numerical results
have shown that a flap spanning the outer 20% of the blade can reduce the standard deviation of the root bending
moment by 15%-24%. Similar to what was also found for rigid flaps, these articles corroborate the capacity of
ATEG for load alleviation.

Conclusions

To maximize the operational power yield of wind turbines, designs need to accommodate for the effect of instantaneous
flow perturbations. Given the practical requirements to do so, for example low inertia and high frequency
actuation, morphing technologies represent a fitting candidate. In particular for this study, published TE morphing
studies were surveyed. Based on the available literature, all studies appear to have been focused on load alleviation.
Thus, no research appears to have been conducted with the main goal of using morphing technologies for
maximizing the power of large rotors subjected to the dynamic inflow that can be expected in real-life applications
for future-generation, large-rotor wind turbines. To fill this research gap, a detailed plan will be formulated in
preparation for the PhD Seminar. Based on the literature, another research question pertains to fundamental aerodynamic
phenomena associated with dynamically modifying the shape of the blade. From a design perspective,
these behaviours could potentially be leveraged to increase the performance of all morphing aerodynamic devices.

From a modelling point of view, their impact is not yet implemented in any of the low-fidelity numerical tools
expected to be used in the project's design phase. Consequently, to simplify future design procedures for morphing
technologies, it is desired that within this project unsteady aerodynamic phenomena are also studied. Finally, given
the early development stage of morphing technologies for wind turbines, it is also of interest that these unsteady
phenomena are contained within a low-fidelity numerical tool based on blade-element momentum (BEM) theory
or panel methods that can be used in the initial design stages of all future morphing solutions.

References

(1) Paris agreement to the united nations framework convention on climate change. T.I.A.S. No. 16-1104, dec
2015.
(2) M. Z. Akhter and F. K. Omar. Review of flow-control devices for wind-turbine performance enhancement.
Energies, 14(5):1268, 2021.
(3) P. B. Andersen, C. Bak, M. Gaunaa, and T. Buhl. Wind tunnel test of a closed loop controller for an airfoil
with trailing edge flaps. In TORQUE 2010, pages 127–134. European Wind Energy Association (EWEA),
2010.
(4) P. B. Andersen, M. Gaunaa, C. Bak, and T. Buhl. Load alleviation on wind turbine blades using variable
airfoil geometry. In Proceedings of the EWEC, 2006.
(5) T. Barlas and M. Lackner. Smart rotor blade technology applied to the upwind reference turbine. In Proceedings
of the IEA topical expert meeting on the application of smart structures for large wind turbine rotor
blades, Sandia National Labs, Alberquerque, USA, 2008.
(6) T. Barlas and G. van Kuik. Review of state of the art in smart rotor control research for wind turbines.
Progress in Aerospace Sciences, 46(1):1–27, 2010.
(7) T. Barlas, J.W. VanWingerden, A. Hulskamp, and G. Van Kuik. Closed-loop control wind tunnel tests on an
adaptive wind turbine blade for load reduction. In 46th AIAA aerospace sciences meeting and exhibit, page
1318, 2008.
(8) L. Bergami and N. K. Poulsen. A smart rotor configuration with linear quadratic control of adaptive trailing
edge flaps for active load alleviation. Wind Energy, 18(4):625–641, 2015.
(9) L. O. Bernhammer, G. A. van Kuik, and R. De Breuker. Fatigue and extreme load reduction of wind turbine
components using smart rotors. Journal ofWind Engineering and Industrial Aerodynamics, 154:84–95, 2016.
(10) T. Buhl, D. C. Bak, M. Gaunaa, and P. B. Andersen. Load alleviation through adaptive trailing edge control
surfaces: Adapwing overview. In 2007 European Wind Energy Conference and Exhibition, pages 20–23.
European Wind Energy Association (EWEA), 2007.
(11) T. Buhl, M. Gaunaa, and C. Bak. Potential Load Reduction Using Airfoils with Variable Trailing Edge
Geometry. Journal of Solar Energy Engineering, 127(4):503–516, 06 2005.
(12) A. Buljan. Mingyang commissions 16 mw offshore wind turbine with 260-metre rotor diameter in china,
July 2023. Accessed: 2024-06-06.

(13) X. Cai, Y. Wang, B. Xu, and J. Feng. Performance and effect of load mitigation of a trailing-edge flap in a
large-scale offshore wind turbine. Journal of Marine Science and Engineering, 8(2), 2020.
(14) D. Castaignet, T. Barlas, T. Buhl, N. Poulsen, J. Wedel-Heinen, N. Olesen, C. Bak, and T. Kim. Full-scale
test of trailing edge flaps on a vestas v27 wind turbine: active load reduction and system identification. Wind
Energy, 17(4):549–564, 2014.
(15) EWEA. UpWind-Design limits and solutions for very large turbines. EWEA, 2011.
(16) M. Gaunaa and P. B. Andersen. Load reduction using pressure difference on airfoil for control of trailing
edge flaps. In 2009 European Wind Energy Conference and Exhibition. EWEC, 2009.
(17) J. Jonkman. The new modularization framework for the fast wind turbine cae tool. In 51st AIAA Aerospace
Sciences Meeting including the new horizons forum and aerospace exposition, page 202, 2013.
(18) D. Y. Kim, Y. H. Kim, and B. S. Kim. Changes in wind turbine power characteristics and annual energy
production due to atmospheric stability, turbulence intensity, and wind shear. Energy, 214:119051, 2021.
(19) D. Li, S. Zhao, A. Da Ronch, J. Xiang, J. Drofelnik, Y. Li, L. Zhang, Y. Wu, M. Kintscher, H. P. Monner,
A. Rudenko, S. Guo, W. Yin, J. Kirn, S. Storm, and R. D. Breuker. A review of modelling and analysis of
morphing wings. Progress in Aerospace Sciences, 100:46–62, 2018.
(20) N. Troldborg. Computational study of the risø-b1-18 airfoil with a hinged flap providing variable trailing
edge geometry. Wind Engineering, 29(2):89–113, 2005.
(21) J. Vaningen. Transition, pressure gradient, suction, separation and stability theory. In AGARD Laminar-
Turbulent Transition 15 p (SEE N78-14316 05-34), 1977.
(22) W. Yu, M. M. Zhang, and J. Z. Xu. Effect of smart rotor control using a deformable trailing edge flap on load
reduction under normal and extreme turbulence. Energies, 5(9):3608–3626, 2012.

Session 213: Aero-elastic and blade technology
20th EAWE PhD Seminar on Wind Energy
24 - 26 September 2023
Visby, Sweden

Enhanced characterization and modeling of structural damping in Wind Turbine Blade Composites

Marjan Noroozi [a], Abbas Mehrad Kazemi Amiri[a], Euan Brough[a],

[a] CDT in Wind and Marine Energy Systems and Structures, Department of Electronic and Electrical Engineering, University of Strathclyde, Glasgow, UK

E-mail: abbas.kazemi-amiri@strath.ac.uk

Keywords: EMA, DMA, Damping, Vibration, Loss Factor, Composite Materials

1. Introduction

Tackling climate change and relying on secure energy supplies are two integral factors in making future decisions in the energy area that have attracted the attention of the governments. Wind power generation technology is mature enough with a low levelized cost of electricity, but more improvements are in progress. The levelized cost for onshore and offshore wind energy production is anticipated to be 0.02-0.03 $/kWh and 0.03-0.07 $/kWh, respectively, by 2050 [1]. The electricity generation can be adversely affected by the vibration of the blades. Edgewise and flapwise vibrations are the most important modes of vibrations in wind turbine blades, and in the majority of blades the edgewise vibration, in the absence of significant aerodynamic damping, is the main problem [2-4]. Damping decreases vibration, noise, and fatigue and boosts the structural integrity, performance, and stability of the wind turbines [5-7]. Accordingly, the importance of damping undesired vibrations through a sufficient degree of structural damping becomes obvious. This will then require efficient and accurate methods to estimate material damping as well as modeling it for the sake of blade load simulation and a proper design.

Among the current methods, Dynamic Mechanical Analysis (DMA) and Experimental Modal Analysis (EMA) are widely used for quantifying structural damping. DMA involves applying a small amplitude oscillatory stress or strain to a material and measuring its mechanical response, providing the loss factor ($\tan(\delta)$) which quantifies viscoelastic behavior with temperature and frequency change [8]. The damping capability of the material can be characterized by the phase difference ($\tan(\delta)$) between the applied stress and the resultant strain. The real part of the complex modulus is the storage modulus representing the elasticity of the material, while the imaginary part represents the energy loss ability of the material [9]. The loss associated with microstructural variations is known as material internal damping [10]. EMA involves measuring a structure's response to applied excitation to determine its dynamic characteristics, providing the damping ratio and natural frequency [11]. There are various techniques to apply modal testing from lab scale to the field application and there exist many different post-processing methods in the time or frequency domain, each of DMA or EMA methods has its limitations, particularly in the context of composite materials and materials with high elastic moduli. DMA results can introduce errors due to shear effects and boundary conditions, while EMA results can be affected by boundary conditions and post-processing methodologies.

2. Main objectives

One objective of this study is to identify the material damping of carbon UD composite material by conducting experiments via DMA and EMA methods and studying the effects of frequency, temperature, and geometry on the damping results and verification of the results through comparison with damping of aluminum, which a well-known isotropic material.

The other objective is understanding both DMA and EMA processes and what methods and procedures are used in carrying out them. For instance, comparing the effects of the presence of air in the experiment (aerodynamic damping) to the vacuum condition on the damping results. The difference between vacuum and air presence condition results will show the effect of aerodynamic damping.

Making a correlation between the obtained results from DMA (loss factor) and EMA (damping ratio) is another objective of this study. The fundamental difference between DMA and EMA makes direct comparison challenging, as EMA focuses on vibrational energy dissipation, whereas DMA quantifies viscoelastic behavior through the stress-strain relationship. This discrepancy can lead to difficulties in integrating and comparing results from the two methods accurately. Many DMA and EMA results have been obtained for various materials, but the results of these two methods for a particular material are not yet properly comparable. As a result, making a correlation is practical as it facilitates the comparison and provides more accurate results.

3. Methodology

DMA and EMA experiments are conducted to determine the damping characteristics of a carbon UD material. The effective control of the aerodynamic damping is not possible as vacuum conditions cannot be applied in the DMA process. According to Table 1, the test mode is a three-point bend for specimens with 1-4.5 mm thickness to realize the impact of thickness on the damping properties. The test is repeated for each specimen 10 times.

Table 1. DMA test setup parameters.

Parameter	Test Mode	Strain Applied	Temperature Range	Frequency Range	Sample Thickness Tested	Number Of Tests per Sample	Material Nature
Description or Value	Three-point Bend	100 Micro-strains	Constant (30°C)	Varied (0.01, 0.1, 0.5, 1:20 HZ)	1- 4.5 mm (0.5 mm increments)	10	Anisotropic (Carbon Fiber-UD)

Based on the conducted experimental DMA analysis, the variation in the viscoelastic damping materials' mechanical properties with frequency is obtained as shown in Fig.1. These loss factor values will be further post-process to obtain the damping contributions from different strati-stress deformation and loading directions to assess the net damping values and the correlation with those of EMA tests.

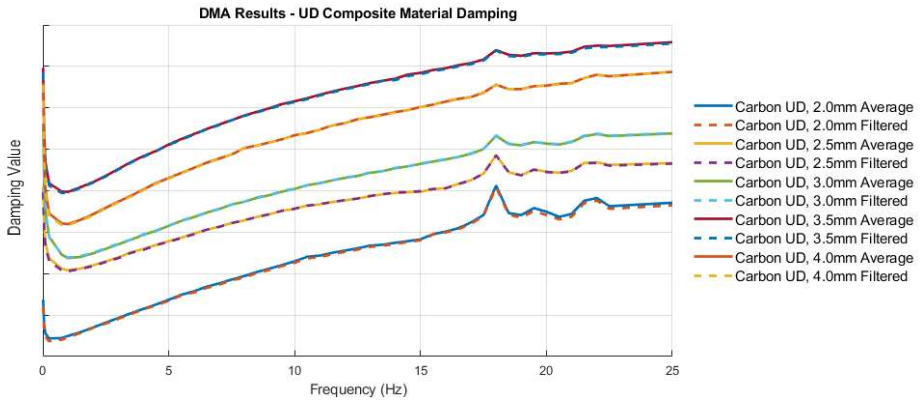

Figure 1: Loss Factor according to the different frequencies for the various thicknesses of the carbon UD viscoelastic damping material.

A test rig is developed at the University of Strathclyde, Glasgow, to conduct experimental modal analysis to investigate the damping ratio of carbon composite materials [12]. The test rig is equipped with an automatic

modal hammer mechanism to apply the impact excitations in the vacuum with strain gauges to enable the control of the incurred strain-stress in the specimen hence, keeping the loading strike in check. The design condition is as presented in Table 2, with a free-free boundary, and -0.9 bar vacuum condition. The vacuum condition is created to eliminate the effect of aerodynamic damping. Excitation is conducted via a hammer with a 20-100 N strike force. Multiple post-processing system identifications and modal analysis methodologies for this experimental process are possible, such as the POLYMAX or Poly Least Squared Complex Frequency Methods (PLSCF) to obtain the damping ratios. The EMA tests plan aims at varying the natural frequencies of the test specimen within a range of normal stress to investigate the dependency of damping ratio to both frequency and mechanical stress for carbon UD and aluminum. Furthermore, the correlation between EMA and DMA damping metrics will be studied and compared with those available in the literature. The output of this research is expected to provide robust testing techniques to obtain reliable structural damping metrics and shed light on how to feed these metrics to effective computational modeling of damping (e.g. in FE analysis) for accurate dynamic response analysis of sensitive systems such as wind turbine blades.

References

[1] M. Bošnjaković, M. Katinić, R. Santa and D. Marić. Wind turbine technology trends. *Applied Sciences,* 12:8653, 2022.

[2] K. Thomsen, J. T. Petersen, E. Nim, S. Øye and B. Petersen. A method for determination of damping for edgewise blade vibrations. *Wind Energy: An International Journal for Progress and Applications in Wind Power Conversion Technology,* 3:233-246, 2000.

[3] D. Qiu, J. Chen and Q. Xu. Dynamic responses and damage forms analysis of underground large scale frame structures under oblique SV seismic waves. *Soil Dynamics and Earthquake Engineering,* 117:216-220, 2019.

[4] S. R. Sandanshiv and U. S. Chavan. Vibration suppression effects on rotating wind turbine blade using a particle damping method. *Vibroengineering Procedia,* 29:43-48, 2019.

[5] M. Capaldo and P. Mella. Damping analysis of Floating Offshore Wind Turbine (FOWT): a new control strategy reducing the platform vibrations. *Wind Energy Science Discussions,* 2022:1-29, 2022.

[6] B. B. Prasad, F. Duvigneau, D. Juhre and E. Woschke. Application of particle dampers on a scaled wind turbine generator to improve low-frequency vibro-acoustic behavior. *Applied Sciences,*12:671, 2022.

[7] Y.-S. You, K.-Y. Song and M.-Y. Sun. Variable natural frequency damper for minimizing response of offshore wind turbine: principle verification through analysis of controllable natural frequencies. *Journal of Marine Science and Engineering,* 10: 983, 2022.

[8] F. Wang, J. Liao, C. Huang, H. Yu, J. Yan and H. Li. Study on the damping dynamics characteristics of a viscoelastic damping material. *Processes,* Vol. 10:635, 2022.

[9] M. Lahelin, I. Aaltio, O. Heczko, O. Söderberg, Y. Ge, B. Löfgren, S.-P. Hannula and J. Seppälä. DMA testing of Ni–Mn–Ga/polymer composites. *Composites Part A: Applied Science and Manufacturing,* 40:125-129, 2009.

[10] Q.-F. Fang, Z.-G. Zhu, T.-S. Ge and T. Ke. Characterization and mechanism of high damping materials. *WULI-BEIJING-,* 29:541-545, 2000.

[11] L. B. Ibsen and M. Liingaard. Experimental modal analysis, 2006.

[12] E. Brough, D. Nash, A. M. Kazemi Amiri, P. Couturier and V. L. Reis. Development of a test rig for improved estimation of structural damping of wind turbine composite materials. in *Proceeding of American Society of Mechanical Engineers,* 87141:V001T01A026.

6.3 Session 313: Aero-elastic and blade technology

26.09.2024, 9:0, Room 3

Chair:

Isaac Bensignor

Presenters:

Nazari Samira	Enhancing Antifouling Efficiency of Superhydrophobic Surfaces on Wind Turbine Applications: Micro-Texture and Spreading Diameter Analysis
Kellaris Konstantinos	Study of the three-dimensional coherent structures in the wake of flatback airfoils

20th EAWE PhD Seminar on Wind Energy
24 - 26 September 2023
Visby, Sweden

Enhancing Antifouling Efficiency of Superhydrophobic Surfaces on Wind Turbine Applications: Micro-Texture and Spreading Diameter Analysis

Samira Nazari[a], Lilibeth A. Zambrano M.[a], David Culliton[a]

[a] Department of Aerospace and Mechanical Engineering, South East Technological University (SETU), Carlow Campus, Ireland
E-mail: david.culliton@setu.ie

Keywords: Biofouling; Superhydrophobic surfaces; CFD; spreading diameter.

1 Introduction

Biofouling poses significant challenges across various sectors, including marine, industrial and renewable energy applications. Biofouling refers to the undesirable accumulation of microorganisms, plants, algae, and animals on wet surfaces [1]. In renewable energy systems, such as offshore wind turbines and tidal energy converters, biofouling can cause severe operational issues, including structural degradation, increased aerodynamic and hydrodynamic drag, reduced efficiency, and accelerated material deterioration [1].

One of the most attractive strategies to combat these issues is the use of passive antifouling coatings [2]. These coatings are engineered to prevent the adhesion and growth of fouling organisms by modifying the surface energy of materials and their topology [3].Control of the surface energy of antifouling coatings offers functional effectiveness and offers a useful approach to managing biofouling in renewable energy installations. This enhances operational efficiency and extends the lifespan of the infrastructure. This study focuses on superhydrophobic (SHB) surfaces, which are considered low-energy surfaces. They are effective coatings in various applications including drag-reduction [4], anti-icing [5], anti-corrosion [6], anti-fouling [7], and self-cleaning [8]. They exhibit extreme water repellence, causing water droplets to form spherical shapes and easily roll off from the surface. This characteristic reduces the droplet's contact time with the surface, preventing initial settling and the formation of biofilm. This characteristic helps prevent microorganisms and biofouling substances from sticking to the surface on offshore wind turbines, both blades and tower parts. [9].

In this study, we investigated cubic micro-textured SHB surfaces, exhibiting a contact angle of 150°. Our primary focus was on the spreading diameter, a key parameter for assessing the hydrophobicity

of these surfaces. By comparing the spreading diameters with a flat surface, we aimed to evaluate the effectiveness of the cubic micro-texture SHB surface.

2 Methodology

This study aims to investigate how the density of the cubic micro-texture affects the spreading diameter, ultimately identifying the optimal configuration for wind turbine applications. Three-dimensional Volume of Fluid (VOF) multiphase models were conducted using ANSYS Fluent 2021 R1 to simulate cubic micro-textured SHB surfaces with a constant contact angle of 150° and the initial water droplet diameter considered 0.5 mm. Figure 1 (a) illustrates the geometry of the pillars. In all cases, the edge dimension of and the height of the pillars are equal, 50 μm, while the distance between adjacent micro-textures varies, d, set at 10, 20, and 30 μm. Table 1 represents the models and dimensions.

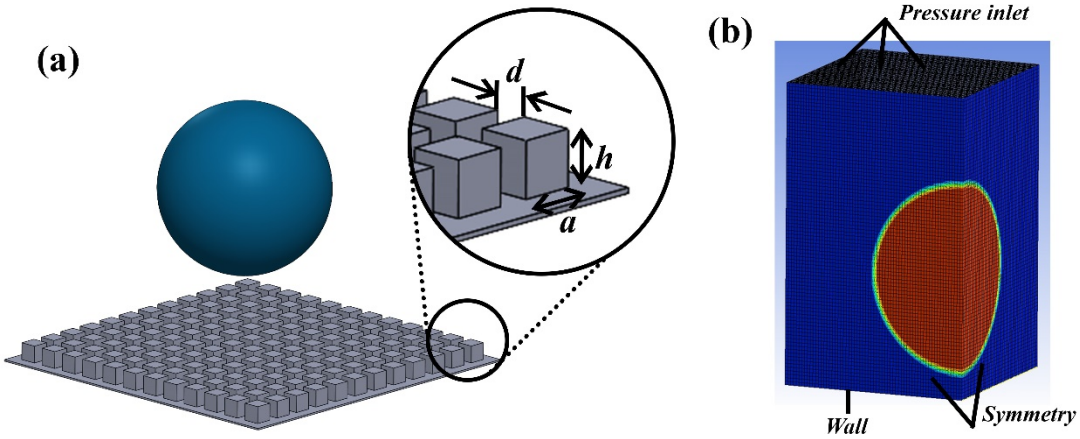

Figure 1: (a) Geometry of cubic micro-texture SHB surface. (b) Boundary condition and mesh elements

Table 1: Dimension of three cubic microtextured SHB surfaces

Models number	Name of Models	a (µm)	d (µm)	h (µm)	Density of micro-texture (numbers/mm²)
1	SHB-C-10	50	10	50	289
2	SHB-C-20	50	20	50	255
3	SHB-C-30	50	30	50	156

The Weber number in this study is considered zero, and droplets in all cases were released from the same height (3.2×10^{-4}m) above the surface. To reduce the computational complexity, only a quarter of the domain was simulated. The domain geometry is 0.5 × 0.5 × 0.75 mm³, with boundary conditions shown in Figure 1 (b). A surface tension model was adapted to simulate the SHB surface.

A pressure-based solver was used to perform the transient simulations, with PISO, QUICK, and Compressive methods employed to discretise the pressure, momentum, and volume fraction

respectively. The structured hexahedron elements were adopted, and the number of elements was selected between 400,000-500,000 based on mesh sensitivity analysis for cubic micro-textured surfaces.

3 Validation

Validation was conducted on a flat surface using settings adapted from Sun et al. [10]. The study investigated the impact of a 1.6 mm diameter droplet, focusing on the spreading factor defined as D/D_0, where D represents the droplet diameter at each time step and $D0$ is the initial diameter. Our simulation results showed good agreement with both the simulations and experiments of Sun et al. in terms of capturing the droplet shape over time (figure 2). A comparison with their experimental data revealed an average error of 7.7% in the spreading factor, which is 1.7% lower than reported in their simulation.

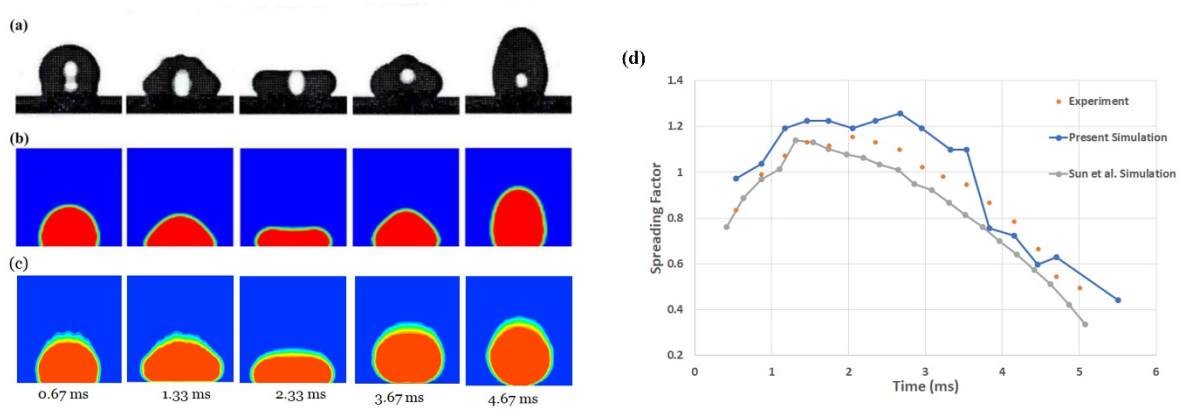

Figure 2: Impact of a water droplet on a superhydrophobic (SHB) surface. (a) Experimental model by Sun et al. [10] (b) Numerical model by Sun et al. [10] (c) Our present numerical model at five different time points (d) Comparison of the spreading factor among Sun et al.'s experimental and numerical model [10], and our present numerical study.

4 Result and discussion

In this study, the effectiveness of superhydrophobic (SHB) surfaces in reducing the spreading diameter of water droplets was evaluated using cubic micro-textures. The primary reason for focusing on spreading diameter is that a lower spreading diameter indicates a more hemispherical droplet shape. This shape facilitates the rolling off of water droplets from the surface, which in turn reduces the likelihood of microorganism attachment, thereby mitigating biofouling in offshore wind turbines. Three cubic micro-textured SHB surfaces were analysed and compared. The spreading diameters of these surfaces were compared with a flat SHB surface. The results show all SHB-C models cause a significant decrease in spreading diameters compared to the flat surface model. The results demonstrated small differences in among the micro-textured surfaces (Figure 3):

- **SHB-C-10:** This model showed a great reduction in spreading diameter compared to the flat surface by 43.54%.
- **SHB-C-20:** This surface exhibited a slightly more pronounced reduction in spreading diameter compared to SHB-C-10 (44.9%).
- **SHB-C-30:** Notably, the SHB-C-30 model achieved a 54.2% lower spreading diameter compared to the flat surface, making it the most effective in promoting water repellence and reducing microorganism attachment [11].

5 Conclusion

1. The comparative effectiveness of three SHB surfaces with inter-pillar distances of 10, 20, and 30 micrometres (SHB-C-10, SHB-C-20, and SHB-C-30) was successfully evaluated using the Spreading Diameter as an indicator of hydrophobicity (lower is better). Performance was benchmarked against a flat SHB surface.
2. The SHB-C-30 model demonstrated the most significant reduction in spreading diameter, (54.4% lower than the flat surface).
3. The optimal micro-texture spacing in the SHB-C-30 surface enhances water repellence, making it highly suitable for applications in renewable energy systems.

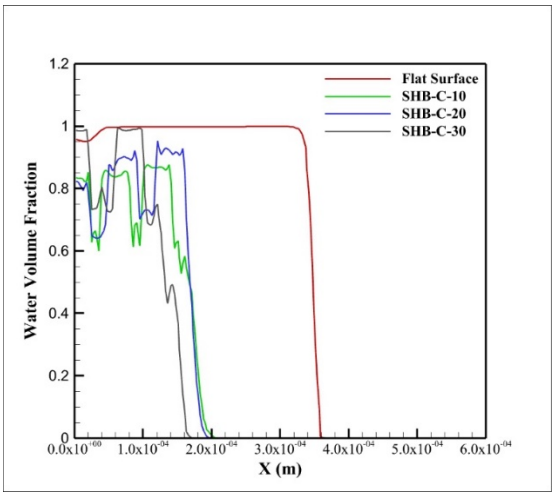

Figure 3: Comparison of spreading diameter in three cubic SHB models.

Acknowledgements

This study is supported by the Sustainable Energy Authority of Ireland under the SEAI Research, Development & Demonstration Funding Programme 2021 (Grant number 21/RDD/671 as part of the project SPOTBlade Strategies for Erosion and |Fouling Protection of Offshore Turbine Blades)

References

1. Guo, H., et al., *Direct formation of amphiphilic crosslinked networks based on PVP as a marine anti-biofouling coating.* Chemical Engineering Journal, 2019. **374**: p. 1353-1363.

2. Jin, H., et al., *Bioinspired marine antifouling coatings: Status, prospects, and future.* Progress in Materials Science, 2022. **124**: p. 100889.
3. Qiu, H., et al., *Functional polymer materials for modern marine biofouling control.* Progress in Polymer Science, 2022. **127**: p. 101516.
4. Liravi, M., et al., *A comprehensive review on recent advances in superhydrophobic surfaces and their applications for drag reduction.* Progress in Organic Coatings, 2020. **140**: p. 105537.
5. Li, W., Y. Zhan, and S. Yu, *Applications of superhydrophobic coatings in anti-icing: Theory, mechanisms, impact factors, challenges and perspectives.* Progress in Organic Coatings, 2021. **152**: p. 106117.
6. Vazirinasab, E., R. Jafari, and G. Momen, *Application of superhydrophobic coatings as a corrosion barrier: A review.* Surface and Coatings Technology, 2018. **341**: p. 40-56.
7. Jin, H., et al., *Recent advances in emerging integrated antifouling and anticorrosion coatings.* Materials & Design, 2022. **213**: p. 110307.
8. Fürstner, R., et al., *Wetting and self-cleaning properties of artificial superhydrophobic surfaces.* Langmuir, 2005. **21**(3): p. 956-961.
9. Otitoju, T., A. Ahmad, and B. Ooi, *Superhydrophilic (superwetting) surfaces: A review on fabrication and application.* Journal of industrial and engineering chemistry, 2017. **47**: p. 19-40.
10. Sun, J., et al., *Three-dimensional VOF simulation of droplet impacting on a superhydrophobic surface.* Bio-Design and Manufacturing, 2019. **2**: p. 10-23.
11. Yuan, Y., et al., *Surface characteristics influencing bacterial adhesion to polymeric substrates.* RSC advances, 2017. **7**(23): p. 14254-14261.

20th EAWE PhD Seminar on Wind Energy
24-26 September 2024
Visby, Sweden

Study of the three-dimensional coherent structures in the wake of flatback airfoils

Konstantinos Kellaris[a], **George Papadakis**[b], and **Marinos Manolesos**[a]

[a]School of Mechanical Engineering, National Technical University of Athens
[b]School of Naval Architecture and Marine Engineering, National Technical University of Athens

Email: kkellaris@mail.ntua.gr

Keywords: flatback airfoils, low-drag regime, secondary wake instabilities, DES, modal analysis

1 Introduction

As wind turbine (WT) rotor diameters increase, aiming to lower the Levelized Cost of Energy (LCOE), flatback (FB) airfoils, i.e., airfoils with a blunt trailing edge (TE), have gained traction recently. FB airfoils are placed at the root of WT blades, providing various aerodynamic, structural, and aeroelastic benefits. From an aerodynamics point of view, FB airfoils can provide higher lift values due to the reduced adverse pressure gradient over the aft part of the suction side [1]. In addition, their aerodynamic performance is insensitive to surface roughness compared to traditional sharp TE airfoils [1]. Early studies indicated that blades with flatpack airfoils can be up to 16% lighter than blades that use traditional airfoils without inducing any performance penalty [2]. Additionally, due to the blunt TE and increased blade cross-sectional area, FB blades have increased flapwise stiffness. However, FB airfoils come with an increase in drag force and noise [1, 3]. Consequently, several TE flow control devices have been proposed to improve their aerodynamic performance and decrease the associated drag penalty [3, 4, 5].

Most of the studies regarding FB airfoils have focused either on their aerodynamic/aeroacoustic performance [3, 6] or the wake characteristics of their flow [7, 5, 8] at $a = 0^{\circ}$, or relatively low angles of attack (AoA). Recently, studies were performed up to near-stall or post-stall [9, 10] AoA to provide new insights regarding the three-dimensional wake behaviour using high-fidelity tools. In experiments [11, 12, 13, 3, 4] and in simulations [14, 3, 9], a low-drag "pocket" arises in a region of AoA before stall, however, no one has yet sufficiently explained it.

2 Methods

2.1 Computational Fluid Dynamics

The present investigation focused on the LI30-FB10 airfoil, i.e., an airfoil with a maximum thickness of $0.3c$ and a trailing edge height of $h_{TE} = 0.106c$, where c is the chord length, also investigated in [4, 5, 9]. High-fidelity simulations were performed with the in-house solver MaPFlow [15] to solve the three-dimensional incompressible unsteady Navier-Stokes equations using the artificial compressibility method [16] and the Finite Volume discretization. An O-type grid spanning 50 chord lengths with approximately 10 million cells was used following previous computational studies [5, 9]. The grid had a spanwise length of one chord, while the non-dimensional distance of the first cell from the airfoil was $y^{+} = 0.1$. The airfoil was investigated at a high Reynolds number, namely $Re = 1.5 \times 10^{6}$, using the IDDES method [17]. This hybrid turbulence modelling approach blends the Spalart-Almaras RANS model with the Smagorinsky LES model. Specifically, the RANS variant of the model is employed near the airfoil, while the LES variant is employed away from the airfoil. The necessary grid layers and refinement around the airfoil (RANS region) are shown in Figure 1(a), while Figure 1(b) demonstrates the low-drag pocket discussed in the previous section.

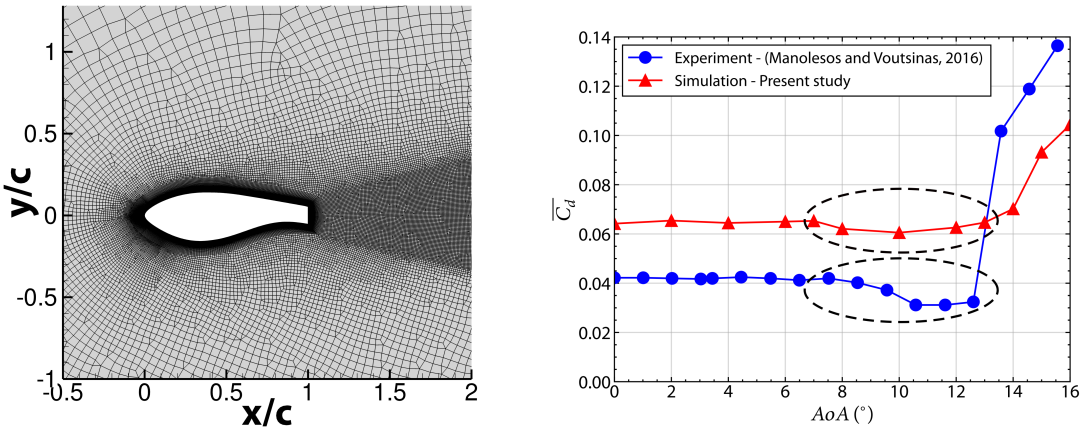

(a) (b)

Figure 1: (a): Detail of the grid refinement layers around the LI30-FB10 airfoil. (b): The variation of the drag coefficient C_d with the angle of attack and the low-drag regime is denoted with dashed ellipses.

2.2 Modal Analysis of Wake Structures

In order to extract the three-dimensional wake coherent structures/modes, the multiscale Proper Orthogonal Decomposition (mPOD) method [18] was utilized for two angles of attack—one inside $(12°)$ and one outside $(0°)$ of the low-drag pocket. At each simulation timestep, the grid data are interpolated onto a Cartesian grid spanning one chord length at the streamwise and spanwise directions and half chord length at the y-normal direction. Afterward, the dataset is organized into a large matrix where each column represents a timestep and each row a point in time. Then, by applying suitable band-pass filters to the temporal correlation matrix and performing POD for each filtered scale, mPOD yields a representation of the dataset modes that retain the energy optimality of the POD while simultaneously presenting more pure spectral content compared to the plain POD. For visualization purposes, we utilize Q-criterion [19] isosurfaces of the spatial coefficients of each mode coloured by either streamwise or spanwise vorticity. Finally, we extract the dominant frequency of each mode from the spectral behaviour of the temporal coefficients of each mode.

3 Results

The vortical structures found in the two cases are shown in the left panels of Figure 2 using Q-criterion isosurfaces coloured with spanwise vorticity. Firstly, the Bénard-von Kármán (primary) instability is evident for both cases. Additionally, the secondary instabilities, i.e. pairs of counterrotating vortices in the streamwise direction that connect two consecutive primary spanwise vortices (white Q-criterion isosurfaces) are also shown in Figure 2. The wake is more organized for the low-drag $(12°)$ case, and the structure of the secondary instability observed in both cases is more apparent compared to the high-drag $(0°)$ case.

The primary instability dominates the first (most energetic) mPOD modes and is omitted from this abstract in the interest of brevity. Specifically, the primary instability and its harmonics appear throughout the first 10 and 6 modes for the $(0°)$ and $(12°)$ cases, respectively.

As shown in the right panels of Figure 2, the first modes that exhibit dominant spanwise behaviour are the 11th and 7th modes for the high-drag $(0°)$ and low-drag $(12°)$ cases, respectively. At $(0°)$ the associated Strouhal number $(St = 0.018)$ is an order of magnitude smaller than the one at the $(12°)$ case $(St = 0.106)$. In addition, the vortical pairs appear to be distorted along the span, an effect that is possibly introduced by the oblique shedding of the primary instability. We estimate the spanwise wavelength of the secondary instabilities, counting the number of vortex pairs along the span, leading to a spanwise wavelength of approximately $\lambda_z = 1h_{TE}$ and $\lambda_z = 1.4h_{TE}$ at $(0°)$ and $(12°)$, respectively.

Finally, while a comprehensive framework exists for characterizing the secondary instabilities in the wake of cylindrical bluff bodies, this is not the case for elongated bluff bodies. The characterization of the secondary

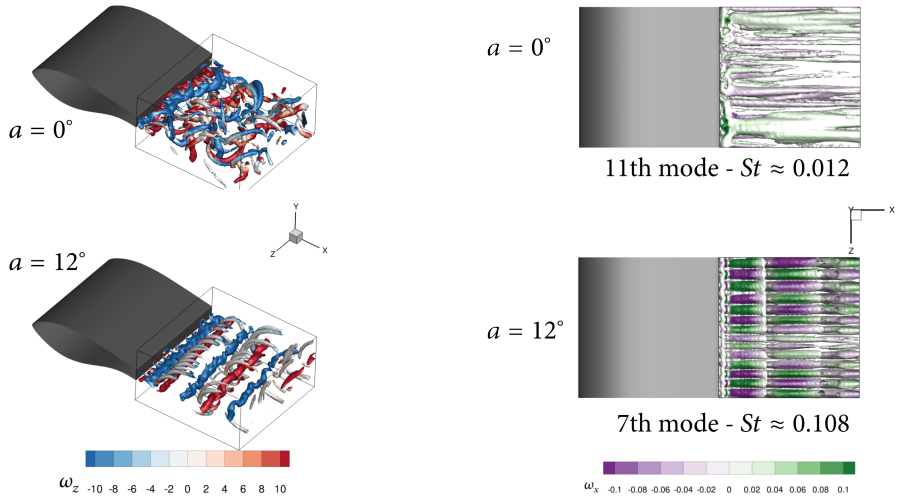

Figure 2: Q-isosurfaces coloured with vorticity. Left: Indicative snapshots for the high-drag (0°) (top) and the low-drag (12°) (bottom) cases coloured with spanwise vorticity. Right: The first mPOD modes exhibiting dominant spanwise behaviour at (0°) (top) and (12°) (bottom) coloured with streamwise vorticity.

instability at (0°) does not correspond to a previously identified coherent mode, as the oblique shedding and the vortex dislocations significantly affect the topology of the wake. On the other hand, at (12°), the modes have a frequency that is a subharmonic of the primary instability. In addition, as shown in the bottom right panel of Figure 2, the streamwise vortical pairs' rotation direction changes at each primary vortex-shedding cycle. Therefore, the instability is characterized as the Mode S′ identified by [20].

4 Conclusions

In summary, the three-dimensional coherent structures for the flow past a flatback airfoil were investigated for two angles of attack—one inside (12°) and one outside (0°) of the low-drag pocket. Namely, the primary instability (Bénard-von Kármán vortex street) dominates the wake for the most energetic modes in both cases. However, the wake is more organized at the (12°) case. The first modes demonstrating spanwise behaviour for the high-drag (0°) and the low-drag (12°) cases are the 11th and 7th modes, respectively. However, the behaviour identified in these modes differs significantly for both cases. In the low-drag case (0°), the instability corresponds to the mode S′ described for the flow past elongated bluff bodies [20], while the instability at the high-drag (0°) case cannot be characterized under a pre-existing framework. These new insights about the wake behaviour and organization, in combination with the existence of the low-drag pocket, can potentially be used to formulate a passive drag reduction strategy based on spanwise excitation using the wavelength identified for the Mode S′ instability.

Acknowledgements

Computational resources were provided by HPC Wales, which is gratefully acknowledged. Additionally, this work was supported by computational time granted from the National Infrastructures for Research and Technology S.A. (GRNET S.A.) in the National HPC facility - ARIS - under project 'HPC4FAIR' with ID pr014018_thin. Furthermore, K. Kellaris and M. Manolesos kindly acknowledge the financial support of the European project 'TWEET-IE' funded by the European Union's Horizon 2020 Research and Innovation Programme (Grant Agreement 101079125).

References

[1] J. P. Baker, E. A. Mayda, and C. P. Van Dam. Experimental analysis of thick blunt trailing-edge wind turbine airfoils. *Journal of Solar Energy Engineering*, 128(4):422–431, Nov. 2006.

[2] D. Griffith and P. Richards. The SNL100-03 Blade: Design Studies with Flatback Airfoils for the Sandia 100-meter Blade. Technical Report SAND2014-18129, 1159116, 537751, Sandia National Lab, Albuquerque, NM (United States), Sept. 2014.

[3] M. F. Barone, D. E. Berg, W. J. Devenport, and R. A. Burdisso. Aerodynamic and aeroacoustic tests of a flatback version of the DU97-W-300 airfoil. Technical Report SAND–2009-4185, 1504612, Aug. 2009.

[4] M. Manolesos and S. G. Voutsinas. Experimental study of drag-reduction devices on a flatback airfoil. *AIAA Journal*, 54(11):3382–3396, Nov. 2016.

[5] G. Papadakis and M. Manolesos. The flow past a flatback airfoil with flow control devices: Benchmarking numerical simulations against wind tunnel data. *Wind Energy Science*, 5(3):911–927, July 2020.

[6] M. Fuchs, P. Weihing, T. Kuehn, M. Herr, A. Suryadi, C. Mockett, H. Knobbe-Eschen, F. Kramer, and T. Knacke. Two computational studies of a flatback airfoil using non-zonal and embedded scale-resolving turbulence modelling approaches. In *28th AIAA/CEAS Aeroacoustics 2022 Conference*, Southampton, UK, June 2022. American Institute of Aeronautics and Astronautics.

[7] G. Wang, L. Zhang, and W. Z. Shen. LES simulation and experimental validation of the unsteady aerodynamics of blunt wind turbine airfoils. *Energy*, 158:911–923, Sept. 2018.

[8] L. Hongpeng, W. Yu, Y. Rujing, X. Peng, and W. Qing. Influence of the modification of asymmetric trailing-edge thickness on the aerodynamic performance of a wind turbine airfoil. *Renewable Energy*, 147:1623–1631, Mar. 2020.

[9] M. Manolesos and G. Papadakis. Investigation of the three-dimensional flow past a flatback wind turbine airfoil at high angles of attack. *Physics of Fluids*, 33(8):085106, Aug. 2021.

[10] G. Bangga, F. Seel, T. Lutz, and T. Kühn. Aerodynamic and acoustic simulations of thick flatback airfoils employing high order DES methods. *Advanced Theory and Simulations*, 5(8):2200129, May 2022.

[11] H. A. Smith and R. F. Schaefer. Aerodynamic characteristics at reynolds numbers of 3.0 x 10 (exp 6) and 6.0 x 10 (exp 6) of three airfoil sections formed by cutting off various amounts from the rear portion of the NACA 0012 airfoil section. Technical report, 1950.

[12] M. Post, R. Jones, A. Denton, and R. Millard. Characterization of a flatback airfoil for use in wind power generation. In *46th AIAA Aerospace Sciences Meeting and Exhibit*, page 1330, 2008.

[13] J. Baker and C. P. van Dam. Drag reduction of blunt trailing-edge airfoils. In *BBAA VI International Colloquium on: Bluff Bodies Aerodynamics & Applications*, Milano, Aug. 2008.

[14] T. Winnemöller and C. P. Van Dam. Design and Numerical Optimization of Thick Airfoils Including Blunt Trailing Edges. *Journal of Aircraft*, 44(1):232–240, Jan. 2007.

[15] G. Papadakis. *Development of a Hybrid Compressible Vortex Particle Method and Application to External Problems Including Helicopter Flows*. PhD thesis, National Technical University of Athens, 2015.

[16] D. Ntouras and G. Papadakis. A coupled artificial compressibility method for free surface flows. *Journal of Marine Science and Engineering*, 8(8):590, Aug. 2020.

[17] P. R. Spalart, S. Deck, M. L. Shur, K. D. Squires, M. Kh. Strelets, and A. Travin. A New Version of Detached-eddy Simulation, Resistant to Ambiguous Grid Densities. *Theoretical and Computational Fluid Dynamics*, 20(3):181–195, July 2006.

[18] M. A. Mendez, M. Balabane, and J.-M. Buchlin. Multi-scale proper orthogonal decomposition of complex fluid flows. *Journal of Fluid Mechanics*, 870:988–1036, May 2019.

[19] J. C. R. Hunt, A. A. Wray, and P. Moin. Eddies, streams, and convergence zones in turbulent flows. Dec. 1988.

[20] K. Ryan, M. C. Thompson, and K. Hourigan. Three-dimensional transition in the wake of bluff elongated cylinders. *Journal of Fluid Mechanics*, 538(-1):1, Aug. 2005.

TOPIC 7

Electrical conversion, energy system and wind power-to-X

7.1 Session 123: Electrical conversion, energy system and wind power-to-X

24.09.2024, 13:10, Room 3

Chair:

Jean Bastin

Presenters:

Jiménez-Ruiz Javier	Modelling ofWind Turbines within the Framework of IEC 61400-27 Standard
Bruninx Max	Reinforcement learning based control for the next-generation offshore wind-hydrogen farm
Zheng Fanning	Assessing the impact of wind farm control strategies on the integrated electricity grid

20th EAWE PhD Seminar on Wind Energy
24-26 September 2024
Visby, Sweden

Modelling of Wind Turbines within the Framework of IEC 61400-27 Standard

J. Jiménez-Ruiz[a], **A. Honrubia-Escribano**[a], and **E. Gómez-Lázaro**[a]

[a]Renewable Energy Research Institute, Department of Electrical, Electronic, Automatic and Communications Engineering of ETSII-AB, University of Castilla-La Mancha (UCLM)

E-mail: javier.jimenezruiz@uclm.es

Keywords: DIgSILENT PowerFactory; generic models; neural networks; power systems stability; wind energy

1 Introduction

In the past years, wind energy has become one of the most predominant technologies used to achieve carbon free power systems. Integrated into power systems around the world, it's a major source of renewable energy for many countries and a critical step towards achieving net-zero emissions. By 2050, global energy consumption is expected to rise by 14% compared to 2020 levels [1], hence the implementation of new power plants in power systems is an urgent need. The surge in global energy demand is fueled by two key factors: a growing population and a push to electrify industries, replacing combustion engines. This not only increases total energy needs but also alters the demand profile as well.

The Global Wind Energy Council (GWEC) reports that a significant 77.6 GW of new wind power capacity was added in 2022. This brings the total installed wind power capacity to 906 GW worldwide [2]. The distribution of said new capacity is concentrated mainly in five countries, which are China, USA, Brazil, Germany and Sweden [3]. Driven by concerns over pollution and a commitment to environmental sustainability, the European Union (EU) has implemented stringent regulations to reduce greenhouse gas emissions from energy generation. To achieve this goal, the EU has set ambitious wind power targets for 2030. These targets aim for a total installed capacity of 323 GW, with a specific focus on 100 GW from offshore wind farms [4]. Wind energy has emerged as a dominant renewable energy source in many countries, particularly across Europe. Spain exemplifies this trend. In 2023, wind energy claimed the top spot within the nation's power mix, contributing the highest share of annual electricity production among all renewable sources. Notably, it covered 22.2% of the country's total electricity demand [5].

As wind power plants were introduced into power systems, the need to develop wind turbine models to carry out simulations to ensure grid stability grew with urgency. Initially, dynamic wind turbine models were developed and implemented by the manufacturers, so only vendor-specific models were available [6]. As wind farms are made up of a large number of individual units, which often differ from farm to farm, this led to a large number of supplier-specific models, making it difficult for grid operators to run simulations in which a large number of wind farms are connected to the grid. In response to this situation, the International Electrotechnical Commision (IEC) embarked on the task of creating generic models capable of simulating the real behaviour of wind turbines independently of the manufacturer. The work performed by IEC finally bore fruit with the publication of the 61400-27 standard in 2015 (which was later updated in 2020). IEC 61400-27 allows to model wind turbines using generic models, which greatly help grid operators to simulate the behaviour of large wind farms connected to the grid, specially under fault situations.

2 IEC 61400-27 generic models

IEC 61400-27 describes generic models for both Type I, II, III and IV wind turbines, providing sufficient parameters to accurately represent the dynamic behaviour of these systems under grid perturbations (such as short circuits or voltage dips). Figure 1 represents the block diagram corresponding to Type I and Type II wind turbines, black arrows represent the elements that are both found in Type I and Type II, while gray arrows indicate elements which

are only present in Type II wind turbines. Figure 3.5 represents the block diagrams defined by IEC used to model Type III and Type IV wind turbines, black arrows represent the elements that are both found in Type III and Type IV wind turbines, while gray arrows represent elements which are only present in Type III wind turbines. The block diagrams presented in Figures 1 and 2 are furthermore composed of a number of modules, which vary according to the type of wind turbine used, and which have adjustable parameters in order to adjust the behaviour of the generic models as closely as possible to the actual field behaviour of the wind turbines.

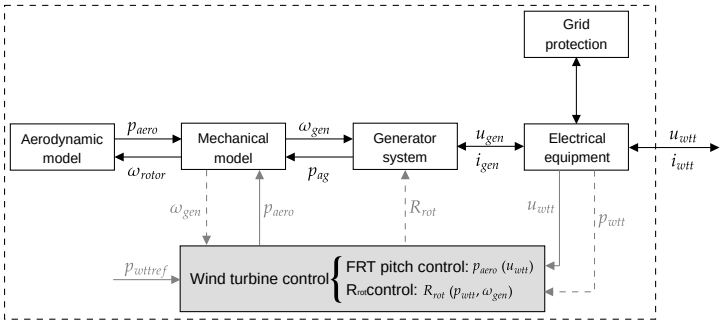

Figure 1: Block diagram of generic wind turbine Type IA, Type IB & Type II.

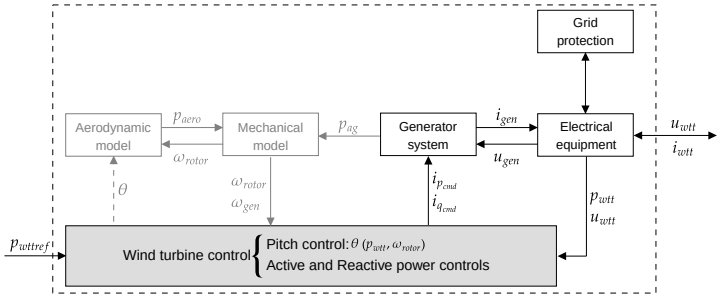

Figure 2: Block diagram of generic wind turbine Type III & Type IV.

2.1 Type III wind turbines

Type III wind turbines, also known as doubly fed asynchronous generators (DFIG), are an improvement on the Type II wind turbines. Type III wind turbines are equipped with a converter which is connected to the rotor of the electrical generator and to the grid, so an additional excitation current can be injected into the rotor, which provides the ability to control the magnitude and phase of the rotor current almost instantaneously [7]. Inverter power typically varies between 25 % and 30 % of the total wind turbine capacity, allowing a speed range of approximately 60 % to 110 % of rated speed [8]. Since the current in the rotor can be changed rapidly, the speed of the wind turbine can be modified to extract the maximum possible power for a given wind speed. In this type of wind turbine, the generator can operate both above and below the synchronous speed, so the power flow through the converter is bi-directional; above the synchronous speed, power is generated in both the rotor and the stator, while if the speed is below the synchronous speed, the rotor will draw power from the grid (if the DFIG rotates exactly at the synchronous speed, the power flow to the rotor is only due to the compensation of ohmic losses in the rotor winding resistance) [9]. The fact that Type III wind turbines have the ability to modify their rotational speed to match the wind speed in order to extract maximum power, together with their high reliability, has made these turbines the most widely used in both onshore and offshore applications [10]. Since most of the installed wind turbines are of this type, the analysis that is being carried out focuses on this model.

The complexity of Type III wind turbine modelling can be inferred by observing Figure 3, which represents the generic IEC 61400-27 model implemented in DIgSILENT PowerFactory (one of the most used software to perform electrical dynamical simulations).

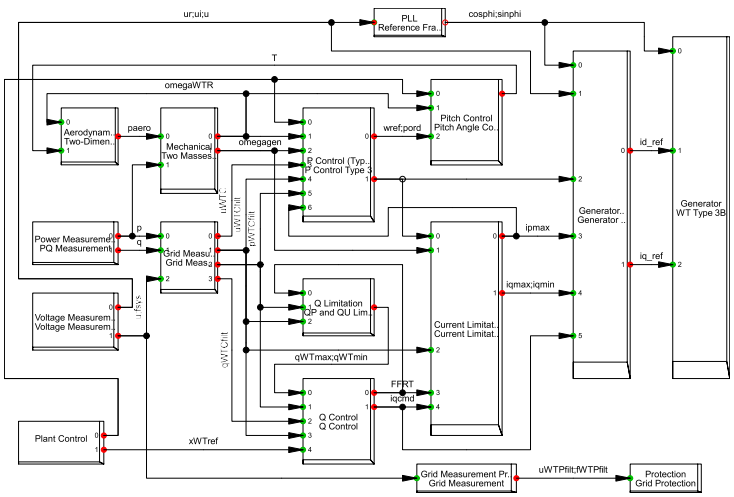

Figure 3: IEC 61400-27 Type III wind turbine implemented in DIgSILENT PowerFactory

Each of the submodules that can be observed in Figure 3 represent a different component of the wind turbine, said submodules have a wide range of parameters which have to be modified in order to accurately represent the actual behaviour of the wind turbine that is being analysed. Figure 4 represents the active power output of a simulated Type III wind turbine during a voltage dip. It can be clearly observed by comparing Figure 4(a) and Figure 4(b) that different parameters result in extremely different active power responses.

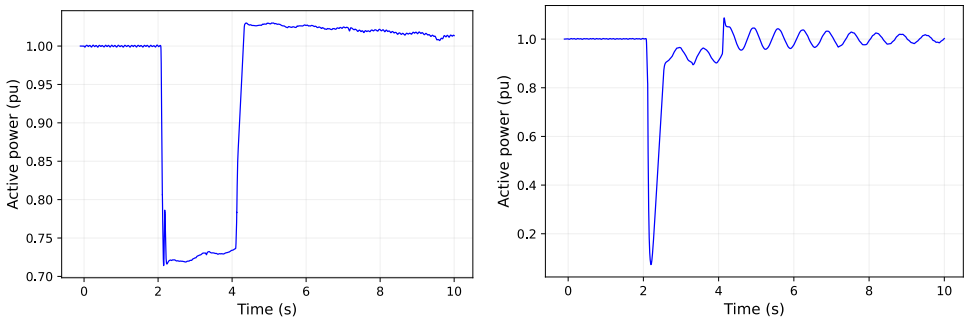

(a) Active power (not adjusted)

(b) Active power (adjusted)

Figure 4: Active power output under voltage dip

3 Parameter tuning of generic wind turbine models with neural networks

As it was mentioned in Section 2.1, Type III wind turbine generic models are composed of different modules, which also contain a large number of adjustable parameters. This high number of parameters (over a hundred of them), although it allows a faithful description of the behaviour of Type III wind turbines, makes the adjustment of all of them an arduous and complex task.

The aim of the proposed work is to create a model which is able to characterise the equivalent model of a wind turbine by means of the real response of a wind turbine to a voltage dip. As can be seen in Figure 5, a previously trained neural network will be used to determine the adjustable parameters of the generic model that best emulate the real behaviour of the wind turbine, using as inputs the voltage dip experienced by the wind turbine and its active and reactive power response. This will provide a model capable of adjusting any wind turbine to the generic models proposed by the IEC 61400-27 standard, which will facilitate the integration of wind energy into the grid and therefore help to create carbon free power systems.

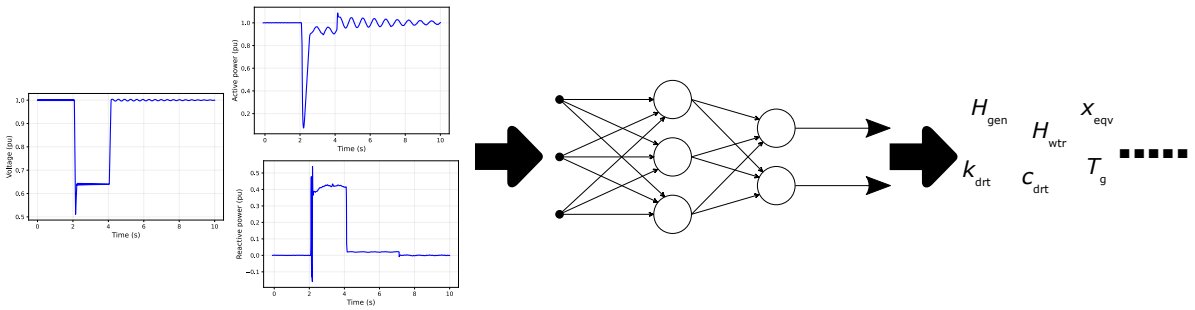

Figure 5: Parameter tuning methodology for Type III wind turbines using neural networks

The simulation software DIgSILENT PowerFactory is used to develop the work. This software has an Application Programming Interface (API) that allows to interact with DIgSILENT PowerFactory through the Python programming language, which means that we can use the large number of existing packages of said language (many of them oriented towards data analysis and machine learning) to characterise wind turbines according to IEC 61400-27 standard. The results to be obtained will be of great help to grid operators, as they will allow the widespread application of the generic wind turbine models proposed in IEC 61400-27, creating a common and reliable framework to ensure the stability of power grids with a large integration of wind energy.

References

[1] D. Raimi, E. Campbell, R. Newell, B. Prest, S. Villanueva, and J. Wingenroth, "Global energy outlook 2022: turning points and tension in the energy transition," *Resources for the Future: Washington, DC, USA*, 2022.

[2] IRENA, "Wind energy — irena.org." `https://www.irena.org/Energy-Transition/Technology/Wind-energy`, 2024. [Accessed 04-06-2024].

[3] Alex, "Global Wind Report 2023 - Global Wind Energy Council — gwec.net." `https://gwec.net/globalwindreport2023/`, 2023. [Accessed 04-06-2024].

[4] E. P. Soares-Ramos, L. de Oliveira-Assis, R. Sarrias-Mena, and L. M. Fernández-Ramírez, "Current status and future trends of offshore wind power in europe," *Energy*, vol. 202, p. 117787, 2020.

[5] "Aee anuario 2023 - asociación empresarial eólica — aeeolica.org." `https://aeeolica.org/aee-anuario-2023/`. [Accessed 04-06-2024].

[6] T. García-Sánchez, I. Muñoz-Benavente, E. Gómez-Lázaro, and A. Fernández-Guillamón, "Modelling types 1 and 2 wind turbines based on iec 61400-27-1: Transient response under voltage dips," *Energies*, vol. 13, no. 16, p. 4078, 2020.

[7] S. Feleke, R. Satish, B. Pydi, D. Anteneh, A. Y. Abdelaziz, and A. El-Shahat, "Damping of frequency and power system oscillations with dfig wind turbine and de optimization," *Sustainability*, vol. 15, no. 6, p. 4751, 2023.

[8] A. Jabal Laafou, A. Ait Madi, A. Addaim, and A. Intidam, "Dynamic modeling and improved control of a grid-connected dfig used in wind energy conversion systems," *Mathematical Problems in Engineering*, vol. 2020, pp. 1–15, 2020.

[9] Z. Din, J. Zhang, Z. Xu, Y. Zhang, and J. Zhao, "Low voltage and high voltage ride-through technologies for doubly fed induction generator system: Comprehensive review and future trends," *IET Renewable power generation*, vol. 15, no. 3, pp. 614–630, 2021.

[10] B. P. Ganthia, S. K. Barik, and B. Nayak, "Wind turbines in energy conversion system: Types & techniques," *Renewable energy and future power systems*, pp. 199–217, 2021.

20th EAWE PhD Seminar on Wind Energy
24-26 September 2024
Visby, Sweden

Reinforcement learning based control for the next generation offshore wind-hydrogen farm

Max Bruninx[a], **Timothy Verstraeten**[a], **Pieter-Jan Daems**[a], **Ann Nowé**[a], and **Jan Helsen**[a]

[a]Vrije Universiteit Brussel, Pleinlaan 2, 1050 Brussels, Belgium

E-mail: max.bruninx@vub.be

Keywords: reinforcement learning, probabilistic forecasting, hybrid power plants, electricity markets

1 Introduction

The increased integration of renewable energy sources into the electricity grid presents a significant challenge. The intermittent nature of these resources complicates the forecasting of their energy output, and the resulting forecast errors can lead to imbalances within the electricity market. From the perspective of the wind farm, this results in additional costs, i.e. balancing costs, imposed by the transmission system operator (TSO). In case of overproduction, curtailment of the wind turbines is often employed as a strategy to mitigate balancing costs. However, curtailment results in a loss of potential energy and also impacts the lifetime of the turbine [10].

The use of probabilistic forecasts, instead of point forecasts, presents an alternative approach to reducing balancing costs resulting from the day-ahead schedule. By incorporating the forecast error in the optimization problem, a trading strategy can be determined that maximizes expected revenue rather than minimizing imbalance. The solution can be found using techniques from the field of stochastic optimization.

Hybrid power plants, where the wind farm is coupled to an electrolyzer, could be employed as an alternative to curtailments. During periods of surplus electricity generation, excess energy can be channelled towards the production of green hydrogen. This hydrogen can then be sold to a third party or consumed during periods of insufficient power output. Furthermore, active trading in the intraday market presents an alternative strategy for managing imbalances. However, optimizing control in this context becomes a multi-agent problem in continuous time-space. This characteristic significantly complicates the application of stochastic optimization techniques, thereby introducing the need for a data-driven approach.

The goal of this research project is to combine techniques from the field of stochastic optimization and reinforcement learning for hybrid power plant control. More specifically, we aim to employ a Newsvendor strategy for day-ahead bidding and then train an RL agent that, given the resulting day-ahead schedule, can maximize revenues using intraday control. While data-driven and stochastic optimization-based approaches have been proposed in past research, there is, to the best of our knowledge, no research that investigates the combination of both techniques to construct an end-to-end control system which maximizes revenue. To evaluate the proposed approach, the following research questions will be addressed:

1. What are the current state-of-the-art techniques for probabilistic forecasting? How do different forecasts impact the outcome of the (constrained) Newsvendor solution?
2. Which day-ahead bidding strategy would an RL agent, that uses the probabilistic forecasts as input, learn? How do these compare to the strategies obtained by the (constrained) Newsvendor solution?
3. Can an RL agent learn an intraday hydrogen plant control strategy which considers the day-ahead schedule, electricity prices, updated wind forecasts and efficiency losses?
4. How can we extend our approach to combine intraday trading and hydrogen plant control?

2 Related works

[9] show that probabilistic forecasts can be used to determine a day-ahead bidding strategy that maximizes expected revenue using a Newsvendor model. The advantage of this approach is that it has an analytical solution under the assumption that there is only one decision moment, i.e. no intraday markets. However, even though this strategy is optimal in the long run, they found that it could introduce large imbalances in the short term. To that end, [15] introduce a constrained version of the Newsvendor model. Furthermore, it should be noted that the solution of this model is highly dependent on the quality of the probabilistic forecasts [14], [8], [5]. Other techniques from the field of stochastic optimization have also been applied to solve more complex versions of this problem, such as robust optimization to include energy storage [11] or two-level stochastic optimization for day-ahead and intraday markets [3]. However, these strategies do require a complete mathematical formulation of the problem and rely on assumptions such as independence between decisions in different time intervals.

Data-driven approaches, on the other hand, relax these assumptions and learn the optimal strategy from historical data, allowing to optimize more complex systems such as hybrid power plants. Examples are a scalable optimization approach for wind farm control which using Multi-Agent Multi-Armed Bandits and Gaussian Mixture Models [12]; a direct reinforcement learning (RL) approach for day-ahead strategic bidding [7]; a feature-driven approach to control a hybrid power plant [4] and proximal policy optimization to control an energy storage device [6].

3 Methodology

This study proposes the development of wind power production forecasting models utilizing transformer-based neural networks. These architectures are recognized as the current state-of-the-art in sequential prediction tasks, such as time series forecasting. In addition, various techniques for probabilistic forecasting, including conformal prediction [13] and (non-)parametric probabilistic forecasting (e.g. [2]), will be studied.

Incorporating the probabilistic forecasts, we propose a two-step revenue optimization approach:

1. *Day-ahead bidding strategy*
   Based on day-ahead forecasts of wind power production and expected balancing costs, employ the (constrained) Newsvendor bidding strategy in the day-ahead market.

2. *Intraday control strategy*
   Train an RL agent which decides whether to produce (or consume) hydrogen or trade in the intraday market such that revenue is maximized under the day-ahead schedule. The inputs to the RL agent will be the current market prices, a hydrogen electrolyzer model and updated wind power production forecasts.

The aim is to first carefully construct and evaluate every component of the approach and then combine everything together to evaluate the strategy as a whole. The models will be trained and evaluated based on real data from Belgian offshore wind farms and market data of the Belgian energy exchange (EPEX SPOT Belgium) and balancing markets (managed by Elia).

4 Results

As a first step, the power model proposed by [1] was re-implemented using data from a different wind farm in the Belgian North Sea cluster. In addition, a baseline model that does not consider sequential data was created. The model was trained and evaluated with a training set consisting of data from 2023, a validation set from Jan-Feb 2024 and a test set from Mar-Apr 2024. Mean Absolute Percentage Error (MAPE) and Mean Absolute Error (MAE) normalized by the installed capacity were used as performance metrics. The results can be found in Figure 1.

It was found that the performance was considerably worse compared to the results of [1], with a test MAE of $\pm 7\%$ compared to $\pm 2\%$. However, four possible reasons could explain the discrepancy in results: First and foremost, curtailments and downtime of the wind farm were not excluded in our training and evaluation set. As shown in Figure 2, the four worst predictions based on MAPE were strongly impacted by these manual control actions in

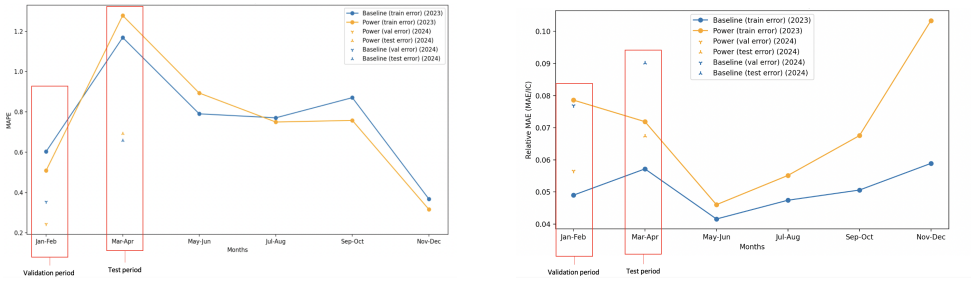

(a) MAPE (b) Normalized MAE

Figure 1: Performance metrics over time

the data. Second, a different train-test split method was applied: [1] constructs its test set using randomly selected days for each month, whereas we employ a time-based split. As seen in Figure 1, the performance of our model is time-variant and therefore it is hard to compare our results against a training set that is spread over time. In addition, random splitting of data might result in an overestimation of performance in the case of time-series data. Third, turbulence intensity has been calculated using a different time window: [1] uses a centred time window whereas we use a backward-looking time window. The issue with the former is that information about the future is given to the model, which is impossible in a real-time prediction context. However, we assume that the impact of this difference in time-window is minor. Last, the power capability signal was not included in our models whereas it was included in [1]. As shown in Figure 3, this variable corresponds to the power production in the case of no down-regulation and will therefore significantly impact the model performance in estimating power production.

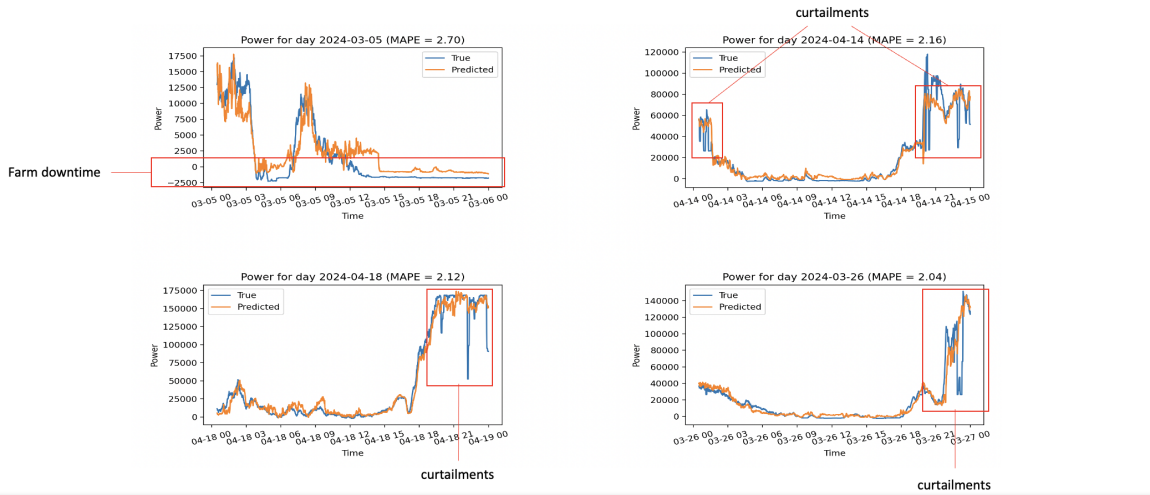

Figure 2: Four worst predictions based on MAPE

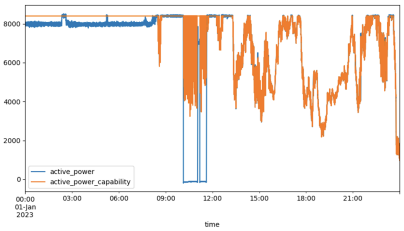

Figure 3: Power capability signal of a wind turbine

References

[1] S. Ally, P.-J. Daems, T. Verstraeten, A. Nowé, and J. H. Vub. Modular deep learning approach for wind farm power forecasting and wake loss prediction. *Authorea Preprints*, 2023.

[2] Y. Chen, Y. Kang, Y. Chen, and Z. Wang. Probabilistic forecasting with temporal convolutional neural network. *Neurocomputing*, 399:491–501, 2020.

[3] T. Dai and W. Qiao. Optimal bidding strategy of a strategic wind power producer in the short-term market. *IEEE transactions on sustainable energy*, 6(3):707–719, 2015.

[4] E. Helgren, J. Kazempour, and L. Mitridati. Feature-driven strategies for trading wind power and hydrogen. *arXiv preprint arXiv:2310.01385*, 2023.

[5] J. Huber, S. Müller, M. Fleischmann, and H. Stuckenschmidt. A data-driven newsvendor problem: From data to decision. *European Journal of Operational Research*, 278(3):904–915, 2019.

[6] J. Jeong, T.-Y. Ku, and W.-K. Park. Time-varying constraint-aware reinforcement learning for energy storage control. *arXiv preprint arXiv:2405.10536*, 2024.

[7] N. Mazzi and P. Pinson. Purely data-driven approaches to trading of renewable energy generation. In *2016 13th International Conference on the European Energy Market (EEM)*, pages 1–5. IEEE, 2016.

[8] A. Oroojlooyjadid, L. V. Snyder, and M. Takáč. Applying deep learning to the newsvendor problem. *IISE Transactions*, 52(4):444–463, 2020.

[9] P. Pinson, C. Chevallier, and G. N. Kariniotakis. Trading wind generation from short-term probabilistic forecasts of wind power. *IEEE transactions on Power Systems*, 22(3):1148–1156, 2007.

[10] K. Robbelein, P.-J. Daems, T. Verstraeten, N. Noppe, W. Weijtjens, J. Helsen, and C. Devriendt. Effect of curtailment scenarios on the loads and lifetime of offshore wind turbine generator support structures. In *Journal of Physics: Conference Series*, volume 2507, page 012013. IOP Publishing, 2023.

[11] A. A. Thatte, L. Xie, D. E. Viassolo, and S. Singh. Risk measure based robust bidding strategy for arbitrage using a wind farm and energy storage. *IEEE Transactions on Smart Grid*, 4(4):2191–2199, 2013.

[12] T. Verstraeten, P.-J. Daems, E. Bargiacchi, D. M. Roijers, P. J. Libin, and J. Helsen. Scalable optimization for wind farm control using coordination graphs. *arXiv preprint arXiv:2101.07844*, 2021.

[13] V. Vovk, A. Gammerman, and G. Shafer. *Algorithmic learning in a random world*, volume 29. Springer, 2005.

[14] C.-H. Yang, H.-T. Wang, X. Ma, and S. Talluri. A data-driven newsvendor problem: A high-dimensional and mixed-frequency method. *International Journal of Production Economics*, 266:109042, 2023.

[15] M. Zugno, T. Jónsson, and P. Pinson. Trading wind energy on the basis of probabilistic forecasts both of wind generation and of market quantities. *Wind Energy*, 16(6):909–926, 2013.

20th EAWE PhD Seminar on Wind Energy
24-26 September 2024
Visby, Sweden

Assessing the impact of wind farm control strategies on the integrated electricity grid

Fanning Zheng, **Abhinav Anand**, and **Carlo L.Bottasso**

Wind Energy Institute, Technische Universität München, Garching bei München, Germany

E-mail: fanning.zheng@tum.de

Keywords: wind farm control, power flow simulation, integrated electricity grid

This work evaluates the impact of wind farm control strategies on the electricity grid. A comprehensive modeling framework integrating renewable generation sub-models, conventional generation, variable load, and various associated controllers is developed. Within a case study, application scenarios are simulated to assess the effects of wind farm control techniques on the grid.

Advanced wind farm control strategies are crucial for the large-scale integration of wind energy into the power system [3]. While many research projects have been focusing on power maximization, future optimization objectives will increasingly prioritize economics, turbine lifetime, and ecological considerations. For instance, future wind farm operations will aim for profit maximization while minimizing environmental impact rather than simply maximizing wind farm annual energy production (AEP) [1]. Ongoing international research projects in multi-objective wind farm control highlight the relevance and timeliness of this work.

Currently, a significant share of power generation is provided by conventional generators connected to the transmission grid. Hence, grid ancillary services provided predominantly by conventional power plants are managed by the transmission system operator. Power generation from photovoltaic (PV) and wind plants are mostly connected to the distribution grid and are characterized by uncertainty due to strong weather dependency [2]. This results in a high variability of power generation in grids with large renewable share. The energy transition towards predominantly renewable generation requires additional flexibility and regulating options in the distribution grid. As future principal electric power suppliers [4], wind farms will be required to provide grid-supporting services and contribute to system stability. In the future, various factors including grid codes, electricity market, balancing market and environmental constraints will have an impact on wind farm operation. Switching between control strategies enables responding to current conditions and generating new revenue streams beyond the pure production of electricity.

This work proposes a modular framework for modeling a realistic distribution grid with integrated wind farm and PV plant sub-models. It incorporates greedy, maximum power, maximum profit, and active power wind farm control utilizing offline-generated lookup tables. The framework serves as a tool for grid integration and power flow studies, accommodating various research questions. Figure 1 provides an overview of the electricity grid layout used for power flow simulations. The grid model is a modified version of the MV Oberrhein grid, available in Python. The model has been extended by conventional generation and a wind farm. The 179-bus system covers a surface area of 105 km^2 and includes 147 load elements, 153 renewable and conventional generators, 2 external grids, and 181 lines.

The model follows the novel approach of considering multiple wind farm control strategies within one framework and explores switching of control techniques, which is implemented using scheduled signals. The case study simulates and assesses relevant application scenarios, considering greedy and maximum power wind farm control as baseline cases. The proposed future scenario includes a maximum profit strategy, which considers turbine damage while respecting minimum lifetime constraints. Additionally, primary and secondary frequency response by the wind farm can be enabled. Analogously to current practise in the transmission grid, primary frequency control is implemented through droop response, whereas secondary frequency control is based on the area generation error of the grid.

Various performance indicators are assessed to analyze the impact of wind farm control strategies. These indicators include line loading, line losses, active power, and power exchange with the external grid, all obtained from power flow simulation. The parameters are analysed to investigate the direct interactions within the grid. Furthermore, the impact on grid frequency is evaluated in the context of primary frequency support. Based on

the power flow results, CO_2 equivalent emissions, referred to as line emissions, are calculated from per-line active losses. The most important performance indicator for future wind farm operations is the expected profit. The profit is computed using revenue and a cost function that accounts for turbine component damage, following the approach of [1]. Finally, the results from different application scenarios are compared to each other to identify potential gains and showcase the benefits of various wind farm control strategies.

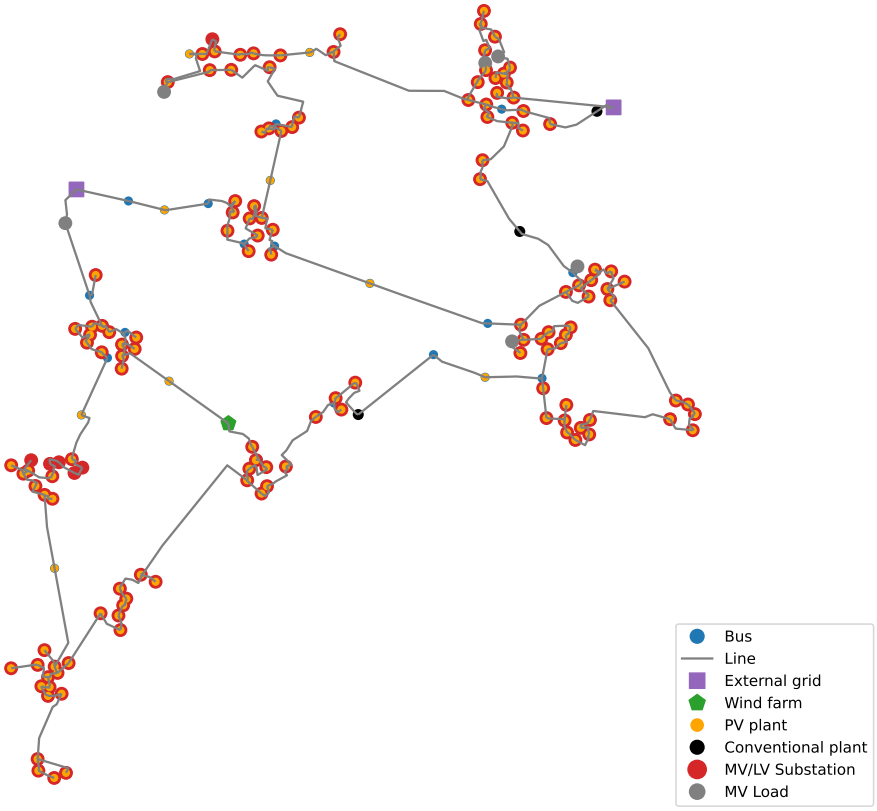

Figure 1: Layout of modified MV Oberrhein grid model

Acknowledgements

The continuation of this work will be supported by the SUDOCO project, and the TWAIN project, both funded by the European Union.

References

[1] R. Braunbehrens, A. Anand, F. Campagnolo, and C. L. Bottasso. First experimental results on lifetime-aware wind farm control. *Accepted for Publication in IOP Journal of Physics: TORQUE Conference Proceedings*, 2024.

[2] K. Korotkiewicz, P. Steinbusch, M. Modemann, F. Paulat, M. Zdrallek, S. Hetzel, U. Dietzler, J. Vormelker, and U. Schlüter. Medium-voltage grid state control as a basis towards a holistic automation in smart distribution systems. *CIRED - Open Access Proceedings Journal*, 2020(1):473–476, 2020.

[3] J. Meyers, C. Bottasso, K. Dykes, P. Fleming, P. Gebraad, G. Giebel, T. Göçmen, and J.-W. van Wingerden. Wind farm flow control: prospects and challenges. *Wind Energy Science*, 7(6):2271–2306, 2022.

[4] C. R. Shapiro, J. Meyers, C. Meneveau, and D. F. Gayme. Wind farms providing secondary frequency regulation: evaluating the performance of model-based receding horizon control. *Wind Energy Science*, 3(1):11–24, 2018.

7.2 Session 323: Electrical conversion, energy system and wind power-to-X

26.09.2024, 10:30, Room 3

Chair:

Keeta Smith	Chapman-

Presenters:

Nenoff Carl	Influence of floating offshore wind turbine dynamics on bubble covering in proton exchange membrane electrolysers
Castro Bernardo	Valerio Analysis of HVDC interconnectors in the North Sea Grid for offshore wind integration
Useche Mario	AC Energy Islands for the optimal integration of offshore wind energy resources: Operation Strategies using Multi-Objective Nonlinear Programming

20th EAWE PhD Seminar on Wind Energy
24-26 September 2024
Visby, Sweden

Influence of floating offshore wind turbine dynamics on bubble covering in proton exchange membrane electrolysers

Carl Nenoff[a]

[a]Fraunhofer Institute for Wind Energy Systems IWES

E-mail: carl.nenoff@iwes.fraunhofer.de

Keywords: Floating offshore wind turbines (FOWT); proton exchange membrane electrolysis (PEMEL); bubble dynamics; hydrogen production; marine conditions

1 Introduction

Hydrogen production by electrolysis with power from renewable energy systems (RES) is a key element for the decarbonisation of the energy sector, transportation, and several industrial sectors. To scale up the availability of green hydrogen and increase the utilisation factor of RES, placing electrolysers in close proximity of RES is considered beneficial due to minimized infrastructure. Large potential for new RES comes from offshore wind turbines. The use of floating offshore wind turbine (FOWT) opens up areas in deeper waters worldwide. Almost 40 GW have been announced through 2030 [6]. One concept for the production of offshore hydrogen is the decentralized hydrogen production directly on offshore platforms at the tower bottom of wind turbines [4]. FOWT experience challenging load dynamics under marine conditions where the load profile is dominated by a combination of loads from turbulent wind and waves. Load dynamics of FOWT on their tower bottom might affect hydrogen production systems in several ways.

The most advanced green hydrogen production technologies, proton exchange membrane electrolyser (PEMEL) and alkaline electrolyser (AEL), are both influenced by the development, propagation, and detachment of gas bubbles on the porous layer of their membranes or electrodes. As of today, PEMEL is the favoured technology for offshore wind and power-to-x use [1]. Bubble dynamics in PEMEL have been investigated using numerical and experimental setups [3, 5, 8].

Their influence on performance under marine dynamics may affect hydrogen production by influencing bubble covering on the cathode side of the electrolyser. In [2] the authors describe prevention of bubble build-up and quicker removal from the electrode, among other effects, by inducing higher frequency excitation. It might be reasonable that low frequency excitation found in FOWT affect bubbles similarly.

2 Methods

Effects of changed bubble dynamics in PEMEL due to marine movements are evaluated by modelling and simulation. The simulation is done in two parts as shown in Figure 1: simulation of the FOWT dynamics and simulation of the PEMEL.

First, the publicly available openFAST model of the IEA Wind 22 MW Offshore Reference Wind Turbine [9] is used to simulate the structural dynamics and power production. The PEMEL is supposed to be placed on the semi-submersible platform of the turbine and experiencing the same movements as the tower bottom of the turbine. Tower bottom acceleration and power production of the turbine are simulated and passed to the PEMEL model.

In [8] a PEMEL model shows that bubble covering makes up to a 2.17 % reduction in efficiency at the highest current density of 1.5 A/cm^2. It is a MATLAB/Simulink model consisting of four parts, namely cathode, anode, PEM membrane and voltage module. Presence of bubbles influences the active area and effective resistance of the PEMEL.

Bubble coverage is found to increase with increasing current density, bubble detachment radius, and temperature and decreases with increasing cathode pressure and water velocity. In a simplified approach according to [8],

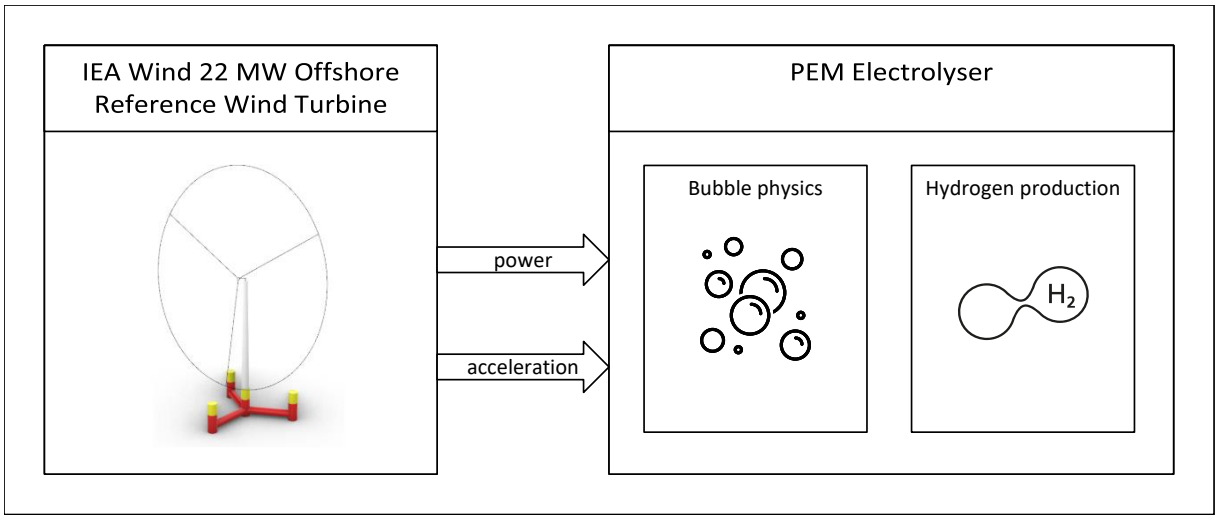

Figure 1: Diagram showing the simulation setup used to evaluate the influence of FOWT movements on bubble physics and thus hydrogen production. Power and acceleration are simulated with the FOWT model [9] and passed to the PEMEL model considering the influence of bubble covering [8].

the bubble buoyancy force F_b and the tension force of the bubble F_s form the combined force on the bubble in Equation 1.

$$\sum F_{total} = F_b - F_s \tag{1}$$

Bubble detachment happens If the buoyancy force exceeds the tension force of the bubble. To consider the effects of marine motion of the FOWT, an additional time dependent dynamic force F_d is introduced to the combined force on the bubble shown in Equation 2.

$$\sum F_{total} = F_b - F_s + F_d \tag{2}$$

In this simplified approach, all forces act in vertical direction. Acceleration in z-direction a_z from the FOWT simulation results, the growing bubble volume V_b and the gas density ρ_g make up the resulting additional force F_d shown in Equation 3 that suppresses (in negative z-direction) or speeds up (in positive z-direction) bubble detachment from the membrane. To get the actual Volume of the bubble V_b, the spherical radius r_b and contact angle with the porous layer of the membrane θ are used in Equation 4.

$$F_d = V_b \cdot a_z \cdot \rho_g \tag{3}$$

$$V_b = \frac{4}{3}\pi r_b^3 (2 + 3\cos\theta - \cos^3\theta) \tag{4}$$

3 Results

The simulation results will provide insights into how the dynamics and movements of a FOWT affect bubble dynamics and hydrogen production in a PEMEL placed on the FOWT platform.

To post-process the results, the bubble coverage and electrolyzer efficiency will be analyzed with different inputs from the FOWT operating under varying conditions according to design load case (DLC) scenarios [7]. The additional time-dependent dynamic force on the bubbles due to the FOWT acceleration will be a key factor in determining how the marine motion affects bubble detachment.

Comparisons will be made between the PEMEL performance with and without the influence of FOWT dynamics to quantify the impact. Visualizations such as bubble plots could be used to gain insights into the bubble dynamics under different conditions.

The results will likely be presented through a combination of:

- time series plots showing the variation of key parameters like bubble coverage and electrolyzer efficiency,
- bar charts or tables comparing PEMEL performance metrics with and without FOWT motion,
- contour plots or animations visualizing the spatiotemporal evolution of bubbles in the electrolyzer.

4 Conclusion

In summary, the study aims to characterize the coupled dynamics between a FOWT and a PEMEL hydrogen production system, in order to assess the feasibility and impacts of offshore application of electrolysis using floating wind power. The findings could help guide the design and optimization of such systems by mitigating negative effects and determining potential benefits of electrolysis under marine conditions.

Acknowledgements

Supported by:

on the basis of a decision
by the German Bundestag

References

[1] M. Dörenkämper, T. Meyer, D. Baumgärtner, J. Borowski, C. Deters, E. Dietrich, J. Fricke, F. Hans, T. Jersch, M. Leimeister, M. Neshati, G. Pangalos, T. Quiroz, G. Quistorf, N. Requate, K. Schalk, J. Schmidt, M. Schnackenberg, S. Schwegmann, S. Hoffmann, P. Thomas, L. Vollmer, J. Walgern, V. Widerspan, and H. Zotieieva. Weiterentwicklung der rahmenbedingungen zur planung von windenergieanlagen auf see und netzanbindungssystemen: Endbericht, 2023.

[2] Y. Ehrnst, P. C. Sherrell, A. R. Rezk, and L. Y. Yeo. Acoustically–induced water frustration for enhanced hydrogen evolution reaction in neutral electrolytes. *Advanced Energy Materials*, 13(7), 2023.

[3] J. C. Garcia-Navarro, M. Schulze, and K. A. Friedrich. Detecting and modeling oxygen bubble evolution and detachment in proton exchange membrane water electrolyzers. *International Journal of Hydrogen Energy*, 44(50):27190–27203, 2019.

[4] O. S. Ibrahim, A. Singlitico, R. Proskovics, S. McDonagh, C. Desmond, and J. D. Murphy. Dedicated large-scale floating offshore wind to hydrogen: Assessing design variables in proposed typologies. *Renewable and Sustainable Energy Reviews*, 160:112310, 2022.

[5] G. Li. Lattice boltzmann simulations of gas bubble transport in proton exchange membrane water electrolysis cells. *Journal of Physics: Conference Series*, 2280(1):012048, 2022.

[6] W. Musial, P. Spitsen, P. Duffy, P. Beiter, M. Shields, D. Mulas Hernando, R. Hammond, M. Marquis, J. King, and S. Sathish. Offshore wind market report: 2023 edition.

[7] A. Natarajan, M. H. Hansen, and S. Wang. Design load basis for offshore wind turbines: Dtu wind energy report no. e-0133.

[8] X. Su, L. Xu, and B. Hu. Simulation of proton exchange membrane electrolyzer: Influence of bubble covering. *International Journal of Hydrogen Energy*, 47(46):20027–20039, 2022.

[9] F. Zahle, A. Barlas, K. Loenbaek, P. Bortolotti, D. Zalkind, L. Wang, C. Labuschagne, L. Sethuraman, and G. Barter. Definition of the iea wind 22-megawatt offshore reference wind turbine.

20th EAWE PhD Seminar on Wind Energy
24-26 September 2024
Visby, Sweden

Analysis of HVDC interconnectors in the North Sea Grid for offshore wind integration

Bernardo Castro Valerio[a,b], **Oriol Gomis-Bellmunt**[a], **Vinicius Lacerda**[a], **Marc Cheah**[a], and **Pieter Gebraad**[b]

[a]CITCEA-UPC
[b]YouWind Renewables

E-mail: bernardo.castro@upc.edu

Keywords: HVDC, Interconnector, Offshore Wind, Optimal Power Flow

The North Seas Energy Cooperation back in 2020 had proposed to support the long term goal of reaching 60 GW of offshore wind by 2030 and 300 GW by 2050. In September 2022 the numbers got revisited on the immediate targets of 76 GW by 2030 and 193 GW by 2040 to reach at least 260 GW by 2050 [1]. The ambitious objectives create a need for grid development and market design. As front runners of offshore wind the TSOs of Belgium, Denmark, Germany and The Netherlands got together in 2023 and proposed the first MTDC in the North Sea in *Expert paper : The Esbjerg Cooperation* . Following the first draft, Great Britain, Luxembourg, Ireland and Norway joined in to form a nine country committee to progressively develop the power goal in the North Sea. In [2] the committee present the hybrid interconnects to be built in the 2030s. The projects as they stand at the moment are set to be built in point to point connections. However, as they all share the same voltage rating, Multi Terminal Direct Current (MTDC) grids have been proposed as a solution [4].

In this work we study the preliminary design of the future North Sea Grids. We analyze the utilization of the proposed grid with a hybrid optimal power flow (OPF). This is the first step in order to propose improvements enhancing efficiency and reducing costs. The rest of this extended abstract will be formed by a description of the OPF in section 1, a description of the case to be studied in 2. In section 3 we vary the offshore wind availability and study how the system would operate.

1 AC/DC Hybrid optimal power flow model

The objective of the OPF is to minimize the expenditure in power consumption over the different generators. Additionally, due to various converters being able to be connected to a same AC node, a constrain is added to prevent that the mathematical model gives resulting opposite reactive powers in each converter. The constraint is only added for nodes with two or more converters connected and is multiplied by a factor $\kappa = 10^{-3}$ to not affect the main cost function. The full optimization function is shown in equation 1.

$$min \sum_{g=1}^{\mathscr{G}_{ac}} (P_g \cdot C_{m(g)}) + \kappa \sum Q_{c_i}^2 [n_{ac_i} \geq 2\ conv] \tag{1}$$

The OPF is built in per unit system as a non linear model. It combines an AC OPF formulation which limits the voltage and angle of all nodes, while ensuring an operable power rating of the lines. The model contains two types of generation units. One being renewable sources where a power availability is set and a curtailment variable is added to it. Secondly, the other generation unit will have a minimum and maximum value and a cost designated to it.

The DC branches are modeled according to Fig.1a where the voltage is measured from pole to ground. Following a similar formulation as in AC, for the DC power flow equations are expressed as equation 2.

$$P_{c_d} - P_{l_d} = U_d \sum_{f=1;f\neq d}^{\mathscr{N}_{dc}} \left((U_f - U_d) \cdot p_e \cdot Y_{bus_{DC_{df}}} \right) \qquad \forall d \in \mathscr{N}_{dc} \tag{2}$$

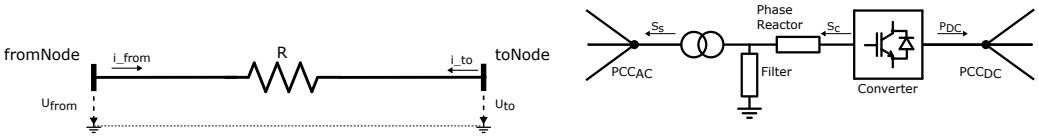

(a) DC branch model.

(b) Converter model.

Figure 1: Models used in the AC/DC OPF

Where P_{c_d} is the power into the node by an AC/DC converter and P_{l_d} a load's consumption. p_e is the polarity of the DC branch connecting nodes $d\&f$ and takes value of $p_e = 1$ for assymetrical links, and $p_e = 2$ for symmetrical and bipolar links. This formulation allows to include assymetrical monopolar taps in bipolar MTDC systems, as long as they share the same voltage rating.

The AC/DC converter model is connected between one AC node and one DC node. In this study it is modelled as Fig.1b comprising four elements. A transformer modeled as a series impedance represented in admittance mode $G_{tf} + jB_{tf}$, a filter as a shunt susceptance B_f, a phase reactor a series impedance represented in admittance mode $G_{pr} + jB_{pr}$ and a power electronic AC/DC converter. Internal AC voltages in the model are subject to limitations similar to the AC nodes. For the converters four sets of equation to relate the real power, reactive power, voltages and angles. These constrains will depend on the utilization of the full model or transformer-less or filter-less model.

To model the power electronics, a relation between the power injected into the AC passive elements $P_{c_{AC}}$ and the power injected $P_{c_{DC}}$ into the DC node d and the power loss in the elements is described as equation 3. P_{loss} is calculated by parameters a b & c, such parametrization will always return a positive number, resulting in the relation of $P_{c_{AC}}$ and $P_{c_{DC}}$ sign will maintain power flow direction.

$$P_{c_{AC}} + P_{c_{DC}} + \left[a + b\frac{\sqrt{P_{c_{AC}}^2 + Q_{c_{AC}}^2}}{V_{c_{AC}}} + c\left(\frac{P_{c_{AC}}^2 + Q_{c_{AC}}^2}{V_{c_{AC}}^2}\right)\right] = 0 \tag{3}$$

The model to be presented has been implemented in python under the package name *PyFlow ACDC* available online. The OPF model is built with Pyomo [3] and it is solved by the use of the ipopt solver. Continuous integration is set up on the repository.

2 Case Study

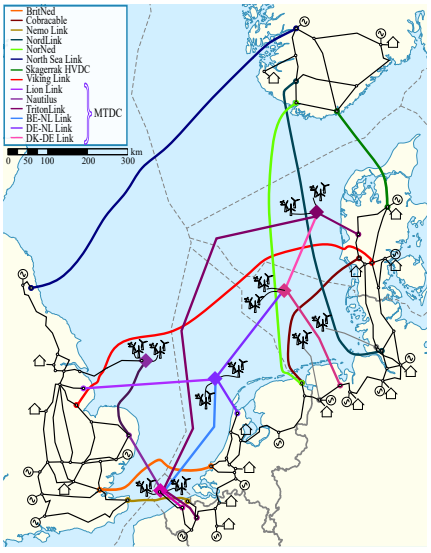

Figure 2: North Sea grid with interconnectors and possible MTDC.

Table 1: Overview of HVDC connections in the North Sea

Name	Acronym	From Market	To Market	Rating
BritNed	BN	GB	NL	1.0 GW
CobraCable	CC	NL	DK	1.4 GW
Nemo Link	NM	GB	BE	1.0 GW
Nord Link	ND	NO	DE	1.4 GW
NorNed	NN	NL	NO	0.7 GW
NorthSea Link	NS	GB	NO	1.4 GW
Skagerrak	Sk	NO	DK	1.6 GW
Viking Link	VL	GB	DK	1.4 GW

(a) HVDC interconnectors in the North Sea

Name	Acronym	From Market	To Market	Rating
Lion Link	LL	GB	NL	1.8 GW
Nautilus	NA	BE	GB	1.4 GW
Triton Link	TL	BE	DK	2.0 GW
BE-NL link	BN	BE	NL	2.0 GW
DE-NL link	DN	DE	NL	2.0 GW
DE-DK link	DD	DE	DK	2.0 GW

(b) HVDC MTDC in the North Sea

The case study is a construction of the North Sea HVDC development area, based on the market areas of Belgium (BE), Denmark 1 (DK) , Germany (DE), Great Britain (GB), Netherlands (NL) and Norway 2 (NO).

The aim of the case study is to analyze the behaviour of power flows and curtailment of offshore developments. The offshore developments considered in the study are: Princess Elizabeth Island (PEI) in BE with an installed power of 3.5GW, NL Energy Hub (NLH) with an initial power rating of 2 GW, German Offshore Interconnection Cluster (GOC) with 4GW of installed capacity, Danish Energy Island (DK_{EI}) with 3.5 GW and Hornsea (HS) 1& 2 with 2.6 GW. In addition, German developments that already are connected through HVDC are combined into two clusters, Germany North (DE_N) with 2.13 GW and Germany South (DE_S) with 4.7 GW of installed capacity.

The study is divided into three scenarios. Each scenario will add on the previous one. In the first scenario (SI) the market areas are interconnected only by AC branches. One AC interconnector between BE and NL, one AC interconnector between NL and DE and two AC interconnectors between DE and DK. For the second scenario (SII) HVDC existing interconnectors are added to the case study. The HVDC links used in the study are presented in table 1a.

For the third scenario (SIII) a multi terminal DC grid (MTDC) based on [2]. The MTDC grid is formed by the projects that have a Memorandum of Understanding (MoU) and an Agreement of Interconnection (AoI) with the aim to be operational by mid 2030s. The aim of the MTDC is to have HVDC lines have dual functionality. One to connect the offshore developments of the different energy Hubs and secondly to act as interconnectors between markets. The projects that would interconnect in the MTDC are presented in table1b. SIII map distribution is shown in Fig. 2. An additional assymetrical monopole link is included in the study to connect the Horn Sea development to the MTDC.

3 Full load analysis

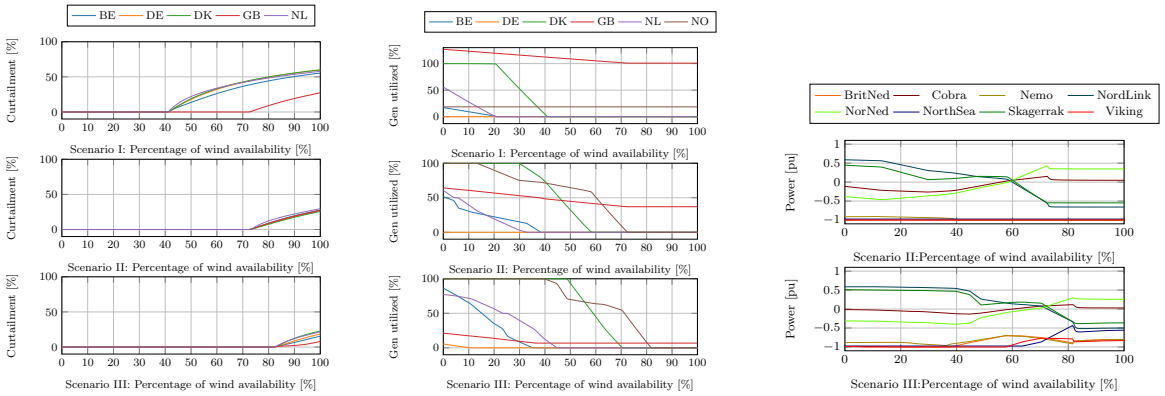

(a) Curtailment of offshore developments (b) Power generation in each market (c) Power flow in the HVDC interconnectors

Figure 3: Results of power generation and curtailment on percentage of wind availability

In section the case study is analysed with full load, it takes the price and load for each market as presented in Table 2. This part of the analysis focuses on changing the wind availability as a percentage of the wind capacity of each market area. The aim is to identify the different threshold of each scenario for curtailment and power generated.

Table 2: Power capacity in each market

Market	Wind capacity [MW]	Generation Capacity [MW]	Load [MW]	Average Price [€/ MWh]
BE	3500	3144	1850	97.27
DE	10846	18680	3215	96.67
DK	3500	4074	1160	81.26
GB	2600	7701	8975	108.23
NL	2000	6026	1640	95.82
NO	0	4346	800	79.44

In Fig.3a when comparing the results on all three scenarios, we can note that the main difference is on SI. In SI, the offshore wind developments in the European markets start to be curtailed at 41 % and the offshore development of GB at 73 %. When comparing SII and SIII, in SII the curtailment starts evenly in all markets at 73%. On the other hand in SIII, most offshore developments start being curtailed at 82%.In addition, GB offshore development stays at low curtailment. The differences between SII and SIII can be a result of the increased transmission capacity and the addition of a converter station ton GB offshore development which allows for reactive power compensation on the station.

In Fig.3b the power generation per market area is shown over the percentage of wind availability. It is important to note that in SI, so that the optimization problem is solvable, the generation capacity of GB had to be increased. When comparing all three scenarios we can see that GB power generated is decreased as the scenarios progress. As NO has the lowest price for power produced, it is the last one to not be utilized when wind capacity increases in SII and SIII. However, it is also shown that not in all percentages NO will have the highest percentage of power utilized. This is due to the fact that, the location of the generation nodes and load nodes are also important to consider. This is also corroborated as BE and DE have very similar average price, but they defer completely on power production profile.

In Fig. 3c the power transmitted by each HVDC interconnector is shown. The power transmitted is positive when the power flows from the market *from* to the market *to* according to Table. 1a. It can be noted that the power transmitted through the Skagerrak, NorNed and NordLink have the same power dependancy on wind availability. With low wind availability the three HVDC links are used to transmit power produced in NO to the different markets, whilst with high wind availability they are used to supply power to NO so that it can then be transmitted to GB by the North Sea cable. Cables that connect GB such as VL, NL,NS,BN in SII are always maxed to transmit power into GB. However, in SIII around 65% VL and NS no longer transmit power at full capacity.

4 Conclusion and Future Work

To conclude, the increased interconnection of the MTDC grid allows for a more efficient power distribution of offshore wind power generation reducing the curtailment of offshore developments. This study also shows that a correct analysis of the possible utilization of new interconnectors is needed as some interconnectors such as Cobra Cable could have little utilization. Further work on this theme would include a variable load, price and wind power availability according to time series data. Lastly, as the installed offshore power increments in the North Sea are timed increments, an optimized development and expansion of this MTDC has to be tough out taking into account such increments.

Acknowledgements

This work has received funding from the ADOreD project of the European Union's Horizon Europe Research and Innovation program under the Marie Skłodowska-Curie grant agreement No 101073554.

References

[1] The north seas energy cooperation, 2022.

[2] Expert paper ii : Offshore tso collaboration unlocking the potential of the north seas, 2024.

[3] M. L. Bynum, G. A. Hackebeil, W. E. Hart, C. D. Laird, B. L. Nicholson, J. D. Siirola, J.-P. Watson, and D. L. Woodruff. *Pyomo–optimization modeling in python*, volume 67. Springer Science & Business Media, third edition, 2021.

[4] O. Gomis-Bellmunt, J. Liang, J. Ekanayake, R. King, and N. Jenkins. Topologies of multiterminal hvdc-vsc transmission for large offshore wind farms. *Electric Power Systems Research*, 81(2):271–281, 2011.

20th EAWE PhD Seminar on Wind Energy
24-26 September 2024
Visby, Sweden

AC Energy Islands for the optimal integration of offshore wind energy resources: Operation Strategies using Multi-Objective Nonlinear Programming

Mario Useche-Arteaga[a,b], **Oriol Gomis-Bellmunt**[a], **Marc Cheah**[a], **Vinicius Lacerda**[a], and **Pieter Gebraad**[b]

[a]Centre d'Innovació Tecnològica en Convertidors Estàtics i Accionaments, Departament d'Enginyeria Elèctrica, Universitat Politècnica de Catalunya, Barcelona, Spain.
[b]Youwind Renewables, Barcelona, Spain.

E-mail: mario.useche@upc.edu

Keywords: Energy islands, energy storage systems, high-voltage transmission systems, hydrogen Production, offshore wind energy, wind power integration.

Energy islands refer to systems located in artificial offshore structures or natural islands that serve as a point of connection for offshore energy and facilitate the interconnection of those assets to onshore grids. These systems have emerged as a promising solution for the integration of large amount of offshore wind generation capacity into power systems. Such islands also could incorporate responsive infrastructure such as energy storage and hydrogen production systems, which can contribute to a flexible and adaptive power system that can efficiently respond to wind power intermittency, power grid constraints and curtailments. AC energy islands could be particularly cost-benefit effective for short distances between wind power parks and onshore grids. However, the implementation of AC energy islands require reactive power compensation systems to maintain voltage stability and reduce power losses. This research develops optimal operation strategies for AC energy islands through the optimal reactive power dispatch, as well as the optimal management of battery energy storage systems (BESS), hydrogen production systems and active power dispatch of offshore wind power systems. The research proposed to address the optimal operation of AC energy islands as follows: i) a nonlinear approach for controlling the reactive power compensation systems and addressing the grid power system model, thermal line constraints, and safety operational limits; ii) a finite horizon mathematical programming approach for the optimal management of battery energy storage and hydrogen production systems; and iii) a multi-objective programming approach for maximizing the active power delivered to the onshore power grid while minimizing the nodal voltage deviations simultaneously.

1 Optimal Real and Reactive Power Dispatch of AC Energy Islands

High Voltage Alternating Current (HVAC) systems have been the dominant technology in power systems, and therefore, there is extensive knowledge concerning their development, operation, and continuous technological evolution, positioning them as the best techno-economic solution for the majority of power system applications. Nevertheless, this technology faces challenges in the implementation of transmission systems for energy islands [2]. In such applications, the capacitive effect of cables utilized in underwater transmission systems could substantially elevates their currents, voltage deviations and power losses. Specifically, the losses incurred by HVAC systems are intrinsically linked to reactive power flows, which escalate significantly in offshore systems [1]. In such scenarios, the capacitive effect of cables utilized in underwater transmission systems substantially elevates their currents.Therefore, reactive power compensation systems and control strategies are imperative to maintain voltage stability and reduce power losses. This section presents the proposed mathematical programming model for the optimal operation of the AC energy island shown in Fig. 1.

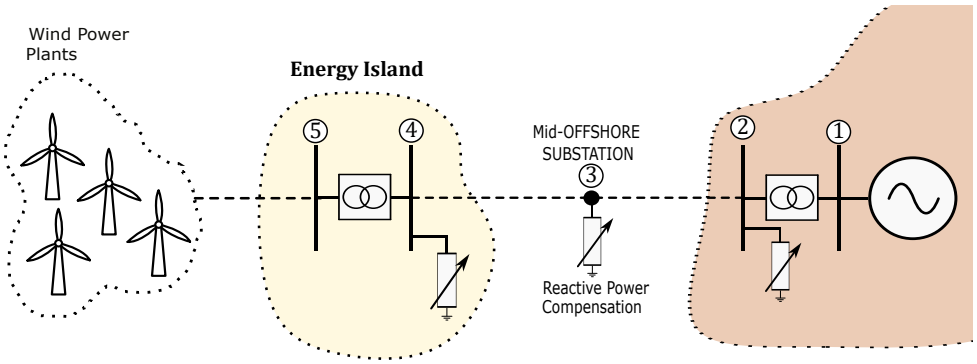

Figure 1: AC Energy Island Test System.

1.1 Objective Function

The objective function proposed for the optimal operation of the energy islands shown in Fig. 1 is presented in (1). This objective function aims to maximize the active power injected into the onshore grid at node 1.

$$\max \sum_{t=t_i}^{t_f} \Re(s_g(t)) \tag{1}$$

1.2 Constraints: Grid Model

The approach proposed in this research considered the Grid model by using the nonlinear power flow equations in the polar representation, separating the power balance equations in their real and imaginary parts. Specifically, by utilizing the polar representation of nodal voltages ($v_k = V_k \angle \theta_k$), we derive equations (2)-(3).

$$P_k = V_k \sum_m (y_{km} V_m [g_{km} cos(\theta_k - \theta_m) + b_{km} sin(\theta_k - \theta_m)]) \tag{2}$$

$$Q_k = V_k \sum_m (y_{km} V_m [g_{km} sin(\theta_k - \theta_m) - b_{km} cos(\theta_k - \theta_m)]) \tag{3}$$

where P_k is the entry k of the active power vector $P = [P_g, 0, 0, 0, P_w]$. Similarly, Q_k is the entry k of the reactive power vector $Q = [Q_g, Q_{on}, Q_l, Q_{off}, Q_w]$. In addition, P_g and Q_g represents the slack active and reactive power, respectively. Q_{on} is the reactive power compensation in the onshore substation, Q_l is the mid-offshore substation reactive power compensation, Q_{off} is the reactive power compensation in the offshore substation and Q_w is the reactive power dispatched by the energy island. In addition, the nodal voltage constraints are model through the equations (4)-(5).

$$v_g = 1.0 \tag{4}$$

$$v_{min} \leq \|v_k\| \leq v_{max} \tag{5}$$

1.3 Constraints: Nominal Power Limits

The optimization model for the energy island may also consider the constraints imposed by nominal power of the reactive power compensation systems and power electronics converters. These constraints are model through the set of equations (6)-(12):

$$\Re(s_w) \leq f(t).P_{wpp}^{nom} \tag{6}$$

$$\|s_w(t)\| \leq s_w^{max} \tag{7}$$

$$Q_g \leq Q_g^{max} \tag{8}$$

$$Q_{on} \leq Q_{on}^{max} \tag{9}$$

$$Q_l \leq Q_l^{max} \tag{10}$$

$$Q_{off} \leq Q_{off}^{max} \tag{11}$$

$$i_{km}(t) \leq i_{km}^{max}(t) \tag{12}$$

where the set of equations (8)-(11) are the reactive power compensation limits. The set of constraints (6) and (7) represents the wind power availability constraint and the apparent power constraint of the wind power plant, respectively. In addition, $f(t)$ is the wind power availability function in p.u. for the period t. The set of equations (12) represents the thermal transmission lines constraints, which are defined in the following equations:

$$i_{imag} = B_{sh}V_k cos(\theta_k) + G_{km}V_m sin(\theta_k) - G_{km}V_m sin(\theta_m) + B_{km}V_k cos(\theta_k) - B_{km}V_m cos(\theta_m)$$
$$i_{real} = -B_{sh}V_k sin(\theta_k) + G_{km}V_k cos(\theta_k) + G_{km}V_m cos(\theta_m) - B_{km}V_k sin(\theta_k) + B_{km}V_m sin(\theta_m)$$
$$i_{km}^2 = i_{imag}^2 + i_{real}^2; \quad i_{km} \leq i_{km}^{max}$$

2 Optimal management of Battery Energy Storage and Hydrogen Production Systems: A Finite Horizon Mathematical Approach

Battery energy storage and hydrogen production are dynamic systems that require a time horizon control approach. In this context, finite horizon mathematical programming over predicted time windows emerges as a suitable approach for the optimal management of battery energy storage and hydrogen production systems. The main idea of this approach is to use predicted values of wind power availability and power demand to determine the optimal operation actions for BESS and hydrogen production using a mathematical programming model over the predicted time window. This process could be applied in the real-time operation of energy islands using a rolling horizon strategy. Consequently, the models for incorporating BESS (Battery Energy Storage Systems) and hydrogen production systems in the proposed optimal operation of AC energy islands are presented in the following subsections.

2.1 BESS Model

The model proposed for the energy storage system uses two decision variables for charging and discharging power rates, p^c and p^d respectively. The model proposed also considers the charging and discharging efficiency rates of energy storage (η^c and η^d). The full model is presented in the set of equations (13)-(18):

$$e(t) = e(t-1) + \eta^c p^c(t) - \frac{1}{\eta^d} p^d(t) \tag{13}$$
$$e(t = t_{ini}) = E_0 \tag{14}$$
$$e(t = t_{fin}) = E_f \tag{15}$$
$$\underline{E} \leq e(t) \leq \bar{E} \tag{16}$$
$$0 \leq p^c(t) \leq \bar{P}^c \tag{17}$$
$$0 \leq p^d(t) \leq \bar{P}^d \tag{18}$$

where e is the state of energy (SoE), E_0 is the initial state of energy, E_f is the final state of energy, $\underline{E}$ is the minimum energy storage capacity, $\bar{E}$ is the maximum energy storage capacity, $\bar{P}^c$ is the maximum power charging rate and $\bar{P}^d$ is the maximum power discharging rate. In addition, conventional Battery Energy Storage Systems (BESS) have integrated power converters, which have the capacity to control the reactive power. This capacity could be used as a control variable in our optimization problem to support reactive power requirements of power systems, which is included in our approach considering the apparent power limits of the power converter.

2.2 Green Hydrogen Production Models

Green hydrogen is usually produced through alkaline electrolizers. This hydrogen production equipment exhibits non-linear behaviours. Different approaches has been proposed for modeling the green hydrogen production, which includes constant efficiency models, polynomial approximations, piece-wise linear approximations and convex approximations. This work considers a linear model for the hydrogen production system, which is based on the model proposed in reference [3]. The model is presented in the as follows:

$$h(t) = (P/\eta^e).r(t) \tag{19}$$

where $h(t)$ is the hydrogen produced at period t, P is the rated power of the electrolyzer, η^e is the efficiency of the electrolizer, defined as the energy required to produce 1 kg of hydrogen, and $r(t)$ is the hourly load factor of the electrolyzer at period t.

3 Multi-Objective Optimization

Since the thermal limits of the transmission lines impose a constraint for a maximum current, the power injected into the grid could be increased by increasing the nodal voltages. However, power systems elements and loads are designed to work close to the nominal voltage, therefore it is important for the operation of the system to reduce voltage deviations. This problem represents a multi-objective programming model with non-dominated objective functions, where no single objective can be improved without worsening another. This type of mathematical programming problems could be address through the Pareto front concept. The Pareto front concept can be applied in our optimization model using the weighting factor α, as shown in the multi-objective function (20).

$$\max \ \alpha.F_P + (1-\alpha).F_V \tag{20}$$

where the F_P is the objective function for maximizing the active power injected into the onshore grid and F_V is the objective function regarding the voltage deviation. It is important to highlight that the sign of the objective function F_V is changed in order to include the minimization of the voltage deviation.

$$F_P = \frac{\sum_{t=t_i}^{t_f} \Re(s_g(t))}{\sum_{t=t_i}^{t_f} \left(f(t).P_{wpp}^{nom}\right)} \tag{21}$$

$$F_V = -\frac{\sum_{t=t_i}^{t_f} \sum_{k=1}^{N} \|v_k(t) - v_{max}\|}{\tau \sum_{k=1}^{N} \left(\|v_k^{nom} - v_{max}\|\right)} \tag{22}$$

where τ is the time window length of the proposed approach, v_k^{nom} is the nominal voltage at node k and v_{max} is the maximum allowed voltage deviation. In order to get the most convenient weighting factor for the optimal operation of AC energy islands, the Pareto front is constructed by varying the weighting factor from 0% to 100%.

4 Results and Conclusions

This research proposed a multi-objective nonlinear programming strategy for optimizing the operation of AC energy islands with the objective of addressing curtailments associated with power flow constraints, maximizing power generation injected into the onshore power system and minimizes nodal voltage deviations. The strategy applies a nonlinear approach for controlling the reactive power compensation systems and a finite horizon approach for the optimal management battery energy storage and hydrogen production systems. The results demonstrate that BESS and Hydrogen production are effective solutions for addressing the power curtailments imposed by thermal power line limits and grid constraints. In addition, the results demonstrate that proposed strategy significantly reduces the nodal voltage deviations while maximizing the power injected into the onshore grid, demonstrating that the proposed reactive-active power dispatch and the rolling finite horizon approach are suitable for the optimal operation of AC Energy islands.

References

[1] J. Dakic, M. Cheah-Mane, O. Gomis-Bellmunt, and E. Prieto-Araujo. Hvac transmission system for offshore wind power plants including mid-cable reactive power compensation: Optimal design and comparison to vsc-hvdc transmission. *IEEE Transactions on Power Delivery*, 36(5):2814–2824, 2021.

[2] M. Jansen, C. Duffy, T. C. Green, and I. Staffell. Island in the sea: The prospects and impacts of an offshore wind power hub in the north sea. *Advances in Applied Energy*, 6:100090, 2022.

[3] G. Matute, J. Yusta, J. Beyza, and L. Correas. Multi-state techno-economic model for optimal dispatch of grid connected hydrogen electrolysis systems operating under dynamic conditions. *International Journal of Hydrogen Energy*, 46(2):1449–1460, 2021.

TOPIC 8

Support structures and geotechnics

8.1 Session 215: Support structures and geotechnics

25.09.2024, 13:0, Room 5

Chair:

Ansh Patel

Presenters:

Vandegar Gabriel	Modeling structural damage for ship collisions against spar floating offshore wind turbines using a deep learning approach
Abdullah Mahmoud	A Supervised Data-Driven Methodology for Damage Classification in Jacket-Type Wind-Turbine Foundations
Reinhardt Tim	Ensuring accurate modal properties of blades for the estimation of the second tower mode in offshore wind turbines
Eichner Lukas	LUKAS' JACKET: A test structure for model and monitoring based lifetime management of offshore jacket support structures
Nordtorp Frederik	Force Control in Hybrid Testing

20^{th} EAWE PhD Seminar on Wind Energy
24-26 September 2024
Visby, Sweden

Modeling structural damage for ship collisions against spar floating offshore wind turbines using a deep learning approach

Gabriel Vandegar, **Priscilla Salazar L**, and **Philippe Rigo**

ANAST, Department of ArGEnCo, University of Liège, Belgium

E-mail: gvandegar@uliege.be

Keywords: Ship Collisions, Offshore Wind Turbines, Finite Element Analysis, Neural Network

1 Introduction

Despite the promising prospects of floating offshore wind farming, its widespread deployment is not without challenges. Currently, a few collision cases between ships and offshore wind turbines (OWT) have been reported. One example is the drifting of a rudderless cargo ship into the Hollandse Kust Zuid offshore wind farm in the Dutch North Sea during a storm [1] (Figure 1a). Similarly, a cargo ship collided with a OWT installed at the German Gode Wind farm [2] (Figure 1b). As floating wind farms expand, the likelihood of collisions between ships and floating offshore wind turbines (FOWT) is expected to increase. The consequences of such collisions can be significant, on the ship's side, perforation of tanks resulting in pollution or even an explosion in the case of a methane tanker or a hydrogen-propelled ship. On the side of the wind farms, local damage on the turbine support structure, collapse of the entire tower, rupture of the anchoring lines leading to the drift of the platform and a collision with other wind turbines in the park.

Analyzing the structural impacts of such accidents is critical for the wind energy industry, and these are currently evaluated using the nonlinear finite element method (NLFEM). Although the NLFEM allows for a high-fidelity representation of the complex physical phenomena that take place in a ship-FOWT collision event, including large deformations, plasticity, complex contact, and fluid-structure interaction (Figures 2a and 2b), its implementation remains challenging in terms of computation time and the expertise needed for model preparation. Simplified methods are thus very useful to assess the damage of both the striking ship and the struck offshore wind turbine, especially at the preliminary design stage associated with risk assessment, where structural optimization and damage stability analysis require simulating hundreds of collision scenarios involving different striking ships and impact conditions. [3].

Figure 1a: A 37200-tons rudderless cargo ship drifted into the HollandseKustZuid offshore windfarm in the Dutch North Sea. [1]

Figure 1b: The cargo ship Petra L. stroke an offshore wind turbine at GodeWind 1 wind farm (Germany). [2]

This study presents and compares two different approaches to rapidly estimate the elasto-plastic response of a spar FOWT subjected to ship collision. A series of preliminary NLFEM simulations are performed to build a

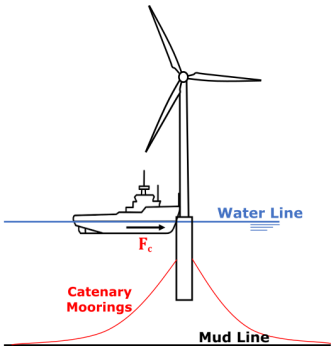

Figure 2a: Schematic representation of the main components to consider when studying ship-FOWT collision. [4]

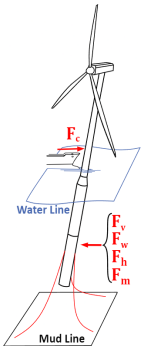

Figure 2b: Schematic representation of the main interactions occurring in the system during a ship-FOWT collision. [4]

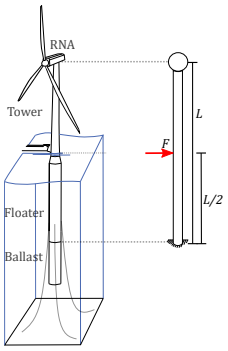

Figure 2c: Schematic representation of the simplifications done on the proposed models. [4]

database and establish what is considered in this work as the ground truth to train, validate and compare the two proposed approaches. The first, is the development of an analytical model based on existing formulations developed following the so-called Super Element (SE) method [5] and validated with observations from the NLFEM results. The second, is the development of a neural network (NN) model trained with the results obtained by the NLFEM simulations. Finally, the resulting force-penetration and energy balance curves computed with both models are compared to NLFEM results showing that the NN model provides good approximations in most cases, while the SE model's performance is limited to certain conditions.

2 Description of the Models

2.1 Analytical model

The analytical model, or the SE model, is an iterative algorithm where at each iteration, the contact force between the FOWT's tower and the striking ship is computed as a function of the penetration of the striking ship into the FOWT. Three distinct deformation phases are considered: (i) Local elastic indentation at the contact zone; (ii) Local plastic indentation; and (iii) Buckling mechanism at the base of the FOWT tower. For each phase, analytical formulae are derived to compute the contact force. The inputs of this model are geometrical data of the tower (radius R, thickness t, and height L) and material properties of the FOWT tower, as well as the mass and the initial velocity of the ship. The outputs are the history plot of the force, kinetic energy of the ship, internal energy of the FOWT, and penetration of the ship into the FOWT. The SE model is fully described in [4].

2.2 Neural network model

The deep learning model follows the Transformer architecture introduced in [6]. This architecture is renowned for its effectiveness in handling sequential data, particularly in the context of natural language processing. However, its versatility makes it suitable for various other applications, including sequence estimation tasks. The model is developed and trained to estimate the history plot of the force, kinetic energy of the ship, internal energy of the FOWT, overall displacement of the ship, local crushing of the FOWT's tower, and global bending of the FOWT. The inputs used by the NN model are the same as those of the SE model, with the addition of the impact position. The SE model is limited to mid-length impact, so this additional input will ensure more versatility for NN model.

3 Numerical experiments

The NLFEM simulations are performed for collisions of ships against spar floaters, considering different geometries of the floater by varying the radius R, thickness t, and height L, rotor nacelle assembly (RNA) mass m_{RNA}, impact location h, ship mass m_{ship}, impact velocity v_{ship}, and material yielding strength σ_y. The variables are randomly selected in the range presented in Table 1.

Simplifications of the FOWT and ship were used in this preliminary study to reduce the simulation time as a large amount of data is required for training neural networks. The hydrodynamics are not incorporated in the NLFEM simulations, and the ship was modeled as a perfectly rigid wedge. Similarly, the ballast of the spar FOWT

was assumed to be rigid. The FOWT tower was simplified to a cantilever tube with a tip mass representing the RNA at its free end (Figure 2c), a common assumption in the structural design of OWTs and fixed offshore platforms [7, 8]. Details on the numerical model used in this study can be found in [4]. Approximately 1000 numerical simulations were conducted using LS-DYNA software to generate the necessary data to train the NN model where the outputs are structured as sequences, with each sequence consisting of 201 equally spaced points representing the time domain between 0 and 10 seconds. This approach ensures that the temporal evolution of the outputs is comprehensively captured over the duration of the event.

Table 1: Choice of the parameters used to generate the dataset

	R [m]	t [mm]	L [m]	m_{RNA} [tons]	σ_y [MPa]	v_{ship} [m/s]	m_{ship} [tons]	h [%]
min	2.5	30	100	272	235	0.5	6000	25
max	5	60	200	820	390	5	24000	70

4 Results

Hereafter is an example of the results obtained for collisions between a 6000-ton offshore service vessel (OSV) colliding into the NREL 5MW OC3 FOWT with initial ship velocities of 2 m/s and 5 m/s. The FOWT geometrical dimensions are a radius of 3.5 m, a wall thickness of 39 mm, a length of 140 m, and a RNA mass of 350 tons. The two proposed approaches are evaluated using the coefficient of determination, commonly referred to as R^2. The computed score for each model is given in Table 2 (δ, δ_{loc}, δ_{glo}, U_{fowt}, and K_{ship} denote the overall penetration, the local penetration, the global penetration, the internal energy of the FOWT, and the kinetic energy of the ship respectively.). In addition, the history plots of the computed outputs are given in Figures 3 and 4 for impact at 2 m/s and 5 m/s, respectively.

Table 2: Comparison of R^2 scores, expressed as percentages, for the SE model and the NN model relative to the numerical model.

Velocity [m/s]	Force		δ		δ_{loc}		δ_{glo}		U_{fowt}		K_{ship}	
	SE	NN	SE	NN	SE	NN	SE	NN	SE	NN	SE	NN
2	82.9	85.3	99.7	99.6	-	96.0	-	71.5	98.2	99.7	99.4	99.9
5	0.0	77.5	92.8	99.0	-	82.0	-	95.4	86.1	99.8	98.1	99.8

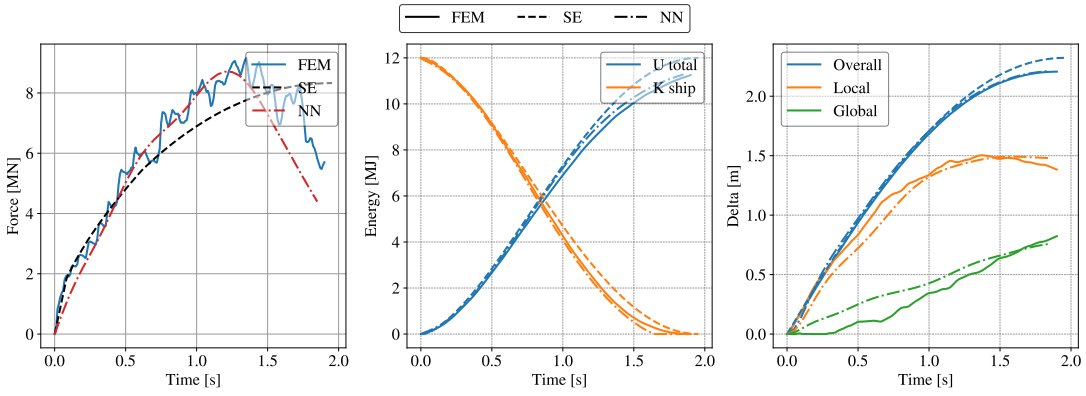

Figure 3: Comparison of the history plot of the force, energy balance, and penetration obtained numerically, with the SE model and with the NN model for a 2 m/s impact at mid-length.

As depicted in Figures 3 and 4, both models generally yield satisfactory results, yet the NN model appears to outperform the SE model overall. The NN model is able to differentiate between local and global penetration, while the SE model combines the two deformations. Additionally, the NN model can estimate collisions along the entire length of the FOWT's tower, whereas the SE model is limited to impacts at mid-length.

It is important to note that the results presented here are selected to highlight both accurate and less accurate approximations by the SE model. Generally, the SE model was found to perform poorly for FOWT towers with an

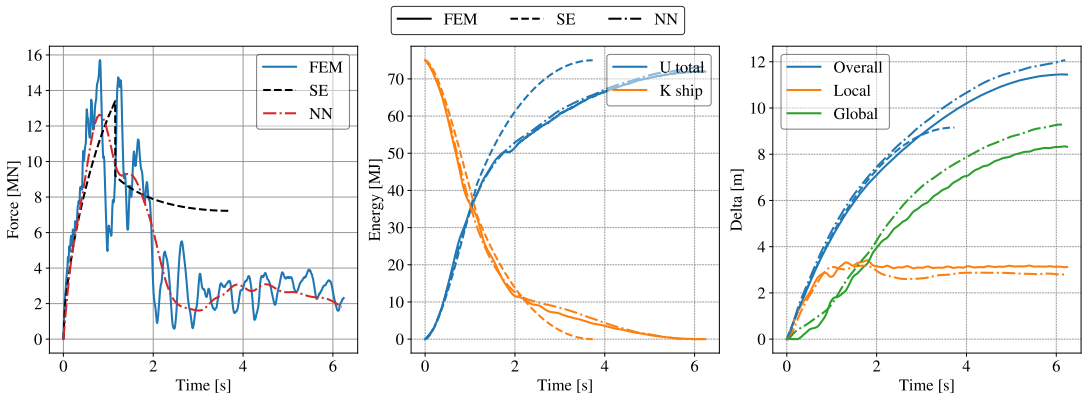

Figure 4: Comparison of the history plot of the force, energy balance, and penetration obtained numerically, with the SE model and with the NN model for a 5 m/s impact at mid-length.

aspect ratio of $length/radius < 15$. On the other hand, the NN model's performance remained consistent across various configurations.

5 Conclusion

Two simplified approaches to assess the crashworthiness of FOWTs are presented: one based on the SE method and the other employing a NN model trained with numerical results. The comparative analysis showed that both models can approximate the contact force, energy dissipation, and damage done to the FOWT's tower. However, the NN model has more versatility due to its broader range of application and, in most cases, more accurate performance than the SE model.

Additionally, it should be noted that the NN model trained with NLFEM simulations relies not only on access to specialized software but also on the expertise required to perform these simulations correctly. In other words, the NN model is only as reliable as the numerical model used for its training.

References

[1] Margientimmer. Rudderless Julietta D causes damage to foundation of wind farm Hollandse Kust Zuid - Windpark Hollandse Kust South., 9 2022.

[2] J. O. Mandra. Cargo ship strikes turbine at Orsted's Gode Wind 1 offshore wind farm, suffers massive damage, 5 2023.

[3] S. Echeverry. *Numerical and analytical study of a spar-like floating offshore wind turbine impacted by a ship*. PhD thesis, University of Liege, 2021.

[4] I. Ladeira, S. Echeverry, and H. Le Sourne. A simplified method to assess the elasto-plastic response of standalone tubular offshore wind turbine supports subjected to ship impact. *Ocean Engineering*, 279:114313, 2023.

[5] H. Le Sourne, N. Besnard, C. Cheylan, and N. Buannic. A ship collision analysis program based on upper bound solutions and coupled with a large rotational ship movement analysis tool. *Journal of Applied Mathematics*, 2012.

[6] A. Vaswani, N. Shazeer, N. Parmar, J. Uszkoreit, L. Jones, A. N. Gomez, L. Kaiser, and I. Polosukhin. Attention is all you need. *CoRR*, 2017.

[7] W. Tong. *Wind power generation and wind turbine design*. WIT press, 2010.

[8] J. Travanca and H. Hao. Dynamics of steel offshore platforms under ship impact. *Applied Ocean Research*, 47:352–372, 2014.

A Supervised Data-Driven Methodology for Damage Classification in Jacket-Type Wind-Turbine Foundations

Mahmoud Abdullah*[1], Abdollah Malekjafarian[1], and Ramin Ghiasi[1]

[1]Structural Dynamics and Assessment Laboratory, School of Civil Engineering, University College Dublin, Dublin, Ireland – Ireland

Abstract

Structural health monitoring (SHM) of offshore structures offers a promising approach to detect and diagnose structural damage promptly, making it paramount for their development. This paper introduces a robust data-driven framework for detecting structural damage in offshore jacket foundations. The methodology involves a comprehensive process including data preprocessing, data segmentation, feature extraction, and selection, as well as the application of supervised machine learning algorithms for damage detection. Experimental acceleration response data from eight triaxial sensors mounted on a laboratory model of offshore jacket structure under healthy and damaged conditions are utilized. Data from 20 experiments is segmented into various time windows to capture the structural response over time. The statistical features are extracted from segmented data, and then the top ten features with the highest variance are selected using the Analysis of Variance (ANOVA) algorithm. The features extracted from a healthy state and three damage states of loosening the bolt under two noise conditions are used for the training and testing of the classification model. To ensure robustness damage detection, four classification algorithms of naïve Bayes (NB), K-Nearest Neighbour (KNN), Support Vector Machine (SVM), and Artificial Neural Network (ANN) are employed. The results demonstrate the efficiency of the proposed methodology in predicting the damage type in offshore jacket structures, with performance measures exceeding approximately 97.5%. Additionally, the study indicates the capacity of the indicated classification algorithms to identify structural damage types under various wind speeds, ensuring accurate real-time prediction.

*Speaker

20th EAWE PhD Seminar on Wind Energy
24-26 September 2024
Visby, Sweden

Ensuring accurate modal properties of blades for the estimation of the second tower mode in offshore wind turbines

T Reinhardt[a], **C Sastre Jurado**[a,b], **W Weijtjens**[a], and **C Devriendt**[a]

[a]Vrije Universiteit Brussel, OWI-lab, Pleinlaan 2, Elsene, 1050, Belgium
[b]UGent, Geotechnical Laboratory, Technologiepark 68, Zwijnaarde, 9052, Belgium

E-mail: tim.reinhardt@vub.be

Keywords: blade scaling, digital twin, structural modelling

1 Introduction

The structural design of offshore wind turbines is typically driven by the fatigue limit state. In the past a mismatch was observed between measured and the as-designed eigenfrequencies of offshore wind turbines with monopile foundations [1]. For the first tower mode this mismatch was reduced through the enhancement of the soil-structure interaction modelling in the Pisa project [2], [3]. However, a mismatch in the second tower mode still persisted resulting from the modelling approach of the rotor nacelle assembly [4], see Figure 1. Monitoring strategies such as scour monitoring [5] can be improved when this mode is also taken into account. Moreover, the second tower mode gains relevancy in the fatigue design of offshore wind turbines subjected to sea ice loading [6].

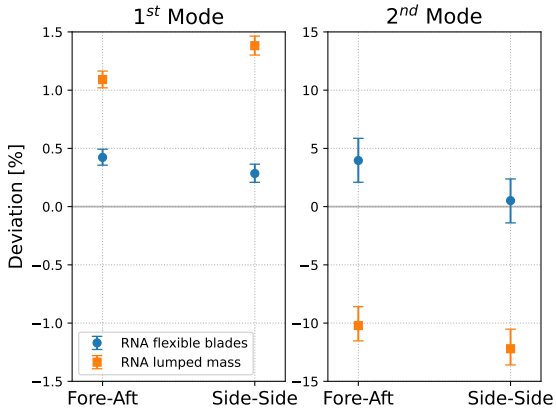

Figure 1: Comparison between lumped mass and flexible blades modelling of the RNA [4].

In foundation design the fatigue limit is typically assessed modelling the rotor nacelle assembly as a lumped mass; neglecting the flexibility of the blades. A significant challenge for inclusion of flexible blades in foundation design models is the lack of blade properties available from turbine manufactures. Alternatively, blades of reference turbines can be used. However, reference turbine blades might not agree with the design philosophy of the turbine manufacturers raising the question; how can the properties of reference turbine blades be scaled to fit the modal properties of their counterpart on the actual turbine?

In this contribution, two approaches to scale reference blades are investigated to answer this question. The first approach is based on reevaluating blade scaling laws by including the technological evolution of reference blade design into account, while the second approach seeks to scale the blade properties to match the modal properties of the actual blade known from measurements.

2 Integrated finite element model of the turbine

The structural model of the wind turbine is set up through the finite element solver *OpenSees* [7] using the *Python*-interpreter *OpenSeesPy* [8]. The substructure is modelled using Timoshenko beams to account for combined bending and shear deformations. Effects of enclosed and added water are simplified as nodal lumped masses that are evenly distributed along the water depth.

A linear elastic foundation model is assumed for the monopile foundation, based on the 1D *PISA* design method [2]. The initial soil stiffness is assumed, as the scope of this contribution is limited to the computation of eigenfrequencies in parked condition of the turbine.

The blades are modelled using beam elements connected to the rotor hub node. Each beam element has a constant cross section with cross sectional properties being derived from given blade properties. Rotor hub and nacelle node are linked via beam elements with rigid flexibility to a master node. The master node itself is linked to the tower top node via a rigid link.

3 Ensuring accurate modal dynamics of the blades

Two approaches are investigated, to ensure that the scaled reference blades included in the turbine model have a similar modal dynamic behaviour as their real life counterpart.

The first approach relies solely on the scaling of reference blades. Technological advances in blade design render scaling based on rules of similarity overly conservative, see for example the scaling of the blade mass in Table 1 and Figure 2. Therefore, updated scaling laws will be derived for the blade properties from the evolution of blades of common reference turbines. An advantage of this approach is that neither the exact blade properties nor measurements are needed. However, this approach fails to take differences in the design philosophies in blade design into account and might thus not be able to completely fit the modal properties of the blades of the real life turbine.

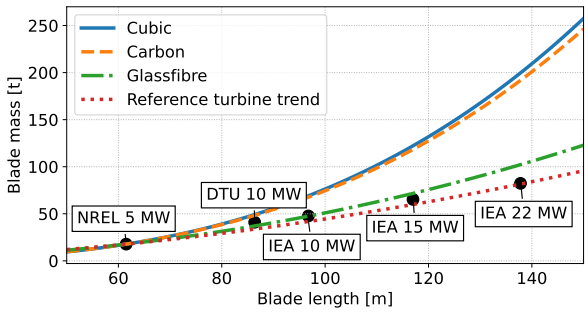

Figure 2: Scaling approaches for blade mass.

Table 1: Geometric scaling factors n_l for blade mass

Scaling rule	Scaling factor
Cubic	n_l^3
Carbon	$n_l^{2.95}$
Glasfibre	$n_l^{2.17}$
Reference turbine trend	$n_l^{1.89}$

Instead of scaling laws, the scaling factors in the second approach are used to tune the properties of the reference blade to match the blade modes in measurements of the real life turbine. This approach is able to overcome any difference in design philosophy between the reference and real life blade. However, measurements might not always be available, especially in the design process.

Both approaches will be benchmarked with measurements of an offshore wind turbine in the Belgian North Sea.

Acknowledgements

The authors would like to acknowledge the support of the Belgian Ministry of Economic Affairs through the ETF project WINDSOIL. The support of VLAIO through the De Blauwe Cluster SBO SOILTWIN project is also acknowledged.

References

[1] D Kallehave, B W Byrne, C LeBlanc Thilsted, and K Kousgaard Mikkelsen. Optimization of monopiles for offshore wind turbines. *Philosophical Transactions of the Royal Society A: Mathematical, Physical and Engineering Sciences*, 373:20140100, 2015.

[2] B W Byrne, G T Houlsby, H J Burd, K G Gavin, D J P Igoe, R J Jardine, C M. Martin, R A McAdam, D M Potts, D M G Taborda, and L Zdravković. Pisa design model for monopiles for offshore wind turbines: application to a stiff glacial clay till. *Géotechnique*, 70(11):1030–1047, 2020.

[3] C Sastre Jurado, B Stuyts, W Weijtjens, and C Devriendt. Impact of calibrated soil-monopile-interaction model on resonance frequencies. *Journal of Physics: Conference Series*, 2265:032098, 2022.

[4] T Reinhardt, C Sastre Jurado, W Weijtjens, and C Devriendt. On the influence of rotor nacelle assembly modelling on the computed eigenfrequencies of offshore wind turbines. *Journal of Physics: Conference Series*, 2767(5):052034, 2024.

[5] M Weil, C Sastre Jurado, M Chaar, K Winkler, W Weijtjens, and C Devriendt. Quantifiable scour detection for offshore wind turbines using resonance frequency monitoring and a digital twin. In *Proceedings of the 14th International Workshop on Structural Health Monitoring*, page 2739 – 2749, 2023.

[6] T C Hammer, T Willems, and H Hendrikse. Dynamic ice loads for offshore wind support structure design. *Marine Structures*, 87:103335, 2023.

[7] F McKenna. Opensees: A framework for earthquake engineering simulation. *Computing in Science & Engineering*, 13(4):58–66, 2011.

[8] M Zhu, F McKenna, and M Scott. Openseespy: Python library for the opensees finite element framework. *SoftwareX*, 7:6–11, 2018.

LUKAS' JACKET: A test structure for model and monitoring based lifetime management of offshore jacket support structures

Lukas Eichner[a,b]

[a] Bundesanstalt für Materialforschung und -prüfung (BAM)
[b] Technische Universität Berlin

E-mail: lukas.eichner@bam.de

Keywords: offshore jacket support structure; test structure; fatigue life; lifetime management; risk-based inspection; maintenance planning; structural health monitoring

The current generation of offshore wind turbines has a planned operational lifetime of 20 to 25 years. Throughout this duration, all components of the assets, including the support structures, are intended to operate reliably. Design specifications for these structures are determined to maintain the system within defined reliability limits. The design focuses on fatigue aspects, as the structures are subjected to cyclic loads from wind and waves. Particularly at the joints of jacket support structures made of steel, damage from fatigue loading must be considered. Welded joints connect the hollow tube profiles, leading to highly stressed points known as hotspots. These locations are therefore focal points in the recurring inspections, as well as other inspection and monitoring procedures conducted on site. As part of operation and maintenance (O&M), these costly, and sometimes safety-critical, measures contribute to the operational expenditures (OPEX) of an installation. The proportion of costs from O&M costs to the levelized cost of energy (LCoE) of an offshore wind farm ranges from 15% to 30% [1]. Therefore, wind farm operators are interested in optimizing inspection and maintenance planning [2]. This work aims to contribute to this goal by applying scientific methods experimentally to a realistic test structure.

Figure 1: Jacket support structure in offshore wind farm Borkum Riffgrund 2 (Source: Ørsted).

At the EAWE PhD Seminar 2023, the author presented the design of such a test structure, called LUKAS' JACKET. The structure represents a scaled-down version of a jacket support structure of an offshore wind turbine,

such as those found in the Borkum Riffgrund 2 wind farm (see Figure 1:). Chords and braces connect the three legs of the structure on each side, resulting in several different nodes. The designed structure represents one level of the "multi-story" frame and, with a height of 2.30 meters and a leg spacing of 1.92 meters, is scaled at a ratio of 1:10 to reality (see Figure 2:, left). The test structure has since been manufactured and prepared for initial experiments (see Figure 2:, right). This contribution aims to provide an update on the status of the structure and to introduce the models and methods behind the experimental execution.

Figure 2: Design of test structure (left) / Manufactured test structure at BAM test facility with removed X joint (right).

The goal of the experiments is to demonstrate that systems like three-dimensional jackets possess redundancies that, despite the reduced fatigue life of individual components, enable reliable operation if an appropriate maintenance concept is in place. In practice, individual potentially faulty components in the structure have been handled conservatively so far. To move away from this approach, methods and strategies in the field of life cycle management that enable economically optimal and reliable operation must be transferred from scientific research to practice. Experiments are the preferred method to establish the proof of concept.

Figure 3: Facility setup for horizontal cyclic loading of test structure (left) / Removable Y joints (middle) / Manufactured test structure at BAM test facility with removable joints inserted (right).

To realistically simulate the operational lifetime of a jacket structure through an experiment, cyclic loads must be applied to the structure to replicate typical fatigue processes (see Figure 3:, left). To ensure that the test structure is not a "disposable product" and can undergo multiple test cycles, the experimental concept includes system-level and component-level tests. The latter are conducted on removable joints (see Figure 3:, middle). These elements at the nodes of the structure have been manufactured in multiple variations, both to potentially contain mentioned flaws and to undergo more load cycles individually than the main structure. Once the removable joint is sufficiently pre-damaged and thus the reduced remaining fatigue life is established, the element is inserted into the overall structure (see Figure 3:, right). The defined maintenance strategy is then implemented on the entire system. This strategy consists of structural health monitoring (SHM), inspections, and repairs. At defined intervals, cyclic

loading is interrupted to apply dynamic loads. Using the installed monitoring system and coupled operational modal analysis (OMA), the modal parameters of the structure are determined, which can help identify potential system damage [3]. Optimal sensor placement (OSP) can be determined based on a maximum value of information (VoI) across the entire pre-posterior predicted service life [4]. For detailed investigations at the hotspots, inspections are conducted using non-destructive methods, among others. Overall global and local information about the structure's condition is gathered these methods, which are then incorporated into models describing the structure through Bayesian updating (see Figure 4:) [5, 6, 7]. This allows for initial system identification based on different system responses and later updating of the predicted parameters of analytical and numerical models. Utilizing the updated models, decisions regarding maintenance actions, such as further inspections or repairs, are made, which are subject to uncertainties. The probabilistic models enable a reliability- and risk-based maintenance strategy, where, for example, maximum failure rates can act as triggers for maintenance actions. These decisions are relevant for the planned duration of the simulated operational lifetime, as well as for potential lifetime extensions, which are currently of significant importance in practice. Optimizing the maintenance strategy for the operational lifetime of the structures with these methods will lead to a higher utility of the offshore wind farm.

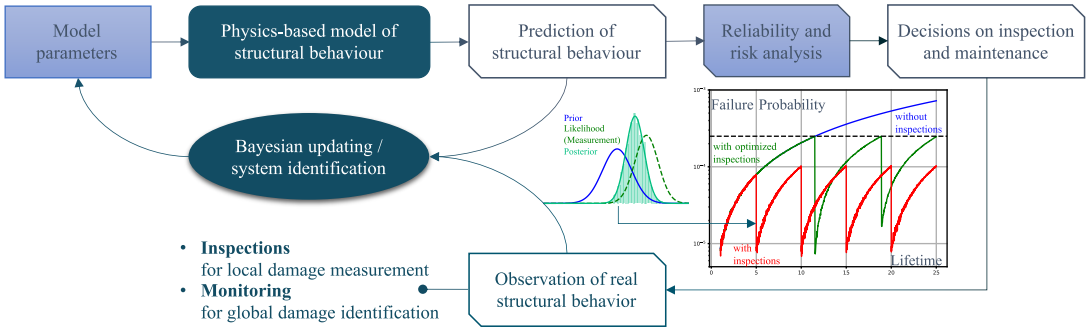

Figure 4: Framework for reliability- and risk-based maintenance planning using structural models updated with information from maintenance measures (adopted from [8]).

The work associated with the test structure encompasses a variety of topics (including fatigue, damage detection and identification, reliability, Bayesian updating, system identification, SHM, maintenance planning, decisions under uncertainties), which are integrated through corresponding models and methods. All these models have been and are being applied in the numerical accompaniment of the experiments. By applying them to a structure that includes the relevant locations and aspects of real-world structures, both well-functioning and suboptimal parts of the established framework will be revealed.

Acknowledgements

The author thanks Professor Yuri Petryna from Technische Universität Berlin for supervision and Ronald Schneider and Matthias Baeßler from BAM for their help during the doctoral studies.

References

1. S. Ambühl and J. D. Sørensen. *Sensitivity of Risk-Based Maintenance Planning of Offshore Wind Turbine Farms.* Energies. **10**(4): p. 505, 2017.
2. M. Farhan, R. Schneider, S. Thöns and M. Gündel. *Probabilistic cost modeling as a basis for optimizing the inspection and maintenance of support structures in offshore wind farms (Preprint).* Wind Energy Science. 2024.
3. B. Peeters and G. de Roeck. *Stochastic System Identification for Operational Modal Analysis: A Review.* Journal of Dynamic Systems, Measurement and Control. **123**(4): p. 659-667, 2001.

4. L. Eichner, R. Schneider and M. Baeßler. *Optimal vibration sensor placement for jacket support structures of offshore wind turbines based on value of information analysis.* Ocean Engineering. **288**(2): p. 115407, 2023.
5. M. W. Vanik, J. L. Beck and S. K. Au. *Bayesian Probabilistic Approach to Structural Health Monitoring.* Journal of Engineering Mechanics. **126**(7): p. 738-745, 2000.
6. J. L. Beck and S. K. Au. *Bayesian updating of structural models and reliability using markov chain monte carlo simulation.* Journal of Engineering Mechanics. **128**(4), 2002.
7. R. Schneider, S. Thöns and D. Straub. *Reliability analysis and updating of deteriorating systems with subset simulation.* Structural Safety. **64**: p. 20-36, 2017.
8. L. Eichner, R. Schneider, P. Simon and M. Baeßler. *Optimal sensor placement for vibration-based structural health monitoring obtained via value of information analysis as part of a digital structural integrity management of offshore structures*. in *3rd International Conference on Health Monitoring of Civil & Maritime Structures (HeaMES 2022)*, 2022.

20th EAWE PhD Seminar on Wind Energy
24-26 September 2024
Visby, Sweden

Force Control in Hybrid Testing

Frederik Nordtorp[a], **Elif Ecem Baş**[b], **Cláudio Ângelo Gonçalves Gomes**[c], and **Giuseppe Abbiati**[a]

[a]Department of Civil and Architectural Engineering, Aarhus University, Denmark
[b]R&D Test Systems A/S, Hinnerup, Denmark
[c]Department of Electrical and Computer Engineering, Aarhus University, Denmark

E-mail: fnk@cae.au.dk

Keywords: Hybrid testing, hardware-in-the-loop testing, force control, differential algebraic equation

1 Introduction

The evolution of wind turbine (WT) technology has led to a complication in the structural testing of increasingly larger components and efficient experimental methods are needed. Hybrid testing (HT), which is also called hardware-in-the-loop testing, is an experimental method that allows testing a physical substructure (PS) of an engineering system while simulating its interaction with the rest of the system in a numerical substructure (NS). The methodology was originally proposed for the purpose of seismic testing of civil engineering structures.

Recent improvements in actuation have facilitated HT of WT components. Sauder et al. [3] apply physical hydrodynamic loading on floaters within an ocean basin while simulating the rest of the floating wind turbine. Likewise, Belloli et al. [2] propose the application of physical aerodynamic loading on rotor systems within wind tunnels, while simulating hydrodynamic loads on floaters. In the majority of work related to hybrid testing, the PS is tested in displacement control mode. Specifically position commands are sent to a test setup, while force feedback is fed back to the coordination algorithm. A coordination algorithm which could be either a time-integration or control scheme ensures that NS and PS are in equilibrium and coupling conditions (for example displacement compatibility) are verified.

There are fewer examples of HT in force control mode. In the author's opinion, this is because position control is safer than force control, and actuation systems are designed to operate in displacement control mode. However, for PS that have stiffness of a similar order of magnitude as the stiffness of the actuation system, position control is problematic. This system is typically subjected to very small displacements so the compliance of the actuation system as well as the noise of feedback signals are not negligible. In this case, it is recognized by the HT community, that force control mode shall be adopted.

This extended abstract presents a force control hybrid testing framework for the structural testing of wind turbine components. The numerical framework is intended to simulate multi-body dynamic hybrid models. However, in this work, the validation of the framework is conducted on a linear dynamical system. The PS is tested using a small-scale single-degree-of-freedom test bench for a double mass-spring-damper system.

2 Coordination algorithm for force control

The coordination algorithm for force-controlled hybrid testing is applied to derive a hybrid model for a simplified system. Specifically, the framework is demonstrated for a two-mass-spring-damper system, where one spring is represented by a PS, as shown in Figure 1.

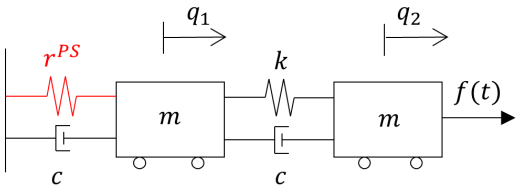

Figure 1: Hybrid model of double mass-spring-damper system

In this system, q_1 and q_2 are the generalized coordinates for the horizontal translation of the masses m. The damping coefficient is denoted by c, and f represents a force acting on the second mass. The stiffness of the springs is defined by k, but for the PS, the restoring force from the stiffness is represented by λ.

This restoring force is commanded from the NS to the PS within a pseudo-dynamic time-scheme, with position feedback p_λ^{PS} being fed back into the NS, as illustrated in Figure 2

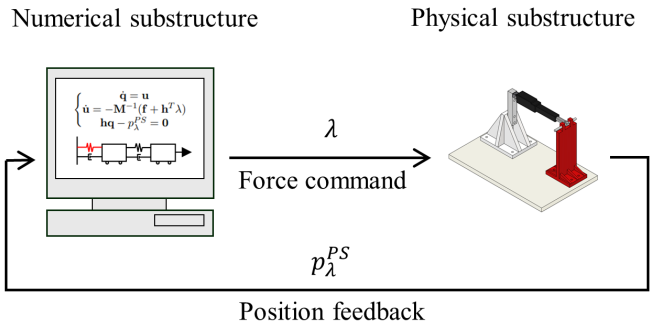

Figure 2: Schematic overview of force-controlled hybrid test

The coordination algorithm enables the NS to compute a force command from position feedback by introducing the restoring force as a Lagrange multiplier λ into the state-space equation, constraining the position feedback. This results in the differential algebraic equation (DAE),

$$\begin{cases} \dot{\mathbf{q}} = \mathbf{u} \\ \dot{\mathbf{u}} = -\mathbf{M}^{-1}(\mathbf{f} + \mathbf{h}^T \lambda) \\ \mathbf{hq} - p_\lambda^{PS} = 0 \end{cases} \tag{1}$$

where $\mathbf{h}$ is a mapping vector. The mass matrix $\mathbf{M}$ and the generalized force vector $\mathbf{f}$ are for the specific case defined as,

$$\mathbf{M} = \begin{bmatrix} 2m & m \\ m & m \end{bmatrix}, \quad \mathbf{f} = \begin{bmatrix} cu_1 - f \\ cu_2 - f + kq_2 \end{bmatrix} \tag{2}$$

To solve the Heesenberg index-2 DAE [1] and transform it back into a differential equation, the first and second time derivative of the constraint in (1) are taken,

$$\mathbf{hu} - v_\lambda^{PS} = 0 \tag{3}$$

$$-\mathbf{hM}^{-1}\mathbf{f} - \mathbf{hM}^{-1}\mathbf{h}^T\lambda - a_\lambda^{PS} = 0 \tag{4}$$

where v_λ^{PS} and a_λ^{PS} are constraints on the velocity and acceleration, respectively.

Using the Baumgarte stabilization theorem to avoid the drift-off phenomena, which is present for (4), it is summed with weighted contributions from (1) and (3),

$$-\mathbf{hM}^{-1}\mathbf{f} - \mathbf{hM}^{-1}\mathbf{h}^T\lambda - a_\lambda^{PS} + \gamma_2(\mathbf{hu} - v_\lambda^{PS}) + \gamma_1(\mathbf{hq} - p_\lambda^{PS}) = 0 \tag{5}$$

where tuning parameters γ_1 and γ_2 are chosen as $\gamma_1^2 = 2\gamma_2$ for critical damping. Baumgarte highlights that a suitable choice of tuning parameters should be attained from numerical experiments.

Finally, the Lagrange multiplier λ, representing the restoring force command, is isolated in (5),

$$\lambda = (\mathbf{h}\mathbf{M}^{-1}\mathbf{h}^T)^{-1}\left(-\mathbf{h}\mathbf{M}^{-1}\mathbf{f} - a_\lambda^{PS} + \gamma_2(\mathbf{h}\mathbf{u} - v_\lambda^{PS}) + \gamma_1(\mathbf{h}\mathbf{q} - p_\lambda^{PS})\right) \tag{6}$$

Applying the expression for the restoring force from (6), the DAE in (7) transforms into the state-space equation,

$$\begin{cases} \dot{\mathbf{q}} = \mathbf{u} \\ \dot{\mathbf{u}} = -\mathbf{M}^{-1}(\mathbf{f} + \mathbf{h}^T(\mathbf{h}\mathbf{M}^{-1}\mathbf{h}^T)^{-1}\left(-\mathbf{h}\mathbf{M}^{-1}\mathbf{f} - a_\lambda^{PS} + \gamma_2(\mathbf{h}\mathbf{u} - v_\lambda^{PS}) + \gamma_1(\mathbf{h}\mathbf{q} - p_\lambda^{PS})\right)) \end{cases} \tag{7}$$

The computation of a restoring force command requires position, velocity, and acceleration feedback. Since only position feedback is available from the PS, velocities and accelerations are approximated based on recent position feedback p_λ^{PS} and previous generalized coordinates $\mathbf{q}_{i-2}$-$\mathbf{q}_i$ and speeds $\mathbf{u}_{i-2}$-$\mathbf{u}_i$ obtained from simulation results. Using least square regression of a cubic polynomial from the trajectory history, the specific constants $\hat{A}$, $\hat{B}$, $\hat{C}$ and $\hat{D}$ are obtained by,

$$\hat{A},\hat{B},\hat{C},\hat{D} = \min_{A,B,C,D} \left\| \begin{bmatrix} p(-2\Delta t) - \mathbf{h}\mathbf{q}_{i-2} \\ \frac{d}{dt}p(-2\Delta t) - \mathbf{h}\mathbf{u}_{i-2} \\ p(-\Delta t) - \mathbf{h}\mathbf{q}_{i-1} \\ \frac{d}{dt}p(-\Delta t) - \mathbf{h}\mathbf{u}_{i-1} \\ p(0) - \mathbf{h}\mathbf{q}_i \\ \frac{d}{dt}p(0) - \mathbf{h}\mathbf{u}_i \\ 100(p(\Delta t) - p^{PS}) \end{bmatrix} \right\|, \qquad p(t) = At^3 + Bt^2 + Ct + D \tag{8}$$

where Δt is the time-step.

Based on the specific cubic polynomial parameters, the velocity v_λ^{PS} and acceleration a_λ^{PS} feedback are derived,

$$v_\lambda^{PS} = \frac{d}{dt}p(\Delta t), \qquad a_\lambda^{PS} = \frac{d^2}{dt^2}p(\Delta t) \tag{9}$$

3 Experimental implementation of pseudo-dynamic hybrid test

The hybrid model has been implemented on a small-scale single-degree-of-freedom test bench at Aarhus University. The PS is represented by a 3D printed PLA cantilever beam with dimensions $8 \times 50 \times 100mm$. The tip of the cantilever beam is subjected to displacements by an electromechanical mini-actuator, and a force transducer measures the restoring force.

Using an Arduino UNO Wifi board, the actuator position is managed in an iterative loop to achieve the target restoring force. This forms a force-controlled setup capable of sending force commands and receiving position feedback, which can be operated from a Python environment. An image of the test setup is presented in Figure 3.

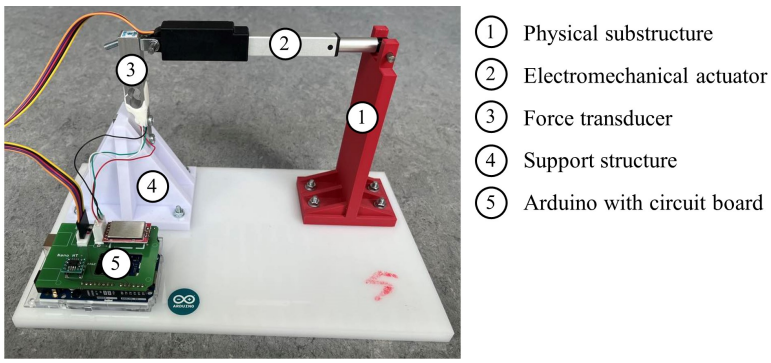

Figure 3: Small-scale single-degree-of-freedom test-bench for hybrid testing at Aarhus University

For the hybrid model the mass $m = 0.5kg$, the damping $c = 5.0\frac{Ns}{m}$, the stiffness $k = 3780\frac{N}{m}$ and the load $f = 8N$. The equation of motion was solved using a 2^{nd} order Runge-Kutta time integration scheme with a fixed time step of $h = 1\ ms$.

4 Results and discussion

To verify the hybrid model and tune the parameters γ_1 and γ_2, a dummy HT was conducted where the PS was temporally substituted by a NS with $p_\lambda^{NS} = -\lambda/k$. During this process, the tuning parameters were adjusted, and the results from the dummy hybrid test were compared to a numerical simulation of the same system. A fairly good match was achieved with $\gamma_1 = 100$ and $\gamma_2 = 2500$. Applying the same tuning parameters, the results for a force controlled hybrid test are presented in Figure 4.

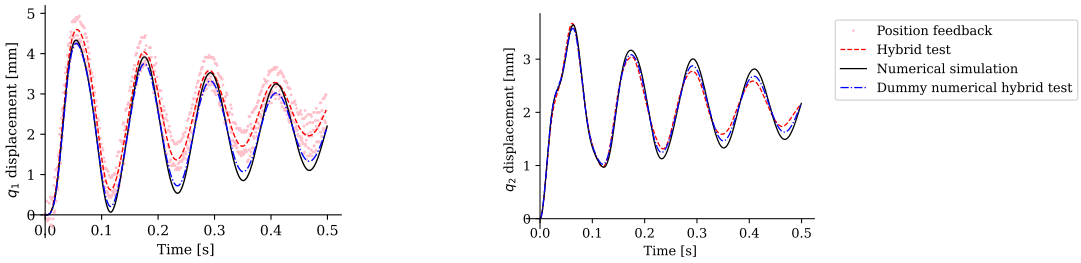

(a) (b)

Figure 4: Simulation and test results for a) q_1 and b) q_2

Overall, the hybrid test shows a fairly good agreement with the numerical simulation, despite a significant amount of noise from the test-bench. The noise could originate from inaccuracies in the force transducer response, which distort the control loop at each time step. Another indication of a successful coordination algorithm is the close match between the dummy hybrid test and the numerical simulation. This match improves further with a smaller time step.

5 Conclusion

The presented coordination algorithm successfully linked the NS to the PS in force control mode. The implemented HT achieved fairly good agreement with numerical simulations, despite noise from the test setup. The dummy hybrid test further confirmed the algorithm's effectiveness, but emphasised the hurdle of picking the tuning parameters.

References

[1] U. M. Ascher and L. R. Petzold. *Computer Methods for Ordinary Differential Equations and Differential-Algebraic Equations*. Society for Industrial and Applied Mathematics, USA, 1st edition, 1998.

[2] M. Belloli, I. Bayati, A. Facchinetti, A. Fontanella, H. Giberti, F. La Mura, F. Taruffi, and A. Zasso. A hybrid methodology for wind tunnel testing of floating offshore wind turbines. *Ocean Engineering*, 210:107592, 2020.

[3] T. Sauder, V. Chabaud, M. Thys, E. Bachynski-Polić, and L. Sæther. Real-time hybrid model testing of a braceless semi-submersible wind turbine: Part i — the hybrid approach. 06 2016.

8.2 Session 322: Support structures and geotechnics

26.09.2024, 10:30, Room 2

Chair:

Jean Bastin

Presenters:

Sudhakaran Nikhil	Assessing True Brinelling and Its Implications for Wind Turbine Bearings
Petry Alice	Challenges with ice basin tests for offshore wind turbine substructures in Arctic conditions
Napier Aidan	Load mitigation devices for wind turbine supports and foundations – an early feasibility study

20th EAWE PhD Seminar on Wind Energy
24 - 26 September 2023
Visby, Sweden

Assessing True Brinelling and Its Implications for Wind Turbine Bearings

Nikhil Sudhakaran[a], Yi Guo[a], Asger Bech Abrahamsen[a]

[a] DTU Wind and Energy Systems, Frederiksborgvej 399 DK- 4000 Roskilde
E-mail: niksu@dtu.dk

Keywords: wind turbine bearings, true brinelling, experimental testing

1 Introduction

Roller bearings are essential elements for the operation of wind turbines because failures of any of these bearings can cause detrimental damage to the turbine. Therefore, understanding bearing life and failure mechanisms is critical. One primary failure mode is true brinelling, which occurs under extreme loads, causing indents or regions of plastic deformations in bearing subcomponents such as the raceway[1]. This failure mode is particularly relevant for wind turbine pitch and main shaft bearings due to increased loads caused by scaling up the rotor diameter of modern wind turbines[2], [3].

2 Methodology

2.1 Indentation Standardisation

This study investigates the impact of true brinelling on bearing performance and lifespan. To achieve this, bearing life tests will be conducted on both indented and non-indented bearings. Initially, the indentation process will be standardised by applying a fixed load to a roller placed on the raceway of the bearing to ensure reproducibility. The indent formed will also be studied using optical microscopes to understand its variance using the same applied load and compared with Finite element modelling of the expected deformation of the raceway

2.2 Bearing Lifetime Tests

The experiments are carried out for a cylindrical thrust roller bearings on two FE8 test rigs, which will rotate the bearing at T ~ 100 ºC at 100-250 rpm and constant axial loads of F = 50-80 kN until an accelerometer will indicate a bearing damage as an increased vibration level. These tests will be repeated under varying load levels and with different lubricants to explore the relationship between applied load, lubricant type, and bearing failure due to indentations.

3 Analysis and outcomes

The test results will be analysed to evaluate the impact of indentations on bearing performance, focusing on metrics such as bearing lifetime under different load and lubrication conditions. Additionally, the failure modes will be examined by visually inspecting the surfaces of bearing components and assessing the roughness of damaged parts.

Overall, this study investigates how indentations affect bearing life and performance, contributing to a better understanding of bearing failures and preventing them in wind turbines.

20th EAWE PhD Seminar on Wind Energy
24 - 26 September 2023
Visby, Sweden

References

[1] "ISO 15243:2017 - Rolling bearings — Damage and failures — Terms, characteristics and causes." Accessed: Jun. 21, 2024. [Online]. Available: https://www.iso.org/standard/59619.html

[2] J. Kenworthy *et al.*, "Wind turbine main bearing rating lives as determined by IEC 61400-1 and ISO 281: A critical review and exploratory case study," *Wind Energy*, vol. 27, no. 2, pp. 179–197, Feb. 2024, doi: 10.1002/WE.2883.

[3] A. Rezaei, Y. Guo, J. Keller, and A. R. Nejad, "Effects of wind field characteristics on pitch bearing reliability: a case study of 5 MW reference wind turbine at onshore and offshore sites," *Forschung im Ingenieurwesen/Engineering Research*, vol. 87, no. 1, pp. 321–338, Mar. 2023, doi: 10.1007/S10010-023-00654-X

20th EAWE PhD Seminar on Wind Energy
24-26 September 2024
Visby, Sweden

Recent developments in model-scale ice basin experiments for offshore wind turbine substructures

Alice Petry[a] and **Arttu Polojärvi**[a]

[a]Aalto University, School of Engineering, Department of Mechanical Engineering, FI-00076 Aalto, Finland

E-mail: alice.petry@aalto.fi

Keywords: Substructure design, ice loads, model-scale experiments

Introduction

Finland plans to expand its offshore wind production capacity. The European Commission estimates Finland's offshore wind potential to be 8 GW [6]. The Gulf of Bothnia has been identified as a well-suited area for large scale wind power deployment [23], despite the occurrence of sea ice [7]. A recent analysis suggests that the ice conditions in the Northern Baltic Sea are too severe for monopile foundations [22]. The planned offshore wind turbines may require substructures fitted with ice mitigating measures, such as ice cones. Possible substructures include sloping gravity-based structures (GBS) or jacket and monopile structures fitted with ice cones (Figure 1).

Ice actions from drifting sea ice and ridges can result in large loads on offshore structures. Turbine substructures and foundations need to be designed to withstand the possible ice conditions. Design load estimates require knowledge of the local ice conditions, e.g., level ice thickness with a 50-year return period, as outlined in IEC-61400-3 [13]. Consequently, accurate met-ocean conditions at the planned wind farm site are needed. To complicate the matter, connecting given ice conditions to ice loads on offshore wind turbines remains a challenge. Some ice load data exists for hydrocarbon extraction platforms (e.g., [5]), lighthouses (e.g., [16]), and navigational aids (e.g., [15]) in the Baltic Sea. Offshore wind turbines face different challenges, as they are slender and flexible, which makes them prone to ice-induced vibrations [11]. Existing design experience stems from smaller offshore wind turbines located in the Southern Baltic Sea with relatively light ice conditions, or from the Bohai Sea [24].

Model-scale ice basin experiments can be used to address some of these challenges, such as estimating expected loads and the occurrence and severity of ice-induced vibrations, in a controlled and systematic manner. This paper discusses some developments in ice basin model-scale experiments for offshore wind turbine substructures.

Figure 1: Three substructures with ice cones: a) GBS at Tahkoluoto [20], b) GBS of a 0.5 MW wind turbine at Tunoe Knob [17], c) jacket substructure with two ice cones at Baltic 2 [12].

Methods

The Aalto Ice and Wave Tank (Figure 2) is a water basin equipped with a cooling system to produce model sea ice [1]. The basin is 40 m by 40 m in area and 2.8 m deep. The ice is generated from a water-ethanol mixture,

which freezes with reduced flexural and compressive strength (in comparison to sea ice). To grow the model ice, the water mixture is sprayed layer-by-layer at an ambient temperature of $-16\,^{\circ}\mathrm{C}$ to $-10\,^{\circ}\mathrm{C}$. Once the model ice has the target thickness, it is kept at an ambient temperature of $-11\,^{\circ}\mathrm{C}$ until it has reached the desired strength. The ice is then tempered at $-2\,^{\circ}\mathrm{C}$ to $0\,^{\circ}\mathrm{C}$ to maintain the desired ice properties during the testing day. The final model ice has a fine-grained microstructure. The mechanical properties of model ice are measured following the guidelines of the International Towing Tank Committee (ITTC) [14]. It is typical to record the ice thickness, strain modulus, flexural strength, and compressive strength throughout the testing day.

The targeted mechanical properties of the model ice and the design of the structure model depend on the chosen scaling factor for the planned experiments. These scaling laws are often derived using dimensional analysis. The goal of scaling is to maintain geometric, kinematic, and dynamic similarity. Most experiments that focus on conical substructures use a scaling law based on the dimensionless Froude and Cauchy numbers. Froude similitude maintains the ratio between inertial forces and gravitational forces, while Cauchy similitude maintains the ratio between elastic forces and inertial forces. Consequently, it is assumed that ice deforms elastically until failure, and that gravity and ice-structure interaction velocity play a role in the ice failure process.

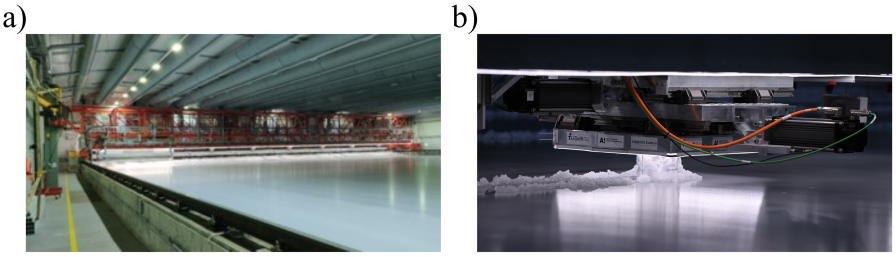

Figure 2: a) Aalto Ice and Wave Tank with an ice sheet, b) hybrid test setup with a cylindrical structure model.

Results and discussion

The scalability of a model-scale experiment relies on the scalability of the model ice and the ice-structure interaction. Froude and Cauchy scaling focuses on scaling the strength of the model ice, even though not all strength measurements are repeatable. For example, the compressive strength of ice can depend on the size of the indenter [14] and the testing method [3]. Flexural strength measurements are less dependent on specimen size and testing method [19]. Moreover, it may not be possible to scale the flexural strength and the compressive strength at the same time. As a result, the ratio of compressive strength to flexural strength can differ from the expected ratio, which might cause the ice to fail in a different failure mode than expected.

The ice-ice and ice-structure friction coefficients may also be different for model ice and for sea ice. When ice fails against wide conical structures, large rubble piles can form which affect the load on the structure. This was observed at the Kemi-I lighthouse in the Bay of Bothnia [4] which has a width comparable to monopile foundations. Forming the rubble piles in a laboratory scale experiment is challenging, likely due to a low ice-ice friction coefficient. Note that friction coefficients are not scaled under Froude and Cauchy scaling.

Challenges related to scaling model ice properties force researchers to make compromises when designing experiments. For example, even though the ice-structure friction coefficient should remain unchanged, model structures may be made of different materials than the full-scale structure for manufacturing convenience, e.g., using wooden cones [2] or 3D-printed conical [18] and cylindrical [8] structures. Earlier research on dynamic ice-structure interaction have included connecting the structure model to a compliant support [2], [21] or using a flexible structure model [25]. A drawback of such techniques is that they often only take into account one possible natural frequency of the structure. Recent experiments used a hybrid test setup (Figure 2) based on replica modelling [9] to study the dynamic response of an offshore wind turbine with a cylindrical waterline profile [10]. This setup can take into account multiple natural frequencies of a structure, which makes it possible to observe multi-modal ice-induced vibrations.

Lastly, there is no universal set of scaling laws, as they depend on the chosen research questions. Froude and Cauchy scaling is an example of a set of scaling laws which can be applied to rigid conical structures where the

ice is expected to fail predominately in bending. Recent experiments studying ice-induced vibrations of offshore wind turbines with monopile substructures proposed a new set of scaling laws based on a theoretical understanding of the energy transfer during ice-structure interaction [8]. These scaling laws focus on scaling ice behaviour as opposed to ice strength. The scaling constant is based on the mean brittle crushing load level in full-scale and in model-scale. The use of mean crushing load, as opposed to the compressive strength of ice, circumvents known problems in the availability and repeatability of compressive strength measurements.

Conclusion

Ice basin tests and model-scale experiments are useful techniques to understand ice interaction with offshore wind turbine substructures. The challenges presented above are (1) differences in the mechanical properties and the behaviour of model ice and sea ice, and (2) limited variety in tested (and validated) scaling laws. Recent developments in the design of model structures and new scaling laws are promising avenues to improve estimates of ice loads and dynamic ice-structure interaction. In addition to the continued development of model ice and structure models, future research should focus on exploring new scaling laws to investigate dynamic ice-structure interaction on conical structures and to study ice loads related to various ice conditions, including those related to ice ridges.

Acknowledgements

The authors wish to acknowledge funding from the European Union–NextGenerationEU instrument through Research Council of Finland under grant number (348586) WindySea – Modelling engine to design, assess environmental impacts, and operate wind farms for ice-covered waters. A Petry would like to thank Vegard Hornnes for proofreading this paper during a nice cabin trip to Eastern Finland.

References

[1] Aalto University. Aalto ice and wave tank. `https://www.aalto.fi/en/iwt`, Apr 2018. Accessed: 28.06.2024.

[2] A. Barker, G. Timco, H. Gravesen, and P. Vølund. Ice loading on Danish wind turbines: Part 1: Dynamic model tests. *Cold regions science and technology*, 41(1):1–23, 2005.

[3] A. M. Böhm, H. Herrnring, and F. von Bock und Polach. Lessons learned: The influence of testing properties on uniaxial compression tests of ice. In *Proceedings of the ASME 2022 41st International Conference on Ocean, Offshore and Arctic Engineering: June 5-10, Hamburg, Germany*, volume 6: Polar and Arctic Sciences and Technology. V006T07A019. ASME, 2022.

[4] T. G. Brown and M. Määttänen. Comparison of Kemi-I and Confederation Bridge cone ice load measurement results. *Cold Regions Science and Technology*, 55(1):3–13, 2009.

[5] A. Cornett and G. Timco. Ice loads on an elastic model of the Molikpaq. *Applied ocean research*, 20(1-2):105–118, 1998.

[6] European Commission and Directorate-General for Energy. *Study on Baltic offshore wind energy cooperation under BEMIP – Final report*. Publications Office, 2019. `https://data.europa.eu/doi/10.2833/864823`.

[7] M. Granskog, H. Kaartokallio, H. Kuosa, D. N. Thomas, and J. Vainio. Sea ice in the Baltic Sea – A review. *Estuarine, coastal and shelf science*, 70(1-2):145–160, 2006.

[8] T. C. Hammer, O. Puolakka, and H. Hendrikse. Scaling ice-induced vibrations by combining replica modeling and preservation of kinematics. *Cold Regions Science and Technology*, 220:104127, 2024.

[9] T. C. Hammer, C. van Beek, J. Koning, and H. Hendrikse. A 2d test setup for scaled real-time hybrid tests of dynamic ice-structure interaction. In *Proceedings of the 26th International Conference on Port and Ocean Engineering under Arctic Conditions: June 14-18, 2021, Moscow, Russia*. POAC, 2021.

[10] T. C. Hammer, T. Willems, and H. Hendrikse. Dynamic ice loads for offshore wind support structure design. *Marine Structures*, 87:103335, 2023.

[11] H. Hendrikse and T. S. Nord. Dynamic response of an offshore structure interacting with an ice floe failing in crushing. *Marine Structures*, 65:271–290, 2019.

[12] J. Hoek. Dynamic ice-structure interaction for jacket substructures - Fig. 1-3. MSc thesis, Delft University of Technology, 2021.

[13] International Electrotechnical Commission. *Wind energy generation systems - Part 3-1: Design requirements for fixed offshore wind turbines*, 5 2019. IEC 61400-3-1:2019.

[14] International Towing Tank Conference. *ITTC Quality System Manual - Recommended Procedures and Guidelines - Procedure - Test Methods for Model Ice Properties - 7.5-02-04-02*, 6 2021. Rev. 03.

[15] M. Määttänen and E. Järvinen. Baltic aids-to-navigation ice-induced vibration measurements 2003. *Report, Helsinki University of Technology*, 2003.

[16] T. S. Nord, I. Samardžija, H. Hendrikse, M. Bjerkås, K. V. Høyland, and H. Li. Ice-induced vibrations of the Norströmsgrund lighthouse. *Cold Regions Science and Technology*, 155:237–251, 2018.

[17] N.-E. Ottesen Hansen and H. Gravesen. Engineering practice for ice force design in denmark. In *Proceedings of the 16th International Conference on Port and Ocean Engineering under Arctic Conditions: August 12-17, 2001, Ottawa, Canada*. POAC, 2001.

[18] A. Petry, T. Hammer, A. Polojärvi, H. Hendrikse, and O. Puolakka. Ice basin experiments on mixed-mode failure on ice cones. In *Proceedings of the 27th International Conference on Port and Ocean Engineering under Arctic Conditions: June 12-14, 2024, Glasgow, Scotland*. POAC, 2023.

[19] A. Petry, M. Suominen, R. Matala, T. Skogström, and E. Seppänen. Impact of testing method on measured flexural strength of model-scale ice. In *Proceedings of the 27th International Conference on Port and Ocean Engineering under Arctic Conditions: June 12-14, 2024, Glasgow, Scotland*. POAC, 2023.

[20] Suomen Hyötytuuli Oy. ImageBank - Merituuli. `https://media.hyotytuuli.fi/category/20`, 6 2022. Accessed: 28.06.2024.

[21] Y. Tian and Y. Huang. The dynamic ice loads on conical structures. *Ocean Engineering*, 59:37–46, 2013.

[22] F. L. van der Stap, M. B. Nielsen, C. C. Owen, P. van der Male, and H. Hendrikse. On the feasibility of monopile foundations for offshore wind in the baltic sea. In *Proceedings of the 27th International Conference on Port and Ocean Engineering under Arctic Conditions: June 12-14, 2024, Glasgow, Scotland*. POAC, 2023.

[23] E. A. Virtanen, J. Lappalainen, M. Nurmi, M. Viitasalo, M. Tikanmäki, J. Heinonen, E. Atlaskin, M. Kallasvuo, H. Tikkanen, and A. Moilanen. Balancing profitability of energy production, societal impacts and biodiversity in offshore wind farm design. *Renewable and Sustainable Energy Reviews*, 158:112087, 2022.

[24] G. Wang, D. Zhang, Q. Yue, and S. Yu. Study on the dynamic ice load of offshore wind turbines with installed ice-breaking cones in cold regions. *Energies*, 15(9):3357, 2022.

[25] N. Xu, Q. Yue, X. Bi, K. Tuomo, and D. Zhang. Experimental study of dynamic conical ice force. *Cold Regions Science and Technology*, 120:21–29, 2015.

Load mitigation devices for wind turbine supports and foundations – an early feasibility study

Aidan Napier [a], Abbas Mehrad Kazemi Amiri 2[a], Luis Recalde-Camchao 3[a], Matthew Cole 4[a], Euan Brough 5[a]

[a] University of Strathclyde

E-mail: aidan.napier.2021@uni.strath.ac.uk

Keywords: Wind Turbine, Foundation, Damping, Isolator, Load Mitigation, FEA

1 Introduction:

With the increase in wind turbine size to meet higher renewable energy demand, larger turbines are exposed to higher ultimate loads, which require larger structural support or load mitigation techniques through load dampening devices, load isolation devices or through control mechanisms. The main aim of this project is to investigate the feasibility of the adaptation and novel application of base isolation-damper device(s) for the mitigation of the ultimate and fatigue loads acting on the wind turbines foundation structure. Energy dissipative devices have been widely used in the past to protect infrastructure and improve lifetime performance. Potential advantages of this technology in the context of wind energy application can be viewed from the ultimate and fatigue loads perspectives, where the former will be beneficial to the design of the geotechnical foundations and latter to the tower and support structures, in terms of cost-effectiveness of manufacturing by reducing weight, welding demand, whilst reducing the requirements of maintenance, transport and installation.

The use of load mitigation in all man-made infrastructure can be found in bridges, buildings and space exploration structures, used to reduce loads for improved structural integrity and reduced cost. Historically, wind turbines have explored the use of tower mass dampers, tuned liquid dampers, brace systems [1] and many more systems which implore active, semi active and passive dampening or isolating devices. Paolo Di (2021) recently proposed a Rotational friction dampener, as seen in figure 1, which can reduce loads up to 40% of bending moment, this was numerically assessed against the NREL 5MW turbine models. Other unique systems of self-centring and moment resisting frames used for earthquake fatigue load mitigation have been explored [2 and 3] for application in the project. However, the primary focus will be to identify more dampeners that have yet to be applied to wind turbines, spanning from new elastoplastic compounds to new methods of restraint at the connection point.

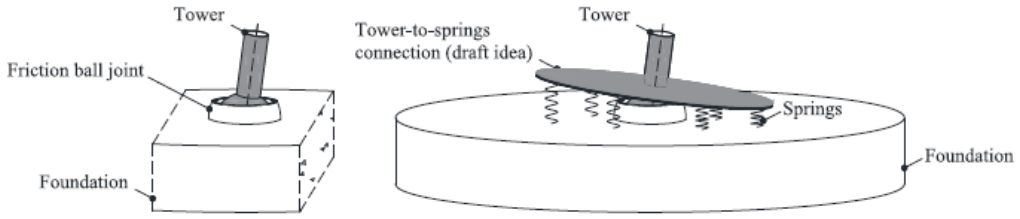

Fig. 4. Draft idea of a 3D setup for real world applications.

Figure 1: Di Paolo RFD concept [1]

2 Project objectives and Methodology:

The study will focus on the adaptation for parametric design and application of load mitigation tower-base connection devices such as structural isolator connections for turbine tower and foundation. With quantitative assessment of the connection device and review of potential other load isolation devices the project further aims to detect how to improve the device's performance, possibly through combination of devices that work based on different energy dissipation mechanics. The primary objective is then to produce a computational model of the load mitigation devices which will indicate which device has the largest load reduction in tower base bending moment, maximum shear forces and tower top acceleration. The model will be designed in an FEA tool (Ansys) and calibrated against an aerodynamic Bladed model. The overall outcome of the study is to identify and quantify the effects of using load mitigation devices on wind turbine loads for the purpose of extending life of towers or reutilising foundations for repowering of existing power plants [1].

The project methodology is as follows:

- Review literature on existing and novel structural isolators and dampening device application in structural and mechanical engineering.
- Create FEA model of candidate damper devices based on its design parameters and/or characteristic curves and integration with the turbine tower and foundation equipped with the damper device/ devices for assessment against an aeroelastic turbine loading regime.
- Assess, ascertain parameters and recommend guidance for improving performance of damper device under turbine loading that are obtained from an existing aeroelastic turbine model in Bladed aerodynamic model and FEA models.

With the project taking shape from previous work done to identify which load mitigation techniques are the most favourable for a wind turbine tower. This project will utilise turbine rotor hub loads models from an existing multi-MW turbine aeroelastic model and load analysis results from previous work to inform the direction and load mitigation systems to be focused on. Whereby, new finite element model representative for turbine tower (with and without connection devices) will be created, these models will be numerically tested against ultimate and fatigue loads to investigate alleviation of the bending moment, shear force and displacement load absorption or mitigation. It is well expected that such devices are capable of reducing the turbine loads on the tower and foundation. However, the extent and effectiveness of load mitigation need to be closely studied within this project for recommendations on the practical feasibility and device performance enhancement.

Acknowledgements:

Acknowledgements, thank you to the EPSRC CDT for Wind and Marine Systems and structures who are the primary sponsor for the project, providing research tools and assistance. Thank you to Mehrad, Luis and Euan for their support as co-authors in the project. They put the foundations of the project together and provided support in their specific expertise of Mechanical engineering, Control engineering, Aerodynamic and FEA modeling.

References

[1] Di Paolo, M., Nuzzo, I., Caterino, N., & Georgakis, C. T. (2021). A friction-based passive control technique to mitigate wind induced structural demand to wind turbines. Engineering Structures, 232, 111744. https://doi.org/https://doi.org/10.1016/j.engstruct.2020.111744

[2] Freddi, F., Dimopoulos, C. A., & Karavasilis, T. L. (2017). Rocking damage-free steel column base with friction devices: design procedure and numerical evaluation. Earthquake Engineering & Structural Dynamics, 46(14), 2281-2300. https://doi.org/https://doi.org/10.1002/eqe.2904

[3] Kam, W.Y., Pampanin, S., Palermo, A. and Carr, A.J., 2010. Self-centering structural systems with combination of hysteretic and viscous energy dissipations. *Earthquake engineering & structural dynamics*, *39*(10), pp.1083-1108.Di Paolo, M., Nuzzo, I., Caterino, N., & Georgakis, C.

TOPIC 9

Floating wind turbines

9.1 Session 223: Floating wind turbines

25.09.2024, 15:10, Room 3

Chair:

Maksims Pogumirskis	

Presenters:

Silwal Kimon	Investigation of Wake Meandering of a Floating Wind Turbine
Messmer Thomas	Coherent flow structures in the wake of a floating wind turbine
Rappe Victor	Fatigue analysis of floating offshore wind turbines
Firpo Agnese	Actuator Line Modelling of Multi-turbine Interaction in Floating Offshore Conditions

Investigation of Wake Meandering of a Floating Wind Turbine

Kimon Silwal[a,b], Thomas Messmer[a,b], Michael Hölling[a,b]

[a] Carl von Ossietzky Universität Oldenburg, School of Mathematics and Science, Institute of Physics

[b] ForWind - Center for Wind Energy Research, Küpkersweg 70, 26129 Oldenburg, Germany

E-mail: kimon.silwal@uni-oldenburg.de

Keywords: *Wake meandering, active grid, Stewart platform, hot wires, stereo PIV*

Wind resources get stronger and relatively more stable as one moves further offshore. Thus, harnessing wind power in such areas is preferable except for one issue posed by the sea depth. Floating offshore wind turbine (FOWT) presents an effective means to harness wind power for sea depths larger than 60m compared to the bottom fixed wind turbine [1]. FOWT's, however, move in six degrees of freedom with motion influenced by the wind, waves, current, platform design, mooring and other factors adding to the complexity of the motion [2]. The motion affects the aerodynamics around the turbine and influences the development of the wake behind it.

Understanding the wake dynamics of a floating wind turbine is an ongoing area of research. Research findings from the last decade are available, but the understanding is inadequate to explain the wake development under different conditions of motion and atmospheric conditions. Wake meandering behaviour due to the platform's motion is of specific interest as it is linked to the recovery and its effect on the downstream turbines. Li et al. have shown that the earlier onset of wake recovery is due to sway motion [3] through simulation and experimentally by Messmer et al. [4] through wind tunnel experiments using a Stewart platform with six degrees of freedom. The platform's motion results in instabilities in wake structures, characterised by skewness and tilting, and wake meandering from dynamic wake effects. These instabilities lead to time-varying velocity deficits and turbulence intensities, impacting wake recovery and downstream turbines' performance in a wind farm. Studies have shown that power loss in the wind farm due to wake interaction can go up to 20% [5] and the fatigue load on the tower can increase by a factor of two [6]. Therefore, study of wake meandering through experiments under realistic conditions of inflow and floating motion is essential to improve the accuracy of the wake models and for design and operation of wind farms.

The following research questions are framed.

1. How does the platform motion of the FOWT influence the wake meandering?

2. How can the experimental data be used to identify key parameters to develop and refine wake meandering models?

3. What effect does the waked wind field have on the dynamic loading and the structure response of the FOWT?

The study aims to investigate the wake meandering of a floating wind turbine through experiments in the wind tunnel using a scaled model of a wind turbine, MoWiTO 0.6 [7]. A schematic diagram of the test set-up is shown in Figure 1. The motion of the model wind turbine platform is generated using a Stewart platform with six degrees of freedom. The active grid in the wind tunnel will be used to create different inflow conditions with different

turbulent intensities and scales. Stereoscopic particle image velocimetry and hot wires will be used to capture the detailed wake dynamics and turbulence characteristics.

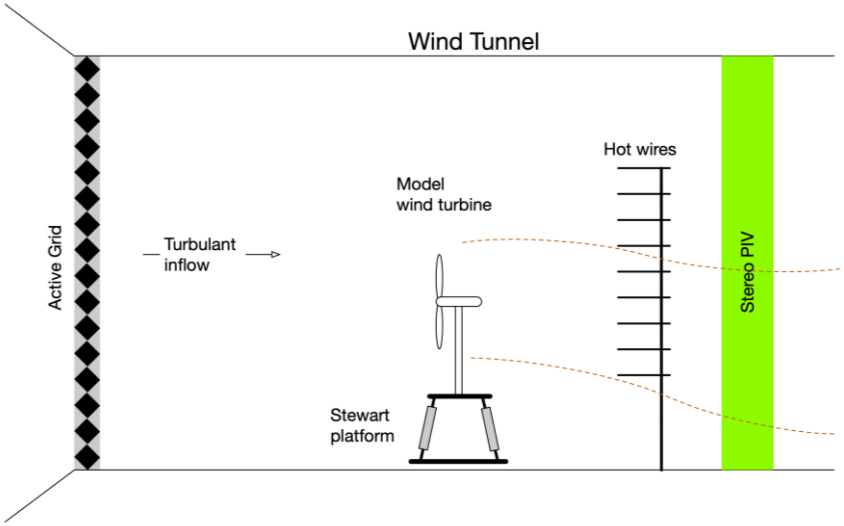

Figure 1: Schematic diagram of the wind tunnel test setup showing the model turbine mounted on the Stewart platform operating in a turbulent inflow controlled by the active grid

The experimental results from the wind tunnel experiments will be used to develop and refine the wake meandering model. The process involves identifying key parameters to create wind fields that best represent wake meandering behaviour. The wind field generated by the meandering wake model will be used in the Laboratory of Research in Hydrodynamics, Energetics, and Atmospheric Environment's (LHEEA) wave basin test facility, which uses an actuator emulated model of a wind turbine in a Software-in-the-Loop (SiL) system. The actuator emulated model of the wind turbine consists of six fans that replicate the aerodynamic forces acting on the blade, with the whole set-up allowing for a realistic turbine response to wind and wave conditions. Finally, the OpenFAST simulation tool will be used to conduct a fully coupled simulation of the floating wind turbine under various wake conditions to analyse the effect of aerodynamic load, hydrodynamic load, mooring load and elastic behaviour of the wind turbine.

The study aims to enhance the understanding of the floating wind turbine's wake meandering through wind tunnel experiments and the development of simulation models. The integration of the model-generated wind field, SiL system, and OpenFAST simulation will allow for precise turbine behaviour in different conditions. This will enable the assessment of different loading on the wind turbine. The methodology and some preliminary results will be presented in the seminar.

Acknowledgements

This work is part of the project FLORIDA funded by the Deutsche Forschungsgemeinschaft (DFG, German Research Foundation) – project number 529978479.

References

[1] H. Díaz and C. Guedes Soares. Review of the current status, technology and future trends of offshore wind farms. Ocean Engineering 209:107381, 2020.

[2] J. M. Jonkman and D. Matha. Dynamics of offshore floating wind turbines—analysis of three concepts. *Wind Energy* 14(4):557–569, 2011.

[3] Z. Li, G. Dong, and X. Yang. Onset of wake meandering for a floating offshore wind turbine under side-to-side motion. *J Fluid Mech* 934, 2022.

[4] T. Messmer, M. Hölling, and J. Peinke. Enhanced recovery and non-linear dynamics in the wake of a model floating offshore wind turbine submitted to side-to-side and fore-aft motion. *J. Fluid Mech.* (submitted) arXiv:2305.12247, 2023.

[5] R. J. Barthelmie and L. E. Jensen. Evaluation of wind farm efficiency and wind turbine wakes at the Nysted offshore wind farm. *Wind Energy* 13(6):573–586, 2010.

[6] T. J. Larsen, H. Aa. Madsen, G. C. Larsen, and K. S. Hansen. Validation of the dynamic wake meander model for loads and power production in the Egmond aan Zee wind farm. *Wind Energy* 16(4):605–624, 2013.

[7] J. Schottler, A. Hölling, J. Peinke, and M. Hölling. Design and implementation of a controllable model wind turbine for experimental studies. *J Phys Conf Ser* 753(7):072030, 2016.

20th EAWE PhD Seminar on Wind Energy
24-26 September 2024
Visby, Sweden

Coherent flow structures in the wake of a floating wind turbine

T Messmer[a], J Peinke[a], and M Hölling[a]

[a]Carl von Ossietzky Universität Oldenburg, School of Mathematics and Science, Institute of Physics, ForWind - Center for Wind Energy Research, Küpkersweg 70, 26129 Oldenburg, Germany

E-mail: thomas.messmer@uni-oldenburg.de

Keywords: turbulence, FOWT, wake, aerodynamics, wind tunnel experiment

1 Introduction

The need to increase the share of renewable energies worldwide requires a significant growth in installed offshore wind energy. In addition to well developed bottom-fixed wind turbine, floating offshore wind turbine (FOWT) is an upcoming technology. Mounted on an moored floating platform, a FOWT can move freely in 6 additional degrees of freedom (DoF) compared to a fixed wind turbine. These movements depend on the operating conditions (wind and wave), type of platform, moorings, etc [1]. They cover different range of frequencies and amplitudes, usually expressed in terms of platform Strouhal number, St and reduced amplitude, A^*. These are expressed as follows:
$St = f_p D/U_\infty$, $A^* = A_p/D$
with f_p the platform motion's frequency, D the rotor diameter, U_∞ the incoming wind speed and A_p the amplitude of the motion.

Previous works showed that floater motions impact rotor aerodynamics as well as the wake generated [2, 3]. The larger effect are especially seen for low level of turbulence in the inflow [3]. In [4] we analysed the wake of an idealised floating wind turbine and showed that motions enable a faster wake recovery. We also found that movements lead to the formation of coherent flow structures in the wake. The role of these coherent patterns on the transition to the far-wake and enhanced recovery is still to be better understood.
In this present study, we analyse results from wind tunnel experiments of a simplified floating wind turbine model. We tested idealised motion of the platform and low level of turbulence and measured the wake of the turbine. We used hot-wire anemometers and stereoscopic PIV to record with high spatial and temporal resolution the wake generated. The purpose is to depict the evolution of the coherent structures in the wake and their role on the enhanced wake recovery.

2 Methodology

For this research, wind tunnel measurements were carried out using the Model Wind Turbine Oldenburg (MoWiTO 0.6) mounted on a Stewart platform to mimic motions of a floating wind turbine [5]. This set-up was installed in the closed-loop wind tunnel (3×3 m^2 inlet section) of the university of Oldenburg. The tests were done with different turbulent conditions, including laminar inflow ($TI \approx 0.3$ %) and cases with higher turbulence intensity ($TI \in [0.8, 3]$ %). The turbine was moved by the platform following harmonic motions in fore-aft and side-to-side degrees-of-freedom (DoFs).

A total of 19 hot wire anemometers, arranged horizontally, were installed on an array to measure the wind speed in the wake of the turbine at different downstream positions ranging from 2D to 10D downstream, with D, the rotor diameter equal to 0.58 m. This set-up enabled to measure horizontal wind profiles of velocity in the wake of the turbine with a high sampling frequency of 6 kHz. In addition, stereoscopic

PIV was used to measure at $x \approx 3D,\ 5D,\ 7D$ the wake of the wind turbine.

We measured the wake of a surging and swaying turbine with $St = 0.38$ and $A^* \in 0.007, 0.017$, $C_T \approx 0.8$.

3 Results

At the conference, the impact of the direction of motion, amplitude of motion and inflow turbulence on the formation of the coherent structures will be presented and discussed. The spatially and temporally resolved wind speed data measured in the wake will be used to quantify energy, shaped and evolution of the flow structures. Their role on the enhanced recovery and faster transition to far-wake will be depicted.

Acknowledgements

This project has received funding from the European Union's Horizon 2020 research and innovation programme under the Marie Sklodowska-Curie grant agreement N°860879 as part of the FLOAting Wind Energy netwoRk (FLOAWER) consortium. The authors would like to thank J. Jüchter for his valuable help with MoWiTO 0.6 and J. Puczylowski for his continuous support in the development of the experimental set-up.

References

[1] Jonkman, J. M., Matha, D. (2011). Dynamics of offshore floating wind turbines—analysis of three concepts. Wind Energy, 14(4), 557-569.

[2] Sebastian, T., Lackner, M. A. (2013). Characterization of the unsteady aerodynamics of offshore floating wind turbines. Wind Energy, 16(3), 339-352.

[3] Li, Z., Dong, G., Yang, X. (2022). Onset of wake meandering for a floating offshore wind turbine under side-to-side motion. Journal of Fluid Mechanics, 934, A29.

[4] Messmer, T., Hölling, M., Peinke, J. (2024). Enhanced recovery caused by nonlinear dynamics in the wake of a floating offshore wind turbine. Journal of Fluid Mechanics, 984, A66.

[5] T. Messmer, C. Brigden, J. Peinke, M. Hölling. A six degree-of-freedom set-up for wind tunnel testing of floating wind turbines. J. Phys.: Conf. Ser. 2265, 042015. 2022

20th EAWE PhD Seminar on Wind Energy
24-26 September 2024
Visby, Sweden

Fatigue analysis of floating offshore wind turbines

Victor Rappe[a], **Kris Hectors**[a], and **Wim De Waele**[a]

[a]Ghent University / OWI-Lab, Faculty of Engineering and Architecture, Department of Electromechanical, Systems and Metal Engineering, Laboratory Soete, Technologiepark 46, 9052 Zwijnaarde, Belgium

E-mail: Victor.Rappe@UGent.be

Keywords: Fatigue, finite element analysis, Floating offshore wind turbines

1 Introduction

As the world transitions towards sustainable energy, offshore wind energy is becoming increasingly critical. However, conventional fixed-bottom wind turbines face economic limitations in depths greater than 60 meters, rendering approximately 80% of global offshore wind resources inaccessible to them [1]. To overcome this challenge, floating offshore wind turbines (FOWTs) present a viable solution. These turbines can be deployed at much greater depths, allowing them to be placed farther offshore where winds are stronger and more consistent, and where they are not visible from the shoreline.

Despite currently accounting for only about 0.2% of total wind power worldwide [2], floating wind power is projected to grow to over 6% by 2030 [3]. This rapid expansion is driven by extensive research and development efforts, exemplified by projects like the TetraSpar [4]. However, while the (hydro-)dynamics of FOWT substructures are well-documented in literature, studies on the structural fatigue of these FOWTs are relatively scarce. Addressing this gap, the BEL-Float project [5], funded by the Energy Transition Fund of the Belgian federal government, aims to develop an open-source numerical method to assess fatigue loads, to evaluate the (local) accumulation of fatigue damage, and ultimately to predict the fatigue lifetime of the floater substructure with high accuracy. The OC4 DeepCWind FOWT [6], illustrated in Figure 1, is used as a reference to develop this method.

Figure 1: Illustration of the OC4 DeepCWind semi-submersible FOWT, as defined in [6]

2 Challenges and proposed methodology

Conducting a fatigue analysis of the substructure of a FOWT presents several challenges. In typical dynamic modeling approaches, such as those used in software packages like OpenFAST [7], a flexible tower is coupled with a rigid floater. However, this means that no internal forces and moments, and thus stresses can be extracted for the floater. As a result, most studies in literature that consider the fatigue of FOWT substructures focus solely on the fatigue at the tower base [8, 9], where forces and moments can easily be extracted from the dynamic analysis. On the other hand, only one research paper [10] exists to the authors knowledge that considers the fatigue of other critical locations, such as welded joints, of a FOWT substructure.

To perform a detailed fatigue analysis of these critical regions, knowledge of local stresses is required. This necessitates the development of a finite element (FE) model that considers the distributed pressure loads on the wetted surface due to waves and current acting on the structure, instead of the resultant forces at the centre of gravity (CoG), which are used in the rigid body analyses. To address this, a method is developed to accurately determine and implement the governing distributed hydrodynamic pressures onto a shell-based FE model, as illustrated on Figure 2. The method presented here is inspired by the works of Lee et al. [10] and Gao et al. [11].

First, a global (hydro-)dynamic time domain analysis is conducted using the open-source software OpenFAST. This analysis provides the following time domain outputs:

- the forces and moments at the transition piece between the tower and the floating platform;
- the forces at the mooring fairleads;
- the position and acceleration of the CoG of the floating platform in all six degrees of freedom (DOFs);
- the sea elevation at a reference point.

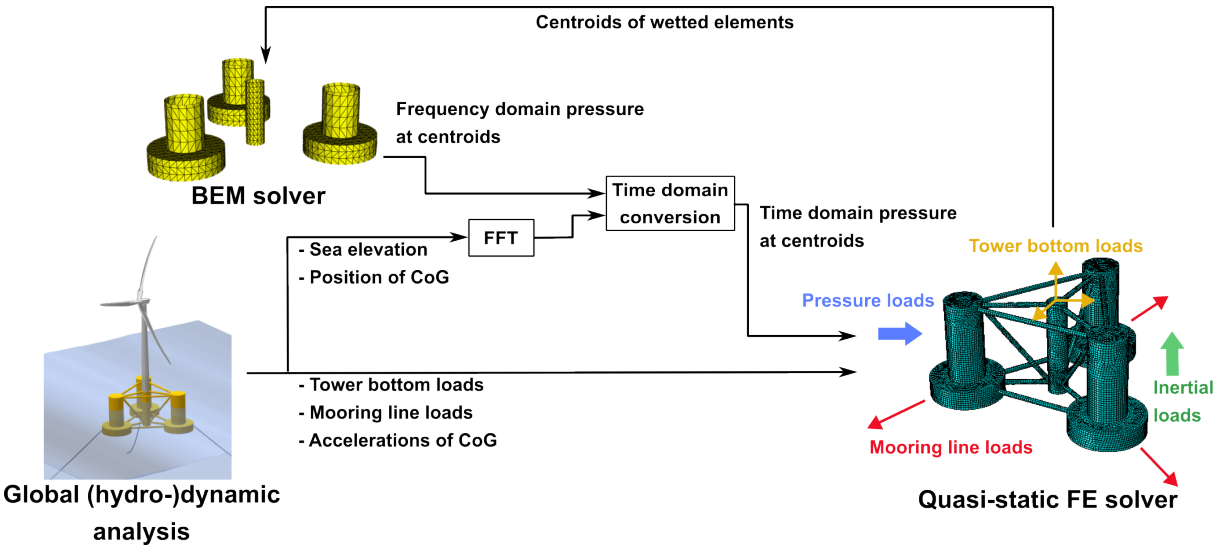

Figure 2: Schematic showing the method used to extract, calculate, and map the loads on an FE model

Next, a frequency domain simulation is conducted using Capytaine [12], an open source boundary element method (BEM) solver for linear potential flow, to determine complex pressure values across a range of frequencies. This is done at the centroid of all wetted elements in the FE mesh for Froude-Krylov, diffraction, and radiation loads. The reasoning behind selecting these locations will be explained later in this section. Since linear potential flow is being considered, the BEM solver disregards the cross braces. Their slender shape allows to assume that their contributions are negligible.

To transform the frequency domain pressures into useful time domain data, the following steps are performed for the diffraction problem, using the sea elevation $h(t)$ as input to the method:

1. it is assumed that the input $h(t)$ can be described as a finite Fourier series, i.e.:

$$h(t) = \Re\left[\sum_{n=1}^{N} h_n \exp(i(\omega_n t + \phi_n))\right] \tag{1}$$

with N the number of frequencies, and h_n and ϕ_n respectively the amplitude and phase angle corresponding to the angular frequency ω_n.

2. a fast Fourier transform (FFT) is used to extract the amplitudes h_n, angular frequencies ω_n, and phase angles ϕ_n from $h(t)$;

3. since a linear problem is considered, the complex pressure values $p_{\text{diffraction}}(\omega)$ calculated in the BEM solver can be regarded as a transfer function;

4. the time domain diffraction pressure $p_{\text{diffraction}}(t)$ is then determined via:

$$p_{\text{diffraction}}(t) = \frac{1}{N}\Re\left[\sum_{n=1}^{N} h_n |p_{\text{diffraction}}|(\omega_n)\exp[i(\omega_n t + \phi_n + \angle p_{\text{diffraction}}(\omega_n))]\right] \tag{2}$$

where $|\cdot|$ denotes the absolute value and $\angle\cdot$ represents the phase angle.

The same method is used for the Froude-Krylov and radiation loads, using the sea elevation and the position of the CoG in all six DOFs, respectively, as input, and treating $p_{\text{Froude-Krylov}}(\omega)$ and $p_{\text{radiation}}(\omega)$, respectively, as transfer function.

As mentioned above, these time domain pressures are determined for the centroid of each wetted shell element of the FE mesh. This allows to directly assign each pressure component to their corresponding element, creating a distributed pressure field on the FE model. It is important to note that this method permits the use of different meshes for the BEM and FE analyses. Once the hydrodynamic loads have been applied, the accelerations of the CoG of the platform are used to calculate the inertial loads and are assigned to the model. Subsequently, the tower bottom loads, mooring loads, gravity loads, and hydrostatic pressure are applied. Finally, a quasi-static FE analysis is performed.

3 Progress and Future Work

The method described above is being developed in the context of the BEL-Float project. At this time, linear potential flow theory is considered, but the drag term of the Morison equation will additionally be implemented in the future. Afterwards, a multi-dimensional fatigue modelling strategy will be developed, as shown in Figure 3. From the shell element FE analysis of the substructure, fatigue critical welds will be identified and solid element submodels will be developed of the regions surrounding these welds. The hot spot stress approach [13] will be used to extract fatigue governing stress spectra, after which the rainflow counting method combined with the Palmgren-Miner damage rule will be employed to determine the local fatigue damage.

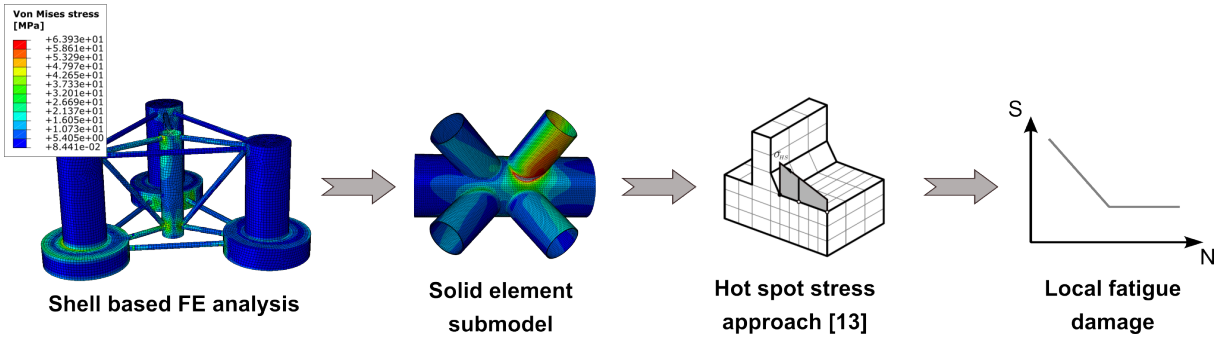

Figure 3: Schematic showing the multi-dimensional fatigue modelling strategy

Acknowledgments

This work is financially supported by the FPS Economy (FOD Economie) under the call 2022 of the Energy Transition Fund of the Belgian Federal Government through the BEL-Float project.

References

[1] Aegir-Insights, Floating offshore wind – a global opportunity (2022).
URL https://gwec.net/wp-content/uploads/2022/03/GWEC-Report-Floating-Offshore-Wind-A-Global-Opportunity.pdf

[2] J. Lee, F. Zhao, Gwec — global wind report 2024 (2024).
URL https://gwec.net/wp-content/uploads/2024/04/GWR-2024_digital-version_final.pdf

[3] A. Subbulakshmi, M. Verma, M. Keerthana, S. Sasmal, P. Harikrishna, S. Kapuria, Recent advances in experimental and numerical methods for dynamic analysis of floating offshore wind turbines — an integrated review, Renewable and Sustainable Energy Reviews 164 (2022) 112525. doi:10.1016/J.RSER.2022.112525.

[4] M. Borg, M. W. Jensen, S. Urquhart, M. T. Andersen, J. B. Thomsen, H. Stiesdal, Technical definition of the tetraspar demonstrator floating wind turbine foundation, Energies 2020, Vol. 13, Page 4911 13 (2020) 4911. doi:10.3390/EN13184911.
URL https://www.mdpi.com/1996-1073/13/18/4911/

[5] M. Mahieu, Bel-float (May 2024).
URL https://www.owi-lab.be/bel-float

[6] A. Robertson, J. Jonkman, M. Song, A. Goupee, A. Coulling, C. Luan, Definition of the semisubmersible floating system for phase ii of oc4 (2014).
URL https://www.nrel.gov/docs/fy14osti/60601.pdf

[7] J. Jonkman, Openfast.
URL https://www.nrel.gov/wind/nwtc/openfast.html

[8] X. Li, W. Zhang, Long-term fatigue damage assessment for a floating offshore wind turbine under realistic environmental conditions, Renewable Energy 159 (2020) 570–584. doi:10.1016/J.RENENE.2020.06.043.

[9] C. Luan, T. Moan, On short-term fatigue analysis for wind turbine tower of two semi-submersible wind turbines including effect of startup and shutdown processes, Journal of Offshore Mechanics and Arctic Engineering 143 (2 2021). doi:10.1115/1.4047542/1084660.
URL https://dx.doi.org/10.1115/1.4047542

[10] D. C. Lee, S. kwon Na, S. Kim, C. wan Kim, Deterministic fatigue damage evaluation of semi-submersible platform for wind turbines using hydrodynamic-structure interaction analysis, International Journal of Precision Engineering and Manufacturing - Green Technology 9 (2022) 1317–1328. doi:10.1007/S40684-021-00326-7/TABLES/5.
URL https://link.springer.com/article/10.1007/s40684-021-00326-7

[11] Z. Gao, D. Merino, K. J. Han, H. Li, S. Fiskvik, Time-domain floater stress analysis for a floating wind turbine, Journal of Ocean Engineering and Science 8 (2023) 435–445. doi:10.1016/J.JOES.2023.08.001.

[12] M. Ancellin, A python-based linear potential flow bem solver (2022).
URL https://capytaine.github.io/stable/

[13] K. Hectors, H. D. Backer, M. Loccufier, W. D. Waele, Numerical framework for fatigue lifetime prediction of complex welded structures, Frattura ed Integrita Strutturale 14 (2020) 552–566. doi:10.3221/IGF-ESIS.51.42.

20th EAWE PhD Seminar on Wind Energy
24-26 September 2024
Visby, Sweden

Actuator Line Modelling of Multi-turbine Interaction in Floating Offshore Conditions

Agnese Firpo[a]

[a]Laboratory of Fluid-Machines, Department of Energy, Politecnico di Milano, Via Lambruschini 4, I-20156 Milano, Italy

E-mail: agnese.firpo@polimi.it

Keywords: Actuator Line Model (ALM), wake interaction, FOWTs

1 Introduction

The development of numerical models capable of accurately representing the physics of a wind turbine wake, especially under platform motions, is crucial for the advancement of floating offshore wind farms. In wind farms, the majority of turbines operate within the wake of upstream turbines, a condition that notably influences their loads and performance, especially when platform motions are involved. Therefore, having numerical models capable of efficiently analysing these operational conditions is essential. In this context, the medium-fidelity Actuator Line Model (ALM) proves particularly suitable. This model combines the advantages of both low-fidelity and high-fidelity models. By substituting the blades with rotating forces, it avoids the need to resolve the boundary layer, thereby reducing computational time. Moreover, by resolving the flow using a standard CFD approach, it ensures high accuracy.

2 Research question

In this research, the primary objective is to provide a detailed analysis of turbine-wake interaction in a configuration with two turbines aligned in series at a distance of 5 diameters. Specifically, the study considers a case with fixed-bottom turbines and a case where platform motion is applied to the upstream turbine. The focus is on the operational conditions of the downstream turbine, analysing global and blade loads, with particular attention to the characteristics of the flow field it experiences.

Using the velocity sampling method implemented in the ALM model, detailed information can be obtained on the actual velocity perceived by the actuator points of the downstream turbine. Therefore the CFD simulation of the flow field provides a precise estimate of the velocity experienced by the downstream turbine, resulting from the combined effects of the upstream wake velocity deficit and the induction effect of the downstream turbine. This is particularly crucial, especially when the upstream turbine experiences platform motion. In such scenarios, the presence of velocity pulsations in the wake affecting the downstream turbine further complicates the flow dynamics. These considerations are valuable for developing analytical wake models, offering insights to devise appropriate approaches for estimating the velocity experienced by the downstream turbine under floating conditions.

3 Methodology

This study is conducted using an in-house Actuator Line Model (ALM) implemented in OpenFOAM. The combination of an internal ALM code with an open-source CFD software provides the authors with complete freedom for implementation and control. This ALM code has recently been modified to allow the simulation of multiple turbines, each subject to prescribed platform motions. Preliminary analyses simulate two turbines aligned at a distance of 5 diameters.

As an initial step, URANS simulations were performed to limit computational time and to analyse the effect of the mean velocity on the second rotor. Future developments will involve transitioning to LES simulations to

investigate the contribution of wake instability due to turbulence. In any case, the authors have confirmed in [3] that the URANS simulation is capable of accurately capturing the average velocity defect in the near wake, thereby ensuring the validity of the results obtained here. The turbulence model used is k-ω SST and the validation of the model in estimating blade loads for a single fixed and floating turbine was carried out in [5]. Validation for a single turbine was achieved by comparing the numerical results with the experiments of the UNAFLOW campaign (Fontanella et al. [4] and Bayati et al. [1]) and the results from various computational models used in the OC6 Phase III project (Bergua et al. [2]).

To maintain consistency with these previous simulations, also this study simulates the same scaled-down model of the DTU 10 MW turbine tested in the UNAFLOW experimental campaign conducted in the wind tunnel of Politecnico di Milano ([4], [1]). The numerical simulation replicates the wind tunnel dimensions and the same operating conditions tested, including freestream velocity, upstream turbine position, rotational speed, and platform motions. The key difference is the addition in the numerical domain of a second turbine, identical to the upstream one, placed 5 diameters downstream.

4 Preliminary results

This section presents the initial preliminary results. More detailed analyses of the loads and flow field will be conducted to complete the work, especially in the case of platform motion.

4.1 Fixed-bottom case

The first case involves two fixed turbines and serves to provide a baseline assessment of the operational conditions of the downstream turbine without platform motion. Figure 1 shows the temporal trends of thrust and torque for both turbines, highlighting the performance reduction of the downstream turbine when impacted by the upstream wake.

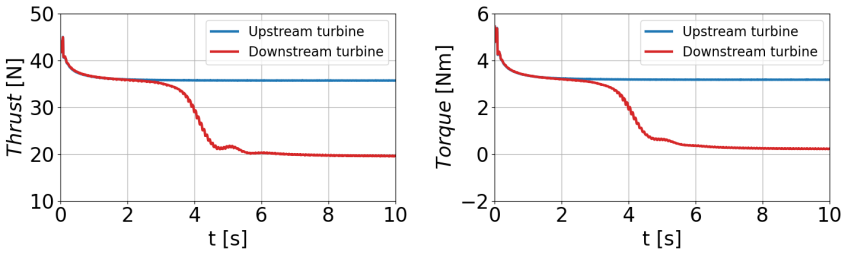

Figure 1: Thrust and torque convergence over simulated time.

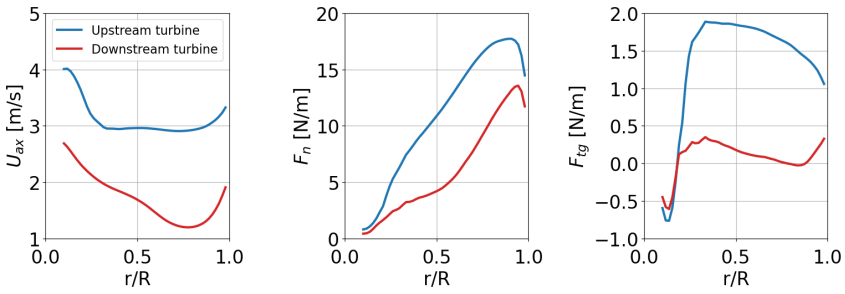

Figure 2: Axial velocity, normal and tangential force along the blade span.

To delve deeper into the load analysis, the span-wise trends of some fundamental quantities are examined. Figure 2 illustrates the span-wise profiles of the absolute velocity sampled at the AL points by the ALM code, along with the normal and tangential forces for both the downstream and upstream turbines. The absolute velocity on the downstream rotor shows the influence of the upstream wake, displaying not only an overall reduction but also

a different distribution along the blade. The reduced velocity experienced by the downstream turbine, combined with its different blade distribution, leads to a decrease and redistribution of the normal and tangential forces. Analysing the flow field affecting the second turbine will help better understand the velocity distribution at the AL points and quantify the induction effect of the downstream turbine on the upstream velocity deficit.

4.2 Surge motion on the upstream turbine

In this case the upstream turbine is subjected to a prescribed sinusoidal surge platform motion with a frequency of 1 Hz and an amplitude of 0.035 m. In this case, platform motion generates wake velocity pulsations that require detailed analysis. Figure 3 displays the temporal trends of the global thrust and torque loads. It is clear that the URANS simulation effectively captures the wake velocity pulsations, leading to oscillations in the downstream turbine loads once the interaction begins.

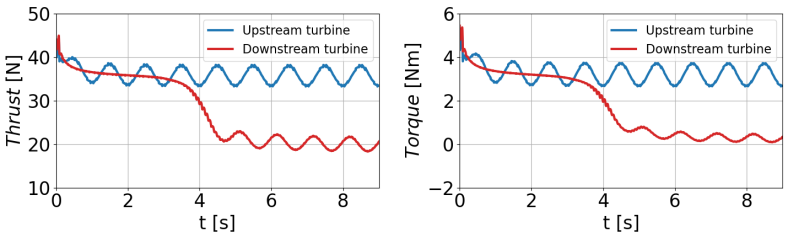

Figure 3: Thrust and torque convergence over simulated time.

In Fig. 4, the trend of global loads during a surge period is depicted. To enhance clarity in comparison, each curve has been adjusted by subtracting the corresponding mean value ($< * >$). The image reveals not only a lower amplitude of the downstream turbine loads but also a phase shift of approximately 113°compared to the upstream turbine. Further insight into this behaviour will require a detailed analysis of the flow field to examine the temporal evolution of the upstream turbine wake.

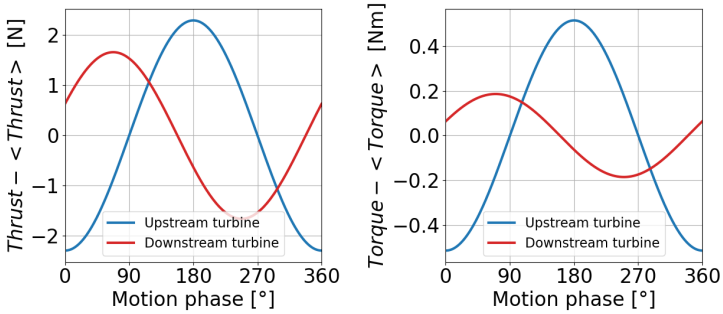

Figure 4: Thrust and torque convergence over one surge period.

As an additional level of detail, attention will also be given to the span-wise distribution of various quantities. In Fig. 5 the absolute velocity sampled at the AL points, the normal force, and the tangential force are presented for both the upstream turbine (solid lines) and the downstream turbine (dashed lines).

For each turbine, four time instants evenly distributed over a surge period (0T, 1/4 T, 1/2 T, 3/4 T) are provided to capture the variability due to platform motion. The distribution of forces on the upstream turbine aligns with the imposed platform motion: minimum forces at the 0T instant (indicating the maximum leeward velocity of the turbine and thus the minimum relative velocity) and maximum forces at the 1/2 T instant (indicating the maximum windward velocity of the turbine and thus the maximum relative velocity). Forces on the downstream turbine exhibit a trend consistent with global loads over time and similar to the fixed-bottom scenario. The absolute velocity is minimally affected by platform motion for both turbines; therefore, it becomes crucial, especially in this scenario, to analyse the flow field to gain further insights into the induction effects of the two turbines.

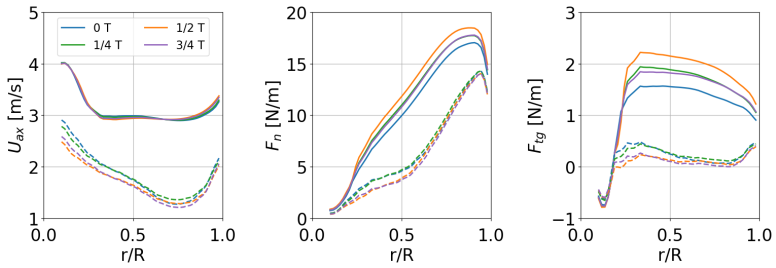

Figure 5: Axial velocity, normal and tangential force along the blade span for four time instants evenly distributed over a surge period. Solid lines represent the upstream turbine and dashed lines the downstream one.

5 Conclusions

The observations outlined in this abstract serve as the initial step towards a thorough analysis of the operational conditions of a rotor operating within the wake of an upstream turbine, particularly in case of platform motion. Future analyses will rely on a more comprehensive assessment of blade loads and the flow field experienced by the second turbine, especially during surge motion. As previously mentioned, this study aims to elucidate aspects related to estimating the induction of the downstream turbine, which combines with the velocity deficit of the upstream wake, particularly in the presence of wake velocity pulsations. These insights could prove useful in developing superimposition analytical wake models, particularly for floating turbines.

Acknowledgements

This study was carried out within the NEST- Network 4 Energy Sustainable Transition (D.D. 1243 02/08/2022, PE00000021) and received funding under the National Recovery and Resilience Plan (NRRP), Mission 4 Component2Investment 1.3, funded from the European Union- NextGenerationEU. This manuscript reflects only the authors' views and opinions, neither the European Union nor the European Commission can be considered responsible for them.

References

[1] I. Bayati, M. Belloli, L. Bernini, D. Boldrin, K. Boorsma, M. Caboni, M. Cormier, R. Mikkelsen, T. Lutz, and A. Zasso. Unaflow project: Unsteady aerodynamics of floating wind turbines. *Journal of Physics: Conference Series*, 1037(7):072037, jun 2018.

[2] R. Bergua, A. Robertson, J. Jonkman, E. Branlard, A. Fontanella, M. Belloli, P. Schito, A. Zasso, G. Persico, A. Sanvito, E. Amet, C. Brun, G. Campaña Alonso, R. Martín-San-Román, R. Cai, J. Cai, Q. Qian, W. Maoshi, A. Beardsell, G. Pirrung, N. Ramos-García, W. Shi, J. Fu, R. Corniglion, A. Lovera, J. Galván, T. A. Nygaard, C. R. dos Santos, P. Gilbert, P.-A. Joulin, F. Blondel, E. Frickel, P. Chen, Z. Hu, R. Boisard, K. Yilmazlar, A. Croce, V. Harnois, L. Zhang, Y. Li, A. Aristondo, I. Mendikoa Alonso, S. Mancini, K. Boorsma, F. Savenije, D. Marten, R. Soto-Valle, C. W. Schulz, S. Netzband, A. Bianchini, F. Papi, S. Cioni, P. Trubat, D. Alarcon, C. Molins, M. Cormier, K. Bruker, T. Lutz, Q. Xiao, Z. Deng, F. Haudin, and A. Goveas. Oc6 project phase III: validation of the aerodynamic loading on a wind turbine rotor undergoing large motion caused by a floating support structure. *Wind Energy Science*, 8(4):465–485, 2023.

[3] A. Firpo, A. G. Sanvito, G. Persico, V. Dossena, P. Schito, and A. Zasso. Multi-fidelity actuator-line modelling of fowt wakes. In *Journal of Physics: Conference Series*, volume 2767, page 052050. IOP Publishing, 2024.

[4] A. Fontanella, I. Bayati, R. Mikkelsen, M. Belloli, and A. Zasso. Unaflow: a holistic wind tunnel experiment about the aerodynamic response of floating wind turbines under imposed surge motion. *Wind Energy Science*, 6(5):1169–1190, 2021.

[5] G. Persico, A. Sanvito, A. Firpo, P. Schito, V. Dossena, and A. Zasso. A novel vortex-based velocity sampling method for the actuator-line modeling of floating offshore wind turbines. *Available at SSRN 4625595*.

9.2 Session 324: Floating wind turbines

26.09.2024, 10:30, Room 4

Chair:

Thea Vanelli

Presenters:

De Pascali Marco	Influence of platform motion on the energy production of a floating wind farm
Al-Ghuwaidi Abdulelah	Assessing and monitoring low frequency dynamics of floating offshore wind turbines using operational modal analysis
Kämmerling Max	On the Generalization of Machine Learning Algorithms for Mooring Line Tension Estimation of Floating Wind Turbines under Unknown Sea Conditions

20th EAWE PhD Seminar on Wind Energy
24-26 September 2024
Visby, Sweden

Influence of platform motion on the energy production of a floating wind farm

M. De Pascali

E-mail: marco.depascali@polimi.it

Keywords: Floating wind farm, wakes, power production

1 Introduction

In recent years the first utility-scale floating wind farms have been installed and others are expected to go online in the next years. Compliance of the floating foundation allows large-amplitude low-frequency motions which interact with the turbine controller and influence in a significant manner the wind speed experienced by rotor. Due to this difference with bottom-fixed offshore turbines, it is crucial to understand the physics of the energy conversion process taking place in floating wind farms to quantify their energy production with low uncertainty. Waves excitation has been shown to have negligible effects on the energy production of an isolated wind turbine [5]. In [6] a two-turbine floating wind farm is examined and it is shown how large scale movements of the platform result in increased wake meandering which excites the yaw motion of the downstream turbine and increases the blades fatigue loads. A two-turbine wind farm is also studied in [4], where it is found the floater motion triggers a faster breakdown of the wake improving the power production of the downstream machine compared to the case with bottom-fixed foundation.

2 Objectives

The objective of this work is to investigate the impact of platform motion on the power production of floating wind farms. We clarify how the power curve of the isolated turbine changes when a floating support platform is used in place of a bottom-fixed one. Then, we analyze the influence of platform movement driven by site-specific wind and wave conditions on the flow field inside a wind farm of seven turbines with regular layout. Finally, we show the influence of the floating foundation on the farm energy production.

3 Methodology

We model in FAST.Farm two small wind farms, each of seven 15 MW wind turbines (IEA 15 MW), one with monopile foundations and one with floating platforms (VolturnUS semisubmersible). FAST.Farm combines the Dynamic Wake Meandering model with structural dynamics, hydrodynamic excitation, mooring lines, turbine control, and full-field turbulent wind. The wind turbines are arranged in a regular staggered layout with 5D distance between rows and columns [2]. We examined one below rated scenario with a mean wind speed of 10 m/s because in this condition wind turbines are operated at nearly maximum thrust and wake effects are significant. 16 wind directions (φ) equally spaced of 22.5° are considered. The wind fields of the simulations are generated in TurbSim. The wind is calculated based on the Kaimal turbulence model, the turbulence intensity is 0.12, the wind speed vertical profile follows a power law with a shear exponent of 0.14. Waves in the simulations are of irregular type based on the JONSWAP spectrum. The wave height and the peak spectral period are defined from linear correlation with the average wind speed following the same procedure of [3], resulting in a $H_s = 2$ m and a $T_p = 5.5$ s. Only aligned wind/wave conditions have been considered. Each FAST.Farm simulation has a time length of 4200 s, the first 600 s were discarded in the post-processing to remove transient effects, resulting in an effective simulation length of 1 hour which is necessary to capture the slow dynamics of the floating foundation. Six 1-hour simulations with different realizations of the turbulent wind field and waves are run for every wind direction to reproduce the stochastic variability of environmental excitation.

4 Results and discussion

Power production at farm level is affected by the behavior of individual wind turbines. In Sect. 4.1 we show the use of a floating platform modifies the steady-state response of a wind turbine rotor. These differences at the turbine level combine with those rising at the farm level due to wakes, and this is presented in Sect. 4.2.

4.1 Response of the isolated wind turbine

The steady-state operating points of generated power and rotor aerodynamic thrust force of the IEA 15 MW, with monopile foundation and the VolturnUS semi-submersible, regulated with the control strategy described in [1], are visualized in Fig. 1. The peak-shaving routine of the floating wind turbine controller reduces the maximum thrust force near the rated wind speed at the expense of a lower generated power. At 10 m/s, the peak shaving reduces the thrust force of 10% compared to the monopile case and due to the momentum conservation, this leaves a slightly larger amount of kinetic energy in the wind turbine wake. In the below-rated region, the thrust force and generated

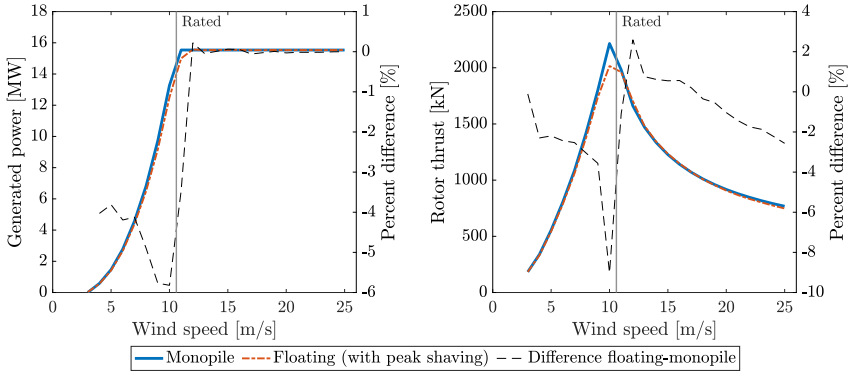

Figure 1: Steady-state power curves of generated power and rotor aerodynamic thrust force of the wind turbines with monopile and floating foundations. The floating wind turbine controller has a peak shaving routine limiting the maximum thrust force at the expense of a lower power output.

power are lower for the floating wind turbine compared to the monopile case. This is due to the platform static tilt and the consequent reduction of rotor area projection on the vertical plane. In the above-rated region, the generated power is saturated to its rated value and is equal for the monopile and floating wind turbines. The thrust force is slightly higher for the floating wind turbine compared to the monopile for wind speeds just above rated, and is lower for higher wind speeds.

4.2 Response of the wind farm

The symmetry of the wind farm layout is reflected in the generated power that has a similar behaviour in the four quadrants of the wind direction. In the first quadrant ($0^\circ \leq \varphi \leq 90^\circ$) we distinguish three situations that are summarized in Table 1. For $\varphi = 0^\circ$, the monopile wind farm exhibits a similar power compared to the floating wind farm; when $\varphi = 45^\circ$, the monopile wind farm exhibits a higher power; when $\varphi = 90^\circ$, the monopile wind farm exhibits a lower power.

Table 1: Power generated by the bottom-fixed and floating wind farms obtained averaging the 6 simulations with different realization of stochastic wind and waves for every wind direction.

Wind direction [°]	Power monopile [MW]	Power floating [MW]
0	78.86	77.97
45	87.88	84.29
90	58.64	60.88

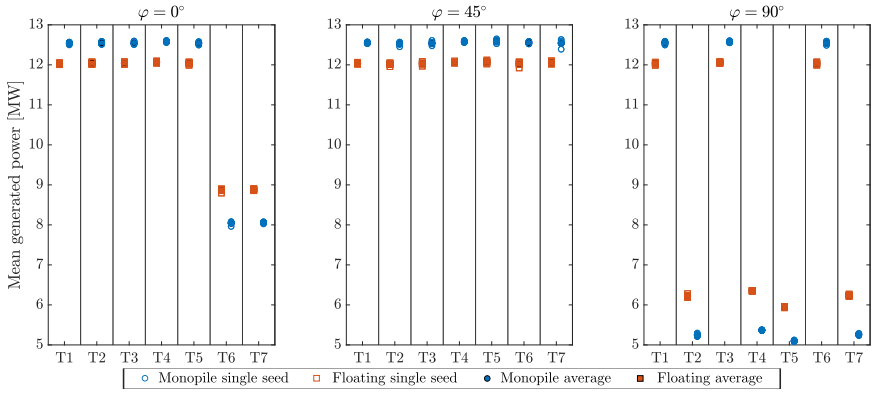

Figure 2: Power generated by the seven wind turbines (T), in the monopile and floating cases, for three wind directions φ.

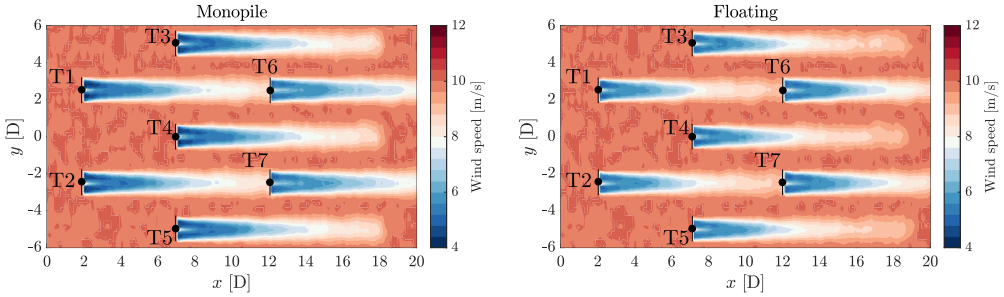

Figure 3: Time averaged flow fields of longitudinal wind speed across the wind farm, on a plane at 150 m from the water level, for the monopile and floating foundations with wind coming from $\varphi = 0°$.

The contributions of individual wind turbines to the total generated power is examined in Fig. 2. We distinguish two situations: some turbine units generate a power close to 12 MW, corresponding to the output of the isolated case (see Fig. 1), whereas others, that are waked, have a reduced power output. In the first condition, the generated power with a floating platform is lower than with a monopile, and this is attributed to the wind turbine static tilt. In the other case it is the opposite: the floating wind turbines produce more power. To explain the differences in terms of power generated by the waked wind turbines we analyze the wake losses and their impact on the energy-conversion process at rotor level. Wake losses depend on the wind direction since for some incoming wind angles there are turbines working in a more pronounced waked condition. This is visualized in Fig. 3 showing the instantaneous flow field across the farm for $\varphi = 0°$. For $\varphi = 90°$ four wind turbines (T2, T4, T7, T5) operate in the wake of upstream units, for $\varphi = 0°$ two wind turbines (T6, T7) are waked, when $\varphi = 45°$, wakes are directed between rotors of downstream units and there are no wake losses. For $\varphi = 45°$ the response of the isolated turbine drives the wind farm performance, while for $\varphi = 0°$ or $90°$ wakes affect the power production of some units, triggering a different behavior of floating wind turbines compared to bottom-fixed ones. Figure 3 shows the longitudinal wind speed in the turbine wakes is generally higher for the floating wind farm compared to the monopile case. The higher wind speed in the wake of floating wind turbines is mainly due to these factors: slightly less energy is extracted from the flow with peak shaving; the large low-frequency motions of the floating platform affect the wake meandering; the wake is deflected upwards due to the increased rotor tilt given by platform static pitch.

In the floating case, the low-frequency motion of the rotor and the use of peak shaving may leave more energy in the wake compared to the monopile case. This is explored in Fig. 4 which shows the mean wind speed (ambient wind disturbed by wakes) at hub-height for three wind directions, with monopile and floating wind turbines. For $\varphi = 0°$, T6 and T7 experience the wake of upstream wind turbines; for $\varphi = 90°$ T2, T4, T5, and T7 are in waked condition; for $\varphi = 45°$ wake effects are minimized by the layout geometry and all wind turbines experience the free stream wind speed. In general floating wind turbines in waked conditions experience a higher mean wind speed compared to the monopile case. The mean power generated by the wind turbines, which is reported in Fig. 2, follows approximately the same trend of the mean wind speed of Fig. 4. When operating in an undisturbed

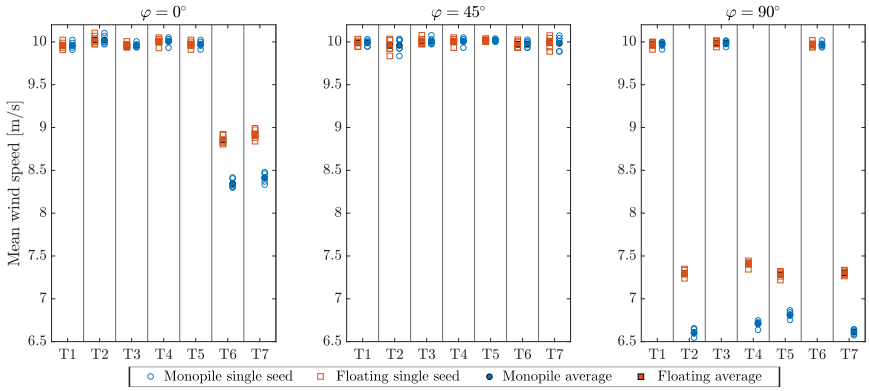

Figure 4: Mean wind speed at hub height for the seven wind turbines (T), in the monopile and floating cases, for three wind directions φ.

wind field (i.e., with a wind speed of 10 m/s) the monopile wind turbines exhibit a larger generated power. This is because they have a better efficiency compared to the floating case: they do not use the peak shaving controller and do not suffer of the reduction of rotor area projection on the plane normal to wind. Conversely, when in the wake of an upstream unit, floating wind turbines produce more power. Although they have a lower efficiency, this is offset by the higher wind speed they experience.

5 Conclusions

In this study, we investigated the energy production of a small floating wind farm and how this is influenced by the low-frequency movements of floating foundations. We modeled a seven-turbine wind farm in the multi-physics simulator FAST.Farm and we studied how the farm response changes when conventional bottom-fixed foundations are replaced with semi-submersibles. Our results show that, when operating in an undisturbed wind, floating wind turbines have a lower power-conversion efficiency compared to their bottom-fixed equivalent. This is due to the reduction of rotor area projection normal to wind caused by the floater tilt and the use of a peak-shaving control strategy. However, a reverse trend has been found for waked wind turbines, that exhibit a higher power output in the floating case. We linked the higher generated power of waked floating turbines to the higher wind speed found in their wake, which is mainly due to dynamic conditions at rotor created by platform motion, the wake upward deflection associated with platform static tilt, and the use of a thrust clipping controller.

References

[1] N. J. Abbas, D. S. Zalkind, L. Pao, and A. Wright. A reference open-source controller for fixed and floating offshore wind turbines. *Wind Energy Science*, 7(1):53–73, 2022.

[2] S. Andersen, A. Madariaga, K. Merz, J. Meyers, W. Munters, and C. Rodriguez. Advanced integrated supervisory and wind turbine control for optimal operation of large wind power plants. Technical report, SINTEF Energy Research.

[3] A. Fontanella, G. Colpani, M. De Pascali, S. Muggiasca, and M. Belloli. Assessing the impact of waves and platform dynamics on floating wind turbine energy production. *Wind Energy Science Discussions*, 2023:1–33, 2023.

[4] N. Ramos-García, S. González Horcas, A. Pegalajar-Jurado, S. Kontos, and H. Bredmose. Investigation of the floating IEA wind 15-MW RWT using vortex methods Part II: Wake impact on downstream turbines under turbulent inflow. *Wind Energy*, 25(8):1434–1463, 2022.

[5] A. Saenz-Aguirre, A. Ulazia, G. Ibarra-Berastegi, and J. Saenz. Floating wind turbine energy and fatigue loads estimation according to climate period scaled wind and waves. *Energy Conversion and Management*, 271:116303, 2022.

[6] A. S. Wise and E. E. Bachynski. Wake meandering effects on floating wind turbines. *Wind Energy*, 23(5):1266–1285, 2020.

20th EAWE PhD Seminar on Wind Energy
24-26 September 2024
Visby, Sweden

Assessing and monitoring low frequency dynamics of floating offshore wind turbines using operational modal analysis

A Al-Ghuwaidi[a], **W Weitjens**[a], and **C Devriendt**[a]

[a]Vrije Universiteit Brussel, OWI-lab, Pleinlaan 2, Elsene, 1050, Belgium

E-mail: abdulelah.al-ghuwaidi@vub.be

Keywords: Floating Offshore Wind Turbines, Operational Modal Analysis, Low-frequency modes, Structural Health Monitoring, Damage detection.

1 Introduction

Marine Renewable Energies (MRE) has exhibited huge potential in recent years, with more expansion to the open sea [1]. By using Floating Offshore Wind Turbines (FOWTs), a huge potential in harvesting wind energy will be unlocked for sites with deeper water depth (more than 50m) [2]. Despite the various advantages of FOWTs, their commercialization has been slow. Currently, only a few FOWTs are installed in real-world settings, mostly for testing purposes [3].

2 Scope of Research

One significant drawback of FOWTs is the high operation and maintenance costs (OPEX). For example, predicting the dynamics of moored systems is more complex than for fixed systems, leading to greater uncertainties and higher costs for floating turbines compared to fixed turbines [4]. A potential solution to reduce these uncertainties and OPEX is the implementation of remote structural health monitoring (SHM) system.

The absence of fixed foundations results in an additional 6 degrees of freedom (DOFs) when using a floating foundation. Due to their substantial weight and reliance on flexible mooring systems, floating offshore wind turbines tend to exhibit very low natural frequencies in their horizontal degrees of freedom, such as surge, sway, and yaw. Figure 1 shows these low frequency modes (i.e. $0-0.05$ Hz) compared to the 1st tower Fore-Aft (FA) and Side-Side (SS) frequencies for NREL OC4 semi-submersible. The aim of this work is to investigate the challenges when assessing the low-frequency modes of floating wind turbines using Operational Modal Analysis. Also, to use the algorithm for monitoring the health of structures to identify damage at its early stage.

3 Methodology

Time-domain software like OpenFAST will be used to generate the time-series signal at different desired points on the FOWT resembling the placement of a accelerometer sensors. The 5MW reference wind turbine mounted on NREL OC4 semi-submersible model [5] will be used. The developed algorithm will then be tested by running a sensitivity analysis simulating different damage scenarios (i.e. loss of a mooring line) for damage detection. The developed algorithm will be fed by real-time data from instrumented turbines to validate its functionality which then will be used for SHM system.

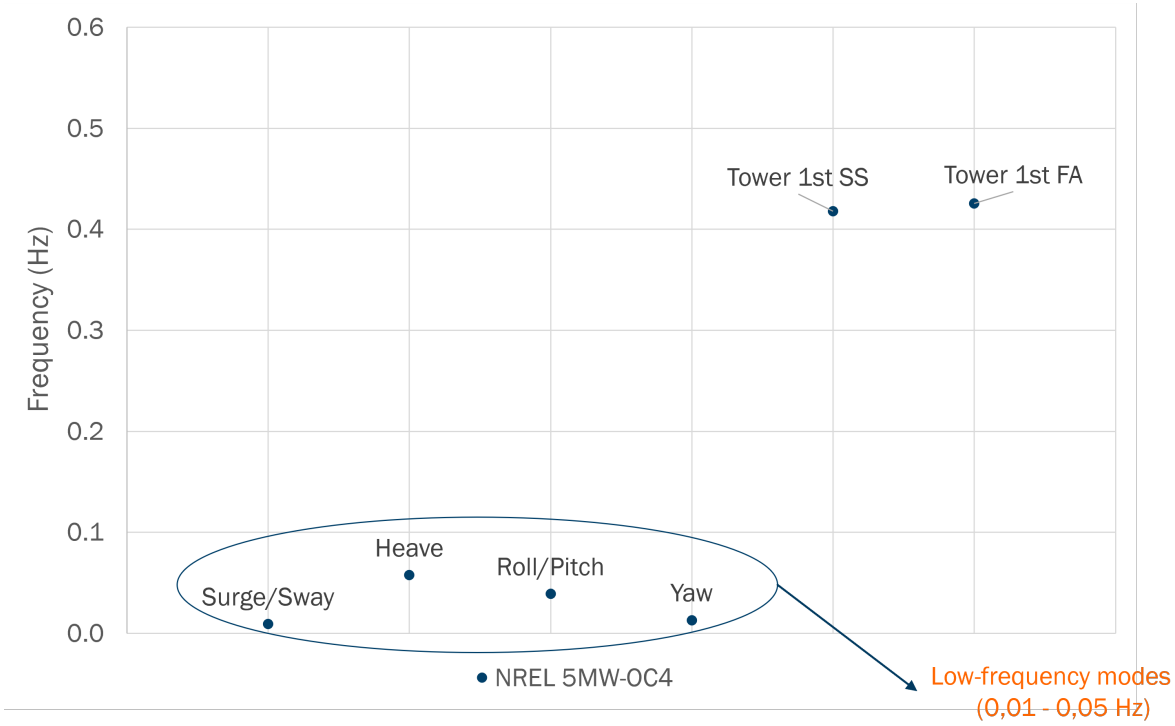

Figure 1: Low-frequency modes of NREL OC4 semi-submersible floating turbine [6].

Acknowledgements

The authors would like to thank the Belgian Ministry of Economic Affairs for their support with the ETF project BEL-Float.

References

[1] V.C. Carlos, Weiss, R. Guanche, B. Ondiviela, Castellanos F.O, and J. Juanes. Marine renewable energy potential: A global perspective for offshore wind and wave exploitation. *Energy Conversion and Management*, 177:43–54, 2018.

[2] B. Nuno and F. Margarida. Emergence of floating offshore wind energy: Technology and industry. *Renewable and Sustainable Energy Reviews*, 99:66–82, 2019.

[3] K. Hyoung-Chul, K. Moo-Hyun, and C. Do-Eun. Structural health monitoring of towers and blades for floating offshore wind turbines using operational modal analysis and modal properties with numerical-sensor signals. *Ocean Engineering*, 188:106226, 2019.

[4] Y.H. Bae, M.H. Kim, and H.C. Kim. Performance changes of a floating offshore wind turbine with broken mooring line. *Renewable Energy*, 101:364–375, 2017.

[5] A. Robertson, J. Jonkman, M. Masciola, H. Song, A. Goupee, A. Coulling, and C. Luan. Definition of the semisubmersible floating system for phase ii of oc4.

[6] A. Robertson, J. Jonkman, F. Vorpahl, W. Popko, J. Qvist, L. Froyd, X. Chen, J. Azcona, E. Uzungoglu, C. Guedes Soares, C. Luan, H. Yutong, F. Pengcheng, A. Yde, T. Larsen, J. Nichols, R. Buils, L. Lei, T. Anders Nygard, and et al. Offshore code comparison collaboration, continuation within iea wind task 30: Phase ii results regarding a floating semisubmersible wind system: Preprint.

On the Generalization of Machine Learning Algorithms for Mooring Line Tension Estimation of Floating Wind Turbines under Unknown Sea Conditions

Max Kämmerling[a], Vincenzo Nava[a,b], Javier Del Ser[a,c]

[a] TECNALIA, Basque Research & Technology Alliance (BRTA), 48160 Derio, Spain
[b] Basque Center for Applied Mathematics (BCAM), 48009 Bilbao, Spain
[c] University of the Basque Country (UPV/EHU), 48013 Bilbao, Spain

E-mail: maximilian.kammerling@tecnalia.com

Keywords: Floating Offshore Wind, Structural Health Monitoring, Mooring Lines, Machine Learning

Although they are more difficult to exploit, offshore wind resources promise higher average wind speeds and increased social acceptance when compared to resources onshore. Wind resources in deep-water are often characterised by even more stable and higher average wind speeds. Accessing these regions will enable higher average capacity factors, highlighting their potential for harnessing wind energy [1].
A bottom fixed installation of offshore wind turbines is only economically viable in water depths up to 50-60m, leading to the need for the development of Floating Offshore Wind Turbines (FOWTs)for deeper water in areas with no continental shelf. Consequently, reliable station-keeping systems with mooring lines are imperative for FOWTs. However, economic drivers within the renewable energy sector often result in non-redundant designs, making each mooring line failure a catastrophic event and might result in the loss of the whole system. Consequently, mooring lines emerge as one of the most critical subsystems of FOWTs. The primary causes of mechanical failures in mooring lines are extreme loads and fatigue, both of which depend on the axial tension in the mooring lines at the pad eyes, hereinafter referred to as 'mooring tension'. Therefore, monitoring mooring tension becomes paramount in assessing the Remaining Useful Life (RUL) and implementing Structural Health Monitoring (SHM) systems of FOWTs.
Direct measuring the mooring tensions is challenging for various reasons. The submerged and harsh offshore conditions make these methods expensive and prone to durability issues. Additionally, marine growth, which naturally accumulates on these submerged components, necessitates regular removal. Therefore, direct measurement of mooring tensions is costly and unreliable without substantial maintenance, frequent inspections, and replacements.
An alternative approach consists of the indirect estimation of the mooring tensions. For example, platform movements are easier to measure, and these measurements often offer greater robustness. For instance, the six Degrees of Freedom (DoFs) of a floating platform can be accurately measured using Global Positioning System (GPS) sensors and Inertial Measurement Units (IMUs), technologies that offer stable measurements with small errors proved in many engineering applications. Placing the sensor inside the hull, away from the harsh offshore environmental conditions, is possible and enhances its longevity.
Considering the significant correlation between mooring tensions and motions, utilizing the motion responses of the floating structure for predicting mooring tension emerges as a viable and efficient option.

To find a transfer function for mapping motions to mooring tensions of floating structures, machine learning (ML) techniques have been applied in recent research, including studies conducted by [2], [3], and [4].
Our doctoral research, which commenced in October 2023, aims to elaborate on the generalization of ML algorithms for mooring line tension estimation of FOWTs under unknown sea conditions. In the following, we will present the results of a baseline study conducted during the initial phase of the doctoral project. This study seeks to outline the key problems that will be addressed throughout the remainder of our PhD research.

For the baseline study, *HarshLab2*, a floating laboratory owned and operated by Tecnalia Research & Innovation [5], is selected as the initial use case. *HarshLab2* is a moored buoy without an installed tower or wind turbine. Consequently, the buoy's movements are not influenced by aerodynamics, control and electrical system (servo) dynamics, or the structural dynamics of an installed wind turbine and its tower.
HarshLab2 is anchored at the Biscay Marine Energy Platform (BiMEP) [6], situated in the Gulf of Biscay, 2.96 km offshore from the village of Armintza (Bizkaia, Spain), at a depth of 65 meters, and can be seen in Figure 1a. For the initial phase of our research, we are focusing on measurement data from a 1/13.6 scaled wave tank model of *HarshLab2*. This approach simplifies the use case further, as wave tank experiments provide a controlled environment. In our experiments, the model was not subjected to wind or current, resulting in buoy motions driven solely by wave loads and the behavior of the mooring system. The *HarshLab2* wave tank model, which can be seen in Figure 1b, consists of three parts: A lower, larger diameter cylinder, an upper cylinder with a smaller diameter, and a landing deck. It is anchored by three catenary mooring lines made of steel chains, as shown in Figure 1c.

Figure 1a:
Real scale floating laboratory HarshLab2

Figure 1b:
Small scale wave tank model of *HarshLab2* that provided training data for this study

Figure 1c:
Chain and load cell of HarshLab2 wave tank model's mooring system

In the wave tank experiments, 15min runs of 12 different sea states were conducted. Several parameters were measured, including the floater's motions in the six DoFs using an optical tracking system and the mooring tensions in the three mooring lines using load cells. In this preliminary study, a Support Vector Regressor (SVR) with a nonlinear kernel was used. The inputs to the models were the current, the precedent 15 and succeeding 10 timesteps of the three DoFs: surge, heave, and pitch. The model's output was the current timestep of the mooring tension of one of the mooring lines. A Robust Scaler, that uses median and interquartile range to scale input and output variables, was used for normalization. The exact configuration of the regression model, including sits hyperparameters are included in Table 1. The model was trained with data from nine sea states, while data from three sea states were held out for testing. The parameters of these sea states are listed in Table 2.

Table 1: Hyperparameters of regression model

Hyperparameter	Value
Output feature y	Tension in Mooring Line 1
Input features X	Surge, Heave, Pitch
Input time window	[-1.5s, 1.0s]
Sampling frequency f	10Hz
SVR epsilon-tube parameter ε	0.1
SVR regularization parameter C	5
SVR kernel	Radial Basis Function
SVR kernel parameter γ	$1/n_{features} * \sigma_X^2$

The parameterized SVR model was evaluated individually on each sea state in both the training and test datasets. The coefficient of determination R^2, root-mean-square error (RMSE) and mean absolute percentage error (MAPE) for different sea states were calculated and are also presented in Table 2.
Overall, the model demonstrates strong performance, achieving an R^2 greater than 92%, an average RMSE below 0.9N and a MAPE below 2.6% for all sea states. The model exhibits particularly robust performance when tested with data under wave conditions (H_s and T_p) close to the average conditions of the sea states used in the training data. For instance, in test sea state 62, the model attained an R^2 of 98.48%, a RMSE of 0.1667N, and a MAPE of 0.76%. The good agreement between estimations and observations of the Mooring Tensions can be seen in Figure 2a.
However, for test sea state 59, which features H_s and T_p at the lower end of the training data's condition range, the model's performance was reduced, with an R^2 of 92.18%. A detailed analysis of the predictions reveals that the regressor slightly underestimates both the peaks and troughs of the mooring tension, with a small observable lag in the estimations, as shown in Figure 2b.
Conversely, for the test sea state 69, which has H_s and T_p at the upper end of the training data's condition range (H_s = 4.3m and T_p = 12.3s real scale), the model's performance was again reduced, achieving an R^2 of 94.01% and a very high MAPE of 2.59% The regressor significantly underestimates the peaks and overestimates the troughs of the mooring tension, particularly affecting the highest peaks and troughs in the experiment, as illustrated in Figure 2c. Similar observations can be made for Runs 67-68, the sea state with the highest H_s value (5.6m real scale) in the training data.
Despite the model's overall strong performance across most sea states, it is evident that its performance diminishes for sea conditions not well represented in the training data, thus showing limited generalization capability. Specifically, for larger sea states resulting in high mooring tension peaks, the model shows potential for improvement.

Our next steps will include an optimization of the architecture of the current model and an exploration of different machine learning models to determine if the identified problem is independent of the algorithm and its hyperparameters. For the remainder of our PhD research, we will address the identified generalization problem of ML algorithms for mooring line tension estimation of FOWTs under unknown sea conditions. We will focus on enhancing the model's performance for rare, extreme sea states, which significantly contribute to the fatigue life of the mooring system. Additionally, to the *HarshLab2* floating laboratory, several other use cases, such as wave tank models of FOWTs and, if available, real scale devices installed in offshore conditions will be investigated.

Table 2: Characteristics of sea states in training and test data and corresponding performance metrics of the SVR model

Run N°	H_s [m, real scale]	T_p [s, real scale]	Dataset	R^2 [%]	RMSE [N]	MAPE [%]
58	1	5.79	train	98.98	0.1405	0.64
59	1	7.72	test	92.18	0.2188	1.11
60	1.36	9.65	train	98.45	0.0927	0.42
61	1.88	6.87	train	99.44	0.1432	0.64
62	1.88	9.15	test	98.48	0.1667	0.76
63	1.88	11.44	train	98.44	0.1000	0.45
71	2.04	14	train	97.97	0.1016	0.46
64	3	7.79	train	99.56	0.1923	0.85
65	3	10.39	train	99.22	0.1653	0.70
66	3	12.98	train	99.21	0.1672	0.72
69-70	4.3	12.29	test	94.01	0.7102	2.59
67-68	5.6	9.22	train	97.99	0.8792	1.94

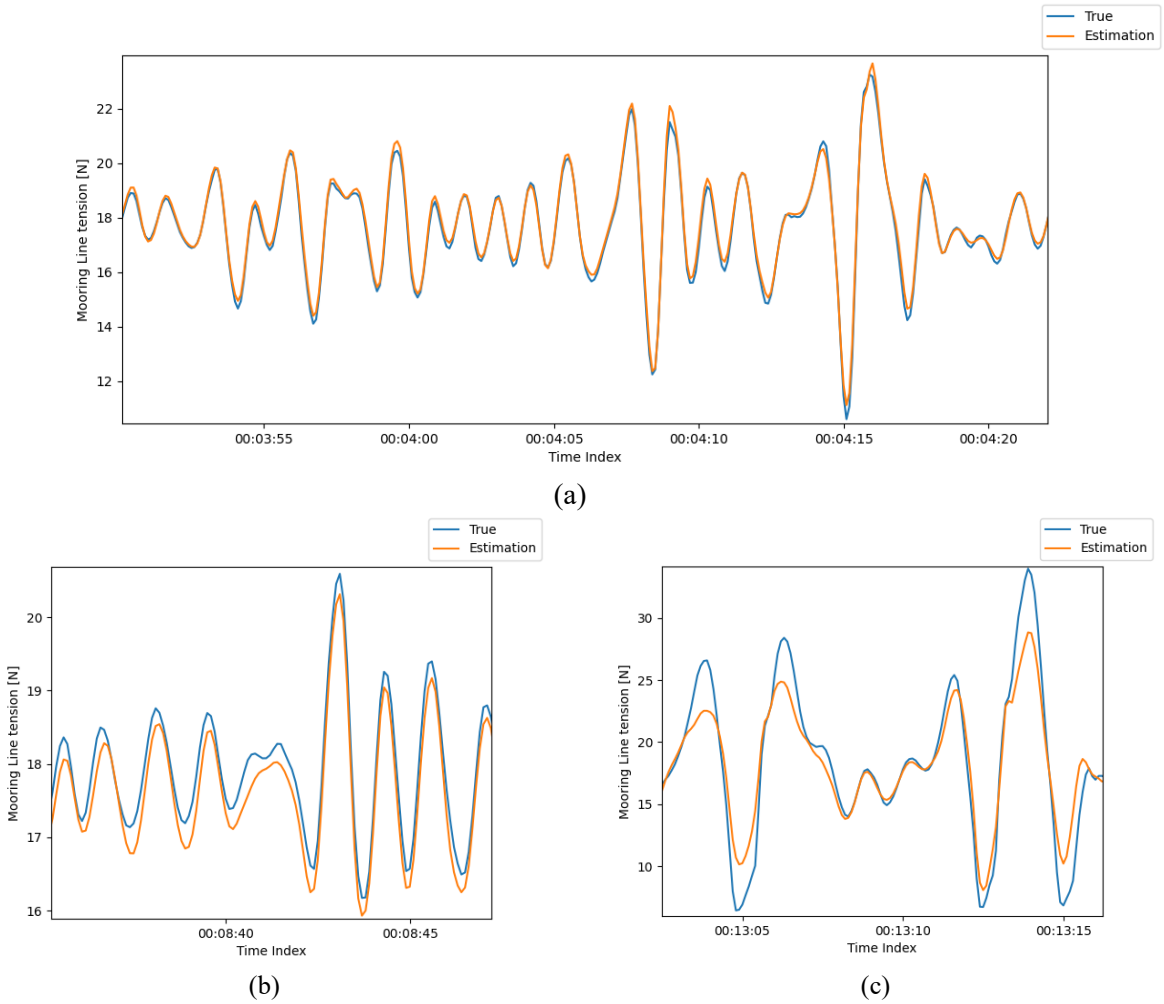

Figure 2: Time series segment of estimations (orange lines) and observed values (blue lines) of mooring line tension of test sea states 62 (a), test sea state 59 (b) and test sea state 69 (c)

References

[1] M. Hannon, E. Topham, J. Dixon, D. McMillan, and M. Collu. Offshore Wind, Ready to Float? Global and UK Trends in the Floating Offshore Wind Market. 2019.

[2] J. Walker, A. Coraddu, M. Collu, and L. Oneto. Digital twins of the mooring line tension for floating offshore wind turbines to improve monitoring, lifespan, and safety. *Journal of Ocean Engineering and Marine Energy*, 8:1 – 16, 2022

[3] G. Ma, C. Jin, H. Wang, P. Li, and H.-S. Kang. Study on dynamic tension estimation for the underwater soft yoke mooring system with LSTM-AM neural network. *Ocean Engineering*, 267: 113287, 2023

[4] Y. Yang, T. Peng, S. Liao. Predicting future mooring line tension of floating structure by machine learning. *Ocean Engineering*, 269: 113470, 2023

[5] Fundación Tecnalia Research & Innovation. HarshLab. Available online on https://harshlab.eu/, accessed on 09/06/2023, last updated on 29/03/2023.

[6] BiMEP Biscay Marine Energy Platform, S.A. Measurements Met-ocean Reference Buoy. 2022

TOPIC 10

Emerging Technologies

10.1 Session 124: Emerging technologies

24.09.2024, 13:10, Room 4

Chair:

Maksims Pogumirskis	

Presenters:

Calzoni Lucrezia	Mitigation Strategies to Counteract the Fluid-Structure Interference in the Connection Area between the Blade and the Rotor Arm of a Vertical Axis Wind Turbine
Zulfazli Muhammad Mutthanna Amjad Bin	X-Rotor Secondary Rotor Aerodynamic Modelling
Sharma Dishant	Numerical Investigation of Deep Dynamic Stall on 2 Bladed H-Rotor VAWT using Scaled Resolved Turbulence Model

20th EAWE PhD Seminar on Wind Energy
24-26 September 2024
Visby, Sweden

Mitigation Strategies to Counteract the Fluid-Structure Interference in the Connection Area between the Blade and the Rotor Arm of a Vertical Axis Wind Turbine

L. Calzoni[a]

[a]Department of Aerospace Science and Technology, Politecnico di Milano, Via La Masa 34, 20156 Milan, Italy

E-mail: lucrezia.calzoni@polimi.it

Keywords: Vertical Axis Wind Turbine, Aerodynamics.

Introduction and Motivations

For years, the European Union has been taking a proactive approach, striving to achieve climate neutrality by 2050 and leading the way as the first continent to commit zero climate impact. This commitment was renewed during the COP28 meeting held in December 2023, where global leaders reiterated their pledge to reduce net greenhouse gas emissions by at least 55% by 2030 [1], and to triple renewable energy capacity within the same timeframe [3], marking a significant milestone in the European Green Deal. Renewable energy plays a critical role in this era of transformation. By 2030, renewable sources are forecasted to generate 68% of total energy production, a substantial increase from the 28% observed in 2021. Within this renewable energy spectrum, wind energy is anticipated to make up approximately one-third of the total energy output, highlighting its pivotal role in steering towards a sustainable energy future [6]. However, unlocking the full potential of wind energy and other renewables requires further technological innovation to drive cost reduction and enhance competitiveness within the energy market.

In this context, Vertical-Axis Wind Turbines (VAWTs) emerge as leading technologies, offering significant advantages due to their unique design. A key feature that makes them particularly appealing is their ability to adapt to wind direction without needing blade orientation, unlike Horizontal-Axis Wind Turbines (HAWTs). VAWTs feature a cylindrical actuation surface perceived as omnidirectional, always perpendicular to the wind flow, ensuring consistent energy capture efficiency regardless of the wind direction [6]. This eliminates the need for complex blade orientation control mechanisms that are inherent in HAWTs, thus leading to significant system complexity and cost reduction [4].Additionally, having a lower centre of gravity compared to an equivalent HAWT, VAWTs can be better suited to future offshore applications. This flexibility, combined with their scalability, makes VAWTs well-suited to a wide range of environmental and geographical settings, including urban areas and offshore applications, where wind conditions may vary unpredictably. Despite their long-standing history and significant advantages, VAWTs' behaviour and complex three-dimensional force field are still not fully understood within the wind energy community. This has erroneously led to the misconception that VAWTs are inherently less efficient than HAWTs and do not have commercial viability. Advancing the understanding and modelling of VAWT aerodynamics for design purposes is therefore essential for accurately assessing their potential future applications.

A common issue that affects the performance of VAWTs, which has not yet been thoroughly investigated, is the aerodynamic interference between the VAWT blade and the rotor arm. As explored in [2], both wind tunnel tests conducted on a scaled model of the blade-rotor arm connection, as well as CFD analysis, revealed a peculiar fluid-structure interaction. Further analysis of this interaction reveals an abrupt flow detachment from the cylindrical connecting element (Figure 1a), resulting in the formation of a distinctive asymmetric bubble-like separation region with downstream vortex structures (Figure 2a).

This anomaly, as highlighted from the wall shear stress distribution using Line Integral Convolution (LIC) surfaces (Figure 1b), influences the deviation of the flow on the blade surface, leading to the formation of a separation zone at the end of the root on both the suction and pressure sides.

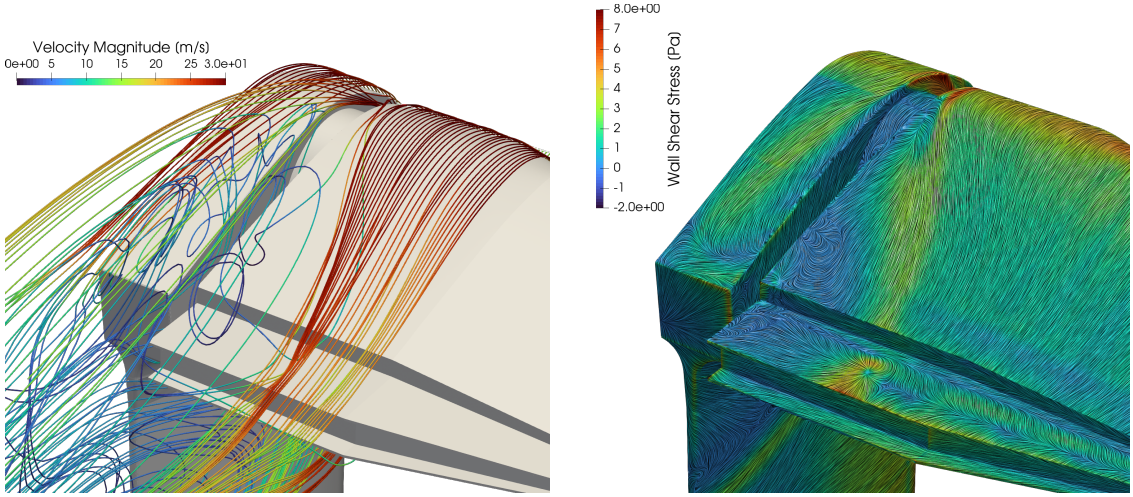

(a) (b)

Figure 1: 3D streamlines within the blade-rotor arm connection zone (a) and LICs visualisation of wall shear stress distribution along the model's surface (b) at α=0°.

Nevertheless, this separation region, as shown in Figure 1b where the presence of limiting streamlines on the surfaces of both the blade and rotor-arm is readily apparent, is confined to a specific and well-defined section of the blade. This unusual flow pattern significantly impacts the aerodynamic characteristics of the blade, causing initially symmetric profiles to behave as antisymmetric ones, leading to the generation of lift even at a zero angle of attack (Figure 2b).

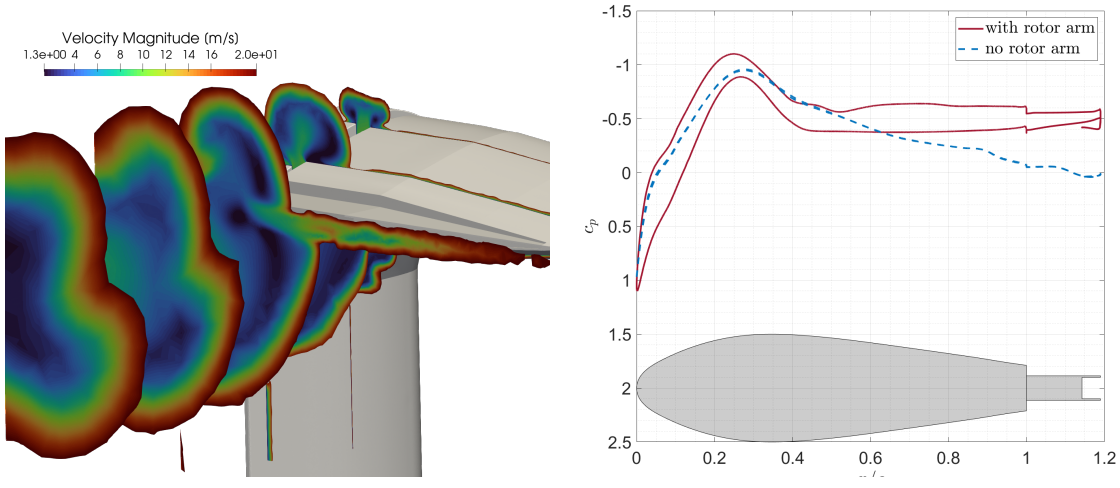

(a) (b)

Figure 2: (a) Velocity iso-contours on cross-sectional slices along the wake (a) and C_p distribution at 4% of the span with and without the rotor arm (b) at α=0°.

Research Outline

In this scenario, the following research question naturally arises:

"How can the adverse effects associated with the unique fluid-structure interaction on VAWT blades, caused by blade-rotor arm interference, be mitigated to enhance blade efficiency?"

To address this question, the research is structured into three main parts.

First Research Stage

The initial stage of the research is guided by the observation of the anomalous behavior of blade profiles, which, despite their symmetry, exhibit antisymmetric behaviour. This prompts a pivotal question:

"How would blade performance be affected by adopting antisymmetric profiles instead of symmetric ones to counteract fluid-structure interaction effects?"

Consequently, the research focuses on redesigning blade airfoils, considering the influence exerted by the presence of the rotor arm, and exploring the feasibility of using not only symmetric but also antisymmetric airfoils. This approach holds significant importance as it enables a thorough examination of the potential impacts of antisymmetric profiles on VAWT performance.
The proposed methodology involves mainly numerical optimisation techniques, primarly using a Genetic Algorithm (GA) with appropriate models of aerodynamic and structural objective functions. Particular emphasis will be placed on modelling the aerodynamic objective function, aiming to enclose, through a simplified mathematical model, the effect due to the presence of the rotor arm. When using a Genetic Algorithm, it is crucial to start with a robust initial population of individuals. In this context, the initial population will be constructed based on a comprehensive analysis of how the rotor presence affects the geometry of the original airfoils, exploiting inverse airfoil design techniques [5]. By examining the airfoils pressure coefficient curves, it is possible to trace back to the corresponding airfoil shape, thereby understanding which airfoil geometric parameters are most significantly influenced by the fluid-structure phenomena. This methodical approach ensures that the resultant airfoil designs are finely tailored to mitigate adverse fluid-structure interactions, thereby enhancing overall VAWT blade performance.

Second Research Stage

With a clear research goal, the second stage naturally follows the work previously conducted in [2], where potential mitigation strategies were explored through a wind tunnel test campaign. Initially, the strategies focused on closing the gap in the connection region (Figure 3a), identified as a significant factor influencing flow deviation on the blade, and subsequently adding small aluminium barriers, known as fences (Figure 3b), at the blade root. Among the various configurations tested, the most promising involved fences positioned on both the suction and pressure sides of the VAWT blade. This configuration effectively countered flow deviation, thereby enhancing blade efficiency while minimising drag.

Building on these findings, the goal of the second part of this research can be framed as follows:

"How can the shape and position of the small barriers placed at the blade root impact the mitigation of adverse fluid-structure interaction effects and enhance VAWT blade efficiency?"

To address this guiding question, a detailed study using CFD tools needs to be conducted on the most promising fence configurations, previously tested in the wind tunnel, to thoroughly understand their mitigation mechanisms. Following this, the research will focus on determining the optimal shape and position of the fences by developing a simplified mathematical model to represent the behaviour of these small barriers on VAWT blades. This model will consider two key parameters, expected to influence the mitigation action: fence position and height. A specific range for these two parameters will be defined for exploration, and an optimisation algorithm will be employed to systematically analyse potential configurations. This algorithm will finely tune the parameters based on specified criteria such as maximizing blade efficiency, minimizing flow deviation, and reducing blade drag, while also considering the drag generated by the fences themselves. This iterative process will aim to identify the optimal configuration for fence height and position, thereby achieving the initial goal.

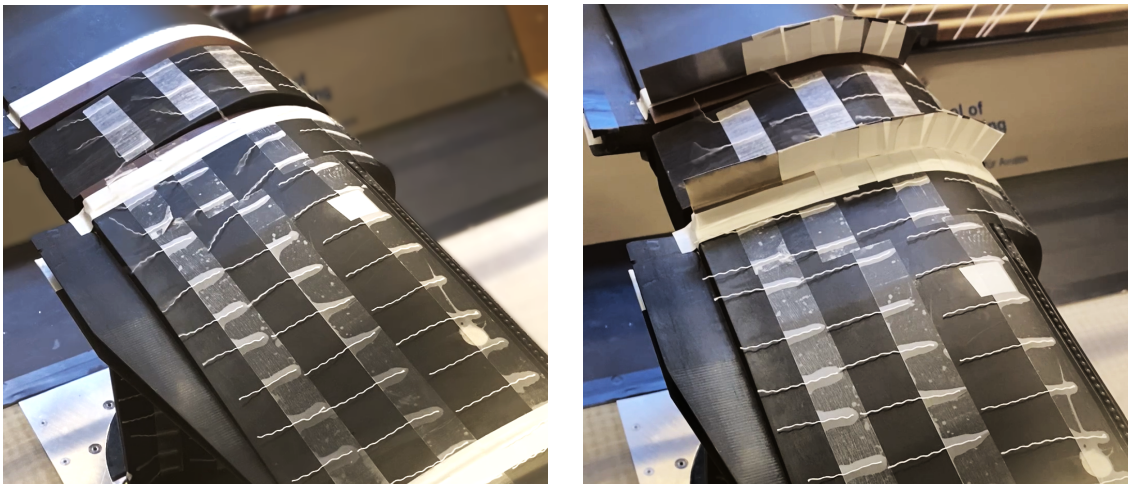

(a) (b)

Figure 3: Tufts visualisation of the gap closed configuration (a) and of the configuration with the fences on both sides (b) at α=0° and at a wind speed of 22 m/s ($Re = 2.3 \cdot 10^5$).

Third Research Stage

Finally, the last part of the research involves integrating the previously established solutions to leverage their combined effects effectively mitigating fluid-structure interaction phenomena. By combining the flow deviation-blocking abilities of fences with the inherent capacity of the newly designed antisymmetric profiles to counteract the induced effects, a substantial reduction in interference, surpassing the effect of just adopting each solution individually, is expected. This integrated approach not only aims to restore the problem symmetry but also promises notable enhancements in blade performance, particularly in terms of efficiency.

References

[1] The european green deal : Striving to be the first climate-neutral continent, 2024. Accessed on June, 2024.

[2] L. Calzoni. Experimental and numerical investigation of the aerodynamic interference at the root of a pitch-controlled vawt blade. Master's thesis, Politecnico di Milano, lucrezia.calzoni@polimi.it, December 2023. An optional note.

[3] COP28, IRENA, and GRA. Tripling renewable power and doubling energy efficiency by 2030: Crucial steps towards 1.5°c, 2023.

[4] S. Eriksson, H. Bernhoff, and M. Leijon. Evaluation of different turbine concepts for wind power. Renewable and Sustainable Energy Reviews, 12(5):1419–1434, 2008.

[5] B. Gardner and M. Selig. Airfoil design using a genetic algorithm and an inverse method. AIAA 41st Aerospace Sciences Meeting and Exhibit, 2003.

[6] S. Watson, A. Moro, V. Reis, C. Baniotopoulos, S. Barth, G. Bartoli, F. Bauer, E. Boelman, D. Bosse, A. Cherubini, A. Croce, L. Fagiano, M. Fontana, A. Gambier, K. Gkoumas, C. Golightly, M. I. Latour, P. Jamieson, J. Kaldellis, A. Macdonald, J. Murphy, M. Muskulus, F. Petrini, L. Pigolotti, F. Rasmussen, P. Schild, R. Schmehl, N. Stavridou, J. Tande, N. Taylor, T. Telsnig, and R. Wiser. Future emerging technologies in the wind power sector: A european perspective. Renewable and Sustainable Energy Reviews, 113, 2019.

X-Rotor Secondary Rotor Aerodynamic Modelling

Muhammad Mutthanna Amjad[a], Laurence Morgan[a], Abbas Kazemi Amiri[a], William Leithead[a], and James Carroll[a]

[b] EEE, University of Strathclyde, Glasgow, G1 1XW, Scotland

E-mail: mutthanna.amjad@strath.ac.uk

Keywords: power take-off, secondary rotor, vertical axis, X-Rotor

The X-Rotor is a novel wind turbine concept that combines a vertical axis primary rotor with horizontal axis secondary rotors, aiming to reduce the levelised cost of energy from offshore wind by 26% through capital and maintenance cost reductions [1]. The unique feature of the X-rotor concepts is that power take-off occurs on the secondary horizontal rotors to maximise energy capture. Previous studies have demonstrated that the X-Rotor design can effectively transfer between 87% and 90% of the power captured by the primary rotor to the secondary rotors, significantly reducing nacelle mass by 85% to 87% compared to conventional horizontal wind turbine drivetrains [2]. This research does not focus on the cost of energy but will explore the aerodynamic performance differences between low and mid-fidelity models based on the Blade Element Momentum Theory (BEM) and the Lifting Line Free Vortex Wake (LLFVW) approach using the Qblade software [3]. Furthermore, it investigates the aerodynamic interactions between multiple secondary rotors and their wake. The expected findings will assist in the investigation of aerodynamic coupling between the primary and secondary rotors.

Figure 1: X-Rotor Concept

References

[1] W. Leithead, A. Camciuc, A. K. Amiri, and J. Carroll, 'The X-Rotor Offshore Wind Turbine Concept', in *Journal of Physics: Conference Series*, Institute of Physics Publishing, Oct. 2019. doi: 10.1088/1742-6596/1356/1/012031.

[2] L. Morgan, W. Leithead, and J. Carroll, 'On the use of secondary rotors for vertical axis wind turbine power take-off', *Wind Energy*, Jun. 2024, doi: 10.1002/we.2901.

[3] 'QBlade - Next Generation Wind Turbine Simulation'. Accessed: Jun. 17, 2024. [Online]. Available: https://qblade.org/

20th EAWE PhD Seminar on Wind Energy
24 - 26 September 2023
Visby, Sweden

Numerical Investigation of Deep Dynamic Stall on 2 Bladed H-Rotor VAWT using Scaled Resolved Turbulence Model

Dishant Sharma[a], Rahul Goyal 2[a]

[a] Department of Energy Science and Engineering, Indian Institute of Technology Delhi, New Delhi 110016, India
E-mail: rahulgoyal@dese.iitd.ac.in

Keywords: Vertical Axis Wind Turbine, Self-start, Dynamic stall, Scale resolve simulation

Abstract: Increasing adaptation in renewable source of energy in urban areas, especially in wind power sector, raises the researcher's interest in optimizing and enhancing the performance of small-scale vertical axis wind turbines. The self-starting, lower performance, and dynamic stability are the major challenges in wind turbines that need to be explored. The present research article focuses on the accurate prediction of the performance and formation of dynamic stall phenomenon in a 2 bladed H-rotor wind turbine involving Transition Shear Stress Transport (TSST), Scaled Adaptive Simulation (SAS) and Detached Eddy Simulation (DES) modelling techniques. Due to overprediction of the reverse-flow in the upstream turbulent boundary layer by the conventional turbulent model, scale resolved technique has been utilized for capturing the accurate flow characteristics. Results are discussed on the impact of tip speed variation on the performance and flow characteristics of the H-rotor at modest Reynolds number (0.85 to 1.95 × 105). A nonuniform structured mesh has been generated satisfying averaged y+<1 criterion for both the airfoils followed by performing a validation that shows 0.15% error utilizing TSST model compared to an experimental result. The results show that at tip speed ratio value 4, the maximum power coefficient is obtained as 0.4046. Furthermore, the aerodynamic performance of the H-rotor is extensively investigated at a lower tip speed ratio of 2 with all the different turbulence models, where deep dynamic stall is the dominating factor, and compared to the performance under high tip speed ratio conditions.

1. Introduction

Wind energy stands out as an abundant and readily available source that has received significant attention among the broad spectrum of renewable resources [1]. In the growing field of wind energy, the adoption of Vertical Axis Wind Turbines (VAWTs) emerges as a captivating potential alternative. These turbines are distinctive from conventional horizontal axis wind turbine's design and offer certain advantages like omnidirectional, scalability, being adaptable to fluctuations in wind patterns that make them suitable for intricate terrains and urban areas [2], [3]. However, there are several challenges associated with VAWTs such as flow instability due to blade wake interactions, rapid and cyclic changes in the angle of attack (AoA) leads to undesired dynamic stall condition. This dynamic stall phenomenon dominates for the low tip speed ratio (TSR) range and significantly affect the self-starting capability, power coefficient (C_p), and deteriorate the overall aerodynamic performance of the H-type VAWTs. Thus, to analyse the complex aerodynamics of H-rotor for optimising its performance and stability, computational fluid dynamics (CFD) simulations has been conducted.

It has been observed that for H-rotor VAWT researchers [4] commonly used URANS or LES to understand the important aspects of formation and progression of dynamic stall during the complete revolution of the turbine at low TSR. However, URANS poorly captured the vortices/small-scale bubbles whereas LES is computationally more expensive and not feasible in most of the situation. Hence, usage of a hybrid/bridging model which required low computational cost, capture flow physics and producing better results would be an ideal solution. The present study is an attempt to involve a hybrid and scale resolving bridging model (TSST, SAS, DES) to inspect the flow characteristics over a blade and to precisely predict the aerodynamic performance of a H-rotor, for a wide working range.

2. Numerical Methodology

One of the most important steps in the modelling process is to create an appropriate computational domain for a fluid dynamics problem. It's important to optimize the domain size: minimum inlet distance from the rotor centre for avoiding the overestimation of turbine's performance, minimum outlet distance for maintaining the pressure recovery, and minimum domain width for minimizing the blockage effects on the turbine performance. Figure 1(a) shows the 2-Dimensional computational domain of 2 bladed (NACA 0018) H-rotor configuration based on the experimental work of Tescione et al. [5]. A non-uniform structured grid (Fig. 1(b)) has been generated in the computational domain followed by generating a fine mesh near the blade wall. The average dimensionless wall distance $y+$ value < 1 and maximum $y+$ (Table 1) is maintained < 5 for all the blades that helps to accurately predict the aerodynamic coefficients and capture the viscous sublayer, visualize the flow reversal and vortices movement over the blade. The geometrical and operational parameters of an H-rotor system are described in Table 2.

Table 1 *$y+$ at the wall adjacent cell of both the blades*

Wall $y+$ maximum	Blade 1	1.4725
	Blade 2	1.1287
Wall $y+$ average	Blade 1	0.4347
	Blade 2	0.2446

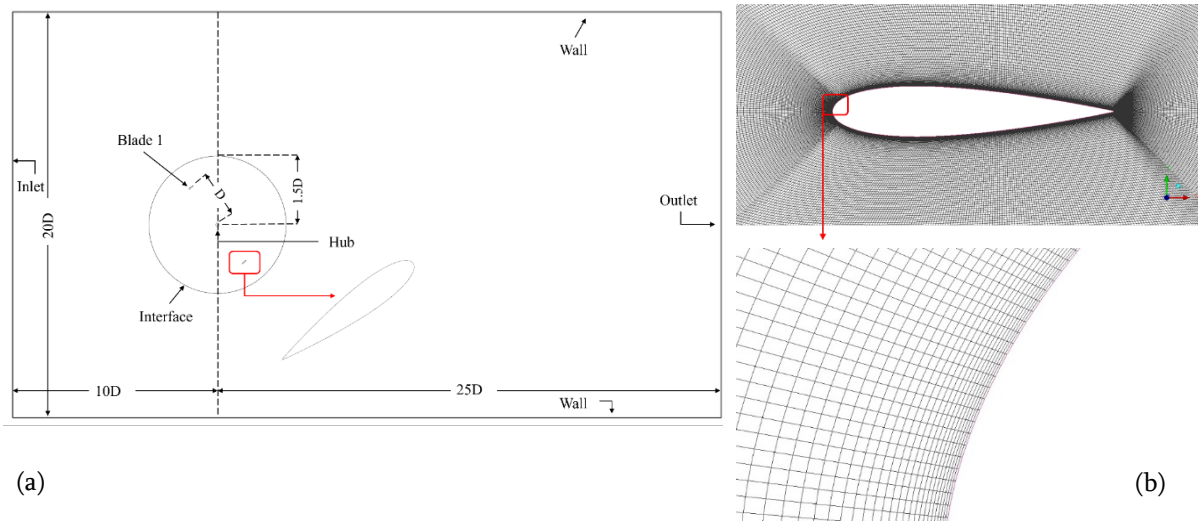

Figure 1(a) *Schematic of computational domain,* ***(b)*** *Structured grid of airfoil and its close-up view*

Table 2 *H-rotor parameters.*

Parameter	Value
Number of blades	2
Blade airfoil	NACA 0018
Blade chord, c [m]	0.06
Rotor and Shaft diameter, D [m]	1, 0.04
Aspect ratio [-]	1
Blade solidity [-]	0.12
Wind speed, V [m/s]	9.3
Chord based Reynolds number, Rec ($\times 10^5$)	0.85 to 1.95
Rotational speed, Ω [rpm]	800
Turbulence intensity [%]	5

3. Preliminary Results

To ensure the reliability, accuracy, optimisation of computation time and resources, grid and time independency test has been conducted as shown in Figs. 2(a) and (b). The current computational work using the Transition SST turbulence model was validated using the experimental results of Tescione *et* al. [5] and a negligible deviation of 0.15% in Cp has been observed. The values of Cp obtained at TSRs ranging from 2 to 5 are plotted (Fig. 2(c)), with TSR 4.0 yielding the highest value of 0.4046. The interest zone of the present analysis is 2 to 3 since the deep stall can be identified in this range. Further, analysis is performed at TSR 2 and compared with the validated TSR 4.5 moment profile, as shown in Fig. 2(d). It can be seen that as the TSR is reduced, the amplitude of the upstream section decreases, and more significant fluctuations in the moment are noticed, indicating the occurrence of bubble creation, bursting, and separation from the suction surface of the blade. As the figure illustrates, at λ equal to 4.5 (83.7 rad/s), number of fluctuations in the complete rotor revolution is 5 and the total positive area in the cycle is 92.09%. When the turbine is operated at λ equal to 2 (37.2 rad/s), number of fluctuations in the complete rotor revolution increases to 13 with a decrement of positive area to 60.16%. At low TSR of 2 the magnitude of initial torque value is not sufficient to rotate the rotor and can be seen from figure the percentage of area is more than 5 times compared to 4.5 TSR.

Table 3 *Influence of tip speed ratio on the moment coefficient during entire rotor rotation.*

TSR	No. of fluctuations	Positive (%)	Negative (%)
2	13	60.16%	39.83%
4.5	5	92.09%	7.90%

Further results and conclusions including turbulence models comparison, z-vorticity contours and pressure coefficient variation will be incorporated into the final oral presentation.

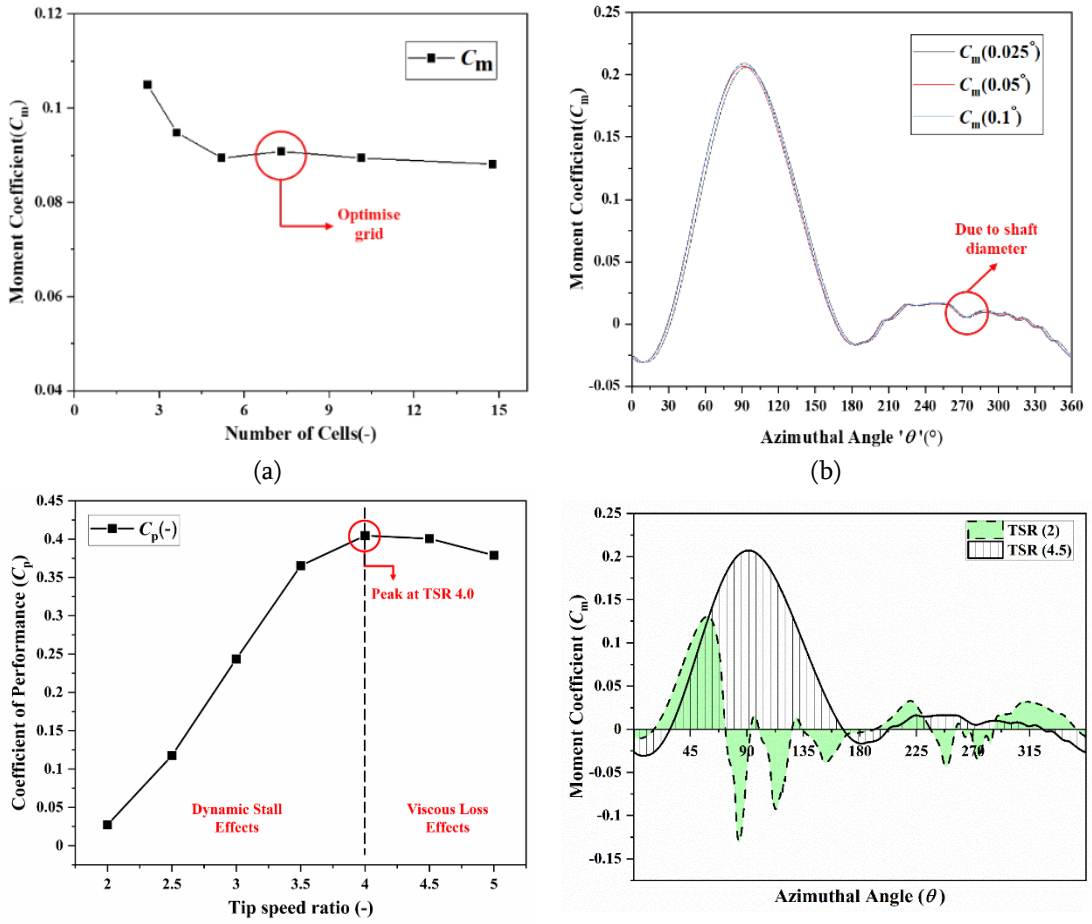

Figure 2 (a) *Mesh independency,* ***(b)*** *Time independency,* ***(c)*** *Performance variation with TSR, and* ***(d)*** *Moment variation for different TSR in a complete turbine revolution*

4. Concluding Remarks

The current study explores the estimation of the performance of dynamic stall and its formation in a two bladed H-rotor wind turbine system. Hybrid and scale resolving turbulent models are utilized to capture the flow behaviour. Simulations are performed for generating initial results and based on that following points are concluded:

- The validation of the present model with the experimental data shows 0.16% error, which shows the reliability of the computational model.
- For a given TSR range 2-5, the C_p value indicates that TSR range 2-3 is the zone of interest as deep stall can be identified in that region.
- For a given azimuthal angle ($0 \leq \theta \leq 360$), as the TSR value is reducing from 4.5 to 2, the moment co-efficient diminishes in the upstream section followed by generating an abrupt fluctuation in the downstream section.
- At low TSR of 2 the magnitude of initial torque value is not sufficient to rotate the rotor and the percentage of area is more than 5 times compared to 4.5 TSR.

Acknowledgements

Dishant Sharma and Rahul Goyal are thankful to the Ministry of Education, India, and the IIT Delhi HPC facility for computational resources.

References

[1] A. Evans, V. Strezov, and T. J. Evans, "Assessment of sustainability indicators for renewable energy technologies," *Renew. Sustain. Energy Rev.*, vol. 13, no. 5, pp. 1082–1088, 2009, doi: 10.1016/j.rser.2008.03.008.

[2] A. Bianchini, G. Ferrara, and L. Ferrari, "Design guidelines for H-Darrieus wind turbines: Optimization of the annual energy yield," *Energy Convers. Manag.*, vol. 89, pp. 690–707, Jan. 2015, doi: 10.1016/j.enconman.2014.10.038.

[3] M. Douak, Z. Aouachria, R. Rabehi, and N. Allam, "Wind energy systems: Analysis of the self-starting physics of vertical axis wind turbine," *Renew. Sustain. Energy Rev.*, vol. 81, no. March 2017, pp. 1602–1610, 2018, doi: 10.1016/j.rser.2017.05.238.

[4] C. J. Simão Ferreira, A. Van Zuijlen, H. Bijl, G. Van Bussel, and G. Van Kuik, "Simulating dynamic stall in a two-dimensional vertical-axis wind turbine: verifi cation and validation with particle image velocimetry data," *Wind Energy*, no. May 2009, pp. 1–20, 2013, doi: 10.1002/we.

[5] G. Tescione, D. Ragni, C. He, C. J. Simão Ferreira, and G. J. W. van Bussel, "Near wake flow analysis of a vertical axis wind turbine by stereoscopic particle image velocimetry," *Renew. Energy*, vol. 70, pp. 47–61, 2014, doi: 10.1016/j.renene.2014.02.042.

10.2 Session 314: Emerging technologies

26.09.2024, 9:0, Room 4

Chair:

Mohammadreza Manami

Presenters:

Pourmirasghariyan Mirhamed	Synchronous control of X-Rotor secondary rotors using a virtual synchronous machine
Bordignon Matteo	Estimation of the Absolute Wind Vector for AWE Systems
Tan Yoke Wang	X-Rotor Scaling and Operation with Primary Rotor Generator

Synchronous control of X-Rotor secondary rotors using a virtual synchronous machine

Mirhamed Pourmirasghariyan[a], David Campos-Gaona [a],Panagiotis Papadopoulos [b]

[a] University of Strathclyde
[b] University of Manchester

E-mail: Mirhamed.pourmirasghariyan@strath.ac.uk

Keywords: X-rotor, Virtual Synchronous Generator (VSG), Microgrid

I. Introduction

Wind Turbine Energy Generation Systems (WTEGS)s are playing an important role in the renewable energy section and Net-Zero carbon ambitions. The ambitions are not restricted to Net-Zero carbon or expanding wind farms. Still, manufacturers are also aiming to bring about radical innovations in terms of the structure, operation, and supply chain of WTEGSs to screen out obstacles in the industry. The main obstacles in industry are turbine tower transportation challenges, maintenance difficulties, and operation principles which hinder robust operation for various scenarios [1].

A novel X-Rotor concept as a new wind turbine structure has been developed at the University of Strathclyde to address these concerns, see Fig. 1.

The above-shown X-Rotor comprises one primary rotor and two secondary rotors with Permanent Magnet Synchronous Generators (PMSG)s. While the primary rotor rotates freely (i.e. it is not connected to any conversion device), the secondary rotors oversee power generation. One of the novelties of the X-Rotor wind turbine is the introduction of high-speed secondary rotors to produce energy which significantly reduces the turbine size for the same rating of a Horizontal Axis Wind Turbine (HAWT). The X-Rotor turbine combines the advantages of HAWT and Vertical Axis Wind Turbine (VAWT). Some of the main benefits can be summarized below:

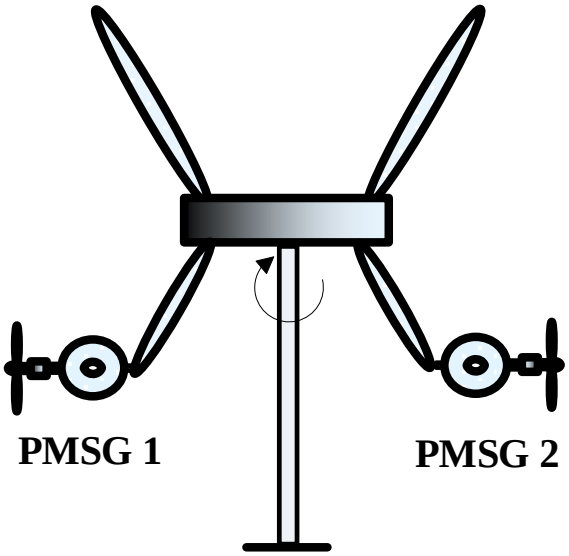

Fig. 1. X-Rotor WTEGS with Secondary Rotors.

- The high-speed secondary rotors will pave the way for smaller generators. Based on (1), for constant power and constant angular force on the rotor, the radius of the rotor must be reduced. Therefore, the size of the wind turbine will be reduced noticeably.

$$T \downarrow .\Omega \uparrow = P(cte) \Rightarrow T \downarrow = r \times F(cte) \qquad (1)$$

where the parameters P , T , r , F and Ω are power, torque, rotor radius, angular force on the rotor, and rotor speed, respectively

- As the X-Rotor structure takes advantage of HAWT and VAWT, the rated speed of the secondary generators is satisfied at lower heights [2]. The lower the tower is, the less material is needed. This will lead to low construction costs, as well as other issues (transportation). More importantly, the lower tower height eases the maintenance of the turbine, and accessibility to the turbine (OPEX is reduced).
- Since the X-Rotor is smaller than the HAWTs with small and high-speed secondary rotating generators, the wake effects are also reduced because of the different mixing with the atmospheric flows which in turn causes a more efficient structure [3]. This will increase the efficiency of the wind farm.

II. Problem Statement

As the primary rotor is not connected to a converter or a generator, only two PMSGs oversee energy generation. Having two different converters to control each PMSG is pricey. In this regard, by having only one converter controlled as a Virtual Synchronous Generator (VSG), a virtual Micro Grid (MG) is conceivable. Further, considering the nominal rating of the converter to be twice that of a single PMSG, it will act as a slack-bus Conventional Synchronous Generator (CSG). Overall, by the proposed concept, the frequency, produced active and reactive power, DC-Link voltage can be easily controlled, see Fig. 2.

III. Conclusion

In this project, a control structure will be proposed to control both PMSGs of the X-rotor with the VSG concept. This will bring about some benefits as follows:

- Cost-effectiveness: Instead of one single converter for each PMSG, only one converter can be operated as VSG
- Controllability: Every important parameter including active and reactive powers, frequency, DC-link voltage, etc. is controllable.

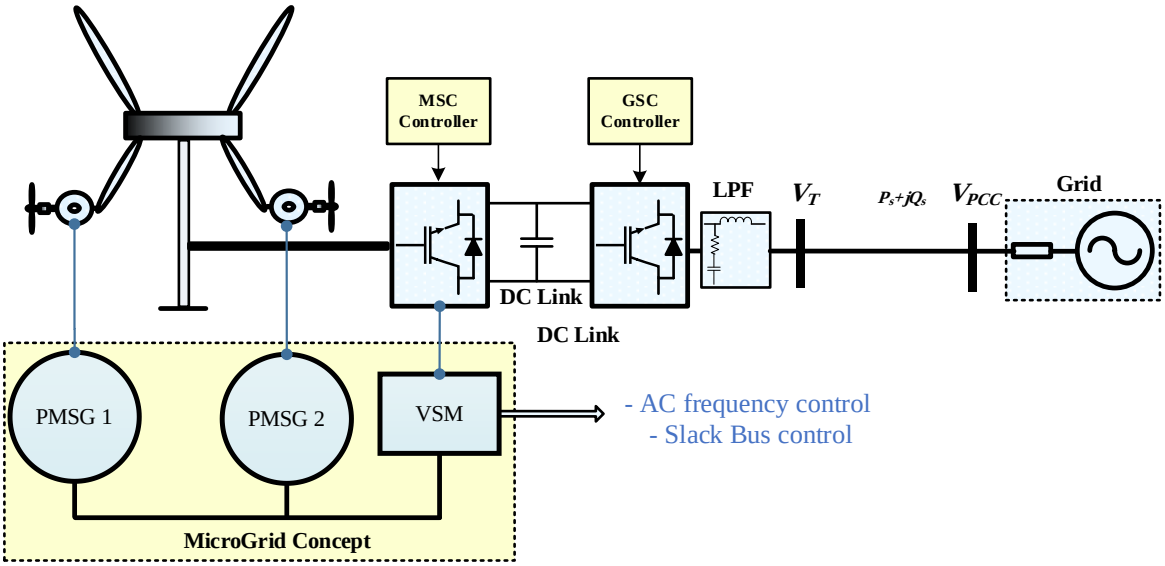

Fig. 2. Conceptual MG operation of X-rotor via VSG.

- Simplicity: The proposed MG conceptual grid is simple because there is only one converter and two PMSGs in which all of them are operated as CSGs.
- The VSG will enhance the stability of the system as there is no Phase Locked Loop (PLL). Moreover, it is operable in islanded modes because of VSG advantages.

References

[1] J. Carroll, A. McDonald and D. McMillan, "Reliability Comparison of Wind Turbines With DFIG and PMG Drive Trains," in *IEEE Transactions on Energy Conversion*, vol. 30, no. 2, pp. 663-670, June 2015.
[2] https://xrotor-project.eu/
[3] David Bensason *et al* , *J. Phys.: Conf. Ser.* 2505 012040, 2023.

20th EAWE PhD Seminar on Wind Energy
24-26 September 2024
Visby, Sweden

Estimation of the Absolute Wind Vector for AWE Systems

M. Bordignon[a], **A. Croce**[a], and **L.M. Fagiano**[b]

[a]Department of Aerospace Science and Technology, Politecnico di Milano
[b]Deparment of Electronics, Information and Bioengineering, Politecnico di Milano
E-mail: matteo.bordignon@polimi.it

Keywords: Estimation, AWE, Optimization

1 Introduction

Airborne Wind Energy (AWE) is a technology able to harness wind power by employing an autonomous tethered aircraft, usually referred to as a kite. Systems within this category can harvest high-altitude wind energy (approximately 200-500 m from the ground), resulting in an high power yield, as first introduced by Loyd [7]. This advantage however comes at the cost of a higher system complexity. The role of automation is therefore crucial in order to exploit the theoretical benefits of this technology. Figure 1 summarises the main employed layouts.

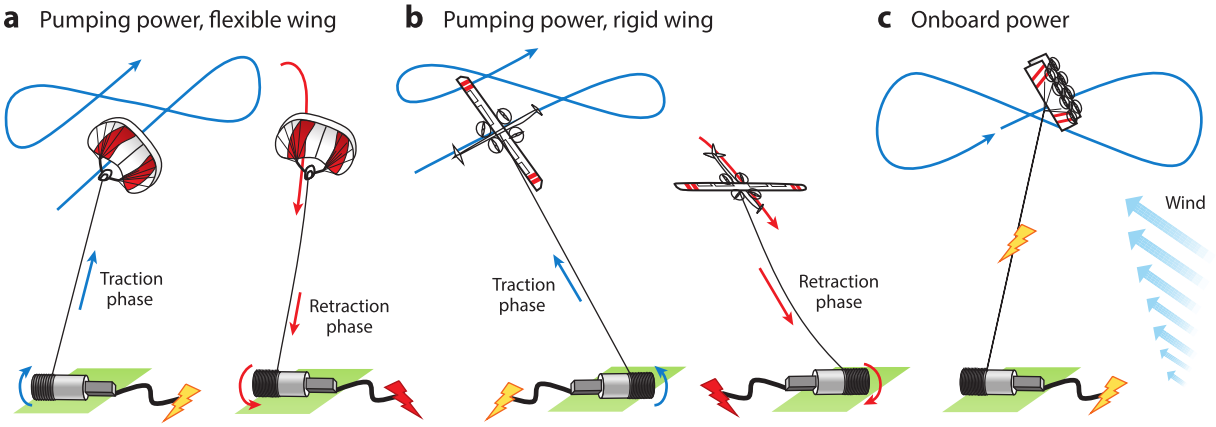

Figure 1: Operation principles of the three airborne wind energy system layouts that are currently at an advanced development stage: (a) on-ground (pumping power) conversion with a flexible aircraft, (b) on-ground conversion with a rigid aircraft, and (c) onboard power conversion. taken from [4], reprinted with permission

One of the main challenges of this system is its reliability [4]. In particular, the lack of an accurate wind speed measurement at the flight altitude degrades the control systems' effectiveness, as wind is the main source of power while simultaneously being the main source of disturbance in the system. To improve inaccurate currently employed methodologies, mainly based on the interpolation of ground-level measurements, this work proposes a novel wind estimation method based on the solution of an optimization problem. The algorithm is fed only by the kite position data, along with its derivatives, and the tether force. All of the measurements are easily retrievable in a real-world setting, therefore making the method practically feasible. In a simulation setting, the results of this approach suggest a promising application in the field.

2 Modelling

Due to the simulative nature of this work, this first section depicts the models exploited during this research.
The simulation model will be introduced, providing a foundational understanding of the structure and compo-

nents of the model exploited to create feasible flight data, in an attempt to replicate real-world scenarios. Only an overview of the model will be presented since a detailed explanation can be found in the Ph.D. thesis of Professor Lorenzo Fagiano [3].

When describing the aerodynamic model, consider a scenario where a flexible wing is connected to the ground via one or multiple tethers. To ensure the model's versatility, a single equivalent point mass, denoted with m, was employed to represent the combined effects of various forces acting on the system. This point is positioned at the kite's aerodynamic center, denoted with vector r, and concentrates both the kite's mass and the mass of the tether, similar to the approach outlined in [8], from which the picture in the following section was taken.

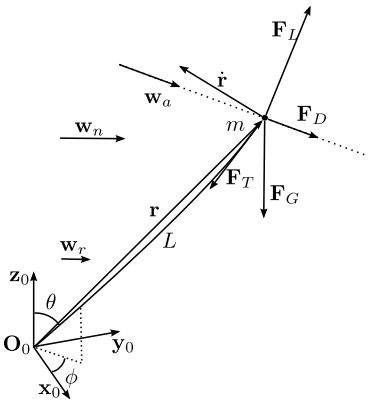

Figure 2: AWE System diagram

The system will be described within an inertial reference frame fixed to the ground station, where the tether is attached. This reference frame, denoted as $R = (X, Y, Z)$, is right-handed, with X representing the primary wind direction, Z pointing upwards, and Y completing the coordinate system. In Figure 2, this reference frame is illustrated using its unit vectors x_0, y_0, and z_0.

The equations of the forces governing such system can be summarized as

$$F_L = \frac{1}{2}\rho A C_L \|w_a\|^2 z_l \tag{1}$$

$$F_D = \frac{1}{2}\rho A C_D \|w_a\|^2 \frac{w_a}{\|w_a\|} \tag{2}$$

$$F_G = (m_k + \frac{1}{2}m_t)\begin{bmatrix} 0 \\ 0 \\ -g \end{bmatrix} \tag{3}$$

The system trajectory is controlled with two inputs. The first one is the steering effort applied on the kite and the second one is the tether force F_T. Considering the latter, while its direction is always defined by r, its magnitude is modified based on the difference between the actual and the reference length of the tether.
Albeit simple, this approach can describe the dynamics of the system with the necessary accuracy for the problem at hand, while reducing the simulation burden.

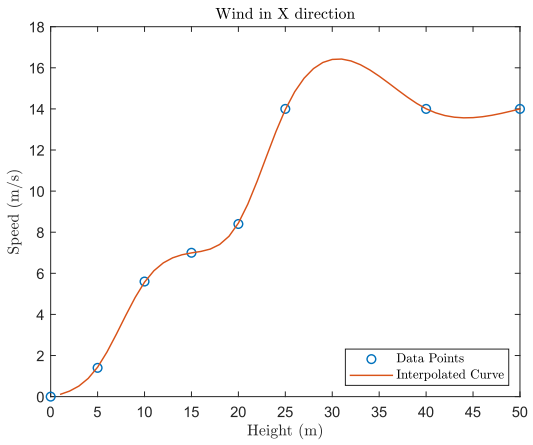

Figure 3: Wind profile in the X direction

Lastly, the wind model can be introduced. In the literature, it is possible to find different valid models, such as *log-law* and *power law* [1]. However, these models produce small changes in wind magnitude when subjected to minimal changes in the altitude of the system flights. In order to improve the scenario coverage of the estimation approach, a novel wind model was utilized in this work. The wind magnitude in its principal direction, namely X, was generated using an interpolation function, implementing a Cubic Spline method based on arbitrarily selected data points. This procedure created an irregular wind field, improving the robustness of the results. Similarly, in the Y direction, the wind magnitude will be linearly proportional to the height and the wind in the X direction. The generated wind speed in this direction can be described with Equation 4, where α and β are arbitrary coefficients to be selected to generate different scenarios.

$$W(Y) = \alpha W(X) + \beta r_z \tag{4}$$

3 Estimation

While wind estimation has been extensively explored in traditional wind energy, particularly in papers like [5] and [6], there's limited research addressing this issue in the context of AWE. Notably, [8] stands out as a significant contribution where researchers make use of an Extended Kalman Filter (EKF) framework to estimate aerodynamic parameters and wind data.
This study addresses the wind estimation problem using a Gradient-Based Optimization approach. This technique belongs to a group of methods that leverage first- and second-order optimality conditions to identify the minimum of a given cost function. In particular, this work employed a *Sequential Quadratic Programming* (SQP) method, that uses *Broyden–Fletcher–Goldfarb–Shanno* (BFGS), a quasi-newton method, to approximate the Hessian matrix, in order to check if the best candidate meets the second-order optimality condition. Through the use of BFGS, this crucial approximation can be computed by using only information on the gradients of the cost function and constraints. A detailed mathematical derivation of these methods can be found at [2].

In this technique, an estimation model is employed. It can be summarised as

$$\ddot{r} = f_{est}(\tilde{r}, \tilde{\dot{r}}, \|\tilde{F}_t\|, \overline{p}, W, z_l) \tag{5}$$

where $\overline{p} = [\rho, A, \overline{C_L}, \overline{C_D}, m_k, n_t, d, \mu_t]$ represents the modified vector of constant parameters.
This model is a simplification of the simulation one, emphasizing the model mismatch inevitably present in a real-world application.

By defining the direction of the lift vector z_l thought its directional components and the vector of optimization variables as

$$z_l = \begin{bmatrix} z_{lx} & z_{ly} & z_{lz} \end{bmatrix}^T \tag{6}$$

$$u = \begin{bmatrix} W_x & W_y & z_{lx} & z_{ly} & z_{lz} \end{bmatrix}^T \tag{7}$$

at each time step, the following nonlinear optimization problem is solved. It tries to minimize the difference between the measured accelerations of the kite and computed ones from an estimation model. An additional term is added to the cost function, based on the difference between the solution at the current and previous step.

$$\begin{aligned} \underset{u}{\text{minimize}} \quad & (\tilde{\ddot{r}} - \ddot{r})^T Q (\tilde{\ddot{r}} - \ddot{r}) + (u - u_{old})^T Q_{diff} (u - u_{old}) \\ \text{subject to} \quad & \ddot{r} = f_{est}(\tilde{r}, \tilde{\dot{r}}, \|\tilde{F}_t\|, p, u), \\ & \underline{u} \leq u \leq \overline{u}, \\ & \|z_l\| - 1 = 0, \\ & {z_l}^T w_a = 0 \end{aligned}$$

Simulating the system and applying the estimation algorithm on the flight data produced yield satisfactory results, which can be depicted in Figure 4.

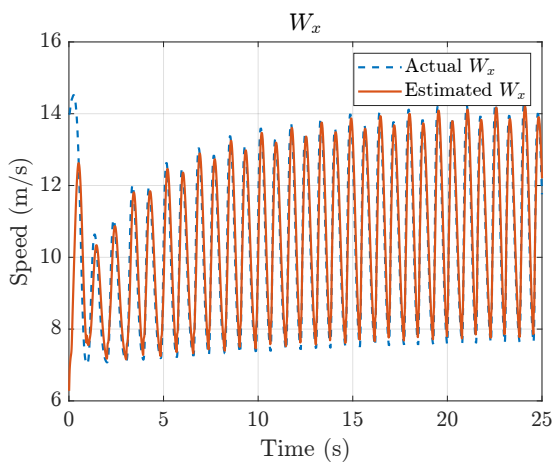

(a) Estimated wind in time

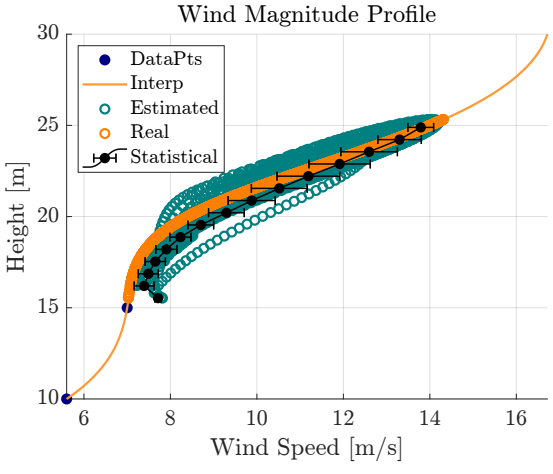

(b) Estimated wind profile

Figure 4: Estimation results

The statistical analysis shown in Figure 4b was produced by grouping the estimated wind points by different height ranges. By flying repetitively in the same area, as commonly done by AWES systems, the estimation approach proposed is able to accurately reconstruct the input wind profile.

4 Conclusions and Further Developments

Absolute wind vector estimation is crucial for optimizing AWE systems. This work introduces a novel methodology that improves existing techniques by employing optimization techniques, yielding excellent results despite its simplicity. The approach is easily replicable across different systems and robust to uncertainties, making it flexible for various constraints.
Further research could involve testing with real-world data, reconstructing wind fields using the estimated vectors, and implementing kites as sensors to enhance wind field models and flight zone selection, with the objective of steering the system to more profitable areas.

References

[1] C. L. Archer. *An Introduction to Meteorology for Airborne Wind Energy*, pages 81–94. Springer Berlin Heidelberg, Berlin, Heidelberg, 2013.

[2] L. Fagiano. Constrained numerical optimization for estimation and control.

[3] L. Fagiano. *Control of tethered airfoils for high-altitude wind energy generation*. Ph.d. dissertation, Politecnico di Torino, Turin, Italy, 2009. Available: http://hdl.handle.net/11311/1006424.

[4] L. Fagiano, M. Quack, F. Bauer, L. Carnel, and E. Oland. Autonomous airborne wind energy systems: Accomplishments and challenges. *Annu. Rev. Control. Robotics Auton. Syst.*, 5:603–631, 2021.

[5] G. Hafidi and J. Chauvin. Wind speed estimation for wind turbine control. In *2012 IEEE International Conference on Control Applications*, pages 1111–1117, 2012.

[6] A. W. H. Lio and F. Meng. Effective wind speed estimation for wind turbines in down-regulation. *Journal of Physics: Conference Series*, 1452(1):012008, jan 2020.

[7] M. L. Loyd. Crosswind kite power. *J. Energy*, 4:106–11, 1980.

[8] E. Schmidt, M. De Lellis Costa de Oliveira, R. Saraiva da Silva, L. Fagiano, and A. Trofino Neto. In-flight estimation of the aerodynamics of tethered wings for airborne wind energy. *IEEE Transactions on Control Systems Technology*, 28(4):1309–1322, 2020.

X-Rotor Scaling and Operation with Primary Rotor Generator

Yoke Wang Tan, Laurence Morgan, William Leithead, James Caroll, Mehrad Kazemi Amiri

E-mail: tan.yoke.wang@strath.ac.uk

Keywords: X-Rotor, QBlade

The X-rotor is a novel wind turbine concept which combines a vertical axis primary rotor with horizontal axis secondary rotors with the potential to reduce the levelized cost of energy from offshore wind by 20-30% [1]. This project aims to investigate the 1:10 scaled free vortex wake model with turbulent vorticity of 2-bladed X-rotor wind turbine using Qblade simulation software. An aero-elastic model of the primary rotor will also be developed to investigate the aeroelastic effects on the power production and load distribution of the primary rotor of the X-rotor concept. The scaled model study will be used to support the fabrication of 1:10 scaled prototype of 2-bladed X-rotor concept.

Figure 1: Design Representation of the X-Rotor Concept.

References

[1] W. Leithead, A. Camciuc, A. K. Amiri and J. Carroll, "The X-Rotor Offshore Wind Turbine Concept," *Journal of Physics: Conference Series,* 1356:1 – 012031, 2019.